# DIAGNOSTICS AT THE MAX IV 3 GeV STORAGE RING DURING COMMISSIONING

Å. Andersson†, J. Breunlin, B. N. Jensen, R. Lindvall, E. Mansten, D. Olsson, J. Sundberg, P. F. Tavares, S. Thorin, MAX-IV Laboratory, Lund University, Lund, Sweden

*Abstract*

The MAX IV 3 GeV storage ring based on a multibend achromat lattice allows for horizontal emittances from 330 pm rad down to 180 pm rad, depending on the number of insertion devices. The diagnostics used during commissioning will be described, with emphasis on the emittance diagnostics. This will involve two diagnostic beam lines to image the electron beam with infrared and ultraviolet synchrotron radiation from bending magnets, in order to determine also beam energy spread. The scheme for horizontal emittance measurements looks promising also for an order of magnitude lower emittance. Bunch lengthening with harmonic cavities is essential for the low emittance machine performance. We have used a radiation-based sampling technique to verify individual bunch distributions.

## THE MAX IV FACILITY

The MAX accelerator facility is shown in Fig. 1. A more detailed description can be found in [1]. As an injector, a 3 GeV S-band linac has been chosen. Admittedly, a booster synchrotron is a more economical choice as a ring injector, but a linac injector opens up for Short-Pulse Facility (SPF) operation [2] and also paves the way for possible Free-Electron Laser operation [3]. A smaller ring at 1.5 GeV, MAX V, was also introduced at the laboratory to increase the spectral range of high-quality undulator radiation. This ring has just started (fall 2016) to be commissioned.

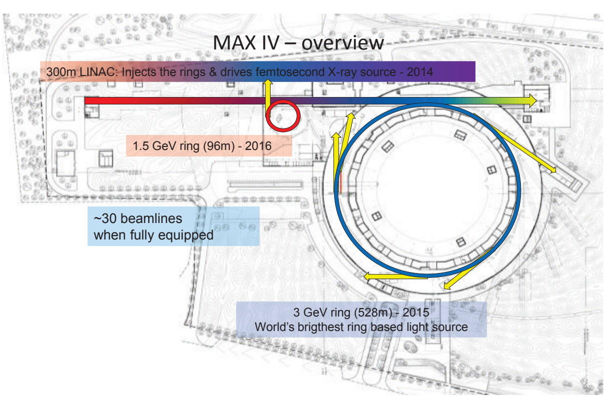


Figure 1: The MAX IV facility.

## THE LINAC INJECTOR AND ITS MAIN DIAGNOSTICS FOR INJECTION

The 3 GeV injector linac is described in more detail in [1] and [4]. Two electron guns are used; one thermionic RF gun used for injections into the rings and one photo-cathode RF gun for short pulse operation for the SPF. Our experience with the former is positive regarding robustness and long cathode lifetime. However, recent experience with the photo-cathode gun operation exceeds the expectations, and in future it might be used as injector gun as well. In this paper we limit the description to the diagnostics relevant for ring injections.

Linac commissioning started in August 2014 when the installation of the MAX IV 3 GeV ring started. After one year the linac commissioning was completed and the 3 GeV ring commissioning started. Some parameters for the MAX IV linac can be found in Table 1.

Table 1: Injector Linac Parameter Values

| | |
|---|---|
| End energy | 3 GeV |
| RF | 2.9985 GHz |
| Field gradient | 17 MV/m |
| Acc cell length | 5.2 m |
| No of structures | 39 |
| Bunch compressors | Double achromats |

### *Current Transformers*

The beam current and the electron bunch train envelope are resolved by twelve current transformers (CTs). Three of them are strategically placed after the RF thermionic gun, just after the chopper system [5], and just after an energy filter designed to cut away the low energy tail of the emitted pulse. Examples of these pulses are shown in Fig. 2. The chopper system efficiently creates a 100 MHz time structure, matching the ring RF, or a 500 MHz structure for maximum ring BPM sensitivity. Further, two CTs surround each bunch compressor achromats, and two CTs are placed at the beginning and at the end of each transfer line going up to the two rings. The CT signals are used continuously by the radiation protection system generating alarms in case of non-acceptable losses.

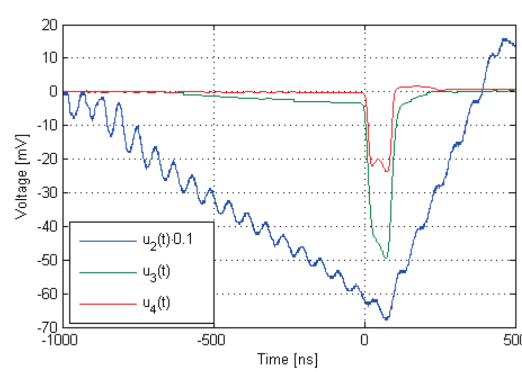


Figure 2: CT signals (Z=1 Ω) after thermionic gun (blue), chopper system (green) and energy filter (orange).

ISBN 978-3-95450-177-9

# BEAM COMISSIONING OF SuperKEKB RINGS AT PHASE 1

M. Tobiyama*, M. Arinaga, J. W. Flanagan, H. Fukuma, H. Ikeda, H. Ishii, K. Mori, E. Mulyani[1], M. Tejima, KEK Accelerator Laboratory, 1-1 Oho, Tsukuba 305-0801, Japan
[1]also at SOKENDAI (The Graduate University for Advanced Studies), 1-1 Oho, Tsukuba, Japan
G.S. Varner, U. Hawaii, Dept. Physics and Astronomy, 2505 Correa Rd., Honolulu HI 96822 USA
G. Bonvicini, Wayne State U., 135 Physics Bldg., Detroit MI 48201, USA

*Abstract*
The Phase 1 commissioning of SuperKEKB rings without superconducting final focus magnets or Belle-II detector began in Feb., 2016. A total of 1010 mA (LER) and 870 mA (HER) stored beam has been achieved close to the design emittance and x-y coupling. Most of the beam diagnostics, including new systems such as gated turn-by-turn monitors and X-ray beam size monitors, have been commissioned with beam and proved to be essential to the success of machine commissioning. The results of the beam commissioning, including the evaluation and difficulties of the beam diagnostics are shown.

## INTRODUCTION

The KEKB collider has been upgraded to the SuperKEKB collider with a final target of 40 times higher luminosity than that of KEKB. It consists of a 7 GeV high energy ring (HER, electrons) and a 4 GeV low energy ring (LER, positrons). About 2500 bunches per ring will be stored at total beam currents of 2.6 A (HER) and 3.6 A (LER) in the final design goal.

The first stage of commissioning (Phase 1 operation) without the Belle-II detector started in Feb. 2016 and continued until the end of June [1]. The major purposes of this operation were start-up of each hardware components, establishment of beam operation software and tools, low-emittance and x-y coupling tuning, and background studies with the BEAST detector. The Belle-II group requested an integrated beam dose of 360 to 720 Ah to achieve a very low beam-gas background when the Belle-II detector is installed at Phase 2.

The beam instrumentation has played a very important role at each step of commissioning, such as establishing the circulating orbit in the very early stage of commissioning, accumulating large beam currents, and so on. At the same time the performance of the beam instrumentations has been evaluated by the beam.

In this paper we describe the results of the beam commissioning of SuperKEKB rings with the obtained performance of the beam instrumentations. The main parameters of the Phase 1 operation of SuperKEKB HER/LER and the types and number of main beam instrumentations are shown in Table 1.

## OUTLINE OF THE COMMISSIONING

Figure 1 shows the Phase 1 commissioning history [2].

* email address: makoto.tobiyama@kek.jp

Table1: Main Parameters and Beam Instrumentations of SuperKEKB HER/LER in Phase 1 Operation

| | HER | LER |
|---|---|---|
| Energy (GeV) | 7 | 4 |
| Circumference(m) | 3016 | |
| Max. Beam current (mA) | 1010 | 870 |
| Max. Number of bunches | 2455 | 2363 |
| Single bunch current (mA) | 1.04 | 1.44 |
| Min. bunch separation(ns) | 4 | |
| Bunch length (mm) | 5 | 6 |
| RF frequency (MHz) | 508.887 | |
| Harmonic number (h) | 5120 | |
| Betatron tune (H/V) | 44.54/46.56 | 45.54/43.56 |
| Synchrotron tune | 0.02 | 0.018 |
| T. rad. damping time (ms) | 58 | 43 |
| L. rad. damping time (ms) | 29 | 22 |
| x-y coupling (%) | 0.27 | 0.28 |
| Natural emittance (nm) | 3.2 | 4.6 |
| Beam position monitor | 486 | 444 |
| BPM Displacement sensor | 110 | 108 |
| Gated turn-by-turn monitor | 58 | 59 |
| Transverse FB system | 2 | 2 |
| Longitudinal FB system | 0 | 1 |
| Visible SR size monitor | 1 | 1 |
| X-ray size monitor | 1 | 1 |
| Betatron tune monitor | 2 | 2 |
| DCCT | 1 | 1 |
| CT | 1 | 1 |
| Bunch current monitor | 1 | 1 |

The commissioning started with the tuning of the beam transfer lines. Injection to the LER started on Feb. 8th and beam was successfully stored on the 10th. The HER



ISBN 978-3-95450-177-9

# DIAGNOSTIC SYSTEMS FOR THE PAL-XFEL COMMISSIONING

Changbum Kim*, Sojeong Lee, Gyujin Kim, Bonggi Oh, Haeryong Yang, Juho Hong, Hyo-Jin Choi, Geonyeong Mun, Soungyoul Baek, Dongchul Shin, Youngjin Suh, Byoung Ryul Park, Jihwa Kim, Heung-Sik Kang, and In Soo Ko
Pohang Accelerator Laboratory, POSTECH, Pohang 790-834, Korea

*Abstract*

In 2011, an X-ray Free-Electron-Laser project was started in the Pohang Accelerator Laboratory (PAL-XFEL). The construction of the PAL-XFEL was finished at the end of 2015, and the commissioning was started from April 2016. The electron beam energy of 10 GeV was achieved at the end of April and the bunch compression was tried in May. The undulator commissioning was started from June. During the commissioning process, various kinds of instruments were used for the beam parameter monitoring including beam position monitors, beam profile monitors, beam charge monitors, beam arrival-time monitors, and beam loss monitors. This work will introduce the PAL-XFEL diagnostic system which was used in the commissioning process.

## INTRODUCTION

The PAL-XFEL is a fourth-generation light source to produce hard X-ray radiation with a femto-second pulse width by using the Self Amplification of Spontaneous Emission (SASE) [1]. In the PAL-XFEL, electron beams with 200 pC can be generated from a photocathode RF gun and accelerated to 10 GeV energy by using a 780 m long linear accelerator. After the linear accelerator, the electron beam passes through a 250 m long undulator section to produce hard X-ray of 0.1 nm wavelength. Finally, the FEL radiation come into the beamline of which length is 80 m long. Figure 1 shows a bird's eye view of the PAL site. The PAL-XFEL is shown as a long line in the left and the storage ring of the PLS-II is shown in the right.

The PAL-XFEL building construction was started from September 2012 and it was finished in December 2014. After that, the installation of the linac, the undulator, and the beamline components were continued to the end of 2015 as shown in Fig. 2. The RF conditioning started from November 2015 and it was continued about six months. The commissioning was started in the mid of April 2016, and 10 GeV electron beam was achieved in the end of April. The first spontaneous radiation of the undulator was obtained on 12th of June, and the first SASE FEL was observed on 14th of June 2016. The wavelength of the SASE FEL radiation was 0.5 nm with the electron beam energy of 4 GeV.

For the successful commissioning of the PAL-XFEL, various kinds of diagnostics along the linac and undulator section were used to measure beam parameters such as the beam position, the beam charge, the beam size, the bunch length, et cetera. These parameters for the beam operation and instruments for measurements of them are listed in Table 1. In this paper, diagnostic system of the PAL-XFEL will be presented. It will include the beam position monitor, the beam profile monitor, the beam charge monitor, the beam arrival-time monitor, and the beam loss monitor.

## PAL-XFEL DIAGNOSTICS

### *Beam Position Monitor*

Figure 3 shows the stripline Beam-Position-Monitor (BPM) pickup of the PAL-XFEL. For the beam operation of an accelerator, it is important that the electron beam passes through the center of the quadrupole magnet to keep the beam shape symmetrically, and to make the orbit close to the ideal one as much as possible. In the PAL-XFEL, stripline BPMs were installed along the linear accelerator to monitor the beam position inside the vacuum chamber. The measured resolution of the stripline BPM was 3 $\mu$m. For the BPM

Figure 1: A bird's eyes view of the PAL. The PAL-XFEL and the PLS-II are shown in the left and the right, respectively.

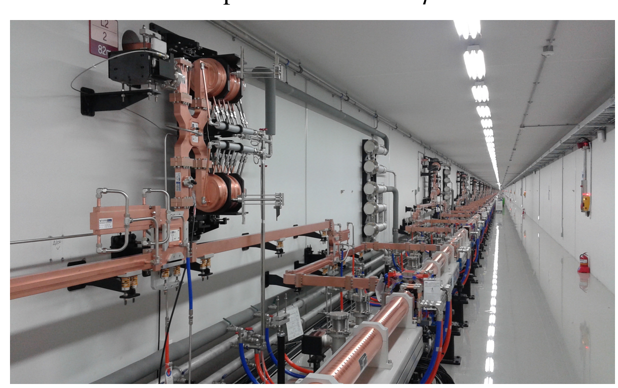

Figure 2: Accelerating structures inside the PAL-XFEL linac tunnel.

* chbkim@postech.ac.kr



ISBN 978-3-95450-177-9

# FIRST EXPERIENCE WITH THE STANDARD DIAGNOSTICS AT THE EUROPEAN XFEL INJECTOR

D. Lipka*, A. Affeldt, R. Awwad, N. Baboi, R. Barret, B. Beutner, F. Brinker, W. Decking, A. Delfs, M. Drewitsch, O. Frank, C. Gerth, V. Gharibyan, O. Hensler, M. Hoeptner, M. Holz, K. Knaack, F. Krivan, I. Krouptchenkov, J. Kruse, G. Kube, B. Lemcke, T. Lensch, J. Liebing, T. Limberg, B. Lorbeer, J. Lund-Nielsen, S. Meykopff, B. Michalek, J. Neugebauer, Re. Neumann, Ru. Neumann, D. Noelle, M. Pelzer, G. Petrosyan, Z. Pisarov, P. Pototzki, G. Priebe, K. Rehlich, D. Renner, V. Rybnikov, G. Schlesselmann, F. Schmidt-Foehre, M. Scholz, L. Shi, P. Smirnov, H. Sokolinski, C. Stechmann, M. Steckel, R. Susen, H. Tiessen, S. Vilcins, T. Wamsat, N. Wentowski, M. Werner, C. Wiebers, J. Wilgen, K. Wittenburg, R. Zahn, A. Ziegler,
DESY, Hamburg, Germany
O. Napoly, C. Simon, CEA Saclay, France
A. Ignatenko, DESY, Zeuthen, Germany
R. Baldinger, R. Ditter, B. Keil, W. Koprek, R. Kramert, G. Marinkovic, M. Roggli, M. Stadler, D. M. Treyer, PSI, Villigen, Switzerland†
A. Kaukher, European XFEL, Hamburg, Germany

*Abstract*

The injector of the European XFEL started beam operation in December 2015. Besides the gun and the accelerating section, containing a 1.3 and a 3.9 GHz accelerating module, it contains a variety of standard diagnostics systems specially designed for this facility. With very few exceptions, all types of diagnostics systems of the whole XFEL are installed in the injector. Therefore the injector operation allows validating and proving of the diagnostics performances for the entire facility. Most of the standard diagnostics have been available from the very beginning of the beam operation and have been used for the monitoring of the first beam. In the following months the diagnostics have been optimized and used for improvements of beam quality. In this contribution, the first results and the operation experience of the standard beam diagnostics of the European XFEL are reported.

## INTRODUCTION

The European X-ray Free-Electron Laser (E-XFEL) [1] is the 3.4 km long international facility, running from DESY in Hamburg to the town of Schenefeld (Schleswig-Holstein) in Germany. To construct and operate the E-XFEL, international partners agreed on the foundation of an independent research organization – a non-profit limited liability company under German law named the European XFEL GmbH. DESY is leading the accelerator construction consortium and will be in charge of the accelerator operation.

The accelerator is based on superconducting TESLA Radio-Frequency (RF) technology. Within one RF pulse of up to 600 $\mu$s length, a train with up to 2700 bunches will be generated. This results in a bunch minimal spacing of 222 ns. The repetition rate of the RF pulses is 10 Hz, so that a maximum number of 27000 X-ray pulses per second can be produced. The operation charge varies from 20 pC to 1 nC to provide different characteristics of the output radiation, i. e. the average power or the bunch length, as requested by the users. Therefore diagnostics components have to monitor the beam properties within this dynamic range.

Beam operation of the photocathode gun started already in February 2015, the complete injector became operable in December 2015. In this first accelerator part of the facility, several diagnostics systems are installed, commissioned and have been optimized for the measurement of the electron beam properties. This paper focuses on standard electron beam diagnostics for the E-XFEL injector. Special and higher-order mode diagnostics systems are described in [2–8].

## STANDARD DIAGNOSTICS FOR THE EUROPEAN XFEL

The standard diagnostics contains a variety of position, charge and loss monitors and screen stations. It is also planned to use wire scanners at positions with high electron energies. The full list of monitoring systems is given in Table 1. A description of the different systems with results of their laboratory and beam tests can be found in [9–24].

Table 1: Diagnostics System Numbers for the Complete E-XFEL and for the Gun with Injector

| System | Total number | Gun and injector |
|---|---|---|
| BPMs | ~460 | 14 |
| Charge monitors | ~50 | 10 |
| Screens | ~70 | 11 |
| Wire scanners | 12 | 0 |
| Loss monitors | ~490 | 20 |

* dirk.lipka@desy.de

† This work was partially funded by the Swiss State Secretariat for Education, Research and Innovation SERI

# LHC ONLINE CHROMATICITY MEASUREMENT - EXPERIENCE AFTER ONE YEAR OF OPERATION

K. Fuchsberger, G.H. Hemelsoet (CERN, Geneva, Switzerland)


## *Abstract*

Hardware and infrastructural requirements to measure chromaticity in the LHC were available since the beginning. However, the calculation of the chromaticity was mostly made offline. This gap was closed in 2015 by the development of a dedicated application for the LHC control room, which takes the measured data and produces estimates for the chromaticity values immediately online and allows to correct chroma and tune accordingly. This tool proved to be essential during commissioning as well as during every injection phase of the LHC. It became particularly important during the intensity ramp up with 25ns where good control of the chromaticity became crucial at injection. This paper describes the concepts and algorithms behind this tool, the experience gained as well as further plans for improvements.


## INTRODUCTION

A very good control of chromaticity is critical for LHC operation to counteract instabilities and resulting emittance blowup. During standard operation a big part of this is achieved by model based feed-forward during injection and ramp [1, 2]. However, in numerous operational scenarios (e.g. commissioning periods, machine development, non-standard cycles), a manual way for the operations crew to check and correct chromaticity is indispensible.

Additionally, the measurement data for the feed-forward and for tuning the models have to be qualified and at the beginning of each filling of the LHC, the chromaticity is systematically checked by the operations team. Therefore, such means have to be quick and simple in order reduce turnaround time and operational mistakes, respectively.

Already in LHC run 1, a simple online chroma display was available, based on radial modulation. At the start of run 2, with the big amount of software changes on different layers, this display became dysfunctional and was not maintained anymore. To fill this gap, a more integrated application was introduced, which not only allowed measuring and tracking chroma through the cycle, but also allowed direct calculations of corrections and sending them to the hardware.

The following sections are describing the principles and features of this application, its usage and future improvements as well as some more general outlook on the future of LHC online chroma measurement.

## FEATURES AND OVERVIEW

Figure 1 shows a screenshot of the LHC chroma application displaying traces of measured chroma during a ramp. The top panel of this application shows the actually measured chroma values, allows to set target values, calculate


Figure 1: LHC Chroma Application, showing chroma traces throughout a ramp, dedicated chroma measurement.

corrections and send them to the hardware. The bottom panel of the application can display various traces of input- and calculated data:

- raw tunes,
- raw RF modulation signal,
- fits to both (see below) and
- calculated chroma values.

Further, the same application also allows to trim tune values (placed on a second tab).

Since no direct measurement of the chromaticity is yet available at the LHC, the chroma app follows the 'usual procedure' as if measuring the chroma manually: Changing the RF frequency (corresponding to an energy change) and measuring the tune change resulting from this energy change. Therefore, two signals are required: The frequency change (wrt the centered frequency) and the actual tune of the machine.

### *Raw Data Flow*

While the RF frequency is a direct input to the machine and can therefore directly be acquired from the RF systems in high precision, the tune has to be derived (measured) from the transverse beam motions. The state-of-the-art devices to accomplish a high sensitivity tune signals are the so-called BBQ devices [3], which deliver a very good tune signal under various different conditions. Without going into the detailed complexity of the full LHC tune acquisition chain, we only want to mention here, that these are the same systems which are also used for the LHC tune realtime feedback systems. Several instances of such BBQ devices are available, which are pre-configured for different scenarios (mainly driven by



ISBN 978-3-95450-177-9

# HARMONICALLY RESONANT CAVITY AS A BUNCH LENGTH MONITOR

B. Roberts, M. Pablo, Electrodynamic 4909 Paseo Del Norte Ne suite D, Albuquerque, NM 87113
E. Forman, J. Grames, F. Hannon, R. Kazimi W. Moore, M. Poelker, Thomas Jefferson National Accelerator Facility, 12000 Jefferson Ave., Newport News, VA 23606,
M. M. Ali, Department of Physics, Old Dominion University, Norfolk, Virginia 23529

*Abstract*

A compact, harmonically-resonant cavity with a fundamental resonant frequency of 1497 MHz was used to evaluate the temporal characteristics of electron bunches produced by a 130 kV dc high voltage spin-polarized photoelectron source at the Continuous Electron Beam Accelerator Facility (CEBAF) photoinjector, delivered at 249.5 and 499 MHz repetition rates and ranging in width from 45 to 150 picoseconds (FWHM). The cavity's antenna was attached directly to a sampling oscilloscope that detected the electron bunches as they passed through the cavity bore with a sensitivity of ~ 1 mV/µA. The oscilloscope waveforms are a superposition of the harmonic modes excited by the beam, with each cavity mode representing a term of the Fourier series of the electron bunch train. Relatively straightforward post-processing of the waveforms provided a near-real time representation of the electron bunches revealing bunchlength and the relative phasing of interleaved beams. The non-invasive measurements from the harmonically-resonant cavity were compared to measurements obtained using an invasive rf-deflector-cavity technique and to predictions from particle tracking simulations [1].

## THE HARMONIC CAVITY

The Harmonic cavity was designed to resonate at many harmonic $TM_{0N0}$ modes, and to suppress or displace TE and non-axially symmetric TM modes within or beyond its operational bandwidth. The shallow saucer-shaped cavity (Fig 1) has a mode spectrum free of TE modes for several tens of GHz because TE modes resonate at frequencies greater than $c/2h$ where $c$ is the speed of light and $h$ is the cavity length along the beam's direction of motion. Radial slits cut into the cavity walls do not affect the $TM_{0N0}$ modes which have purely radial wall currents while the $TM_{MNP}$ modes with azimuthal mode numbers, M, less than the number of discontinuities are suppressed. Finally, the shape of the cavity was tuned to yield harmonic TM0N0 modes. This was accomplished in the design phase by iteratively modifying the cavity geometry and solving for the $TM_{0N0}$ mode frequencies with the field solver POISSON/Superfish [2]. The $TM_{0N0}$ cavity modes are axially symmetric and have a field maximum on the cavity axis, i.e., along the direction of the electron beam motion.

Electron bunches at a pulse repetition rate $w_0$ can be described using a Fourier series expansion:

$$i_{beam}(t) = a_1 \cos(w_o t + \theta_1) + a_2 \cos(2w_o t + \theta_2) \ldots + a_n \cos(n w_o t + \theta_n) \quad (1)$$

where $a_n$ and $\theta_n$ describe the relative amplitudes and phases of each contributing harmonic term. The non-invasive bunchlength monitor cavity was designed to measure each term of the Fourier series expansion:

$$v_{detected}(t) = a_{TM_{010}} \cos(w_0 t + \theta_{010}) + a_{TM_{020}} \cos(2w_0 t + \theta_{020}) \ldots + a_{TM_{0n0}} \cos(n w_0 t + \theta_{0n0}) \quad (2)$$

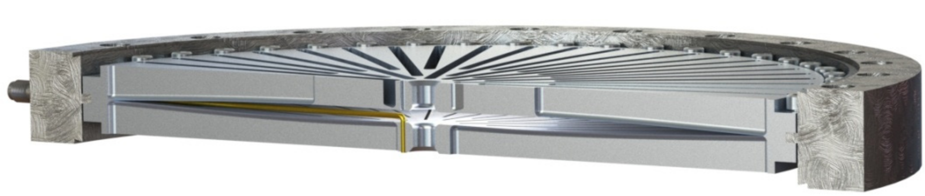

Figure 1: (top) A cut-away drawing of the harmonically-resonant cavity showing the antenna and the curvature of the cavity surfaces. (bottom) A photograph of the cavity nested inside the bore of a 10” double-sided knife edge Conflat flange. Two additional 10” Conflat flanges attach to either side to form the UHV-compatible vacuum vessel.



ISBN 978-3-95450-177-9

# DESIGN, PRODUCTION AND TESTS OF BUTTON TYPE BPM FOR TAC-TARLA IR FEL FACILITY

M. T. Gundogan, O. Yavas, Dept. of Engineering Physics, Ankara University, Ankara, Turkey
A.Aydin, E.Kasap, Dept. of Physics, Gazi University, Ankara, Turkey
C.Kaya, Institute of Accelerator Technologies, Ankara University, Ankara, Turkey

*Abstract*

Turkish Accelerator and Radiation Laboratory in Ankara (TARLA) facility is an IR FEL and Bremsstrahlung facility as the first facility of Turkish Accelerator Center (TAC) that is under construction in Golbasi Campus of Ankara University. TARLA is proposed to generate oscillator mode FEL in 3-250 microns wavelengths range and Bremsstrahlung radiation. It will consist of normal conducting injector system with 250 keV beam energy and two superconducting RF accelerating modules in order to accelerate the beam 15-40 MeV. The electron beam will be in both continuous wave (CW) and macro pulse (MP) modes. The bunch charge will be limited by 77pC and the average beam current will be 1 mA.

To detect electron beam position, BPM (Beam Position Monitor) has to use through beam line. Wall current monitor based system button type TARLA BPM are briefly mentioned.

In this study, simulation results of design in CST, production and test studies for button type TARLA BPM are presented. Mechanical and electronic design, antenna simulations, and the latest testing procedures are given for a button type BPM.

## INTRODUCTION

The Turkish Accelerator Center (TAC) Collaboration is established in 2006 as an inter-university collaboration with 12 Turkish Universities under the coordination of Ankara University by support of Ministry of Development of Turkey. Main aim of the collaboration is to study on technical design and construction of proposed accelerator facilities in Turkey for accelerator based scientific research and technological developments in basic and applied sciences [1].

Turkish Accelerator and Radiation Laboratory in Ankara (TARLA) facility is under construction as a first facility of TAC which is proposed to generate infrared FEL beams in 3-250 micrometers wavelength range based on superconducting electron linac with 15-40 MeV beam energy [2]. TARLA electron source is a thermionic DC gun with 250 keV energy. It is planned that the TARLA facility will provide electron beam in continuous wave (CW) and macro pulse (MP) modes based on SRF modules. Longitudinal electron bunch length will be change between 6ps and 0.4 ps along to accelerator. Repetition rate of electron bunches will be 13 MHz. The bunch charge will be limited by 77pC and the average beam current will be 1 mA. The schematic diagram of TARLA facility is shown in Figure 1 [3].

The facility will contain also IR FEL and Bremsstrahlung radiation production halls and experimental stations. It is planned that the facility will produce two FEL beams by two different undulator magnets U25 and U90 with 2.5 cm and 9 cm period lengths, respectively. The main aim of the facility is to use IR FEL beams for research and application in material science, nonlinear optics, semiconductors, biotechnology, medicine and photochemical processes. In addition, a bremsstrahlung station is planned for nuclear spectroscopy studies up to 35 MeV. The main parameters of TARLA Facility are given in Table 1[3].

Table 1: The Main Parameters of TARLA Facility

| Parameters | Value |
|---|---|
| Energy [MeV] | 15-40 |
| Bunch charge [pC] | 77 |
| Average beam current [mA] | 1.0 |
| Bunch repetition rate [MHz] | 13 (16.25) |
| Bunch length [ps] | 0.4-6 |
| Norm. RMS trans. emit. [mm mrad] | < 16 |
| Norm. RMS long. emittance. [keV.ps] | < 100 |
| Macro pulse duration [µs] | 50 - CW |
| Macropulse reputation rate [Hz] | 1- CW |
| Wavelength [µm] | U25:3-20<br>U90:18-250 |

## BEAM POSITION MONITORS FOR TARLA

Beam diagnostics is an essential part for all types of accelerators; because it should be known different beam characteristics such as beam position, beam current, beam charge etc. Beam characteristics have been kept under control by diagnostic devices. Beam position monitors are one of important online diagnostics devices to measure the position of the beam in the beam line. They are designed in order to provide reliable and accurate beam position readings. Typical BPM is composed of four opposite mounted plates called electrodes or antenna.

The difference of signal from opposite electrodes gives information about the beam position and average beam current in the beam line and report it to the control system [4].

ISBN 978-3-95450-177-9

# INVESTIGTION OF TRANSVERSE BEAM INSTABILITY INDUCED BY AN IN-VACUUM UNDULATOR AT SPEAR3*

K. Tian†, J. Sebek, J. L. Vargas, SLAC National Accelerator Laboratory, Menlo Park, USA

*Abstract*

Vertical beam instabilities have been observed at SPEAR3 when a newly installed in-vacuum undulator (IVUN) is operated at a set of narrow gap settings. The source of the instabilities is believed to be vertically deflecting trapped modes inside the IVUN tank that are excited by the beam. We have used beam-based measurements to characterize the frequencies and strengths of the excited modes using both our bunch-by-bunch feedback system and a spectrum analyzer. Using numerical simulations of our IVUN structure, we have found modes with high shunt impedance near the measured frequencies. Recently, we have successfully measured these IVUN modes during our current downtime. In this paper, we will report on the measurements, simulations, and plans to damp these modes.

## INTRODUCTION

Transverse beam instabilities at intermittent IVUN pole gap positions have previously been reported by other facilities [1-3]. However, the sources of the instabilities have never been well understood. Recently, we have observed similar beam instabilities associated with one of our IVUNs, the BL15 insertion device (ID).

The 2-meter-long BL15 insertion device in SPEAR3 is the second IVUN in the storage ring and is still under commissioning for full user operation. The undulator period is 22 mm with 86 full strength periods and 2 end periods with reduced strength. When in operations, it will close down to a minimum 6.82 mm pole gap. During early commissioning tests of BL15 ID, we encountered several problems. We found that the injection efficiency of the storage ring degraded significantly when the ID gap was closed to the minimum gap. Therefore, we temporarily raised the lower limit of the ID gap to 8 mm in the control system. Later, we found that the beam size blew up when the gap was set to 8.4 mm during 500mA operation. Upon further investigation, we have discovered that these problems are likely caused by vertical beam instabilities that have occurred at these and other intermittent pole gaps.

The cross section of the ID chamber is shown on the left of Fig. 1. As a standard means of decreasing the resistive wall impedance of the ID, two 70mm wide nickel-plated copper foils (current sheets) are attached to both the top and bottom rows of the magnets through the magnetic attractive force of the nickel to the pole pieces. Since the electron beam is shielded by the current sheet, we can simplify the complicated ID chamber assembly by approximating it by a round ridge waveguide shown on the right of Fig. 1. The width and height of the narrow gap at the center of the ridge waveguide represent the width of the current sheets and the pole gap, respectively. Based on the theory of the ridge waveguide [4], the cutoff frequency of the waveguide will decrease with the gap height. Because the ID gap opens up to 34 mm at the end of the transition, a small gap means that the cut-off frequency for the cross-sections of the central part of the ID will be lower than that for the cross-sections at the ends of the ID. As a result, the beam can excite low frequency modes which are trapped inside the ID chamber. We believe that these trapped modes are the sources of the beam instabilities we observed at SPEAR3. In the following, we will present the results from beam based measurements, numerical simulations, and RF measurements to support our theory.

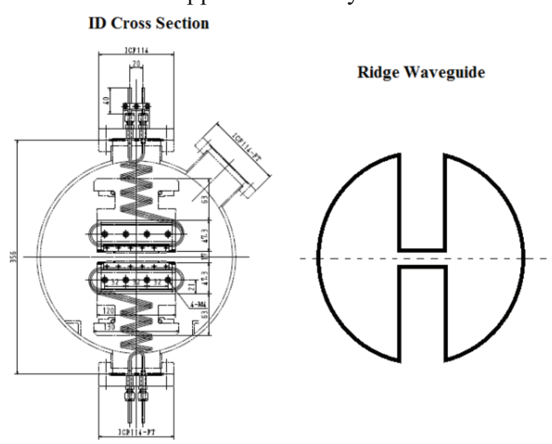


Figure 1: Cross section of SPEAR3 BL15 ID (left) and a round ridge waveguide (right).

## BEAM BASED MEASURMENT

To reveal all the instability modes at different gaps, we scanned the ID gap from 6.82mm to 8.6mm at 10 μm per step. Then we conducted modal analysis using the bunch-by-bunch (BxB) data taken by the feedback system [5] to characterize the mode number and potential frequencies of the modes at different ID gaps. The results are shown in Table 1. The pole gap in the table is the rough midpoint for each instability mode. For the transverse beam instability, the lower betatron sideband drives the instability while the upper sideband damps it [6], so the instability modes and frequencies shown in the table all correspond to the lower sideband of the lowest potential driving frequency. Starting from 6.82mm, we observed a series of instability modes, each of which covered ~100 μm gap range and was separated by ~300 μm from its neighbors. This indicates that the resonant frequency of the problematic mode in the ID chamber reduces by one

* Work supported by DOE contract DE-AC02-76SF00515
† email address: ktian@slac.stanford.edu

ISBN 978-3-95450-177-9

# TRANSIENT STUDIES OF THE STRIPLINE KICKER FOR BEAM EXTRACTION FROM CLIC DAMPING RINGS

C. Belver-Aguilar, M.J. Barnes, CERN, Geneva, Switzerland

*Abstract*

Stripline kickers are generally assumed to have equal contributions from the electric and magnetic field to the total deflection angle, for ultra-relativistic beams. Hence parameters of the striplines, such as the characteristic impedance, the field homogeneity and the deflection angle are typically determined by simulating the striplines from an electrostatic perspective. However recent studies show that, when exciting the striplines with a trapezoidal current pulse, the magnetic field changes during the flat-top of the pulse, and this can have a significant effect upon the striplines performances. The transient solver of Opera2D has been used to study the magnetic field, for the striplines to be used for beam extraction from the CLIC Damping Rings (DRs), when exciting the electrodes with a pulse of 1 $\mu$s flat-top and 100 ns rise and fall times. The time dependence of the characteristic impedance, field homogeneity and deflection angle are presented in this paper. In addition, two solutions are proposed to improve the flatness of the magnitude of the magnetic field throughout the flat-top of the pulse, and the predicted results are reported.

## STUDIES IN THE TIME DOMAIN

DRs for high energy $e^+e^-$ colliders, such as CLIC, have a significant role for achieving high luminosity at the interaction point. Two RF baselines are considered for the CLIC DR operation: 1 GHz and 2 GHz RF systems. The injection and extraction process from the DRs will be carried out using one injection and one extraction system, respectively, in each ring, with only one pulse stored in the rings per cycle: this pulse contains either one single train of 156 bunches with 1 GHz RF structure, or two trains of 312 bunches with 2 GHz RF structure. For the extraction system, a pulse of 560 ns rise/fall time and 900 ns pulse flat-top is required for the 1 GHz baseline, whereas the 2 GHz RF system demands a pulse of 1 $\mu$s rise/fall time and 160 ns flat-top [1].

Inductive adders will be used to generate the pulses for the striplines for the CLIC DRs [2]. In order to limit the electrical and thermal stresses on the system, the goal is to achieve output current pulse rise and fall times of approximately 100 ns.

The deflecting field of the striplines has been previously studied considering only an electrostatic field [3] and an AC magnetic field [4]. Now, transient simulations with Opera2D [5] have been carried out, and a pulse of 100 ns rise and fall time and 1 $\mu$s flat-top has been considered (values close to the 1 GHz RF system goals). The prototype electrodes are made of aluminium Al6063, with an electrical conductivity $\sigma = 3.03 \times 10^7$ S/m. The magnetic field at the centre of the striplines aperture has been calculated and the results are shown in Fig. 1. For these simulations terminating resistors of 50 Ω are assumed, which results in a nominal current of ± 250 A with ± 12.5 kV driving voltage.

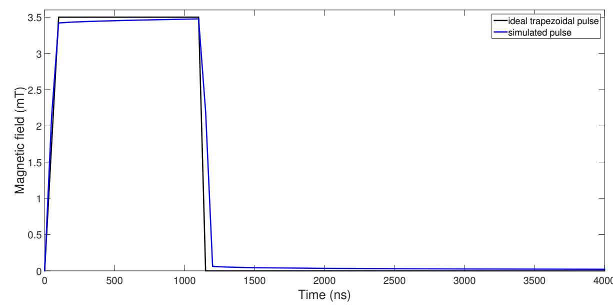


Figure 1: Magnetic field calculated with Opera2D (blue line), compared with an ideal trapezoidal current pulse (black line).

The odd mode characteristic impedance, field inhomogeneity and deflection angle have been studied when considering ideal trapezoidal voltage and current pulses. The characteristic impedance is calculated from inductance and capacitance: these quantities are derived from predicted stored magnetic and electrostatic energy, respectively. The odd mode characteristic impedance increases from 40.57 Ω at the beginning of the flat-top to 41.01 Ω at the end of the flat-top, corresponding to an increase of 1.1%. The field inhomogeneity at 1 mm radius, from the centre of the striplines aperture, increases from ±0.0028% to ±0.0112%, which is close to the maximum limit imposed by beam dynamics requirements (±0.01%). The total deflection angle increases from 1.3597 mrad to 1.3697 mrad, as shown in Fig. 2, which corresponds to an increase of 0.73%.

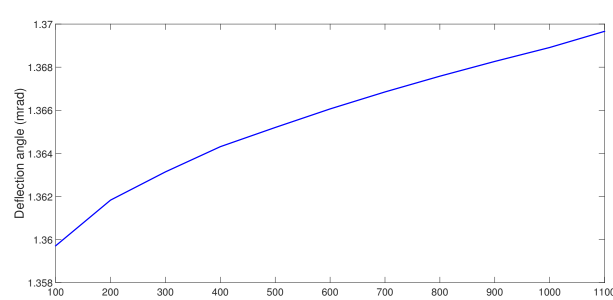


Figure 2: Total (sum of electric and magnetic) deflection angle, during the pulse flat-top.

The increase of the characteristic impedance and hence the increase of the magnetic field and deflection angle, during the pulse flat-top, is greater than specified. In an attempt to flatten the "flat-top" field two proposals are pre-

ISBN 978-3-95450-177-9

# FIRST BEAM TESTS OF THE APS MBA UPGRADE ORBIT FEEDBACK CONTROLLER*

N. S. Sereno†, N. Arnold, A. Brill, H. Bui, J. Carwardine, G. Decker, B. Deriy, L. Emery, R. Farnsworth, T. Fors, R. Keane, F. Lenkszus, R. Lill, D. Paskvan, A. Pietryla, H. Shang, S. Shoaf, S. Veseli, J. Wang, S. Xu, B. X. Yang,
ANL, Argonne, IL, USA 60439

*Abstract*

The new orbit feedback system required for the APS multi-bend acromat (MBA) ring must meet challenging beam stability requirements. The AC stability requirement is to correct rms beam motion to 10 % the rms beam size at the insertion device source points from 0.01 to 1000 Hz. The vertical plane represents the biggest challenge for AC stability which is required to be 400 nm rms for a 4 micron vertical beam size. In addition long term drift over a period of 7 days is required to be 1 micron or less at insertion device BPMs and 2 microns for arc bpms. We present test results of the MBA prototype orbit feedback controller (FBC) in the APS storage ring. In this test, four insertion device BPMs were configured to send data to the FBC for processing into four fast corrector setpoints. The configuration of four bpms and four fast correctors creates a 4-bump and the configuration of fast correctors is similar to what will be implemented in the MBA ring. We report on performance benefits of increasing the sampling rate by a factor of 15 to 22.6 kHz over the existing APS orbit feedback system, limitations due to existing storage ring hardware and extrapolation to the MBA orbit feedback design. FBC architecture, signal flow and processing design will also be discussed.

## INTRODUCTION

Figure 1 shows the layout of the “4x4-test” in sectors 27 and 28 of the APS storage-ring (SR). In green are shown the new orbit feedback hardware including the new FBC to process bpm data and generate corrector setpoints. Four insertion device A:P0 and B:P0 bpms are connected to commercial Libera Brilliance+ (LB+) bpm electronics from Instrumentation Technologies, Solkan, Slovenia to obtain beam position for processing in the FBC. The FBC receives the turn-by-turn (TBT) or 271 kHz beam position data, decimates it by twelve to 22.6 kHz and processes it to obtain corrector setpoints. The corrector setpoints are then applied using an interface (CMPSI-2) between the FBC and the existing fast corrector power supply (PS) controls. The four horizontal and vertical fast correctors used are the A:HV3s and B:HV4s in sectors 27 and 28. In addition the FBC is able to send its bpm and corrector data to a data acquisition system (DAQ) which allows the data to be captured and provides a convenient interface to perform step response measurements (at the 22.6 kHz corrector update rate).

Additional diagnostics shown in the figure include the mechanical motion system (MMS) system [1] and the next generation, grazing incidence insertion device (GRID) XBPM [2]. In these tests, we were most concerned with seeing what is required of the system to meet the AC stability specification so the MMS system data was not used by the FBC to correct for long term drift of the bpms. The GRID, also was not used but is presently used in the APS operations orbit feedback system. Table 1 lists the AC and long term beam stability requirements for the MBA ring.

To begin each study, the SR was filled to 102 mA in 324 equally spaced single bunches. Use of this bunch pattern is twofold: first, the LB+ bpms will have a clean, nearly CW signal at their rf inputs and hence all ADC samples in one turn can be used to compute the average beam position; second, this fill pattern has the longest lifetime (60 h) and there is no need for top-up. During top-up injection transients were expected to corrupt some of the data. Every so often, usually when the beam current dropped below 90-95 mA, we would do a fill-on-fill to 102 mA in the 324 bunch fill pattern.

We used the LB+ with its switching feature off so as to not corrupt the fast data stream (at TBT rates as sent to the FBC) with switching noise. The LB+ was operated in its time-domain processing (TDP) mode so as to reduce the latency as much as possible for data processing and transmission through the device (latency is 2 turns in this mode compared to its digital down-conversion (DDC) processing mode where the latency is 4 turns). Toward the end of the testing program reported here, we also implemented notch filtering to eliminate LB+ switching noise and a low-pass (LP) anti-alias filter in the LB+ to remove switching transients and prevent aliasing of signals above 11.3 kHz. The experiments reported in this note were all performed in the horizontal plane since the vertical plane response matrix was ill-conditioned when using all four singular values (SVs) to construct the inverse response matrix (irm).

## FEEDBACK CONTROLLER SIGNAL FLOW, PROCESSING, CONTROL AND HARDWARE

Figure 2 shows the signal flow from bpm data to processed and applied fast corrector setpoints. After forming the bpm error by subtracting the orbit setpoint, the bpm data is multiplied by an irm calculated using standard SR high level software tools. The corrector errors can then be filtered and sent through a PID regulator to produce corrector

* Work supported by the U.S. Department of Energy, Office of Science, under Contract No. DE-AC02-06CH11357

† sereno@aps.anl.gov



ISBN 978-3-95450-177-9

# FIRST OPERATIONAL EXPERIENCE WITH THE LHC DIODE ORBIT AND OSCILLATION (DOROS) SYSTEM

M. Gasior, G. Baud, J. Olexa, G. Valentino, CERN, Geneva, Switzerland

*Abstract*

The LHC started high-energy operation in 2015 with new tertiary collimators, equipped with beam position monitors embedded in their jaws. The required resolution and stability of the beam orbit measurements linked to these BPMs were addressed by the development of a new Diode ORbit and OScillation (DOROS) system. DOROS converts the short BPM electrode pulses into slowly varying signals by compensated diode detectors, whose output signals can be precisely processed and acquired with 24-bit ADCs. This scheme allows a sub-micrometre orbit resolution to be achieved with robust and relatively simple hardware. The DOROS system is also equipped with dedicated channels optimised for processing beam oscillation signals. Data from these channels can be used to perform betatron coupling and beta-beating measurements. The achieved performance of the DOROS system triggered its installation on the beam position monitors located next to the LHC experiments for testing the system as an option of improving the beam orbit measurement in the most important LHC locations. After introducing the DOROS system, its performance is discussed through both, beam and laboratory measurements.

## INTRODUCTION

The Diode ORbit and OScillation (DOROS) system has been primarily designed and optimised for processing signals from the beam position monitors (BPMs) embedded into the jaws of the LHC collimators [1-3]. The system provides orbit readings used for the automatic positioning of the collimator jaws symmetrically around the beam, which reduces drastically the time needed to set-up the collimators and ensures that the collimation hierarchy is always maintained [4].

The DOROS processing for one BPM electrode pair is schematically shown on the block diagram in Fig. 1. It contains four main parts, namely RF processing, orbit processing, oscillation processing and the FPGA controller. The role of the RF processing is to deliver signals with sufficiently large amplitudes to the orbit processing, whose key components are the compensated diode detectors [1]. The detectors convert the amplitude of RF beam pulses into DC voltages which can be measured with very high resolution by the system ADCs. As the orbit processing does not have sufficient bandwidth to cope with signals at LHC betatron frequencies (around 3 kHz), the system is also equipped with a dedicated circuitry optimised for beam oscillation signals.

The RF processing starts with 80 MHz non-reflective filters to reduce the peak amplitudes of the BPM signals, followed by an isolation RF transformer. The transformer cuts ground loops between the LHC machine and the racks where DOROS front-ends are installed, allowing a very clean transmission of the BPM signals. The signals then pass through a calibration switch, which periodically swaps the BPM electrode signals. This way each electrode

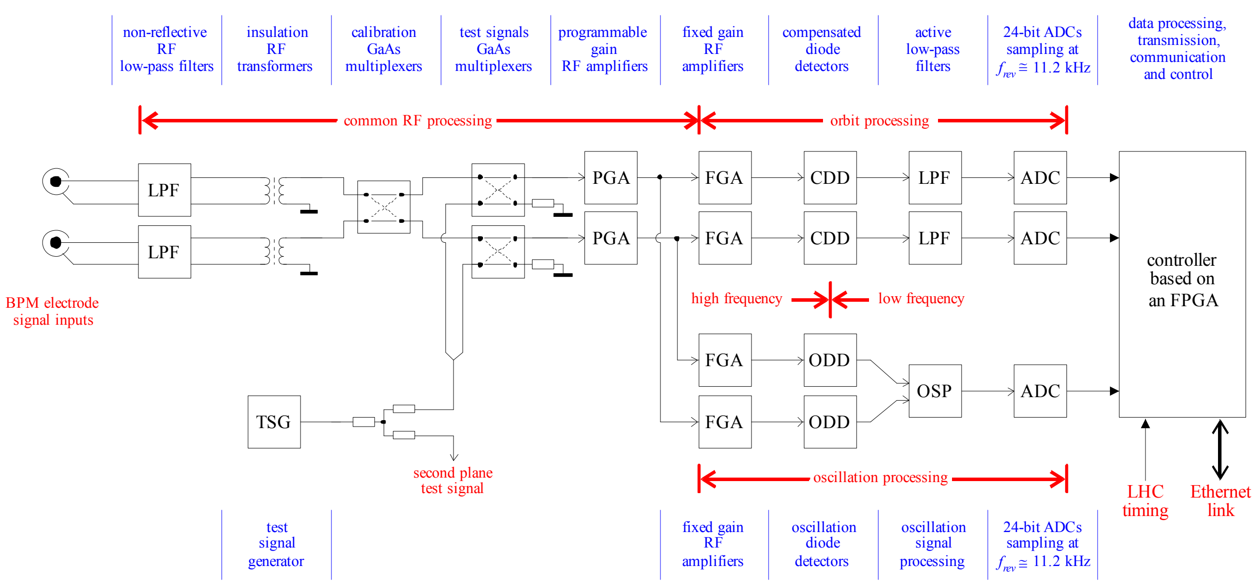


Figure 1: Block diagram of two channels of a DOROS front-end processing signals from one pair of BPM electrodes. LPF – low-pass filter, TSG – test signal generator, PGA – programmable gain amplifier, FGA – fixed gain amplifier, CDD – compensated diode detector, ODD – oscillation diode detector, OSP – oscillation signal processing.

ISBN 978-3-95450-177-9

# BEAM POSITION MONITORS FOR LEReC*

Z. Sorrell†, P. Cerniglia, R. Hulsart, K. Mernick, R. Michnoff
Brookhaven National Laboratory, Upton, NY, USA

*Abstract*

The operating parameters for Brookhaven National Laboratory's Low Energy RHIC Electron Cooling (LEReC) project create a unique challenge. To ensure proper beam trajectories for cooling, the relative position between the electron and the ion beams needs to be known to within 50µm. In addition, time of flight needs to be provided for electron beam energy measurement. Various issues have become apparent as testing has progressed, such as mismatches in cable impedance and drifts due to temperature sensitivity. This paper will explore the difficulties related to achieving the level of accuracy required for this system, as well as the potential solutions for these problems.

## INTRODUCTION

The LEReC project has strict requirements for position and phase measurements. The ion beam has a repetition rate of 9 MHz and the electron beam has a repetition rate of 704 MHz. Two sets of electronics are planned for handling the low frequency and high frequency signals. The typically operation will have 704 MHz bunch trains to overlap the ion beam (Fig. 1). For the electrons to properly cool the ion beam they must be travelling at the same speed with an angle of less than 100 µrad between the beams [1]. To ensure sufficient cooling, the difference between the electron beam and the ion beam must be measured with 50 um accuracy. The challenge with this level of accuracy is the difference between the frequencies of the two beams which creates disparate responses in signal processing. Due to difficulties associated with absolute calibration of BPM electronics, a relative measurement between the two beams is planned.

. During the initial testing, the BPM system will also be responsible for making phase measurements that can be used to calculate the energy of the electron beam. These phase measurements must have a resolution of 0.25 degrees at 704 MHz to give the necessary 1ps resolution for time of flight between BPMs placed several meters apart, in order to provide the required energy resolution of roughly 2E-4 at 400KeV [1].

Several design challenges exist including, synchronous phase measurements across all BPMs, unacceptable errors due to temperature sensitivity of the cables which affect attenuation and cable delays, and matching the high and low frequency signal responses for relative position measurements.

* Work supported by BSA under DOE contract DE-AC02-98CH10886
† zsorrell@bnl.gov

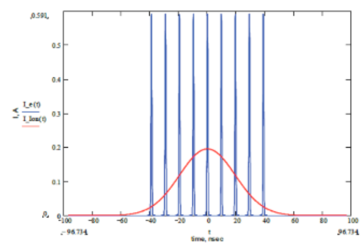

Figure 1: Electron bunches (blue) overlapping with ion bunches (red). [2]

## HARDWARE ARCHITECTURE

The LEReC BPM pickups use 9mm, 15 mm and 28mm buttons oriented along the x and y planes of the machine [2]. The electronics for processing the data from the buttons will be located in a nearby equipment building and will require cable lengths greater than 200 feet, partially routed outdoors. The long cable lengths introduce severe attenuation of the higher frequency 704 MHz electron signal.

Due to the difficulties associated with accurately measuring electron and ion beam signals with different base frequencies, two different analog front ends planned to be used to pre-process the signals. The most significant difference between the two sets of analog front ends is the filters. For low frequency ion and electron measurements a 39 MHz low pass filter will be used and for electrons a 707 MHz band pass filter will be used (Fig. 2). The 9 MHz macrobunch structure of the electron beam signal creates a strong response when the signal is processed at 9 MHz, allowing the electron and ion beam signals to be processed with the same electronics. Diplexers will be mounted in the racks to separate the low and high frequency signals. There will be an RF switch module mounted in the tunnel, the purpose of this module will be explained later in the paper.

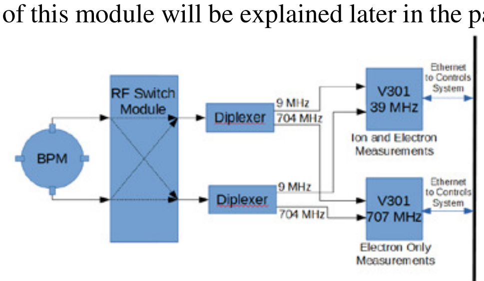


Figure 2: The basic configuration showing how BPM signals are connected to the processing electronics. The 39 MHz electronics measures both electrons and ions.

Libera BPM electronics from a previous project will process the signals in the transport section of the electron beam line. The remaining BPM signals will be processed using in-house designed V301 modules, which are based

ISBN 978-3-95450-177-9

# THE ORBIT CORRECTION SCHEME OF THE NEW EBS OF THE ESRF

E. Plouviez †, F. Uberto, ESRF, Grenoble, France


*Abstract*

The ESRF storage ring is going to be upgraded into an Extremely Bright Source (EBS). The orbit correction system of the EBS ring will require 320 BPMs and 288 correctors instead of 224 BPMs and 96 correctors for the present ring. On the new ring, we are planning to reuse 192 *Libera Brilliance* [1] electronics and 96 fast corrector power supplies and the 8 FPGA controllers of the present system and to add 128 new BPMs electronics and 196 new corrector power supplies. These new BPM electronics and power supplies will not have the fast 10 KHz data broadcast capability of the components of the present system. So we plan to implement a hybrid slow/ fast correction scheme on the SR of the EBS in order to reuse the present fast orbit correction system on a reduced set of the BPMs and correctors and combine this fast orbit correction with an orbit correction performed at a slower rate using the full set of BPMs and correctors. We have made simulations to predict the efficiency of this scheme for the EBS and tested on the present ring a similar orbit correction scheme using only 160 BPMs and 64 correctors for the fast correction. We present the results of our simulations and experiments.


## ISSUES

We aim at achieving a horizontal orbit stability consistent with the 100 pm horizontal emittance of the new ring (instead of 4 nm for the present storage ring). One cell of the new lattice including BPMs and correctors is shown on Figure 1.

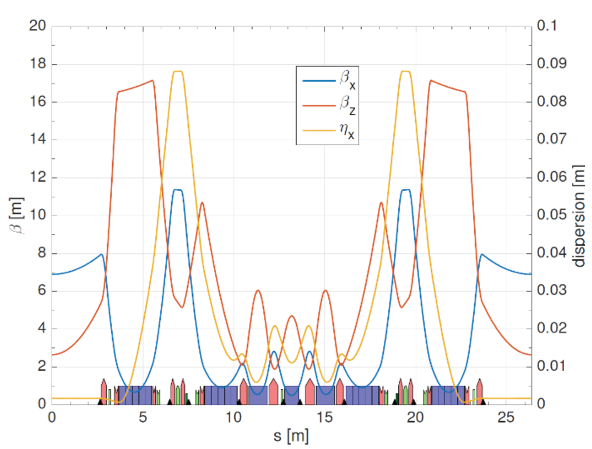


Figure 1: BPMs and correctors in the EBS lattice.
Black triangle: BPM
Small green rectangle: fast corrector
Large green rectangle: slow corrector (sextupole)

The orbit distortion in the frequency range going from .1Hz to 1Hz will come from changes of the parameters (gap and phase) of the ID insertion devices if they are not perfectly corrected against field integral defects. In the 1 Hz to 100Hz range the distortion will first come from the ground vibration filtered by the girder supporting the magnets. We expect that the frequency of the first resonance of the girder will be above 40Hz. The other source of orbit distortion are the spurious fields at the AC mains frequencies (50Hz and its harmonics) and the spurious fields coming from the booster operation (250ms ramp). The correction of these orbit distortions requires operating the orbit correction system in a wide bandwidth. The present fast orbit correction system cannot be easily upgraded to include the larger number of BPMs used on the new ring. Concerning the correctors, among the 288 correctors, 192 correctors will be embedded in the sextupoles; the core of the sextupoles will not be laminated; this will limit drastically the bandwidth of these correctors; the 96 others correctors will have laminated core and will be able to achieve a bandwidth of 500Hz and can reuse the power supplies of the present system. Given the tight time schedule of the project we wanted to avoid as much as possible any unnecessary risky development for the implementation of this fast orbit correction system. For this reason, we are testing an orbit correction scheme using the components of the fast orbit correction system working at 10 KHz of the present ring [1] combined with extra BPMs and correctors power supplies operated at a lower rate. The layout is shown on figure 2.

## ORBIT CORRECTION LAYOUT

The orbit control of the new EBS ring will use 10 BPMs and 9 correctors per cell in order to get a closed orbit, averaged in a bandwidth of a fraction of Hertz, close enough to the ideal orbit to allow the required lifetime and coupling control (this orbit correction is not perfect but only optimal since the number of correctors is less than the number of BPMs); the corrector settings for this optimal correction are obtained by multiplying the orbit distortion vector by a correction matrix $M_{cors}$ obtained by inverting the $M_{res}$ response matrix of the system using the SVD method. The 320 BPM pickups will be connected to two types of electronics: 192 *Libera Brillance* electronics of the type used on our present orbit correction system which will used be both for the slow and fast orbit correction; the others 108 BPMs will be connected to new and simpler electronics. The design of these new BPM electronics will most likely be an evolution of the simple *Spark* electronics [2] already used on the BPMs of our booster. Two types of magnets will be used for the orbit correction: 96 dedicated corrector magnets which will be driven by the power supplies used on the present system with a bandwidth of about 500Hz for

ISBN 978-3-95450-177-9

# BPM STABILTIY STUDIES FOR THE APS MBA UPGRADE*

R. Lill, N. Sereno, B. Yang
Advanced Photon Source, Argonne National Laboratory, Argonne, IL 60439 USA

*Abstract*

The Advanced Photon Source (APS) is currently in the preliminary design phase for the multi-bend achromat (MBA) lattice upgrade. Beam stability is critical for the MBA and will require long term drift, defined as beam motion, over a seven-day timescale to be no more than 1 micron at the insertion device locations and beam angle change of no more than 0.25 micro-radian. Mechanical stability of beam position monitor (BPM) pickup electrodes mounted on insertion device vacuum chambers place a fundamental limitation on long-term beam stability for insertion device beamlines. We present the design and implementation of prototype mechanical motion system (MMS) instrumentation for quantifying this type of motion, specifically in the APS accelerator tunnel and experiment hall floor under normal operating conditions. The MMS presently provides critical position information on the vacuum chamber and BPM support systems. Initial results of the R&D prototype systems have demonstrated that the chamber movements far exceed the long-term drift tolerance specified for the APS Upgrade MBA storage ring.

## INTRODUCTION

In order to achieve the MBA beam stability requirements, an extensive R&D program has been planned and is presently being implemented. The beam diagnostics required for the APS MBA are driven largely from a small electron beam size and the requirements for those systems are outlined in Table 1. The minimum beam size for the MBA lattice is expected to approach 4 microns at the insertion device (ID) source points. AC rms beam stability requirements are defined as 10% the minimum source size at the ID in the band 0.01-1000 Hz. The vertical plane stability requirement is the most ambitious, requiring a stability of 400 nm at the ID source point. In addition, long term drift, defined as motion over a seven-day timescale, can be no more than 1 micron.

Table 1: MBA Beam Stability Requirements

| Plane | AC rms Motion (0.01-1000 Hz) | Long-term Drift (100s-7 days) |
|---|---|---|
| Horizontal | 1.7 μm 0.25 μrad | 1.0 μm 0.6 μrad |
| Vertical | 0.4 μm 0.17 μrad | 1.0 μm 0.5 μrad |

* Work supported by U.S. Department of Energy, Office of Science, under Contract No. DE-AC02-06CH11357.

## BEAM STABILITY R&D OVERVIEW

We have approached the MBA diagnostics R&D in two phases. The first phase, outlined in Figure 1, prototypes new, higher risk diagnostics and their interfaces. This R&D includes an MMS, BPM electronics, Grazing Incidence Insertion Device (GRID) X-Ray BPM [1], and new feedback processing electronics [2]. This phase is presently near completion and has provided the foundation for the next phase of R&D [3].

The MMS system shown on the lower section of Figure 1 will be discussed in greater detail in the paper. This diagnostic has been designed to monitor critical in-tunnel beam position monitoring devices. The mechanical motion generated from changes in chamber cooling water temperature, tunnel air temperature, beam current, and undulator gap position causes erroneous changes in beam position measurements, creating drift in the x-ray beam position. Research to quantify mechanical motion specifically for the APS accelerator tunnel has been ongoing for over five years [4,5].

The second phase of the R&D effort advances the design and integrates all systems required to qualify beam stability. The integrated beam stability testing will require 16 new rf BPMs and 8 new corrector power supplies and interfaces. The integrated beam stability effort will be required to operate transparent to normal APS operation and is planned to start in the late summer of 2016. This testing will greatly reduce risks and qualify many diagnostic systems and their related interfaces.

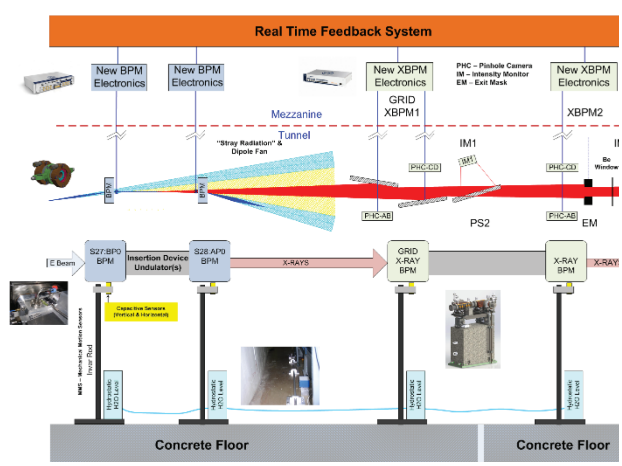


Figure 1: APS-U beam stability R&D.



ISBN 978-3-95450-177-9

# BEAM COMMISSIONING OF TPS FAST ORBIT FEEDBACK SYSTEM

P. C. Chiu, Y. S. Cheng, K. T. Hsu, K. H. Hu, C.H. Huang
NSRRC, Hsinchu 30076, Taiwan

*Abstract*

TPS (Taiwan Photon Source) is a 3 GeV synchrotron light source which had be successfully commissioning with SRF up to 500 Amp in 2015 and Phase I beamline commissioning have followed soon. It has been scheduled to open user operation in 2016. To provide stable and reliable beam, the fast orbit feedback system is indispensable. Due to the vacuum chamber material made of aluminum with higher conductivity and lower bandwidth, extra fast correctors mounted on bellows will be used for FOFB correction loop and DC correction of fast correctors would be transferred to slow ones and avoid fast corrector saturation. Besides, the path length compensation by RF feedback is also tested. This report summarizes the infrastructure of the FOFB and the preliminary beam test is also presented.

## INTRODUCTION

The TPS is a state-of-the-art synchrotron radiation facility which consists of a 150 MeV S-band linac, linac to booster transfer line (LTB), 0.15–3 GeV booster synchrotron, booster to storage ring transfer line (BTS), and 3 GeV storage ring. This synchrotron machine featuring ultra-high photon brightness with low emittance [1] requires beam position stability less than 1/10 beam size. FOFB is therefore implemented to achieve sub-micron orbit stability and it has been tested together with beamline commissioning since 2015. The orbit stability had been effectively improved with FOFB and it showed that the suppression bandwidth could achieve 250 Hz in both horizontal and vertical plane. This had been considered quite helpful for beamline commissioning, especially that TPS had strong 3 Hz booster ramping disturbance and 60 Hz power line noise. After applying RF feedback and resolving long-term reliability related problem, FOFB would be officially operated in September 2016.

## FOFB INFRASTRUCTURE

The design of the TPS storage ring has 24 cells, each cell is equipped with 7 BPMs and 7 horizontal/vertical correctors winding on the sexupoles. These kinds of slow correctors could provide about 500 μrad kick while their bandwidth could be limited only several tens of Hertz due to the eddy effect of the alumina vacuum chamber. This bandwidth is not sufficient to eliminate perturbation with frequency above several hundreds of hertz. Therefore, extra four horizontal/vertical correctors per cell are installed on the bellows site to obtain higher correction bandwidth. These horizontal/vertical correctors have fast response but smaller kick strength around 100/50 μrad. Thus the orbit feedback system would adopt two kinds of correctors simultaneously. The DC component of the fast correctors will transfer from fast to slow correctors smoothly and avoid saturation of the fast correctors as well as provide capability to suppress orbit disturbance. The overall infrastructure of FOFB is as Fig. 1. It is mainly implemented by three parts: BPM, feedback computation unit and corrector power supply control interface. TPS BPM electrical system will adopt the latest I-tech product: Brilliance+ [2]. It also offers a large playground for custom- written applications with VirtexTM 5, Virtex 6 in the gigabit data exchange module (GDX) to be used as orbit feedback computation. The corrector power-supply controller (CPSC) is designed for FOFB corrector control interface. This module is embedded with Intel XScale IOP and Xilinx Spartan-6 FPGA which will interface the fast setting from feedback engines. It was contracted to D-TACQ [3].

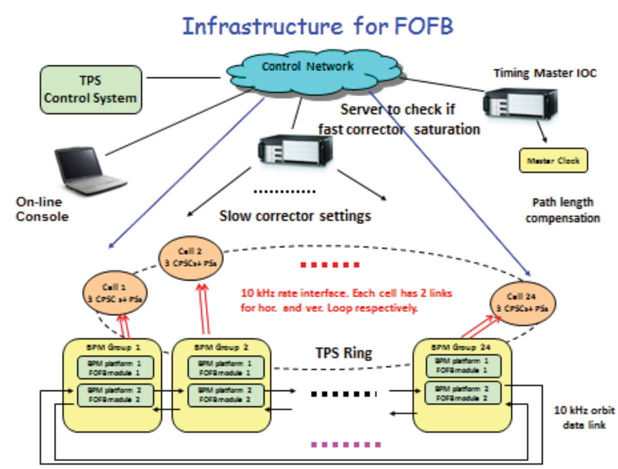


Figure 1: FOFB infrastructure.

### *BPM and GDX Interface*

The TPS BPM electronics had commission with TPS beam commissioning in 2014 [4, 5]. It consists of four kinds of modules: The timing module for clock locking and trigger; up to four BPM modules for receiving button pick-ups and signal processing, the inter-connection board (ICB) module for SW and HW interface; the GDX (Gigabit data exchange) module as Fig. 2 shown for FA data grouping and FOFB computation which could support at most 256 BPMs and 128 correctors feedback computation. The magnet correction output is transmitted to CPSC (corrector power supply controller) based on AURORA protocol of Xilinx. It also provides 10 kHz BPM grouping data through Gigabit Ethernet to support the angle interlock functionalities of TPS. The functional block of FOFB is shown as Fig. 3.

ISBN 978-3-95450-177-9

# A WIRE-BASED METHODOLOGY TO ANALYSE THE NANOMETRIC RESOLUTION OF AN RF CAVITY BPM

S. Zorzetti[1]*, K. Artoos, F. N. Morel, P. Novotny, D. Tshilumba, M. Wendt
CERN, Geneva, Switzerland
L. Fanucci, University of Pisa, Pisa, Italy
[1]also at University of Pisa, Pisa, Italy

*Abstract*

Resonant Cavity Beam Position Monitors (RF-BPMs) are diagnostic instruments capable of achieving beam position resolutions down to the nanometre scale. To date, their nanometric resolution capabilities have been predicted by simulation and verified through beam-based measurements with particle beams. In the frame of the PACMAN project at CERN, an innovative methodology has been developed to directly observe signal variations corresponding to nanometric displacements of the BPM cavity with respect to a conductive stretched wire. The cavity BPM of this R&D study operates at the TM110 dipole mode frequency of 15GHz. The concepts and details of the RF stretched wire BPM test-bench to achieve the best resolution results are presented, along with the required control hardware and software.

## INTRODUCTION

The CLIC experiment at CERN is an international study of a future Compact LInear Collider. The main purpose is to achieve both high efficiency and luminosity at the Interaction Point (IP) at a beam energy up to 1.5 TeV. Therefore, the required beam size at the IP is in the range of a few nanometres. To achieve this, the beam emittance needs to be maintained over the whole 30 km length of the main linac, implying Beam Position Monitor (BPM) technologies capable of measuring nanometric displacements and a precise alignment between the main accelerator components in the micrometric range. In this scenario, the PACMAN project [1], funded by the European Union's Seventh Framework Programme, aims to prove the feasibility of innovative, high precision alignment methods for BPMs, quadrupoles and accelerating structures, based on stretched and vibrating wire technologies.

## CLIC CAVITY BPM AND TESTS

The CLIC cavity BPM design is based on the combination of a monopole TM010 mode reference cavity and a dipole TM110 position cavity, resonating at $\sim$ 15 GHz (a 3D model of the position cavity and pickups is shown in Fig. 1). The initial design in stainless steel was studied through beam measurements in the CLIC Test Facility (CTF3) at CERN and it was later improved to achieve an higher Q value through a copper construction. Five cavity BPM prototypes of the new design are now being studied at CERN. Three BPMs are installed in CTF3 [2] and two others are used by the PACMAN project in a laboratory environment to test stretched-wire methods.

* silvia.zorzetti@cern.ch

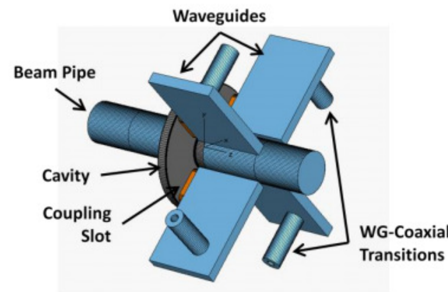


Figure 1: BPM moodel.

The BPM resolution depends on many factors. A relevant signal deterioration is caused by manufacturing imperfections, leading to monopole mode leakage to the position cavity, asymmetries between the lateral pickup ports, or cross coupling between adjacent ports. To avoid a significant degradation of the performances and accuracy, the fabrication tolerances were set very tight. Taking into account the weakest manufacturing aspects, RF simulations of the BPM design anticipated a 50 nm spatial resolution, for 50 ns measurement time with beam [3].
So far, cavity BPM resolution results have mainly been achieved through beam-based techniques. The traditional approach is to pre-align three BPMs in a straight line on a common support, and to predict the position of the central BPM out of the position of the other two. The resolution is extrapolated by the residuals' standard distribution, returned by the difference between the measured position and the calculated one [4].

BPM experiments using particle beams are essential tests for calibrations purposes, e.g. analysing the sensitivity of the cavity as a function of the beam position or the number of charges. However, RF tests, without requiring beam, present a simple way for characterizing first prototypes and pre-align the BPM and its associated quadrupole. The proposed stretched-wire analysis is particularly valuable for finding the electrical center of the position cavity or analysing its high spacial resolution capability.

## STRETCHED-WIRE SETUP

To study the BPM resolution, a standalone test bench has been assembled. The main bench components, and measurement procedure are shown in Fig.2, 3. A Vector Network Analyser (VNA) is added for signal read-out. The scattering parameters acquired through this setup allow the measure



ISBN 978-3-95450-177-9

# MICROTCA.4 BASED OPTICAL FRONTEND READOUT ELECTRONICS AND ITS APPLICATIONS

K. Przygoda†, L. Butkowski, M. K. Czwalinna, H. Dinter, C. Gerth, E. Janas, F. Ludwig, S. Pfeiffer, H. Schlarb, C. Schmidt, M. Viti, Deutsches Elektronen-Synchrotron, Hamburg, Germany
R. Rybaniec, Warsaw University of Technology, Warsaw, Poland

*Abstract*

In the paper the MicroTCA.4 based optical frontend readout (OFR) electronics and its applications for beam arrival time monitor (BAM) and fast beam based feedback (BBF) is presented. The idea is to have a possibility to monitor the modulation density of the optical laser pulses by the electron bunches and apply this information for the BBF. The OFR composed of double width fast mezzanine card (FMC) and advanced mezzanine card (AMC) based FMC carrier. The FMC module consists of three optical channel inputs (data and clock), two optical channel outputs (beam arrival time), 250 MSPS ADCs, clock generator module (CGM) with integrated 2.8 GHz voltage control oscillator (VCO). The optical signals are detected with 800 MHz InGaAs photodiodes, conditioned using 2 GHz current-feedback amplifiers, filtered by 3.3 GHz differential amplifiers and next direct sampled with 16-bit 900 MHz of analog bandwidth ADCs. The CGM is used to provide clock outputs for the ADCs and for the FMC carrier with additive output jitter of less than 300 fs rms. The BAM application has been implemented using Virtex 5 FPGA and measured with its performance at Free Electron LASer in Hamburg (FLASH) facility.

## INTRODUCTION

The Micro Telecommunication Computing Architecture (MicroTCA) is a standard in Telecommunication from several years. Nowadays more often high energy physics research centres are trying to migrate from commonly used Versa Module Europa (VME) to more compact, modular, redundant solutions offered by MicroTCA, especially generation four of the standard. The Deutsches Elektronen-Synchrotron (DESY) in Hamburg in Germany is a leading institute which developing, designing, testing and even commercializing general purpose and application specific modules using this modern technology. Moreover, the next generation light sources such FLASH and European X-Ray Free Electron Laser (E-XFEL) accelerators have been decided to be fully controlled and monitored with its crucial parameters by MicroTCA.4 [1].

The scope of the paper is to summarise the several year research and development (R&D) program on developing direct sampling OFR electronics [2]. The OFR electronics have been optimized to get the best achievable performance when considering the optical to RF conversion of the laser pulses, ADC stability and fast data processing by FPGA's. Fast digital feedback information can be sent out using small form-factor pluggable (SFP) optical modules allowing data transfers up to 10 Gbps. The OFR electronics can be efficiently applied for several applications. Within the paper we are presenting its usage for BAM and BBF experiments.

† konrad.przygoda@desy.de

## BEAM ARRIVAL MONITOR AND BEAM BASED FEEDBACK APPLICATIONS

The BAM signal creation, detection and analysis in the electron bunch arrival time monitor is split into several subsystems, each fulfilling a particular function as shown in Fig. 1.

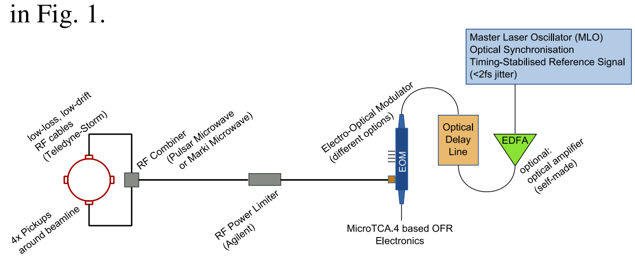


Figure 1: The block diagram of BAM detector.

The RF module which consists of four broadband pickups mounted in the beam tube is applied in order to capture the electric field induced by the passing electron bunches. The signals of opposite pickups are combined for a reduced position dependence of the measurement, resulting in two independent RF channels for the arrival time detection: course and fine. Than the electro-optical modulator (EOM) unit is introduced mainly for translating the RF signals into an amplitude modulation of time-stabilized, ultra-short laser pulses provided by the Master Laser Oscillator (MLO) synchronization system in order to achieve a high temporal sensitivity. The optical frontend electronics need to be installed at the end of the system for signal processing and control of the individual subsystems [3].

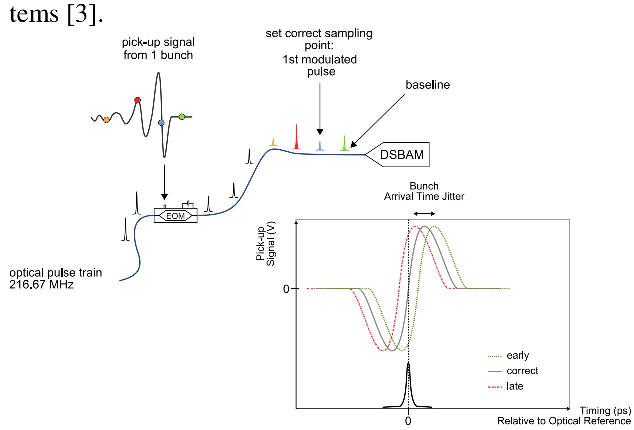


Figure 2: The block diagram of BAM signal detection and calibration.

The beam arrival time is calculated using peak and baseline values of the first modulated (mod) and first unmodu-

ISBN 978-3-95450-177-9

# THE USE OF SINGLE-CRYSTAL CVD DIAMOND AS A POSITION SENSITIVE X-RAY DETECTOR

E. Griesmayer†, P. Kavrigin, C. Weiss, CIVIDEC Instrumentation, Vienna, Austria
C. Bloomer, Diamond Light Source Ltd, Didcot, UK

*Abstract*

Synchrotron light sources generate intense beams of X-ray light for beamline experiments, and the stability of these X-ray beams has a large impact on the quality of the experiments that can be performed. User experiments increasingly utilise micro-focus techniques, focusing the X-ray beam size to below 10 microns at the sample point, with beamline detectors operating at kHz bandwidths. Thus, there is a demand for non-invasive diagnostic techniques that can reliably monitor the X-ray beam position with sub-micron accuracy in order to characterise X-ray beam motion, at corresponding kHz bandwidths. Reported in this paper are measurements from single-crystal CVD diamond detectors, and a comparison with the previous-generation of polycrystalline CVD diamond detectors is offered. Single-crystal diamond is shown to offer superior uniformity of response to incident X-rays, and excellent intensity and position sensitivity. Measurements from single-crystal diamond detectors installed at Diamond Light Source are presented, and their use in feedback routines in order to stabilise the X-ray beam at the sample point is discussed.

## INTRODUCTION

Diamond radiation detectors typically utilise diamond films or plates, some 50 μm thick. Electrodes are deposited on opposite surfaces of the plate (the “front” and “back” of the device), with wire-bonded connections to a PCB frame or holder for the diamond. Standard lithography techniques allow the size and shape of the electrodes to be controlled: dots, quadrants, strips, and pixels can all be realised on the diamond surface. Figure 1 shows a typical arrangement.

Sufficiently energetic incident radiation absorbed by carbon atoms promote electrons from the valence band into the conduction band, forming electron hole pairs. Under the influence of a bias voltage these charge carriers travel to one of the electrodes, where this current can be amplified and measured.

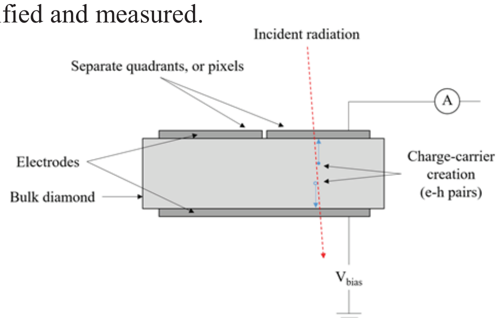


Figure 1: A schematic layout of a diamond X-ray detector

† erich.griesmayer@cividec.at

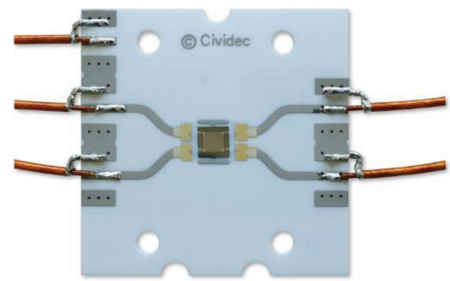


Figure 2: A photograph of the single-crystal diamond detector tested at DLS. The detector is a 4.5 mm x 4.5 mm square diamond in the centre of the image, and is mounted on a ceramic PCB.

Experiments carried out at Diamond Light Source Ltd. (DLS) have been performed to evaluate the performance single-crystal diamond X-ray detectors. Maintaining the spatial stability of the X-ray beam relative to the sample point for the duration of user data collection is vitally important for synchrotron beamlines. Sub-micrometer beamsizes at the sample point are increasing common, and the typically required beam stability is some 10% of beamsize [1]. Reliable X-ray diagnostics are essential during beamline commissioning, during routine “start-up”, and during data collection itself as, increasingly, beamline detectors at DLS operate in the kHz regime. Single-crystal diamond detectors offer the ability to make correspondingly high precision position measurements at these bandwidths.

Results presented in this paper are from quadrant detectors, with four square electrodes (metallised “quadrants”, or “pads” on the surface of the diamond, less than 100 nm thick) deposited onto one face of the diamond, and a single electrode deposited onto the opposite face of the diamond. These sensors can be used to provide both spatial and intensity measurements. Commonly, this type of detector is referred to as an X-ray Beam Position Monitor (XBPM).

## SIGNAL LINEARITY VS INCIDENT FLUX

The signal produced by diamond detectors is typically a current of a few nanoamps to microamps. The signal produced (i.e. the number of charge carriers created in the bulk diamond) is directly proportional to the number of absorbed photons, and thus proportional to the incident light. Signal-crystal diamond has been shown to exhibit a linear signal response to incident flux over many orders of magnitude.

The I04 beamline at DLS has the ability to attenuate the incident light using a series of calibrated absorption materials, inserted into the X-ray beam path. In this way, the

ISBN 978-3-95450-177-9

# BPM ELECTRONICS FOR THE ELBE LINEAR ACCELERATOR - A COMPARISON

U. Lehnert, A. Büchner, B. Lange, R. Schurig, R. Steinbrück
Helmholtz Center Dresden-Rossendorf, PF 510119, 01328 Dresden, Germany

*Abstract*

The ELBE linear accelerator supports a great variety of possible beam options ranging from single bunches to 1.6 mA CW beams at 13 MHz bunch repetition rate. Accordingly high are the dynamic range requirements for the BPM system. Recently, we are testing the Libera Spark EL electronics to supplement our home-built BPM electronics for low repetition rate operation. Here, we discuss the advantages and disadvantages of the two completely different detection schemes. For integration of the Libera Spark EL into our accelerator control system we are implementing an OPC-UA server embedded into the device. The server is based on the free Open62541 protocol stack which is available as open source under the LGPL.

## THE HZDR BPM ELECTRONICS

Figure 1: The HZDR BPM electronics comes in a 1U 19" rack-mount enclosure.

The BPM electronics currently used at ELBE is an in-house design which has been presented at IBIC2013 [1]. It's RF front-end detects the fundamental frequency of 1.3 GHz from the $\lambda/4$ strip-line sensors used at ELBE. This signal after some filtering and amplification/attenuation (see Fig. 2) is mixed down to a 19.5 MHz intermediate frequency. The IF signal is sampled and digitized at 52 MS/s rate. The digital signal is then processed with an $I/Q$-demodulation over 512 samples yielding a system bandwidth of 95 kHz. This bandwidth was chosen to give a sufficiently fast response but at the same time to integrate the least possible amount of noise

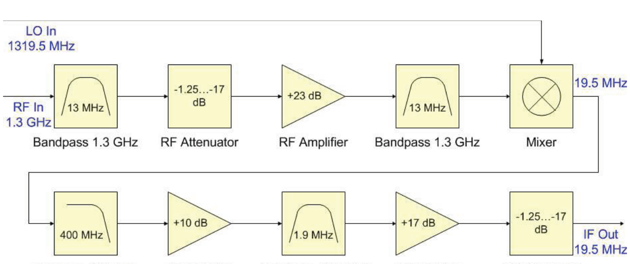


Figure 2: The analog front-end of the HZDR BPM electronics.

in order to reach a high signal-to-noise ratio and dynamic range. A difference-over-sum formula is used to convert the measured signal amplitudes into a position information.

ELBE ist mostly run at 13 MHz bunch repetition rate but frequencies down to 100 kHz or single pulses with arbitrary repetition rates are available. At all frequencies above 100 kHz more than a single bunch is detected in every acquisition frame. The according averaging effect further improves the signal-to-noise ratio. This signal processing, however, is not optimized for low bunch repetition rates. The duration of a single-bunch signal is less than 1 $\mu$s according to the 1.9 MHz bandwidth of the analog front-end while the noise is integrated over the full 10 $\mu$s duration of the sample frame.

## THE LIBERA SPARK EL BPM ELECTRONICS


Figure 3: The Libera Spark EL BPM Electronics.

The Libera Spark EL [2] manufactured by Instrumentation Technologies in the tests reported here was connected to an identical strip-line pickup mounted back-to-back with the one used for the HZDR electronics. This device uses a rather different analog front-end and detection scheme. Right at the input the signal is filtered with a SAW resonator centered at a frequency of 500 MHz. The filtered and amplified/attenuated signal is then directly sent to an ADC with a fast sample-and-hold input stage. Sub-sampling at 117 MS/s the signal is mirrored to a 32 MHz base-band frequency. The signal amplitude is then determined by integrating over a fixed number of samples including a few pre-trigger samples. We have chosen 100 post-trigger samples to capture the waveform shown in Fig. 4. Again, we use a linear difference-over-sum formula to derive the position information from the 4 channel amplitudes.

The bandwidth of the whole system is solely determined by the filter bandwidth which is specified in the datasheet to 8 MHz full width. The time-domain approach to the signal detection is very well suited to the measurement of single bunches at low repetition rates. One may note that actually no harmonic of the 13 MHz bunch repetition rate falls into

ISBN 978-3-95450-177-9

# PERFORMANCE TEST OF THE NEXT GENERATION X-RAY BEAM POSITION MONITOR SYSTEM FOR THE APS UPGRADE*

B.X. Yang, Y. Jaski, S.H. Lee, F. Lenkszus, M. Ramanathan, N. Sereno, F. Westferro
Advanced Photon Source, Argonne National Laboratory, Argonne, IL 60439 USA

*Abstract*

The Advanced Photon Source is developing its next major upgrade (APS-U) based on the multi-bend achromat lattice. Improved beam stability is critical for the upgrade and will require keeping short-time beam angle change below 0.25 µrad and long-term angle drift below 0.6 µrad. A reliable white x-ray beam diagnostic system in the front end will be a key part of the planned beam stabilization system. This system includes an x-ray beam position monitor (XBPM) based on x-ray fluorescence (XRF) from two specially designed GlidCop A-15 absorbers, a second XBPM using XRF photons from the Exit Mask, and two white beam intensity monitors using XRF from the photon shutter and Compton-scattered photons from the front end beryllium window or a retractable diamond film in windowless front ends. We present orbit stability data for the first XBPM used in the feedback control during user operations, as well as test data from the second XBPM and the intensity monitors. They demonstrate that the XBPM system meets APS-U beam stability requirements.

## INTRODUCTION

The Advanced Photon Source (APS) storage ring will receive a major upgrade based on multi-bend achromat lattice [1]. The storage ring emittance will be under 70 pm-rad and the x-ray beam divergence will be dominated by the natural opening angle of the undulator radiation, as expected from a diffraction-limited source. The angular beam stability tolerance is chosen to be a fraction of the beam angular spread. For example, the long-term drift tolerance is 0.6 µrad RMS. For an XBPM at 20 m from the source, this specification translates to an x-ray beam position tolerance of 12 µm. We can assign 70% of this value, 8.5 µm, to the XBPM's total error budget. Table 1 lists the XBPM tolerance for RMS AC beam motion (0.01 – 1000 Hz) and long-term drift (7 days) derived in this manner from the beam stability specifications of the new storage ring.

The first XBPM system designed with these specifications were installed in Sector 27 of the APS storage ring in 2014 [2]. Figure 1 shows the XBPM system which includes the following components: (A) The first XBPM (XBPM1) measures the transverse x-ray beam positions at 18.6 m from the source, which is dominated by the angular motion of the e-beam; (B) the first intensity monitor (IM1) measures the beam intensity when the photon shutter (PS2) is closed; (C) the second XBPM (XBPM2) measures the x-ray beam position at the Exit Mask; and (D) the second intensity monitor (IM2) measures the beam intensity entering the user beamline. The two intensity monitors are used as alignment aids.

* Work supported by U.S. Department of Energy, Office of Science, under Contract No. DE-AC02-06CH11357.

In this work, we will present the performance data of the XBPM1 in user operations, and discuss the design and performance of the XBPM2, IM1 and IM2.

Table 1: APS-U XBPM Tolerance (Z = 20 m)

| | Plane | AC motion | Long-term drift |
|---|---|---|---|
| X-ray beam position tolerance | X | 5.3 µm | 12 µm |
| | Y | 3.4 µm | 10 µm |
| Total XBPM error budget | X | 3.7 µm | 8.5 µm |
| | Y | 2.4 µm | 7.1 µm |

## GRID-XBPM PERFORMANCE

The first XBPM is a grazing-incidence insertion-device XBPM (GRID-XBPM) based on XRF from two GlidCop absorbers. Since it is sensitive only to hard x-rays, the bend magnet background is less than 3% of the XBPM signal at the maximum undulator gap (30 mm) or minimum undulator power ($K$ ~ 0.4) for user operations. In the vertical plane, the XBPM calibration is independent of the undulator gap due to pinhole camera geometry used in x-ray readout optics. In the horizontal plane, the calibration is gap dependent but the offset is small due to symmetry in XBPM design [3,4].

Figure 2 shows the beam stability performance during user operations, as measured by the XBPM1. The data includes 60-days of operations in Summer 2015:

- In the week of June 30, only RFBPMs are used in the orbit feedback control and the x-ray beam is stabilized within +10 µm and −5 µm range, a reasonably good performance.
- After the July 4, the XBPM1 is added into the feedback loop. The black traces show 324-bunch mode of operations where the storage ring is filled twice daily. In these two weeks, we can see small saw tooth shape representing beam motion of 2 µm when the stored current decays from 102 mA to approximately 85 mA.
- After July 21, the blue trace shows operations in 24-bunch top-up mode, and the ring is filled every 2 – 3 minutes. The fuzzy traces represent the beam motion excited by the top-up shots. The severe reduction of the motion amplitude shows the effect of heavy filtering of the XBPM data in signal processing.
- When the XBPM is in the feedback loop, the x-ray beam motion is well within the boundary defined by the red and green lines, which represents the tolerance specifications in Table 1.
- No big jumps of beam positions are found in the gaps on Tuesday machine study days. This indicates that the XBPM helps the beam position return after studies, a feature important to beamline users.



ISBN 978-3-95450-177-9

# DIAMOND MONITOR BASED BEAM LOSS MEASUREMENTS IN THE LHC

C. Xu*, B. Dehning, F. S. Domingues Sousa, CERN, Geneva, Switzerland
E. Griesmayer, CIVIDEC Instrumentation, Vienna, Austria

*Abstract*

Two pCVD Diamond based Beam Loss Monitors (dBLM) are installed near the primary collimators of the LHC, with a dedicated, commercial readout-system used to acquire their signals. The system is simultaneously able to produce a high sampling rate waveform and provide a real-time beam loss histogram for all bunches in the machine. This paper presents the data measured by the dBLM system during LHC beam operation in 2016.

## INTRODUCTION

Diamond detectors with nanosecond time resolution and high dynamic range have been successfully tested and used in the LHC [1,2]. Two diamond detectors are installed next to the primary collimators in the insertion region 7 (IR7) of the LHC for both beam1 (B1) and beam2 (B2).

The initial acquisition system used oscilloscopes to digitize the output of these diamond detectors, however, due to the lack of dedicated software, the beam loss measurements performed with this set-up was neither systematically logged nor analysed since the start of LHC Run2.

A dedicated commercial readout-system was therefore installed in order to better utilize the high time resolution provided by the diamond detectors. The data acquisition software was developed so that automatic data logging would be possible, and the system could provide valuable multipurpose data for accelerator studies.

## SYSTEM DESCRIPTION

### *Diamond Beam Loss Monitor*

The diamond based detector system is comprised of polycrystalline diamond detectors (CIVIDEC Instrumentation GmbH) with a size of 10 mm × 10 mm × 0.5 mm [3]. Each detector is connected to an AC-DC splitter, where the AC-part of the signal is amplified by a current amplifier with 40 dB gain and bandwidth of 2 GHz (both the AC-DC splitter and the preamplifier are provided by CIVIDEC Instrumentation GmbH). The detector system is mounted on a metal panel on top of the beam pipe, 6 meters downstream of the primary collimators (TCP) in IR7 (shown in Fig. 1). The coaxial cable which connects the detector system to the readout system is about 250 m long. The diamond detectors are operated with a bias voltage of 500 V.

### *Readout System*

The detector signals are read out by the ROSY® data acquisition system also provided by CIVIDEC Instrumentation GmbH. The ROSY® system comes with all the acquisition and triggering functionalities of a digital oscilloscope. In addition, an integrated FPGA provides dead-time-free online signal processing. The ROSY® system has an embedded Linux operating system and provides a programmable interface to control the system and transfer the acquired data. This system is installed in the LHC service tunnel and is connected to the CERN technical network via an Ethernet cable.

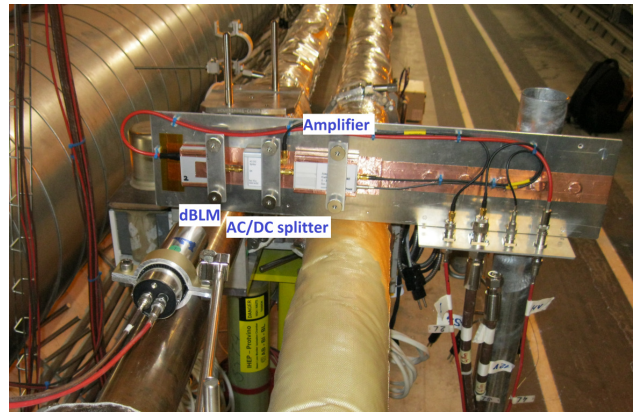


Figure 1: dBLM installation in the LHC IR7.

The ROSY® system is simultaneously able to produce a high sampling rate waveform and provide a real-time beam loss time histogram. In the histogram mode, the system synchronizes to the LHC turn clock and increases the corresponding bin when the loss signal exceeds a user defined threshold. The bin width is 1.6 ns. Figure 2 explains the operational principle of the histogram mode.

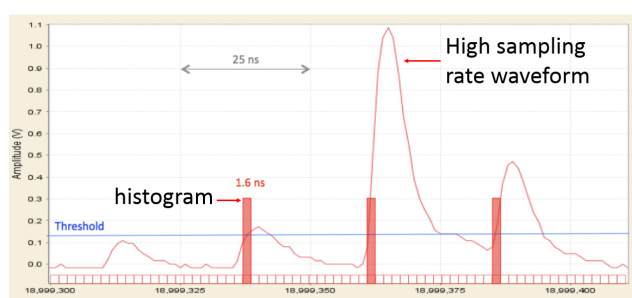


Figure 2: Beam loss signals exceeding a threshold causes the corresponding bin to increase in value [4]. The data is captured using the post-mortem application from CIVIDEC Instrumentation GmbH.

The ROSY® system has 4 analog input channels for the waveform measurement, each channel having a maximum

* chen.xu@cern.ch

ISBN 978-3-95450-177-9

# OPTIMIZED BEAM LOSS MONITOR SYSTEM FOR THE ESRF

B.K. Scheidt, F.Ewald, ESRF, Grenoble, France
P.Leban, Instrumentation Technologies, Solkan, Slovenia

*Abstract*

Monitoring of the 6 GeV electron losses around the ESRF storage ring is presently done by a hybrid system consisting of ionization chambers and scintillators. It allows a rough localization of the losses, but has numerous limitations: size, weight, time-resolution, sensitivity, versatility, and costs. A new system was developed consisting of a detector head (BLD) and the electronics for signal acquisition and control (BLM). The BLD is compact, based on a scintillator coupled to a small photo-multiplier module. The BLM controls 4 independent BLDs and acquires data with sampling rates up to 125 MHz Measurements performed on different configurations of BLD prototypes have lead to an optimized design that allows, together with the flexible signal processing performed in the BLM, to cover a wide range of applications: measurement of fast and strong losses during injection is just as well possible as detection of very small variations of weak losses during the slow current decay. This paper describes the BLD/BLM design, its functionality and performance characteristics, and shows results from prototypes installed in the injection zone and in close vicinity to in-vacuum undulators.

## PURPOSES AND APPLICATIONS OF BEAMLOSS MONITORING

### *Historic Situation*

The ESRF produces synchrotron light for its 40 beamlines by operating as its source a 6GeV electron beam in a Storage Ring of 844m circumference. The nominal values for the current and the emittances are respect. 200mA and 4nm (hor.) & 5pm (vert.). The typical lifetime of the electron beam is about 50hrs, meaning an electron loss rate of about 20 million/sec.

The localization of these losses is monitored & surveyed since long by different systems: A total of 64 ionization chambers of 2 different kinds, and a further set of (also 64) detectors that are based on a scintillator, optically coupled to a photo-multiplier-tube [1]. This total of 128 detectors is positioned identically in the ring structure with its 32 cells, i.e. the 4 detectors have the same position in each cell. For the bulky and heavy ionization chambers this is on the floor underneath each of the 64 dipoles, while the scintillator based detectors are placed at the beam height, radially about 40cm on the internal side of each dipole, and roughly in the middle of the dipole length. Each type of the above detectors employ a 1cm thick lead shielding to avoid detecting the inevitable scattered X-rays inside the tunnel.

### *Essential Diagnostic Tool in the Storage Ring*

This comprehensive set of BLDs has been very helpful in the history of the ESRF in rapidly, and unambiguously, detecting and localizing any excessive electron losses. It is to be noted that the usual loss pattern does not show 128 values of roughly equal values: the loss values among these 128 units can have strong deviations due to numerous non-regular structures in the ring like e.g. the injection-zone elements (septum), scrapers, insertion device vacuum chambers with small apertures, especially for in-vacuum undulators, chambers for different modules of RF-cavities, etc.

In general, the 3 most common causes of strong or excessive losses are:

-1- Aperture-limiting effects by e.g. a miss-aligned chamber, or a non-optimum trajectory of the injected beam.

-2- A locally poor vacuum quality by e.g. a vacuum leak or a reduced conductance (e.g. a newly installed chamber with a different UHV pumping structure), or a poorly conditioned chamber (after its installation).

-3- The characteristics of the electron beam itself (variations in dynamic aperture, resonances, Touschek scattering, etc.)

These, more or less drastic, changes in the loss pattern can occur at different moments. For those mentioned under 1) it is often after installation work in the ring, so directly at the restart after a shut-down period. Those linked with vacuum leaks are obviously occurring when such leaks develop, and usually soon afterwards confirmed by the increase of the pressure gauges in the affected zone. The variations induced by beam dynamics are numerous and these variations in the beamloss readings are directly correlated with other measurements on the beam's lifetime, emittance and injection efficiency.

For all of the above uses the data rate of all these loss detectors was low, in the order of 1Hz. This speed limitation is imposed by both (some of the used) detectors, their cables for signal transmission and in particular their electronics for signal treatment and digitization. Although the detectors posses a gain control that can be set to low gain at e.g. time of injection, it is insufficient to verify that no saturation occurs in the early stage (and fast outputs) of these detectors.

## IMPROVEMENTS WITH THE NEW AND OPTIMIZED SYSTEM

One of the main aims of the new system was to drastically improve the speed and bandwidth up to a time resolution of sub-orbit time (2.816us). This concerns both the BLD detector (and notably its photon-detection-electronics) and the acquisition electronics (BLM).



ISBN 978-3-95450-177-9

# DEVELOPMENT OF A METHOD FOR CONTINUOUS FUNCTIONAL SUPERVISION OF BLM SYSTEMS

C. F. Hajdu, CERN, Geneva, CH; Budapest University of Technology and Economics, HU
C. Zamantzas, CERN, Geneva, Switzerland
T. Dabóczi, Budapest University of Technology and Economics, Hungary

*Abstract*

It is of vital importance to provide a continuous and comprehensive overview of the functionality of beam loss monitoring (BLM) systems, with particular emphasis on the connectivity and correct operation of the detectors. At CERN, a new BLM system for the pre-accelerators of the LHC is currently at an advanced stage of development. This contribution reports on a new method which aims to automatically and continuously ensure the proper connection and performance of the detectors used in the new BLM system.

## INTRODUCTION

At CERN, the scheme for machine protection and optimization relies heavily on beam loss monitors (BLMs). Therefore, a continuous functional supervision of the BLM system is essential. To our knowledge, no particle accelerator in the world has this feature at present.

Currently, one of the most advanced solutions for supervising the functionality of a BLM system is in operation at the LHC. This method enforces a connectivity check of each detector channel every 24 hours, which can only be executed while the accelerator is offline.

The LHC Injectors Upgrade (LIU) project, presently underway at CERN, is a major accelerator upgrade project targeting the pre-accelerators of the LHC. Among other activities, this program mandates the deployment of an upgraded BLM system with extended functionality in the injectors, which is at an advanced stage of development at the time of writing.

This paper reviews the present state of a project aimed at building on LHC experience to develop a process capable of ensuring an uninterrupted supervision of the entire beam loss monitor signal chain from the detector to the acquisition electronics.

## DETECTOR CONNECTIVITY CHECKS AT THE LHC

Ionization chambers are the most frequently used detector type in the LHC BLM system [1]. The bias high voltage applied to the chamber gives rise to an output current proportional to the energy deposited in the volume of the chamber by incident ionizing radiation. This current is acquired and digitized by the front-end electronics [2], then further processed by the back-end electronics [3] responsible for deciding whether the machine is operating under safe conditions. These modules can trigger the safe extraction of circulating beams or inhibit further injections as required.

At the LHC, the method for checking the connectivity of the detectors relies on inducing a sinusoidal modulation at a frequency on the order of 50 mHz in the bias high voltage. The chamber responds as a capacitor and a corresponding sinusoidal signal is generated in its output current, which can then be digitized through the standard signal acquisition chain. The signal is then detected in the time domain using a matched filtering algorithm executed on an FPGA device.

The absence of the modulation in the digitized data stream indicates a defective cabling connection, while variations in the amplitude and the phase of the modulation have been shown to correspond to various other degradations of the signal chain. The connectivity check thus also acts as a component integrity survey [4,5]. Such a check is performed without beam before the start of each physics fill.

## SYSTEM SUPERVISION AT THE INJECTORS

### *System Architecture in Brief*

The new BLM system under development will be common to all injectors. These accelerators impose widely varying requirements, thus the acquisition frequency and input dynamic range of the new system must surpass those of its predecessors. In most locations, ionization chambers will be employed but the use of other detector types such as Cherenkov monitors, diamond detectors and secondary emission monitors is also foreseen. Therefore, the system needs to be able to handle all these various types of detectors [6].

These considerations imply that a new acquisition front-end module had to be designed for the new BLM system. It can digitize input currents ranging from 10 pA to 200 mA using a novel measurement method based on a fully differential integrator [7]. The digitized samples are forwarded to the back-end processing and triggering (BLEPT) modules at 500 ksps for further processing. These modules calculate several moving window integrals referred to as running sums for the digitized current of each detector and are responsible for revoking the beam circulation permit if required.

### *The Suggested Method*

For checking the integrity of the main ionization chamber beam loss monitoring system of the injectors, a modulation-based scheme like the one used in the LHC might be a viable option. However, that scheme requires the accelerator to be offline as the checks, lasting about 6 minutes, are executed during the injection preparation phase, i.e. long periods with no beam characterizing the operation of the LHC. In



ISBN 978-3-95450-177-9

# STUDIES AND HISTORICAL ANALYSIS OF ALBA BEAM LOSS MONITORS

A. A. Nosych, U. Iriso, ALBA-CELLS, Barcelona, Spain

*Abstract*

During 5 years of operation in the 3 GeV storage ring of ALBA, the 124 beam loss monitors (BLMs) have provided stable measurements of relative losses around the machine, with around 10% breakdown of units. We have analyzed these BLM failures and correlated the integrated received dose with any special conditions of each BLM location which might have led to their breakdown.

We also show studies of beam losses in the insertion devices, with particular attention to the results in the multipole wiggler (MPW), where the vacuum chamber is (suspected to be) misaligned and high BLMs counts are detected.

## INTRODUCTION

ALBA is a 3 GeV 3$^{rd}$-generation synchrotron light source, operational since 2011. Currently it is running in top-up mode with beam current of up to 150 mA and the horizontal emittance of 4.6 nmrad. During 5 years of operation the 124 beam loss monitors have been generally doing a very good service in measuring the loss distribution around the 269 m storage ring (SR). Nevertheless, several units did get out of order, some others did get detuned and some more did change their positions over time. A campaign to re-organize the BLM units and understand their health state has been conducted.

## LAYOUT OF ALBA BLMS

Common to other synchrotrons [1], the beam loss detection system of ALBA consists of a pair of compact PIN-diode Bergoz BLMs connected to a two-channel beam signal conditioner (BSC). The BSC provides electrical power and signal readout to- and from- the BLMs. The BLMs are evenly spread around the storage ring at approximately every 2.5 m, coinciding with BPM locations. For maximum sensitivity the active part of BLMs has been positioned in the beam orbit plane and is perpendicular to the beam direction. Besides, placed in the inner side of the ring, they are subjected from the X-ray background.

In total there are 66 BSCs and 124 corresponding BLMs spread around 16 sectors of the machine: 7 or 8 per sector (depending on sector type), plus a few additional units around the injection line from booster. A typical 8-BLM connectivity schematic per sector is shown in Fig. 1.

The BLM detector is sensitive to minimum ionizing particles (MIP) produced when an accelerated particle hits the vacuum chamber [2]. The detector is composed of two PIN-diodes mounted face to face to form a 2-channel coincidence detector. When an ionizing particle hits a PIN-diode, an electric charge is produced, and a bias voltage allows collection of this charge. A particle energy of > 700 keV is

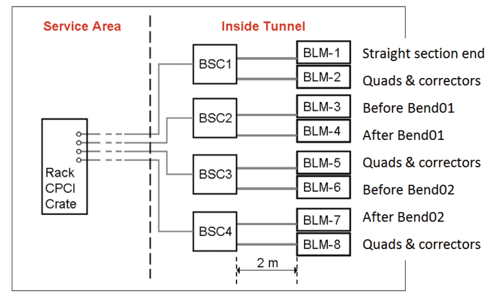


Figure 1: Beam loss detection system of ALBA per storage ring sector.

required to get the PIN-diode ionized and it is detected with an efficiency of > 30%. MIPs cause ionization in both PIN-diodes, while photons do not, which excludes BLMs from being affected by synchrotron radiation.

The size of the PIN-diodes mounted on the circuit determines the detector's solid angle. The coincidence scheme effectively rejects the spurious noise from each channel well below 1 counts per second (cps). The amplification gain of each channel is adjusted with a potentiometer [2].

### *Beam Loss Monitors in Operation*

The nominal counts in the majority of BLM locations during SR operation is around 10-20 cps, which slightly rise during injections, reaching some 10s and 100s in the vicinity of the booster-to-storage transfer line and the injection kickers.

Figure 2 shows a typical loss distribution map around the ring during decay and injection modes, updated at 1 Hz rate. In each sector the lowest losses correspond to the beginning/end of the sector (straight sections), while the highest are systematically read downstream of both dipoles in each sector.

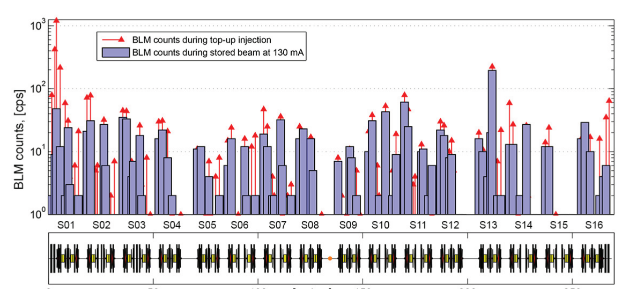


Figure 2: Operational beam loss distribution (log scale) on the ALBA storage ring as observed in the control room.



ISBN 978-3-95450-177-9

# INDUSTRIALISATION OF CAVITY BPMS

E. Yamakawa*, S. Boogert, A. Lyapin,
John Adams Institute at Royal Holloway, University of London, Egham, UK
S. Syme, FMB Oxford, Oxford, UK

*Abstract*

The industrialisation project of a cavity beam position monitor (CBPM) has been commissioned aiming at providing reliable and economical CBPM systems for future Free Electron Lasers (FEL) and similar linac-based facilities. The first prototype of a CBPM system was built at Versatile Electron Linear Accelerator (VELA) in Daresbury Laboratory. We report on the measurement results from the first prototype of our system at VELA and current developments of CBPMs, down-converter electronics and Data Acquisition (DAQ) system.

## INTRODUCTION

CBPMs have gradually moved from an exotic extreme spatial resolution tool designed for use in final focus collider systems [1] to an FEL workhorse [2, 3] providing sub-micrometre resolutions even at low, typically less than 100 pC bunch charge. An industrialisation project had been started jointly by the John Adams Institute (at Royal Holloway, University of London), FMB-Oxford and Daresbury Laboratory in 2014 with support by the Science and Technology Facilities Council (STFC) Innovations Partnership Scheme (grant number ST/L00013X/1). The aim of the project is to design a low-cost, easy in operation and reliable CBPM system that could be deployed even in smaller high brilliance light facilities with no direct access to the required expertise.

A basic CBPM system typically consists of 2 cavities: one position (dipole) and one reference (monopole) cavity for charge and phase normalisation, a set of down-converter electronics, high-speed digitisers for data acquisition and digital processing. In order to kick-start the project, cavity, electronics, DAQ and processing development, as well as setting up the beam experiment started in parallel, with an existing cavity [4] used as a test subject to set up the beam measurements while the new cavities are still in development. The beam test has been set up at STFC Daresbury Laboratory in VELA test facility.

## CBPM TEST SYSTEM AT VELA

We built the first prototype of CBPM system at VELA in Daresbury Laboratory. Currently, the system includes one position and one reference cavity, and is planned to be extended to 3 position cavities plus reference in 2017. There are 2 precision position stages moving a single CBPM horizontally and vertically with respect to the beam (Fig.1). The motion stages are controlled remotely via a MINT motion controller coupled with a PC running LabVIEW code. Three channels of homodyne down-converting electronics reduce the frequency of the signal down to about 20 MHz (Fig. 2).

Two Red Pitaya [5] open source SoC (system on a chip) boards are deployed for DAQ. Red Pitaya hosts a single processor plus FPGA (field-programmable gate array) chip, two 125 MHz 14-bit ADC and 2 DAC channels and a number of GPIO pins. The native code has been modified in order to acquire signals with external trigger and include EPICS (Experimental Physics and Industrial Control System) API modules for seamless interfacing with VELA for DAQ and control.

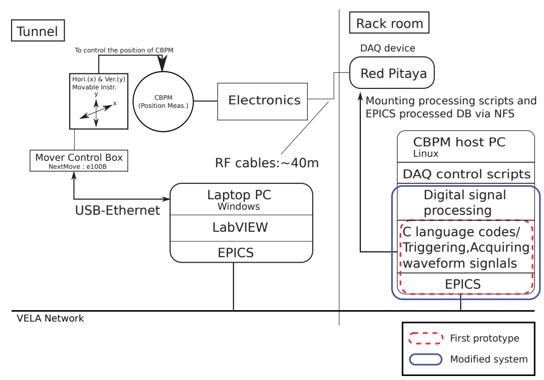


Figure 1: The layout of CBPM system in VELA.

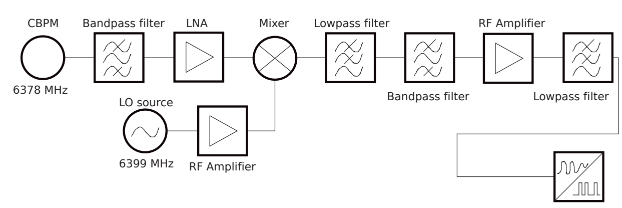


Figure 2: Schematic of the signal down-converting electronics for the C-band system.

In the first instance, we installed a single existing position cavity (Fig. 3) to commission the test system and start working on the electronics and DAQ, the data were taken on the 8th of July 2015.

We measured CBPM signals while moving the stages first in horizontal and then in vertical in order to measure the sensitivity of the cavity in hand. The digitised waveform signal was processed by the digital down-conversion (DDC) algorithm [6] on the host PC to detect the amplitude of the signal using a digital LO (Local Oscillator) of the same frequency as the incoming CBPM signal. A Gaussian filter was applied to remove the noise and up-converted component of the IF signal. For measuring the sensitivity of the cavity, the maximum amplitude of the demodulated signal

* Emi.Yamakawa@rhul.ac.uk

# THE DESIGN, CONSTRUCTION AND OPERATION OF THE BEAM INSTRUMENTATION FOR THE HIGH INTENISTY AND ENERGY UPGRADE OF ISOLDE AT CERN

W. Andreazza, E. Bravin, E.D. Cantero, S. Sadovich, A.G. Sosa, R. Veness,
CERN, Geneva, Switzerland
J. Carmona, J. Galipienzo, P. Noguera Crespo, AVS, Elgoibar, Spain

*Abstract*

The High Intensity and Energy (HIE) upgrade to the online isotope separation facility (ISOLDE) facility at CERN is currently in the process of being commissioned. The very tight space available between the superconducting acceleration cavities used and a challenging specification led to the design of a compact 'diagnostic box' (DB) with a number of insertable instruments on a common vacuum chamber. The box was conceived in partnership with the engineering firm AVS and produced as a completed assembly in industry. 14 diagnostic boxes have been installed and are now operational. This paper will describe the design, the construction and first results from operation of these HIE-ISOLDE diagnostic boxes.

## INTRODUCTION

The High Intensity and Energy (HIE) ISOLDE project is a major upgrade of the ISOLDE and REX-ISOLDE facilities at CERN. The aim of the HIE-ISOLDE project is to greatly expand the physics programme compared to that of REX-ISOLDE. The energy of the post-accelerated radioactive beams will be increased from 3 MeV/u to 10 MeV/u. At the same time the intensity of the source will be increased with higher beam power on the production target, from 2 kW to 10 kW.

The HIE-ISOLDE diagnostic boxes are installed in the Linac between the cryomodules and in the High Energy Beam Transport (HEBT) line, between the quadrupoles of the doublet transport channel, in the dispersive sections of the double-bend achromats and before the experimental target positions.

## BEAM DIAGNOSTIC REQUIREMENTS

The beam diagnostic system must provide a wide range of possibilities for measuring properties of the beam during set-up and operation of the HIE-ISOLDE facility, specifically: measurement of beam intensity using a Faraday cup; measurement of beam transverse profile and beam position using a Faraday cup in parallel with a scanning slit; collimation of the beam using collimator slits; charge-state cleaning using stripping foils; measuring energy and longitudinal profile using silicon detectors [1].

## DESIGN

The design of the diagnostic boxes (DB) was driven by the very tight space available between the superconducting acceleration cavities installed in the LINAC (Fig. 1 & 2). Two cryomodules have been installed so far with four more units planned to be added over the next few years. The LINAC layout allowed a maximum inter-cryomodule distance of 250 mm, where the DBs are located. Two different versions of boxes were designed and produced, equipped with various selections of the same instruments. Five so-called "short DBs" are installed in the HIE-ISOLDE LINAC and eight "long DBs" provide beam instruments in the HIE-ISOLDE experimental lines.

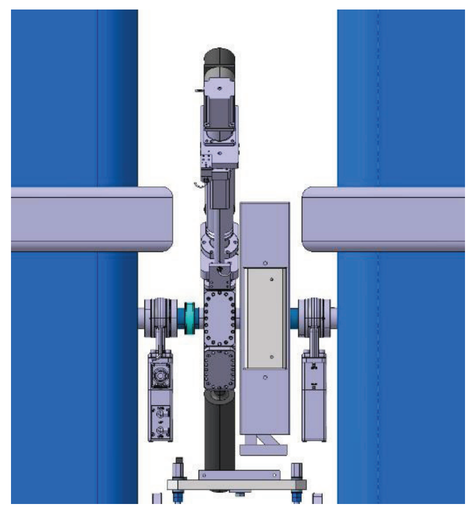

Figure 1: Schematic of the inter-cryomodule region with a short diagnostic box installed.

The design had to allow for installation of the following ultra-high vacuum (UHV) compatible instruments:

- Faraday cup
- Scanning slit
- Collimating slit
- Silicon detector
- Stripping foil

Two edge welded bellows allow the diagnostic box to be aligned with the surrounding components, with a permanently installed survey target used for fiducialisation.

ISBN 978-3-95450-177-9

# THE BROOKHAVEN LINAC ISOTOPE PRODUCTION (BLIP) FACILITY RASTER SCANNING SYSTEM FIRST YEAR OPERATION WITH BEAM*

R. Michnoff#, Z. Altinbas, P. Cerniglia, R. Connolly, C. Cullen, C. Degen, R. Hulsart, R. Lambiase, L. Mausner, W. Pekrul, D. Raparia, P. Thieberger, Brookhaven National Laboratory, Upton, NY

*Abstract*

Brookhaven National Laboratory's BLIP facility produces radioisotopes for the nuclear medicine community and industry, and performs research to develop new radioisotopes desired by nuclear medicine investigators. A raster scanning system was recently completed in December 2015 and fully commissioned in January 2016 to provide improved beam distribution on the targets, allow higher beam intensities, and ultimately increase production yield of the isotopes. The project included the installation of horizontal and vertical dipole magnets driven at 5 kHz with 90 deg phase separation to produce a circular beam raster pattern, a beam interlock system, and several instrumentation devices including multi-wire profile monitors, a laser profile monitor, beam current transformers and a beam position monitor. The first year operational experiences will be presented.

## INTRODUCTION

The purpose of the recently completed raster system at BNL's BLIP facility is to "paint" the proton beam on the target in a circular pattern in order to provide a more even distribution of beam on the target material. At IBIC 2014 we reported on the overall system architecture and presented specific details for each system component [1]. This report will focus on results with beam during the first year of operation with the new system.

The beam instrumentation devices were installed in the fall of 2014 and commissioned with beam during the 2015 beam run from January to July 2015. The raster magnet and associated power supplies were installed during the fall of 2015, and full system commissioning was quickly completed in January 2016, four months ahead of the schedule that was already shortened by one year. The system was reliably operated with beam for the entire 2016 beam run from January to July 2016.

The new BLIP beam-line layout is shown in figure 1.

## BEAM RASTER PATTERNS

The horizontal and vertical raster magnets are driven continuously with sine waves at 5 kHz and 90 deg. phase separation to provide a circular or elliptical beam pattern [2]. The amplitude of the magnet current controls the amplitude of the beam motion.

The raster pattern is programmed using a circular table of horizontal and vertical magnet current amplitudes. The output current changes to the next amplitude in the table after each 450 µs long Linac beam pulse, which occurs every 150 ms. The table size can contain more than 100 values and the amplitudes of the horizontal and vertical values do not need to be equal, thus allowing both circular

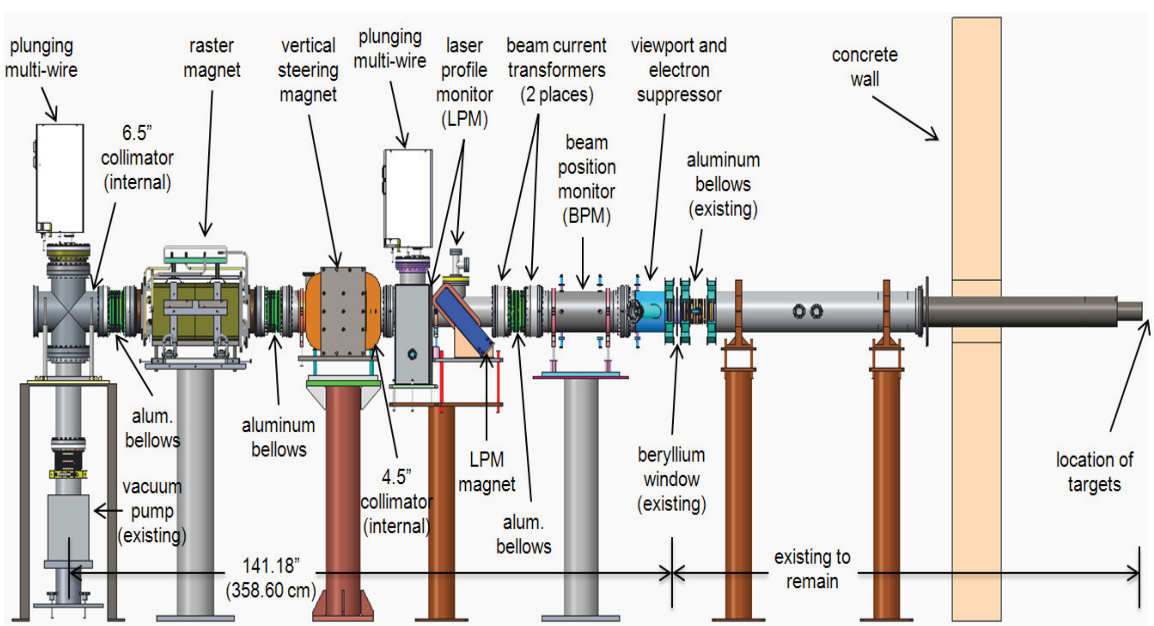


Figure 1: New BLIP beam-line layout.

* Work supported by Brookhaven Science Associates, LLC under Contract No. DE-AC02-98CH10886 with the U.S. Dept. of Energy
#michnoff@bnl.gov

ISBN 978-3-95450-177-9

# BEAM DIAGNOSTICS DESIGN FOR A COMPACT SUPERCONDUCTING CYCLOTRON FOR RADIOISOTOPE PRODUCTION*

R. Varela†, P. Abramian, J. Calero, P. Calvo, M. Domínguez, A. Estévez, L. García-Tabarés, D. Gavela, P.Gómez, A. Guirao, J.L Gutierrez, J.I. Lagares, D. López, L. M. Martínez, D. Obradors, C. Oliver, J.M. Pérez, I. Podadera, F. Toral, C. Vázquez, CIEMAT, Madrid, Spain

*Abstract*

The aim of the AMIT cyclotron is to deliver an 8.5 MeV, 10 μA CW proton beam to a target to produce radioisotopes for PET diagnostics. Such a small cyclotron poses some challenges to the diagnostics design for commissioning and normal operation due to its small size, so miniaturized devices should be built in order to fit in the available space. Two sets of diagnostics have been designed, each one aiming at a different phase of the machine lifecycle. During normal operation the stripping foil and the target will be used to measure the current, a dual transverse profile monitor based on a scintillating screen will be used for interceptive measurements and a Fluorescence Profile Monitor will measure the beam position and the horizontal profile without intercepting the beam. During first stages of commissioning the dual transverse profile monitor and the target will be substituted by an emittance monitor based on a pepper-pot to characterize the beam at the cyclotron exit. Also a movable interceptive Beam Probe will be located inside the cyclotron to give information about the beam during acceleration. Additionally, a test bench for the characterization of the beam right after the exit of the ion source has been built with different instruments to measure the beam current and the transverse profile. In this paper the present status of the design, simulation and tests of the diagnostics for the AMIT cyclotron are described.

## INTRODUCTION

The use of PET as a diagnostic tool in the cancer diagnostic field has rised the demand of suitable radionuclides. Some of the most used radioactive atoms have relatively short lifetimes (few hours at max), which constrains the distance of the medical diagnoses centers to the radioisotope producing facilities. To overcome this limitation a compact cyclotron provides a good solution to this problem, because its small size makes it easy to allocate in small medical centers, allowing the distribution of the radioisotopes to cover as much area as possible.

The AMIT cyclotron (Fig. 1) tries to improve the size and cost efficiency limitations by a careful study of the beam dynamics [1] and the electromagnetic design [2]. It uses two superconducting coils to provide the 4 T magnetic field and a 180º Dee attached to the RF cavity to accelerate H- ions produced by a cold cathode Penning Ion Source. The machine aims to deliver a 10 uA beam of 8.5 MeV protons to irradiate two different targets (one at a time) in order to produce the required amount of $^{11}C$ and $^{18}F$.

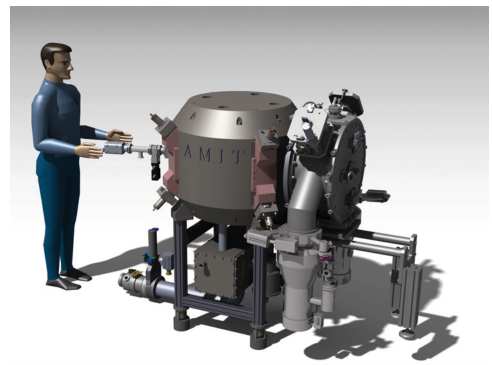

Figure 1: CAD design of AMIT cyclotron.

## MACHINE OPERATION

The main challenge of this cyclotron with respect to the beam diagnostics is compactness. At 4 T and 8.5 MeV the proton bending radius is about 10 cm, limiting enormously the beam diagnostics which can fit inside the cyclotron. Different sets of diagnostics were proposed for the cyclotron's different phases [3]:

1. **Phase 1: Ion Source Characterization.** In this first stage a special test bench (Fig. 2) has been constructed to measure different beam parameters right after the exit of the ion source. This will help to verify and optimize the ion source prior to the assembly in the cyclotron.
2. **Phase 2: Beam Commissioning.** This phase consists of a few subphases, corresponding each one of them at different energy ranges:
   (a) Low energy: In this phase the proper operation of the ion source and the correct alignment between puller and source and first turns is checked.
   (b) Intermediate energy: Optimization of the acceleration from the injection up to the stripping foil.
   (c) Beam delivery at target: Comissioning of the stripping foil and beam transport up to the target and its commissioning.
3. **Phase 3: Operation.** Normal run of the machine with the continuous production of the required radioisotopes.

* This work has been funded by the Spanish Ministry of Economy and Competitiveness under project FIS2013-40860-R.

† rodrigo.varela@ciemat.es

ISBN 978-3-95450-177-9

# BEAM DIAGNOSTICS FOR THE MULTI-MW HADRON LINAC IFMIF/DONES *

I. Podadera †, B. Brañas, A. Guirao, A. Ibarra, D. Jiménez, E. Molina,
J. Molla, C. Oliver, R. Varela, CIEMAT, Madrid, Spain
P. Cara, Fusion for Energy, Garching, Germany

*Abstract*

In the frame of the material research for future fusion reactors, the construction of a simplified facility of IFMIF [2], the so-called DONES (Demo-Oriented Neutron Early Source) [1], is planned to generate sufficient material damage for the new design of DEMO . DONES will be a 40 MeV, 125 mA deuteron accelerator. The 5 MW beam will impact in a lithium flow target to yield a neutron source. The detailed design of the DONES accelerator is being pushed forward within EUROFUSION-WPENS project. One of the most critical tasks of the accelerator will be to identify the layout of beam diagnostics along the accelerator. This instrumentation shall guarantee the high availability of the whole accelerator system and the beam characteristics and machine protection. This contribution will describe the beam diagnostics selected along the accelerator, focusing on the High Energy Beam Transport line, in charge of shaping the beam down to the high power target. The main open questions will be analyzed and the path to obtain the detailed design by the end of the project described.

## ACCELERATOR DESCRIPTION

The linear accelerator for the DONES facility [1] will serve as a neutron source for the assessment of materials damage in future fusion reactors. Unlike the two coupled accelerators for the final IFMIF [2], DONES will be one accelerator, instead of two, accelerating deuterons up to 40 MeV at full CW current of 125 mA (Tab. 1). DONES is divided in three major systems: the particle accelerator, the target and the experimental area. The accelerator system is based on the design of LIPAC [3], which is currently in its commissioning phase [4]. The main sections are (Fig. 1):

- A Low Energy Beam Transport (LEBT) section at 100 keV to guide the low energy ions up to the RadioFrequency Quadrupole (RFQ) and match its injection acceptance.
- An RFQ to accelerate the ions from 100 keV up to 5 MeV.
- A Medium energy Beam Transport Line (MEBT) to match the RFQ extracted beam to the injection of the SRF Linac. It will also be used for matching the RFQ beam with the requirements of the Diagnostics Plate during the RFQ commissioning.
- An SRF Linac to bring the energy of the deuterons up to 40 MeV. It is made of four cryomodules, bringing the energy from 5 MeV up to 9 / 14.5 / 26 and 40 MeV respectively at the exit of each cryomodule.
- A High Energy Beam Transport (HEBT) lines to transport the beam from SRF Linac towards the lithium target or the beam dump transport line (BDTL, in pulse mode).
- A Diagnostics Plate (DP) to commission the beam at medium and high energies. It will be located at the exit of the RFQ and SRF LINAC cryomodules during each beam commissioning stage.

* This work has been carried out within the framework of the EUROfusion Consortium and has received funding from the Euratom research and training programme 2014-2018 under grant agreement No 633053

† ivan.podadera@ciemat.es

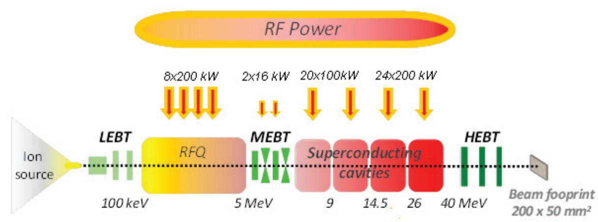


Figure 1: Layout of the DONES accelerator system.

Table 1: DONES Main Beam Parameters

| | |
|---|---|
| Peak current | 125 mA |
| RF frequency | 175 MHz |
| Beam energy | 0.1/5/9/14.5/26/40 MeV |
| $\beta$ | 0.01/0.073/0.097/0.12/0.165/0.2 |

## BEAM DIAGNOSTICS REQUIREMENTS

The requirements of DONES pose several challenges to the beam diagnostics [5]. The normal operation mode of the accelerator will be in continuous (CW) mode, with an average beam current of 125 mA at a bunch frequency of 175 MHz. An additional pulsed mode operation must be taken into account during the commissioning. The use of special interceptive diagnostics is required for this case (e.g. wire scanners, Faraday cups…). A 0.1 % duty factor is estimated for the pulsed mode, with a minimum pulse of 50 μs and a maximum one of 200 μs, as defined for LIPAC. The present plan assumes the operation with deuterons from the earliest stage. However a preliminary operation with protons is highly probable/almost mandatory, as it has been

ISBN 978-3-95450-177-9

# DESIGN OF RISP RFQ COOLER BUNCHER

R. Boussaid†, S. Kondrashev, Young-Ho. Park
Rare Isotope Sciences Project, Institute for Basic Science, Republic of Korea

*Abstract*

Under RISP project, wide variety of intense rare isotope ion beams will be provided. An EBIS charge breeder has been designed to charge breed these beams. Its optimum operation requires injection of bunched beam with small emittance and energy spread. An RFQCB is designed to meet these requirements. In this respect, the RFQCB should efficiently accept high intensity continuous beams and deliver to EBIS bunched beams with emittance around 3 π.mm.mrad, energy spread < 10 eV and short bunch width (~10 µs). A new design concept to be implemented in this RFQCB have been developed, including a novel injection/extraction electrodes geometry with improved differential pumping system. Simulations have shown high efficiency of transmission more than 93 % of incoming ions for beam intensities up to 1 µA with improved beam quality. A set of beam diagnostics tools including Faraday cups, pepper-pot emittance-meter with MCP based detector are designed to characterize the ionbeams.

## RISP PROJECT

A heavy ion accelerator facility called RAON [1] is being designed to produce various rare isotopes under the Rare Isotope Science Project (RISP) [2]. Using the ISOLand IFbeam production methods [3], as well as a combination of these methods RAON will provide wide variety of intense rare isotope ion beams [4] for nuclear physics experiments and applied science.

An efficient and cost effective acceleration of rare isotope beams requires utilization of charge breeder as an interface between ion source and linear accelerator to convert a singly-charged ion beam into the highly-charged ion beam. An Electron Beam Ion Source (EBIS) charge breeder (CB) has been designed [5] and is being built to charge breed rare isotope ion beams for further acceleration. EBIS CB is preferable choice for the most ongoing projects, including RISP, because of its high breeding efficiency, short breeding time, and in particular, high purity of charge bred ion beams. The optimum operation of EBIS CB requires injection of bunched beam with small emittance and low energy spread. An RFQ Cooler/Buncher (RISP-RFQCB) is designed to meet these requirements.

## RFQ COOLER-BUNCHER

At present, RFQCB is operational at multiple rare isotope facilities like CARIBU, ISCOOL, NSCL and others [6]. In order to meet requirements of modern ISOL facilities, it is necessary to increase the beam intensity limit of such device from typically several tens of pico-amperes (~$10^6$ pps) to several tens of nano-amperes (~$10^9$ pps) and to accumulate the ions during time determined by the required EBIS charge breeding time (~10-1000ms). As the existing devices are not able neither to handle high beam current nor to accumulate ions for long period of time, a new RISP-RFQCB device is being developed. In order to meet the EBIS beam requirements, the RISP-RFQCB should efficiently accept high intensity continuous beams from ISOL ion source and deliver to the EBIS charge breeder bunched ion beams with small emittance (~3 π.mm.mrad), low energy spread (<10 eV) and short bunch width (~10 µs).

The RISP-RFQCB is designed to handle intense ion beams with large emittances and wide range of ion masses (6-180 a.m.u), and to deliver bunches with high rep-rate (1-100 Hz). A new design concept to be implemented in the RISP RFQCB have been developed, including a novel injection/extraction electrodes geometry. An overview of the RISP RFQCB design concept will be presented. Simulated performance of the device and design of different sub-systems will be presented and discussed as well.

### *Optics Design*

The RFQCB must accept up to few tens nAmps continuous beam with energy <=60keV and transverse emittance going up to 40 π.mm.mrad over a mass range between 6 and 180 uma. It must also deliver bunched beams in agreement with EBIS injection beam requirements. To conform a conceptual design capable of satisfying these requirements, several ion optical simulations were performed using SIMION 8.1 to model ion optics, including RF/DC fields, buffer gas and space charge effects.

As for all RFQCB devices, ion optical system of the present device can be divided into three sections [7]: injection section, cooling section and extraction section. These sections have to ensure an efficient transmission of the input beams. To efficiently cool RISP beams, the injection energy that will bring the ions to the cooling section should be of ~20-100 eV. Therefore, the relatively high energy of beam should be decreased using a DC electric field. The deceleration can be done by the injection plate electrode setting at high voltage (HV) platform and grounded input electrode, Figure 1. Other injection electrodes provide a fine-tuning of beam transmission. The cooling section consists of the main RFQCB chamber placed at HV platform. This chamber is filled with helium buffer gas and it accommodate the radiofrequency quadrupole (RFQ). It is devoted to trap efficiently the injected beam and to cool it progressively with the buffer gas. To guide the ions along the RFQ up to the extraction section, the RFQ electrodes are segmented and a DC potentials are applied to these segments. The structure is 800 mm in length and is separated into 27 segments of various length. Several electrodes are placed at RFQCB exit to extract and accelerate cooled and bunched ion beam back to the same energy as that of the

†nounaramzi@ibs.re.kr

ISBN 978-3-95450-177-9

# SINGLE PULSE SUB-PICOCOULOMB CHARGE MEASURED BY A TURBO-ICT IN A LASER PLASMA ACCELERATOR

F. Stulle*, J. Bergoz, Bergoz Instrumentation, Saint-Genis-Pouilly, France
W.P. Leemans, K. Nakamura, Lawrence Berkeley National Laboratory, Berkeley, CA 94720, USA

*Abstract*

Experiments at the Berkeley Lab Laser Accelerator (BELLA) verified that the Turbo-ICT allows high resolution charge measurements even in the presence of strong background signals. For comparison, a Turbo-ICT and a conventional ICT were installed on the BELLA petawatt beamline, both sharing the same vacuum flanges. We report on measurements performed using a gas-jet and a capillary-discharge based laser plasma accelerator. In both setups the Turbo-ICT was able to resolve sub-picocoulomb charges.

## INTRODUCTION

Imaging plates and scintillating screens are widely used in laser plasma accelerators (LPAs) for beam diagnostics [1-3]. They allow accurate measurements of the transverse profiles and the bunch charges even in the presence of strong background signals, which often accompany the beam signal due to the LPA working principle. For example, the laser – plasma interaction creates a strong electromagnetic pulse. However, plates and screens are obstacles for the particle beam, degrading beam quality or even capturing particles. And they are susceptible to X-rays. Complementing them by non-destructive charge diagnostics would be highly desirable.

One possibility would be to use integrating current transformers (ICTs) [4]. Previous studies comparing an ICT to a scintillating screen at a gas-jet based LPA [5] have shown that an ICT can provide accurate charge information for this type of accelerators [6]. However, the measurement setup needed to be carefully arranged to reduce the detrimental influence of electromagnetic pulses and other background signals. Capillary-discharge based LPAs [7-10] create even stronger background signals. Consequently, the beam diagnostic must be even less sensitive to such influences.

Examples of ICT signals recorded at a gas-jet based LPA and a capillary-discharge based LPA are shown in Fig. 1 and 2. Note that the background signals were highly variable.

At the gas-jet based LPA the background is a mostly constant offset. For the deduction of the charge a constant background is irrelevant. At the capillary-discharge based LPA the background contributes higher frequency components to the measured signal. This background signal has an important impact on the deduction of the charge.

*stulle@bergoz.com

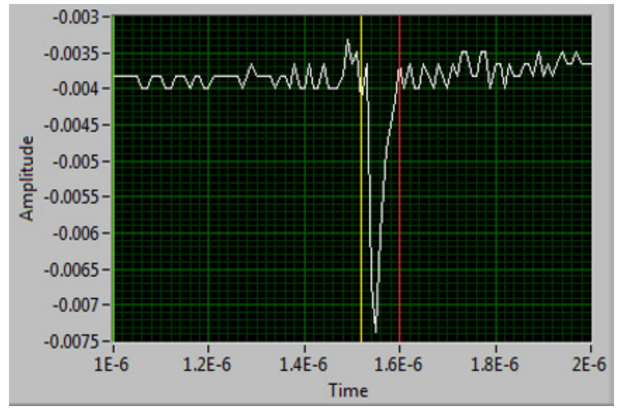


Figure 1: ICT signal recorded in a gas-jet based LPA. The peak between the yellow and red lines is the signal induced by a 10 pC bunch. The constant offset is irrelevant for the deduction of the charge.

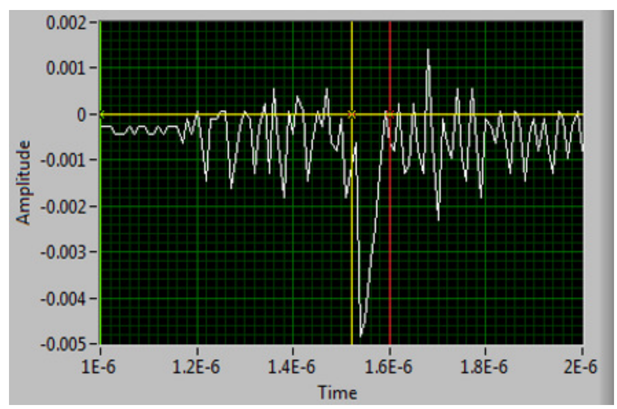


Figure 2: ICT signal recorded in a capillary-discharge based LPA. The peak between the yellow and red lines is the signal induced by a 18 pC bunch.

The Turbo-ICT current transformer and the corresponding BCM-RF electronics have been developed to address the requirements of X-ray free-electron lasers (X-FELs) and LPAs. Thanks to narrow band-pass filtering at a high center frequency, typically 180 MHz, they show little susceptibility to background signals, including electromagnetic pulses, dark current and long particle bunch tails.

To demonstrate the Turbo-ICT advantages for LPAs, a Turbo-ICT was installed in the Berkeley Lab Laser Accelerator (BELLA) petawatt beamline at the Lawrence Berkeley National Laboratory [10]. For comparison, a normal ICT was included in the same vacuum flanges as the Turbo-ICT.

ISBN 978-3-95450-177-9

# TIMING WINDOW AND OPTIMIZATION FOR POSITION RESOLUTION AND ENERGY CALIBRATION OF SCINTILLATION DETECTOR

Jing Zhu, Meihau Fang, Jing Wang, Zhiyong Wei§,
Nanjing University of Aeronautics and Astronautics, Nanjing 210016, P. R. China

*Abstract*

We studied fast plastic scintillation detector array. The array consists of four cuboid bars of EJ200， each bar with PMT readout at both ends. The geometry of the detector, energy deposition in the scintillator， signal generation and energy response have been simulated based on Monte Carlo. The detection efficiency and the real events selection have been obtained while the background noise has been reduced by using two-end readout timing window coincidence. We developed an off-line analysis code, which is suitable for massive data from the digitizer. We set different coincidence timing windows, and did the off-line data processing respectively. It can be shown that the detection efficiency increases as the width of the timing window increases, and when the width of timing window is more than 10 ns, the detection efficiency will slowly grow until it reaches saturation. Therefore, the best timing window parameter τ as 16 ns is obtained for the on-line coincidence measurement. When exposure to $^{137}$Cs $\gamma$ -ray irradiation, a 12 cm position resolution can be achieved while reaching the timing resolution of 0.9 ns. The pulse integration of signals of the detector is in proportion to the energy of incident particles. Furthermore, the geometrical mean of the dual-ended signals, which is almost independent of the hit position, could be used as the particle energy. Therefore, this geometrical mean as the energy of incident particle is calibrated via the Compton edges of $^{60}$Co source, $^{137}$Cs source and the natural $^{40}$K, $^{208}$Tl, and the reliability of the calibration results has been improved. Besides, the energy response is linear.

## INTRODUCTION

When an incident particle interacts in a scintillator, it can cause ionization and excitation of the atoms and molecules of the scintillator. The energy of the incident particle is deposited in the scintillator [1]. The decay of excited atoms and molecules back to their ground states results in a emission of photons with two decay components: the fast one with decay time less than a nanosecond， and the slow one has decay time of hundreds of nanoseconds. The photons are collected on photocathode of the photomultiplier tube (PMT), and then these photons are converted to photoelectrons and amplified. The output signals of the scintillation detector depend on both the energy and the hit position of the incident particle. Besides, false signals come from the dark current and noise also. When the dual-ended readout is taken, we need methods to get hit position and energy of the particles, and also need to select the real events [2]. In this paper, we got real events from incident particles with the background noise reduced by using two-end readout timing window coincidence.

EJ-200 plastic scintillation detector array and its data acquisition system have been set up for radiation measurement in our laboratory. The scintillation detector array consists of four EJ-200 plastic scintillators which have dual-ended PMTs. The EJ-200 plastic scintillator combines two main benefits of long optical attenuation length and fast timing. On the basis of coincidence measurement, we picked out the real events from the timing window of signals, and optimized the timing resolution, position resolution and energy response of the detector.

## SCINTILLATION DETECTION AND DATA ACQUISITION SYSTEM

The plastic scintillator used in this work was provided by the ELJEN Enterprises, USA. The scintillator (denoted by the ELJEN number EJ-200) had dimensions: 5 cm × 5 cm × 125 cm. The decay time of the scintillator is at the level of ns, and the rise time is less than 1 ns. The EJ-200 plastic scintillator was coupled to an ET Enterprises 9813B PMT. A VME bus system was used in our laboratory, and a schematic diagram of the detection system is shown in Fig. 1.

The DT5751 is a 4 channels 10 bit 1 GS/s Desktop Waveform Digitizer with 1 Vpp input dynamic range on single ended MCX coaxial connectors. The DT5751 Waveform Digitizer, which is taken in on-line coincidence measurement, has replaced some complex modules in the traditional coincidence circuits.

The V6533 is a 6 channels High Voltage Power Supply in 1 unit wide VME 6U module.

The online Digital Pulse Processing for Pulse Shape Discrimination firmware (DPP-PSD) was used in this study. Under the frame of DPP-PSD, we got the on-line waveforms and the energy histograms. Besides, the lists for the on-line data were obtained from the digitizer, and were further processed by ROOT, an off-line data-analysis software.

§ email address: wzy_msc@nuaa.edu.cn



ISBN 978-3-95450-177-9

# COMPARATIVE STUDY OF MAGNETIC PROPERTIES FOR CERN BEAM CURRENT TRANSFORMERS

S. Aguilera[1,*], H. Hofmann[1], P. Odier
CERN, Geneva, Switzerland
[1]also at École Polytechnique Fédérale de Lausanne, Lausanne, Switzerland

*Abstract*

At CERN, the circulating beam current measurement is provided by two types of transformer, the Direct Current Current Transformer and the Fast Beam Current Transformer. Each transformer is built based on toroidal cores made from a soft magnetic material. Depending on the type of measurement to be performed these cores require different magnetic characteristics for parameters such as permeability, coercivity and the shape of the magnetisation curve. In order to study the effect of changes in these parameters on the current transformers, several interesting raw materials based on their as-cast properties were selected. The materials have been characterised to determine their crystallisation, melting and Curie Temperatures in order to determine suitable annealing processes to tailor their properties. They have been analysed by several techniques including Electron Microscopy and X-ray Diffraction. As-cast magnetic properties such as the permeability, the B-H curve and Barkhausen noise have also been measured to enable the study of the effect of thermal treatment in the microstructure of the alloys, and the correlation of this with the change in the magnetic properties.

## INTRODUCTION

The total electrical charge of the beam circulating in CERN's accelerators is measured by a family of devices that include current transformers, such as the DC Current Transformers (DCCT) and Fast Beam Current Transformers (FBCT) [1]. This measurement is especially crucial for tuning the beam transfer efficiency between accelerators, monitoring beam losses leading to possible radiation-related issues, assessing beam lifetime, as well as for safety measures to be taken based on the readings. There are a total of 96 transformers at CERN out of which 22 are DCCTs and 74 are FBCTs, coming in various sizes in order to adapt to different vacuum chamber dimensions.

The transformer cores are made out of wound ribbons of soft magnetic material which couple to the electro-magnetic fields accompanying the motion of the charged particle beams. Each type of transformer requires different magnetic materials in terms of permeability, coercivity and the shape of the magnetisation curve to obtain an optimal response for the differing beam parameters of each machine. The choice of material and the associated magnetic characteristics affects transformer parameters such as resolution in the case of the DCCT and bandwidth in case of the FBCT.

The study of commercially available soft magnetic materials, including physical properties such as crystallisation and melting temperatures, and magnetic properties like their Curie temperature and the magnetisation curve, will determine their suitability for each kind of instrument. With this information, a suitable annealing procedure can then be designed for each material. Thermal or thermo-magnetic annealing can drastically change the magnetic properties of the raw materials. The time and heating rate of annealing are the two key parameters that play a crucial role in the final result, enabling for example, the fabrication of nanocrystalline material. By being able to fabricate different cores, it is possible to study how these properties affect the final beam response of such systems in order to find the best solution for each type of application.

## MATERIALS USED

For this study, the materials used were iron-based amorphous and nanocrystalline alloys and cobalt-based amorphous alloys. Two iron-based alloys were purchased from Qinhuangdao Yanqin Nano Science & Technology Co., Ltd., Nanocrystalline 107A1 and amorphous 2065, with the Iron-based amorphous alloy FINEMET® FT-3 bought from Hitachi Metals Europe GmbH. The amorphous cobalt-based materials were purchased from Nanostructured & Amorphous Materials (Nanoamor), Inc., VACUUMSCHMELZE GmbH & Co. KG as VAC 6025 G40 Z and alloy Metglas 2705M from Hitachi Metals. Several cores made out of iron-based nanocrystalline material NANOPERM® were also bought from MAGNETEC GmbH, to be used as a reference material in the study.

## MATERIAL CHARACTERISATION

In order to thermally anneal the samples properly and understand the changes in their magnetic properties, it is first necessary to thoroughly characterise the alloys. Magnetic measurements like permeability, B-H curve and Barkhausen Noise will give an indication of the final performance of the material when in use in the instrument. Repeating these measurements after the annealing process then allows us to understand how the magnetic properties change during the treatment. The main goal being to tune the final magnetic properties through annealing.

### *Permeability and B-H Curve Measurements*

The relative complex permeability was calculated from the impedance measured with the Agilent Vector Impedance Analyser 4294 in the range of 40 Hz to 110 MHz. Cores of

* silvia.aguilera@cern.ch



ISBN 978-3-95450-177-9

# CHARACTERIZATION AND SIMULATIONS OF ELECTRON BEAMS PRODUCED FROM LINAC-BASED INTENSE THz RADIATION SOURCE

N. Chaisueb†, N. Kangrang, S. Rimjaem, J. Saisut, Plasma and Beam Physics Research Facility, Department of Physics and Materials Science, Faculty of Science, Chiang Mai University, Chiang Mai 50200, Thailand

*Abstract*

Electron beams with a maximum kinetic energy of around 2.5 MeV and a macropulse current of about 1 A are produced from an S-band thermionic cathode RF-gun of the linear accelerator system at the Plasma and Beam Physics (PBP) Research Facility, Chiang Mai University (CMU), Thailand. An RF rectangular waveguide input-port and a side coupling cavity of the PBP-CMU RF gun introduce asymmetric electromagnetic field distribution inside the gun cavities. To investigate the effect of the asymmetric field distribution on electron beam production and acceleration, measurements and simulations of the electron beam properties were performed. In this study we use well calibrated current transformers, alpha magnet energy slits, and a Michelson interferometer to measure the electron pulse current, the beam energy, and the bunch length, respectively. This paper presents the measurement data of the electron beam properties at various location along the beam transport line and compares the results with the beam dynamic simulations by using the particle tracking program ELEGANT. Moreover, the RF field feature and the cathode power were optimized in order to achieve the high qualities of the electron beam produced from the RF gun. This result implies and correlates to the electron back-bombardment effect inside the gun cavities.

## INTRODUCTION

The electron linear accelerator at the Plasma and Beam Physics Research Facility (PBP-CMU Linac), Chiang Mai University, Thailand, is used to generate short electron bunches for generation of intense coherent THz radiation in forms of transition radiation and undulator radiation [1-4]. The PBP-CMU Linac transport line consists of two main parts that are the Gun-to-Linac (GTL) section and the Linac-to-Experimental station (LTE) section. In the GTL section, electron bunches are produced from a thermionic RF-gun and are transported to an alpha magnet by using three quadrupoles and two pairs of steering magnets to focus and guide the beam to centre of the alpha magnet entrance.

The alpha magnet is used as a magnetic bunch compressor and also as an energy measuring instrument by utilizing high and low energy slits installed inside its vacuum chamber. Furthermore, the energy slits are used to filter out low energy electrons in order to decrease the energy spread before the beam is post-accelerated in an S-band travelling-wave linear accelerator (linac) structure. In the LTE section, relativistic electron bunches exiting from the post-accelerated linac are currently used to generate the coherent THz radiation at the transition radiation station. To measure the electron beam energy after the linac acceleration, the beam is guided through a $60^{\circ}$ dipole magnet and a beam dump equipped with a Faraday cup at the end of the beam transport line.

Various beam diagnostic instruments are installed along the PBP-CMU Linac system to measure and analyse electron beam properties. Firstly, the current and pulse length of the electron macropulse were monitored with a non-destructive device called a current transformer. This device consists of a ferrite-core toroid with a ceramic tube enclosing the electron beam path and a loaded resistor. Secondly, the electron beam energy and energy spread were measured by using the alpha magnet energy slits and the current transformer for the beam after the RF-gun acceleration and a combination of a dipole magnet, a view screen, and a Faraday cup for the beam after the linac acceleration. Thirdly, a screen station, which consists of a phosphor screen and a CCD camera, is used to capture the transverse distribution of the electron beam. The beam image is then analysed with MATLAB code to obtain the transverse size and profile. Lastly, the bunch length measurement is performed by using an autocorrelation technique with a Michelson interferometer and a pyroelectric detector.

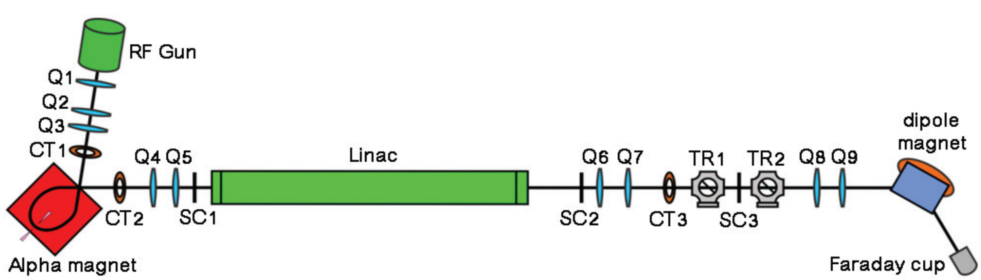


Figure 1: Schematic setup of the PBP-CMU linac system and the beam transport line. The letters Q, CT, SC and TR represent quadrupole magnets, current transformers, screen stations and transition radiation stations.

† Corresponding author: natthawut_chai@cmu.ac.th

ISBN 978-3-95450-177-9

# UPGRADE OF THE LHC BUNCH BY BUNCH INTENSITY MEASUREMENT ACQUISITION SYSTEM

D. Belohrad*, D. Esperante Pereira, J. Kral, S. B. Pedersen, CERN, Geneva, Switzerland

*Abstract*

The fast beam intensity measurement systems for the LHC currently use an analogue signal processing chain to provide the charge information for individual bunches. This limits the possibility to use higher level correction algorithms to remove systematic measurement errors coming from the beam current transformer and the associated analogue electronics chain. In addition, the current measurement system requires individual settings for different types of beams, implying the need for continuous tuning during LHC operation. Using modern technology, the analogue measurement chain can be replaced by an entirely digital acquisition system, even in the case of the short, pulsed signals produced by the LHC beams. This paper discusses the implementation of the new digital acquisition system and the calculations required to reconstruct the individual LHC bunch intensities, along with the presentation of results from actual beam measurements.

## INTRODUCTION

The existing beam intensity measurement system for the LHC was designed some 15 years ago and fully operational at the LHC start-up in 2008. At this time, the available analogue-to-digital (ADC) converters did not have the analogue bandwidth, sampling speed and precision to directly convert short, pulsed signals from LHC beams. Using such ADCs to provide data for the digital integration would have resulted in a much lower measurement accuracy than using analogue integration. Hence the existing system uses an integrator ASIC. The chip integrates the incoming signal at 40 MHz using two integrators working in multiplexed manner. Even if both integrators share the same silicon die, the manufacturing process causes them perform slightly differently when exposed to the same signal. Offset, gain, and the time of integration have to be compensated for each individual integrator. This is done in the FPGA once the integrated data stream has been converted to the digital domain.

Analogue integration also causes a loss of information as the baseline of the signal is integrated together with the beam signal. Once the integrated signal is converted into the digital domain, the algorithm restoring the DC component is unable to separate the baseline from the total integrated value, making it bunch pattern dependent.

The continued progress in ADC technology now enables us to investigate whether fast ADCs can now be used to sample the LHC bunched beam signals, so the complete bunch-by-bunch intensity measurement is performed in the digital domain. This would not only avoid complicated compensation techniques to reduce the problems associated with the integrator ASIC, but it would also allow the use of more sophisticated base-line restoration methods and bunch apex tracking, making the measurement technique more robust.

Further studies confirmed, that when using two dynamic ranges, an ADC with ENOB better than 10.5 bits and sampling rate greater than 500 MHz is needed to limit single shot digital integration error to 1% when a full scale signal is applied. For circulating beam measurements averaging can be used to reduce the ENOB requirements of the ADC.

## IMPLEMENTATION

### *Hardware Layer*

Several requirements have to be satisfied in order to achieve the desired measurement precision:

1. the bandwidth and the impulse response of the measurement device has to be sufficient to fully contain the bunch signal within the 25 ns spacing between LHC bunches (Bandwidth≥800 MHz, Impulse response≪25 ns),
2. the analogue front-end has to shape the bunch signal such that it entirely fills the 25 ns spacing between LHC bunches, but decaying fully to zero before the next bunch signal arrives,
3. the amplitude of the shaped signal must be adapted to optimally use the ADC dynamic range. This involves injection of an offset voltage $V_{ofs}$ and gain optimisation to increase the measured signal amplitude to cover ≈80% of the ADC dynamic range.

The final requirements for this signal shaping can be seen in Fig. 1.

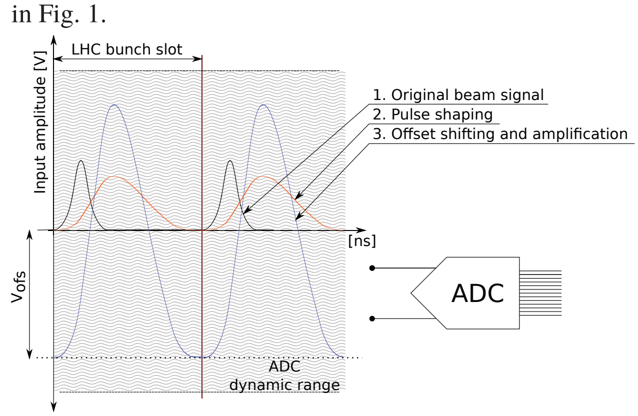


Figure 1: The BCTW signal shaping.

The first condition, concerning the bandwidth and impulse response, could not be satisfied using the original fast beam current transformers (FBCT) installed in the LHC due to the leakage of signal from one bunch into that of a neighbouring bunch slot, and the fact that the signal obtained was position

* david.belohrad@cern.ch

ISBN 978-3-95450-177-9

# PERFORMANCE STUDIES OF A SINGLE VERTICAL BEAM HALO COLLIMATION SYSTEM AT ATF2

N. Fuster-Martínez, IFIC (CSIC-UV)*, Valencia, Spain
A. Faus-Golfe, IFIC (CSIC-UV), Valencia, Spain and LAL, Université Paris-Sud,Orsay, France
P. Bambade, R. Yang, S. Wallon, LAL, Université Paris-Sud, Orsay, France
I. Podadera, F. Toral CIEMAT, Madrid, Spain
K. Kubo, N. Terunuma, T. Okugi, T. Tauchi, KEK and SOKENDAI, Tsukuba, Japan

*Abstract*

In order to reduce the background that could limit the precision of the diagnostics located in the ATF2 post-IP beamline a single vertical beam halo collimation system was installed and commissioned in March 2016. In this paper, we present the measurements done in March and May 2016 in order to characterize the collimation system performance. Furthermore, the collimator wakefield impact has been measured and compared with theoretical calculations and numerical simulations in order to determine the most efficient operation mode of the collimation system in terms of halo cleaning and negligible wakefield impact.

## INTRODUCTION

ATF2 is a scaled-down version of the Beam Delivery System (BDS) of the Future Linear Colliders (FLCs) Final Focus System (FFS) [1] built after the ATF Damping Ring (DR) (see Fig. 1). The ATF2 main objective is to achieve a vertical beam size at the virtual IP of 37 nm within a nanometer level stability.

The control and reduction of the beam halo distribution that could be intercepted by different components in the beamline producing undesired background is a crucial aspect for the FLCs and also for ATF2. In ATF2 the beam halo is formed mainly in the ATF DR and goes into the ATF2 beamline hitting at some locations the beam pipe. The most critical regions are the IP and post-IP were a Shintake monitor (IPBSM) is located used for measuring the nanometer vertical beam size (see Fig. 1). The IPBSM measures the modulation pattern photons produced in the interaction of a laser with the electron beam. Additional background photons in this region may be mixed with the IPBSM signal and limit its precision. Experimentally and by means of tracking simulations the vertical aperture of the last bending magnet (BDUMP) has been identified as the main source of background photons limiting the IPBSM signal to noise ratio. A transverse beam halo collimation system feasibility and design study for reducing the background in ATF2, specially in the last bending magnet, was done and reported in [2]. In March 2016, the vertical beam halo collimation system was installed and commissioned [3].

In this paper, we present the performance studies carried out in the ATF2 spring run. Secondly, we present the comparison of these measurements with realistic tracking simulations performed with the tracking code BDSIM [4]. Furthermore, the collimator wakefield impact on the orbit has been measured using the cavity BPMs system of ATF2 in order to verify the wakefield impact induced, to determine the optimum operation mode of the system and to perform benchmarking between analytical calculations, numerical simulations and measurements. These measurement are relevant for the FLCs because the ATF2 collimator design is based on a first mechanical design of the International Linear Collider (ILC) [5] spoilers. In addition, these measurements could be crucial to understand the discrepancies observed between measurements and predictions for similar geometries in the past experiments performed at ESA [6].

* Work supported by IDC-20101074, FPA2013-47883-C2-1-P and ANR-11-IDEX-0003-02

## COLLIMATION EFFICIENCY STUDIES

The vertical collimation system was constructed and first tested at LAL without beam at the end of 2015. Then, in March 2016 the system was installed in ATF2 (see Fig. 2). More details about the installation and commissioning can be found in [3].

In the March and May 2016 runs the performance of the vertical collimation system with beam has been studied. First, beam halo measurements were performed with the post-IP Wire Scanner (WS) and the Diamond Sensor (DS) [7] located in the post-IP region to study the beam-jaws movement and alignment (see Fig. 1). During these runs the beam energy was 1.3 GeV, the intensity ranging from 0.1-1 $\times 10^{10}$ electrons per bunch and the optics configuration used was the $(10\beta_x^* \times 1\beta_y^*)$ being $\beta_x^*$ and $\beta_y^*$ the value of the nominal betatron functions at the IP. Fig. 3 shows the vertical beam halo distribution measured with the vertical DS with the collimator opened and close to 3 mm half aperture. The DS is located after the BDUMP as can be seen in Fig. 1. The DS measurements are limited by the BDUMP elliptical full aperture which is 26 mm in the vertical plane and 56 in the horizontal one. In order to observe the effect of the collimator on the DS we need to close the collimator at least to 4 mm.

The ATF2 studies required different beam and machine conditions. Because of that, the relative efficiency of the vertical collimation system has been studied for different beam intensities, DR vacuum pressures and ATF2 optics. The intensity ranging from 0.1-1 $\times 10^{10}$, the DR vacuum pressures was changed from $4.99 \times 10^{-7} Pa$ to $1.06 \times 10^{-6} Pa$ and the optics used were the nominal one $(10\beta_x^* \times 1\beta_y^*)$ and the

ISBN 978-3-95450-177-9

# A NEW WALL CURRENT MONITOR FOR THE CERN PROTON SYNCHROTRON

J.M. Belleman*, W. Andreazza, CERN, Geneva, Switzerland
A.A. Nosych, ALBA-CELLS Synchrotron, Cerdanyola del Vallès, Spain

*Abstract*

Wall Current Monitors are the devices of choice to observe the instantaneous beam current in proton accelerators. These entirely passive transformers deliver a high-fidelity image of the beam intensity in a bandwidth spanning from about 100kHz up to several GHz. They serve as a signal source for a diverse set of applications including Low Level RF feedback and longitudinal diagnostics such as bunch shape measurements and phase-space tomography. They are appreciated for their excellent reliability, large bandwidth and unsurpassed dynamic range. We describe the design of a new Wall Current Monitor for the CERN Proton Synchrotron with a useful bandwidth of 100kHz to 4GHz. Two such devices have been installed in the PS machine and are now used in regular operation. Some usage examples will be shown.

## THE CERN PROTON SYNCHROTRON

CERN's Proton Synchrotron is a 628 m circumference, 26 GeV accelerator operating since 1959. Over the years, it has served to accelerate protons and electrons and their anti-particles, as well as several ion species. Today it is an important part of the CERN injector complex, delivering both protons and lead ions to the Large Hadron Collider via the Super Proton Synchrotron, as well as serving many other clients with its dedicated experimental area.

## WALL CURRENT MONITOR PRINCIPLE

As a beam of particles travels through a conducting vacuum tube, it is accompanied by an image charge of equal magnitude but opposite sign flowing along the inside wall of the tube [1]. This co-moving wave of charge constitutes a localised current. If we were to cut the vacuum tube and place an impedance across the gap, this current would develop a voltage which is an accurate replica of the beam current.

To confine signal currents to a well-defined geometry, the gap is surrounded by a conducting shell. In this design the gap is empty, so the shell also holds the vacuum. Inside the shell are ferrite toroid cores that increase the WCM inductance and thereby extend the lower cut-off frequency downwards (Fig. 1). The whole arrangement is basically a single-turn transformer with the beam in the role of the primary 'winding', the conducting shell and the inner chamber as the secondary and the ferrite toroids as the core (Fig. 2).

* jeroen.belleman@cern.ch

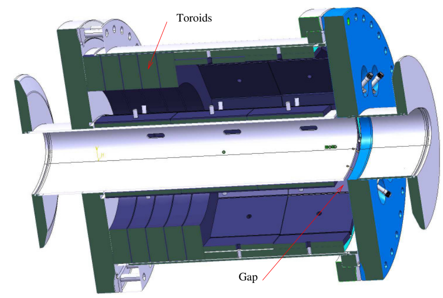


Figure 1: Cut-away view of the Wall Current Monitor.

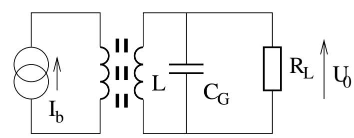


Figure 2: Simplified WCM equivalent circuit.

The WCM's low frequency cut-off is $\omega_L = \frac{R_L}{L}$, with $L$ the inductance of the ferrite toroids and $R_L$ the gap load resistance. The ferrite toroids are Ferroxcube T240/160/20-8C11, with a single-turn inductance of about 2 $\mu$H. Five toroids supply a total of about 10 $\mu$H. With the gap load resistance of 6 Ω, this yields a lower cut-off frequency of about 100 kHz.

The inner surfaces of the shell, as well as the outer surface of the beam pipe, are covered in Ferroxcube 4S60 absorptive ferrite tiles. This does not contribute substantially to the transformer inductance, but it muffles the EM energy propagating into the space between the shell and the beam pipe, which would otherwise look like a coaxial shorted stub in parallel with the gap load resistance.

Despite the liberal use of absorptive ferrite, the high frequency response is dominated by various EM wave effects —cavity resonances— well before it finally drops off because of the gap capacitance $C_G$. A lower gap load resistance would widen the WCM's bandwidth at both ends of the frequency response, but reduce the output signal for a given beam intensity.

Since the ferrites are installed inside the vacuum, they were all subjected to chemical degreasing, followed by a bake-out at 1000 °C in air. The bake-out does not discernably affect the ferrite properties [1]. The main residual gas source was adsorbed water. Although the outgassing rate is not enormous, a WCM has a dedicated ion pump.

ISBN 978-3-95450-177-9

# TEST RESULTS FROM THE ATLAS HYBRID PARTICLE DETECTOR PROTOTYPE*

C.A. Dickerson[#], B. DiGiovine, L.Y. Lin, Argonne National Laboratory, Lemont, IL 60439, USA
D. Santiago-Gonzalez, Louisiana State University, Baton Rouge, LA 70806, USA

*Abstract*

At the Argonne Tandem Linear Accelerator System (ATLAS) we designed and built a hybrid particle detector consisting of a gas ionization chamber followed by an inorganic scintillator. This detector will aid the tuning of low intensity beam constituents, typically radioactive, with relatively high intensity (>100x) contaminants. These conditions are regularly encountered during radioactive ion beam production via the in-flight method, or when charge breeding fission fragments from the CAlifornium Rare Isotope Breeder Upgrade (CARIBU). The detector was designed to have an energy resolution of ~5% at a rate of $10^5$ particles per second (pps), to generate energy loss and residual energy signals for the identification of both Z and A, to be compact (retractable from the beamline), and to be radiation hard. The combination of a gas ionization chamber and scintillator will enable the detector to be very versatile and be useful for a wide range of masses and energies. Design details and testing results from the prototype detector are presented in this paper.

## INTRODUCTION

At the Argonne Tandem Linear Accelerator System (ATLAS) we built and tested a fast, compact particle detector to aid the tuning of low intensity beam constituents with relatively high intensity (>100x) contaminants. These conditions are regularly encountered during radioactive ion beam production via the in-flight method, or when charge breeding fission fragments from the CAlifornium Rare Isotope Breeder Upgrade (CARIBU). The in-flight method of RIB production at ATLAS generally produces beams of interest with energies 5-15 MeV/u and masses less than 30 AMU, while reaccelerated fission fragments from CARIBU, 80 < A < 160, are typically accelerated to energies of 4-10 MeV/u. Our goal is to achieve ~5% energy resolution at a total rate of $10^5$ pps over these energy and mass ranges without significant performance degradation after extended use.

The detector combines a gas ionization chamber (IC) with an inorganic scintillator, Fig. 1, to generate energy loss, ΔE, and residual E signals, which enable the identification of both the Z and the A of the beam constituents. The IC configuration followed designs for similar Tilted Electrode Gas Ionization Chambers (TEGIC) [1-2] – closely spaced parallel grids normal to the beam direction. Resolutions of ~4% and ~2% were reported for A and Z identification, respectively. GSO:Ce, the chosen scintillator, is the most radiation hard of any well characterized scintillator [3], has a 60 ns decay time, and 3-5% energy resolution for heavy ions [4-5]. The scintillator will provide residual E for particles not stopped in the gas, and enables the flexibility to tune the gas properties for the best signal while largely ignoring the gas' stopping power. An avalanche photo diode (APD) was selected as the photoelectric device mainly due to the device's compactness. A more detailed discussion of the design considerations was previously reported [6].

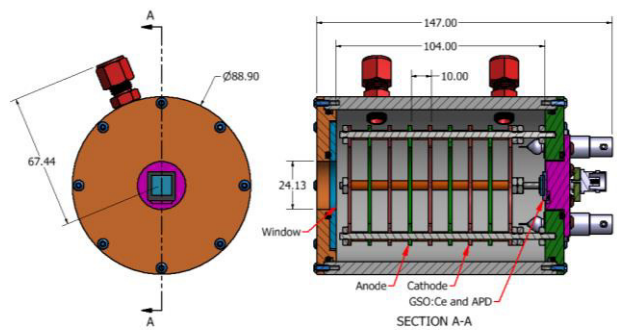


Figure 1: A model of the ATLAS hybrid detector. Dimensions are in mm.

## EXPERIMENT

For the results reported here the scintillator and the gas IC were tested separately; the GSO:Ce was not incorporated into the assembly of the IC. Additionally, an insertion mechanism and vacuum chamber for the hybrid detector have not been designed yet, so the front plate of the IC was adapted to fit directly on a 6 in. CF flange at the end of the beamline.

The ion beam used in these tests was a cocktail of 7.28 MeV/u $^{18}O^{4+}$, $^{27}Al^{6+}$, and $^{36}Ar^{8+}$, corresponding to 131 MeV $^{18}O$, 197 MeV $^{27}Al$, and 262 MeV $^{36}Ar$. The $^{36}Ar$ and $^{18}O$ were injected into the ECR source via gas metering valves, and were delivered at similar intensities. The $^{27}Al$ was a contaminant from the ECR plasma chamber walls, thus it was much less intense and only identified upon analysis.

The gas IC window was 1.14 mg/cm$^2$ (8 μm) Kapton epoxied to an aluminum window mount to facilitate replacement in the event a window broke, Fig. 2.a. The electrical grids were made using ø20 μm gold plated W wire spaced 1 mm apart, Fig. 2.a, which allowed ~98% transmission. The grid frames are printed circuit boards with the appropriate solder traces to mount the grid wire and solder pads to make inter-grid connections. Kapton

*Work supported by U.S. Department of Energy, Office of Nuclear Physics, under contract DE-AC02-06CH11357
#cdickerson@anl.gov

ISBN 978-3-95450-177-9

# BEAM TUNING FOR LONGITUDINAL PROFILE AT J-PARC LINAC

A. Miura†
J-PARC Center, Japan Atomic Energy Agency, Tokai, Ibaraki, JAPAN
Y. Liu, T. Maruta, T. Miyao
J-PARC Center, High Energy Accelerator Research Organization, Tsukuba, Ibaraki, JAPAN

*Abstract*

Using bunch shape monitors (BSMs), we measured the longitudinal bunch lengths of negative hydrogen ion beams in the J-PARC linac. A BSM was installed between two linacs, separate-type drift tube linac (SDTL) and an annular-ring-coupled structure linac (ACS), having acceleration frequencies of 324 and 972 MHz, respectively. We used radio-frequency amplitude modulation of bunches in the beam transport between the SDTL and ACS to minimize emittance growth and beam loss. We conducted amplitude scanning and compared the results with the twiss-parameters obtained from the transverse profiles. In this paper, we discuss the results of amplitude tuning of the buncher cavity at the point of beam loss and emittance. We also discuss the measurement results for various equipartitioning settings of quadrupole magnets.

## INTRODUCTION

At the energy upgrade project in the J-PARC linac, we installed an annular-ring-coupled structure linac (ACS) whose acceleration frequency of 972 MHz can be used to obtain beam energies ranging from 191 to 400 MeV downstream of the separate-type drift tube linac (SDTL). The acceleration frequency of the ACS is three times that of the SDTL; as this frequency jump may lead to beam loss owing to longitudinal (phase spread) mismatch, conducting phase-width matching between the SDTL and ACS sections is critical. To implement this matching strategy, we developed bunch shape monitors (BSMs) to follow the beam behavior in the two ACS-type buncher cavities. A tuning method involving phase-width matching of the three BSMs along with transverse profile matching was proposed. To establish equipartitioning conditions that would meet the beam dynamics design of the J-PARC linac, we use both the transverse profile and the phase width. In this paper, we explain and discuss the measurement results for the various equipartitioning settings.

## BUNCH SHAPE MONITOR IN J-PARC LINAC

### *Bunch Shape Measurement*

In collaboration with the Institute for Nuclear Research of the Russian Academy of Sciences (INR/RAS), a device for the beam phase width measurement was designed based on the observation of secondary electrons from a single wire intersecting a beam. After a series of beam bunches under measurement intersect a target wire having a diameter of 0.1 mm, low-energy secondary electrons are emitted owing to the beam–wire interaction [1, 2]. The wire is held at a negative potential of typically −10 kV. The secondary electrons move almost radially and enter a radio frequency (RF) deflector through collimators. An RF field with the same frequency as the accelerating RF (324 MHz) is applied to deflect the excess secondary electrons by an angle that depends on the phase of the deflecting field. By adjusting the deflecting field phase with respect to the accelerator RF reference, the phase widths of the bunches can be obtained.

### *Installation Layout*

Three BSMs were installed upstream of the ACS section and two ACS-type bunchers were installed between the SDTL and ACS sections, as shown in Fig. 1. We implemented a tuning method involving phase-width matching using the three BSMs along with transverse profile matching. During the BSM measurements, the two 972-MHz ACS-type buncher cavities served as control knobs for phase-width matching [3]. Later, all three BSMs were removed and disassembled for out-gas conditioning. Currently, only one BSM has been reinstalled in front of the ACS01 cavity using additional vacuum pumps [4]. In this study, we used all three BSMs for amplitude scanning of the two ACS type-bunchers, while the single reinstalled BSM in front of the ACS01 was primarily used for an equipartitioning study. We set the longitudinal direction as the direction for phase spreading.

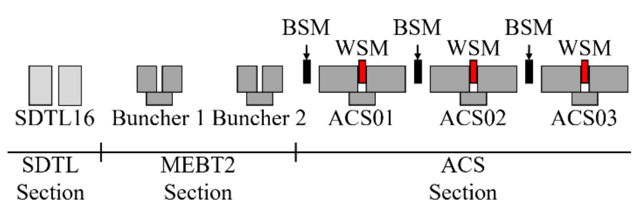


Figure 1: BSM and WSM layout around the upstream ACS section. Positions of WSMs and BSMs are indicated with arrows.

## BUNCH SHAPE MEASUREMENT

During BSM calibration, a full scan was performed wherein the RMS beam width was measured as a function of SDTL15 cavity amplitude and compared with simulations performed using IMPACT and TraceWin. The results for the most upstream BSM (BMS#1) in Fig. 1, which was used further to measure emittance, can be seen in Fig. 2, wherein a close agreement between simulation and measurement is observed.

With the synchronous phase of SDTL15 set to bunching mode (−90°), the root-mean-square (RMS) phase width was measured at the BSMs as a function of the cavity

† akihiko.miura@j-parc.jp



ISBN 978-3-95450-177-9

# SNS RFQ VOLTAGE MEASUREMENTS USING X-RAY SPECTROMETER

A.P. Zhukov, ORNL, Oak Ridge, TN 37830, USA

*Abstract*

Absolute measurement of vane voltage is essential to understand RFQ transmission. We used a non-intrusive technique of bremsstrahlung X-ray measurement. Several windows were installed in different locations of the RFQ to allow measurement of the X-ray spectrum. A CdTe spectrometer was used to estimate spectrum cutoff energy that corresponds to the vane voltage. Different device setups are described as well as measurement accuracy and interpretation of experimental data.

## INTROUDUCTION

An RFQ is a crucial part of the SNS accelerator. It's performance directly affects beam power on target. The history of RFQ detuning issues [1] increased importance of full understanding and extensive characterization of RFQ parameters. These issues are identified as critical for successful upgrades of the SNS accelerator. The Beam Test Facility (BTF) has been constructed for validation of the new spare RFQ [2]. One of the key parameters is the actual RFQ vane voltage. X-ray spectra measurement is a common technique used to obtain vane voltage independently, not relying on design parameters and magnetic field probes [3, 4]. We first reported the preliminary results of such measurements in 2014 [5].

## EXPERIMENTAL SETUP

### *Theory of Operation*

There is always a stream of electrons between RFQ vanes due to the field emission. These emitted electrons are accelerated to the energy corresponding to RFQ voltage and bombard the copper vane. Electrons produce radiation in the form of X-rays with energy spectrum extending up to the energy of an incident electron. Thus measuring the maximum energy of bremsstrahlung X-rays one can obtain the vane voltage.

### *X-ray Spectrometer*

We use an off the shelf X-123 CdTe X-ray spectrometer [6]. Spectroscopy is the main application of this device so one of the main parameters is FWHM (Full Width at Half Maximum). The spectrometer has an internal amplifier that has to be calibrated for a particular energy range. We used Am-241 source for calibration. It has a peak at 69.5 keV that is close enough to maximum expected energy of X-rays – around 80 keV. The FWHM contributes to error of our measurements and is close to 0.8 keV for this energy. The amplifier's settings were optimized to allow binning in 1024-channel MCA with maximum energy 90 keV. The calibration error was estimated to be 0.5 keV at 100 keV for spectrum shown on Fig. 1.

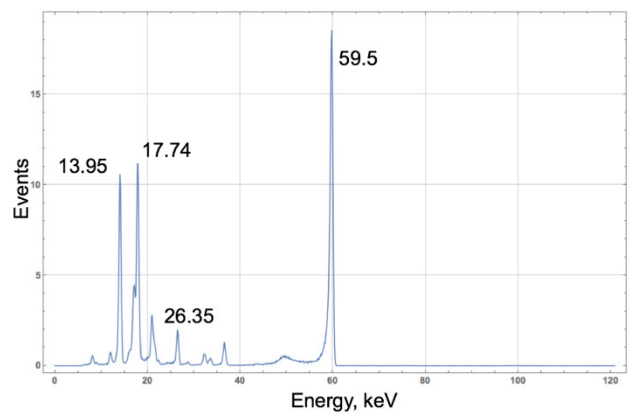


Figure 1: Spectrometer calibration with Am-241 source.

### *RFQ Ports*

Special quartz windows were added to RFQ to allow X-rays reach the spectrometer that is mounted outside of the port looking at the window. The production RFQ that is currently used at the SNS accelerator has four windows. We used one spectrometer and attached it to different

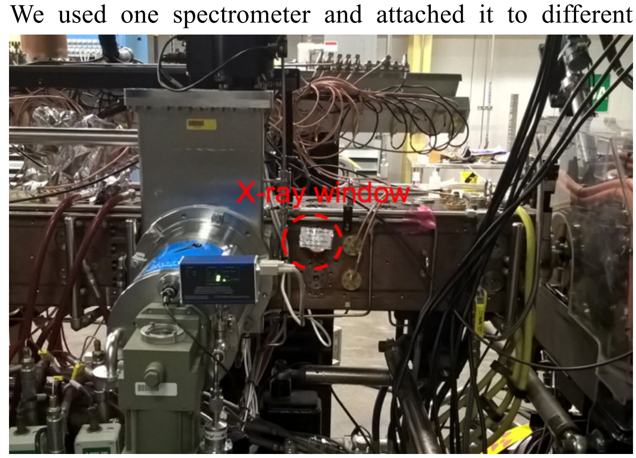


Figure 2: Quartz X-ray window installed in RFQ.

### *Proof of Principle Measurements*

The first set of measurements was done without any shielding enclosure, using vendor calibration and the main goal was to observe correlation of RFQ set point (proportional to vane voltage) and X-rays spectrum. The Fig. 3 shows typical spectrum.

There are different ways of quantifying the cut-off energy [3, 4]. To obtain cut-off energy of the tail we used following procedure: the tail consisting of 0.5% of total events was considered background (shaded grey on Fig. 3), the adjacent 1.5% events were selected and the spectrum was linearized for this part (green shading and red line), intersection of the line with X – axis is called the maximum energy of this distribution.



ISBN 978-3-95450-177-9

# BETA FUNCTION MEASUREMENT FOR THE AGS IPM*

H. Huang†, L. Ahrens, C. Harper, F. Meot, V. Schoefer
Brookhaven National Laboratory, Upton, New York, 11973, USA

*Abstract*

Emittance control is important for polarization preservation of proton beam in the Alternative Gradient Synchrotron (AGS). For polarization preservation, two helical dipole partial Siberian snake magnets are inserted into the AGS lattice. In addition, the vertical tune has to run very high, in the vicinity of integer. These helical dipole magnets greatly distort the optics, especially near injection. The beta functions along the energy ramp have been modeled and measured at the locations of the Ion Profile Monitor (IPM). For the measurements to be valid, the betatron tune, dipole current and orbit responses have to be carefully measured. This paper summarize the experiment results and comparison with the model. These results will lead to understanding of emittance evolution in the AGS.

## INTRODUCTION

Emittance control is important for high luminosity in colliders. For polarized proton operation in Relativistic Heavy Ion Collider (RHIC), emittance preservation is advantageous due to its link to polarization preservation. In general, larger emittance results in larger depolarizing resonance strength and consequently, larger polarization loss. Several techniques have been employed in the AGS to preserve polarization, such as dual partial snakes [1], horizontal tune jump quadrupoles [2] and harmonic orbit corrections. To further reduce polarization loss in the accelerator chain, it is necessary to control the emittance growth. As the first step, we need to measure emittance reliably.

The main device in the AGS to measure emittance is the ion collecting IPM [3], which has been put in use for more than 20 years. They are installed at $\beta_{max}$ locations to measure both horizontal and vertical emittances. The device shows that vertical emittance increases four times in the AGS during polarized proton acceleration. However, some reported emittance growth is not real. There are several problems with this measurement. First, polarized proton operation requires two partial snake magnets which are helical dipole magnets with constant fields during the whole AGS cycle. The high magnet field near injection causes significant optical distortion. Several compensation quadrupoles have been installed on both sides of each helical dipole to mitigate the optical effect but their effects are limited. The expected beta beating may distort the reported emittance values at low energies. Second, the space charge of bunched beam is stronger at higher energy due to smaller beam size which causes larger reported emittance [4]. The profiles obtained from the AGS IPM has known effects from space charge of bunched beam, which can only be mitigated at a flattop by turning off RF cavities.

The real currents of all active magnets and other beam radius can be logged for each AGS cycle. The AGS can be modeled by MAD-X with these input information. Using the lattice model with the helical magnets included, the beta functions at the IPM locations can be calculated along the AGS magnet ramp. One example of measured emittance for polarized protons with the modeled beta functions in both vertical and horizontal in AGS magnet cycle is shown in Fig. 1. Polarized protons are injected into the AGS at 150ms from the start of the magnet cycle (AGS T0) and is ramped immediately. The acceleration is finished at 582ms and about one second at flattop is used for extraction manuevers. For the measurement shown in Fig.1, the RF cavity was shut off at 1000ms and beam was debunched after 1000ms. The drop of reported emittance at 1000ms indicates the effects of space charge. The distortion of the beam profile is due to space charge force and is mitigated with RF off. The bunch intensity for these measurements was $2 \times 10^{11}$. The modeled vertical beta function near injection is less than half of the value at flattop. There are fluctuations in the measurements, but it is clear that the vertical emittance seems doubled from injection to the flattop, even taking into account the new beta functions and removing the space charge effect. On the other hand, the horizontal emittance growth is not so strong, if any. Since the helical dipole partial snake magnets

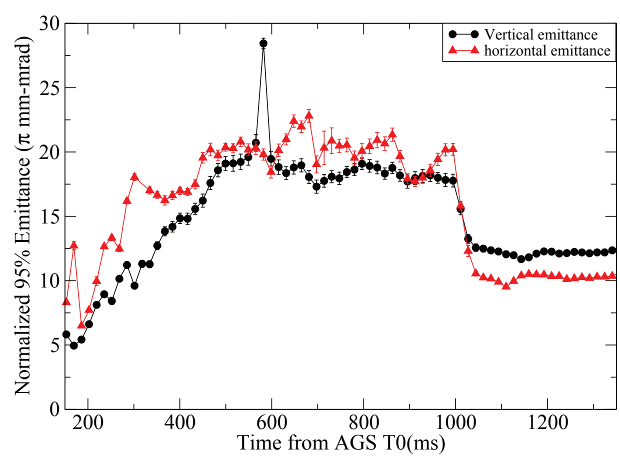


Figure 1: The normalized 95% emittance of both planes along the AGS magnet cycle. The energy ramp finishes at 582ms. The RF cavities are shut off at 1000ms and the "true" emittance at flattop is reported after that.

are hard to model, there is some doubt if the model gives the correct beta functions along the energy ramp. At higher energies, as the beam rigidity is higher, the effect from the helical dipoles are smaller. The model predicts that with

* Work supported by Brookhaven Science Associates, LLC under Contract No. DE-AC02-98CH10886 with the U.S. Department of Energy.
† huanghai@bnl.gov

ISBN 978-3-95450-177-9

# OPTIMIZED CRYOGENIC CURRENT COMPARATOR FOR CERN'S LOW-ENERGY ANTIPROTON FACILITIES

M. Fernandes*, The University of Liverpool, U.K. & CERN, Geneva, Switzerland
A. Lees, D. Alves, T. Koettig, E. Oponowicz, J. Tan, CERN, Geneva, Switzerland
C. Welsch, Cockcroft Institute & The University of Liverpool, U.K
R. Geithner, R. Neubert, T. Stöhlker, Friedrich-Schiller-Universität & Helmholtz Institute Jena, Jena, Germany
M. Schwickert, GSI, Darmstadt, Germany

*Abstract*

Non-perturbative measurement of low-intensity charged particle beams is particularly challenging for beam diagnostics due to the low amplitude of the induced electromagnetic fields. In the low-energy Antiproton Decelerator (AD) and the future Extra Low ENergy Antiproton (ELENA) rings at CERN, an absolute measurement of the beam intensity is essential to monitor operational efficiency and provide important calibration data for all AD experiments. Cryogenic Current Comparators (CCC) based on Superconducting QUantum Interference Device (SQUID) have in the past been used for the measurement of beams in the nA range, showing a very good current resolution. However these were unable to provide a measurement of short bunched beams, due to the slew-rate limitation of SQUID devices and their strong susceptibility to external perturbations. Here, we present the measurements and results obtained during 2016 with a CCC system developed for the Antiproton Decelerator, which has been optimized to overcome these earlier limitations in terms of current resolution, system stability, the ability to cope with short bunched beams, and immunity to mechanical vibrations.

## CURRENT MEASUREMENT OF LOW-INTENSITY BEAMS

Low-intensity charged particle beams present a considerable challenge for existing beam current diagnostic devices. This is particularly true for beams with average currents below 1 µA which is the resolution limit of standard DC Current Transformers [1]. Other monitors, such as AC Current Transformers or Schottky monitors are able to measure low-intensity beam currents, but neither can simultaneously provide an absolute measurement, with a high current and time resolution, which at the same time is independent of the beam profile, trajectory and energy.

At CERN's low-energy antiproton ($\bar{p}$) decelerators, the AD and ELENA (currently under construction) rings, both bunched and coasting beams of antiprotons circulate with average currents ranging from 300 nA to 12 µA. The AD cycle consists of alternate phases of deceleration, where the beam is bunched, and beam cooling, when the beam is debunched and its velocity is kept constant. The beam is also bunched at injection and extraction. The AD current profile during the whole deceleration and cooling cycle along with the maximum slew-rate during phases where the beam is bunched is shown in Fig 1. The $\bar{p}$'s are injected in the AD with a momentum of 3.5 GeV corresponding to $\beta = 0.967$, and are extracted with 100 MeV and $\beta = 0.106$.

Having a current measurement able to cope with these characteristics would greatly help the optimisation of the machine operation. To meet these requirements, a low-temperature SQUID-based Cryogenic Current Comparator (CCC) system is currently under development [2]. Similar devices have already been developed for electrical metrology [3], and have already been used for beam current measurements in particle accelerator [4]. The current project, is a collaboration between CERN, GSI, Jena University and Helmholtz Institute Jena to develop this technique further.

The main design specifications for the monitor are: beam current resolution < 10 nA; and a measurement bandwidth of 1 kHz.

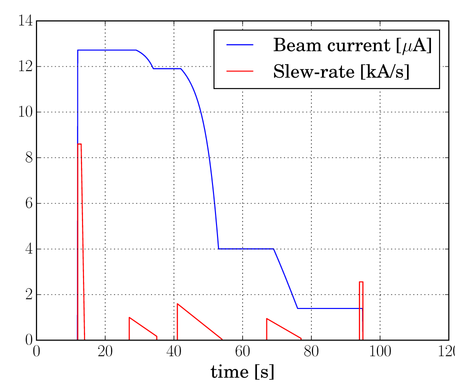


Figure 1: Nominal beam current during an AD cycle, and maximum beam current slew-rate in bunched beam phases.

## OVERVIEW OF THE FUNCTIONING PRINCIPLE OF THE CCC

The CCC (see schematic in Fig. 2) works by measuring the magnetic field induced by a charged particle beam. This field is concentrated in a high-permeability ferromagnetic pickup core, from which it is coupled into the SQUID sensor via a superconducting flux transformer. The SQUID's are highly sensitive magnetic flux sensors that permit the measurement of the weak fields created by the beam. The superconducting magnetic shield structure around the pickup-core

* e-mail: miguel.fernandes@cern.ch

ISBN 978-3-95450-177-9

# A PRECISE PULSED CURRENT SOURCE FOR ABSOLUTE CALIBRATION OF CURRENT MEASUREMENT SYSTEMS WITH NO DC RESPONSE

M. Krupa*[1], M. Gasior
CERN, Geneva, Switzerland
[1] also at Lodz University of Technology, Lodz, Poland

*Abstract*

Absolute calibration of systems with no DC response requires pulsed calibration circuits. This paper presents a precise pulsed current source designed primarily for remote calibration of a beam intensity measurement system. However, due to its simple and flexible design, it might also prove interesting for other applications. The circuit was designed to drive a load of 10 Ω with current pulses lasting a few hundred microseconds with an amplitude of 1 A and precision in the order of 0.01 %. The circuit is equipped with a half-bridge for precise determination of the absolute output current using the 0 V method. This paper presents the circuit topology and discusses in detail the choice of the critical components along with their influence on the final achieved accuracy. The performance of the built prototype of the current source is presented with laboratory measurements.

## INTRODUCTION

Many modern measurement systems have no low-frequency response so that their calibration cannot be achieved with DC signals. One of the available possibilities to calibrate such systems is to use a circuit generating long pulses with a well-defined and stable amplitude.

The pulsed current calibration unit described in this paper consists of two main circuits: a current source generating the calibration current and a half-bridge circuit for measuring the current with high accuracy. Similar circuitry was developed in the past for the inductive beam position monitors of the CERN CLIC Test Facility (CTF3) [1].

This paper describes the principle of operation and discusses the choice of the most critical components. A brief description of additional features, extending the field of potential applications, is also given.

All measurements shown in this paper were obtained with a prototype circuit built and optimised for calibrating the new bunch-by-bunch intensity measurement system of the Large Hadron Collider (LHC) [2, 3]. The source was designed to deliver a current pulse of 1 A into 10 Ω load for a few hundred microseconds. However, the system can easily be adapted for other values of the current and a wide range of loads by simply adjusting the values of a handful of components.

* michal.krupa@cern.ch

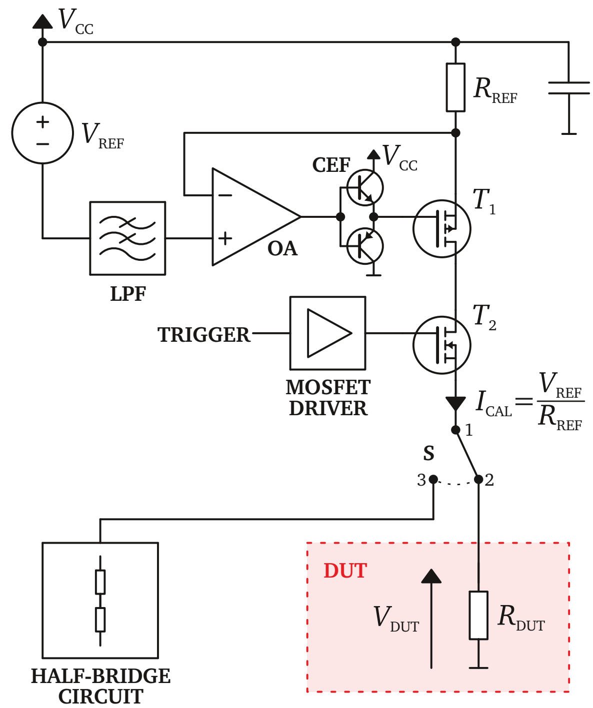


Figure 1: A simplified circuit diagram of the current source. LPF - Low-Pass Filter; OA - Operational Amplifier; CEF - Complementary Emitter Follower; DUT - device being calibrated

## CURRENT SOURCE

The principle of operation of the current source can be explained using the circuit diagram shown in Fig. 1. During normal operation the switch S is in position 1-2 to send the calibration current $I_{CAL}$ to the grounded load $R_{DUT}$ of the device to be calibrated.

The value of $I_{CAL}$ is determined by the ratio of the reference voltage $V_{REF}$ and the reference resistance $R_{REF}$, both being part of the regulation loop. The non-inverting input of the operational amplifier (OA) is set to $V_{CC} - V_{REF}$ and additionally filtered by a low-pass filer (LPF). OA regulates its output voltage such that its inverting input virtually matches the voltage of the non-inverting input. Hence, the voltage at the inverting input of OA also equals $V_{CC} - V_{REF}$ which in turns yields a voltage drop of $V_{REF}$ across the reference resistor $R_{REF}$. The complementary emitter-follower (CEF) buffers the output of OA to drive the large gate capacitance of the top p-channel MOSFET $T_1$ to improve the response time

ISBN 978-3-95450-177-9

# DEFLECTING CAVITY DYNAMICS FOR TIME-RESOLVED MACHINE STUDIES OF SXFEL USER FACILITY*

M. Song, H. Deng†, B. Liu, D. Wang, SINAP, Shanghai, 201800, China

*Abstract*

Radio frequency deflectors are widely used for time-resolved electron beam energy, emittance and radiation profile measurements in modern free electron laser facilities. In this paper, we present the beam dynamics aspects of the deflecting cavity of SXFEL user facility, which is located at the exit of the undulator. With a targeted time resolution around 10 fs, it is expected to be an important tool for time-resolved commissioning and machine studies for SXFEL user facility.

## INTRODUCTION

Free electron laser (FEL) in the X-ray spectral region is a highly fruitful field ranging from ultra-fast scale probe to molecular biology, and from material science to medical science. Currently, the first X-ray FEL (8.8 nm) facility in China driven by 840 MeV LINAC is under construction at Shanghai, namely SXFEL test facility [1-2]. A soft X-ray user facility [3] has been proposed on the basis of SXFEL test facility. With a straightforward beam energy upgrade to 1.5 GeV, the FEL wavelength will extend to 2.0 nm and fully cover the water-window region [3]. In order to guarantee the FEL lasing performance at short wavelength, besides cascading HGHG [4], EEHG [5] and PEHG [6], a SASE [7] undulator line which consists of in-vacuum undulator and the insertion is also raised up.

For such an ultra-short bunch required for excellent FEL performance, one of the great challenges is the measurement and diagnosis with high temporal resolution. Up to now, many techniques have been developed, including zero RF phasing and streak camera. Transverse RF deflecting cavity is introduced to diagnose longitudinal profile of the electron bunch and FEL radiation, which is capable of resolving the temporal structure as short as sub-fs level under the circumstance of high deflecting voltage and frequency [8]. Since this method can effectively convert time-correlated longitudinal profile into the transverse profile, thus the bunch could be revealed and analysed in more detail. In terms of high efficiency and resolution, this technique would become key diagnostic system in the future. Therefore, a pair of X-band RF deflectors is planned at the exit of the undulator section of SXFEL user facility.

## DIAGNOSTIC BEAMLINE OPTIMIZATION

The preliminary designed deflector beamline of SXFEL user facility is shown in Fig. 1. Four quadruple magnets can be used for the beam optics optimization within the system, in which, one quadruple magnet downstream the RF deflecting cavity can be used for additional beam focusing in case of relative large beam size on the screen. The bending magnet located about 6 m downstream the undulator exit, is used for beam momentum and spread measurement. The transverse deflecting structure (TDS) installed in the beam line provide the performance to measure the longitudinal phase space, and thus the longitudinal bunch distribution.

The main goal of the whole TDS beamline is achieving high temporal resolution and allowing precious longitudinal measurement of ultra-short bunch. When the electron bunch passes through the RF deflecting cavity with the bunch centre at the zero-phase, the high frequency and time-resolved deflecting fields will kick the bunch and broaden its transverse size on the screen. According to the basics of the deflecting concept, the analytical formula of resolution can be deduced as follows [9]:

$$\Delta_s = \frac{c(E/e)}{\omega V_0} \frac{\sqrt{\varepsilon_x}}{\sqrt{\beta_d \sin \Delta\psi \cdot \gamma}} \tag{1}$$

On the basis of the formula, it is found that the resolution not only depends on the beam emittance and TWISS parameters but also influenced by the phase advance and deflecting force induced by the RF deflecting. Considering the time-resolved ability and the intrinsic beam profile, the beamline optimization could be achieved by adjusting four quadruple magnets gradient with ELEGANT [10] simulation under the condition that $\beta$ function at the screen ranging from 2 m to 4 m. The main parameters of TDS and optimized beamline are summarized in Table 1. It should be pointed out that the parameters are tentative and still need to be optimized.

Table 1: Main Parameters of TDS and Optimized Beamline

| | | | |
|---|---|---|---|
| RF deflecting frequency | $f$ | 11.424 | *GHz* |
| RF deflector voltage | $V_0$ | 10 | *MV* |
| RF deflector length | $L$ | 1 | *m* |
| RF deflector number | | 2 | |
| Nominal beam size | $\sigma_{x0}$ | 31.5 | *μm* |
| Beam size with TDS on | $\sigma_x$ | 971.6 | *μm* |
| Beta at TDS | $\beta_d$ | 8.8 | *m* |
| Beta at screen | $\beta_s$ | 2.9 | *m* |
| Phase advance | $\Delta\varphi$ | 79 | *degree* |
| Normalized emittance | $\varepsilon_n$ | 1.015 | *μm* |
| RMS bunch length | $\sigma_z$ | 55.797 | *μm* |

*Work supported by Natural Science Foundation of China (11475250 and 11322550) and TenThousand Talent Program.
†denghaixiao@sinap.ac.cn

ISBN 978-3-95450-177-9

# ELECTRON BEAM LONGITUDINAL DIAGNOSTIC WITH SUB-FEMTOSECOND RESOLUTION

G. Andonian[1], M. Harrison, F. O'Shea, A. Ovodenko, RadiaBeam Technologies, Santa Monica, CA, USA
M. Fedurin, K. Kusche, I. Pogorelsky, M. Polyanski,
C. Swinson, Brookhaven National Laboratory, Upton, NY, USA
M. Weikum, DESY, Hamburg, Germany
J. Duris, J. Rosenzweig, N. Sudar, UCLA, Los Angeles, CA, 90095
[1] also at UCLA, Los Angeles, CA 90095

*Abstract*

In this paper, we describe the status of prototype development on a diagnostic for high brightness electron beams, that has the potential to achieve sub-femtosecond longitudinal resolution. The diagnostic employs a high-power laser-electron beam interaction in an undulator magnetic field, in tandem with a rf bunch deflecting cavity to impose an angular-longitudinal coordinate correlation on the bunch which is resolvable with standard optical systems. The fundamental underlying angular modulation that is the basis of this diagnostic has been tested experimentally at the Brookhaven National Laboratory Accelerator Test Facility (BNL ATF) with a high-brightness electron beam and >100GW IR laser operating in the $TEM_{10}$ mode. Here we provide an update on the status of the experimental program with details on the undulator testing, and initial results that include a study of the effects of the laser mode, and energy, on the beam angular projection.

## INTRODUCTION

The precise characterization of the longitudinal profile of high-brightness electron beams is crucial for applications in light source development and advanced accelerator applications. Current techniques to measure the beam bunch profile include rf zero phasing methods, pulse reconstruction using interferometry of beam-based coherent radiation [1], and transverse deflecting cavities [2]. Deflecting cavities are very attractive because the presently attainable resolution with modern cavities in the x-band is on the order of a few fs. This paper describes a method to further enhance the resolution of the transverse deflecting cavity with the addition of an orthogonal transverse angular modulation on the beam correlated to the longitudinal coordinate. The correlation is generated by an interaction of the electron beam with a high-power laser in a resonant undulator. The interaction, similar to a higher-order inverse free-electron laser interaction, provides a correlated angular modulation that is resolvable on a distant screen with standard diagnostics and is schematically pictured in Fig. 1.

The interaction of the $TEM_{10}$ laser mode, operating at high power and an electron beam in an undulator field yields an angular modulation on the beam. The detailed physical description is presented in Ref. [3]. For the system sketched in Fig. 1, the total angular modulation $\Delta x'$ is a function of

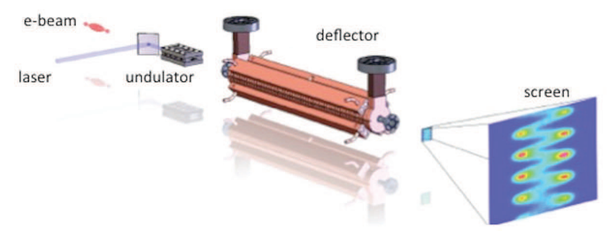


Figure 1: The electron beam interacts with a high-power, IR laser in the $TEM_{10}$ mode, in a resonant undulator to provide a "fast", sinusoidal transverse angular modulation. The deflecting cavity provides a "slow" streak in the orthogonal dimension. The resultant combined downstream pattern yields information on the bunch profile with enhanced longitudinal resolution.

the longitudinal coordinate, $s$, and is given by the expression [4],

$$\Delta x' = Ak \sin(ks + \phi) \tag{1}$$

where $k$ is the wavenumber of the driving laser, $\phi$ is the relative phase, and the amplitude of the oscillation, $A$, is proportional to

$$A \sim \frac{2K}{\gamma^2}\sqrt{\frac{P_L}{P_0}}[JJ] \tag{2}$$

In the expression for the amplitude $A$, $K$ is the scaled undulator parameter, $\gamma$ is the beam Lorentz factor, $P_L$ is the laser power, and the coupling factor $[JJ] = J_0(K^2/(4+2K^2)) - J_1(K^2/4+2K^2))$. For application as a bunch length diagnostic, it is important to maximize this amplitude because the angular modulation projection on a downstream profile monitor is the direct observable. From the expression above, it is clear the oscillation amplitude scales as the $\sqrt{P_L}$ and inversely with $\gamma^2$. Therefore the interaction favors high power, long wavelength lasers, and low-moderate energy beams. Based on this scaling, an experiment was designed for the Brookhaven National Laboratory Accelerator Test Facility (BNL ATF). The BNL ATF has a long history in experiments based on laser-electron beam interactions due to the availability of a high-brightness beam and high-power, $CO_2$ based IR laser. The expected interaction based on relevant BNL ATF parameters for the electron beam ($\epsilon_n$=1mm-mrad, $E$=48MeV, $Q$=300 nC) and high power laser operations ($\lambda$ = 10.6$\mu m$, $P_L$= 100GW) is shown in Fig. 2 using

ISBN 978-3-95450-177-9

# SIMULATION OF THz STREAK CAMERA PERFORMANCE FOR FEMTOSECOND FEL PULSE LENGTH MEASUREMENT

I. Gorgisyan*, PSI, Villigen, Switzerland, EPFL, Lausanne, Switzerland
R. Ischebeck, P. Juranic, E. Prat, S. Reiche, PSI, Villigen, Switzerland

*Abstract*

Extremely bright short-pulsed radiation delivered by the free electron laser (FEL) facilities is used in various fields of science and industry. Most of the experiments carried out using FEL radiation are dependent on the temporal durations of these photon pulses. Monitoring the FEL pulse lengths during these experiments is of particular importance to better understand the measurement results. One of the methods to measure the temporal durations of the FEL pulses is the THz streak camera. This contribution presents simulation of the THz streak camera concept that allows better understanding of the measurement technique and estimating measurement accuracies achievable with this method.

## INTRODUCTION

The ultrashort pulses of FEL radiation are used to study the dynamic processes in ultrafast temporal domain. The advancement of the FEL technologies enables delivery of photon pulses with durations in the femtosecond region or shorter. Measuring the lengths of the photon pulses is useful both for the users performing measurements at FEL facilities and the machine operators to monitor the performance of the accelerator itself.

Various techniques are currently used in different facilities to measure the temporal duration of the FEL pulses [1–6]. Among these methods is THz streak camera [2, 7–10] that is able to measure the pulse durations of FEL pulses with photon energies from UV to hard X-ray. To better understand the performance of THz streak cameras, to estimate the possible measurement accuracy of this method and to optimize the data analysis method used to retrieve the pulse lengths from the THz streaking measurements, a Matlab code was developed to simulate the streaking effect and the pulse length calculation procedure. The results delivered by the simulation demonstrate that the THz streak camera method is able to measure the length of the FEL pulses with an accuracy of about a femtosecond and indicate ways towards achieving sub-femtosecond accuracies. More comprehensive information about the simulation procedure and the obtained results is provided in [11].

## CONCEPT

The theory of the THz streak camera is presented in detail in [7, 12]. The idea of the method is to encode the temporal duration of an FEL pulse into the energy spectra of the photoelectrons produced by this pulse. This is done by ionizing the electrons in presence of an external THz radiation. Depending on the time of the ionization, the created electron experiences different phase of the THz pulse. Due to the interaction of the electron with the electric field of the THz pulse, its final kinetic energy changes. This change is dependent on the phase of the THz at the moment of the ionization. Electrons created by different parts of a photon pulse have different ionization times and, therefore, experience different energy shifts due to the interaction with the external streaking field. As a result, the energy spectrum of the streaked electrons is the convolution of the non-streaked electron spectrum and the temporal profile of the photon pulse. In case of convolution the rms widths of the two profiles add quadratically, meaning that the spectral width of the streaked photoelectrons can be written in the following form:

$$\sigma_{st}^2 = \sigma_0^2 + \tau_X^2(s^2 \pm 4cs). \tag{1}$$

Here $\sigma_0$ is the rms width of the non-streaked spectrum, $\tau_X$ is the duration of the ionizing pulse and $s$ is the streaking strength of the THz pulse. The term $c$ in equation 1 represents the linear energy chirp along the photon pulse. The sign $\pm$ corresponds to the electrons traveling along the electric field of the THz and opposite to it. By comparing the two streaked spectra of the electrons to their non-streaked spectra, one can calculate the spectral broadening $\Delta\sigma_\pm$ due to streaking in opposite directions. Using these two amounts of broadening, it is possible to exclude the chirp from equation 1 and obtain the pulse duration as

$$\tau_X = \sqrt{\frac{\Delta\sigma_+^2 + \Delta\sigma_-^2}{2s^2}}. \tag{2}$$

This expression is used in the simulation process to retrieve the rms lengths of FEL pulse using the photoelectron spectra.

## SIMULATION PROCEDURE

The simulation procedure uses energy spectra and temporal profiles of different FEL pulses generated by code Genesis [13] to reproduce the ionization of the electrons and their consequent streaking by the THz pulse. Once the non-streaked spectrum and the two streaked spectra of the electrons are obtained, the pulse lengths are calculated using equation 2. The reconstructed rms durations of the pulses are compared to the rms lengths of the input FEL pulses, and the accuracy and the precision of the calculations are estimated for each of the FEL pulses.

Overall, 178 FEL pulses were generated using the Genesis code. The pulse lengths were in range from about 1 fs up to 40 fs. The pulses of lengths from 1 fs to 15 fs were in the hard X-ray radiation range with photon energies of 12.4 keV,

* ishkhan.gorgisyan@psi.ch



ISBN 978-3-95450-177-9

# ELECTRON BEAM PROBE DIAGNOSTIC FOR BESSY II STORAGE RING

D. Malyutin, A. Matveenko, Helmholtz-Zentrum Berlin, Berlin, Germany


*Abstract*

A low energy electron beam can be used to characterize the high energy ultra-relativistic bunches. This technique allows one to obtain the bunch transverse profiles as well as the bunch length within a non-destructive single shot measurement.

In this paper the bunch length measurement technique based on the interaction of the low energy electron beam with an ultra-relativistic bunch is described. Results of numerical simulations of measurements related to BESSY II are presented. A possible setup of such diagnostic system for BESSY II and in future for BESSY VSR is proposed.


## INTRODUCTION

For better understanding of the beam dynamics in particle accelerators detailed bunch characterization is required. This includes, for example, the bunch length measurements.

The bunch length can be measured, for example, using a standard method with a streak camera which analyses a synchrotron light from a dipole magnet [1, 2] or using a low energy electron beam crossing the electron bunch trajectory in the accelerator [3]. Both methods are non-destructive, i.e. does not affect the bunch, and therefore they can be used during the standard routine operation at user facilities or at others accelerators where destructive diagnostic methods cannot be used. Each method has its own advantages and disadvantages.

### *Streak Camera*

A streak camera measures length and structure of an ultra-fast light signal by representing it as a two-dimensional image. In particle accelerators the light comes, for example, from the synchrotron radiation or optical transition radiation.

A light pulse hits the photocathode causing it to emit a bunch of photoelectrons, Fig. 1 [4]. The time structure of this bunch is identical to the structure of the light pulse.

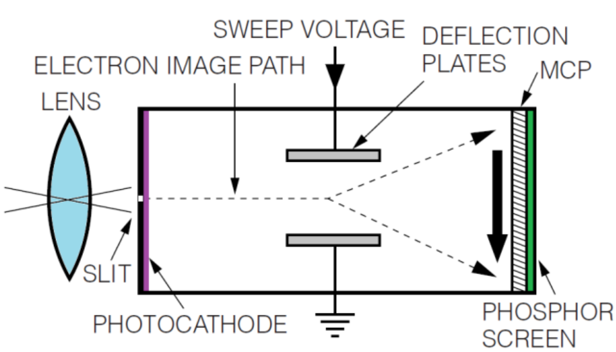


Figure 1: Streak camera basics [4].

These electrons are accelerated and then deflected by a ramped transverse electric field between the deflection plates. Afterwards the number of electrons is multiplied by the microchannel plate (MCP) and imaged on the phosphor screen. The resulted transverse profile of the screen image will represent the temporal profile of the light pulse. The minimal achieved resolution by available commercial streak cameras is in the order of 200 fs [4, 5].

### *Electron Beam Probe*

Electron beam probe diagnostic is based on interaction of the low energy electrons with the strong electric and magnetic fields of the relativistic bunch. Measuring the result of such interaction the bunch length or transverse bunch profile can be obtained [3].

A probe electron beam (3) is generated and accelerated in the electron gun (1) up to about 100 keV energy, Fig. 2.

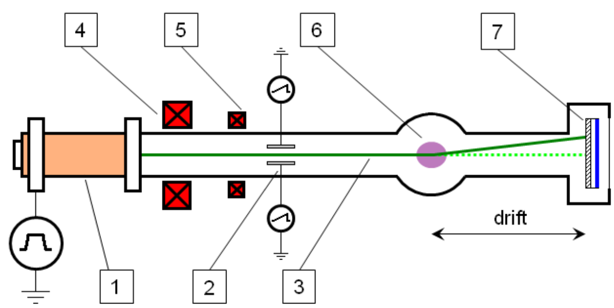


Figure 2: Electron Beam Probe layout: 1 – electron gun, 2 – horizontal deflecting plates, 3 – probe electron beam, 4 – focusing solenoid, 5 – magnetic correctors, 6 – electron bunch to be measured, 7 – detector (MCP and phosphor screen).

The beam is focused by the lens (4) and adjusted vertically and horizontally by a two-coordinate corrector (5). Time correlation in the beam is introduced by horizontal deflecting plates (2). After interaction with the ultra-relativistic bunch (6) the beam is projected on the observation screen (7). The horizontal axis on the screen will correspond to the time and the vertical axis will contain information about the bunch length. In Fig.2 the orientation of the deflecting plates is misleading: they are drown as the view from the top and all others components are drown as the side view.

The additional amplification scheme for the electron detection is required due to the low electron density of the probe beam on the observation screen. It can be realized as an electron-optical assembly of a microchannel plate (MCP) and a phosphor screen, in a similar way as it is done for the streak camera. The resulting image of the probe beam on the phosphor screen is recorded by a CCD camera. The vertical deflection angle is calculated from the image vertical size divided by the drift length, Fig. 2.

The maximal deflection angle of the probe electrons can be a parameter which can be used to characterize the bunch length. The deflection angle depends on the distance from

ISBN 978-3-95450-177-9

# LASER-BASED BEAM DIAGNOSTICS FOR ACCELERATORS AND LIGHT SOURCES*

C.P. Welsch#, Cockcroft Institute and The University of Liverpool, UK
on behalf of the LA³NET Consortium

*Abstract*

The Laser Applications at Accelerators network (LA³NET) was selected for funding within the European Union's 7th Framework Programme. During its 4 year duration the project has successfully trained 19 Fellows and organized numerous events that were open to the wider laser and accelerator communities. The network linked research into lasers and accelerators to develop advanced particle sources, new accelerating schemes, and in particular beyond state-of-the-art beam diagnostics. This paper summarizes the research results in laser-based beam diagnostics for accelerators and light sources. It discusses the achievable resolution of laser-based velocimeters to measure the velocity of particle beams, the resolution limits of bunch shape measurements using electro-optical crystals, position resolution of laser wire scanners, and limits in energy measurements using Compton backscattering at synchrotron light sources. Finally, it also provides a summary of events organized by the network and shows how an interdisciplinary research program can provide comprehensive training to a cohort of early career researchers.

## OVERVIEW

The primary aim of the LA³NET project [1] was to train 19 early stage researcher within a multidisciplinary network of academic and research-focused organizations across Europe. The network was awarded 4.6 M€ by the European Commission in 2011 and joined more than 30 institutions from around the world. The secondary aim was to establish a sustainable network and generate new knowledge through the research carried out by the Fellows. The LA³NET Fellows were hosted by 11 partner institutions all over Europe and although their work focuses on research, they are provided not only with scientific supervision and opportunities of secondments to other institutions involved in the project, but also complementary training through network-wide events. This includes international schools and topical workshops, as well as a final project conference and numerous outreach events. Through the involvement of almost 30 associated and adjunct partners the project gains an interdisciplinary dimension including strong links to industry. In the following section examples of research results from across the consortium in the beam diagnostics work package are given.

* This project has received funding from the European Union's Seventh Framework Programme for research, technological development and demonstration under grant agreement no 289191.
# c.p.welsch@liverpool.ac.uk

## RESEARCH

The Fellows carried out research within one out of five thematic work packages. These are particle sources, beam acceleration, beam diagnostics and instrumentation, system integration and detector technology.

### *Laser Velocimeter*

Pencil or curtain-shaped neutral gas jet targets are important for a number of accelerator-based experiments, either as cold targets or for example for diagnostic purposes [2]. However, only very few studies have addressed the optimization of these jets towards their respective application. The development of a laser velocimeter for an in-detail characterization of the gas jet and investigations into the jet dynamics, probing simultaneously its density, velocity, and temperature, was the aim of an ESR project at University of Liverpool [3]. For this purpose, laser self-mixing has been developed by Alexandra Alexandrova. The theoretical and experimental analysis of factors influencing the performance of the self-mixing laser diode sensor was compared. Variables that influence the resulting spectrum were investigated, primarily the velocity of the target, and the concentration of the seeders to assess the performance of the sensor. It has been shown that the spectrum of the signal directly depends on these factors. Experiments have demonstrated the possibility to use the self-mixing technique for measuring the velocity of fluids up to 1.5 m/s with a low level of seeders from 0.03% which would provide sufficient feedback of light. It has also been shown that increasing the target velocity reduces the amplitude of the peak of the spectrum and broadens the peak itself [4]. Analysis of the spectrum allows information to be obtained of the distribution of the velocities within the volume of the flow illuminated by laser light. The outlook of the project focused on characterization of different gas jets, studies into 3D position and motion detection in an UHV environment, using different lasers and benchmarking of numerical studies.

### *Laser Emittance Meter*

The optimum exploitation of the LHC ultimately depends on the quality and availability of the beams prepared in the injector complex. To set up new machine and achieve the best performance, it is important to measure the transverse emittance of the beam as it exits LINAC4 [5, 6]. A new technique has been proposed, based on the "slit & grid" technique, but using a laser beam rather than a physical slit. The project based at CERN was focused on the development of a laser emittance meter and carried out by Thomas Hofmann. Photo-detachment of electrons in an H- ion beam provides an interesting way of non-

ISBN 978-3-95450-177-9

# STREAK CAMERA CALIBRATION USING RF SWITCHES

U. Iriso, M. Alvarez, A.A. Nosych, ALBA-CELLS, Barcelona, Spain
A. Molas, Universitat Autónoma de Barcelona, Spain

*Abstract*

The streak camera has been used to measure the bunch length since the ALBA storage ring commissioning in 2011. Previously, we developed an optical calibration system based on the Michelson interferometry. In this report, we show the electronic calibration system based on the work in DLS [1], and compare both calibration systems. Finally, we show measurements of the longitudinal impedance obtained with the new calibration.

## INTRODUCTION

ALBA is equipped with a beam diagnostics beamline (BL34- Xanadu) that uses the visible part of the synchrotron radiation to characterize both longitudinal and transversely the electron beam profile [2, 3]. In the longitudinal plane, the key instrumentation is the Streak Camera (SC), which allows precise bunch length measurements and longitudinal beam dynamics studies. The camera is the Optronis SC-10 model, with a synchroscan frequency working at 250 MHz to distinguish the beam bunches spaced by 2 ns [4].

In order to perform precise measurements using the streak camera, it is necessary to determine the calibration factor that provides the relationship between the number of pixels and the corresponding time units. Moreover, Ref. [2] shows that depending on the speed sweep unit of the streak camera, this calibration might not be completely linear and a multi-linear calibration is required. This is especially the case for the slowest synchroscan speed of 50 ps/mm, while the speeds of 25 and 15 ps/mm show a very linear behaviour.

At ALBA, this factor was calibrated in 2012 using an optical set-up based on the Michelson interferometry [2]. The goal in those experiments was to include an optical delay of a known amount in the path of the synchrotron radiation, and measure it using the streak camera. This solution faces two main limitations: on one side, it is not easy to assemble the calibration setup (proper alignment of the optical systems); and secondly, it only provides calibration in the fast (in our case, vertical) sweep speeds.

Instead, the solution developed at Diamond Light Source [1] is based on delaying the reference RF signal used for the fast sweep unit with respect to the synchrotron radiation. This is achieved using RF switches, which change the path length of the RF signal by a known amount. Moreover, since the switching frequency is also known, a calibration pattern for the slow (in our case, hor) scale is also given.

## ELECTRONIC CALIBRATION KIT

The layout of the calibration kit is shown in Fig. 1. The $f_{rf}/2$=250 MHz reference signal is introduced in the crate, where two RF switches alternate the signal path between

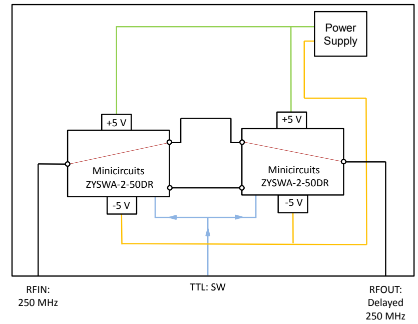


Figure 1: Schematic illustration of the crate used in order to introduce a delay in the 250MHz signal using the PIN diodes switching with a frequency set by the TTL signal and two cables with a certain different length.

a longer or a shorter way, whose difference is called $\Delta\tau$. By precisely measuring the difference in the path length, we can calibrate the streak camera. The RF switches are triggered by an Event Receiver producing TTL square waves, whose switching frequency $f_{sw}$ can be changed at will. The calibration process is disabled if we disable the output on the Event Receiver.

The image obtained in the SC when the calibration kit is in use has the zigzag shape shown in Fig. 2. The image has a symmetry top/bottom, since the SC sends odd bunches to the top half of the image, and bottom bunches to the bottom.

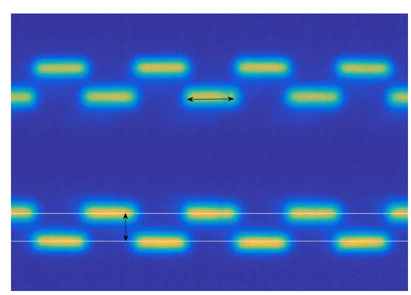

Figure 2: Output image of the streak camera after performing the delay of the 250MHz signal with the RF switches.

Note that:

- The horizontal scale is calibrated using the distance between streaks, which corresponds to $0.5/f_{sw}$ (see horizontal arrow in Fig. 2).
- The vertical scale is calibrated using the distance between the zigzag streaks, which corresponds to the time delay given by the cable difference, $\Delta\tau$ (see vertical arrow in Fig. 2).



ISBN 978-3-95450-177-9

# DEVELOPMENT OF ACCELERATOR SYSTEM AND BEAM DIAGNOSTIC INSTRUMENTS FOR NATURAL RUBBER AND POLYMER RESEARCH

E. Kongmon†, N. Kangrang, S. Rimjaem, J. Saisut, C. Thongbai, Plasma and Beam Physics Research Facility, Department of Physics and Materials Science, Faculty of Science, Chiang Mai University, Chiang Mai 50200, Thailand
M.W. Rhodes, Thailand Center of Excellence in Physics, Commission on Higher Education, Bangkok 10400, Thailand
P. Wichaisirimongkol, Science and Technology Research Institute, Chiang Mai University, Chiang Mai 50200, Thailand

*Abstract*

This research aims to design and develop an electron linear accelerator system and beam diagnostic instruments for natural rubber and polymer research at the Plasma and Beam Physics Research Facility, Chiang Mai University, Thailand. The accelerator consists of a DC thermionic electron gun and an S-band standing-wave linac. The system can produce electron beams with the energy range of 0.5 to 4 MeV for the pulse repetition rate of 30 to 200 Hz and the pulse duration of 4 µs. Commissioning of the accelerator system and development of beam diagnostic instruments to measure electron beam energy, electron pulse current and electron dose are underway. This contribution presents and discusses on the RF commissioning progress as well as status of design and construction of the beam diagnostic system.

## INTRODUCTION

A linear accelerator (linac) system for electron beam irradiation on natural rubber and polymeric materials is developed at the Plasma and Beam Physics Research Facility, Chiang Mai University, Thailand. The system consists of a Pierce-type DC gun with a flat circular thermionic cathode with diameter of 4.86 mm, a 5-cell standing-wave linac structure equipped with a driven radio-frequency (RF) system, electron beam diagnostic instruments and an irradiation apparatus. It is foreseen that the irradiation system composes of a beam sweeper with a vacuum horn chamber and a movable stage for the sample container. The layout of the accelerator and irradiation system is shown in Fig. 1.

The electron beam diagnostic instruments are under design and construction. A Faraday cup and an integrated current transformer will be used to measure the electron charge and pulse current. A dipole magnet and phosphor screen equipped with a CCD camera readout system will be utilized for an electron beam energy measurement. The results from the current and energy measurement can be used to estimate the electron dose produced from the accelerator system. The transverse beam size and transverse electron distribution at the sample container location will be observed via an outside vacuum screen station. The electron depth and dose distribution will also be measured with dosimeter [1]. In this paper, we present the results of the RF commissioning, electron beam dynamic simulations and status of preparation for the beam diagnostic instruments.

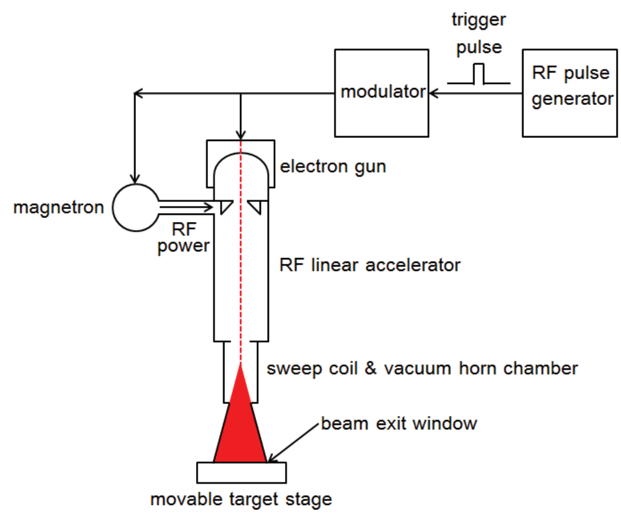


Figure 1: Layout of electron linear accelerator, a related RF power system and an irradiation apparatus.

## HIGH POWER RF COMMISSIONING

The linac system can be used to accelerate electron beam to reach the average kinetic energy of 0.5 to 4 MeV depending on the supplied RF peak power, which can be varied from 0.66 to 2 MW. A diagram of the RF generator and measurement systems are shown in Fig.2. The main components of the RF generator are a high voltage power supply with a variac for voltage variable (VAC), a pulse forming network (PFN) and a pulse modulator system. The RF signal amplitude is generated and amplified by a magnetron to reach the MW level. Then, the RF wave is transported from the magnetron to the linac via a WR-284 rectangular waveguide system with a ceramic RF window to separate the $SF_6$ pressurized part and the vacuum part. A forward and reflected RF powers are measured at a directional coupler prior the ceramic RF window.

As shown in Fig. 2, the forward and reflected RF ports of the directional coupler have the attenuation values of -60 dB. The forward and reflected RF power ports are connected to the cables and the attenuators with total attenuation values of -96.66 dB and -97.89 dB, respectively. The RF signals are converted to analog

†Corresponding author: Ekkachai_kon@cmu.ac.th

ISBN 978-3-95450-177-9

# TEMPERATURE AND HUMIDITY DRIFT CHARACTERIZATION OF PASSIVE RF COMPONENTS FOR A TWO-TONE CALIBRATION METHOD

E. Janas[1,2,*], K. Czuba[1], U. Mavrič[2], H. Schlarb[2]
[1] ISE, Warsaw University of Technology, Poland
[2] DESY, Hamburg, Germany

*Abstract*

Femtosecond-level synchronization is required for various systems in modern accelerators especially in fourth generation light sources. In those high precision synchronization systems the phase detection accuracy is crucial. However, synchronization to a low noise electrical source is corrupted by a phase detection error originating in the electrical components and connections due to thermal and humidity-related drifts. In future, we plan to implement calibration methods to mitigate these drifts. Those methods require a calibration signal injection, called second tone, into the system. Intrinsically, the injection circuit remains uncalibrated therefore it needs to be drift-free. We performed drift characterization of a set of RF components, which could serve for implementation of a signal injection circuit, namely selected types of couplers and splitters. We describe the measurement setup and discuss the challenges associated with this kind of measurement. Finally, we provide a qualitative and quantitative evaluation of the measurements results.

## MOTIVATION

A two-tone calibration method bases on an additional signal injection to the electronics circuits, which should get calibrated; in our case it is a phase detector for synchronization of a laser. Because the second signal properties are known, a drift arising in phase detector circuit can be measured. On this base a drift for an effective signal (being a subject of detection) can be estimated. Naturally, the second signal should be distinguishable from the effective one, therefore slightly apart in frequency. From the other hand, it should also be close enough to allow for comparison of the phase change between the two. A thorough analysis for a proper frequency choice has been presented in [1] and in essence shows, that the smaller the offset, the better calibration. More detailed description or another view on the method can also be found for example in [2, 3].

The injection of a calibration signal requires auxiliary hardware, which consist of at least a small section, where the effective and the calibration signal would not share the same path. An example would be a passive RF combiner, where its two arms are separate for each signal. Consequently, this piece of a circuit remains uncalibrated and introduces an error. In this paper, measurements of drift between two inputs of a combiner are presented, which allow for a rough comparison of different selected components.

* Ewa.Janas@desy.de

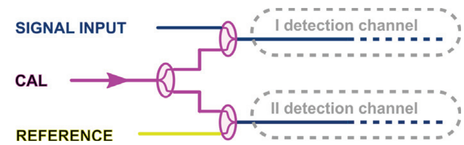

Figure 1: Phase calibration scheme.

## APPLICATION

In our case, the method will be used in a bit more complex setup, where additionally a complete second channel is introduced, injected with a reference signal. As the reference is intrinsically drift-free, it allows, that the drifts of the circuits can also be observed at the original frequency, possibly further improving the drift calibration. The drawback of this additional calibration method is, that the circuits are made equal, but are not very same; there are natural differences between them. These include for example PCB traces lengths inaccuracies or ambient temperature differences. The errors can be reduced by a proper PCB routing and placing both channels close to each other, but they can never be completely removed. Therefore both methods could be seen as supplementary to each other. However, the injection circuit in case of combined methods becomes bigger. Effectively, it has a structure depicted in Fig. 1. The splitters/combiners shown here can be as well implemented by couplers; the most important is, that the arrangement remains symmetrical.

In this configuration, the effective phase difference between the laser and the reference $\Delta\phi_{Eff}$ (which is present at the entrance of a phase detection module, that is yet devoid of parasitic drifts from the detector circuits) is defined by a following equation [1]:

$$\Delta\phi_{Eff} = \Delta\phi_{EffMeas} - A * \Delta\phi_{CalMeas}$$

where:

$\Delta\phi_{EffMeas}$ – phase difference measured by a phase detector between the input signal at the first channel and the reference at the second channel

$\Delta\phi_{CalMeas}$ – phase difference measured by a phase detector between both channels at the calibration signal

$A = \frac{f_{Eff}}{f_{Cal}}$ – coefficient to translate the drift at the calibration frequency into phase difference at the frequency of the measured signal

Besides phase stability, another crucial requirement for the injection circuit components to assure a decent level of calibration, is good isolation. This allows to avoid refer-



ISBN 978-3-95450-177-9

# COHERENT DIFFRACTION RADIATION IMAGING METHODS TO MEASURE RMS BUNCH

R.B. Fiorito†, C. P. Welsch, Cockcroft Institute, University of Liverpool, Daresbury, UK
A.G. Shkvarunets, IREAP, University of Maryland, College Park, MD USA,
C. Clarke, A. Fisher, SLAC National Accelerator Laboratory, Menlo Park, CA

*Abstract*

The measurement of beam bunch length with high resolution is very important for the latest generation light sources and also a key parameter for the optimization of the final beam quality in high gradient plasma accelerators. In this contribution we present progress in the development of novel single shot, RMS bunch length diagnostic techniques based on imaging the near and far fields of coherent THz diffraction radiation (CDR) that is produced as a charged particle beam interacts with a solid foil or an aperture. Recent simulation results show that the profile of a THz image of the point spread function (PSF) of a beam whose radius is less than the image produced by a single electron, is sensitive to bunch length and can thus be used as a diagnostic. The advantages of near (source) field imaging over far field imaging are examined and the results of recent high energy (20 GeV) CDR THz experiments at SLAC/FACET are presented. Plans for experiments to further validate and compare these imaging methods for both moderate and high energy charged particle beams are discussed.

## INTRODUCTION

In previous studies we have shown that the angular distribution (AD) of CDR from a slit or aperture is sensitive to RMS bunch length [1]. The AD can be calculated from the integrated spectral angular density of DR from single electron multiplied by the longitudinal form factor of the pulse integrated over a frequency band in which the integrand is appreciable [2]. Typically this band is limited at low frequencies by the outer radius or boundary of the radiator. At high frequencies it is truncated by the fall off of the longitudinal bunch form factor and, if the radiator is an aperture, by the aperture size. The AD is given by

$$\boxed{\frac{dI_{bunch}^{CDR}}{d\Omega} \approx N_e^2 \int_{\Delta\omega} \frac{d^2 I_e^{DR}}{d\omega d\Omega} S_z(\sigma_z,\omega) d\omega}$$

where $I_e$ is the intensity of the CDR from a single electron, $N_e$ is the number of electrons, $S_z$ is the longitudinal form factor, $\sigma_z$ is the RMS longitudinal size of the bunch, $\omega=2\pi f$ is the angular frequency, and $d\Omega$ is the solid angle of observation.

In a proof of principle experiment, the AD projected on a plane normal to the direction of the CDR from a plate and a slit were observed using a scanning Golay cell at PSI's 100 MeV injector linac for various bunch lengths. The latter was varied by a compressor chicane in the range of 0.5-2 psec. The bunch lengths were inferred fitting scans of the angular distribution obtained from the equation above to the data. The inferred bunch lengths were also compared with those obtained independently with an electro-optical sampling method and were found to be in excellent agreement with the AD measurements in all cases studied.

## OBSERVING THE CDR PSF

According to the virtual photon paradigm [3] the properties of radiation produced by relativistic particles interacting with materials or fields follow those of real photon interactions. For example, when a relativistic charged particle passes through an aperture, diffraction radiation is produced with properties similar to those observed when real photons diffract from the aperture. Applying this paradigm to CDR, the spatial distribution of CDR from a transversely coherent source, i.e. the PSF of the radiation from a coherent source such as a bunch of electrons radiating at a wavelength close to the bunch size, should be related by Fourier transformation to the AD of the photons observed. Then since the AD is related to the longitudinal bunch size, the PSF should also be likewise sensitive to the bunch length.

To observe the PSF, i.e. the spatial form of the CDR from a "single" electron, the transverse size of the beam must be much smaller than the PSF observed of a single electron. In this case the CDR is fully transversely coherent and the CDR PSF will be observed. The PSF of coherent transition radiation (CTR) has been similarly observed in the optical band [4], and under similar beam size conditions should be observable in the THz regime as well (note that CDR and CTR for a finite radiator are closely related via Babinet's principle [5]).

To test this hypothesis we have developed a simulation code to calculate the CDR PSF and explore its sensitivity to bunch length. The CDR produced as an electron passes through a finite sized radiator is intercepted by a lens positioned in the far field of the source which focuses the radiation onto the image plane of the lens.

Simulation results for a 100 MeV beam, interacting with a simple annular aperture oriented normal to the beam are shown in Figure 1 for various bunch sizes in the range of 1-3 picoseconds in the wave band (1-600 GHz). In this example the transverse beam size of the frequency integrated PSF from a single electron has a FWHM ~ 10-20mm (see Figure 1). Note that each of the PSFs shown is

†ralph.fiorito@cockcroft.ac.uk

ISBN 978-3-95450-177-9

# TIME CORRELATED SINGLE PHOTON COUNTING USING DIFFERENT PHOTON DETECTORS

L. Torino, U. Iriso, ALBA-CELLS, Cerdanyola del Vallès, Spain

*Abstract*

Time Correlated Single Photon Counting (TCSPC) is used in accelerators to measure the filling pattern and perform bunch purity measurements. The most used photon detectors are photomultipliers (PMTs), generally used to detect visible light; and Avalanche Photo-Diodes (APDs), which are often used to detect X-rays. At ALBA synchrotron light source, the TCSPC using a standard PMT has been developed and is currently in operation. Further tests have been performed using an APD. This work presents the experimental results using both detectors, and compares their performances.

## INTRODUCTION

The Time Correlated Single Photon Counting (TCSPC) is largely used in several accelerators to perform Filling Pattern (FP), and Bunch Purity measurements [1, 2]. The technique allows real time, and non-destructive FP measurements using the synchrotron radiation and providing high dynamic ranges.

The TCSPC is based on the fact that the number of photons produced when the beam is passing through a bending magnet is directly proportional to the number of electrons in the beam. Therefore, the FP can be obtained by measuring the temporal distribution of the synchrotron radiation, which corresponds to the one of the electron beam.

At ALBA the TCSPC using visible light has been successfully tested (see [3] for details), and more recently, a final setup for the routine operation has been developed. Moreover an Avalanche Photo-Diode (APD) has been also tested to perform TCSPC using x-rays.

The final setup for the visible light, and the new setup for the x-rays are presented in this work, together with a discussion on the obtained results.

Table 1: Manufacturer specification of the PMT and the APD. The Transit Time Spread that is measured in house.

| | PMT H10721-210 | APD C5658 |
|---|---|---|
| Photocathode Material | Ultra Bialkali | Silicon |
| Spectral Response | 230-700 nm | 200-1100 nm |
| Dark Current | 10 nA | 0.1 nA |
| Rise Time | 0.57 ns | 0.5 ns |
| Transit Time Spread | 0.2281 ns | 0.47 ns |

## TCSPC USING VISIBLE LIGHT

The photon-detector used to perform TCSPC in the visible range at ALBA is a Hamamatsu photomultiplier (PMT) H10721-210. The main characteristics of the device are collected in Table 1, and preliminary tests are shown in [3].

The final TCSPC setup has been moved for operation stability reasons inside the tunnel. The light is extracted using the copper absorber located at the end of visible light diagnostic frontend. This is possible since the synchrotron light reaching the ALBA diagnostic beamline Xanadu is extracted through an "half-mirror" which selects only the upper lobe of the radiation generated. In this way the central and the lower lobe reach the copper absorber, which is oriented at 45°with respect to the incident light. Even if the absorber is not polished, it is still able to reflect the visible light which is extracted through an extraction window, after which the PMT is located. A sketch of the light path at the end point of FE01 is presented in Fig. 1.

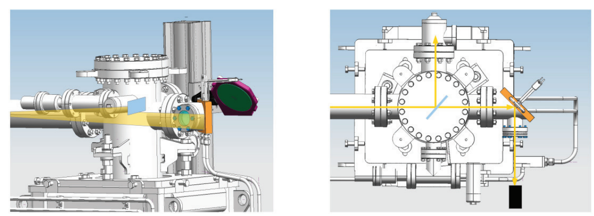

(a) *Front view.* (b) *Top view, the black box represent the PMT.*

Figure 1: Layout of FE01 endpoint and sketch of the light path.

In order to avoid the contaminations from the visible ambient light in the tunnel, a container has been designed to accommodate the TCSPC final setup. The container is a black box fixed on a support, and is directly connected to the secondary extraction window of FE01.

The PMT is contained in a small box in order to make the cabling easier (see Fig. 2(a)). On the front part of the box a c-mount lens tube is mounted, holding a Neutral-Density (ND) filter and a 633 nm band pass filter in order to shield the radiation and low the flux to less than one photon per revolution period, as required from the TCSPC. In front of the PMT box, a motor allows to introduce a gradual ND filter (from 0 to $10^5$) to control the photon flux.

Lead sheets have been located around the PMT to reduce the noise produced by particle losses and to slow down the device aging process.

Figure 2 shows two pictures of the setup. In the first the container is open and all the components are visible, while in the second the box is closed and is mounted in the tunnel at the FE01 location.

The power supply and the required electronics to properly control the components in the container (PMT and motor) are located outside the tunnel. The PMT signal is connected to a Picoharp300, which acquires the data and send them to

ISBN 978-3-95450-177-9

# DEVELOPMENT, CALIBRATION AND APPLICATION OF NEW-GENERATION DISSECTOR WITH PICOSECOND TEMPORAL RESOLUTION

*O. I. Meshkov[1], O. V. Anchugov, V. L. Dorokhov, G. Ya. Kurkin, A. N. Petrozhitsky, D. V. Shvedov, E. I. Zinin, BINP SB RAS, Novosibirsk, 630090, Russia
P.B. Gornostaev, M.Ya. Schelev, E.V. Shashkov, A.V. Smirnov, A.I. Zarovskii, GPI RAS, Moscow, 119991, Russia
[1]also at NSU, Novosibirsk, 630090, Russia

*Abstract*

A dissector is an electron-optical device designed for measurement of periodic light pulses of subnanosecond and picosecond duration. LI-602 dissector developed at BINP SB RAS is widely used for routine measurements of a longitudinal profile of electron and positron beams at BINP electron-positron colliders and other similar installations [1-3]. LI-602 dissector is a part of many optical diagnostic systems and provides temporal resolution of about 20 ps. Recently a new generation of picosecond dissectors were created on the basis of the PIF-01/S1 picosecond streak-image tube designed and manufactured at the GPI Photoelectronics Department [4, 8-10]. The results of the measurements of instrument function of the new dissector based on PIF-01/S1, which were carried out in the static mode [5], showed that temporal resolution of the dissector can be better than 3-4 ps (FWHM). The results of temporal resolution calibration of the new-generation picosecond dissector carried out at the specialized set-up based on a femtosecond Ti:sapphire laser and recent results of longitudinal beam profile measurements at BINP damping ring are given in this work.

## BASIC PRINCIPLES OF DISSECTOR OPERATION

The detailed description of the detector operation can be found in [3, 6]. We will remind just very common ideas of the device operation. The layout of a dissector is shown in Fig. 1. The image section of dissector consists of a photocathode, electron lens, deflection plates and slit aperture.

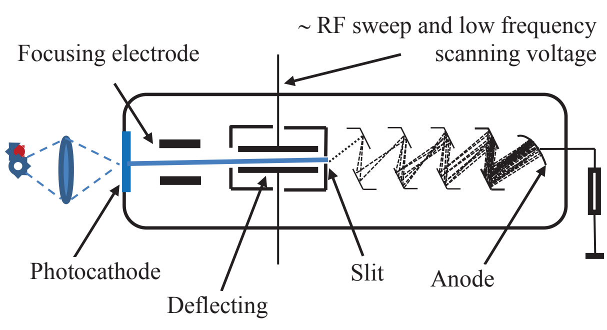


Figure 1: The simplified layout of the dissector.

*O.I.Meshkov@inp.nsk.su

Let the point-like image of a pulse radiation source be projected onto the photocathode of such a device. If radiation pulses and RF deflection voltage are strictly synchronized, then a stationary electron image *Q(x)* appears on the slit plane (Fig. 2). The typical frequency of RF sweep voltage $U_{sw}(t)$ is tens of MHz. The image *Q(x)* reproduces the time structure of the object under observation.

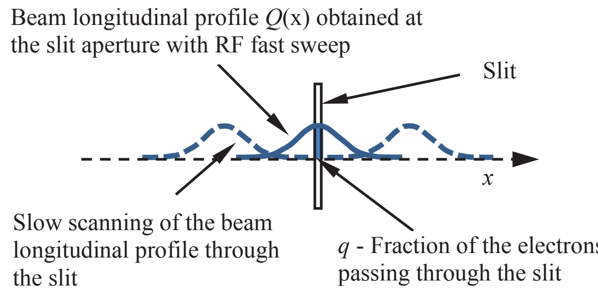


Figure 2: The scheme of slow scanning of *Q*(x) distribution transversely through the slit.

Only the electrons with charge *q,* which pass through the slit, reach the secondary electron multiplier. The average anode current of the secondary electron multiplier is proportional to this charge *q* and is proportional to the luminosity of the process at the given moment. The beam image is scanned transversely through the slit with velocity $V_{sl} << V_{sw}$. When distribution *Q(x)* is scanned, the anode signal of the secondary electron multiplier repeats the shape of the observed signal.

## TIME SCALE OF THE DISSECTOR

A simple way to define a time scale is an important advantage of the dissector. It is achieved with permanent point-like source of the light focused on the photocathode of the dissector. The space distribution $Q_p(x)$, as it is represented in Fig.3, periodically appears on the slit aperture plane and is read out during slow scanning. As a result, the space scale transforms into time scale. The space interval and the corresponding time interval $T_l$ between two distinct marks at the calibration curve depend on $U_0$ at fixed RF frequency $\nu_{RF}$. The same signal appears at the anode of the dissector if to scan slowly this distribution with linear ramp voltage applied to the deflecting plates.

The upper plot in Fig. 3 is an experimental curve obtained for temporal calibration of the dissector. The sweep velocity as well as the time scale of the dissector

ISBN 978-3-95450-177-9

# AXD MEASUREMENTS AT SOLEIL

M. Labat, M. El Ajjouri, N. Hubert, D. Pedeau, M. Ribbens, M.A. Tordeux, Synchrotron SOLEIL, 91 191 Gif-sur-Yvette, France

*Abstract*

A first prototype of in-Air X-ray Detector (AXD) has been installed on the SOLEIL storage ring. An AXD simply consists of a scintillator, an objective and a camera installed in air behind the absorber of the bending magnet's synchrotron radiation layer. The radiation vertical profile analysis easily enables to retrieve the vertical beam size of the electron beam at the source point. This simple diagnostics opens large perspectives of beam size measurement all around the ring for an accurate characterization of the beam and improvement of its stability survey.

## INTRODUCTION

An in Air X-ray Detector (AXD) has been installed at SOLEIL in August 2016 for vertical electron beam position and size measurements. An AXD consists of a scintillator and an imaging system [1] as illustrated in Figure 1. When the electron beam passes in the ring dipole field, it produces synchrotron radiation (SR) over a wide spectral range including hard X-rays. The synchrotron radiation in the X-ray range can pass through the absorber and the dipole vacuum chamber to reach the air in the tunnel. The X-ray SR layer distribution is then transformed into a visible light distribution by a scintillator. Finally, an imaging system enables to record this distribution on a camera. The analysis of the vertical profile of the light distribution enables to retrieve the vertical dimension at the source point, i.e. in the ring dipole. This paper summarizes the design and installation of the AXD at SOLEIL and presents its first measurements obtained in September 2016.

## AXD SOURCE POINT

### AXD Location

The AXD has been installed behind the second dipole of cell 12 at SOLEIL (C12-D2). The geometry of the C12-D2 vacuum chamber enables to mount the scintillator only 1.3 m downstream the source point inside the dipole (see Figure 2).

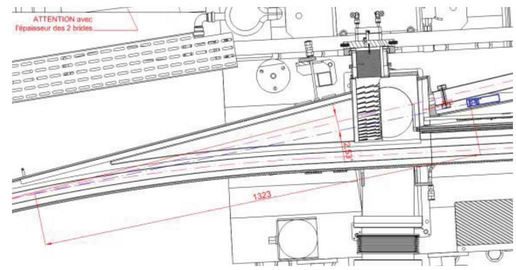

(a) Chamber drawing. Scintillator in blue.

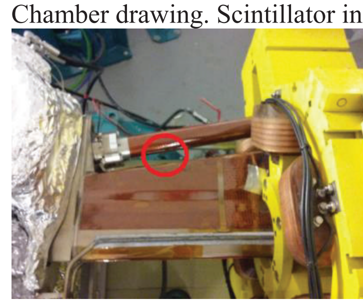

(b) Chamber picture before AXD installation. Red circle: expected scintillator location.

Figure 2: C12-D2 vacuum chamber.

### Beam Parameters at Source Point

The scintillator is in fact in between two vacuum chamber exit branches: the one for the 0° radiation and the one for the electron beam exit, corresponding to an extraction angle of 2.53°. The electron beam parameters at the 2.53° source point are given in Table 1.

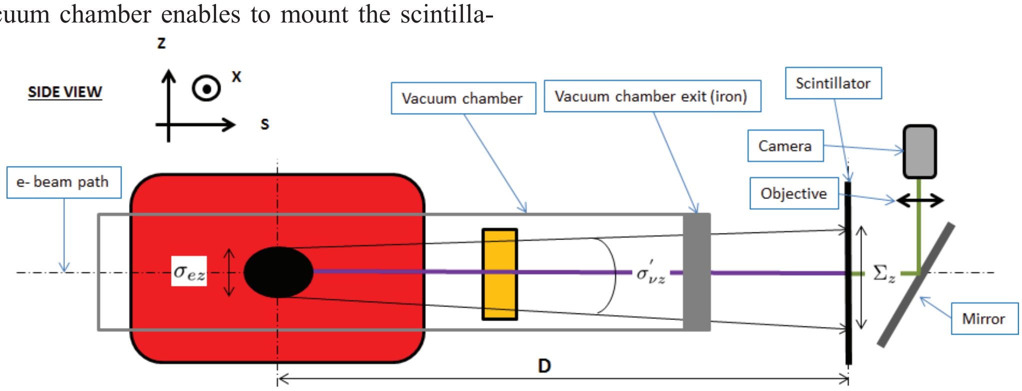


Figure 1: AXD schematic.



ISBN 978-3-95450-177-9

# NOVEL GRATING DESIGNS FOR A SINGLE-SHOT SMITH-PURCELL BUNCH PROFILE MONITOR

A. J. Lancaster*, G. Doucas, H. Harrison, I. V. Konoplev,
John Adams Institute, Department of Physics, University of Oxford, Oxford, OX1 3RH, UK

*Abstract*

Smith-Purcell radiation has been successfully used to perform longitudinal profile measurements of electron bunches with sub-ps lengths [1]. These measurements require radiation to be generated from a series of gratings to cover a sufficient frequency range for accurate profile reconstruction. In past systems the gratings were used sequentially and so several bunches were required to generate a single profile, but modern accelerators would benefit from such measurements being performed on a bunch by bunch basis. To do this the radiation from all three gratings would need to be measured simultaneously, increasing the mechanical complexity of the device as each grating would need to be positioned individually and at a different azimuthal angle around the electron beam. Investigations into gratings designed to displace the radiation azimuthally will be presented. Such gratings could provide an alternative to the rotated-grating approach, and would simplify the design of the single-shot monitor by reducing the number of motors required as all of the gratings could be positioned using a single mount.

## INTRODUCTION

Modern and future particle accelerators provide challenges for longitudinal beam profile monitors by producing short bunches with highly variable profiles. A successful monitor will have to resolve sub-ps bunches in a non-destructive manner on a single-shot (bunch-by-bunch) basis. Possible techniques which could enable such a monitor include electro-optic measurements [2] and the use of coherent radiation spectroscopy [3] [4]. This paper presents a preliminary conceptual design for a single bunch profile monitor based on coherent Smith-Purcell radiation (cSPR), with an emphasis on changes to the design of the metallic grating used to generate the radiation.

## SMITH-PURCELL RADIATION

Smith-Purcell radiation arises when a charged particle bunch travels near to a periodic metallic structure. The electric field of the particles induces a surface charge on the surface of the structure which then follows the particles, giving rise to a surface current. Discontinuities in the structure result in changes to the current and so to the emission of radiation. Each period will emit radiation in the same way, giving rise to a far field dispersion relation which links the wavelength of the radiation to angle of emission.

* andrew.lancaster@physics.ox.ac.uk

To use cSPR as a beam diagnostic it is necessary to predict the intensity of the radiation which will be generated, which requires several functions to be understood. The first step is to calculate the radiation produced by a single particle travelling above a single period of the grating. The effect of the grating periodicity can then be incorporated to give the expected intensity distribution from a single particle travelling above the full Smith-Purcell grating. It is at this stage that the dispersion relation becomes apparent.

The particle bunch must then be modelled. Assuming that the transverse bunch profile remains constant throughout we can describe the charge distribution as $T(x, y)Z(z, t)$, and the intensity of the cSPR is then found to be proportional to the Fourier transform of the longitudinal bunch profile. This means that by measuring the intensity of the cSPR along with other relevant beam parameters it is possible to retrieve the frequency components of the particle bunch and determine the longitudinal profile [5].

Coherent Smith-Purcell radiation has already been used to perform longitudinal bunch profile measurements at FACET, SLAC [1]. The E203 experiment sequentially measured three gratings with different periods, with three additional blank measurements to perform background subtraction. Each grating provided 11 frequency measurements, giving 33 measurement points in total. These measurements had to be taken over an extended period of time as the gratings were mounted on a carousel. As each accelerator will have different measurement requirements 33 frequency measurements has been taken as the target for the design of the single-shot device. The key constraints on the monitor are that background subtraction needs to be performed without the use of blanks and that the device must be compact.

The first constraint can be addressed by taking advantage of the high degree of polarization of Smith-Purcell radiation, which is predicted by theory and has been confirmed experimentally [6]. Previous measurements have shown the background signal to be broadly unpolarized [1]. This means that cSPR will be split asymmetrically by a polarizer but the background radiation will be evenly split. By using a pair of detectors it would therefore be possible to subtract the background radiation from the cSPR signal on a bunch-by-bunch basis. Such a detector layout is shown in Fig. 1.

The second constraint can be met by rotating the three gratings azimuthally around the particle beam. By positioning the three gratings at $\phi$=0° and ±60° there is enough space for the three sets of detectors to be positioned in a compact region along the beam pipe. The layout, shown in Fig. 2, is approximately 160 mm longer than the E203

ISBN 978-3-95450-177-9

# RECENT BEAM SIZE MEASUREMENT RESULT USING SYNCHROTRON RADIATION INTEFEROMETER IN TPS

M.L. Chen, H.C. Ho, K.H. Hsu, D.G. Huang, C.K. Kuan, W.Y. Lai, C.J. Lin, S.Y. Perng, C.W. Tsai, T.C. Tseng, H.S. Wang
NSRRC, Hsinchu, Taiwan

*Abstract*

Taiwan Photon Source (TPS) was under commissioning operation in 2015. An optical diagnostic beam line was constructed in TPS 40th beam port for the diagnostics of the electron beam properties. A synchrotron radiation interferometer, one instrument of this diagnostic beam line, operates for monitoring the beam size. In the beginning, the interferogram of the vertical beam is usually distorted. We found the stray light affected the vertical interferogram obviously while the beam current was raised. This paper describes the problems we met and how to eliminate the stray light for better beam size estimation. In the normal course of events, TPS is driven in 300mA and the horizontal beam size is 56um and the vertical beam size is 32um. The beam current of TPS is maximumly driven to 518mA in June, 2016. This paper also presents the trend of beam size during current running up.

## INTRODUCTION

Taiwan Photon Source (TPS) was commissioned in 2015. The electron beam has stored in the storage ring of current 518 mA and energy 3 GeV in June 2016. The beam is operated at 300 mA for normal operation and the current is also rising up to 518mA for machine study.

To measure the transverse beam size, two monitors are adopted in TPS 40th beam port. One is an X-ray pinhole camera and the other is a synchrotron radiation interferometer (SRI). [1] The X-ray pinehole camera is installed in the vacuumed chamber inside the shielding wall. And the beam line is also extended to the experiment area by using several folding mirrors to transport light to pass through the shielding wall. The SRI is installed on an optical table in a hutch lab outside of shielding wall.

In this paper we present the resent beam size measurement result and the relation of measurement result between two beam size monitors. We also present the problems we met and our countermeasures.

## PRINCIPAL OF SYNCHROTRON RADIATION INTERFEROMETER

The synchrotron radiation interferometer, presented by Dr. T. Mitsuhasi in KEK, is widely applied to monitor beam size of synchrotron light sources [2,3,4].The basic principle of a SR interferometer is to measure the profile of a small beam through the spatial coherency of light, and is known as the Van Citter-Zernike theorem. The distribution of intensity of the object is given by the Fourier transform of the complex degree of first-order spatial coherence. The intensity of interferogram pattern, I, is shown as the function of position,$y_1$,

$$\mathrm{I(y1)} = I_0\left[sinc(\frac{2\pi a}{\lambda R}y_1)\right]^2\left[1+|\gamma(\nu)|\cos\frac{2\pi D}{\lambda R}\,y_1+\varphi\right] \quad (1)$$

Where $\lambda$ denotes the wavelength, $R$ denotes the distance from the light source to the double slit, and $D$ denotes the double slit separation, and $a$ denotes half-height of slits. The visibility $\gamma$ is related to the complex degree of coherence.

$$\gamma = \left(\frac{2\sqrt{I_1.I_2}}{I_1+I_2}\right)\left(\frac{I_{max}-I_{min}}{I_{max}+I_{min}}\right) \quad (2)$$

The beam size is given by

$$\sigma_{beam} = \frac{\lambda \mathrm{R}}{\pi \mathrm{D}}\sqrt{\frac{1}{2}\ln(\frac{1}{\gamma})} \quad (3)$$

According to the above equation (3), the beam size is observed by the visibility of the interferogram.

## MONITOR SYSTEM SETUP

The SRI beam-size monitor is installed at TPS 40th beam port. The beam line structure is shown as fig1. The radiation produced at the dipole magnet propagates 19.2 m to pass through the shielding wall.

The main error of the visible SR interferometer arises from the distortion of the mirror by the radiation power [5]. So the first mirror of the beam line is a cooled beryllium mirror, which was adopted to prevent distortion. After beryllium mirror, the light passes the extraction window and an aluminium reflection mirror, and then it transports through the shielding wall. In the outside of the shielding wall, two folding aluminium mirrors are used to connect the synchrotron light to the optical table in hutch. Synchrotron light is separated to three channels by two beam splitter. 50% light is delicate for SR interferometer and the other 50% light is for streak camera monitoring.

The SRI beam size monitoring system is constructed by a diffraction-limited high-quality lens for focusing; the focusing length of this lens is 2 m; the wavefront error is less than $\frac{1}{10}\lambda$ . A polarizer and a band-pass filter are used to obtain quasi-monochromatic light. The centre wavelength of the bandpass filter is 500 nm with 10 nm bandwidth. An eyepiece is applied to magnify the

ISBN 978-3-95450-177-9

# FRASCATI BEAM-TEST FACILITY (BTF) HIGH RESOLUTION BEAM SPOT DIAGNOSTICS

P. Valente, INFN – Sezione di Roma, P.le Aldo Moro 2, I-00185 Rome, Italy.
B. Buonomo, C. Di Giulio, L. G. Foggetta, INFN – Laboratori Nazionali di Frascati, Via Enrico Fermi 40, I-00044 Frascati (Rome), Italy.

*Abstract*

The DAFNE Beam Test Facility (BTF) is operational in Frascati since 2003, hosting tens of experimental groups for an average of more than 200 beam-days each year. In the last years the beam diagnostics tools have been completely renewed and the services for the users have been largely improved.

We describe here the new transverse beam diagnostics based on GEM compact time projection chambers (TPC) and MEDIPIX Silicon pixel detectors, the upgraded data acquisition and the data caching system based on MEMCACHED, allowing a straight-forward integration of existing and new sub-systems in the renewed data logging. Results on the optimization of the transverse beam spot and divergence are reported, as well as the real-time diagnostics and feed-back user experience.

## INTRODUCTION

The beam parameters of the Beam Test Facility, operational at the Frascati laboratories since 2004 [1], cover a wide range in terms of intensity (from $10^{10}$ particles/pulse down to the single particle regime) and energy (from 30 to 750 MeV), while the transverse beam spot can be adjusted with beam-line optics and collimators [2].

This requires a high-resolution, efficient, robust, reliable, fast, easily manageable transverse diagnostics detector, with online readout capability in order to be effective in the beam setup phases. As additional requirement, the thickness of the detector should be kept at an acceptable level in order not to spoil the beam spot or alternatively the detector should be easily removable from the beam-line.

## TRANSVERSE DIAGNOSTICS

The transverse diagnostics of the BTF beam is an essential tool for the users, especially for detector characterization and calibration purposes.

We have developed both a very light diagnostics, based on micro-pattern gas detectors, namely a compact time-projection chamber (TPC) based on a triple Gas Electron Multiplier (GEM), and a thicker, but higher resolution system based on Silicon pixel detectors with integrated readout.

The two different systems have different limitations and advantages, so that we can choose the best solution depending on the beam parameter required by the users.

### *GEM TPC*

In the framework of the AIDA EU project a triple-GEM TPC has been developed, with the idea of having a very compact and light device, capable of reconstructing in 3D the particle tracks, even though with different resolutions in the three coordinates: if the beam passes in the drift space between the cathode and the first GEM foil, one of the two transverse coordinates will correspond to the drift direction, so that the time of arrival measurement will allow reaching a resolution of the order of 100 μm (limited by the longitudinal diffusion in the drift gap). In our case we have chosen a 4 cm drift length and a standard $Ar\text{-}CO_2\text{-}CF_4$ mixture. The other two coordinates are measured by the 128 pads, 3×6 mm$^2$ over an active area of 50×50 mm$^2$, smaller with respect to the GEM foils, cathode and anode planes, with standard dimensions 100×100 mm$^2$, in order to avoid the effect of electric field lines distorsion at the edges, even though we have introduced a thin kapton foil with Copper surface all around the drift space as Faraday-cage for a better shaping of he field.

A FPGA allows to easily readout the 128 pad times and quickly transfer the data via Ethernet interface. The online display of the GEM TPC acquired beam profiles is shown in Fig. 1.

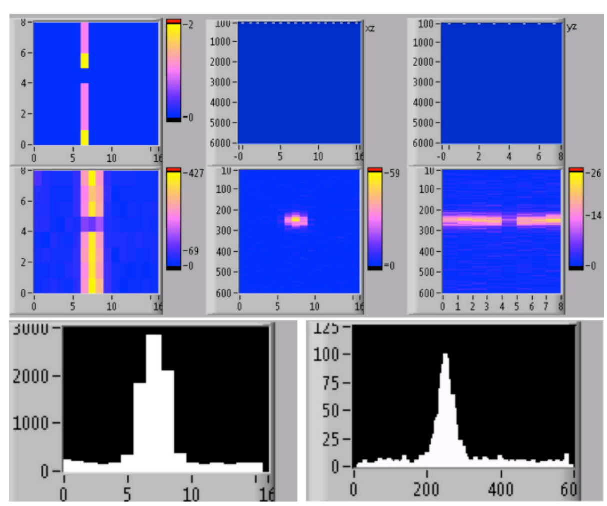


Figure 1: 477 MeV electron beam imaged by the GEM TPC; online display of the six planes view (top) and the two transverse projections (bottom).



ISBN 978-3-95450-177-9

# DESIGN AND EXPERIMENTAL TESTS OF THE SwissFEL WIRE-SCANNERS

G.L.Orlandi*, R.Ischebeck, C.Ozkan Loch, V.Schlott,
Paul Scherrer Institut, 5232 Villigen PSI, Switzerland
M. Ferianis, G. Penco
Elettra Sincrotrone Trieste, 34149 Basovizza, Trieste, Italy

*Abstract*

The SwissFEL wire-scanner (WSC) composes of an in-vacuum beam-probe - motorized by a stepper motor - and an out-vacuum pick-up of the wire-signal. In SwissFEL, WSCs will absolve two main tasks: high precision measurement of the beam profile for determining the beam emittance as a complement to view-screens; routine monitoring of the beam profile under FEL operations. In order to fulfill the aforementioned tasks, the design of the in-vacuum component of the SwissFEL WSCs followed the guidelines to ensure a mechanical stability of the scanning wire at the micrometer level as well as a significative containment of the radiation-dose release along the machine thanks to the choice of metallic wires with low density and Atomic number. Beam-loss monitors have been suitably designed to ensure a sufficient sensitivity and dynamics to detect signals from scanned beams in the charge range 10-200 pC. The design, the prototyping phases, the bench and electron-beam tests - performed at SITF (Paul Scherrer Institut) and FERMI (Elettra, Trieste) - of the entire SwissFEL WSC set-up will be presented.

## PREMISE

The proceeding contents are an extract of an article recently accepted for publication in Physical Review Accelerators and Beams [1]. Aim of the present proceeding is to outline the most relevant aspects of the work done for the development of the SwissFEL WSC which the reader can examine in depth in [1]. The introductory and conclusive sections of the proceeding directly descend from [1].

## INTRODUCTION

SwissFEL will provide coherent X-rays light in the wavelength region $7 - 0.7\ nm$ and $0.7 - 0.1\ nm$ [2]. Electron bunches with charge of 200/10 $\mathrm{pC}$ and transverse normalized slice emittance of 0.4/0.2 $\mathrm{mm.mrad}$ will be emitted by a S-band photocathode gun at a repetition rate of $100\ \mathrm{Hz}$ according to a two-bunches structure with a temporal separation of $28\ \mathrm{ns}$. The electron beam will be then accelerated up to $330\ \mathrm{MeV}$ by a S-band RF booster and, finally, to $5.8\ \mathrm{GeV}$ by a C-band RF linac. Thanks to an off-crest acceleration in the RF Booster, the electron beam will experience a longitudinal compression in two magnetic chicanes from an initial bunch length of $3/1\ \mathrm{ps}$ (rms) down to $20/3\ \mathrm{fs}$ (rms). Two X-band RF cavities will compensate the quadratic distortion of the longitudinal phase space due to the off-crest acceleration of the beam and the non-linear contribution of the magnetic dispersion [3]. In the booster section, a laser-heater will smooth down possible micro-structures affecting the longitudinal profile of the beam [4, 5]. Finally, thanks to a RF kicker - placed after the second bunch-compressor - and a magnetic switch-yard, the second electron bunch of the beam train will be shifted from the main beam line to a secondary one so that the SwissFEL linac, after a further acceleration stage of the two bunches, will supply two distinct undulator chains at a repetition rate of $100\ \mathrm{Hz}$: the hard X-rays line Aramis and the soft X-rays line Athos [2].

In a FEL (Free Electron Laser) driver linac, WSCs are currently used to monitor the transverse profile of the electron beam [6, 7, 8, 9, 10, 11, 12, 13, 14] when the view-screen imaging of the beam is hampered by coherent radiation emission due to microbunching. In SwissFEL, WSCs will be complementary to view-screens for emittance measurements and, thanks to the barely invasive feature, also used for routine monitoring of the transverse profile of the electron beam during FEL operations. Moreover, the beam imaging at SwissFEL being performed by means of YAG:Ce screens [15], only WSCs will be able to discriminate the profile of each single bunch in two-bunches operations. In SwissFEL, the WSC in-vacuum hardware consists of a planar wire fork which can be inserted $45^o$ with respect to the vertical direction into the vacuum chamber by means of a UHV linear-stage driven by a stepper motor, see Fig.(1). The wire-fork is designed to be equipped with two wire triplets, the spare triplet being possibly composed of wires of different material and/or diameter. Each wire of the triplet will separately scan the beam profile along a given direction: the vertical wire (X-scanning, horizontal-scanning), the horizontal wire (Y-scanning, vertical-scanning) and the diagonal wire (XY-coupling). During a WSC measurement, the single wire scanning the beam at a constant speed produces - at every RF shot - a shower of primary scattered electrons and secondary emitted particles in proportion to the fraction of the beam sampled by the wire. In SwissFEL, the forward - high energy and small scattering angle - component of the particle shower (wire-signal) will be out-vacuum detected by means of Beam-Loss-Monitors (BLMs). The beam-loss sensitive material of the SwissFEL BLMs is a scintillator fiber (Saint Gobain BCF-20, decay time 2.7 ns) wrapped

* gianluca.orlandi@psi.ch

ISBN 978-3-95450-177-9

# DEVELOPMENT AND COMMISSIONING OF THE NEXT GENERATION X-RAY BEAM SIZE MONITOR IN CESR *

N.T. Rider, S.T. Barrett, M.G. Billing, J.V.Conway, B. Heltsley, A. Mikhailichenko, D.P. Peterson, D. Rubin, J.P. Shanks, S. Wang, CLASSE, Cornell University, Ithaca, NY 14853, U.S.A

*Abstract*

The CESR Test Accelerator (CESRTA) program targets the study of beam physics issues relevant to linear collider damping rings and other low emittance storage rings. This endeavour requires new instrumentation to study the beam dynamics along trains of ultra-low emittance bunches. A key element of the program has been the design, commissioning and operation of an x-ray beam size monitor capable, on a turn by turn basis, of collecting single pass measurements of each individual bunch in a train over many thousands of turns. The x-ray beam size monitor development has matured to include the design of a new instrument which has been permanently integrated into the storage ring. A new beam line has been designed and constructed which allows for the extraction of x-rays from the positron beam using a newly developed electro magnet pair. This new instrument utilizes custom, high bandwidth amplifiers and digitization hardware and firmware to collect signals from a linear InGaAs diode array. This paper reports on the development of this new instrument and its integration into storage ring operation including vacuum component design, electromagnet design, electronics and capabilities.

## INTRODUCTION

The Cornell Electron Storage Ring (CESR) provides electron and positron beams which are used for accelerator research and as a synchrotron light source. Both of these applications require diagnostic equipment and instrumentation to maintain particle beam and x-ray quality. The Next Generation x-Ray Beam Size Monitor (NGXBSM) is part of a suite of instrumentation developed for this purpose. The NGXBSM is a natural evolution of the instrument which was developed during the early stages of the CESRTA program. This instrument images x-rays from a bending magnet through a pinhole optical element on to a 32x1 pixel linear array detector. Figure 1 shows the basic concept of beam size measurement using x-rays.

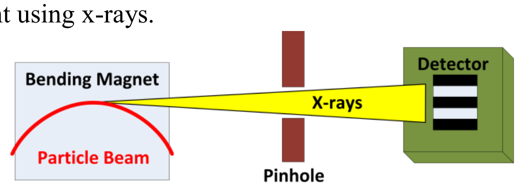


Figure 1: XBSM concept.

The development program has thus far leveraged the existing beam line and support structure of the experimental hutches at the Cornell High Energy Synchrotron Source (CHESS). While this arrangement was convenient, it was also temporary. The instrument was disassembled at the end of every CESRTA run and reinstalled, aligned and calibrated at the beginning of the next run. This prevented the use of the instrument during normal CHESS operations and limited development opportunities. The instrument provides valuable beam tuning information and an effort was undertaken to design and build a permanently installed instrument in CESR. The new instrument is a simplified application of the first generation technology. It provides vertical beam size measurements on a bunch by bunch and turn by turn basis. The available optical elements include a 35 micron vertical pinhole, a 200 micron vertical pinhole and an unlimited opening. These were chosen to support the typical operating energies of CESR, 2.085 GeV and 5.3 GeV. The instrument is capable of operating with CESR beam energies down to 1.8 GeV. First generation data acquisition electronics and software have been utilized to capture and process the x-ray images.

## ACCELERATOR INTEGRATION

In order to reduce the risk to the accelerator vacuum system, it was decided to pursue a windowed beam line design with the optical elements and detector outside of the CESR beam pipe. A beryllium window provides physical separation between the CESR and NGXBSM beam pipes. Usable x-ray intensity across the energy range of the accelerator is maintained by utilizing multiple x-ray sources. At 5.3 GeV an existing normal bend magnet is used as the x-ray source. At 2.085 GeV, a new two pole source magnet has been designed and constructed to provide the x-ray source. This new magnet is required to provide sufficient x-ray flux through the beryllium window at lower CESR beam energies. The spatial requirements of the new beam line coupled with the requirement for the installation of a new source magnet, limited potential instrument locations in the CESR tunnel. The location chosen for this new instrument forced an overall reduction in length of the x-ray path from optical element to detector when compared to the first generation instrument. Since the instrument is effectively a pinhole camera, this serves to reduce the effective magnification from source to detector. In order to offset this effect, the detector has been tilted at a 60 degree angle to functionally reduce the pixel height and increase resolution. The present configuration has a distance from source to optic of 4.4m or 6.76m, depending on which source is used, and a distance from optic to detector of 4.4m. Motorized stages are used to allow for precision alignment of the optical elements and the detector. Figure 2 shows a functional overview of the instrument and key CESR components.

*Work supported by NSF grant PHY-0734867 and DOE grant DE-FC02-08ER41538

ISBN 978-3-95450-177-9

# STUDY OF YAG EXPOSURE TIME FOR LEReC RF DIAGNOSTIC BEAMLINE

S. Seletskiy †, T. Miller, P. Thieberger
BNL, Upton, USA

*Abstract*

The LEReC RF diagnostic beamline is supposed to accept 250 us long bunch trains of 1.6 MeV – 2.6 MeV (kinetic energy) electrons. This beamline is equipped with a YAG profile monitor. Since we are interested in observing only the last bunch in the train, one of the possibilities is to install a fast kicker and a dedicated dump upstream of the YAG screen and related diagnostic equipment. This approach is expensive and challenging from an engineering point of view. Another possibility is to send the whole bunch train to the YAG screen and to use a fast gated camera to observe the image from the last bunch only. In this paper we demonstrate the feasibility of the last approach, which significantly simplifies the overall design of the RF diagnostic beamline.

## LEReC RF DIAGNOSTIC BEAMLINE

The LEReC accelerator [1, 2] includes a dedicated RF diagnostic beamline (Fig. 1). This beamline will be utilized for fine-tuning of the RF required to produce electron bunches with energy spread better than $5{\cdot}10^{-4}$.

The beamline consists of a bending magnet creating dispersion at the location of the YAG screen and a deflecting cavity "crabbing" electron bunches in time domain. Thus, the beam image on the YAG screen represents the longitudinal phase space of the beam.

The temporal structure of the bunch train sent to the diagnostic beamline is as follows. There are N=30 (100 ps long) electron bunches, with nominal charge Q=130 pC, spaced by 1.4 ns and forming a single macro-bunch. The macro-bunches are separated by Δt=110 ns and form the train of any chosen length. The schematic of e-beam temporal structure is shown in Fig. 2.

The overall length of the bunch train required for RF diagnostic is determined by stabilization time of the RF system. It was determined [3] that bunch train of length t=250 us is sufficiently long to study the beam-loading effects in LEReC RF cavities.

We plan to send the whole bunch train to the YAG screen and to use a fast gated camera (such as Imperex B0610 with trigger jitter under 60ns [4]) to observe the image from the last macro-bunch only.

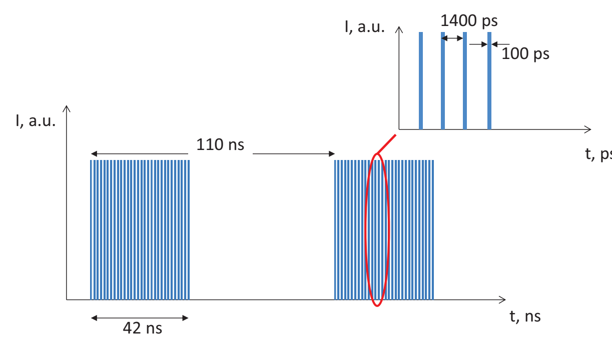


Figure 2: Temporal structure of electron beam.

In this paper we will consider two connected questions of YAG screen performance for the described bunch train.

First, we will study the instantaneous temperature jump in YAG crystal due to deposition of a single bunch train.

Second, we will find the steady-state temperature of YAG screen for various e-beam repetition rates.

## YAG SCREEN PERFORMANCE

The best, known to us, test of YAG screen performance under temperature stress is the RHIC electron lens operation. In this test 5 keV, 97 mA DC beam "chunks" as long as 1.2 ms were deposited on the YAG screen.

The crystal response still was linear for such parameters and the Gaussian transverse distribution with σ=0.133 cm was still observed on the YAG screen.

We calculated that due to deposition of each shot YAG temperature had to jump by 194 K. Numerous shots with 3-5 s repetition rate were sent to YAG crystal without damaging it.

The test [5] of the dependence of YAG crystal performance on temperature corroborates that it is safe to heat the YAG screen up to 200 C.

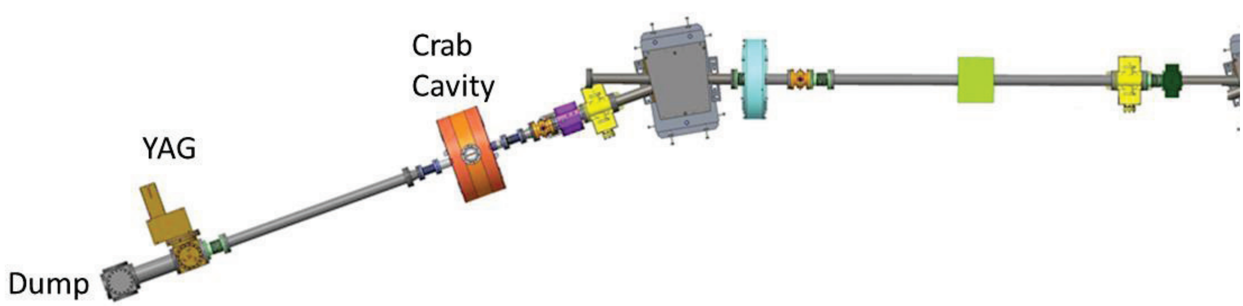


Figure 1: LEReC RF diagnostic beamline layout.

† seletskiy@bnl.gov

ISBN 978-3-95450-177-9

# TRANSVERSE BEAM PROFILING AND VERTICAL EMITTANCE CONTROL WITH A DOUBLE-SLIT STELLAR INTERFEROMETER*

J. Corbett†, X. Huang and J. Wu, SLAC National Accelerator Laboratory, Menlo Park, USA
C.L. Li, East China University of Science and Technology, Shanghai, China
T. Mitsuhashi, KEK, Tsukuba, Japan
Y.H. Xu, Donghua University, Shanghai, China
W.J. Zhang, East China University of Science and Technology, Shanghai, China
and the University of Saskatchewan, Saskatoon, Canada

*Abstract*

Double-slit interferometers are useful tools to measure the transverse the cross-section of relativistic charged particle beams emitting incoherent synchrotron radiation. By rotating the double-slit about the beam propagation axis, the transverse beam profile can be reconstructed including beam tilt at the source. The interferometer can also be used as a sensitive monitor for vertical emittance control. In this paper we outline a simple derivation of the Van Cittert-Zernike theorem, present results for a rotating double-slit measurement and demonstrate application of the interferometer to vertical emittance control using the Robust Conjugate Direction Search (RCDS) optimization algorithm.

## INTRODUCTION

The concept of a double-slit visible light SR interferometer for charged-particle beam size measurement was first developed at KEK [1] and has since been widely used at many accelerator facilities [2]. Compared with an optical telescope, the double-slit interferometer has the advantage of removing aperture diffraction effects thereby improving spatial resolution.

Perhaps the most well-known application of the stellar interferometer was Michelson's measurement of the 0.047" angle subtended by α-Orionis [3]. Subsequently the field of stellar interferometry has advanced to include telescope configurations with sophisticated aperture synthesis [4] and non-redundant aperture arrays which have also been applied to measure charged particle beam cross-sections using synchrotron radiation [5].

SPEAR3 has a dedicated SR diagnostic beam line designed to characterize properties of the electron beam. Within the beam line, unfocused visible light travels 16m to an optical bench where it has a rectangular cross-section of 60mm x 100mm. The vertical acceptance of ±3mrad is sufficient to pass almost all of the 500nm wavelength component with measureable edge diffraction around the perimeter of the beam (Fig. 1, inset).

Figure 1 shows a schematic of the beamline including the interferometer optics. At the dipole source point, the electron beam cross-section is approximately 120µm x 20µm depending on the lattice configuration. A stationary ±0.6mrad beam stop at the accelerator midplane protects the Rhodium-coated SR beam extraction mirror from the high heat flux of the primary x-ray beam. Typical interferometer slit separations for horizontal and vertical beam size measurements are 15 mm and 50 mm, respectively [6]. Both the double-slit mask and the CCD camera can be mounted on rotatable stages to enable measurement at arbitrary angles relative to the beam axis.

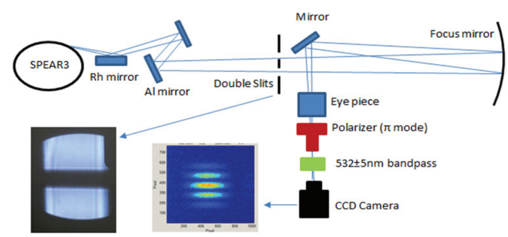


Figure 1: Stellar interferometer on the SPEAR3 visible light diagnostic beam line.

In this paper we first provide a simplified 'conceptual' derivation of the Van Cittert-Zernike theorem to demonstrate the Fourier transform nature of a stellar interferometer operating in the far-field regime. Axial rotation of the interferometer slits about the beam propagation axis is shown to yield the transverse electron beam profile and corresponding beam coherence ellipse in reciprocal space. As an application to machine tuning, vertical interferometer slits are used with a robust optimization program to control vertical beam emittance.

## VAN CITTERT-ZERNIKE THEOREM

Analysis of the fringe pattern from a double-slit interferometer in the far field of an incoherent radiating source is often based on the Van Cittert-Zernike theorem [7,8]. In short, the theorem states that under proper paraxial and monochromatic light conditions the fringe contrast evaluated as a function of spatial frequency defined by the slits is the Fourier transform (FT) of the incoherent intensity distribution of the source, $I(x,y)$:

$$\Gamma(f_x, f_y) = \iint I(x,y) e^{-2\pi i (f_x x + f_y y)} dx dy \qquad (1)$$

In practice, by measuring the fringe contrast Γ as a function of slit separation (spatial frequencies $f_x$ ,$f_y$), one can deduce the source profile $I(x,y)$ via the inverse FT.

* Work supported by US Department of Energy Contract DE-AC03-76SF00515, Office of Basic Energy Sciences and the China Scholarship Council.
† corbett@slac.stanford.edu

ISBN 978-3-95450-177-9

# POLARIZATION MEASUREMENT AND MODELING OF VISIBLE SYNCHROTRON RADIATION AT SPEAR3*

C. L. Li†, East China University of Science and Technology, Shanghai, China
J. Corbett, SLAC National Accelerator Laboratory, Menlo Park, USA
Y. H. Xu, Donghua University, Shanghai, China
W.J. Zhang, East China University of Science and Technology, Shanghai, China
and the University of Saskatchewan, Saskatoon, Canada

*Abstract*

Synchrotron radiation from dipole magnets is linearly polarized in the plane of acceleration and evolves toward circular polarization with increasing vertical observation angle. The intensity of the x-y field components can be modeled with Schwinger's theory for the angular-spectral power distribution. Combined with Fresnel's laws for reflection at a mirror surface, it is possible to model field polarization of visible SR light in the laboratory. The polarization can also be measured with a polarizer and quarter wave plate to yield Stokes' parameters $S_0$-$S_3$. In this paper we present measurements and modeling of the visible SPEAR3 SR beam in terms of Stokes' parameters and plot on the results on the Poincaré sphere.

## INTRODUCTION

Synchrotron radiation (SR) has the unique property of a high degree of field polarization. The SR beam from a dipole magnet, for instance, is linearly polarized in the transverse acceleration plane, and changes to elliptical and finally circular polarization as the vertical observation angle increases [1]. Polarized SR in the UV or X-ray regime is frequently used to probe structural properties of matter [2]. Visible SR, with a relatively large opening angle, provides a unique opportunity to study the SR beam polarization state.

According to Schwinger's theory for synchrotron radiation, the σ- and π mode power density distributions produced from a dipole magnet can be accurately modeled. By combining with Fresnel's equations for reflection of electromagnetic radiation at a material interface, the beam polarization at the SR source and at the optical bench can be modeled.

For this work we constructed an optical measurement system composed of a bandpass filter, field-discriminating polarizer and quarter wave plate (QWP) to characterize the beam polarization state in terms of Stokes's parameters [3,4]. The measurement system is mounted on a continuous-scan vertical stage to record the beam intensity as a function of vertical observation angle and polarizer rotation angle. Preliminary results have been presented in references [5,6]. In this paper, we extend the analysis to a Stokes' parameter representation, extract beam polarization ellipse parameters and display the results on the Poincaré sphere.

* Work supported by US Department of Energy Contract DE-AC03-76SF00515, Office of Basic Energy Sciences and the China Scholarship Council.
† Corresponding author: chunlei520@gmail.com

## THE SPEAR3 DIAGNOSTIC BEAMLINE

As shown in Fig. 1, the unfocused visible SR beam first encounters a Rhodium-coated extraction mirror at an incidence angle of 81 degrees to the surface normal. The beam is then reflected by two near-normal Al mirrors onto the optical bench. An image of the unfocused SR beam at a distance ~16m from the source is seen to the right. A 'cold finger' x-ray beam stop shadows a range of ±0.6 mrad at the accelerator midplane to protect the extraction mirror from high heat loads at 500mA electron beam current.

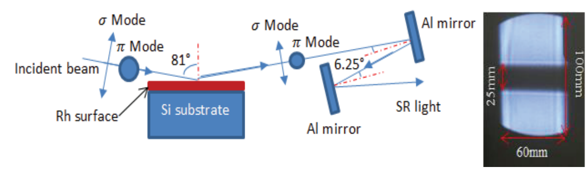


Figure 1: Schematic diagram of the visible-light SR beam transport line at SPEAR3.

Table 1: Reflection Properties of the Rh-coated Mirror

| Parameters | Value |
|---|---|
| Wavelength (nm) | 532 |
| Refractive index ($n_r$) | 2.633 |
| Extinction index ($k_i$) | 3.306 |
| Reflection coefficient $r_s$(π mode) | 0.957 |
| Reflection coefficient $r_p$ (σ mode) | 0.508 |
| Intensity ratio $I_p/I_s$=$(r_p/r_s)^2$ | 0.2818 |
| π mode phase shift $\Delta\emptyset_S$ | -176.726° |
| σ mode phase shift $\Delta\emptyset_P$ | 119.555° |
| Phase difference $\Delta\emptyset_{S-P}$ | above=153.6° |

The visible SR beam extraction mirror was manufactured with 600Å Rhodium deposited on a monolithic Si block [7]. As a result, the refractive index $n_r$ and extinction index $k_i$ exhibit 'thin film' properties as found in [8]. The corresponding reflection coefficients listed in Table 1 were calculated using Fresnel's laws [9] with a complex index of refraction $n$=$n_r$+i$k_i$. The grazing-incidence reflection angle in combination with the thin-film Rh mirror surface properties results in ~75% power loss of the horizontal beam polarization component (σ-mode radiation). The normal-incidence Al mirrors have only a small effect.

Stokes' parameters for the unfocused beam were measured using the continuous-scan data acquisition system to systematically probe the vertical observation



ISBN 978-3-95450-177-9

# DIAGNOSTIC TEST-BEAM-LINE FOR THE INJECTOR OF MESA*

I. Alexander†, K. Aulenbacher
Institut für Kernphysik, Johannes Gutenberg-Universität, D-55099 Mainz, Germany

*Abstract*

With the test-beam-line it is possible to measure the two transverse phase-spaces and the temporal distribution of the electron bunches. It is also possible to investigate the emittance close to the source. The beam-line components will be introduced and a selection of the results will be presented.

## INTRODUCTION

MESA will be a multi-turn Energy Recovery Linac (ERL) which can be operated in two different modes. An ERL Mode (105 MeV) or an External Beam (EB) Mode (155 MeV) [1]. The source will be a 100 kV dc photo gun which delivers polarized electrons with a current of 150 µA and an unpolarized electron beam with a beam current of 1 mA in stage-1 and 10 mA in stage-2. The goal is to operate in c.w.-mode which means a bunch charge ($Q_b$) of 0.8 pC in stage-1 and 8 pC in stage-2. More details on the MESA project and the current status can be found in [1–3].

The task of the diagnostic test-beam-line is to determine if the photo electron source ($PES$) can deliver a smaller normalized emittance ($\epsilon_n$) than the acceptance of the accelerator with a sufficient safety margin - for all $Q_b$ - which requires that $\epsilon_n \leq 1\,\mu m$. For the operation of MESA the source should be reliable and deliver a high extractable charge with a long lifetime.

Semiconductor photo-cathodes have some properties that should be taken into account. When excited with photon energies close to the band gap energy it is possible to create spin polarized electrons with circular polarized photons. However, when operating in this mode one suffers from low quantum efficiency ($QE$) and reduced cathode lifetime. If high currents, but no spin-polarization, are desired it is advantageous to use higher photon energies, since the $QE$ is almost an order of magnitude larger and the lifetime is longer. At around 400 nm the photo-cathodes can have a $QE$ of 10% ≙ 32 mA/W. For higher photon energies not only the $QE$ increases but also the thermal emittance does. This is because of the fact, that the stimulated electrons have not enough time to thermalize while they are traveling through the semiconductor and end up with a wider energy distribution. This additional energy spread gets transferred into larger transverse momenta which leads to a larger thermal emittance [4].

The source in the diagnostic test-beam-line has delivered 700 C [5] within one charge-lifetime at average currents exceeding 1 mA. The experiment needs average current of 1(10) mA corresponding to an extracted charge of 3.6(36) C/h. Therefore, the transmission from $PES$ to target should be as big as possible, to allow long continuous runtimes. To achieve this requirement a RF-synchronized laser must excite photo-emission. We will capture the so-produced bunches by a harmonic buncher system which can accept bunches with an extension of about 160° [6]. This leads to the requirement that the emitted intensity - which is the convolution of the temporal laser intensity profile and the response of the photo-cathode - must fit into this interval. Fractions outside the interval may be suppressed by a chopper system to provide very clean operating conditions for MESA. In the setup described here one of the circular deflecting cavities which were developed for the chopper system of MESA is used as temporal diagnostic instrument - see below.

## COMPONENTS

### *Beam Line*

A schematic overview of the beam-line setup is given in Fig. 1. In the upper left side there is the dc photo gun with a load-lock system and a potential of −100 kV. After the excitation of the electrons by laser light they are accelerated in the vertical direction. 1 m downstream of the source the first analyzing stage (scanner 1) is placed followed by an $\alpha$-magnet which bends the electrons 270° from the vertical to the horizontal direction. Between the both $\alpha$-magnets the second analyzing stage (scanner 2) is mounted. Here the evolution of $\epsilon_n$ with respect to the position of scanner 1 can be studied. If the second $\alpha$-magnet is switched off investigations of the temporal distribution ($TD$) of the electron beam can be done with a deflecting cavity [7, 8] and a Ce:YAG screen. If the second $\alpha$-magnet is switched on the electrons pass by the third analyzing stage (scanner 3) where it is possible to take a closer look to the beam halo with two perforated Ce:YAG screens. Behind scanner 3 there is a Wien-Filter for spin manipulation and a double scattering Mott polarimeter. This device is currently under test and promises to yield very precise polarization measurements [9] for the experiments (P2 [10] and MAGIX [11]) foreseen at MESA. It is, however, not relevant for the contents discussed here. All components between the source and the second $\alpha$-magnet/scanner 3 are UHV compatible and bakeable. There are focusing elements like quadrupoles (blue) and solenoids (green) as well as several steering magnets which are not shown in Fig. 1.

The laser system ($LS$) for unpolarized high average electron current is installed close to the source chamber to create a minimized beam spot on the photo-cathode.

* Work supported by the German Science Foundation (DFG) under the Cluster of Excellence PRISMA
† alexand@kph.uni-mainz.de



ISBN 978-3-95450-177-9

# TRANSVERSE BEAM SIZE DIAGNOSTICS USING BROWNIAN NANOPARTICLES AT ALBA

M. Siano*, B. Paroli, M. A. C. Potenza, Dipartimento di Fisica,
Università degli Studi di Milano and INFN Sezione di Milano, via G.Celoria ,16 ,20133 Milano ,Italy
U. Iriso, A. Nosych, L. Torino, ALBA-CELLS, Cerdanyola del Vallès, Spain
A. N. Goldblatt, S. Mazzoni, G. Trad, CERN, Geneva, Switzerland

*Abstract*

In this work we describe a novel beam diagnostic method based on coherence characterization of broad-spectrum bending magnet radiation through the Heterodyne Near Field Scattering (HNFS) technique. HNFS is a self-referencing technique based on the interference between the transmitted beam and the spherical waves scattered by each particle of a colloidal suspension. The resulting single-particle interferogram shows circular interference fringes modulated by the spatio-temporal Complex Coherence Factor (CCF) of the radiation. Superposition of a number of these patterns results in a stochastic speckle field, from which spatial and temporal coherence information can be retrieved in near field conditions. Here we describe the basics of this technique, the experimental setup mounted along the hard X-ray pinhole at the ALBA synchrotron light source, and the possibility of transverse electron beam size retrieval from the spatial coherence function of the emitted dipole radiation. We also show preliminary results concerning power spectral density of visible synchrotron radiation as obtained from temporal coherence.

## INTRODUCTION

In the ALBA storage ring, electrons are kept circulating to produce hard X-ray synchrotron radiation through bending dipoles and other insertion devices. Transverse beam size measurements are routinely performed with an X-ray pinhole camera [1], while parallel reliable measurements are provided by classical Young interferometry for visible synchrotron radiation in the Xanadu beamline [2]. A novel approach to access the full 2D coherence map and hence the 2-dimensional beam profile, also suitable for X-ray wavelengths, is given by the Heterodyne Near Field Speckle technique (HNFS) [3–5]. It has already been successfully applied to visible ($\lambda$ = 402 nm) SASE FEL radiation at SPARC_LAB, Laboratori Nazionali di Frascati [4] and to soft X-ray ($\lambda$ = 0.1 nm) undulator radiation at ESRF, Grenoble [5]. Recently [6], we have overcome monochromatic requirements and extended the technique to broadband visible radiation. The aim of this work is to describe applicability of HNFS to hard X-ray spatial and temporal coherence measurements at ALBA and to discuss the related transverse beam size diagnostics.

The paper is organized as follows: we first provide the reader with an overview of the HNFS technique and its extension to broadband radiation; then we describe the ALBA facility and the related HNFS diagnostics; we show experimental results regarding temporal coherence measurements of visible synchrotron radiation along the Xanadu beamline; finally, we collect our conclusion.

* mirko.siano@unimi.it

## HETERODYNE NEAR FIELD SPECKLE TECHNIQUE

### *Fundamentals of the Technique*

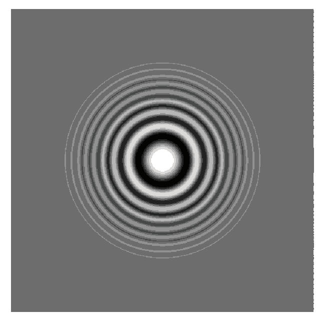

Figure 1: Single particle interferogram described by Eq. 2. Interference fringes have been modulated with a Gaussian coherence factor $e^{-2\left[(x-x_i)^2+(y-y_i)^2\right]/\sigma^2}$ with a coherence area of linear dimension $\sigma$ = 200 $\mu$m. Mesh size 500×500, parameters used for the computation are $\lambda$ = 632.8 nm, $z$ = 5mm, frame dimension 0.7 mm.

Heterodyne Near Field Scattering (HNFS) is a self-referencing interferometric technique based on the superposition of the strong transmitted incident beam ($E_0$) and the weak spherical waves scattered by each particle of a colloidal suspension ($E_s$). The resulting intensity distribution is given by [7]

$$I = |E_0 + E_s|^2 = |E_0|^2 + 2Re\{E_0^* E_s\} \quad (1)$$

where in the last equality we have neglected the term $|E_s|^2$ accounting for multiple scattering and the interference between different scattered spherical waves (heterodyne conditions). The term $2Re\{E_0^* E_s\}$ describes the superposition of many single-particle interferograms, each showing circular interference fringes of the form

$$I_i(x,y) \propto cos\left[\frac{k}{2z}\left[(x-x_i)^2+(y-y_i)^2\right]\right] \quad (2)$$

being $k = 2\pi/\lambda$, $\lambda$ the radiation wavelength, $(x, y)$ the transverse coordinates on the detection plane at a distance $z$ from



ISBN 978-3-95450-177-9

# DESIGN AND PERFORMANCE OF CORONAGRAPH FOR BEAM HALO MEASUREMENTS IN THE LHC

A. Goldblatt*, E. Bravin, F. Roncarolo, G. Trad, CERN, Geneva, Switzerland
T. Mitsuhashi, KEK, Ibaraki, Japan

*Abstract*

The CERN Large Hadron Collider is equipped with two Beam Synchrotron Radiation systems (BSR), one per beam. These systems are used to monitor the transverse distribution of the beam, its longitudinal distribution and the abort gap population. During the 2015-2016 winter shut-down period, one of the two BSR systems was equipped with a prototype beam halo monitor, based on the Lyot coronagraph, classically used in astrophysics telescopes to observe the sun's corona. The system design, as well as part of the optics, was taken from the coronagraph used in the KEK Photon Factory, adapted in order to satisfy the LHC BSR source constraints. This project is in the framework of the HL-LHC project, for which there is the requirement to monitor the beam halo at the level of $10^{-6}$ of the core intensity. This first prototype has been designed as a demonstrator system aimed at resolving a halo-core contrast in the $10^{-3}$ to $10^{-4}$ range. After illustrating the design of the LHC coronagraph and its technical implementation, this contribution presents the result of the first tests with beam and the planned system upgrades for 2017.

## PRINCIPLE OF THE CORONAGRAPH

The coronagraph is an instrument developed in the first half of 20th century by Bernard Lyot, a French astrophysicist, in order to observe the halo of the sun. A sketch of the Lyot coronagraph can be seen in Fig. 1.

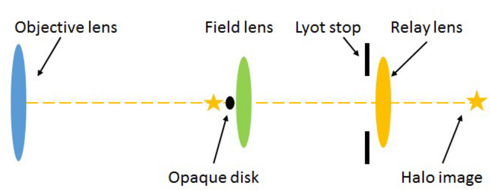


Figure 1: Sketch of the Lyot coronagraph optical layout.

A real image of the object is created by an objective lens. An opaque disk located at the image plane of this lens masks the bright core of the object in order to make the halo visible.
Such a system is however limited by the light diffracted from the limited aperture of the objective lens, which creates a diffraction pattern at the image plane, perturbing the observation of the halo.
Lyot's solution consisted of adding a field lens, which images the objective lens and thus shifts the diffraction fringes out of the center, as shown in Fig. 2.
By placing a well dimensioned aperture stop, the "Lyot stop", at the location where the diffraction fringes are re-imaged, the fringes are blocked and can't propagate to the final image plane, where the halo is observed. [1–4]
A relay lens creates the final image of the beam with a magnification suitable for the camera sensor.

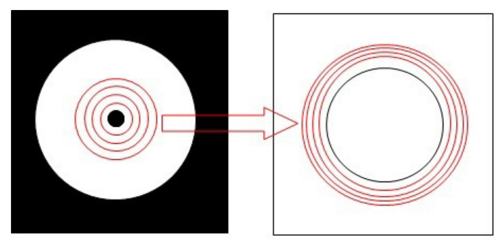

Figure 2: Sketch of diffraction pattern at the objective lens (left) and field lens (right) image planes.

The performance of the coronagraph is defined by its contrast, that is to say the ratio of the halo intensity with respect to the core intensity at image plane. It is limited by the background noise, which has mainly two sources: the first is the diffraction "leakage" to the image plane (i.e. diffraction fringes which are not blocked by the Lyot stop), which depends of the objective lens aperture, the mask size and the Lyot stop aperture. The second is Mie scattering, which is generated mainly by small particles on the optical elements located before the objective lens, and leads to a uniform increase of the background level. The Mie scattering depends on the size of the scattering particles and their distance to the objective lens. Mie scattering after the mask doesn't have a strong impact, since the light is by then strongly attenuated.
These limitations and the expected performance of the LHC coronagraph are quantified in the next section.

## LHC HALO MONITOR DESIGN

### *Layout*

The prototype beam halo monitor installed in the LHC during the winter shut down 2015-2016 is based on the same design and re-uses the optics of the Photon Factory coronagraph tested at KEK. Some modifications were introduced in order to fulfill the specific conditions of the LHC synchrotron light source and mechanical constraints. [5–7]
The coronagraph is designed to be used both at injection and top energy (450GeV and 7TeV respectively).

* Aurelie.Goldblatt@cern.ch

ISBN 978-3-95450-177-9

# SINGLE SHOT TRANSVERSAL PROFILE MONITORING OF ULTRA LOW CHARGE RELATIVISTIC ELECTRON BUNCHES AT REGAE

H. Delsim Hashemi*, DESY, Hamburg, Germany


*Abstract*

Relativistic electron microscopes are increasingly under consideration in dream experiments of observing atomic scale motions as they occur. Compared to ordinary electron microscopes that are with energies limited to few tens of keV, relativistic electrons reduce the space-charge effects strongly. This enables packing more electrons in shorter bunches and thereby capturing atomic scale ultra-fast dynamics even in a single shot. A typical relativistic-electron-microscope, based on an RF-gun, can provide experiments with couple of thousands to millions of electrons bunched in a few $\mu m$ length and a transversal dimension of a fraction of a mm. After scattering from a sample diffracted electrons are distributed over transversal dimensions typically two orders of magnitude larger. For transversal diagnostics before scattering a cost effective solution is implemented while for Diffraction Pattern (DP) detection the goal is imaging the entire pattern with single-electron imaging sensitivity and good signal to noise in single shot and keeping well depth as high as possible.


## INTRODUCTION

Beam quality demands for relativistic electron microscopy are extraordinary. To study e.g. proteins a coherence length of 30 nm is required which translates into a transverse emittance of 5 nm at a spot size of 0.4 mm. In order to study chemical reactions or phase transitions in pump-probe experiments short bunch lengths down to 10 fs and a temporal stability of the same order are required. These are challenging parameters for an electron source, which can only be reached at a low bunch charge of about 100 fC [1]. REGAE (Relativistic Electron Gun for Atomic Exploration) has been commissioned at DESY with the goal to produce electron bunches as required for electron diffraction [2]. REGAE employs a photocathode S-band RF gun that operates at high accelerating fields providing means to suppress space charge induced emittance growth. Space-charge forces that limit the density of electrons too, scale inversely with the energy of electrons squared. This explains the advantage of relativistic electrons. The draw back for scintillator base transversal diagnostics is the reduction of energy loss in a typical energy of 5 MeV. This fundamental problem makes it challenging to image relativistic-electrons. Radiation damage is another draw back with relativistic-electrons.

* hossein.delsim-hashemi@desy.de

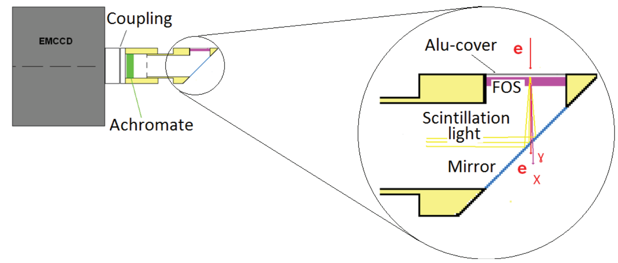


Figure 1: Schematic layout of DP-detector. Electron beam hits the 150 $\mu m$ thick CsI scintillator of FOS in normal angle and generates the scintillation light that gets coupled efficiently to the fiber optics. The image that is formed at the exit of fiber plate is reflected by a mirror towards the camera. This mirror is transparent for x-rays and energetic electrons and reflects the scintillation light to the coupling optics of the camera.

## INDIRECT DIAGNOSTICS USING SCINTILLATORS

Due to high radiation damage in the energy range of 3 to 5 MeV direct electron detection is not an option. Here scintillators can be used to make a copy of electron-beam transversal profile. Geometrically there are two ways to use a scintillator to detect the transversal distribution of electrons; transmissive and reflective. In transmissive option usually scintillator is perpendicular to the electron beam and the light generated in forward direction can be collected by a downstream mirror. This mirror can be a metal coated thin silicon wafer. Such mirror can be transparent for electrons and x-rays and reflect visible scintillation light to be coupled to a camera, see Fig. 1.

In reflective geometry, scintillator is holded with 45° to the electron-beam axis and backward scintillation light is lens coupled toward a camera. This is mainly used for diagnostics at injector part of REGAE [3].

### *Detection System Parameters*

For an electron-imaging system, $N_e$, the total number of electrons generated in one pixel can be expressed as a function of the performance characteristics of the various detection-system parameters. For a lens coupled CCD it can be written as:

$$N_e = n_e \eta\, g\, QE \tag{1}$$

where $n_e$ is the number of electrons per unit area (e.g. the area on the scintillator that is imaged to a pixel of the CCD),

ISBN 978-3-95450-177-9

# A SCINTILLATING FIBRE BEAM PROFILE MONITOR FOR THE EXPERIMENTAL AREAS OF THE SPS AT CERN

I. Ortega Ruiz*, J. Spanggaard, G. Tranquille, CERN, Geneva, Switzerland
A. Bay, G. J. Haefeli, Ecole Polytechnique Fédérale de Lausanne (EPFL), Lausanne, Switzerland

*Abstract*

The CERN Super Proton Synchrotron (SPS) delivers a wide spectrum of particle beams (hadrons, leptons and heavy ions) that can vary greatly in momentum and intensity. The profile and position of these beams are measured using particle detectors. However, the current systems show several problems that limit the quality of such monitoring. We have researched a new monitor made of scintillating fibres read-out with Silicon Photomultipliers (SiPM), which has the potential to perform better in terms of material budget, range of intensities measured and available detector size. In addition, it also has particle counting capabilities, extending its use to spectrometry or Time-Of-Flight measurements. Its radiation hardness is good to guarantee years of functioning. We have successfully tested a first prototype of this detector with different particle beams at CERN, giving accurate profile measurements over a wide range of energies and intensities. It only showed problems during operation with lead ion beams, believed to come from crosstalk between the fibres. Investigations are ongoing on alternative photodetectors, the electronics readout and solutions to the fibre crosstalk.

## INTRODUCTION

In the experimental areas of the SPS, protons are extracted during 4.8 seconds and collided with primary, secondary and sometimes tertiary targets, in order to produce beams of particles that can be selected and sent to the experimental users. These beams can be composed of hadrons (protons, kaons, pions, antiprotons...), leptons (electrons, positrons, muons...) and lead ions. Their momenta can vary greatly, from 1 to 400 GeV/Z/c, and their intensities from $10^3$ to $10^8$ particles per second. The profile and position of these beams are typically measured using Delay Wire Chambers (DWC), Multi Wire Proportional Chambers (MWPC) or Scintillator Finger Scanners (FISC). Replacement detectors for the wire chambers are actively being sought as they are ageing and the expertise to produce them is gradually being lost.

In addition, two new beam lines dedicated to neutrino R&D will be commissioned in 2017, in collaboration with Fermilab and other institutes. The monitors for these lines will form a spectrometer for particle momentum measurement and therefore need to count single particles, while covering an area of $200 \times 200\,\mathrm{mm}^2$.

* inaki.ortega@cern.ch

## SCINTILLATING FIBRES

Scintillating plastic fibres (SciFi) have emerged as one of the best active materials for the monitors of the experimental areas. They are extensively used for charged-particle tracking in high energy physics, for example in the LHCb and ATLAS ALFA experiments at CERN [1, 2].

The scintillating fibres have a core made of polystyrene cladded with one or two layers of lower refractive index material. This gradient of refractive index allows a fraction of the light created inside the fibre to be trapped by total internal reflection. The polystyrene fibre core usually employs a two level doping system: a primary scintillator emitting in the UV and a wavelength shifter to capture the short reach UV photons and re-emit them in the visible wavelength region. This shift in wavelength also enhances the match in terms of quantum efficiency for common photodetectors. The processes of energy absorption, scintillation and wavelength shifting are mediated by very fast quantum processes that yield a photon time distribution with rise time and decay time of 1-3 ns [3]. Light production typically reaches up to 8000 photons per MeV of energy deposited, although the trapping efficiency of square fibres varies between 4.2% and 7.3% [4, 5]. Depending on the amount of dopants, the light emitting properties of the fibres can be changed and their radiation hardness can be improved.

### *Radiation Hardness*

A very important characteristic of a beam monitor is its radiation hardness. The detector should be able to operate continuously and reliably for years with beams of intensities of $10^8$ particles/second or $10^6$ Pb ions/s. The radiation damage is mainly manifested as a shorter attenuation length of the fibre resulting in less light collected by the photodetectors. Data from literature shows that short fibres of less than 40 cm can withstand doses of up to 10 kGy before showing significant damage [6].

Simulations of the SciFi monitor carried out with Geant4 [7] show that for a single beam extraction of $10^8$ particles, an absorbed dose of 100 mGy can be expected per fibre. Such short fibres should therefore withstand up to $10^5$ of such beam extractions, guaranteeing several years of operation before having to be replaced.

### *Material Budget*

It is important for a beam monitor to perturb the measured beam as little as possible. A charged particle traversing a medium of thickness $x$ is deflected due to Coulomb scattering from nuclei, characterized by the radiation length $X_0$ and the nuclear interaction length $\lambda$ [8]. Comparing the

ISBN 978-3-95450-177-9

# DESIGN AND APPLICATION OF THE WIRE SCANNER FOR CADS PROTON BEAMS*

L. D. Yu†, J.S.Cao, H.P. Geng, C. Meng, Y.F. Sui,
Key Laboratory of Particle Acceleration Physics & Technology,
Institute of High Energy Physics, Chinese Academy of Sciences, Beijing 100049, China

*Abstract*

CADS Injector-I accelerator is a 10-mA 10-MeV CW proton linac, which uses a 3.2-MeV normal conducting 4-Vane RFQ and superconducting single-spoke cavities for accelerating. Seven wire scanners are designed and used to measure the beam profile of CADS Injector-I. In this paper, principal of operation, instrumentation and programming of these wire scanners are discussed. Some results of beam profile and emittance measurement with these wire scanners are also presented.

## INTRODUCTION

The ADS project in China (CADS) is a strategic plan to solve the nuclear waste problem and the resource problem for nuclear power plants in China. One of the two front end injectors—injector-I of CADS has been designed and constructed by the Institute of High Energy of Physics(IHEP) [1]. Beam diagnostic and monitoring instruments play an important role during the machine commissioning and operation. One of those instruments is wire scanner which is employed to verify the focusing lattice, verify the functionality of the steering magnets, provide data for quad scan style emittance measurements, and helped to verify beam position diagnostics. A total of 7 wire scanners have been indigenously developed. At several critical points of the injector I linac such a set of wire scanner will be installed. In this paper principal of operation, instrumentation and programming of C-ADS wire scanners are discussed. The measured results are also presented.

## WIRE SCANNER

### Instrumentation

A drawing of the CADS wire scanner is shown in Fig. 1. A 100µm diameter gold plated tungsten wire is stretched simultaneously to X, Y and U directions which is 45 degree tilted from the X direction. The wires are oriented such that when the scanner insertion axis is inclined 45 degree above the beam plane, the three wires are oriented horizontally, vertically and in the 45-degree direction. In this way a single axis of motion allows the beam to be scanned in three axes. The three wires are offset from each other so that no more than one wire at a time is within the beam centre. Figure 2 shows the picture of the wire mover stage and the vacuum chamber.

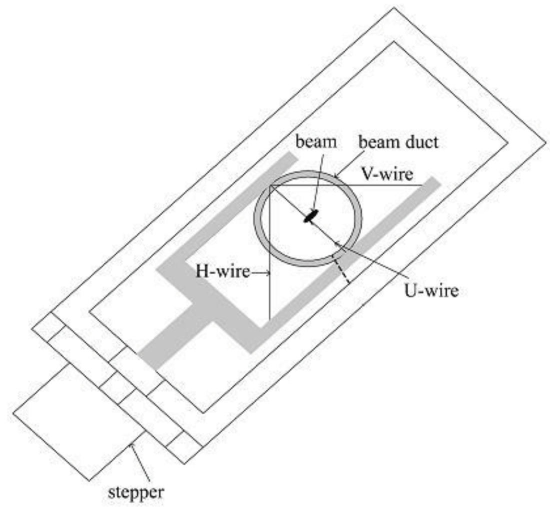


Figure 1: Schematic drawing of the wire scanner.

Figure 2: Overview system of wire scanner.

### Control System

The wire scanner in CADS is controlled through PXI control system [2]. National Instrument (NI) PXI-8115 microcontroller is used for this application. The step motor is

* Work supported by China ADS Project (XDA03020000)
† yuld@ihep.ac.cn

ISBN 978-3-95450-177-9

# SCINTILLATION AND OTR SCREEN CHARACTERIZATION WITH A 440 GeV/c PROTON BEAM IN AIR AT THE CERN HIRADMAT FACILITY

S. Burger†, B. Biskup[1], S.Mazzoni, M.Turner[2], CERN, Geneva, Switzerland
[1]also at Czech Technical University, Prague, Czech Republic
[2]also at Graz University of Technology Theoretical Physics Institute, Vienna, Austria

*Abstract*

Beam observation systems, based on charged particles passing through a light emitting screen, are widely used and often crucial for the operation of particle accelerators as well as experimental beamlines. The AWAKE [1] experiment, currently under construction at CERN, requires a detailed understanding of screen sensitivity and the associated accuracy of the beam size measurement. We present the measurement of relative light yield and screen resolution of seven different materials (Chromox, YAG, Alumina, Titanium, Aluminium, Aluminium and Silver coated Silicon). The Chromox and YAG samples were additionally measured with different thicknesses. The measurements were performed at the CERN's HiRadMat [2] test facility with 440 GeV/c protons, a beam similar to the one foreseen for AWAKE. The experiment was performed in an air environment.

## INTRODUCTION

The accelerators at CERN use more than 250 beam instruments based on scintillation and/or Optical Transition Radiation (OTR) screens. Even though the emission of scintillation and OTR light is very well understood, comparative measurements of commonly used screen types are hard to find.

We tested 13 typical screen materials (see Table 1 and Fig. 1) in the HiRadMat [2] test facility. We used a 440 GeV/c proton bunch from the CERN SPS populated with $10^{11}$ protons with a radial proton beam size of $\sigma = 2$ mm.

## EXPERIMENTAL SETUP

### *Layout*

Figure 2 shows a 3D model of the experimental setup. A linear stage with a stepper motor is used to select screens. The screens are positioned at 45 degrees with respect to the incoming beam. A mirror reflects the light emitted by the screens to a CCD camera (WATEC 902H3) equipped with a 25 mm focal length camera lens. This optical line gives calibration values of ~100µm/pixel in both the horizontal and vertical planes.

Two rotatable optical filter wheels are placed in front of the camera lens to, if necessary, reduce the light transmission from 100% down to 0.00001% in 14 steps.

A second linear translation stage is available to move an aluminium foil of 100µm thickness in front of the screen to prevent any light created upstream from reaching the camera. Additionally, we surrounded the setup with a blackened metal box that has two openings for the entrance and exit of the beam. The presence of a beam dump located approximately 10 meters downstream our setup resulted in an elevated background noise on the camera image due to backscattering.

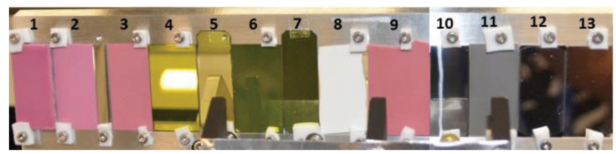


Figure 1: Image of the screen material samples mounted on the screen holder.

Table 1: Material Samples Shown in Figure 1

| Screen Nr. | Material | Thickness [mm] | Supplier |
|---|---|---|---|
| 1 | Chromox ($Al_2O_3$:$CrO_2$) | 3.0 | *CeraQUest* |
| 2 | Chromox ($Al_2O_3$:$CrO_2$) | 1.0 | *CeraQuest* |
| 3 | Chromox ($Al_2O_3$:$CrO_2$) | 0.5 | *CERN stock* |
| 4 | YAG (YAG:Ce) | 0.5 | *Crytur* |
| 5 | YAG (YAG:Ce) | 0.1 | *Crytur* |
| 6 | YAG back-coated (YAG:Ce + Al) | 0.5 | *Crytur* |
| 7 | YAG back-coated (YAG:Ce + Al) | 0.1 | *Crytur* |
| 8 | Alumina (99% purity) | 1.0 | *GoodFellow* |
| 9 | Chromox-old type ($Al_2O_3$:$CrO_2$) | 1.0 | *CERN stock* |
| 10 | Aluminium | 1.0 | *CERN stock* |
| 11 | Titanium | 0.1 | *GoodFellow* |
| 12 | Aluminium coated Silicon | 0.25 | *MicroFabSolutions* |
| 13 | Silver coated Silicon | 0.3 | *Sil'Tronix* |

### *Control and Acquisition*

The measurement setup is controlled via VME based modules. The control of the filter wheels, light for calibration and the image acquisition are made through the standard CERN beam observation electronics [3].

We used an analogue camera that is not synchronized with the proton beam. The camera triggers every 20ms and integrates over a 20ms period. The acquisition is performed by capturing the image in the acquisition board on ever vertical sync. from the video signal (i.e. each 20ms).

† stephane.burger@cern.ch



ISBN 978-3-95450-177-9

# SCINTILLATING SCREENS INVESTIGATIONS WITH PROTON BEAMS AT 30 keV AND 3 MeV

C. Simon*, F. Harrault, F. Senee, O. Tuske, CEA-Saclay/DRF/Irfu, Gif sur Yvette, France
E. Bordas, F. Leprêtre, Y. Serruys, CEA-Saclay/DEN, Gif sur Yvette, France
P. Ausset, INPO, Orsay, France
J. Fils, GSI, Darmstadt Germany

*Abstract*

Luminescent screens hit by accelerated charged particle beams are commonly used as beam diagnostics to produce a visible emitted light, which can be sensed by a camera. In order to investigate the characteristics of the luminescence response of several scintillators, the beam shape and the observation of the transverse position, experiments were done with different low intensity proton beams produced by two different test benches.

This study is motivated by the need to identify scintillator materials for the development of a 4-dimensional emittancemeter which will allow the characterization of the beams, in particular the emittance measurement (size, angular divergence).

This paper describes the experimental setups and our investigations of the optical properties of various scintillating materials at two different proton beam energies respectively about 30 keV and 3 MeV. The light produced by these screens is characterized by yield, flux of the emitted light versus the beam intensity, time response, and long life-time and they are compared.

## INTRODUCTION

The characterization of the beams, in particular the emittance measurement (size, angular divergence) is a key point, both in the understanding of physical phenomena involved, such as space charge compensation, interaction with the residual gas, interaction with solid interfaces, or the dynamics of plasma ion sources, as in the validation of accelerators design.

As part of collaboration with the IPNO, a 4 Dimensions Emittancemeter (EMIT4D) [1] is under development. It will provide, in a single measurement, the beam distribution in the transverse 4-dimensional phase space (X, X', Y, Y'), characterizing the beam with a high accuracy.

The principle of this instrument is simple. A screen drilled with 2D series of holes of very small diameter (called pepper-pot) intercepts the beam. It samples a grid of transverse beam positions. The particles passing through the holes will strike further a scintillator screen that emits light radiation. Physical properties of the original beam are reconstructed through the analysis of this radiation, collected by a dedicated video system (like a digital camera).

As part of this project, some measurements were done with several scintillators at two different proton beam energies respectively about 30 keV and 3 MeV in order to study the properties of each scintillator and determine which one could be used with beam intensity from 0.1 µA to 5 µA and energy from few 10 keV up to few MeV.

* claire.simon@cea.fr

## SCINTILLATORS

The scintillators selection is based on the materials available and on use as diagnostics in proton beam production. Scintillation screens under study, like crystals, powder screens, and ceramics, are presented in Table 1. The "powder" scintillators have been provided by the CEA DAM except the $BaF_2$ provided by GSI. The thickness of the powder layer is also specified. Crystal scintillators YAG:Ce were bought at Crytur [2], BGO and Prelude 420 at St Gobain [3].

Table 1: List of Scintillators Under Study

| Name Composition | Density g/cm$^3$ | Light yield (photons/keV) | Thickness (mm) |
|---|---|---|---|
| P22 $Y_2O_2S$:Eu | | 45 | 0.008 |
| P46 $Y_3AlO_{12}:Ce^{3+}$ | 4.5 | 6 | 0.008 |
| P31 ZnS:Cu | 4.09 | 130 | 0.01 |
| $BaF_2$ | 4.88 | 10 | |
| BGO | 7.13 | 8-10 | 0.25 |
| YAG:Ce | 4.5 | 16.7 | 0.25 & 1 |
| Prelude420 $Lu_{1.8}Y_2Si0_5$:Ce | 7.1 | 32 | 0.25 |
| $Al_2O_3$:Cr | 3.63 | 0.367 | 5 |

## EXPERIENCE SETUPS

The measurements were done on two experimental setups at two different proton beam energies respectively about 30 keV and 3 MeV. The width of the beam spots was about 1 mm and the beam current was not higher than 5 µA in both cases.

### *Low Energy Proton-Beam Production*

The proton beam is produced by the ALISES 2 ion source developed at the CEA Saclay [4]. This ion source prototype delivers a pulsed beam of protons up to 34 mA at 40 keV of extraction energy. The extracted beam is transported to the diagnostic chamber, through the BETSI beam line [5] like shown Fig. 1.



ISBN 978-3-95450-177-9

# A NEW BEAM LOSS MONITOR CONCEPT BASED ON FAST NEUTRON DETECTION AND VERY LOW PHOTON SENSITIVITY

J. Marroncle*, A. Delbart, D. Desforge, C. Lahonde-Hamdoun, P. Legou, T. Papaevangelou, L. Segui, G. Tsiledakis, CEA Saclay, DRF/DSM/IRFU, Gif sur Yvette, France

*Abstract*

Superconductive accelerators may emit X-rays and Gammas mainly due to high electric fields applied on the superconductive cavity surfaces. Indeed, electron emissions will generate photons when electrons impinge on some material. Their energies depend on electron energies, which can be strongly increased by the cavity radio frequency power when it is phase-correlated with the electrons.

Such photons present a real problem for Beam Loss Monitor (BLM) systems since no discrimination can be made between cavity contributions and beam loss contributions. Therefore, a new BLM is proposed which is based on gaseous Micromegas detectors, highly sensitive to fast neutrons, not to thermal ones and mostly insensitive to X-rays and Gammas. This detector uses Polyethylene for neutron moderation and the detection is achieved using a $^{10}B$ or $^{10}B_4C$ converter film with a micromegas gaseous amplification. Simulations show that detection efficiencies > 8 % are achievable for neutrons with energies between 1 eV and 10 MeV.

## INTRODUCTION

This paper deals with the design of a new Beam Loss Monitor based on Micromegas detectors devoted to fast neutron detection.

We will present, firstly, the motivation to develop this new BLM followed by a brief Micromegas working principle description. Then, simulation results will be presented to confirm that all the specifications are fulfilled, which mainly are fast neutron detection with a good efficiency, but very low sensitivity to thermal neutrons as well as to X-rays and γ's. Time response has been investigated to finally propose the addition of a faster monitor for safety purposes. The R&D program will be briefly discussed before to conclude.

## WHY NEW BEAM LOSS MONITORS?

The idea to develop a new kind of BLM was triggered by the construction of new powerful accelerators as ESS for instance. Beam line part of them uses superconductive technology, where their accelerating cavity surfaces are submitted to very huge electric fields. These later release electrons from time to time which are accelerated under the RF electric fields covering an energy spectrum up to few MeV. When these electrons impinge on material, they may generate important photon fluxes with energy range from X-Rays to γ's. These phenomena concern also the RFQ, but at lower energy. Such photons, emitted at the lowest beam energy, contribute particularly as background to the external BLM, since the beam loss signal comes only from neutral particles (neutrons and photons) which are the only ones able to escape from the beam pipes or structures. Therefore, photon-sensitive BLMs may deliver signals which are not correlated to beam losses, but to cavity behaviours. As we can't discriminate between photons coming from beam losses or cavities, we propose a BLM blind to photon contributions. Note that it is less dramatic for higher beam energy where lost particles may have higher energy, producing numerous hadronic by-products which can be efficiently detected by usual BLM like ion chambers.

Another important criterion for BLM is the ability to locate the beam losses. It may be achieved with neutrons, but only with fast neutrons. Indeed, neutrons may be thermalized in the accelerator, particularly on the concrete wall. They will be detected after few rebounds, far from their emission locations.

To summarize, the requirements for BLM used on superconductive accelerator, especially for those working at low beam energy, are the following:

- Fast neutron detection, insensitive to thermalized ones
- Blind to X-rays and gammas.

We propose to design such a BLM, called neutron BLM (nBLM), based on Micromegas detectors [1].

## MICROMEGAS WORKING PRINCIPLE

Micromegas detectors were invented at CEA Saclay in 1995 [2] and have been submitted, since their births, to a lot of improvements, modifications to fulfil new specifications and detection schemes. Micromegas is a Micro-Pattern Gaseous Detector (MPGD) as sketched on Fig. 1.

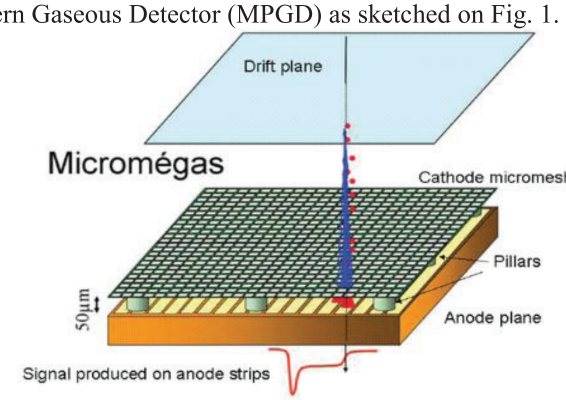


Figure 1: Micromegas scheme.

* Jacques.marroncle@cea.fr

ISBN 978-3-95450-177-9

# BEAM LOSS AND ABORT DIAGNOSTICS DURING SuperKEKB PHASE-I OPERATION

H. Ikeda*, J. W. Flanagan, H. Fukuma, T. Furuya and T. Tobiyama, KEK, High Energy Accelerator Research Organization, Ibaraki 305-0801, Japan

*Abstract*

Beam commissioning of SuperKEKB Phase-I started in Feb., 2016. In order to protect the hardware components of the accelerator against the Ampere class beams, the controlled beam abort system was installed Because of the higher beam intensity and shorter beam lifetime of SuperKEKB than that of KEKB, a beam abort monitor system was prepared aiming to monitor the machine operation and to diagnose the hardware components. The system collected the data of all aborts, totalling more than 1000 in this operation period, and we diagnosed not only the hardware performance but the tuning software by analysing the relations between beam current, loss monitor signals and RF cavity voltages. This paper will give the outline of the monitoring system, and will present typical examples of signal and diagnoses.

Table 1: Machine Parameters of SuperKEKB

| Parameter | LER | HER | DR | unit |
|---|---|---|---|---|
| Energy | 4.0 | 7.0 | 1.1 | GeV |
| No. of bunches | 2500 | | 4 | |
| Circumference | 3016 | | 135.5 | m |
| Max. stored current | 3.6 | 2.6 | 0.07 | A |
| Emittance (h) | 3.2 | 4.6 | 42.5 | nm |
| Emittance (v) | 8.64 | 12.9 | 3150 | pm |
| Bunch length | 6.0 | 5.0 | 6.53 | mm |
| $\beta x/\beta y$ at IP | 32/0.27 | 25/0.30 | | mm |
| Luminosity | $8 \times 10^{35}$ | | | $cm^{-2}s^{-1}$ |
| RF frequency | | 509 | | MHz |

## INTRODUCTION

SuperKEKB [1] is an electron-positron collider with a design luminosity of $8 \times 10^{35}$ $cm^{-2}s^{-1}$. The beam size at the interaction point (IP) will be squeezed to the nm level and the beam currents will be 2.6 A and 3.6 A for electrons and positrons, respectively, to achieve the design luminosity. The machine parameters of SuperKEKB are listed in Table 1.

High current beams may cause damage to sensitive detector and accelerator components. In KEKB, we had several problems and needed to improve the system each time. For example, an IP chamber was melted by strong synchrotron radiation, some collimators were damaged by high intensity beam, and imperfect beam dumps due to the wrong abort timing were observed. The collimators were upgraded and the abort system was improved using fast loss monitor and beam phase signal etc. It is important to check all accelerator systems before installation of the detector for higher current operation. We operated the accelerator without the Belle detector for five months in Phase-I.

## ABORT AND ABORT MONITOR SYSTEM

In order to protect the hardware components of the detector and the accelerator against the high beam currents, we installed the controlled abort system. The abort monitor system was prepared also for diagnosing and optimizing the abort system.

### *Abort Kicker and Trigger System*

The beam abort kicker is composed of a tapered vertical magnet, a horizontal magnet, a Lambertson DC septum magnet, and additional pulsed quadrupole magnets for LER and a sextupole magnet for HER to increase the beam cross-section to avoid damaging the extraction widow [2]. The dump duration corresponds to one revolution time, i.e. 10 μsec. The beam is distributed in every two RF buckets with an empty bucket space of 200 ns which covers build-up time of the abort kicker magnet. It is also required to synchronize the kicker timing with this abort gap for the protection of hardware. This abort trigger system collects four types of abort trigger requests [3].

1. Direct trigger from hardware components such as RF, vacuum, magnet and monitor.
2. Trigger from loss monitor.
3. Trigger from synchrotron oscillation phase.
4. Manual abort which is requested for machine stop and various studies.

The abort request signals from each hardware component are converted to optical signals and collected to VME modules in 12 local control rooms (LCR). The request signals from LCRs, software abort request signals, and manual abort request signals are collected in the central control room (CCR) and sent to the abort kicker within 20 μsec.

### *Abort Monitor System*

Our monitoring system consists of four data loggers. The SuperKEKB ring circumference is 3 km with 12 LCRs as shown in Fig. 1. Loss monitor signals are collected at 4 LCRs, RF signals are collected at 6 LCRs and the data loggers are located in 4 LCRs. Collected signals include beam current measured by a DCCT, beam loss signals from PIN photo-diodes (PINs) and ion chambers (ICs), signals from the RF cavities, i.e. cavity voltages and output power of klystrons, the beam phase signal showing the deviation from the synchronous phase, the injection trigger timing and the abort request signal.

* hitomi.ikeda@kek.jp

# SYNCHRONOUS LASER-MICROWAVE NETWORK FOR ATTOSECOND-RESOLUTION PHOTON SCIENCE

K. Şafak†, F. X. Kärtner[1], A. Kalaydzhyan, O.D. Mücke, W. Wang, M. Xin[1]
CFEL - DESY, Hamburg, Germany
M. Y. Peng, MIT, Cambridge, Massachusetts, USA
[1]also at MIT, Cambridge, Massachusetts, USA

*Abstract*

Next-generation photon-science facilities such as X-ray free-electron lasers and intense-laser beamline centers are emerging worldwide with the goal of generating sub-fs X-ray pulses with unprecedented brightness to capture ultrafast chemical and physical phenomena with sub-atomic spatiotemporal resolution. A major obstacle preventing this long-standing scientific dream to come true is a high precision timing distribution system synchronizing various microwave and optical sub-sources across multi-km distances. Here, we present, for the first time, a synchronous laser-microwave network providing a timing precision in the attosecond regime. By developing new ultrafast timing detectors and carefully balancing optical fiber nonlinearities, we achieve timing stabilization of a 4.7-km fiber link network with 580-attosecond precision over 52 h. Furthermore, we realize a complete laser-microwave network incorporating two mode-locked lasers and one microwave source with total 950-attosecond jitter integrated from 1 μs to 18 h.

## INTRODUCTION

Drift-free and long-distance transfer of time and frequency standards provides high-temporal resolution for ambitious large-scale, scientific explorations. To name a few: sensitive imaging of low temperature black bodies using multi telescope arrays [1]; gravitational deflection measurements of radio waves using very-long-baseline interferometry [2]; synchrotron light sources [3], gravitational-wave detection using large laser interferometers [4], and next-generation photon science facilities such as X-ray free-electron lasers (XFELs) [5] and laser-based attoscience centers [6]. Among these, XFELs and attoscience centers demand the most challenging synchronization requirements with sub-femtosecond precision to generate ultrashort X-ray pulses for the benefit of creating super microscopes with subatomic spatiotemporal resolution [7]. To achieve this, it is necessary to develop an attosecond-precision timing distribution system (TDS) to synchronize various microwave and optical sub-sources across the km-scale facilities to deliver the timing stability required for seeded FEL operation and attosecond pump-probe measurements.

So far, there has been no TDS meeting this strict requirement. Although research in attosecond X-ray pulse generation has progressed rapidly in the past few years [8], sub-atomic-level measurements cannot be performed due to the lack of a high-precision timing control. Hence, low temporal precision provided by the current synchronization systems remains to be a major obstacle from realizing attosecond hard-X-ray photon-science facilities.

There are two general synchronization schemes reported so far. The first scheme uses microwave signal distribution via amplitude modulation of a continuous-wave laser and employs electronic phase-locking techniques to synchronize various microwave and pulsed laser sources [9]. However, this technique cannot deliver better than ~100-fs RMS jitter across the facility [10] due to low phase discrimination with microwave mixers and high noise floor at photodetection. The second scheme [11], which is further developed in this paper, uses ultralow-noise pulses generated by a mode-locked laser as its timing signal to synchronize optical and microwave sources using balanced optical cross correlators (BOCs) [12,13] and balanced optical-microwave phase detectors (BOMPDs) [14,15], respectively. While this pulsed scheme has breached the 10-fs precision level [15-18], realization of sub-femtosecond precision requires further development of the timing detectors (i.e., BOCs and BOMPDs) and deep physical understanding of optical pulses shaping in fiber transmission.

This paper starts with the recent developments achieved in timing detection schemes, and then demonstrates the synchronous laser-microwave network delivering attosecond precision.

## TIMING DETECTORS

The primary elements to realize a high precision TDS are the timing detectors as they dictate the smallest timing errors to be detected by the system.

### *Polarization-noise-suppression in SH-BOCs*

Second-harmonic BOC (SH-BOC) (see Figure 1(a)) operating with 1550-nm input pulses is the most widely used timing detector in our system employed to stabilize the transmission delays of our fiber based timing links.

In this SH-BOC scheme, a polarization beam splitter (PBS) spatially combines two orthogonally polarized pulse trains at 1550-nm central wavelength. The input pulses travel in a double-pass configuration inside a periodically poled potassium titanyl phosphate (PPKTP) crystal. The end facet of the crystal has a dichroic coating (DC), which is highly reflective for 1550 nm and anti-reflective for 775 nm wavelength. In this way, the SH pulse generated during the forward pass of the fundamen-

† kemal.shafak@desy.de



ISBN 978-3-95450-177-9

# ELECTRO-OPTICAL METHODS FOR MULTIPURPOSE DIAGNOSTICS

R. Pompili*, M.P. Anania, M. Bellaveglia, F. Bisesto, E. Chiadroni, A. Curcio, D. Di Giovenale
G. Di Pirro, M. Ferrario, Laboratori Nazionali di Frascati, 00044 Frascati, Italy
A. Cianchi, University of Rome Tor Vergata, 00133 Rome, Italy
A. Zigler, Racah Institute of Physics, Hebrew University, 91904 Jerusalem, Israel

*Abstract*

Electro-Optical Sampling (EOS) based temporal diagnostics allows to precisely measure the temporal profile of electron bunches with resolution of few tens of fs in a non-destructive and single-shot way. At SPARC_LAB we adopted the EOS in very different experimental fields. We measured for the first time the longitudinal profile of a train of multiple bunches at THz repetition rate, as the ones required for resonant Plasma Wakefield Acceleration (PWFA). By means of the EOS we demostrated a new hybrid compression scheme that is able to provide ultra-short bunches (< 90 fs) with ultra-low (< 20 fs) timing-jitter relative to the EOS laser system. Recently we also developed an EOS system in order to provide temporal and energy measurements in a very noisy and harsh environment: the electrons ejected by the interaction of a high-intensity (hundreds TW class) ultra-short(35 fs) laser pulses with solid targets by means of the so-called Target Normal Sheath Acceleration (TNSA) method.

## INTRODUCTION

The research activity of the SPARC_LAB test-facility [1] (LNF-INFN, Frascati) is currently focused on advanced acceleration techniques for electrons, protons and heavier ions. The demand to accelerate particles to higher and higher energies is currently limited by the effective efficiency in the acceleration process that requires the development of large facilities. By increasing the accelerating gradient, the compactness can be improved and costs reduced.

For the acceleration of electrons, the technique that guarantees gradients of the order of GV/m relies on plasma acceleration [2, 3]. In this case a *driver* pulse, consisting in an electron bunch (Plasma Wakefield Acceleration, PWFA) or a laser pulse (Laser Wakefield Acceleration, LWFA), excites a wakefield in a plasma. Such wakefield is then used in order to accelerate electron coming directly from plasma (so-called self-injection schemes [4–6]) or a subsequent *witness* bunch, externally injected by a linac [7, 8]. Both in the particle and laser driven schemes, ultra-short bunches are required in order to produce larger wakefields and avoid an excessive growth of emittance and energy spread. In the latter one, in particular, a very demanding task is represented by the synchronization between the laser and the witness bunch, that requires relative timing-jitters of the order of few femtoseconds [7].

In the field of protons and ions acceleration, energies in multi-MeV range have been obtained in the past decade by means of the so-called Target Normal Sheath Acceleration (TNSA) method [9–11], in which an high-intensity short-pulse laser interacts with solid targets. The typical timescale for particle emission is on the sub-picosecond level but so far no direct and time-resolved measurement was able to determine the exact mechanism of the acceleration process and cross-check the developed theoretical models [12].

From the previous considerations it follows that precise time-resolved measurements with sub-picosecond resolution are of great interest for different aspects of particle acceleration. In the following we report about the use of electro-optic methods in such fields, showing that it represents a valuable tool for a deeper understanding of the physical processes involved.

## TEMPORAL MEASUREMENT FOR TRAINS OF ELECTRON BUNCHES

The Electro-Optical Sampling (EOS [13]) is a temporal diagnostics that allows to measure the bunch longitudinal charge distribution by means of nonlinear crystals like ZnTe and GaP. Being a single-shot and non-intercepting device able to provide temporal resolution of the order of few tens of fs [14, 15], it is widely used in accelerator facilities [16–19]. Its working principle relies on the electro-optic (or Pockels) effect induced in such crystals by the Coulomb field generated by a relativistic bunch. The crystal becomes birefringent, i.e. characterized by two refractive indices $n_{1,2}$ along its principal optical axes. If at the same time a linearly polarized laser crosses the crystal, the crystal birefringence makes its polarization elliptical, i.e. the two orthogonal components of the laser electric field cumulate a relative phase delay given by

$$\Gamma(t) = \frac{\omega_L d}{c}(n_1 - n_2) \propto E_b(t)\,, \qquad (1)$$

where $\omega_L$ is the laser central frequency and $d$ is the crystal thickness. From eq. 1 it follows that the bunch temporal profile $E_b(t)$ is imprinted on the phase delay $\Gamma(t)$.

At SPARC-LAB facility we used Ti:Sa IR laser ($\lambda$ = 800 nm, 70 fs rms pulse duration) in order to measure the longitudinal profile of a 110 MeV comb-like electron beam [20] consisting in two consecutive bunches of 80 pC delayed by 800 fs. The laser is directly derived from the photo-cathode laser system, resulting in a natural synchronization with the electron beam. The bunch longitudinal profile is retrieved by means of the spatially encoding technique [18], in which the laser crosses the nonlinear crystal with an angle of 30°.

Fig. 1(a) shows an electro-optic signal measured by using a 100 $\mu m$-thick GaP crystal. By projecting the signal along

* riccardo.pompili@lnf.infn.it



ISBN 978-3-95450-177-9

# NOVEL ACCELERATOR PHYSICS MEASUREMENTS ENABLED BY NSLS-II RF BPM RECEIVERS*

Boris Podobedov#, Weixing Cheng, Yoshiteru Hidaka, Brookhaven National Laboratory, Upton, NY 11973, USA
Dmitry Teytelman, Dimtel Inc., San Jose, CA 95124, USA


*Abstract*

NSLS-II light source has state-of-the-art RF BPM receivers that were designed and built in-house incorporating the latest technology available in the RF, digital, and software domains. The recently added capability to resolve the orbits of multiple bunches within a turn as well as further improvement in transverse positional resolution for single- and few-bunch fills [1] allowed us to perform a number of novel beam dynamics measurements. These include measuring small impedances of vacuum chamber components, and of extremely small (~1e-5) current-dependent tune shifts, as well as obtaining an amplitude-dependent tune shift curve from a single kicker pulse.

In this paper we briefly review the unique capabilities of NSLS-II BPMs and present examples of beam physics measurements that greatly benefit from them.


## INTRODUCTION

NSLS-II is a recently constructed 3 GeV synchrotron light source at the Brookhaven National Laboratory presently in routine operations for a growing user community. By design, the vertical beam size at NSLS-II could be as low as 3 microns RMS, so a very significant effort went into ensuring that orbit stability is guaranteed to be a small fraction of that. To that extent state-of-the-art RF BPM receivers were designed and built in-house [2-8]. Among many challenging BPM specifications the key ones are related to the resolution and long term stability. The BPMs were commissioned some time ago and all of the design specifications have been confirmed with beam. Reaching turn-by-turn (TbT) resolution of 1 µm and 200 nm for 10 kHz sampled orbit was reported in [4], for measurements with long bunch trains (NSLS-II user operations typically run with ~1000 bunches filling consecutive 500 MHz RF buckets; harmonic number is 1320).

However, with the standard BPM signal processing the resolution for single bunch fills is a lot lower, i.e. ~10 µm TbT at 0.5 mA [4]. Also, standard processing does not resolve the positions of individual bunches within a turn. Since better single-bunch resolution as well as the ability to measure TbT positions of at least a few bunches stored in the ring is strongly desired for some sensitive beam dynamics experiments we have recently addressed both of these issues by special BPM signal processing [1].

Briefly, intra-turn capability was achieved by separately processing fractions of BPM button ADC samples acquired on every turn, with each fraction timed to the bunch of interest. This also provided some resolution improvement for single- and few-bunch fills. Additionally resolution was improved by including multiple revolution harmonics in the TbT position calculation. With this new BPM signal processing we can resolve up to 8 bunches stored in the ring, essentially limited by the bandwidth of the BPM front-end filter that stretches the FWHM duration of a single bunch pulse to ~20 ADC samples out of the total of 310 acquired every turn. The resolution improvement for single bunch fills was about one order of magnitude, down to ~1 µm TbT at 0.5 mA.

* Work supported by DOE contract DE-AC02-98CH10886.
# boris@bnl.gov

## BEAM PHYSICS MEASUREMENTS

The ability to resolve multiple bunches within a turn combined with improved BPM resolution allowed us to carry out a number of novel beam physics measurements. Here we concentrate on the measurements of small relative tune shifts and the related ones for transverse coupling impedances. More are described in the accompanying IBIC'16 talk and in [1].

### *Small Relative Tune Shifts*

The standard way of measuring betatron tunes is by exciting the beam with a pinger magnet. At NSLS-II this measurement is usually done with a short, low current bunch train, typically 1-2 mA in 100 consecutive buckets. TbT positions are recorded on 180 regular RF BPMs around the ring. The data from each BPM is processed individually to obtain 180 tune values. Their average gives the final measured tune while their RMS spread provides the measurement error. If a large number of turns is processed, we typically find that, for each individual measurement, the final tune value could be resolved to better than 1e-6.

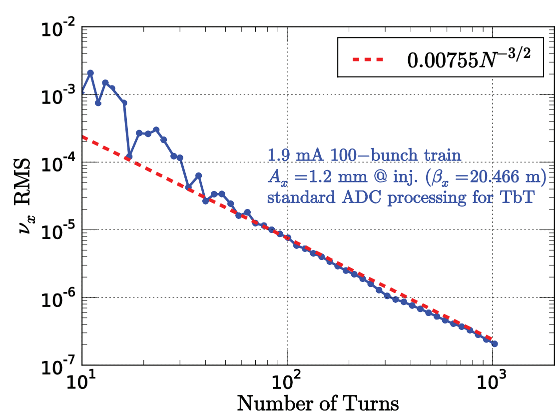


Figure 1: RMS of horizontal tune vs. number of turns.



ISBN 978-3-95450-177-9

# MEASUREMENTS OF LONGITUDINAL COUPLED BUNCH INSTABILITIES AND STATUS OF NEW FEEDBACK SYSTEM

G. Rehm*, M.G. Abbott, A.F.D. Morgan, Diamond Light Source, Oxfordshire, UK

*Abstract*

We have modified the vertical bunch-by-bunch feedback at Diamond Light Source to also provide a longitudinal kick on a separate input. Using our existing drive/damp system and a modulator/amplifier to the required 1.5 GHz we are thus able to characterise the damping rates of all coupled bunch instabilities, while not able to provide feedback. At the same time, we have started the development of a completely new longitudinal feedback system based on commercially available components, providing 500 MS/s, 14 bit conversion in and 16 bit out, powerful Virtex 7 field programmable gate array for digital signal processing and 2 GB of on board buffer for recording data. We report on the status of the development and our plans to bring the new system into use.

## INTRODUCTION

At Diamond we have been working on *transverse* Bunch-by-Bunch Feedbacks (BBFB) for nearly a decade [1–4], and have concluded an major upgrade of the Digital Signal Processing (DSP) in firmware and software in 2014 [5–7] providing unique capabilities. So naturally, when asked to provide a *longitudinal* BBFB system to deal with potential Coupled Bunch Instabilities (CBI) introduced by Higher Order Modes (HOM) of a pair of normal conducting Radio Frequency (RF) cavities which will be installed at Diamond in summer 2017, we preferred to build one ourselves rather than opt for a commercial solution. However, our existing system is built around the *Libera Bunch-by-Bunch Processor* (LBBB) [8,9] which is unfortunately no longer available due to obsolescence of its components. Even if we had spares available in house, it did not appear prudent to build a new system based on 10 year old obsolete electronics, so we searched for an alternative.

After several discussions with potential suppliers we found the best option for us is to put together a system using modular commercially available Printed Circuit Board (PCB) components. We found this to be the better solution compared to having a dedicated PCB designed, as it avoids hardware development and the associated costs, and offers a path to a potential multitude of applications by re-using modular parts of the whole system.

At the same time, we thought what tests we could do before we would install the longitudinal kicker cavity, with its own lengthy development and manufacturing [10, 11]. We concluded that we could use a spare LBBB to provide drive signals and analysis of longitudinal CBI, which we would excite using the parasitic *longitudinal* coupling impedance of a pair of vertical kicker striplines driven in common

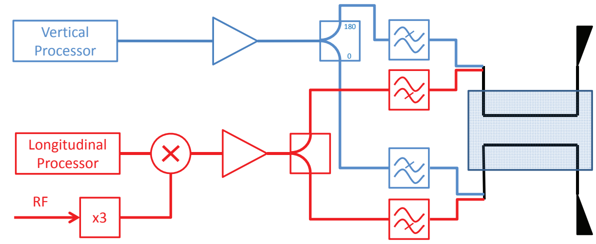


Figure 1: Block diagram of the connections of vertical and longitudinal BBFB to the vertical kicker stripline.

mode (as opposed for the vertical kick which is achieved by driving the pair in differential mode).

Consequently, the first part of the paper will concern the measurement setup and results for longitudinal CBI made so far using the vertical striplines, while the second part will summarise the status of our development of a new feedback processor.

## LONGITUDINAL CBI MEASUREMENT

In search of providing longitudinal kicks with a bandwidth of 250 MHz without the dedicated longitudinal kicker installed, we found that the vertical striplines used as part of the transverse BBFB do provide a coupling as well. This coupling impedance scales with $\sin(\omega l/c)$ where $l$ is length of the striplines (280 mm in our case) [12]. From this we select to excite the 250 MHz bandwidth below $3 f_{RF} \approx$1.5 GHz, which provides a strongly varying though always non-zero impedance.

The block diagram in Fig. 1 illustrates how we manage to continue to provide vertical BBFB while at the same time exciting longitudinal oscillations. The output for the vertical is amplified (at baseband 0-250 MHz) then fed through a 180° splitter to differentially drive the striplines. On the other side, the output for the longitudinal is up-converted to 1.5 GHz, then amplified and fed through a 0° power splitter to the striplines. Both signals are combined using a pair of diplexers with a cross over frequency of 1 GHz, thus allowing concurrent action in both planes.

We then apply a method of 'drive-damp' experiments described in more detail elsewhere [13] using a spare LBBB, with the only difference that on the longitudinal system we are driving at frequencies $\omega = (pM + \mu)\omega_0 + \omega_S$ with $p = 3$ (third RF harmonic), $M = 936$ our harmonic number, $\mu = 0, 1, \ldots, 935$ the scanned modes, $\omega_0$ our revolution frequency and $\omega_S \approx 2\pi \cdot 2$ kHz our synchrotron frequency.

Part of the analysis of CBI is already done in the FPGA as part of our DSP code implemented in the LBBB [6]. We are measuring the complex amplitude of the driven mode

* guenther.rehm@diamond.ac.uk



ISBN 978-3-95450-177-9

# BEAM BASED CALIBRATION OF A ROGOWSKI COIL USED AS A HORIZONTAL AND VERTICAL BEAM POSITION MONITOR

F. Trinkel*, F. Hinder, D. Shergelashvili, IKP, Forschungszentrum Jülich, 52425 Jülich, Germany, RWTH Aachen, 52062 Aachen, Germany
H. Soltner, ZEA-1, Forschungszentrum Jülich, 52425 Jülich, Germany
for the JEDI collaboration†

*Abstract*

Electric Dipole Moments (EDMs) violate parity and time reversal symmetries. Assuming the CPT-theorem, this is equivalent to CP violation, which is needed to explain the matter-over-antimatter dominance in the universe. The goal of the JEDI collaboration (Jülich Electric Dipole moment Investigations) is to measure the EDM of charged hadrons ($p$ and $d$). Such measurements can be performed in storage rings by observing a polarization build-up, which is proportional to the EDM. Due to the smallness of this effect many systematic effects leading to a fake build-up have to be studied. A first step on the way towards this EDM measurements is the investigation of systematic errors at the storage ring COSY (COoler SYnchrotron) at Forschungszentrum Jülich. One part of these studies is the control of the beam orbit with high precision. Therefore a concept of Beam Position Monitors (BPMs) based on pick-up coils is used. The main advantage of the coil design compared to electric-pick-up BPMs is the stronger response to the bunched-beam frequency and the compactness of the coil itself. A single Rogowski BPM measures the beam position in horizontal and vertical direction. Results of such a BPM in an accelerator environment are presented.

## INTRODUCTION

The goal of the JEDI collaboration is to measure the EDMs of charged particles ($p$ and $d$) at the storage ring COSY [1, 2]. To create an EDM signal an RF Wien filter introduces a vertical polarisation build-up of the stored polarized particles. This signal is proportional to the particles' EDM [3, 4]. To handle systematic effects, it is important to control the orbit with high precision. These systematic effects can contribute to an unwanted polarization build-up, which may erroneously be interpreted as an EDM signal [5]. The existing orbit control system at COSY will be improved to fulfil these requirements [6]. Furthermore, an investigation started with the goal to develop a prototype of a SQUID-based BPM [7]. For this SQUID-based BPM Rogowski coils are used as magnetic pick-ups [8]. This SQUID-based BPM development is divided into different steps. A first step is the test of a Rogowski coil, which is used as a BPM. The Rogowski coil consists of a torus, which is divided into four segments. Each segment is wound with a thin copper wire to measure the voltage, induced by the bunched beam. With this configuration it is possible to measure the beam position in the horizontal and the vertical plane. An advantage of the Rogowski coil BPM is its thickness of only 1 cm compared to the length of the existing BPMs with an extent of about 13 cm for one plane. This allows for installations in places with tight spatial constrains.

* f.trinkel@fz-juelich.de
† http://collaborations.fz-juelich.de/ikp/jedi/index.shtml

## DESIGN OF ROGOWSKI PICK-UP COIL AND COSY INSTALLATION

The idea to measure the beam position with a segmented Rogowski coil is based on the measurement of the magnetic field induced by the particle flux. The geometry can be characterised by two radii. The radius $R$ defines the distance from the centre of the tube to the centre of the torus and the radius $a$ is the radius of the torus itself. In the presented setup the radius R is 40 mm and the radius $a = 5$ mm. The sketch of the different segments of the Rogowski coil BPM is shown in figure 1. Each segment is wound with a thin copper wire, which has the diameter of 150 $\mu$m. The number of windings for each segment is about 350. The depicted coordinate system is used in the following mathematical derivation. The segments are labelled with the numbers 1 to 4. The torus consist of vespel, which is vacuum-proofed.

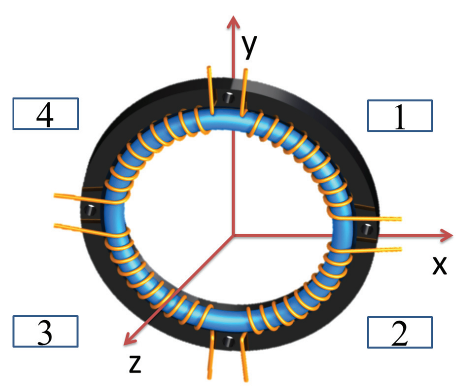


Figure 1: Sketch of a Rogowski coil BPM arrangement, which measures the horizontal and vertical beam position.

Two Rogowski coil BPMs with a distance of 13.3 cm to each other were installed in COSY storage ring to measure beam positions in the horizontal and in the vertical plane. The front Rogowski coil is installed on a fixed frame to use it as a reference BPM to suppress systematic effects like cycle to cycle orbit changes. The rear Rogowski coil is placed on a piezo table. The travel range is from −20 mm to 20 mm in horizontal and vertical plane. The resolution of the piezo



ISBN 978-3-95450-177-9

# A NOVEL ELECTRON-BPM FRONT END WITH SUB-MICRON RESOLUTION BASED ON PILOT-TONE COMPENSATION: TEST RESULTS WITH BEAM

G. Brajnik*, S. Carrato, University of Trieste, 34127 Trieste, Italy
S. Bassanese, G. Cautero, R. De Monte, Elettra-Sincrotrone Trieste, 34149 Trieste, Italy

*Abstract*

In this paper we present a novel and original four-channel front end developed for a beam position monitor (BPM) system. In this work, we demonstrate for the first time the continuous calibration of the system by using a pilot tone for both beam current dependency and thermal drift compensation, completely eliminating the need for thermoregulation. By using this approach, we were also able to investigate several odd and well-known behaviours of BPM systems; the influence of important issues, like the non-linearity of ADCs and the gain compression of amplifiers, which do affect the reliability of the measurement, have been fully understood. To achieve these results, we developed a new radio-frequency front end that combines the four pick-up signals originated by the beam with a stable and programmable tone, generated within the readout system. The signals from a button BPM of Elettra storage ring have been acquired with a 16-bit, 160 MS/s digitizer controlled by a CPU that evaluates the acquired data and applies the correction factor of the pilot tone. A final resolution equal to 1 µm, for a vacuum chamber with an average radius of 19 mm, has been measured with a long-term stability better than 1 µm.

## INTRODUCTION

Accuracy in BPM systems is strongly influenced by the following factors: beam current dependency (to achieve the proper dynamic range, the gains of the preamplifiers have to be adjusted), thermal drifts of electronics (filters, amplifiers, ADCs) and variations of the frequency response of the cables due to changes in temperature or humidity. All of these issues are responsible for inter-channel gain differences, which modify the calculated position.

Typically, every factor has its own compensation method: e.g. gain calibration look-up tables, thermal controlled racks, low-loss cables. The proposed strategy aims to correct all the factors simultaneously: a fixed sinusoidal tone (used as the same reference for all the channels) is added to the original signal coming from the beam (called carrier). A similar technique is already known [1–3], but for the first time experimental results have shown the improvement in resolution due to this method. In order to achieve an effective correction, the pilot tone frequency has to fall near the carrier one, without, however, interfering with the latter. The position of the tone is crucial: only the gaps between the beam harmonics (spaced by the inverse of revolution period) are suitable frequencies [4].

* gabriele.brajnik@elettra.eu

## PROPOSED COMPENSATION

Let $a(t)$ be the input signal coming from the beam, $p(t)$ the pilot tone and $h_A(t)$ the response of channel A. The output of the chain, after the coupler, the filter and the amplifier is a convolution: $s_A(t) = h_A(t) * [a(t) + p(t)]$. Moving to the frequency domain and using the Fourier transforms in calligraphy upper case, the output can be written as $\mathcal{S}_A(f) = \mathcal{H}_A(f) \cdot [\mathcal{A}(f) + \mathcal{P}(f)] = \mathcal{A}_M(f) + \mathcal{A}_P(f)$, where $\mathcal{A}_M(f) = \mathcal{H}_A(f) \cdot \mathcal{A}(f)$ and $\mathcal{A}_P(f) = \mathcal{H}_A(f) \cdot \mathcal{P}(f)$. The complete evaluation of $\mathcal{H}_A(f)$, if $\mathcal{P}(f)$ is used, is not required if we suppose that $f_P$ (the pilot frequency) and $f_C$ (the carrier frequency) are close to each other, allowing us to write $\mathcal{H}_A(f_P) \approx \mathcal{H}_A(f_C)$. In this case, it can be written:

$$\mathcal{A}(f_C) = \frac{\mathcal{A}_M(f_C)}{\mathcal{H}_A(f_C)} = \frac{\mathcal{A}_M(f_C)}{\mathcal{A}_P(f_P)} \cdot \mathcal{P}(f_P) \tag{1}$$

Extracting the amplitudes from $\mathcal{A}(f_C)$ for each channel and substituting them in the typical difference-over-sum (DoS) equation [5, 6] render it possible to calculate compensated spatial coordinates corrected for variations or mismatches of the preamplifiers:

$$X = L \cdot \frac{(A_M/A_P + D_M/D_P) - (B_M/B_P + C_M/C_P)}{A_M/A_P + B_M/B_P + C_M/C_P + D_M/D_P}; \tag{2}$$

$$Y = L \cdot \frac{(A_M/A_P + B_M/B_P) - (C_M/C_P + D_M/D_P)}{A_M/A_P + B_M/B_P + C_M/C_P + D_M/D_P}. \tag{3}$$

where $A_M, B_M, C_M, D_M$ are the amplitudes of the measured carrier and $A_P, B_P, C_P, D_P$ are the amplitudes of the pilot tone.

Obviously, to obtain a continuous and effective correction, care must be taken in treating the analog signals, as well as choosing appropriate computing power to digitally demodulate both carrier and pilot.

## ANALOG RF FRONT END

Figure 1 shows the block diagram of the system: a low-phase-noise PLL generates the pilot tone (whose frequency and amplitude are programmable), which is split into four paths by a high-reverse-isolation splitter that guarantees more than 52 dB of separation between the outputs. A coupler sums the tone with the signal from the pick-ups, adding further 25 dB of isolation to prevent inter-channel crosstalk from the path of the pilot tone. At this point, all the signals pass through a bandpass filter, centered at 500 MHz

ISBN 978-3-95450-177-9

# ACCURATE BUNCH RESOLVED BPM SYSTEM

F. Falkenstern, F. Hoffmann, J. Kuszynski, M. Ries
Helmholtz-Zentrum Berlin, Germany

*Abstract*

Operation of storage rings with multiple beams stored on different closed orbits as well as beam dynamics studies for complex fill patterns require accurate and stable measurement of the beam position for each individual bunch [1].

Analog BPM systems are usually optimized for measuring the closed orbit averaged over all buckets and many turns. Therefore no information about the position of individual bunches is supplied. The new bunch resolved BPM electronics, currently under development at HZB, is based on the analysis of RF-signals delivered by a set of four stripline / pick-up electrodes. These signals in combination with a low jitter master clock and commercially available DAQ cards allow to measure the bunch-resolved beam position with a resolution of a few micrometer.

Experiments performed at BESSY II and MLS demonstrate the performance of the setup and will be discussed.

## INTRODUCTION

HZB operates two electron storage ring based light sources named BESSY II and MLS [2]. BESSY II is operated at an electron energy of 1.7 GeV with a maximum current of 300 mA distributed to 400 buckets. Whereas MLS is operated at 629 Mev with a current of up to 200 mA stored in 80 buckets. The main RF cavities of both rings operate at a frequency of about 500 MHz providing a bucket spacing of approximately 2 ns.

Different fill patterns and optics modes (i.e. low alpha) allow our users to work with optimal synchrotron light conditions at the beamlines. This flexibility of beam conditions leads to high requirements in the field of beam diagnostics.

For measurement of the average orbit the analog BPM system is used. The major advantage of this system is a high position resolution of about 1 micrometer for currents between 1 mA und 300 mA. Due to averaging, no external timing is required. The disadvantages is that there are no information about the position for each individually bunches and turns. In future upgrades of both storage rings this information may become necessary, therefore an alternative approach has to be explored.

## DIAGNOSTICS REQUIREMENTS

What are the main challengers of bunch-resolved BPM diagnostic systems for the storage ring?

A) Capture the position of each individual bunch with an accuracy in the µm range.
B) Measurement results of the bunch position don't depend on temperature drifts.
C) The measurement data has to be linear with the orbit changes.
D) Large dynamic range of bunch currents from 10 µA to 10 mA.
E) The synchronous phase shift over the full fill pattern and small changes of beam phase with respect to the master clock should have no influence.
F) Cross talk between neighboring bunches due to ringing or reflections on the scale of 2 ns should be minimized.
G) Measurement results of the bunch position don't depend on orbit bumps (large displacements).

The following solution was found meeting all requirements.

A) A 14-Bit ADC with an analog BW of more than 500 MHz was chosen. The principle of under sampling allows to achieve a very good amplitude resolution. This technique is already being used in our fill pattern monitor "BunchView" [3].
B) The BPM signal will be multiplexed. So each of 4 signal channel has the same path of filter, amplifier and ADC. In other words only one active detector for all channels is used. This schematic has very good results in relation to thermal drift and aging of electronic parts.
C) A data acquisition card with a very linear 14 Bit ADC for a wide dynamic range of analog amplitudes is applied.
D) Linearity of the DAQ hardware will allow to apply normalization.
E) The approach of a sampling scope with 100 GHz is used for finding the maximum of the amplitude of the bunch signals.
F) A low pass filter (LPF) of about 750 MHz is applied to minimize the cross-talk to following bunches.
G) In the case of driving the orbit bumps it is important to have a good electrical separation between channels of the RF switch. The bad isolation between channels will be affected the X by change Y and vice versa.

The main component of the DAQ system is provided by using standard commercial equipment. A major advantage is the use of LabVIEW for controlling and



ISBN 978-3-95450-177-9

# CERN PS BOOSTER TRANSVERSE DAMPER: 10 kHZ - 200 MHZ RADIATION TOLERANT AMPLIFIER FOR CAPACITIVE PU SIGNAL CONDITIONING

A. Meoli*, A. Blas, R. Louwerse, CERN, Geneva, Switzerland

*Abstract*

After connection to the LINAC4, the beam intensity in the PS Booster is expected to double and thus, an upgrade of the head electronics of the transverse feedback BPM is necessary. In order to cover the beam spectrum for an effective transverse damping, the pickup (PU) signal should have a large bandwidth on both the low and high frequency sides. Furthermore, in order to extend the natural low frequency cut-off from 6 MHz (50 Ω load) down to the required 10 kHz, with no modification of the existing PUs, a high impedance signal treatment is required. The electronic parts should withstand the radiation dose received during at least a year of service. This constraint implies the installation of the amplifier at a remote location. A solution was found inspired by the technique of oscilloscopes' high impedance probes that mitigates the effect of transmission line mismatch using a lossy coaxial cable with an appropriate passive circuitry. A new large bandwidth, radiation tolerant amplifier has been designed. The system requirements, the analysis, the measurements with the present PUs, the design of the amplifier and the experimental results are described in this contribution.

## INTRODUCTION

New pick-up (PU) head amplifiers are needed in the CERN PSB (Proton Synchrotron Booster) for the specific needs of the transverse feedback (TFB) system. This latter feedback was installed in order to damp transverse instability of the beam and it is fully operational with the present beam as injected from the LINAC2 (linear accelerator).

As shown in the Table 1, in 2018 a higher beam intensity (factor 2.5 increase) is expected from the new LINAC4. This will mean a higher voltage on the beam position pick-up installed in the ring and a potential saturation or destruction of the head amplifiers presently installed.

The beam spectrum, as sensed by the beam PUs, is populated at the harmonics of the revolution frequency and at so-called betatron side bands (amplitude modulation) around the revolution lines. The transverse betatron motion is inherently due to the architecture of a synchrotron where the beam experiences a certain number of transverse oscillations at each turn (revolution). This number of oscillations is called the tune and it is a non-integer value (Q.q) with a fractional part q. The side-bands observed in the transverse error signal, calculated as the difference of signals from two opposite pick-up up electrodes of a given H or V plane, are located $q{\cdot}f_{\mathrm{rev}}$ apart from each of the revolution harmonics. $f_{\mathrm{rev}}$ is the beam revolution frequency. With minimum values of $q = 0.1$ and $f_{\mathrm{rev}} = 1$ MHz, the lowest frequency betatron band is located at 100 kHz.

In order to have a good damping rate at 100 kHz, the phase error at this frequency should be minimal; this is why a low-frequency −3 dB cut-off pole is requested at 10 kHz. On the higher end of the spectrum, the limit is mainly technological. The head amplifier is required to have the widest possible bandwidth considering the potential high frequency instabilities. Nevertheless, our present limited knowledge of the machine impedance does not allow for precise specifications in that direction, so we are aiming at amplifiers having a bandwidth equivalent to what the PU itself can supply.

Table 1: CERN PSB Machine Parameters with LINAC4

| | |
|---|---|
| Proton kinetic energy, $E_{\mathrm{k}}$ | 160 MeV → 2 GeV |
| Velocity factor, $\beta$ | 0.533 → 0.948 |
| Revolution frequency, $f_{\mathrm{rev}}$ | 1 MHz → 1.8 MHz |
| Maximum protons per bunch, $N_{\mathrm{p}}$ | $2.5 \cdot 10^{13}$ ppb |
| Minimum bunch length, $4\sigma$ | ≈150 ns |

## PICK-UP

The pick-up is using 4 conductive plates engraved on the inner surface of a ceramic tube inside which the beam will flow. This ceramic tube is enshrined inside a cylindrical stainless steel tube. The capacitance between each plate of the PU and its grounded support is measured to be around 630 pF. Under the presence of beam, the PU plate can be represented as a current generator [1] feeding the electrode capacitance in parallel with the monitoring circuit load.

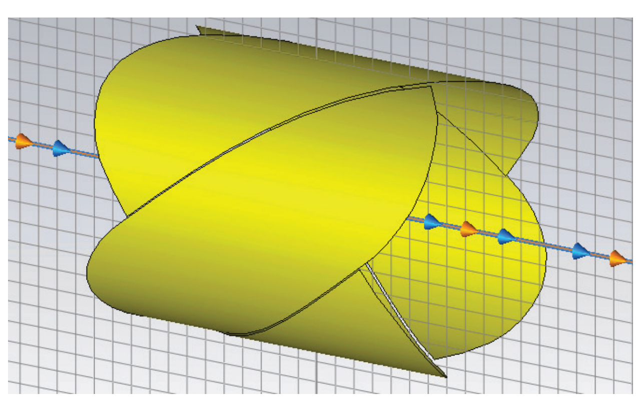

Figure 1: CST PU Model.

* alessandro.meoli@cern.ch

ISBN 978-3-95450-177-9

# SIMULATION OF BUNCH LENGTH AND VELOCITY DEPENDENCE OF BUTTON BPMS FOR LINACS USING CST PARTICLE STUDIO®

M. Almalki* KACST, Riyadh, Saudi Arabia
P. Forck, T. Sieber, R. Singh, GSI, Darmstadt, Germany

*Abstract*

At non-relativistic velocities at a proton LINAC, the electromagnetic field generated by the beam has a significant longitudinal component, and thus the time evolution of the signal coupled to the BPM electrodes depends on bunch length and beam velocity. Extensive simulations with the electromagnetic simulation tool CST Studio® were executed to investigate the dependence of the induced BPM signal on different bunch lengths and velocities. Related to the application, the simulations are executed for the button BPM arrangement as foreseen for the FAIR Proton LINAC. These investigations provide the required inputs for the BPM system and its related technical layout such as analogue bandwidth and signal processing electronics. For the BPM electronics, it is important to estimate the contribution of the harmonic used for the data processing. Additionally, the analogue bandwidth of the BPM system is determined from studying the output signal of the button BPM as a function of bunch length at different beam velocities. This contribution presents the results of the simulations and comments on general findings relevant for a BPM layout and the operation of a hadron LINAC.

## INTRODUCTION

The electromagnetic fields generated by a beam and thus the time evolution of the signal coupled out by a pickup depend on beam velocity. In the limit of relativistic velocities, the generated beam fields are pure transverse electric and magnetic known as Transverse Electric and Magnetic (TEM) mode. A TEM mode has an electric and magnetic field vector perpendicular to the propagation direction. Thus, the electric field is longitudinally concentrated above and below the beam [1]. For moderate beam velocities $\beta > 0.9$ the resulting field can be also approximated to first order by TEM field distribution and the image current mirrors the same time behavior as the beam is traveling. At low beam velocities $\beta < 0.5$, the electromagnetic field is no longer a TEM wave [2]. In this regime the power coupled out by the pickup is much lower than the power carried by the beam due to the reduction in the coupling of high-frequency Fourier components.

On the other hand, it is important to keep in mind that the accurate determination of the bunch length is not trivial. The reason is the presence of the advanced Coulomb-field of the moving bunches, in particular for low $\beta < 0.5$ range [3]. The geometric length of the bunch $\Delta z$ along the $z$−axis depends on the particle velocity $\beta$ which can be calculated from [3]

$$\Delta z = \beta c \Delta t_b \tag{1}$$

where $\Delta t_b = 2\sigma_b$. The reason is that the derivative of a Gaussian Function has the maximum and the minimum exactly at $\pm\sigma$.

## CST STUDIO® SIMULATIONS

The simulations have been carried out using the CST Particle Studio Wakefield solver [4] to study bunch length and velocity dependence of button BPMs for LINACs. The Wakefield solver is the most appropriate for studying the BPM response and the simulations are driven by a bunch of charged particles in the time domain. A 3D model of a BPM of four button pickups has been created in the CST Particle Studio® as shown in Figs. 1.

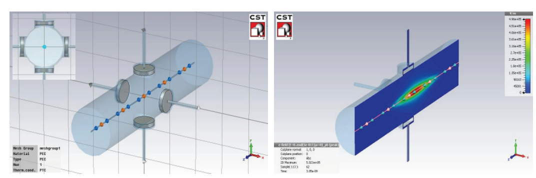

Figure 1: Left: A 3D model of the pick-up monitor as simulated in CST Particle Studio®. Right: The absolute value of the electric field of a bunch of $\sigma$ = 100 ps long and $\beta$ = 0.37

The wakefield has been simulated up to a 150 *mm* length along the beam coordinate. The excitation source is defined by a Gaussian-shaped longitudinal charge distribution with beam bunch charge of 1 nC in the $z$ direction. The pickup response, expressed as the output signal in time and frequency domains, is obtained for each simulation run reflecting the pickup's interaction with the beam. The output voltages convergence versus mesh size has been investigated prior to utilizing the results. The convergence has been examined at three beam velocity $\beta$ = 0.08, 0.27 and 0.37 with a bunch length chosen to be 150 ps. Figs. 2 demonstrates the results of the Wakefield solver at different mesh settings. The results show a solid convergence of the output signals and frequency spectrums in the interesting frequency range for $\beta$ = 0.08, 0.27 and 0.37. A visible difference is only observed in the frequency spectrum for $\beta$ = 0.08 with the mesh setting of 150000.

## SIMULATIONS AND RESULTS

The CST simulations have been carried out to investigate the bunch length characteristics for the interesting dynamic range in proton LINAC which assumed to be between 50 to

* mmmalki@kacst.edu.sa

ISBN 978-3-95450-177-9

# DEVELOPMENT STATUS OF A STABLE BPM SYSTEM FOR THE SPring-8 UPGRADE

H. Maesaka†, RIKEN SPring-8 Center, Kouto, Sayo, Hyogo, 679-5148, Japan
H. Dewa, T. Fujita, M. Masaki, S. Takano[1],
Japan Synchrotron Radiation Research Institute, Kouto, Sayo, Hyogo, 679-5198, Japan
[1]also at RIKEN SPring-8 Center, Kouto, Sayo, Hyogo, 679-5148, Japan

*Abstract*

We are developing a stable and precise BPM system for the low-emittance upgrade of SPring-8. Key requirements for the BPM system are: 1) long-term stability of the radiated photon beam direction well within the intrinsic photon divergence, 2) single-pass resolution better than 100 µm for a 100 pC single-bunch for first-turn steering in the beam commissioning, and 3) BPM center accuracy better than 100 µm rms with respect to an adjacent quadrupole to achieve the design performance of the upgraded storage ring. Based on these requirements, a button-type BPM head and a readout electronics are being developed. Some prototypes of the BPM head were manufactured and the machining accuracy was confirmed to be sufficient. For the readout electronics, a MTCA.4-based system and an upgrade of a commercial BPM electronics are under study. Since radiation damage to the signal cable of the present BPM system was found to be a cause of humidity-dependent drift of BPM offset, measures against the radiation damage are considered for the new BPM cable. The preparation of a beam test of the new BPM system is in progress to confirm the overall performance.

## INTRODUCTION

A low-emittance upgrade of SPring-8 was recently proposed in order to provide much more brilliant x-rays to experimental users [1]. The natural emittance of an electron beam after the upgrade is estimated to be 140 pm rad without any radiation damping by insertion devices (IDs), while the emittance of the present SPring-8 storage ring is 2.4 nm rad. The emittance can be further reduced to 100 pm rad by operating IDs thanks to radiation damping. This low emittance value is realized by using 5-bend achromat lattice and by reducing the beam energy from 8 GeV to 6 GeV. As a result, the brilliance of x-ray radiation is expected to be more than one orders of magnitude higher than the present SPring-8.

Since the horizontal beam size becomes smaller, the stability of the beam position should also be improved. The beam size at the center of an ID is approximately $25 \times 5$ µm$^2$ rms. Therefore, the beam position stability is required to be 1 µm level. Although the vertical beam size is comparable to the present SPring-8, the present BPM system has some drift problems of more than 10 µm [2]. Thus, we plan to replace the present BPM system with new one, which goes for the stability of 1 µm level.

Since the upgraded SPring-8 can provide brilliant x-rays with a small source size, small divergence and a high coherent flux, the stability of the photon beam axis is the most important. The upgraded SPring-8, for example, enables a direct nano-focusing scheme wherein primary x-ray radiation from an undulator can be directly focused to a nanometer spot without any secondary virtual sources by using downstream apertures [3]. In this beamline, the stability of the photon beam axis is critical and it should be well within the intrinsic photon divergence. The required stabilities are sub-µm and sub-µrad for the photon beam position and direction, respectively. Consequently, a stable electron BPM and a photon BPM are necessary [4].

In addition to the stability issue, the BPM system is indispensable to the beam commissioning of the upgraded SPring-8. For the first-turn beam steering, single-pass BPM measurements with high accuracy and high resolution (100 µm rms) are demanded, since the dynamic aperture becomes significantly narrower (< 10 mm) than the present storage ring [1]. After the success of beam storage, the beam orbit is adjusted to the center of each multi-pole magnets in order to achieve the design performance of the upgraded SPring-8. Thus, a BPM system with high single-pass resolution (100 µm rms) and high position accuracy (10 µm rms) is necessary.

In this article, we describe an outline of the BPM system for the SPring-8 upgrade, such as the development status of a BPM head and a readout electronics, and the improvement of the BPM stability. The design of the BPM head is detailed in Ref. [5].

## BPM SYSTEM FOR THE SPring-8 UPGRADE

### *BPM System Overview*

The SPring-8 storage ring consists of 48 unit cells and each cell is equipped with 7 BPMs after the upgrade. In total, 336 BPMs will be utilized for the machine operation. The BPM electrode was selected to be a button type [5]. The readout electronics for each BPM is designed to have measurement functions of both closed-orbit distortions (COD) and single-pass (SP) trajectories with sufficient precision and accuracy.

### *Required Performance*

As mentioned in the introduction, the BPM system for the SPring-8 upgrade should have sufficient stability, high-resolution and high-accuracy. Main specifications of the BPM system are summarized in Table 1.

† maesaka@spring8.or.jp



ISBN 978-3-95450-177-9

# COMMISIONING OF BEAM POSITION AND PHASE MONITORS FOR LIPAc *

I. Podadera †, A. Guirao, D. Jiménez, L. M. Martinez, J. Molla,
A. Soleto, R. Varela, CIEMAT, Madrid, Spain

*Abstract*

The LIPAc accelerator is a 9 MeV, 125 mA CW deuteron accelerator [1] which aims to validate the technology that will be used in the future IFMIF accelerator. Several types of Beam Position Monitors –BPM's- are placed in each section of the accelerator to ensure a good beam transport and minimize beam losses. LIPAc is presently under installation and commissioning of the second acceleration stage at 5 MeV [2]. In this stage two types of BPM's are used: four striplines to control the position at the Medium Energy Beam Transport line (MEBT), and three striplines to precisely measure the mean beam energy at the Diagnostics Plate. The seven pickups have been installed and assembled in the beamlines after characterization in a wire test bench, and are presently being commissioned in the facility. In addition, the in-house acquisition system has been fully developed at CIEMAT. In this contribution, the results of the beam position monitors characterization, the tests carried out during the assembly and the status of the electronics system are reported.

## PICKUP MANUFACTURING

### *MBPM*

Four striplines are installed along the MEBT (Fig. 1) to track the beam from the RFQ to the MEBT. The BPM's chambers are installed in the middle of the combined magnets (quadrupole and two steerers) as seen in Fig 1. This makes the design, installation and assembly quite challenging, due to the very tight space available. In addition, all the materials should be non-magnetic to avoid any perturbance in the quality of the magnetic field.Three vacuum chambers were manufactured: two containing one BPM each, and a longer one containing two BPM's located in consecutive magnets. Compact welded bellows are inserted, shielded inside to protect them to the spray particles of a high CW current hadron accelerator, and welded to rotating flanges. Due to the compact design the fabrication (realized by Vacuum Projects in Spain) was quite complicated. The feedthroughs were very prone to crack due to overheating during TIG welding, although the feedthrough manufacturer supported this technique. After many attempts and empirical studies, laser welding had to be used for the first welding whereas the welding of other pieces in the chamber was kept by TIG. Once each BPM body was fabricated, it was welded to the rest of the vacuum chamber. This was also a challenging process, especially in the last chamber with two BPM's, since the tolerances were quite small. During all the manufacturing process, the machined pieces were metrology controlled, taking especial care to the BPM assembly and the coordinates of the fiducial points with respect to the reference frame. Finally, the chambers underwent an ultrasonic cleaning and a vacuum leak test to verify the tightness for a proper operation in LIPAC.

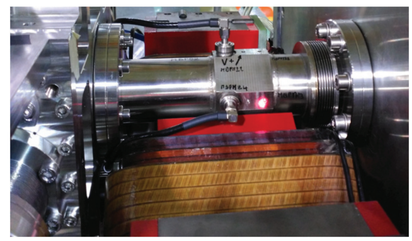

Figure 1: Picture of MBP02 mounted in the MEBT between the poles of the second MEBT magnet.

### *DBPM*

The three units of the Diagnostics Plate BPM (DBPM) have been manufactured and tested (Fig. 2), based in the design presented in [3]. All the units have been manufactured in the CIEMAT workshops. As in the case for the MBPM, metrology was watched along all the procedures. Prior to and after the final welding assembly the unit was measured usign a 3D coordinate machine. Once the assembly was finished several acceptance tests were done. The first one was the test of the vacuum leak of the device. A leak below $10^{-12}$ mbar·l/s was detected, which is far beyond the requirements for the LIPAc.

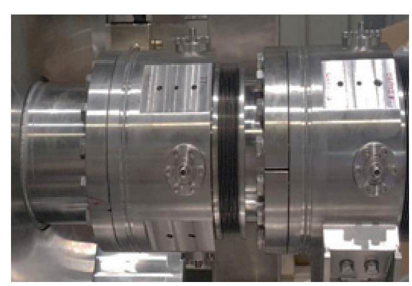

Figure 2: Picture of two of the DBPM's mounted in the Diagnostics Plate.

## RF CHARACTERIZATION

A series of electromagnetic tests were performed to validate each pickup prior to the installation in the beamline. The two main tests that are done to characterize the pickup are: the coupling between the channels in the frequency range of

* Work partially supported by the Spanish Ministry of Economy and Competitiveness under project AIC-A-2011-0654 and FIS2013-40860-R
† ivan.podadera@ciemat.es

ISBN 978-3-95450-177-9

# DESIGN OF THE TRANSVERSE FEEDBACK KICKER FOR ThomX

M. El Ajjouri, N. Hubert, A. Loulergue, R. Sreedharan, Synchrotron SOLEIL, Gif sur Yvette, France
D. Douillet, A.R. Gamelin, D. Le Guidec, LAL, Orsay, France

Abstract

ThomX is a Compton back-scattering source project in the range of the hard X rays to be installed in 2017. The machine is composed of an injector Linac and a storage ring where an electron bunch collides with a laser pulse accumulated in a FabryPerot resonator. The final goal is to provide an X-rays average flux of 1013 ph/s. To keep up with this flux, it is required to install a transverse feedback system to suppress instabilities generated by injection position jitter sources, resistive wall impedance or collective effects. This paper describes the design and simulation studies of the stripline kicker that will be used for the transverse feedback system.

## *Introduction*

ThomX [1] is a demonstrator for a Compton back-scattering source in the hard X-ray range to be installed in Orsay, France, in 2017 [2]. A single electron bunch will be accelerated every 20 ms by a 50 MeV LINAC and stored in a 16 m circumference storage ring to interact with a high energy laser (fig. 1).

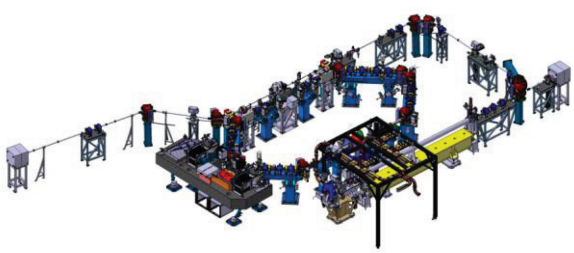

Figure 1: Layout of the ThomX facility.

By operating at low energy (50 MeV) the natural damping effect of the synchrotron radiation is weak and the beam stability becomes a crucial matter. The computed instability growth time and the corresponding kicker strength requirement for the different types of instabilities are listed in table 1. The results indicate that for Thom-X, the most critical effect comes from the injection orbit jitter inducing emittance growth at a growth rate of ~5 μs once the bunch stored in the ring.

Table 1: Instabilities Estimate for ThomX Ring

| **source** | **Growing time** | **Kicker strength Δx'** |
|---|---|---|
| Beam pipe Geometries | 160μs | > 10nrad |
| Resistive Wall | 600μs | > 2 nrad |
| Ions | < 100 μs | > 20nrad |
| Injection Jitter | 5 μs | 2 μrad |

## *ThomX Transverse Feedback*

To cope with these instabilities, it was decided to use a digital transverse feedback system, composed of a wideband detector button beam position monitor (BPM) a RF front-end, a FPGA based processor, a power amplifier and a stripline kicker (fig. 2). The system is capable of detecting a coherent transverse motion and applying a counter kick to damp it, bunch by bunch and turn by turn, with one (or even 2) bunches.

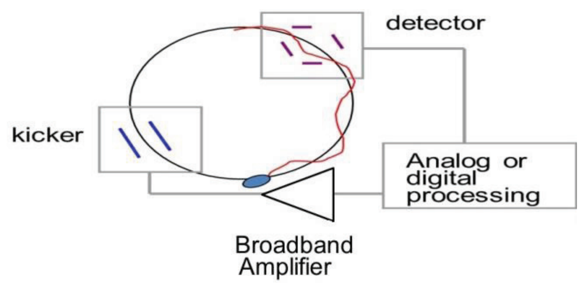


Figure 2: Digital feedback system.

## *Stripline Kicker Impedance Matching*

The stripline kicker has 4 electrodes connected to electrical feedthrough at both ends. The electrodes are 300 mm long that corresponds to λ/2 of RF frequency (500 MHz). To maximize the transmission power, we must adapt the electrode impedance with the external transmission impedance lines (amplifier and cables are 50 ohm).

The formula to calculate the characteristic impedance Z for the different modes is the following [3, 4]:

$$Z = \frac{V^2}{2*E*c} \qquad (1)$$

where c is the speed of light, V is the electric potential between stripline electrode and vacuum pipe, and E is the electric field. We use the Poisson electromagnetics 2D software [5] (fig. 3) to calculate the electric field for different dipole, quadrupole and sum mode (table 2).

Table 2: The Potential Applied to each Electrode to Calculate Electric Field

| **Field mode** | **E1** | **E2** | **E3** | **E4** |
|---|---|---|---|---|
| Sum | +V | +V | +V | +V |
| V Dipole | +V | -V | -V | +V |
| H Dipole | +V | +V | -V | -V |
| Quadrupole | +V | -V | +V | -V |



ISBN 978-3-95450-177-9

# NOVEL ELECTROSTATIC BEAM POSITION MONITORS WITH ENHANCED SENSITIVITY

M. Ben Abdillah†, Institut de Physique Nucléaire, Orsay, France

*Abstract*

Beam Position Monitors (BPM) measure the beam transverse position, the beam phase with respect to the radiofrequency voltage, and give an indication on beam transverse shape. Electrostatic BPMs are composed of four electrodes that transduce the associated electromagnetic field to the beam into electrical signal allowing the calculation of the beam parameters mentioned above. During commissioning and/or experiences phases that needs very low beam current; the precision of the BPM measurements is reduced due to the low sensitivity of electrostatic BPM to beam current. This paper addresses the design, the realization and the testing of a new set of electrostatic BPMs with large electrodes. It emphasizes the strong points of these BPMs in comparison with BPMs present in SPIRAL2 facility.

## INTRODUCTION

The idea of developing a BPM with enhanced sensitivity arose at the qualification of SPIRAL2 BPM that shows weak received signals by the BPM electrodes at low beam currents (less than 150µA). Novel electrostatic BPM were designed taking into account mechanical constraints (space, stability) while offering better current sensitivity.

## BEAM POSITION MONITORS

A BPM has four electrodes that couple to the beam through the image charge produced by the beam [1]. The BPM electrode is considered as capacitor C that is charged by the beam and discharged through a 50Ω resistor connected to ground. As for SPIRAL2 BPM [2], the electrode receives a multi-tone signal due to the beam bunched with an accelerating frequency 88.0525MHz. Only 1st and 2nd harmonic tones are taken into account in this study. A generic example of electrostatic BPM is sketched in Figure 1.

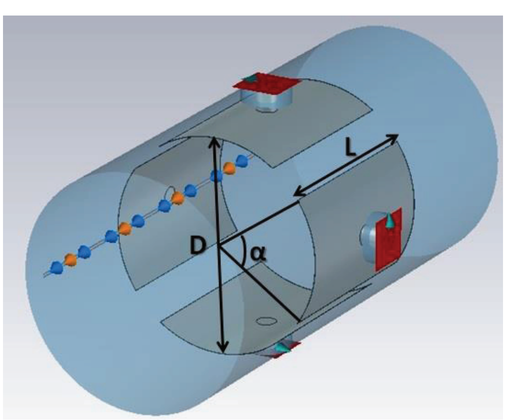


Figure 1 : Generic example of electrostatic BPM.

BPM diameter D, angular length α and length L have direct effects on BPM current and position sensitivities.

For instance, the formula for position sensitivity $K_p$ for Gaussian beams at β=1 is:

$$K_p(dB/mm) = \frac{320}{\ln(10)}\frac{\sin(\alpha/2)}{D\cdot\alpha}$$
$$\alpha \text{ in radians and } D \text{ in mm}$$

Table 1 shows the type of proportional relation between these parameters, this guided the design of SPIRAL2 BPM and the new BPM.

Table 1: Proportional Relation Between BPM Sensitivities and Design Parameters

| Parameter | Current sensitivity | Position Sensitivity |
|---|---|---|
| D | $1/D^2$ | 1/D |
| α | α | sin(α/2)/α |
| L | sin(πL.f/v) | No effect |
| C | 1/C | No effect |

v is the beam speed and f is the accelerating frequency.

As for SPIRAL2 BPM, the design of the new BPM took into account the fact that the BPM will be inserted in the vacuum pipe inside the quadrupoles which will be buried at their turn in the quadrupole magnet. Therefore, BPM diameter D was set to 40mm. the electrode angular length α was set to 63deg as it's a tradeoff between current sensitivity and position sensitivity. Change in BPM diameter should bring 1.5dB enhancement in BPM current sensitivity; it also raises BPM position sensitivity.

Main focus is pointed on the levels of the received signal tones at the first harmonic (176.105MHz) and the second harmonic (352.21MHz). Only BPM length L is modified in order to maximize sensitivity to beam current at the first and the second harmonic while maintaining sensitivity to beam position at these tones.

## BPM ELECTRICAL SIMULATIONS

BPM simulations were run under Mathcad using the method described by Shafer [1]. BPM length L was swept over 180mm range and special focus was put over the level of signal received by BPM electrodes for centered low β (β= 0.08) beams.

Simulations, run with MathCad, show an enhanced output level at the first and second harmonic for L=65mm than the 39mm set for SPIRAL2 BPM (see Figure 2).

†abdillah@ipno.in2p3.fr



ISBN 978-3-95450-177-9

# LCLS-1 CAVITY BPM ALGORITHM FOR UNLOCKED DIGITIZER CLOCK

T. Straumann, S. R. Smith, SLAC, Menlo Park, USA

*Abstract*

Cavity BPMs commonly use the fundamental TM010 mode (excited either in the x/y cavity itself or in a separate “reference” cavity) which is insensitive to beam position as a reference signal, not only for amplitude normalization but also as a phase/time reference to facilitate synchronous detection of the signal derived from the position-sensitive TM110 mode. When taking these signals into the digital domain the reference and position signals need to be acquired by a synchronous clock. However, unless this clock is also locked to the accelerating RF absolute, timing information is lost which affects the relative phase between reference and position signals (assuming they are not carefully tuned to the same frequency).

This contribution presents a method for estimating the necessary time of arrival information based on the sampled reference signal which is used to make the signal detection insensitive to the phase of the digitizer clock. Running an unlocked digitizer clock allows for considerable simplification of infrastructure (cabling, PLLs) and thus decreases cost and eases maintenance.

## INTRODUCTION

Cavity Beam-Position Monitors (BPMs) inherently offer a very high resolution [1, 2]. A beam of charged particles passes a cylindrical cavity and excites the electro-magnetical eigenmodes of the device. The coupling of the beam to some of these modes, in particular the “dipole-mode” TM110 is very sensitive to the transversal beam position. The structures to extract the signals from the cavity are carefully designed to be sensitive to TM110 only and reject other modes [3].

TM110 is also excited by a centered but oblique beam trajectory and “slanted” bunches [1] but the resulting signal is in phase-quadrature to the position signal.

The fundamental TM010 mode of a second, “reference”, cavity which is largely insensitive to the beam-position is also measured so that the position-sensitive signal can be normalized to the beam charge and phase.

Figure 1 shows the typical hardware employed to acquire the cavity-BPM signals. Three RF signals (e.g, X-band), originating at the X- and Y-ports of the main cavity as well as the output of the reference cavity are fed into a analogue receiver and subsequently digitized. The receiver uses multiple mixing stages and/or an image-rejecting configuration.

In order to maintain the highest possible resolution of the system and to reject (or, depending on the application: detect) the effects of an oblique trajectory (or bunch) a phase-synchronous detection algorithm is commonly used [1, 2, 4] with the reference cavity establishing the necessary time or phase reference.

Obviously, the three channels must use a common LO as well as a common ADC clock in order to maintain phase-synchronicity among the channels.

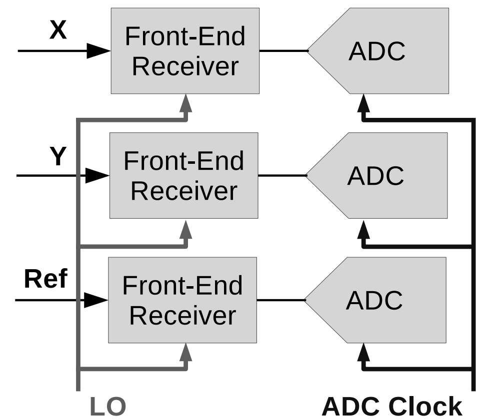


Figure 1: Cavity BPM receiver hardware block diagram.

A synchronous detection algorithm amounts to the estimation of the amplitude of a “known” signal (shape) in the presence of noise [5]. A generic, linear and time-discrete detector for a signal $s(t)$ which is assumed to be time- and band-limited (i.e., it can reasonably approximated by a suitable periodic continuation) can be described by Eq. (1):

$$\hat{A} = \frac{1}{N} \Sigma_{n=0}^{N-1} s(nT_s - t_o) f(nT_s) \quad (1)$$

i.e., the signal is *correlated* with a (normalized[1]) “test”-function $f(t)$.

In addition to the test-function we also must know or estimate the “starting” time $t_o$ of the signal which is also called “Time of Arrival” or TOA.

The subject of this paper is a method for TOA estimation which is suitable for cavity BPMs with a free-running ADC clock. The ADC is usually triggered by the timing system but the TOA depends on the phase of the ADC clock and is unknown to at least $\pm\frac{1}{2}$ sampling period.

## REVIEW OF COMMON METHODS FOR TOA ESTIMATION

In the context of cavity BPMs it is important to consider that one of the advantages of a synchonous detector is its superior SNR when the signal amplitude is small, which is the case when the beam passes close to the electrical center of the main cavity.

[1] so that $\frac{1}{N} \Sigma_{n=0}^{N-1} f^2(nT_s) = 1$.



ISBN 978-3-95450-177-9

# DESIGN FOR THE DIAMOND LONGITUDINAL BUNCH-BY-BUNCH FEEDBACK CAVITY

A. F. D. Morgan, G. Rehm
Diamond Light Source, Oxfordshire, UK

## ABSTRACT

In 2017 it is planned to install some additional normal conducting cavities into the Diamond storage ring. In order to deal with the potential higher order modes in these, we are designing a longitudinal bunch-by-bunch feedback system. This paper will focus on the design of the overloaded cavity kicker, adapted to the Diamond beam pipe cross section. The design has evolved in order to reduce the strong $3^{rd}$ harmonic resonance seen on the introduction of the racetrack beam pipe. Through a combination of geometry optimisation and the addition of integrated taper transitions this harmonic has been greatly reduced while also minimising sharp resonances below 15 GHz. The major features will be described, as well as the expected performance parameters.

## DESIGN

The design comprises a pillbox cavity, with additional coaxial ports coupled via ridged waveguides. In a development on our previous work, the design frequency was moved to 1.875 GHz from the lower 1.625 GHz. This was in order to move more of the higher order modes (HOMs) above the cutoff frequency of the beam pipe and to space out the remaining lines. 2.125 GHz was also considered, but found to generate additional lower frequency HOMs in the structure.

Theoretically, the ridged waveguide structure and the waveguide to coaxial transition both act as high pass filters, and care must be taken to make sure that the overall cutoff frequency is low enough such that all of the higher order modes can be coupled out of the cavity. In practice they behaved more like band pass filters, so the aim was to extend the pass band to as high a frequency as possible.

The coupling structures were originally modelled separately, in order to iterate the model faster. Figure 1 shows a representation of the modelled geometry. The best result was then incorporated into the full model. Figure 2 shows the transmission through the waveguide and coaxial structures. The pass band extended from 1.8 GHz to 8 GHz. Although not ideal it was decided that it was good enough to be incorporated into the full model.

Although useful starting points can be obtained by modelling elements separately, the optimisation must be done on the full model so as to take into account of the interactions between elements. As an example, even with the waveguide and coaxial coupler optimised, there were still unwanted resonances in the wake impedance of the full model. With the original cavity, pipe and couplers, tuning the geometry in various ways could not achieve overall suppression of the

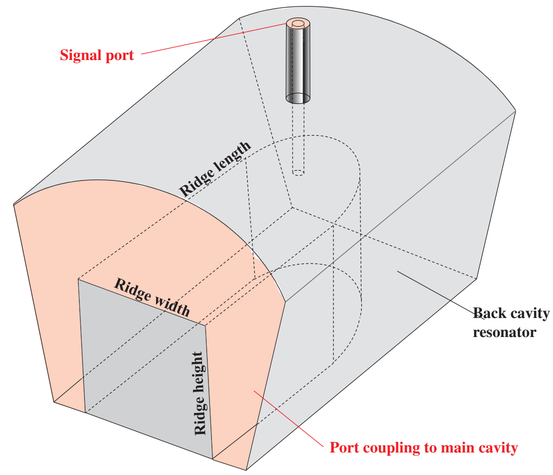


Figure 1: Sketch of the coupler geometry.

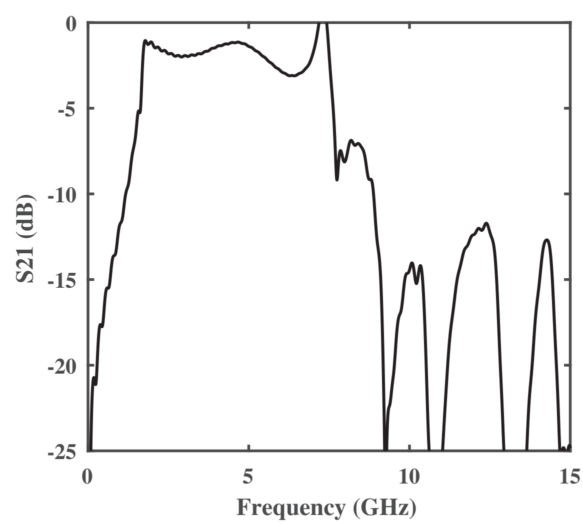


Figure 2: The transmission through the coupling structures as initially added to the full model.

HOM resonances. If one set of resonances was suppressed then another was enhanced.

Only when tapers were added to the model was the overall suppression of these unwanted features realised. After some investigation it was found that tapers moving from the Diamond standard racetrack profile on outer ends of the structure, to a circular profile at the central cavity performed best. Tapers were resisted originally as they are known to

# A NEW STRIPLINE KICKER FOR PF-AR TRANSVERSE FEEDBACK DAMPER

R. Takai*, T. Honda, T. Nogami, T. Obina, Y. Tanimoto, M. Tobiyama
KEK Accelerator Laboratory and SOKENDAI, 1-1 Oho, Tsukuba, Ibaraki 305-0801, Japan

*Abstract*

A feedback damper equipped with a long stripline kicker was used to damp transverse beam oscillation at the Photon Factory Advanced Ring (PF-AR), which is a 6.5-GeV synchrotron radiation source of KEK. Recently, the stripline kicker was renewed to one having shorter electrodes and a smaller loss factor because its insulating support was broken by the beam-induced thermal stress and caused frequent electric discharges inducing dust trapping phenomena. In this paper, we present details of the new stripline kicker, from design to installation, as well as demonstrate results of beam oscillation damping obtained with the new kicker.

## INTRODUCTION

The Photon Factory Advanced Ring (PF-AR), which is a 6.5-GeV electron storage ring of KEK, is known as a unique synchrotron radiation source dedicated to single-bunch operations to provide high-intensity pulsed X-rays. It is operated in decay mode in which the stored beam current is added twice daily up to 60 mA. The principal parameters of the PF-AR are listed in Table 1.

Table 1: Principal Parameters of the PF-AR

| | |
|---|---|
| Operation Energy | 6.5 GeV |
| Injection Energy | 2.85 GeV |
| Stored Current | 60 mA |
| RF Frequency | 508.57 MHz |
| Circumference | 377.26 m |
| Harmonic Number | 640 |
| Number of Bunches | 1 |
| Revolution Frequency | 795 kHz |
| Tunes (x/y/s) | 10.17/10.23/0.05 |
| Damping Time (x/y/s) | 2.5/2.5/1.2 ms |
| Natural Emittance | 294 nm rad |
| Natural Bunch Length | 18.6 mm (62 ps) |

A long stripline feedback kicker comprising four stainless steel pipes with length of about 1.4 m was installed in the west straight section of the ring to damp the transverse oscillations of injected and stored beams. In order to reduce their self-weight deflection, an insulating support made of machinable ceramics "Photoveel [1]" was attached at the midpoint of each electrode. Since user operation commenced in the autumn of 2012, we frequently observed sudden increases in the vacuum pressure accompanied by beam loss around these insulating supports. Inspection of the kicker enabled us to find the damaged insulating supports. We considered this damage to have been caused by thermal stress due to energy loss of the stored single bunch. These supports were previously suspected to cause frequent electric discharges, thereby inducing dust trapping phenomena [2]. Photos of the original kicker electrodes and their insulating support parts taken during the inspection are shown in Fig. 1. Although the time domain reflectometry (TDR) response was acceptable, we found that the head of the bolt supporting the kicker electrode via the Photoveel part discolored to become black due to electric discharges and the Photoveel part itself was partially melted and broken. We continued the user operation by reducing the maximum stored current from 60 mA to 55 mA so as not to exceed the threshold of electric discharges because it was difficult to repair the damaged insulating supports in a short time. A new stripline kicker was designed and fabricated in parallel with this restricted user operation, and finally installed in the summer of 2015.

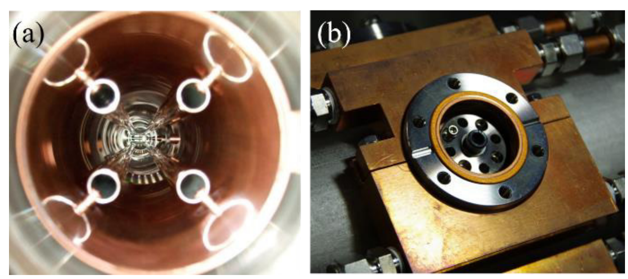

Figure 1: Photos of (a) the original kicker electrodes and (b) their insulating support parts.

In this paper, we describe the details of our new stripline kicker, from design to installation, and show the results of beam oscillation damping with the new kicker.

## DESIGN OF STRIPLINE KICKER

### *Shunt Impedance*

To quantitatively evaluate the stripline kicker performance, we need to calculate the transverse shunt impedance defined as follows [3]:

$$R_{\perp} = \frac{{V_{\perp}}^{2}}{2P}, \tag{1}$$

where $P$ is the rms input power to the kicker electrode, and $V_{\perp}$ is the transverse deflecting voltage generating between the electrodes. This deflecting voltage for a vertical kick is calculated using the following expression:

$$V_{\perp} = \left| \int_0^L [E_y(z) + cB_x(z)]dz \right|, \tag{2}$$

* ryota.takai@kek.jp

ISBN 978-3-95450-177-9

# INTRA-TRAIN POSITION AND ANGLE STABILISATION AT ATF BASED ON SUB-MICRON RESOLUTION STRIPLINE BEAM POSITION MONITORS

N. Blaskovic Kraljevic, T. Bromwich, P. N. Burrows, G. B. Christian, C. Perry, R. Ramjiawan,
John Adams Institute, Oxford, UK,
D. R. Bett, CERN, Geneva, Switzerland

*Abstract*

A low-latency, sub-micron resolution stripline beam position monitoring (BPM) system has been developed and tested with beam at the KEK Accelerator Test Facility (ATF2), where it has been used to drive a beam stabilisation system. The fast analogue front-end signal processor is based on a single-stage radio-frequency down-mixer, with a measured latency of 16 ns and a demonstrated single-pass beam position resolution of below 300 nm using a beam with a bunch charge of approximately 1 nC. The BPM position data are digitised on a digital feedback board which is used to drive a pair of kickers local to the BPMs and nominally orthogonal in phase in closed-loop feedback mode, thus achieving both beam position and angle stabilisation. We report the reduction in jitter as measured at a witness stripline BPM located 30 metres downstream of the feedback system and its propagation to the ATF interaction point.

## INTRODUCTION

The designs for the International Linear Collider (ILC) [1] and the Compact Linear Collider (CLIC) [2] require beams stable at the nanometre level at the interaction point (IP). In support of this, one of the goals of the Accelerator Test Facility (ATF2) at KEK, Japan, is to achieve position stability at the IP of approximately 2 nm. To this end, the Feedback On Nanosecond Timescales (FONT) project [3] operates a position and angle feedback system in the ATF2 extraction line [4]. In order to achieve the required level of position stability at the IP, the FONT feedback system needs to stabilise the beam to 1 μm at the entrance to the final focus system; this requires a BPM processing scheme capable of delivering position signals accurate to the sub-micron level on a timescale of the order of 10 ns.

The FONT beam position monitoring system makes use of three 12 cm stripline BPMs (P1, P2 and P3), which are located in the diagnostics section of the ATF2 extraction line and are placed on individual x, y movers (Fig. 1), and a witness stripline BPM (MFB1FF) located ~30 m downstream (Fig. 2). The BPMs are connected to specially developed analogue processing electronics [6] in order to deliver appropriate position signals to a digital hardware module [7] that digitises the signals and returns the sampled data to a computer where they are logged. The BPM system has achieved a demonstrated resolution of ~300 nm at a charge of $\sim 0.5 \times 10^{10}$ electrons/bunch [6].

## BPM PROCESSOR DESIGN

A schematic of the processor module is shown in Fig. 3 and a photograph of a partially disassembled module is shown in Fig. 6. The operation is as follows: the top ($V_T$) and bottom ($V_B$) stripline BPM signals are subtracted using a 180° hybrid to form a difference ($\Delta$) signal and are added using a resistive coupler to form a sum signal. The resulting signals are then band-pass filtered and down-mixed with a 714 MHz local oscillator (LO) signal phase-locked to the beam before being low-pass filtered

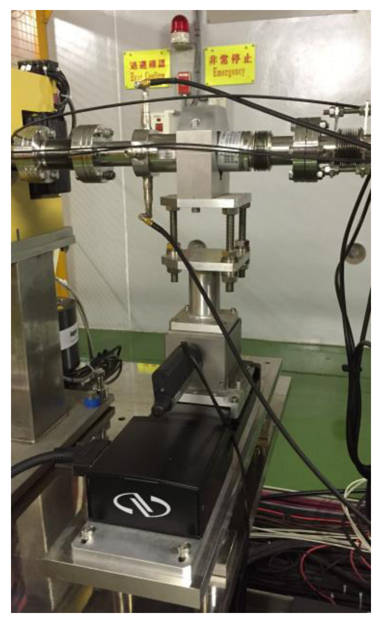

Figure 1: Photograph of the stripline BPM P3 and its mover.

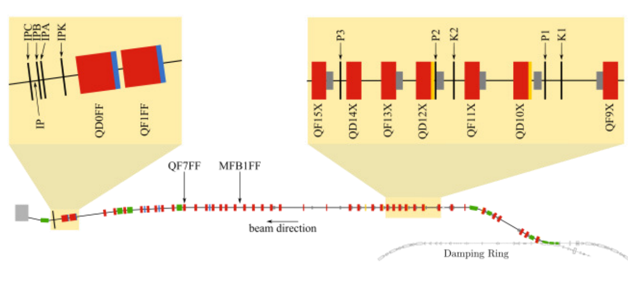


Figure 2: Layout [5] of the ATF2 extraction and final focus beamline with the FONT regions shown in detail.



ISBN 978-3-95450-177-9

# PERFORMANCE OF NANOMETRE-LEVEL RESOLUTION CAVITY BEAM POSITION MONITORS AND THEIR APPLICATION IN AN INTRA-TRAIN BEAM POSITION FEEDBACK SYSTEM

N. Blaskovic Kraljevic, T. Bromwich, P. N. Burrows, G. B. Christian, C. Perry, R. Ramjiawan,
John Adams Institute, Oxford, UK
D. R. Bett, CERN, Geneva, Switzerland
T. Tauchi, N. Terunuma, KEK, Tsukuba, Ibaraki, Japan
S. Jang, Dept. of Accelerator Science, Korea University, Sejong, South Korea
P. Bambade, LAL, Orsay, France

*Abstract*

A system of three low-Q cavity beam position monitors (BPMs), installed in the interaction point (IP) region of the Accelerator Test Facility (ATF2) at KEK, has been designed and optimised for nanometre-level beam position resolution. The BPMs have been used to provide an input to a low-latency, intra-train beam position feedback system consisting of a digital feedback board and a custom stripline kicker with power amplifier. The feedback system has been deployed in single-pass, multi-bunch mode with the aim of demonstrating intra-train beam stabilisation on electron bunches of charge ~1 nC separated in time by c. 220 ns. The BPMs have a demonstrated resolution of below 50 nm on using the raw measured vertical positions at the three BPMs, and has been used to stabilise the beam to below the 75 nm level. Further studies have shown that the BPM resolution can be improved to around 10 nm on making use of quadrature-phase signals and the results of the latest beam tests will be presented.

## INTRODUCTION

A number of fast beam-based feedback systems are required at future single-pass beamlines such as the International Linear Collider (ILC) [1]. For example, at the interaction point (IP) a system operating on nanosecond timescales within each bunch train is required to compensate for residual vibration-induced jitter on the final-focus magnets by steering the electron and positron beams into collision. The deflection of the outgoing beam is measured by a beam position monitor (BPM) and a correcting kick applied to the incoming other beam (Fig. 1). In addition, a pulse-to-pulse feedback system is envisaged for optimising the luminosity on timescales corresponding to 5 Hz.

The Feedback on Nanosecond Timescales (FONT) project has developed ILC prototype systems, incorporating digital feedback processors based on Field Programmable Gate Arrays (FPGAs), to provide feedback correction systems for sub-micron-level beam stabilisation at the KEK Accelerator Test Facility (ATF2) [2]. Demonstration of an upstream closed-loop feedback system that meets the ILC jitter correction and latency requirements is described in [3], together with results demonstrating the propagation of this correction along the ATF2 line. The ultimate aim is to attempt beam stabilisation at the nanometre-level at the ATF2 IP.

In order to achieve the required BPM resolution, three low-Q cavity BPMs have been developed, installed and optimised in the ATF2 IP region. We report here the BPM resolution measured with the ATF2 beam and the results achieved using one of these cavity BPMs to drive local feedback correction at the IP.

## EXPERIMENTAL SET-UP

An overview of the ATF2 extraction and final focus beamlines, showing the positions of the system components in the IP region, is given in Fig. 2. The IP region contains the three C-band cavity BPMs IPA, IPB and IPC, operated on an x, y mover system [5], with IPB being used in the single-loop IP feedback system described below. The cavity BPM design quality factors are shown in Table 1. The IP feedback correction is applied using a stripline kicker (IPK). The final focus magnets (QF1FF, QD0FF) can be used to steer the beam by introducing a position offset or to move the x and y beam waists longitudinally along the beamline. The offset of the QF7FF magnet can be used to change the pitch of the beam trajectory through the IP region.

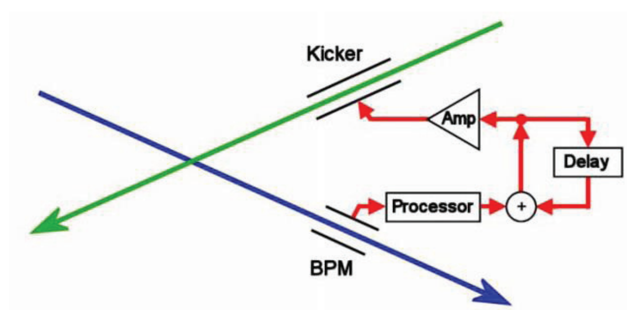


Figure 1: Schematic of IP intra-train feedback system with a crossing angle.

Table 1: Cavity BPM Design Quality Factors [6]

| Quality factor | y dipole mode |
|---|---|
| Loaded quality factor, $Q_L$ | 579 |
| Internal quality factor, $Q_0$ | 3996 |
| External quality factor, $Q_{ext}$ | 677 |



ISBN 978-3-95450-177-9

# DESIGN AND BEAM TEST RESULTS OF THE REENTRANT CAVITY BPM FOR THE EUROPEAN XFEL

C. Simon*, M. Baudrier, M. Luong, L. Maurice, O. Napoly,
CEA-Saclay/DRF/Irfu, Gif sur Yvette, France
N. Baboi, D. Lipka, D. Noelle, G. Petrosyan DESY, Hamburg, Germany
R. Baldinger, B.Keil, G. Marinkovic, M. Roggli, PSI, Villigen, Switzerland

*Abstract*

The European X-ray Free Electron Laser (E-XFEL) will use reentrant beam position monitors (BPMs) in about one quarter of the superconducting cryomodules. This BPM is composed of a radiofrequency (RF) reentrant cavity with 4 antennas and an RF signal processing electronics. Hybrid couplers, near the cryomodules, generate the analog sum and difference of the raw pickup signals coming from two pairs of opposite RF feedthroughs. The resulting sum (proportional to bunch charge) and difference signals (proportional to the product of position and charge) are then filtered, down-converted by an RF front-end (RFFE), digitized, and digitally processed on an FPGA board.

The task of CEA/Saclay was to cover the design, fabrication and beam tests and deliver these reentrant cavity BPMs for the E-XFEL linac in collaboration with DESY and PSI.

This paper gives an overview of the reentrant BPM system with focus on the last version of the RF front end electronics, signal processing, and overall system performance.

Measurement results achieved with prototypes installed at the DESY FLASH2 linac and in the E-XFEL injector are presented.

## INTRODUCTION

The European XFEL [1] is an X-ray free electron laser user facility installed in Hamburg, Germany. The beginning of commissioning is planned by the end of 2016. This accelerator has a superconducting 17.5 GeV main linac based on the TTF technology and its parameters are summarized in Table 1.

Table 1: E-XFEL Accelerator Parameters

| Parameter | Value |
|---|---|
| Typical beam sizes (RMS) | 20 – 200 µm |
| Nominal bunch charge | 0.02 – 1 nC |
| Bunch spacing | ≥ 222 ns |
| Macro-pulse length | 600 µs |
| Number of bunches within macro-pulse | 1 – 2700 |
| Nominal macro-pulse repetition rate | 10 Hz |

Each module includes a string of eight 1.3 GHz RF cavities, followed by a BPM connected to a superconducting quadrupole. Two types of cold BPMs are installed along the machine: cold reentrant BPMs and button BPMs which are not discussed here [2].

The cold reentrant BPM has a beam pipe aperture of 78 mm. It has to measure position and charge, to allow bunch to bunch measurements with a resolution better than 50 µm, a charge between 20 pC and 1 nC and an operating dynamic range of ± 10 mm.

To measure the behaviour of reentrant BPM with the electronics final version in its environment (Modular BPM Unit), beam measurements were done on a reentrant cavity BPM installed in a warm part at FLASH2 [3] and on the first cold reentrant BPM installed in the 3.9 GHz cryomodule during the commissioning of the E-XFEL injector [4].

## REENTRANT BPM SYSTEM

This type of BPM is composed of a radio-frequency reentrant cavity [5], which has to operate in a clean and cryogenic environment, and an analog front end electronic (RFFE) which provides the signals to a digital back end, connected to the control system.

Passing through the cavity, the beam excites electromagnetic fields (resonant modes), which are coupled by four feedthroughs to the outside. The voltage differences (Δ) from two opposite antennas correspond to the voltage of the dipole field in the X and Y axis and the sums (Σ) correspond to the voltage of the monopole field. The Δ and Σ signals are obtained from passive 4-ports 180° hybrid couplers. Each coupler is connected to a pair of opposite antennas and transmits the signals to the radiofrequency Front end electronics via some cables.

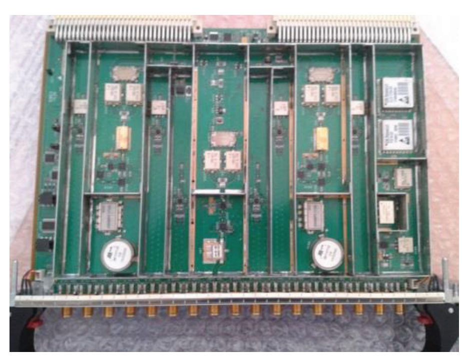

Figure 1: Reentrant RFFE board.

The reentrant Radio-Frequency Front End board (Fig.1) uses a single stage down-conversion to process the Δ/Σ signals. It is based on a Printed Circuit Board (PCB) with surface mount components and uses the VME64x form factor as required by the generic E-XFEL digitizer and

* claire.simon@cea.fr



ISBN 978-3-95450-177-9

# DESIGN OPTIMIZATION OF BUTTON-TYPE BPM ELECTRODE FOR THE SPring-8 UPGRADE*

M. Masaki†,1, H. Dewa[1], T. Fujita[1], H. Maesaka[2], S. Takano[1,2]
[1] Japan Synchrotron Radiation Research Institute, Kouto, Sayo, Hyogo, 679-5198, Japan
[2] RIKEN SPring-8 Center, Kouto, Sayo, Hyogo, 679-5148, Japan

*Abstract*

The design of a button-type BPM electrode for the SPring-8 upgrade has been optimized from the perspectives of 1) mechanical structure, 2) rf characteristics, and 3) thermal issue. We have adopted the electrode structure without a sleeve enclosing a button to maximize the button diameter. To minimize the beam impedance and the trapped mode heating of the electrode, the rf structure has been optimized by 3D electro-magnetic simulations. The reduction of the heating suppresses thermal deformation of the electrode and the BPM block, and improves thermal stability of the BPM system. The mechanical tolerance of the electrode was defined to fit the error budget for the total BPM offset error of 100 μm rms.

## INTRODUCTION

The BPM system of the storage ring for the SPring-8 upgrade [1, 2] has been designed to satisfy the requirements of long-term stability, resolution and accuracy. The specifications of the BPM system are summarized in ref. [3]. For the stability, a drift of the BPM offset less than 5 μm in a month is required. In a beam commissioning phase, a resolution of single-pass (SP) trajectory measurements better than 100 μm rms is necessary for an injected single bunch beam of 100 pC charge. The demanded accuracy for the SP measurement is within 100 μm rms and ±200 μm maximum. We have optimized the design of a button-type electrode for the new BPM system to meet the requirements. The points of the design optimization are 1) the maximization of signal intensity to satisfy the required resolution, 2) the specifications of necessary mechanical tolerances to fit the error budget for the total BPM offset, and 3) the minimization of heating to reduce thermal drift of the BPM offset. This paper focuses on the design of the button-type BPM electrode. The development status of the whole BPM system is described in a separate paper [3].

## MECHANICAL DESIGN

### *Button Diameter*

The vacuum chambers for the new ring have narrow apertures [4] due to small bore diameters of the strong quadrupole and sextupole magnets [5]. A cross-section of the BPM head is shown in Fig.1. The vertical aperture of the beam pipe is 16 mm. The button electrodes are mounted with the horizontal span of 12 mm on 20 mm-wide flat tops of the upper and lower sides. For satisfying the required signal intensity, it is necessary to maximize the button diameter in the narrow mounting space. Hence, we have adopted the electrode structure without a sleeve enclosing the button. No sleeve structure is also beneficial to eliminate the impedance and the trapped modes associated with an annular slot around the sleeve in a housing hole for the electrode. Figure 2 shows a schematic drawing of the designed button electrode. The maximized button diameter is 7 mm.

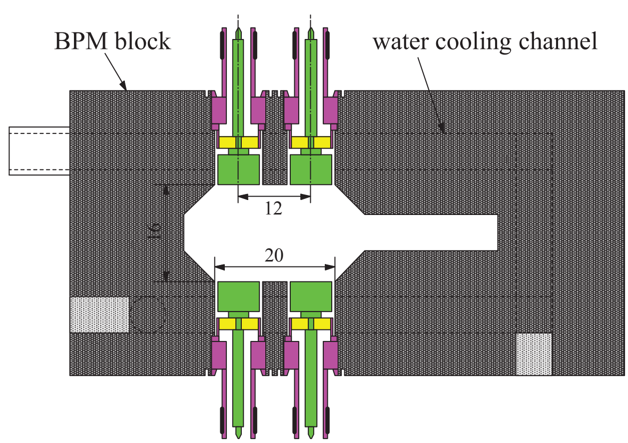


Figure 1: Cross section of the BPM head.

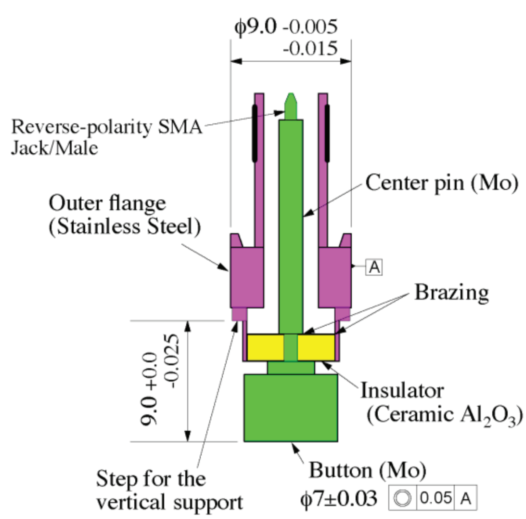


Figure 2: The designed BPM button electrode.

* Work supported by RIKEN SPring-8 Center
† masaki@spring8.or.jp



ISBN 978-3-95450-177-9

# THE CMS BEAM HALO MONITOR AT THE LHC: IMPLEMENTATION AND FIRST MEASUREMENTS

N. Tosi*[1], INFN Bologna, Italy
on behalf of the CMS Collaboration
[1]also at DIFA, Università di Bologna, Italy

*Abstract*

A Cherenkov based detector system has been installed at the Large Hadron Collider (LHC), in order to measure the Machine Induced Background (MIB) for the Compact Muon Solenoid (CMS) experiment. The system is composed of forty identical detector units formed by a cylindrical Quartz radiator directly coupled to a Photomultiplier. These units are installed at a radius of 1.8 m and a distance of 20.6 m from the CMS interaction point. The fast and direction-sensitive signal allows to measure incoming MIB particles while suppressing the much more abundant collision products and albedo particles, which reach the detector at a different time and from a different direction. The system readout electronics is based on the QIE10 ASIC and a $\mu$TCA based back-end, and it allows a continuous online measurement of the background rate separately per each bunch. The detector has been installed in 2015 and is now fully commissioned. Measurements demonstrating the capability of detecting anomalous beam conditions will be presented.

## INTRODUCTION

The increase in beam energy and luminosity in the LHC Run II, started in 2015, also meant an increase in Machine Induced Background (MIB) for the experiments. The Beam Radiation Instrumentation and Luminosity (BRIL) project designed, built and currently operates detectors that measure Luminosity and MIB in several regions of the CMS experiment [1]. Among the MIB detectors are instruments designed for protection of the sensitive inner silicon detectors of CMS from severe beam loss events and others that detect when the MIB reaches levels that would interfere with data taking efficiency. The Beam Halo Monitor (BHM) [2] is the outermost such detector, and it is sensitive to beam gas interactions happening upstream of CMS as well as beam halo interactions with the upstream collimators.

## THE DETECTOR

### *Concept*

The BHM has to be able to detect and correctly identify MIB particles in the context of a particle flux dominated by products of high energy *pp* collisions. Detection and identification are based on techniques that exploit differences between MIB and other particles, combined into a single instrument:

- The MIB flux is dominated by muons, due to absorption and decay of other particle types, while a significant fraction of the *pp*-collision products is composed of neutral particles.
- The MIB originated from the incoming beam and the *pp*-collision products travel in opposite direction.
- At several locations along the beampipe, the MIB and the majority of *pp*-collision products arrive with maximal time separation between each other (exactly half of the bunch spacing, 12.5 ns).

A Cherenkov based detector can make use of all these characteristics, thanks to Cherenkov radiation being emitted promptly and in a known direction with respect to the particle trajectory.

### *Detector Hardware*

Each BHM detector unit is composed of a synthetic quartz cylinder, 100 mm long and 52 mm in diameter, acting as Cherenkov radiator, directly coupled to a fast, UV-sensitive photomultiplier tube (PMT). Particles travelling from the quartz towards the PMT (from right to left in Fig. 1) emit Cherenkov Light that reaches the photocathode. Particles travelling in the opposite direction also emit light, but this is instead absorbed by a layer of black paint applied to the free face of the quartz. These elements are enclosed in a three layer shielding to protect the PMT from the residual field of the CMS solenoid and to absorb the large flux of low energy particles present in the cavern.

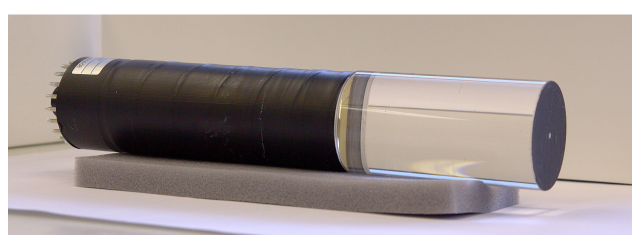

Figure 1: The active elements of the BHM detector unit: a 52 mm diameter quartz cylinder attached to an Hamamatsu R2059 photomultiplier.

The complete detector has twenty units on each end of CMS, mounted around the rotating shielding as shown in Fig. 2. They are located at a radius of 1.8 m and a distance of 20.6 m from the CMS interaction point and pointed towards the incoming beam. The large signal produced by the Hamamatsu R2059 PMT is brought to the readout electronics located in the service cavern via high bandwidth triaxial

* nicolo.tosi@cern.ch



ISBN 978-3-95450-177-9

# BEAM-LOSS MONITORING SIGNALS OF INTERLOCKED EVENTS AT THE J-PARC LINAC

N. Hayashi*, Y. Kato, A. Miura, JAEA/J-PARC, Tokai, Ibaraki, Japan
K. Futatsukawa, T. Miyao, KEK/J-PARC, Tokai, Ibaraki, Japan

*Abstract*

It is important to understand why the beam loss occurs during user operation. It is understandable that the beam loss results from RF cavities failure. However, it would be still useful to study the beam loss detailed mechanism and to know which beam loss monitor (BLM) experiences the highest loss or is most sensitive. This may lead a reduction in the number of interlocked events and a more stable accelerator operation. The J-PARC Linac BLM has a simple data recorder that comprises multiple oscilloscopes. Although its functionality is limited, it can record events when an interlock is triggered. Of particular interest here are the events associated with only the BLM Machine Protection System (MPS). These may reveal hidden problems with the accelerator.

## INTRODUCTION

The Japan Proton Accelerator Research Complex (J-PARC) is a high-intensity proton accelerator facility with three experimental hall, Materials and Life Science Experimental Facility (MLF), Hadron Experimental Facility (HD) and Neutrino Experimental Facility (NU). The accelerator parts are a 400-MeV linac, a 3-GeV Rapid-Cycling Synchrotron (RCS) and the Main Ring (MR), which is operated with 30 GeV. The designed beam power and intensity of the RCS at repetition rate of 25 Hz are 1 MW and $8.3 \times 10^{13}$ protons per pulse (ppp), respectively. On a one-shot basis, this goal was achieved in early 2015 [1]. That same year, there were two MLF target failures at 500 kW. Since then, the nominal operational beam power and intensity of the RCS have been limited to 200 kW and $1.8 \times 10^{13}$ ppp, respectively, for the MLF. The MR is operated with cycles of 2.48 and 5.52 s for the NU and HD, respectively. While most of the RCS beam is supplied to the MLF, four consecutive batches of two bunches each are injected from the RCS to the MR within either of these cycles. Operational MR beam powers of over 425 kW and 42 kW are achieved for the NU and HD.

The designed linac beam current and macro-pulse length are 50 mA and 500 $\mu$s, respectively. However, the peak current of the linac has been kept to 40 mA so far in 2016. The linac bunch structure has also been changed at the request of users. The typical bunch structure for the MLF is 300 $\mu$s macro-pulses in the linac and one bunch in the RCS. For the HD, the macro-pulse length is the same as that for the MLF, but the intensity is typically $1.2 \times 10^{13}$ ppp. For the NU, the macro-pulse is the designed 500 $\mu$s length and a typical RCS intensity is $5 \times 10^{13}$ ppp.

* naoki.hayashi@j-parc.jp

It is important to understand the over-all accelerator behavior, performance and characteristics, particularly in relation to the beam loss. The Machine Protection System (MPS) is usually triggered when a machine or instrument mal-functions or a beam loss monitor (BLM) hits its predefined threshold. The consequence in either case is that the beam is automatically stopped by the MPS.

It is certainly the case that failure of a RF cavity can cause a beam loss. Hence, it is useful to study the detailed correlation between RF cavity failures and the beam-loss pattern. This requires event data from many recorders with time identification. Sometime, a BLM will trigger the MPS without any sign of machine failure. This could be because of beam instability, accidental beam loss, or some other sources. Understanding beam losses and the entire machine characteristics further would help to reduce the number of MPS events and improve accelerator operation.

## LINAC AND BEAM MONITORS

The linac comprises various sub-systems. Its front end is an RF-driven $H^-$ ion source [2] and a 3-MeV RFQ [3]. Three drift-tube-linac (DTL) and 16 separated drift-tube-linac (SDTL) cavities then follow, and the $H^-$ beam reaches 190 MeV at this point. After that, 21 annular-ring coupled structure (ACS) cavities that were added in 2013 accelerate the beam up to 400 MeV [4]. The linac-to-3 GeV RCS beam transport line (L3BT) has a length of 190.5 m[1] and includes a 90 degree arc section in between two straight sections. The final ACS cavity, is showing in Fig. 1, along with debunchers 1 and 2, and 0-degree and 30-degree beam dumps. There are two more beam dumps (100-degree and 90-degree) downstream of the second straight section. These four beam dumps are used during beam tuning. The arc section contains six bending magnets from the marked BM01 to BM06 in Fig. 1.

A proportional chamber type BLM (BLMP) is adapted as the main BLM [5]. Its pre-amplifier is placed either in the sub-tunnel (B1F) or in the machine tunnel (B2F). The signal unit is in the klystron gallery (1F). Its high voltage (HV) is set to 2 kV. The maximum raw output is < 5 V. There are many BLMs distributed all over the linac. In particularly, after $7^{th}$ SDTL, each SDTL and ACS cavity has its own BLMP. In total, 79 BLMPs are connected to the MPS. The number of BLMP is 31 and 5 in the L3BT and in the beam dump area, respectively. $BLMP14$, $BLPM18$, and $BLMP21$ are located between the debuncher cavity 1

[1] It comprises four subsections. Straight section before arc is 33.0 m, Arc section is 44.9 m, Straight section after arc is 59.1 m, and Injection section (to the RCS) is 53.5 m.



ISBN 978-3-95450-177-9

# TIMING WINDOW AND OPTIMIZATION FOR POSITION RESOLUTION AND ENERGY CALIBRATION OF SCINTILLATION DETECTOR

J. Zhu, M.H. Fang, J. Wang, Z.Y. Wei§
Nanjing University of Aeronautics and Astronautics, Nanjing 210016, P. R. China

*Abstract*

We studied fast plastic scintillation detector array. The array consists of four cuboid bars of EJ200， each bar with PMT readout at both ends. The geometry of the detector, energy deposition in the scintillator， signal generation and energy response have been simulated based on Monte Carlo. The detection efficiency and the real events selection have been obtained while the background noise has been reduced by using two-end readout timing window coincidence. We developed an off-line analysis code, which is suitable for massive data from the digitizer. We set different coincidence timing windows, and did the off-line data processing respectively. It can be shown that the detection efficiency increases as the width of the timing window increases, and when the width of timing window is more than 10 ns, the detection efficiency will slowly grow until it reaches saturation. Therefore, the best timing window parameter τ as 16 ns is obtained for the on-line coincidence measurement. When exposure to $^{137}$Cs $\gamma$-ray irradiation, a 12 cm position resolution can be achieved while reaching the timing resolution of 0.9 ns. The pulse integration of signals of the detector is in proportion to the energy of incident particles. Furthermore, the geometrical mean of the dual-ended signals, which is almost independent of the hit position, could be used as the particle energy. Therefore, this geometrical mean as the energy of incident particle is calibrated via the Compton edges of $^{60}$Co source, $^{137}$Cs source and the natural $^{40}$K, $^{208}$Tl, and the reliability of the calibration results has been improved. Besides, the energy response is linear.

## INTRODUCTION

When an incident particle interacts in a scintillator, it can cause ionization and excitation of the atoms and molecules of the scintillator. The energy of the incident particle is deposited in the scintillator [1]. The decay of excited atoms and molecules back to their ground states results in a emission of photons with two decay components: the fast one with decay time less than a nanosecond， and the slow one has decay time of hundreds of nanoseconds. The photons are collected on photocathode of the photomultiplier tube (PMT), and then these photons are converted to photoelectrons and amplified. The output signals of the scintillation detector depend on both the energy and the hit position of the incident particle. Besides, false signals come from the dark current and noise also. When the dual-ended readout is taken, we need methods to get hit position and energy of the particles, and also need to select the real events [2]. In this paper, we got real events from incident particles with the background noise reduced by using two-end readout timing window coincidence.

EJ-200 plastic scintillation detector array and its data acquisition system have been set up for radiation measurement in our laboratory. The scintillation detector array consists of four EJ-200 plastic scintillators which have dual-ended PMTs. The EJ-200 plastic scintillator combines two main benefits of long optical attenuation length and fast timing. On the basis of coincidence measurement, we picked out the real events from the timing window of signals, and optimized the timing resolution, position resolution and energy response of the detector.

## SCINTILLATION DETECTION AND DATA ACQUISITION SYSTEM

The plastic scintillator used in this work was provided by the ELJEN Enterprises, USA. The scintillator (denoted by the ELJEN number EJ-200) had dimensions: 5 cm × 5 cm × 125 cm. The decay time of the scintillator is at the level of ns, and the rise time is less than 1 ns. The EJ-200 plastic scintillator was coupled to an ET Enterprises 9813B PMT. A VME bus system was used in our laboratory, and a schematic diagram of the detection system is shown in Fig. 1.

The DT5751 is a 4 channels 10 bit 1 GS/s Desktop Waveform Digitizer with 1 Vpp input dynamic range on single ended MCX coaxial connectors. The DT5751 Waveform Digitizer, which is taken in on-line coincidence measurement, has replaced some complex modules in the traditional coincidence circuits.

The V6533 is a 6 channels High Voltage Power Supply in 1 unit wide VME 6U module.

The online Digital Pulse Processing for Pulse Shape Discrimination firmware (DPP-PSD) was used in this study. Under the frame of DPP-PSD, we got the on-line waveforms and the energy histograms. Besides, the lists for the on-line data were obtained from the digitizer, and were further processed by ROOT, an off-line data-analysis software.

§ email address: wzy_msc@nuaa.edu.cn



ISBN 978-3-95450-177-9

# USE OF CR-39 PLASTIC DOSIMETERS FOR BEAM ION HALO MEASUREMENTS

I. Eliyahu, A. Cohen, E. Daniely, B. Kaizer, A. Kreisel, A. Perry, A. Shor and L. Weissman†,
Soreq Nuclear Research Center, Yavne 81800, Israel,
O. Girshevitz, BINA, Bar-Ilan University, Ramat-Gan 52900, Israel

*Abstract*

The first testing of CR-39 solid-state nuclear track dosimeters for beam halo measurement were performed at the SARAF phase I accelerator with ~ 2 MeV proton beams. Beam pulses of 90 nA peak intensity of the shortest possible duration (15 ns) available at SARAF were used for direct irradiation of standard CR-39 personal dosimetry tags. The lowest intensity and duration were used to minimize the beam core saturation on CR-39 tags. Other irradiations were done with beam pulses of 200 ns and 1 mA peak intensity. Specially prepared large area CR-39 plates with central hole for the beam core transport were used in the latter tests.

Weak beam structures were clearly observed in both types of irradiation. The tests showed feasibility of low energy beam halo measurements down to resolution level of a single proton. Different CR-39 etching conditions were studied. The advantages and drawback of the method are discussed.

## INTRODUCTION

Beam halo phenomenon and growth of beam emittance are important issues for high-intensity linear accelerators as it directly translated to beam loss and accelerator activation. Special research programs were dedicated to the study of the beam halo formation [1] and appreciable progress was achieved [2]. Nevertheless, beam halo remains difficult to predict, measure and control. Even the definition of halo is a subject of some controversy [3,4]. From theoretical aspect the beam-dynamic predictions of weak beam tails are not always reliable due to complexity of the non-linear and time dependent effects leading to halo formation. From experimental point side the main difficulty is measurement of spatial distribution of weak beam tails at the presence of the many order of magnitude more intense beam core. Development of a simple and reliable tools and methods for beam halo diagnostics is highly desirable.

The first phase of the Soreq Applied Research Facility (SARAF) is operational since 2010 while the second phase is under design and planned to be commissioned starting at 2020. At phase I SARAF linac delivers CW and pulsed proton and deuteron beams at intensity up to 2 mA and at energy up to 4 MeV and 5.5 MeV for protons and deuterons respectively. At full specification SARAF will deliver 5 mA CW proton and deuteron beams at 40 MeV. The facility should satisfy hands-on maintenance requirement which in the case of intense beam require very low beam loss along the accelerator and the beam lines. In this respect understanding and control of the beam halo is a subject of great importance. The exact origin of the beam halo is not known but at least a significant contribution comes from the linac injector [5]. Hence, study of beam halo at the medium energy section is essential for halo tracking over the entire accelerator.

Importance of halo measurements was realized at the early stage of the SARAF project when significant efforts were spent in preparation for the beam halo measurements program [6]. Later on, however, this program was not vigorously pursued due to numerous challenges of the phase I accelerator commissioning and large number of physics experiments requested by the users. At the present, the SARAF team plans on launching only a limited halo research program, with limited beam time.

CR-39, allyl diglycol carbonate, is a plastic polymer commonly used for eyeglass lenses production. This material is also used since the 1970-s for nuclear track detection of cosmic rays, charge particles and fast neutrons [7]. The Soreq dosimetry department uses CR-39 radiation tags for personal radiation monitoring over the course of a few decades. For this halo investigation, we took advantage of significant experience accumulated at our research center with CR-39 and tested possibility of using of these detectors as simple means of beam halo diagnostics.

## TESTS OF CR-39

Several issues should be taken in account when considering using CR-39 material for diagnostics of intense beams. Track detectors have very high sensitivity and thereby capability to detect each individual particle of the beam. On the other hand, the track detectors have a very low level of saturation. Thus, the beam fluence has to be reduced by many orders of magnitudes without changing the peak intensity to ensure successful use of the detectors. A fast beam chopping is an optimal technique for drastically reducing beam current while maintaining the beam profile of the intense beam. In the case of mA beam intensity even a single beam bunch may result in CR-39 saturation in the beam core. The possible way to overcome this problem is to use CR-detectors with a central hole for the beam core transport. Thus, only image of the beam periphery will be taken.

Additional question which should be considered is the conditions of CR-39 development after exposure. The

† weissman@soreq.gov.il



ISBN 978-3-95450-177-9

# ONLINE TOTAL IONISATION DOSIMETER (TID) MONITORING USING SEMICONDUCTOR BASED RADIATION SENSORS IN THE ISIS PROTON SYNCHROTRON

D. M. Harryman*, A. Pertica, Rutherford Appleton Laboratory, Oxfordshire, UK

*Abstract*

During routine operation, the radiation levels in the ISIS proton synchrotron become high enough to permanently affect systems and electronics. This can potentially cause critical components to fail unexpectedly or denature over time, causing disruption for users of the ISIS facility or a loss of accuracy on a number of systems. To study the long term effects of ionising radiation on ISIS systems and electronics, the total dose received by such components must be recorded. A semiconductor based online Total Ionisation Dosimeter (TID) was developed to do this, using pin diodes and Radiation sensing Field Effect Transistors (RadFETs) to measure the total ionisation dose. Measurements are made by feeding the TIDs with a constant current, with the threshold voltage on each device increasing in relation to the amount of radiation that it has received. This paper will look at preliminary offline results using off the shelf Field Effect Transistors (FETs) and diodes, before discussing the development of the RadFET online monitor and the results it has gathered thus far. Finally the paper will look at future applications and studies that this type of monitor will enable.

## INTRODUCTION

ISIS is a pulsed spallation neutron and muon source facility, consisting of a $H^-$ linear accelerator (Linac) and a proton synchrotron. The Linac accelerates $H^-$ ions up to an output energy of 70 MeV, these ions then have their electrons removed with a stripping foil on injection into the synchrotron. The protons ($H^+$ ions) are then accelerated up to 800 MeV before being extracted and directed to one of two target stations. ISIS runs in user cycles, during these cycles the accelerator runs for 24 hours a day for 6-8 weeks, this is when scientists use the neutrons and muons created by the facility to study materials in the target station beam lines. Maintenance operations are carried out during shutdown periods between these cycles, it is best to change components and systems during these shutdown periods, to avoid disrupting the users of the facility.

When the accelerator is being operated, some areas like the synchrotron, become off limits due to the amount of radiation produced. While radiation exposure to personnel has always been monitored at ISIS, historically it has not been done for systems and components. To try and predict when components or systems may fail due to radiation damage, an online TID monitor has been developed, using off the shelf FETs, pin diodes, and application specific RadFETs. The developed TID monitor allows for a number of studies to take place, such as component characterisation, however this paper will primarily focus on the development of the monitor.

Semiconductors are permanently affected by ionising radiation [1]. As high energy particles travel through the gate of a FET, the radiation induced charges get trapped in the gate and create electron hole pairs (see Fig. 1) [1, 2]. Metal Oxide Semiconductor Field Effect Transistors (MOSFETs) have been shown to be more susceptible to radiation effects than the more generic FETs, due to this, they will be the type of FETs used in these experiments.

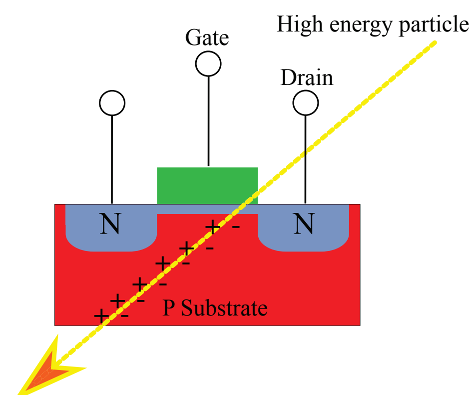


Figure 1: High energy particles creating electron hole pairs and trapping charges in the gate of a Field Effect Transistor (FET) as they travel through.

When biasing a FET or diode that's been irradiated with a constant current the voltage measured back will be proportional to how much radiation the component has been subjected to [2]. This allows for these components to be used as dosimeters. Organisations like the Tyndall Institute have made specific FETs, called RadFETs for just this type of application [3].

The RadFETs used in this experiment were the Tyndall TY1004 [3]. The thicker metal oxide gates of RadFETs have a larger exposed surface area. They are thus by design more susceptible to radiation damage. The TY1004 RadFETs have an 400 nm oxide gate, whereas typical off the shelf FETs will only have an oxide gate of a few nm. FETs with a thinner metal oxide gate will result in components that are less sensitive to radiation damage, but can measure a larger dose capacity. The voltages produced from the TY1004 RadFETs are factory calibrated against precise dose measurements and can be converted using a supplied transfer function Eq. (1) [3].

* daniel.harryman@stfc.ac.uk

ISBN 978-3-95450-177-9

# COSY BPM ELECTRONICS UPGRADE

C. Böhme, A. J. Halama, V. Kamerdzhiev,
Forschungszentrum Jülich, Germany

*Abstract*

The Cooler Synchrotron COSY delivers proton and deuteron beams to the users since the early 90s. The experiments are carried out using the circulating beam as well as the beams extracted from the ring and delivered by three beamlines. The original BPM system still operational in the ring does not fulfill the requirements for new experiments. It utilizes cylindrical and shoe-box type diagonally cut capacitive pick-ups. The most signal processing is done the analog way. Additionally to its age and the increasing failure rate, the analog processing introduces large drifts in e.g. the offset, which regularly require a significant effort for manual calibration. Even then the drifts render it impossible to match the requirements of the planned JEDI experiment, which is an orbit with a maximum of 100 $\mu$m RMS deviation. Therefore an upgrade of the readout electronics was decided. The decision process is described, the implications listed and the current status is reported.

## INTRODUCTION

The COoler SYnchrotron (COSY) of the Forschungszentrum Jülich is a 184 m long racetrack-shaped synchrotron and storage ring for protons and deuterons from 300 MeV/c (protons) or 600 MeV/c (deuterons) up to 3.7 GeV/c. Built in are devices for stochastic as well as electron cooling. The stored ions can be polarized or unpolarized. Commissioned in 1993, the electronic parts of the BPM system are not only outdated, but start failing while spare parts for repair are hard to acquire. In addition, for the planned EDM [1] precursor experiment a higher beam position measurement accuracy is needed than can be reached with the used components. Therefore different upgrade scenarios for the BPM system were investigated.

## CURRENT STATUS

COSY is equipped with 29 shoebox-style BPMs. During commissioning 27 BPMs of two types were installed, a cylindrical type with 150 mm diameter and a rectangular type 150 mm · 60 mm [2]. The selection was made to fit into the beam pipe, which is round in the straight sections and rectangular in the arcs in order to fit into the dipole magnets. Recently 2 BPMs were added with special geometries to fit within the beam pipe of the 2 MeV electron cooler [3]. These two use their own electronics for readout, which is different from the others.

All other BPMs are read out by the same type of electronics [4], whose concept is shown in Figure 1. The readout electronic for each BPM, except for the pre-amplifiers, is housed in one VXI crate, consisting of 2 analog modules, 2 digital modules, one CPU, and one timing receiver. The

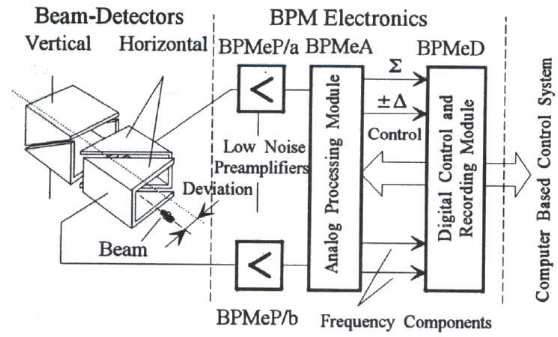


Figure 1: Current Beam Position Monitor electronics assembly [4].

pre-amplifiers are directly connected to the N-type vacuum feedthrough of the pick-ups. This pre-amplifier has a fixed gain of 13.5 dB with an input impedance of 500 $k\Omega$ and a bandwidth of 100 MHz (-3 dB). The gains and offsets of two pre-amplifiers have to be exactly matched for one plane of one BPM in order to avoid incorrect measurements. The preamplified signals are fed into an analog module, where sum and delta signals are produced using a hybrid. These signals are then treated separately and can be further amplified in 6 dB steps from 0 dB to 66 dB. Both the sum and the delta branches have two signal paths. A narrowband path features 3 possible filter settings with bandwidths of 10 kHz, 100 kHz, or 300 kHz and an additional amplifier that can be set from 0 dB to 18 dB in 6 dB steps. The broadband path with 10 MHz bandwidth can be used for turn-by-turn measurements while the narrowband signals are used for closed orbit measurements. The analog outputs are unipolar, the sign of the narrowband delta signal is detected separately and the information is transmitted by a separate TTL signal line. After the analog signal processing the signals are digitized in a digital module. This is done using 20 MHz 8 bit ADCs. For the narrowband signal the sampling frequency is lowered to 1 MHz or 100 kHz, depending on the selected analog bandwidth. For the sum signal only 7 of the 8 bits of the ADC are used, the 8th bit is used to indicate the polarity of the delta signal. The digital module generally has the capability to buffer 4096 data points, while few modules can store up to 64k data points that can be used for turn-by-turn measurements. The CPU in the VXI crate calculates out of the narrowband signal the beam position using a scaling factor for the specific BPM geometry. It is also possible to transfer the raw broadband data to the control system display and export it, for e.g. computation of the turn-by-turn position.

ISBN 978-3-95450-177-9

# BEAM DIAGNOSTICS FOR MEDICAL ACCELERATORS*

C.P. Welsch#, Cockcroft Institute and The University of Liverpool, UK
on behalf of the OMA Consortium

*Abstract*

The Optimization of Medical Accelerators (OMA) is the aim of a new European Training Network that has received 4 ME of funding within the Horizon 2020 Programme of the European Union. OMA joins universities, research centers and clinical facilities with industry partners to address the challenges in treatment facility design and optimization, numerical simulations for the development of advanced treatment schemes, and beam imaging and treatment monitoring. This paper presents an overview of the network's research into beam diagnostics and imaging. This includes investigations into applying detector technologies originally developed for high energy physics experiments (such as VELO, Medipix) for medical applications; integration of prompt gamma cameras in the clinical workflow; identification of optimum detector configurations and materials for high resolution spectrometers for proton therapy and radiography; ultra-low charge beam current monitors and diagnostics for cell studies using proton beams. It also summarizes the network-wide training program consisting of Schools, Topical Workshops and Conferences that will be open to the wider medical and accelerator communities.

## INTRODUCTION

In 1946 R.R. Wilson introduced the idea of using heavy charged particles in cancer therapy. In his seminal paper [1] he pointed out the distinct difference in depth dose profile between photons and heavy charged particles: While photons deposit their energy along the beam path in an exponentially decreasing manner, heavy charged particles like protons and ions show little interaction when they first enter the target and deposit the dominant portion of their energy only close to the end of their range. This leads to an inverse dose profile, exhibiting a well-defined peak of energy deposition (the Bragg Peak). The depth of the Bragg Peak in the target can be selected precisely by choosing the initial energy of the particles. This allows for a significant reduction of dose delivered outside the primary target volume and leads to substantial sparing of normal tissue and nearby organs at risk. The field of particle therapy has steadily developed over the last 6 decades, first in physics laboratories, and starting in the late 90's in dedicated clinical installations. By March 2013 about 110,000 people had received treatment with particle beams, the vast majority having been treated with protons and around 15,000 patients with heavier ions (helium, carbon, neon, and argon). The latter are considered superior in specific applications since they not only display an increase in physical dose in the Bragg peak, but also an enhanced relative biological efficiency (RBE) as compared to protons and photons. This could make ions the preferred choice for treating radio-resistant tumors and tumors very close to critical organs. Proton- and ion therapy is now spreading rapidly to the clinical realm. There are currently 43 particle therapy facilities in operation around the world and many more are in the proposal and design stage. The most advanced work has been performed in Japan and Germany, where a strong effort has been mounted to study the clinical use of carbon ions. Research in Europe, particularly at GSI, Germany and PSI, Switzerland must be considered outstanding. Initial work concentrated predominantly on cancers in the head and neck region using the excellent precision of carbon ions to treat these cancers very successfully [2]. Also, intensive research on the biological effectiveness of carbon ions in clinical situations was carried out and experiments, as well as Monte Carlo based models including biological effectiveness in the treatment planning process were realized [3]. This work has directly led to the establishing of the Heavy Ion Treatment center HIT in Heidelberg, Germany [4]. HIT started patient treatment in November 2009 and continues basic research on carbon ion therapy in parallel to patient treatments. Several other centers offering carbon ion and proton therapy are under construction or in different stages of development across Europe, e.g. five proton therapy centers are being built in the UK, one more has been commissioned in Marburg, Germany and the Medaustron facility has also started patient treatment recently. The OMA network presently consists of 14 beneficiary partners (three from industry, six universities, three research centers and 2 clinical facilities), as well as of 17 associated and adjunct partners, 8 of which are from industry.

## RESEARCH

Continuing research into the optimization of medical accelerators is urgently required to assure the best possible cancer care for patients and this is one of the central aims of OMA [5]. The network's main scientific and technological objectives are split into three closely interlinked work packages (WPs):

- Development of novel beam imaging and diagnostics systems;
- Studies into treatment optimization including innovative schemes for beam delivery and enhanced biological and physical models in Monte Carlo codes;

*This project has received funding from the European Union's Horizon 2020 research and innovation programme under the Marie Skłodowska-Curie grant agreement No 675265.
#c.p.welsch@liverpool.ac.uk

ISBN 978-3-95450-177-9

# ACCELERATOR OPTIMIZATION THROUGH BEAM DIAGNOSTICS

C.P. Welsch#, Cockcroft Institute and The University of Liverpool, UK
on behalf of the oPAC Consortium

*Abstract*

A comprehensive set of beam diagnostics is key to the successful operation and optimization of essentially any accelerator. The oPAC project received 6 M€ of funding within the EU's 7th Framework Programme. This has allowed to successfully train 23 Fellows since 2011. The network joins more than 40 institutions from all around the world, including research centers, universities and private companies. One of the project's largest work packages covers research in beam diagnostics. This includes advanced instrumentation for synchrotron light sources and medical accelerators, enhanced beam loss monitoring technologies, ultra-low emittance beam size diagnostics, diagnostics for high intensity beams, as well as the development of electronics for beam position monitors. This paper presents an overview of the research outcomes from the diagnostics work package and the demonstrated performance of each monitor. It also shows how collaborative research helps achieving beyond state-of-the-art solutions and acts as an ideal basis for researcher training. Finally, an overview of the scientific events the network has been organizing for the wider accelerator community is given.

## INTRODUCTION

The optimization of the performance of particle accelerators was the goal of the Marie Curie Initial Training Network (ITN) oPAC [1]. The project received 6 M€ of funding from the European Union within the 7$^{th}$ Framework Programme, making it the largest-ever ITN. It successfully trained 23 Fellows across 4 scientific work packages (WPs) and allowed them to develop expert knowledge in a number of different fields, such as engineering, physics, electronics, IT and material sciences. Training through network-wide events including schools and topical workshop, participation in international conferences, and secondments for specific skill-building has allowed them to carry out cutting edge research whilst providing them with a broad set of skills that is expected to be an excellent basis for their future careers.

## RESEARCH

The results from the oPAC Fellows' research have resulted in more than 100 contributions to international conferences and workshops. More than 30 papers have already been published in peer-reviewed journals and several more are currently in preparation as results from research projects are being analyzed and Fellows are finalizing their doctoral theses. The following sections present the results from three selected research projects that all formed part of the beam diagnostics work package.

The developments in this WP received additional support by a dedicated hands-on training day in beam instrumentation hosted by Bergoz in June 2013. This familiarized all Fellows in the first year of their project with the particular challenges in carrying out measurements of the detailed characteristics of charged particle beams and allowed them to discuss progress in all sub projects. Of particular importance for instrumentation development is that no single monitor has yet been developed that is able to monitor all properties of a beam, i.e. several different technologies usually need to be combined to get a full understanding of the beam inside its vacuum chamber. Most oPAC projects initially targeted the development of a single detector (prototype) for a specialized purpose. Information from this monitor was then combined with other detectors and linked to the accelerator control and data acquisition system to obtain a full understanding about the beam.

### *Beam Size Measurements at ALBA using Interferometry*

Synchrotron radiation interferometry is now a reliable method to measure the horizontal and vertical beam size at the ALBA storage ring in Barcelona, Spain. The technique, developed by T. Mitsuhashi, allows determining the beam size by measuring the visibility of the interferogram, obtained by making the visible part of the synchrotron radiation interfere using a double slit interferometer. Due to the layout of the ALBA diagnostic beam line Xanadu interferometry measurements were not completely straight forward. Fellow Laura Torino introduced several enhancements to the existing set-up to overcome existing limitations, in particular: The light selected by a photon shutter cuts the light horizontally whilst the first extraction mirror selects only the upper lobe of the produced radiation. This generates a final footprint that is dominated by Fraunhofer diffraction. The use of a double slit system allows the selection of several different fringes of the footprint. Fringes generated by Fraunhofer diffraction don't have necessarily the same phase. This might provoke a loss of contrast affecting the visibility measurements. To reduce this effect the slits were substituted by pinholes to select a more compact region of the footprint and consequently, a reduced number of fringes. Furthermore, the 7 mirrors guiding the light up to the Xanadu optical table are "in-air". The air turbulence in the tunnel or in the beam line can provoke vibrations of the optical elements that are converted in a rigid displacement of the centroid of the interferogram image on the CCD sensor.

*This project has received funding from the European Union's Seventh Framework Programme for research, technological development and demonstration under grant agreement no 289485.

#c.p.welsch@liverpool.ac.uk



ISBN 978-3-95450-177-9

# THE FRASCATI LINAC BEAM-TEST FACILITY (BTF) PERFORMANCE AND UPGRADES*

B. Buonomo, C. Di Giulio, L. G. Foggetta†, INFN – Laboratori Nazionali di Frascati, Via Enrico Fermi 40, I-00044 Frascati (Rome), Italy.
P. Valente, INFN – Sezione di Roma, P.le Aldo Moro 2, I-00185 Rome, Italy.

*Abstract*

In the last 11 years the Beam Test Facility (BTF) of the Frascati DAFNE accelerator has gained an important role in the development of particle detectors development. Electron and positron beams can be extracted to a dedicated transfer line, where a target plus a dipole and collimator system can attenuate and momentum-select secondary particles.

The BTF can thus provide a wide range of beam parameters: energy (from about 50 to 750/540 MeV for electrons/positrons), charge (up to $10^{10}$ particles/bunch) and pulse length (1.5-40 ns), with a maximum repetition rate of 50 Hz.

Beam spot and divergence can be adjusted, down to sub-mm and 2 mrad. Photons can be produced on a target, and energy-tagged inside a dipole by Silicon micro-strip detectors. A shielded Tungsten target is used for neutron production: about $8{\cdot}10^{-7}$/primary, 1 MeV neutrons are produced.

In addition to these activities, a dedicated particle physics experiment (PADME) has been recently approved for running at the BTF, with an intermediate intensity positron beam.

In order to cope with the increasing beam requests, an upgrade program of the facility has been proposed, along three main lines: consolidation of the DAFNE LINAC, in order to guarantee stable operation in the longer term; upgrade of the maximum beam energy to 1 GeV; doubling of the existing beam-line and experimental hall.

## BTF LINE DESCRIPTION AND PRESENT PERFORMANCE

The Beam-Test Facility (BTF) of the INFN Frascati Laboratories is an extraction and transport line, optimized for the production of electrons and positrons in a wide range of intensity, energy, beam spot dimensions and divergence, starting from the primary beam of the DAFNE LINAC. Each of the 50 pulses/s accelerated by the LINAC can be either driven to a small ring for emittance damping (and from there injected into the DAFNE collider rings), or to the BTF line, by means of pulsed dipoles.

A variable depth target (from 1.7 to 2.3 $X_0$) spreads the momentum distribution of the incoming beam, then secondary electrons (or positrons) are momentum selected by means of a 45° dipole and collimators (in the horizontal plane). The beam intensity is thus greatly reduced, depending on the chosen secondary beam energy central value (from about 50 MeV up to almost the primary beam energy) and spread (typically better than 1%, depending on the collimators settings) [1].

The beam is then transported to the experimental hall and focussed by means of two quadrupole FODO doublets. The layout of the beam selection and transport line is shown in Fig. 1, together with the shielded experimental area.

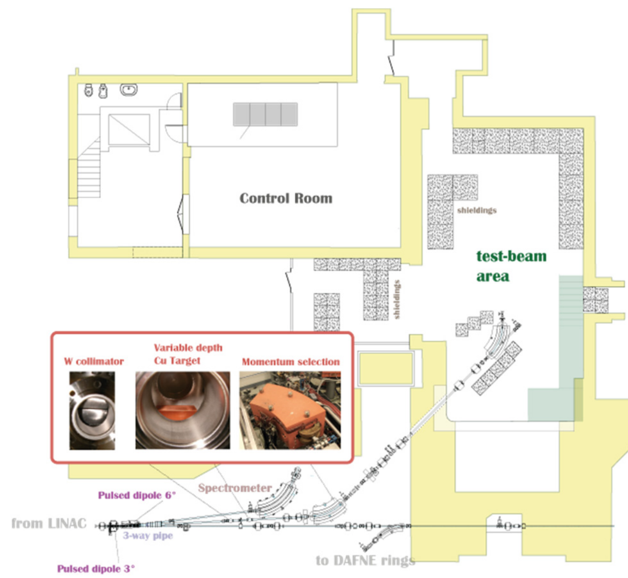


Figure 1: Layout of the BTF line and area, in the inset pictures of (from the left): Tungsten collimators pair, Copper beam-attenuating target, energy-selecting dipole magnet.

### *Availability and Flexibility*

The facility can operate essentially in two different modes: "parasitic", when the DAFNE collider is operating and only LINAC bunches not injected into the rings are available; "dedicated", when the collider is not operating and all LINAC bunches are available for the beam-test. Considering the frequency of electron and positron injections for DAFNE and the number of available bunches, an average of 20 pulses/s is delivered for BTF operation.

The facility has been steadily operating since 2004, with an average of more than 200 beam-days/year, and 25 user groups/year. Beam time is generally allotted in one week shifts (Monday to Monday, 24/7 operation). A small fraction of the shifts have been dedicated to:

- production of tagged photons, by means of a dedicated active Bremsstrahlung target and energy-tagging system, made up of Silicon micro-strip detectors [2];
- electro-production of neutrons on a Tungsten target, shielded by an optimized assembly of polyethylene and Lead [3].

ISBN 978-3-95450-177-9

# TESTING THE UNTESTABLE: A REALISTIC VISION OF FEARLESSLY TESTING (ALMOST) EVERY SINGLE ACCELERATOR COMPONENT WITHOUT BEAM AND CONTINUOUS DEPLOYMENT THEREOF

A. Calia, K. Fuchsberger, M. Hostettler, CERN, Geneva, Switzerland

*Abstract*

Whenever a bug in some piece of software or hardware stops beam operation, loss of time is rarely negligible and the cost (either in lost luminosity or real financial one) might be significant. Optimization of the accelerator availability is a strong motivation to avoid such kind of issues. Still, even at large accelerator labs like CERN, release cycles of many accelerator components are managed in a “deploy and pray” manner. In this paper we will give a short general overview on testing strategies used commonly in software development projects and illustrate their application on accelerator components, both hardware and software. Finally, several examples of CERN systems will be shown on which these techniques were or will be applied (LHC Beam-Based Feedbacks and LHC Luminosity Server) and describe why it is worth doing so.

## INTRODUCTION

An accelerator is a complex system, consisting of many interlinked components, which are typically organized in a control system of different layers from top-level applications to actual hardware.

Fig. 1 shows a vertical slice of a typical accelerator control system stack: On top there is the application layer, consisting of a set of physics-aware applications used by operators, which accesses the hardware through a middle layer. Below, the hardware layer is responsible of actually driving the hardware interacting with the beam.

An accelerator component is typically on one of these layers, and accessing or being accessed by one or more neighbouring components from the other layers. E.g. a top-level software component can access different hardware components through the middle layer, while a hardware component is often accessed by different top-level applications.

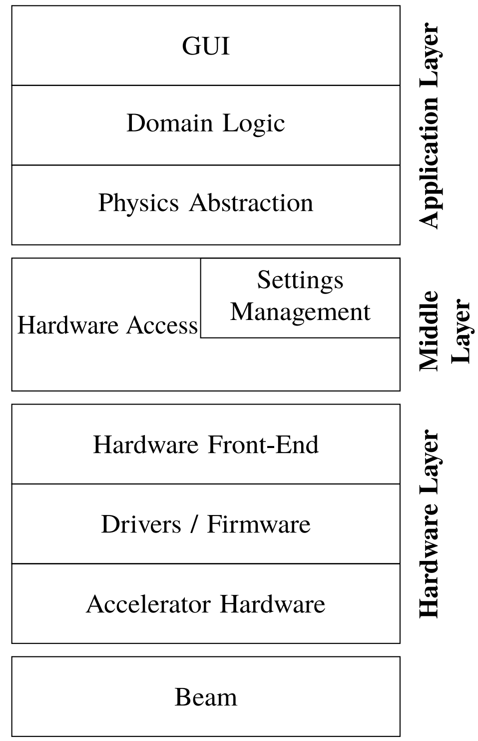


Figure 1: Vertical slice of a typical control system.

## EXECUTION MODE

For testability of individual components or any subset of the whole control system, it is required to reduce the coupling between neighbouring components. To facilitate decoupling, we propose different “execution modes” for an accelerator component, which can make it independent of the input and output of other components for testing and development purposes.

### *Simulation*

In a simulation mode, the component’s inputs are based on a model. This model is dynamic and can be affected by the execution of a component. The purpose of a simulated model is to test the component in a dynamic environment that can be close to the reality (production).

Ideally, it is possible to create various simulation models to effectively test the component under different circumstances. For a web service, a particularly interesting test is to verify the behaviour when network communications are very unstable and randomly slow. In the case of a hardware component, a challenging model can produce random noise in the inputs signals of the hardware cards.

### *Scenario*

A scenario is composed by a set of fixed values that are the inputs of a component. Given the scenario’s input, it is possible to assert the component’s output to spot errors.

Scenarios can be created from particular situations that the component must be able to handle. These situations can be artificially made, based on the component’s design, or can be derived from experience. The latter case is especially true in a high-availability system. In these kind of systems it is precious to not introduce regressions during updates.

ISBN 978-3-95450-177-9

# THE ALIGNMENT OF CONVERGENT BEMLINES AT A NEW TRIPLE ION BEAM FACILITY

O. F. Toader, T. Kubley, F.U. Naab, E. Uberseder, Michigan Ion Beam Laboratory, University of Michigan, Ann Arbor, Michigan, USA

*Abstract*

The Michigan Ion Beam Laboratory (MIBL) at the University of Michigan in Ann Arbor Michigan, USA, has recently upgraded its capabilities from a two accelerator to a three accelerator operation mode. The laboratory, equipped with a 3 MV Tandem, a 400 kV Ion Implanter and a 1.7 MV Tandem, has also increased the number of available beamlines from three to seven with two more in the planning stages. Multiple simultaneous ion beam experiments are already in progress and scientists conduct state of the art experiments involving light and heavy ions. The MIBL staff had to overcome multiple challenges during the physical alignment process of the accelerators, beamlines and experimental end-stages. Not only the position of the accelerators changed, but the target chambers were moved into a different room behind a one meter thick concrete wall. At the same time, a beamline from each accelerator had to converge and connect to a single chamber at a precise angle. This paper focuses on the alignment process of all the equipment involved in triple ion beam experiments and especially on the procedures to align the ion beams on a target.

## INTRODUCTION

Ion beam irradiation experiments, if properly conducted, can simulate the radiation damage that occurs in materials inside a nuclear reactor. While radiation effects induced by neutrons can be successfully emulated by protons and heavy ions irradiations in much shorter times, researchers tried to find a way to also simulate the presence of transmutation products in reactors. Building on the successes of other facilities (TIARA-Japan and JANNUS-France), the Michigan Ion Beam Laboratory (Fig. 1.a,b,c) as part of the Department of Nuclear Engineering and Radiological Sciences at the University of Michigan, is now in the position to deliver dual and triple ion beam irradiations experiments.

## THE PARTICLE ACCELERATORS

The laboratory is equipped with three accelerators: a 3 MV Tandem, a 1.7 MV Tandem and a 400 kV Implanter. The 3 MV Tandem (model 9SDH-2) high current Pelletron accelerator (Fig. 2a) was built by National Electrostatics Corporation (NEC). The 1.7 MV accelerator (Fig. 2b) is a solid-state, gas insulated, high frequency Tandetron built by General Ionex (now HVEE) that operates in the 0.3 MV to 1.7 MV range delivering very stable DC beams. The 400 kV implanter (Fig. 2c) is an air-insulated device also built by NEC that can deliver ion beams from any element in the periodic table, with beam fluences of 1 mA or more for some gas ions, on an area with a diameter in excess of 6 inches (15 cm). The implantation stage can be cooled to LN temperatures or heated up to 800 $^0$C.

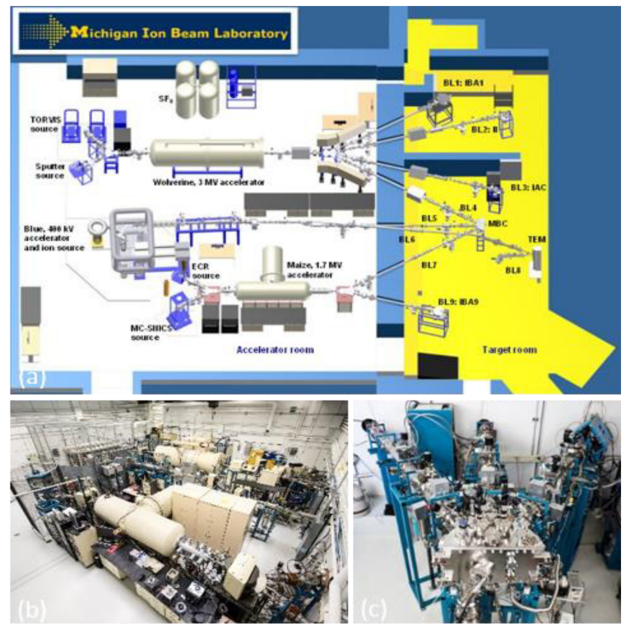


Figure 1: (a) AutoCAD drawing of the lab in the new configuration, (b) Overhead view of the lab (c) View of the multiple ion beam chamber designed to simultaneously accommodate up to three ion beams on a target.

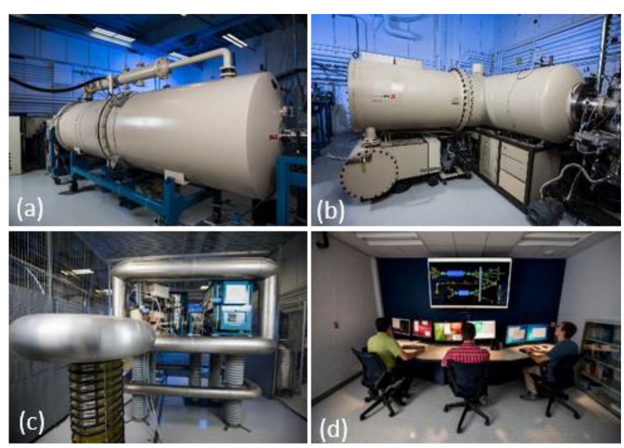


Figure 2: MIBL particle accelerators: (a) 3 MV Tandem – Wolverine (W), (b) 1.7 MV Tandetron – Maize (M), (c) 400 kV ion implanter – Blue (B) and (d) view of the Control Room (CR) of the three accelerators that now operate in remote control mode.



ISBN 978-3-95450-177-9

# BLIP SCANNING SYSTEM POWER SUPPLY CONTROL*

Z. Altinbas†, R. Lambiase, C. Theisen, Brookhaven National Laboratory, Upton, NY, USA

*Abstract*

In the Brookhaven LINAC Isotope Producer (BLIP) facility, a fixed target is bombarded by proton beam to produce isotopes for medical research and cancer treatment. This bombardment process causes spot heating on the target and reduces its lifetime. To mitigate this problem, an upgrade to the beamline has been made by spreading the beam on the target in a circular pattern, which allows the target to heat more uniformly. The beam is steered in a circular pattern by a magnet with orthogonal (X and Y) windings. Each of these two windings is independently powered as part of a resonant circuit driven by a power amplifier. This paper describes the hardware platform used as well as the software implementation of the resonant circuit design and its feedback loop.

## OVERVIEW

The BLIP facility is faced with a high demand for isotopes. To increase the production, the target needs to be bombarded with higher current beam. Focused beam with increased beam current causes heat damage on the target. To prevent this, the heat has to be distributed within the target. This can only be achieved if the target is scanned by the beam in a moving pattern. A set of ferrite core windings was designed to generate a dynamic magnetic field that steers the beam in a circular pattern. Increasing the current into the magnet results in a wider circle. The magnet's two windings are physically perpendicular to each other and are independently powered by two power amplifiers. To minimize the power required to energize these windings, a resonant circuit was designed. Without the resonant circuit, an amplifier with a much higher apparent power would be needed to power each winding. As inherent with resonant circuits, the energy is transferred between the inductor (the winding) and the matching capacitors. The power amplifiers are needed to supply only the initial energy to charge the capacitors at start-up, as well as to make up for the losses in the system. A small portion of these losses is due to the magnet leads. The windings are placed around the beam pipe in the tunnel, about 18 feet in front of the target. Due to high radiation in the tunnel, the resonating capacitors are located in a remote control room. The connections between the resonant capacitors and the windings are made via Kapton insulated litz wires. Kapton was chosen because of its high tolerance to radiation; and litz wire was chosen to mitigate the AC skin effect. The long leads contribute to the resistive losses in the resonant circuit.

The windings and the components of the resonant circuits are required to run at a frequency of 4.9 kHz. This frequency was chosen to spread the beam on the target for specific number of turns (circles) per beam pulse. The pulse width of the beam that is sent to the BLIP facility is 450 µs. At approximately 5 kHz, the beam scribes two and a quarter turns on the target. The scanning system was designed to run continuously as opposed to a pulsed ringing circuit. This is advantageous in two ways. First, running continuously allows for continuous monitoring of proper operation of the equipment. In a ringing circuit, a misfire will not be known until after the beam has been sent to the target. Second, the beam distribution is precisely controlled in the continuous system by a lookup table. In a pulsed system, the only control would be the starting current.

To keep the power amplifier running with minimum power, the load – the inductor and the capacitors (LC) – needs to be matched to the impedance of the power amplifier. This is achieved by adding a transformer in parallel with the capacitors. The turn ratio of the transformer is determined by the ratio of the resistive losses of the resonant circuit to the power amplifier impedance. Since the impedance of the resonant circuit is higher than the power amplifier impedance, the transformer steps up the voltage. Having a matched impedance system ensures the amplifier supplies the minimum power required to run the system.

## HARDWARE

As mentioned in the above section, all the components of the resonant circuit except the windings are located in a remote room. Interface chassis were built to house these components. Each winding has two interface chassis. The first chassis provides access to the litz wire leads and includes the resonant capacitors, while the second chassis contains the impedance matching transformer and connection point to the power amplifier. Each chassis also includes a dedicated current transformer and a dedicated voltage sensor to measure the magnet current and voltage, and the power amplifier current and voltage, respectively. These measurements are acquired by the power supply control system to regulate the feedback loops. A pair of interface chassis is shown in Figure 1.

National Instruments' PXIe hardware platform was chosen as the power amplifier controller. Each power amplifier is controlled by its own function generator module which has the capability to generate 20 MHz sine waves with 14-bit resolution (NI PXI-5402). These modules are configured to generate two separate sine waves. These outputs have adjustable amplitude and have a nominal 90° phase shift, as an input to each power amplifier. To read the current and voltage measurements, an oscilloscope/digitizer module is utilized. The PXIe-5105 is an 8-

* Work supported by Brookhaven Science Associates, LLC under Contract No. DE-AC02-98CH10886 with the U.S. Dept. of Energy.
† ALTINBAS@BNL.GOV



ISBN 978-3-95450-177-9

# BEAM DIAGNOSTICS AT SIAM PHOTON SOURCE

P. Klysubun†, S. Klinkhieo, S. Kongtawong, S. Krainara, T. Pulampong, P. Sudmuang, N. Suradet, SLRI, Nakhon Ratchasima, Thailand

*Abstract*

In recent years the beam diagnostics and instrumentation of Siam Photon Source (SPS), Thailand synchrotron radiation facility, have been significantly improved for both the booster synchrotron and the 1.2 GeV storage ring. Additional diagnostics have been designed, fabricated, and installed, and the existing systems have been upgraded. This paper describes the current status of the beam diagnostics at SPS, as well as their respective performances. These systems include beam position monitors (BPMs), a diagnostics beamline, beam loss monitors (BLMs), real-time tune measurement setups, and others. Apart from the instrument hardware, the acquisition electronics along with the processing software have been improved as well. The details of these upgrades are reported herewith.

## INTRODUCTION AND OVERVIEW

Siam Photon Source [1,2] is the Thailand 1.2 GeV synchrotron light source operated by Synchrotron Light Research Institute (SLRI). The facility is located in the province of Nakhon Ratchasima, approximately 250 km northeast of Bangkok. The accelerator complex comprises of a thermionic electron gun, a 40 MeV linac (LINAC), a low energy beam transport line (LBT) transferring 40 MeV electrons to a 1.2 GeV booster synchrotron (SYN), followed by a high energy beam transport line (HBT) transporting the electron beam to a 1.2 GeV storage ring (STR). The maximum stored beam current has been 150 mA, but soon will be increased after the installation of a new 300 kV RF cavity and a 80 kW solid-state RF amplifier, replacing the old 120 kV cavity and 30 kW amplifier, just completed in August this year. Delivered user beamtime ranges from 4,000 – 4,500 hours per year. Currently there are 10 photon beamlines utilizing the generated synchrotron radiation from infrared to x-ray spectral regions. To ensure stable and reliable operation, as well as to aid machine physicists in maximizing the machine performances, several types of beam diagnostics are placed along the electron beam paths to measure and monitor the characteristics of the electron beam.

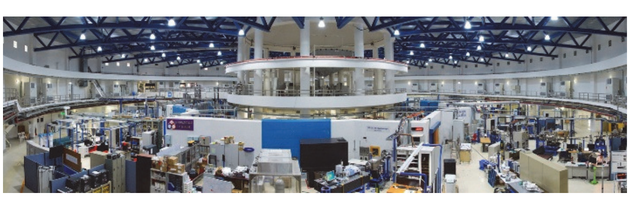

Figure 1: SPS experimental hall.

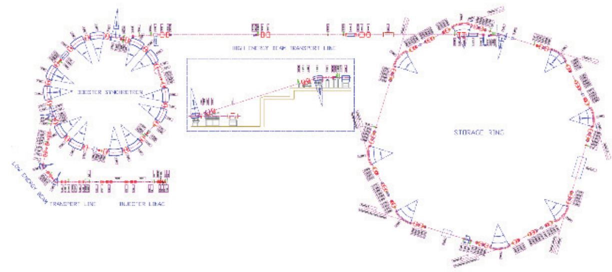

Figure 2: SPS machine layout.

## LINAC AND LBT DIAGNOSTICS

### *Current Monitors (CMs)*

Three wall current monitors (WCMs) placed along the beam path are used to measure the beam current in the linac section. The first CM (CM1) is located between the first and the second pre-bunchers (PB1 and PB2). The second and third CMs (CM2, CM3) are located at the entrance and the exit of the linac, respectively. A Pearson Electronics Model 3100 pulse current transformer (LCT) is located at the end of the LBT just before the beam entering the injection septum.

### *Screen Monitors (SMs)*

The LBT is equipped with 3 SMs to monitor the transverse beam profile as well as the beam position. CCD cameras capture the beam images and send them to the control room. A unified control system controls the screens, the CCD cameras, as well as the lighting.

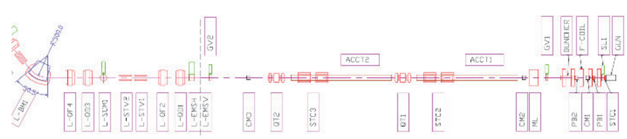

Figure 3: Linac and part of the LBT.

## BOOSTER SYNCHROTRON AND HBT DIAGNOSTICS

### *Direct Current Current Transformer (DCCT)*

The booster synchrotron is equipped with a DCCT capable of measuring 0 – 100 mA (± 0.2 mA) beam current. The output voltage is displayed directly on an oscilloscope in the control room.

† pklysubun@slri.or.th



ISBN 978-3-95450-177-9

# FIRST RESULTS FROM THE IPHI BEAM INSTRUMENTATION

P. Ausset†, M. B. Abdillah, S. Berthelot, C. Joly, J. Lesrel, J.F. Yaniche, IPN 91406 Orsay, France
D. Bogard, B.Pottin, D.Uriot, CEA-Saclay, 91191Gif sur Yvette Cedex

*Abstract*

I.P.H.I. is a High Intensity Proton Injector (CNRS/IN2P3; CEA/Irfu and CERN collaboration) located at Saclay and now on operation. An ECR source produces a 100 keV, 100 mA C.W. proton beams which will be accelerated at 3 MeV by a 4 vanes R.F.Q. operating at 352.2 MHz. Finally, a High Energy Beam Transport Line (HEBT) delivers the beam to a beam stopper. The HEBT is equipped with appropriate beam diagnostics to carry beam current, centroid beam transverse position, transverse beam profiles, beam energy and energy spread measurements for the commissioning of IPHI. These beam diagnostics operate under both pulsed and CW operation. However transverse beam profile measurements are acquired under low duty factor pulsed beam operation using a slow wire scanner. The beam instrumentation of the HEBT is reviewed and the first measurements at 3 MeV are described.

## INTRODUCTION

Since the front end is the most critical part of a High Power Proton Accelerator (HPPA), it was decided to realize a high power proton injector named IPHI under a CNRS/IN2P3, CEA/Irfu and CERN collaboration. IPHI has been designed to be a possible front end for a HPPA devoted to fundamental and applied research: radioactive beams production, neutron sources and transmutation. The aim of IPHI was also to validate the technical choices, to demonstrate operational reliability and to measure the beam parameters of the accelerated beam by the RFQ. IPHI was also designed in the frame of the SPL (Superconducting Proton Linac) study at CERN as a 3 MeV test stand to become the low energy part of the linear accelerator "Linac4" [1]. IPHI consists of an E.C.R. proton source named SILHI (100 mA, 95 keV) followed by a Low Energy Beam Transfer Line (LEBT). A Radio Frequency Quadrupole (length: 6m), operating at 352.2 MHz performs the acceleration of the proton beam up to 3 MeV. Finally the straight section of the High Energy Beam Transfer line (HEBT) may transfer the total power (300 kW) of the beam to a beam stopper (BS) [2]. The deflected section of the HEBT may transfer only a small fraction of the total beam power (few tens of W) for energy dispersion measurement. IPHI is planned to work under C.W. operation but during tests and commissioning periods pulsed mode operation has to be considered to lower the mean power of the beam in order to prevent the accelerator structure and the interceptive beam diagnostics from excessive heating or even from destruction.

## BEAM DIAGNOSTICS

### *General Considerations*

The source ECR source SILHI 100 kV, installed on a high voltage (100 kV) platform produces the required high intensity (100 mA) proton beams either under C.W. or pulsed mode operation according to the selected temporal structure of the radiofrequency signal feeding her magnetron. The LEBT contains the necessary magnetic elements to transport to the RFQ and to centre on the axis of the beam pipe the beam: two solenoids for the focusing of the beam and two pairs (horizontal and vertical) steerers for the beam alignment. An iris controls the beam intensity. The LEBT contains also beam diagnostics for beam current measurements and visualization of the transverse beam profile at the entrance of the cone located on the RFQ.

The general layout of the HEBT is shown in Fig.1. The straight section (dipole "off") is equipped with beam diagnostics in order to:

- Help to the safe transport of the proton beam to a beam stopper able to withstand the full power of the beam: 300 kW under the C.W. mode operation.
- Provide a sufficient characterization of the beam accelerated by the RFQ during the commissioning period and the daily operation: beam current, position, energy, energy dispersion, transverse profile
- Operate under pulsed mode (pulsed mode operation of the ECR source) for machine commissioning or experimental operation and the nominal C.W. mode.
- Test and evaluate non-intrusive techniques for measuring transverse beam profiles of high average power beams. These techniques will have to be brought to operation due to the large quantity of beam energy deposited in any possible intrusive sensor leading to its destruction or to a high activation induced level.

The deflected section (dipole "on") is primarily devoted to energy spread measurements under pulsed mode beam operation (low average beam power operation). For this purpose, an object slit will be located in the straight section before the dipole and an image slit followed by a Faraday cup at the end of the deflected section. The list of the beam diagnostics types in IPHI is given in Table 1.

†ausset@ipno.in2p3.fr



ISBN 978-3-95450-177-9

# LEReC INSTRUMENTATION DESIGN & CONSTRUCTION *

T. Miller†, M. Blaskiewicz, A. Drees, A. Fedotov, W. Fischer, J. Fite, D. M. Gassner R. Hulsart, D. Kayran, J. Kewisch, C. Liu, K. Mernick, R. Michnoff, M. Minty, C. Montag, P. Oddo, M. Paniccia, I. Pinayev, S. Seletskiy K. Smith, Z. Sorrell, P. Thieberger, J. Tuozzolo, D. Weiss, A. Zaltsman, BNL, Upton, NY 11973, USA

*Abstract*

The Relativisitc Heavy Ion Collider (RHIC) at BNL will collide ions with low center-of-mass energies of 7.7 – 20 GeV/nucleon, much lower than 100 GeV per nucleon. The primary motivation is to explore the existence of the critical point on the QCD phase diagram. An electron accelerator is being constructed to provide Low Energy RHIC electron Cooling (LEReC) [1] to cool both the blue & yellow RHIC ion beams by co-propagating a 10 – 50 mA electron beam of 1.6 – 2.6 MeV. This cooling facility will include a 400 keV DC gun, SRF booster cavity and a beam transport with multiple phase adjusting RF cavities to bring the electron beam to one ring to allow electron-ion co-propagation for ~20 m, then through a 180° U-turn electron transport so that the same electron beam can cool the other counter-rotating ion beam, and finally to a beam dump. The injector commissioning is planned to start in early 2017 and full LEReC commissioning planned to start in early 2018. The instrumentation systems that will be described include current transformers, BPMs, profile monitors, multi-slit and single slit scanning emittance stations, time-of-flight and magnetic energy measurements, and beam halo and loss monitors.

## INTRODUCTION

Full operation of LEReC is planned for 2019-20 with cooling of the RHIC ion beams using bunched electron beams of 1.6 – 2.6 MeV [1, 2]. With delivery of a 750 keV DC gun from Cornell University [3] (planned for operation at 400 keV) in October of this year, the injection section is being installed to support commissioning of the gun, followed by installation of the rest of the machine in the summer of 2017. The electron beam has a nested pulse structure [4], where 80 ps bunches at 704 MHz are grouped in macrobunches and positioned to overlap with the 9.1 MHz RHIC ion beam. The macro bunch size varies 30 – 24 bunches and its maximum charge varies 130 – 200 pC (incl. 30% margin) depending on the range of ion bunch length. The machine layout is shown in Fig. 1.

## ELECTRON BEAM INSTRUMENTATION

The parameters measured in each section of the machine layout are quantified in Table 1. Details of each instrument type are elaborated on below.

### *Gun Instrumentation*

In support of HV conditioning of the DC gun, a 24-bit ADC board measuring the voltage across a 350 Ω shunt resistor in series with the HVPS and the cathode and sits at the cathode potential in the $SF_6$ tank. It is powered via a "power over fiber" link [5]. Cathode current is reported during HV conditioning where the current is kept below 100 µA. The gun has a floating anode biased positive to < 1kV to provide ion collection between the gun and booster. A Keithley 6514 electrometer will monitor the anode current.

Table 1: Parameters Measured in Each Machine Section

**Tt**-Total; **Inj**-Injection; **Tr**-Transport; **Mg**-Merger; **Dia**-Diagnostic; **Cl**-Cooling; **Ex**-Extraction

| Tt | Measure | Inj | Tr | Mg | Dia | Cl | Ex |
|---|---|---|---|---|---|---|---|
| **13** | Profile | 3 | 1 | 1 | 1 | 6 | 1 |
| **4** | Charge | 2 | | | 1 | | 1 |
| **7** | Current | 4 | | | 1 | | 2 |
| **41** | Position | 8 | 9 | 2 | 2 | 17 | 3 |
| **1** | Halo | 1 | | | | | |
| **3** | Emittance | 1 | | | | 2 | |
| **2** | Δp/p | | | 1 | | 1 | |
| **1** | Energy | | | | | 1 | |
| **1** | Long. Φ Sp | | | | 1 | | |
| **15** | Beam Loss | 4 | 3 | 1 | | 5 | 2 |

### *Profile Monitors*

Beam profile monitors (PM) employ YAG:Ce crystals and optics for 50-µm resolution. All 13 PMs have low impedance vacuum chambers [6]. YAG:Ce crystals are 100 µm thick with 100 nm Al coatings. All but one PM have 45° polished Cu or SS mirrors that can withstand a single full-power macrobunch @ 1Hz. The PM in the diagnostic section will have a mirrorless design to withstand 250 µs long trains. Tilted lens optics will correct for depth-of-field limitations associated with its 45° YAG crystal. All PM's are pneumatically driven and use GigE digital cameras.

The Prosilica GT1600 camera with iris control is being investigated for use with P-Iris type lenses for remote control of iris settings to help cope with wide macrobunch intensities during commissioning. All PM's have LED illumination and optical features next to and in the same plane as the YAG crystal to assist in focusing of the optics. A 450 nm laser is included to test the response and focus of the YAG crystal by simulated beam scintillation. Two of the PM's in the cooling section are hybrid devices [6] with a horizontal-plane BPM integrated into the chamber.

* Work supported by BSA under DOE contract DE-AC02-98CH10886
† tmiller@bnl.gov

ISBN 978-3-95450-177-9

# A PPS COMPLIANT INJECTED CHARGE MONITOR AT NSLS-II*

A. Caracappa†, C. Danneil, R. Fliller, D. Padrazo, O. Singh, BNL, Upton, USA

*Abstract*

The Accumulated Charge Monitor Interlock (ACMI), a PPS compliant system, was developed to ensure the Accelerator Safety Envelop (ASE) limits for charge generation in the NSLS-II Injector are never violated. The ACMI measures the amount of charge in each injection cycle using an Integrating Current Transformer (ICT). For logistical reasons, adding a redundant ICT was impractical so in order to achieve the high reliability required for PPS this system is designed to perform self-tests by injecting calibrated charge pulses into a test coil on the ICT and analyzing the returning charge signal. The injector trigger rate is 1.97Hz and self-tests are performed 250 msec after every trigger pulse. Despite the lack of a redundant charge measurement the ACMI achieved the high reliability rating required for PPS with a mean time between failure (MTBF) rate greater than $10^6$ hours. The ACMI was commissioned in 2014 and has operated to date without any major problems. In 2015 a second ACMI system was commissioned to monitor charge in another region of the injector system.

## INTRODUCTION

The ASE sets limits on the maximum charge allowed in a single injection shot and the maximum accumulated charge allowed in a one-hour window. The ASE also sets a limit on the one-minute accumulated charge during Top-Off operations at the NSLS-II facility. The ACMI was developed as part of the NSLS-II PPS to ensure that these ASE limits are never violated. The ACMI uses a single ICT to make the charge measurement. It was not practical to install a second ICT which would have allowed redundant charge measurements to be made. Complicating matters further, the ICT (Bergoz ICT-CF6”-60.4-40-70-20:1) is not a safety-rated device and the ACMI must assume that it can fail at any time. Without a redundant measurement the ACMI would have to use a different strategy to ensure that the single charge measurement is accurate. The ICT came equipped with a test coil which is used by the ACMI to perform self-tests between each injector trigger. For each self-test the ACMI launches a calibrated charge pulse to the ICT test coil and analyzes the returning charge signal in the same manner as the actual beam. Any deviation between the expected and measured charge values for the self-tests generates a fault. The LINAC trigger signal is not generated by a PPS compliant system and the ACMI must assume that the trigger signal could fail at any time. The ACMI carefully monitors the trigger timing applying strict limits on the trigger rate. The ACMI also monitors the ICT at all times ensuring that charge is only detected within a proper time window derived from the trigger timing. The ACMI was required to undergo independent reliability analyses and rigorous internal reviews to ensure the system is PPS compliant.

## ACMI SYSTEM

Figure 1 shows the block diagram for the ACMI. The system is built around a safety-rated PLC (Fig. 2: Allen-Bradley 1768-43S). Two PCBs were designed for this system, the Timing Generator and the Analog Processor. An HMI panel allows diagnostic information to be displayed on the ACMI cabinet. The PLC also sends diagnostic information to an EPICS IOC for remote monitoring and data archiving. A few analog and critical timing signals are sent to a VME digitizer for further monitoring. Any fault detected by the ACMI disables the LINAC gun. The only user inputs into the ACMI are PPS compliant reset signals to clear any latched faults.

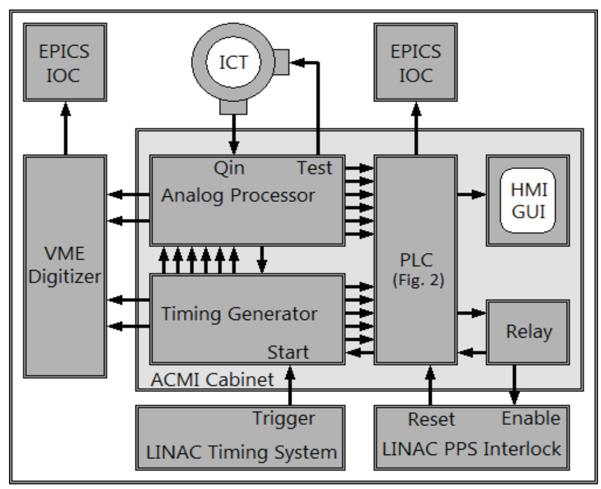


Figure 1: ACMI block diagram.

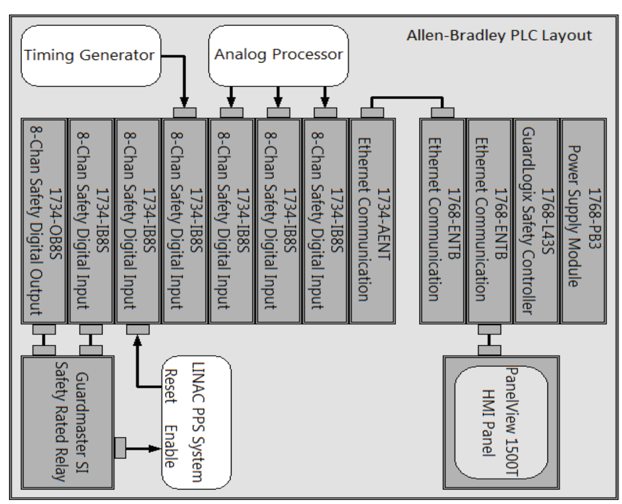


Figure 2: PLC layout.

* Work supported by DOE
† caracapp@bnl.gov



ISBN 978-3-95450-177-9

# A PPS COMPLIANT STORED BEAM CURRENT MONITOR AT NSLS-II*

A. Caracappa†, C. Danneil, A.J. Della Penna, R. Fliller, D. Padrazo, O. Singh, BNL, Upton, USA

*Abstract*

A requirement for top-off operations at the NSLS-II facility is at least 50mA stored ring current. The Stored Beam Current Monitor (SBCM) is part of the NSLS-II Top Off Safety System (TOSS) that determines the storage ring current based on Pick-Up Electrode (PUE) readings. The SBCM downconverts the 500 MHz component of the PUE signal to 2 MHz. The 2 MHz signal is rectified, averaged down to a bandwidth of 500 Hz, and compared to a threshold voltage equivalent to 55mA of stored beam. A redundant SBCM system was also constructed and these two systems must agree that the stored beam is above the threshold to enable top-off operations. The SBCM is also required to remain accurate over wide range of possible fill patterns up to a total current of 500 mA. Under normal conditions for top-off operations the SBCM measurement accuracy is about 1%. The SBCM was commissioned in 2015 as part of the Top-Off Safety System (TOSS) which is responsible for ensuring safe top-off operations at NSLS-II.

## INTRODUCTION

The NSLS-II facility operates primarily in top-off mode where charge is injected into the storage ring at about one minute intervals while beamline safety shutters are open in order to maintain a relatively constant stored current. The TOSS is a multi-levelled interlock designed to ensure that top-off operations at NSLS-II are executed safely. One requirement of the TOSS is that there be at least 50mA of stored beam in the ring. The detection of stored beam indicates that critical ring systems, such as RF and magnet power supplies, are working correctly. The SBCM is a sub-system of the TOSS that performs the stored current measurement. The use of DCCTs or high-speed digitizers in the SBCM design was ruled out because these devices are not safety-rated and their inclusion in a safety rated system would have been difficult to develop.

In order to facilitate meeting the requirements for TOSS the SBCM is designed as a fully analog processor. The SBCM processes PUE signals generated by the beam in order to determine the stored current. The RF cavity frequency of 500 MHz organizes the ring into 1320 RF buckets with the beam typically occupying 80% of these buckets during top-off operations. The gap formed by the empty buckets modulates the 500 MHz PUE signals at the ring rotation frequency of 378.78 KHz (Fig. 1).

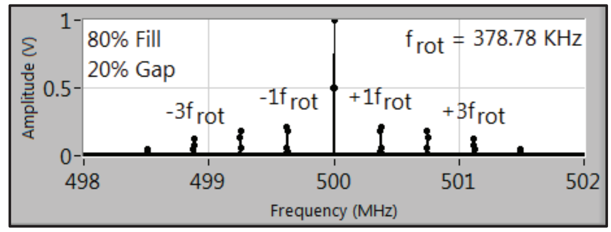


Figure 1: Modulated PUE Signal.

At the frequency range shown in Figure 1 parasitic elements in the analog circuit would make the current measurement difficult to perform. If the PUE signal is mixed with a 498 MHz local oscillator the pattern shown in Figure 1 is regenerated at 2 MHz and at 998 MHz. A 20 MHz low-pass filter blocks the signals centered on 998 MHz. The current information encoded on the PUE signal is preserved on the downcoverted 2 MHz signal. The modulation of the PUE signal is also downconverted as shown in Figure 2.

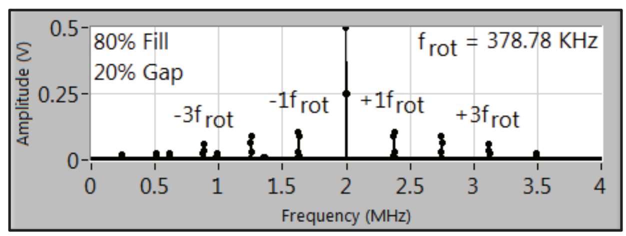


Figure 2: Downconverted PUE Signal.

The downconverted PUE time-domain signal is shown on the left side of Figure 3. The plot shows about 2 ring revolutions of data. The right side of Figure 3 shows the absolute value of the downconverted signal.

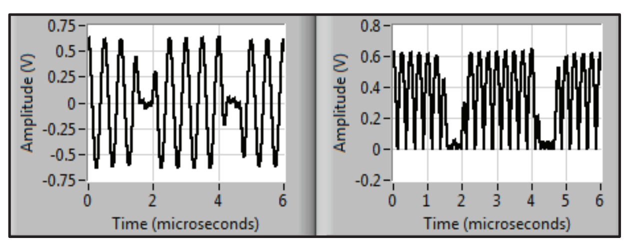


Figure 3: SBCM Time-Domain Signals.

The absolute value is averaged over about 750 ring revolutions to obtain the SBCM reading. For a given fill pattern the relationship between the SBCM reading and the stored current is highly linear with nonlinearities below 1%. Different fill patterns will have slightly different proportionality constants. The fill pattern dependence will be discussed in depth later.

## SBCM SYSTEM

Figure 4 shows the block diagram for the SBCM. A 5:1 combiner module located on the girder with the PUEs performs the passive sum of the PUE signals and allows a

* Work supported by DOE
† caracapp@bnl.gov



ISBN 978-3-95450-177-9

# THE CHERENKOV DETECTOR FOR PROTON FLUX MEASUREMENT (CpFM) IN THE UA9 EXPERIMENT

S. Montesano*, W. Scandale[1], CERN, 1211 Geneva 23, Switzerland
F. M. Addesa, G. Cavoto, F. Iacoangeli, INFN Sezione di Roma, Rome, Italy
L. Burmistrov, S. Dubos, V. Puill, A. Stocchi, LAL, Orsay, France
[1] also at LAL, Orsay, France

*Abstract*

The UA9 experiment at the CERN SPS investigates the possibility to use bent crystals to steer particles in high energy accelerators. In this framework the CpFM have been developed to measure the beam particle flux in different experimental situations. Thin movable fused-silica bars installed in the SPS primary vacuum and intercepting the incoming particles are used to radiate Cherenkov light. The light signal is collected outside the beam pipe through a quartz optical window by radiation hard PMTs. The PMT signal is readout by the WaveCatcher acquisition board, which provides count rate as well as waveform information over a configurable time window. A bundle of optical fibers can be used to transport the light signal far from the beam pipe, allowing to reduce the radiation dose to the PMT. A first version of the CpFM has been successfully commissioned during the data taking runs of the UA9 Experiment in 2015, while a second version has been installed in the TT20 extraction line of the SPS in 2016. In this contribution the design choices will be presented and the final version of the detector will be described in detail.

## INTRODUCTION

Since 2009, the UA9 Experiment investigates the possibility to use bent silicon crystals to steer beams of charged particles, and in particular to improve the performance of a multi-stage collimation system [1]. The main installation of the experiment is in the Long Straight Section 5 (LSS5) of the CERN SPS and includes three goniometers to operate five different crystals, one dedicated movable absorber, several scrapers, detectors and beam loss monitors (BLM) to probe the effect of the crystal on the beam halo [2]. A schematic representation of the layout of the experiment is reported in Fig. 1.

The main process that is investigated is the so-called "planar channeling": particles impinging on a crystals with a direction close to the one of the lattice planes are forced to move between the planes by the atomic potential, with high efficiency; if the crystal is bent, the trapped particles follow the bending and are deflected. When an optimized crystal intercepts the beam halo to act like a collimator, about 80% of the particles are channeled, coherently deflected and dumped on the absorber (see Fig. 1), effectively reducing the beam losses in the sensitive areas of the accelerator [3–8].

* simone.montesano@cern.ch

### *Requirements for the Detector*

In order to fully characterise this system, the flux of the particles diffusing to the crystal should be characterized, as well as the "deflected beam" due to the particles extracted towards the absorber by the crystal. Initial estimations are performed using the variation of the primary beam intensity measured by the Beam Current Transformer (BCT) and intercepting the extracted beam with a Medipix detector enclosed in a Roman Pot [3, 9].

The existing instrumentation allowed to perform several measurements, however, the optimal detector for these measurements would be:

- installed directly in the beam pipe vacuum, to avoid the interaction of the protons with the Roman Pot window;
- able to measure the number of protons extracted from a single SPS bunch (during UA9 operations the bunch length is 3 ns and the minimal bunch distance is 25 ns);
- able to resolve the signal generated by a single proton up to few tens of protons (the estimated extraction rate is of the order of $10^7$ p/s with a revolution time of 23 µs - i.e. few protons extracted per machine turn);
- radiation-hard in order to reliably operate in the accelerator tunnel;
- movable in the direction transversal to the beam, to allow measurements at different apertures of the collimation system and to avoid interfering with the beam during standard machine operations.

## THE CHERENKOV DETECTOR FOR PROTON FLUX MEASUREMENT

In order to comply with the requirements listed above, the concept of the CpFM was conceived. A sketch of the detector is reported in Fig. 2, with its main elements: a radiator that intercept particles inside the beam pipe and create the Cherenkov light, a bellow to allow moving the radiator, an interface transmitting the light outside the beam pipe, a photomultiplier (PMT) to collect the light and electronics to readout the PMT signal. Several investigations and measurements [10] performed in the last few years have allowed to carefully select all the components of the chain.

### *The Cherenkov Radiator*

When choosing the technology of the sensor, different options were considered: silicon and gas detectors posed important issues with respect to operation in the beam pipe vacuum, while scintillator materials were considered not



ISBN 978-3-95450-177-9

# DEVELOPMENT OF HIGH RESOLUTION BEAM CURRENT MEASUREMENT SYSTEM FOR COSY-JÜLICH

Yu. Valdau[1*], L. Eltcov, Rheinische Friedrich-Wilhelms-Universität Bonn, Helmholtz-Institut für Strahlen- und Kernphysik, Nussallee 14-16, D-53115, Bonn, Germany
S. Trusov[2], S. Mikirtytchiants, Forschungszentrum Jülich, Institute für Kernphysik, D-52425, Jülich, Germany,
P. Wüstner, Forschungszentrum Jülich, Zentralinstitut für Engineering, Elektronik und Analytik (ZEA), Systeme der Elektronik (ZEA-2), D-52425, Jülich, German
[1] also at Forschungszentrum Jülich, Institute für Kernphysik, D-52425, Jülich, Germany,
[2] also at Skobeltsyn Institute of Nuclear Physics, Lomonosov Moscow State University, RU-119991 Moscow, Russia

*Abstract*

An experiment to test Time Reversal Invariance at COSY (TRIC) requires a precise beam life-time determination. For this, a high resolution bunched beam current measurement system based on the Fast Current Transformer and Lock-In Amplifier has been build. The first tests of the system, read out by a new DAQ, have been done at COSY and at a test stand in the laboratory where bunched beam current was simulated using a conductive wire. A relative resolution of $1.9 \times 10^{-4}$ for the signal in the wire, equivalent to 1 mA of bunched beam current in COSY, has been obtained in the laboratory. This resolution is sufficient for the realization of the TRIC experiment.

## MOTIVATION

A test of Time Reversal Invariance (TRIC experiment) is under preparation at COSY-Jülich [1]. The experiment is planned as a null transmission experiment in the storage ring using a T-violation sensitive observable $A_{Y,XZ}$ available in double-polarised *pd* scattering. A polarised proton beam, together with a tensor polarised deuterium gas target located in one of the straight sections of COSY, will be used for the TRIC experiment. The $A_{Y,XZ}$ observable will be determined from the difference of beam life-times measured for two independent beam-target spin polarisation states. This is the reason why the TRIC experiment puts very stringent requirements on the precision of beam life-time determination and hence resolution in the beam current measurement. The minimal resolution of $10^{-4}$ integrated over one second in the beam current measurement will allow us to reach the goal of the project after one month of measurement and to improve the present upper limit on the T-violation by an order of magnitude.

## COSY BEAM PARAMETERS

Unfortunately, it is not possible to reach resolution better than $10^{-3}$ in the coasted beam current measurement using a conventional DC Beam Current Transformers (BCT) [2]. But a much higher sensitivity and resolution can be obtained for the averaged bunched beam current measurement using inductive or capacitive pick-ups [3]. Since COSY can provide both bunched and unbunched beams at the energy of the TRIC experiment (see parameters of the COSY beam in Tab. 1) it was decided to construct a new high resolution beam current measurement system for COSY using an inductive sensor, sensitive to the bunched beam, together with modern readout electronics.

Table 1: COSY Beam Parameters During the TRIC Experiment

| Beam Parameter | Expected value |
|---|---|
| Beam momentum | 521 MeV/c |
| Revolution Frequency | 793345 Hz |
| Bunch length | 200 ns |
| Bunch shape | Gaussian |
| Number of protons in ring | $\sim 10^{10}$ |
| Averaged current | 1 mA |

Since TRIC is a precision experiment, which crucially depends on the precision of the beam current measurement, it was decided to build a test stand in the laboratory to have possibility to study parameters of the sensors and the readout chain with conductive wire independently from the availability of the COSY beam.

## FAST CURRENT TRANSFORMER

Two Fast Current Transformers (FCT) with similar parameters have been ordered from the Bergoz Instrumentation company for the TRIC experiment at COSY [4]. Sensors are made in on-flange UHV compatible configuration with a calibration winding. This kind of configuration simplifies sensor installation and requires less than 10 cm of space in the ring. The FCT installed in one of the straight section of the COSY ring is presented in Fig. 1. The device has a conductive break inside and is ready to use after the installation. Since beam intensity in COSY is relatively small, the device installed in the ring is equipped with a custom build low noise preamplifier to work with readout electronics located outside of the accelerator tunnel. Calibration winding

* y.valdau@fz-juelich.de



ISBN 978-3-95450-177-9

# DESIGN OF A VERY COMPACT 130 MeV MØLLER POLARIMETER FOR THE S-DALINAC*

T. Bahlo†, J. Enders, T. Kürzeder, N. Pietralla, J. Wissmann
Institut für Kernphysik, TU Darmstadt, Darmstadt, Germany

*Abstract*

At the **S**uperconducting **Da**rmstadt **Lin**ear **Ac**celerator S-DALINAC [1] it is possible to accelerate electron beams to a maximum energy of up to 130 MeV with a beam current of up to 20 $\mu$A. In the **S**-DALINAC **P**olarized **In**jector SPIN [2] polarized electrons with a polarization of up to 86% can be produced. The polarization can be measured with two already mounted Mott polarimeters in the injector beam line, where the electrons can have energies of up to 10 MeV. To allow a polarization measurement behind the main accelerator a Møller polarimeter suitable for energies between 50 MeV and 130 MeV is currently being developed. The rather low and variable beam energies and the resulting big and also variable scattering angle distribution combined with very strict spatial boundary conditions at the designated mounting area necessitate a very compact set-up for the polarimeter.

## S-DALINAC

The S-DALINAC is a recirculating linear electron accelerator capable of producing cw electron beams with a maximum energy of 130 MeV and beam currents of up to 20 $\mu$A. Its floor plan is shown in Fig. 1. In order to provide electrons with polarizations of over 80%, inside the spin-polarized injector a special GaAs cathodes is illuminated with a laser beam to produce polarized electrons via the photo effect. These electrons are preaccelerated to an energy of 100 keV by a static electric field. To manipulate the spatial spin orientation, the electrons pass a wien filter and solenoid allowing the operator to align the spin orientation to the preferences of the experiment or polarimetry setups. In front of the s.c. injector beam line there is a low energy Mott-Polarimeter usable with electron energies between 100 keV and 250 keV for an incident measurement of the absolute polarization. Additionally there is a Mott-Polarimeter optimized for energies up to 10 MeV behind the s.c. injector and a mountable Compton-Transmission-Polarimeter at the first experimental area. After passing the s.c. main accelerator, it is at this time not possible to measure the polarization until now. Therefore a Møller-Polarimeter for electron energies between 50 MeV and 130 MeV is currently being developed and will be installed at the marked position shown in Fig. 1.

## MØLLER POLARIMETRY

For electron energies of more than 10 MeV Mott polarimetry is not applicable any more. To measure the polarization Møller polarimeters are commonly used for high energy electron beams. Although the Møller scattering crossection is not directly dependent of the participants' spin, one can exploit Pauli's principle that suppresses scattering events with the same orientation of the two involved electrons' spins. It can be shown that this suppression is maximal for a center-of-momentum frame scattering angle of 90° resulting in a maximal analyzing power of the polarimeter if this angle is used. Of course the laboratory frame scattering angle strongly depends on the incident energy of the electrons, what has to be taken into account when positioning the detectors. In Møller Polarimeters the electron beam of unknown absolute polarization scatter on a longitudinally polarized ferromagnetic target. In a first measurement the target material is polarized parallel to the beams polarization and the detected events produced by symmetrical scattered electrons is accumulated. In a second measurement either the target polarization, or the beam polarization is flipped to produce antiparallel spin orientations. The amount of detected events is expected to increase since no Pauli suppression is expected to occur. By comparing the amount of events of both measurements, it is possible to calculate the beams polarization. Generally one finds two different types of Møller polarimeters: One-arm polarimeters only detect and count one of the two scattered electrons making it necessary to strongly collimate the scattered beam. Background radiation represents a big problem for this type of polarimeter making it necessary to shield the detectors very well. Two-armed polarimeters on the other hand detect and count both scattered electrons coincidentally, strongly reducing the random background from the primary beam and activated material in close distance. This allows greater angle acceptances and therefore higher counting rates. The Møller Polarimeter that is currently being designed for the S-DALINAC will be such a two-armed type using coincidence counters.

## POLARIMETER FLOORPLAN

As depicted in Fig. 2 the Møller Polarimeter will be placed right next to the high energy scraper system of the S-DALINAC leaving an area of about two by three meters for scattering, beam separation, detection and dumping. It is not possible to separate the Møller electrons horizontally due to the scraper system blocking the left hand side of the polarimeter. Therefore the Møller electrons have to be separated vertically and additionally be steered further to the right. Since both, target chamber and beam dump, produce a lot of background radiation the detectors have to be positioned carefully to minimize underground events.

* Work supported by the DFG under grant No. SFB 634
† tbahlo@ikp.tu-darmstadt.de



ISBN 978-3-95450-177-9

# THE NEXT GENERATION OF CRYOGENIC CURRENT COMPARATORS FOR BEAM MONITORING*

V. Tympel†, J. Golm[1], R. Neubert, P. Seidel, Institute for Solid State Physics, Jena, Germany
M. Schmelz, R. Stolz, The Leibniz Institute of Photonic Technology IPHT, Jena, Germany
V. Zakosarenko, Supracon AG, Jena, Germany
F. Kurian, M. Schwickert, T. Sieber, T. Stöhlker[1,2], GSI Helmholtz Center for Heavy Ion Research, Darmstadt, Germany
[1]also at Helmholtz Institute, Jena, Germany
[2]also at Institute for Optics and Quantum Electronics, Jena, Germany


## *Abstract*

A new ***C****ryogenic* ***C****urrent* ***C****omparator* with *e****X****tended* ***D****imensions (CCC-XD)*, compared to earlier versions built for GSI, is currently under development for a non-destructive, highly-sensitive monitoring of nA-intensities of beams for larger beamline diameters planned for the new FAIR accelerator facility at GSI. The CCC consists of a:

1) flux concentrator,
2) superconducting shield against external magnetic field and a
3) superconducting toroidal coil of niobium which is read out by a
4) Superconducting Quantum Interference Device (SQUID).

The new flux concentrator (1) comprises a specially designed highly-permeable core made of nano-crystalline material, in order to assure low-noise operation with high system bandwidth of up to 200 kHz. The superconducting shielding of niobium (2) is extended in its geometric dimensions compared to the predecessor CCC and thus will suppress (better -200 dB) disturbing magnetic fields of the beamline environment more effectively. For the *CCD-XD* readout, new SQUID sensors (4) with sub-µm Josephson junctions are used which enable the lowest possible noise-limited current resolution in combination with a good suppression of external disturbances.

The *CCC-XD* system, together with a new dedicated cryostat, will be ready for testing in the CRYRING at GSI in spring 2017. For the application of a CCC in the antiproton storage ring at CERN a pulse shape correction has been developed and tested in parallel. Results from electrical measurements of two components (1 and 4) of the new *CCC-XD* setup will be presented in this work.


## INTRODUCTION

Cryogenic Current Comparator (CCC) is a non-destructive, highly-sensitive charged particle beam measurement system using the magnetic field of the moving charged particles, well described in [1, 2]. Figure 1 shows the general principle with the main parts flux concentrator and flux compensator. Using superconducting components for the coils, the transformer and the Superconducting Quantum Interference Device (SQUID) for the magnetic field measurement it is possible to measure DC currents. That means that it is possible to measure a constant particle flow too. CCCs are in use at GSI [3] and CERN [4]. Figure 2 shows the schematic of a CCC system with the main components: flux concentrator, shielding, pick-up coil and matching transformer, SQUID and cooling.

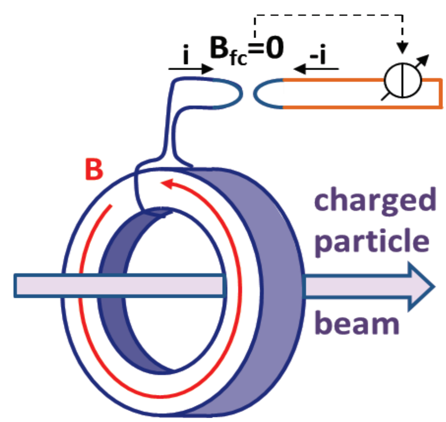


Figure 1: The general principle of a CCC with a flux concentrator and a closed loop current measurement system with compensation current as measurement value.

## *New Challenges*

The CCC application at FAIR leads to two basic challenges: a bakeable ultra high vacuum (UHV) beam tube and a larger beam tube diameter of 150 mm. The required new cryostat is described in [5]. The larger diameter also leads to an extended core diameter of the flux concentrator. Therefore, the new CCC with *eXtended Dimensions* is called *CCC-XD*.

Other challenges of the *CCC-XD* are the desired higher system bandwidth of up to 200 kHz, a higher sensitivity und a better noise immunity. The flux concentrator with its soft magnetic core and the SQUID as magnetic field sensor are the important components to improve the performance of the *CCC-DX* system in this area. Investigation in the field of soft magnetic core materials and the development of a new SQUID design, as described in this work, will ensure the achievement of the forecast targets.

* Work supported by BMBF, project number 05P15SJRBA
† volker.tympel@uni-jena.de

ISBN 978-3-95450-177-9

# DIAGNOSES AND CONTROLS OF SINGLE e-PULSE EXTRACTION AT THE LCLS-I FOR THE ESTB PROGRAM*

J.C. Sheppard †, T. Beukers, W.S. Colocho, F.J. Decker, A.A. Lutman, B.D. McKee, T.J. Smith, M.K. Sullivan, SLAC National Accelerator Laboratory, Menlo Park, CA

*Abstract*

A pulsed magnet is used to kick single electron bunches into the SLAC A-line from the 120 Hz LCLS-1 bunch train. These single bunches are transported to the End Station Test Beam facility. It is mandated that extraction from the LCLS beam does not disturb the non-kicked pulses. An 8.7 mrad kick is required to extract a bunch; without compensation the following bunch experiences a 3 μm kick; with compensation this kick is reduced to less than 0.1 μm which is well within the jitter level of about 0.2 μm. Electron and photon diagnostics were used to identify problems arising from eddy currents, beam feedback errors, and inadequate monitoring and control protocol. This paper discusses the efforts to diagnose, remedy, and control the pulse snatching.

## INTRODUCTION

A set of pulsed magnets are used to horizontally extract single electron bunches at 5 Hz into the SLAC A-line from the 120 Hz LCLS-1 [1] bunch train. These single bunches are transported to the End Station Test Beam facility as either primary beam or secondaries created in a Cu target [2]. An 8.7 mrad kick is required to extract primary beam. Anomalous magnetic fields produced by eddy currents deflect subsequent LCLS-1 pulses. Without compensation, the first bunch following extraction (so-called n+1) experiences a 3 μm normalized kick. This disturbance is exacerbated by improper set up of the undulator launch feedback system which in turn drives the full bunch train away from the nominal kicker off trajectory. With proper setup of the feedbacks the disturbance is limited to the first (n+1) and second (n+2) bunches after extraction. An air core, pulsed post kicker is used to compensate the unwanted deflections. With compensation, the 3 μm normalized kick is reduced to less than 0.1 μm which is well within the undulator launch jitter level of about 0.2 μm.

This paper discusses the actions taken to eliminate the disturbance to the non-extracted LCLS-1 bunches.

## PULSED KICKERS

A set of three pulsed magnets are to kick single LCLS-1 bunches into the SLAC A-Line. The first set of magnets are run with a single pulsed current supply [3] and the third pulsed magnet is powered by a second power supply (a fourth pulsed magnet is being prepared for installation in spring of 2017 and will be powered in series with the existing third magnet). At maximum current, the three magnets are sufficient for extraction of beams with energies up to 16.5 GeV. The pulser also generates a controllable reverse current pulse 1 ms after the primary pulse. This back swing pulse is used in the cancellation of eddy currents.

Each magnet consists of a pair of 1-m long, air core coils. Initially the coils were supported in an aluminum frame and mounted on an Al baseplate. The baseplate was supported in the accelerator housing on a steel girder. After the problems of the eddy currents were identified, 80/20 T-slot™ Al frame members [4] and Al baseplate were replaced with G10 pieces to break up eddy current flow paths and to remove the baseplate "mirror." The effect was to reduce the eddy current fields that affected subsequent bunches by a factor of about 10 from about 10 μm to about 1 μm. Figures 1 a,b,c show the pulsed current waveform; the original magnet with Al frame and baseplate; and the G10 modified magnet.

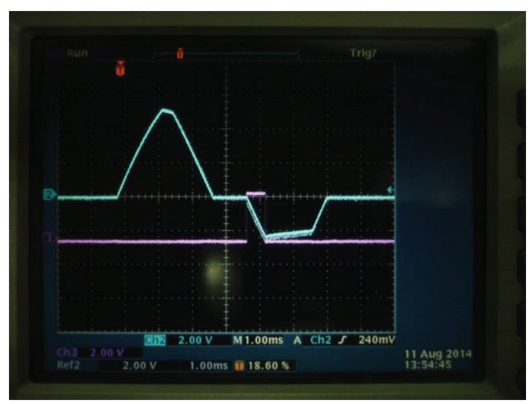

Figure 1a: Pulse kicker current waveform.

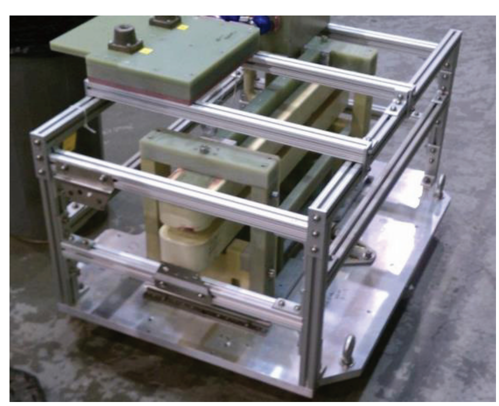

Figure 1b: Original Al frame and baseplate kicker magnet.

* Work supported by DoE Contract DE-AC02-76SF00515, 10/01/2012-09/30/2017

† email address: jcs@slac.stanford,edu



ISBN 978-3-95450-177-9

# THE CERN BEAM INSTRUMENTATION GROUP OFFLINE ANALYSIS FRAMEWORK

B.Kolad, J-J Gras, S. Jackson, S. Bart Pedersen, CERN, Geneva Switzerland.

*Abstract*

Beam instrumentation (BI) systems at CERN require periodic verifications of both their state and condition. An instrument's condition can be diagnosed by looking for outliers in the logged data which can indicate the malfunction of a device. Presently, experts have no generic solution to observe and analyse an instrument's condition and as a result, many ad-hoc Python scripts have been developed to extract historical data from CERN's logging service. Clearly, ad-hoc developments are not desirable for medium/long term maintenance reasons and therefore a generic solution has been developed. In this paper we present the Offline Analysis Framework (OAF), used for automatic report generation based on data from the central logging service. OAF is a Java / Python based tool which allows generic analysis of any instrument's data extracted from the database. In addition to the generic analysis, advanced analysis can also be performed by providing custom Python code. This paper will explain the steps of the analysis, its scope and present the kind of reports that are generated and how instrumentation experts can benefit from them. It will subsequently demonstrate how this approach simplifies debugging, allows code re-use and optimises database and CPU resource usage.

## INTRODUCTION

Both scientific and business domains have witnessed exponential growth of available data. Processing and analysing huge amounts of data is a major problem and has become it's own scientific field leading to the creation of many commercial and open source tools over the years. The need for similar tools in the Beam Instrumentation group at CERN has already been identified in the past [1]. The BI group decided to make their own tool because of the group's very specific constraints (the database can only be accessed via a dedicated java API, and users often need tailor made reports). LHC systems produce large quantities of data which can be used for checking the health of various beam instrumentation systems. OAF aims to simplify and unify the work-flow of the data analysis and problem detection.

After the evaluation of technologies on which we could base our analysis solution, Java, C++ and Python emerged as the primary candidates. These three programming languages have a long history at CERN and are widely used inside the organisation. We finally choose Python, as it offers a rich choice of scientific libraries for numerical and statistical analysis (for example we make heavy use of the Python Panda and Matplot libraries). Furthermore, prototyping in an interpreted language is also much faster than in languages requiring compilation. Python is also beginner friendly and can be used by users with limited programming experience – an important feature for our needs if OAF is to offer a *custom analysis* feature which allows broader analysis via dedicated code supplied by instrument experts.

## STATUS BEFORE OAF

Data logged by the LHC is stored in a so-called logging database [2] and is accessible via a web-based user interface (Timber) which accesses data via a Java API, but provides limited analysis capabilities. This data is regularly extracted and analysed off-line by experts, to elicit useful information about an instruments performance. In the absence of a standard means to do this, instrument specialist inevitably started developing various independent tools. Each of these tools had to support the same set of operations:

- Data extraction
- Statistical analysis
- Production of a report document

The absence of any framework to guide the developers of analysis tools, lead to many problems including:

- Code duplication
- Sub-optimal means of data extraction (by performing an out of process system call, which in turn ran a generic Java command line tool)
- The data extracted by the Java command tool was subsequently dumped into a text file and then parsed into various python data structures
- Some scripts were moved to newer Python / library versions while others remained on out-dated versions
- Very often authors of scripts stayed at CERN for a limited period of time leaving the maintenance burden on newly arrived colleagues.

Dealing with this script *zoo* became a complex software engineering task in itself, and it was soon obvious that the common functionality of these various scripts had to be handled differently so that the maintenance of the infrastructure of the resulting framework should not concern the instrument experts.

## DATA SOURCE

The Logging Service stores data coming from pre-defined signals into an Oracle database, and provides a Java API accompanied by a generic GUI (Timber) which can be used to extract and visualise logged data.

ISBN 978-3-95450-177-9

# IMPROVEMENTS TO THE LHC SCHOTTKY MONITORS

M. Wendt*, M. Betz, O.R. Jones, T. Lefevre, T. Levens, CERN, Geneva, Switzerland

*Abstract*

The LHC *Schottky* monitors have the potential to measure and monitor some important beam parameters, e.g. tune, momentum spread, chromaticity and emittance, in a non-invasive way. We present recent upgrade and improvement efforts of the transverse LHC *Schottky* systems operating at 4.81 GHz. This includes optimization of the slotted waveguide pickups and a re-design of the RF front-end electronics to detect the weak, incoherent *Schottky* signals in presence of large, coherent beam harmonics.

## INTRODUCTION

The theory of bunched beam transverse *Schottky* signals reveals the measurement of machine parameters, such as tune, chromaticity, emittance, etc. based on the observation of coherent and incoherent motion of the bunched particles [1]. The associated dipole moment of each particle, following betatron and synchrotron motion, can be expressed as *Fourier* series, showing upper (usb) and lower (lsb) betatron sidebands around each revolution harmonic $h$, which further splits into synchrotron satellites.

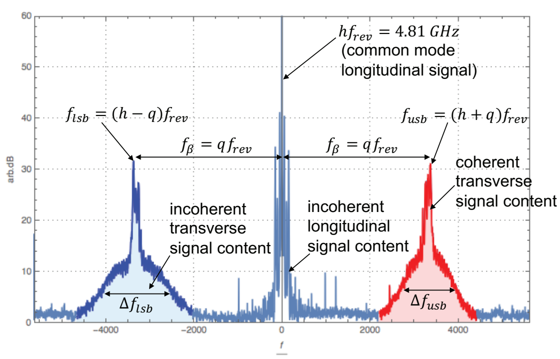


Figure 1: Typical LHC *Schottky* spectrum.

The *Fourier* representation hints to perform the observation of these tiny particle fluctuations in the frequency domain. Figure 1 shows a downconverted *Schottky* spectrum ($h$ = 427746, $f_{\rm rev}$ = 11.245 kHz) for a bunch of $n \approx 10^{11}$ protons (charge state $z$ = 1) in the LHC at injection energy. In practice, even with a very well centered beam, the longitudinal common mode revolution harmonics are always present, and usually dominant. In this low-resolution measurement the synchrotron sideband modulation is "smeared' out" to the usb and lsb incoherent *Schottky* signal "humps". Clearly visible on top of these incoherent signal humps are the coherent betatron sidebands, whose intensity is dependent on the longitudinal bunch shape and amplitude of any residual coherent oscillations. These allows the measurement of the fractional betatron tune $q = f_\beta / f_{\rm rev}$.

* manfred.wendt@cern.ch

The chromaticity $\acute{Q}$ is derived from the different widths $\Delta f_{\rm usb}$, $\Delta f_{\rm lsb}$ of the respective usb and lsb *Schottky* humps.

$$\acute{Q} = \eta \left( h \frac{\Delta f_{\rm lsb} - \Delta f_{\rm usb}}{\Delta f_{\rm lsb} + \Delta f_{\rm usb}} + q \right) \approx \eta h \frac{\Delta f_{\rm lsb} - \Delta f_{\rm usb}}{\Delta f_{\rm lsb} + \Delta f_{\rm usb}} \qquad (1)$$

with $\eta$ being the phase slip factor, which is 3.183e-4 for the LHC, The approximation is true for $h \gg \eta$ and $\Delta f_{\rm lsb} - \Delta f_{\rm usb} \neq 0$. At 4.81 GHz $h \approx 4.28e5$, so that $\eta h \approx 136$, implying that a 1% difference in width represents 1 unit of chromaticity. The momentum spread $\Delta p/p$ is proportional to the average width of the sidebands

$$\frac{\Delta p}{p} \propto \frac{\Delta f_{\rm lsb} + \Delta f_{\rm usb}}{2 f_{\rm rev} h \eta}, \qquad (2)$$

and the emittance can be estimated from the total signal power contained in a given sideband hump, with $A_{\rm usb} \Delta f_{\rm usb} \equiv A_{\rm lsb} \Delta f_{\rm lsb}$. This, however, requires independent calibration.

## THE LHC SCHOTTKY MONITOR SYSTEM

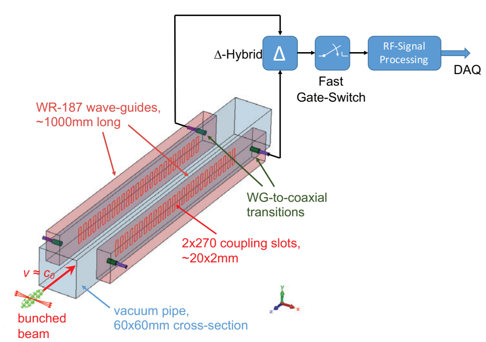


Figure 2: Simplified overview of the LHC *Schottky* monitor system (beam pickup not to scale).

The LHC *Schottky* monitoring system (Fig. 2) was designed and built in frame of the US LARP collaboration with Fermilab [2, 3]. An operation frequency of 4.8 GHz was selected as the best compromise between avoiding overlapping *Schottky* sidebands at very high frequency, and being within the single bunch coherent spectrum at low frequency. A symmetric arrangement of slotted waveguide couplers is used to provide a broadband *Schottky* beam pickup, followed by an RF front-end with narrowband, triple-stage downconversion and a 24-bit audio digitizer based DAQ system. While the 200 MHz bandwidth of the beam pickup offers single bunch time resolution, selected by a fast gate switch, the following low-noise receiver has a final bandwidth of ~15 kHz, slightly larger than the 11 kHz LHC revolution frequency. The LHC is equipped with four such *Schottky* monitoring systems, a horizontal and a vertical unit for each beam.

ISBN 978-3-95450-177-9

# REVIEW OF CHROMATICITY MEASUREMENT APPROACHES USING HEAD-TAIL PHASE SHIFT METHOD AT RHIC *

V.H. Ranjbar, A. Marusic, M. Minty, Brookhaven National Lab, Upton NY 11973, USA

*Abstract*

We review tests of the head-tail phase shift method using various approaches at BNL's RHIC. Both the standard and some more exotic approaches to measure the phase differential between the head and tail of a bunched beam has been attempted at RHIC. The standard kick beam and measured phase evolution of the head and tail of a given bunch has been tried at RHIC. Additionally a more exotic approach to measure the head versus tail phase difference has been tried. In this approach we used a BBQ pickup and kicker with the input stripline signal to the BBQ mixed with a nano second pulse timed to the head and tail of the bunch. In this way we hoped to force the BBQ to sample the head or tail of the bunch depending on the pulse timing. We report on the results and challenges which each approach presented.

## HEAD-TAIL PHASE SHIFT METHOD

The head-tail phase shift approach relies on the measurement of the phase difference that develops between betatron oscillations at fixed longitudinal positions relative to the center of the RF bucket. The maximum phase shift is proportional to the chromaticity and given by the following formula:

$$Q' = \frac{-\eta\Delta\Phi}{2\omega_0\Delta\tau} \tag{1}$$

Here $Q'$ is the chromaticity, $\eta$ the momentum compactions factor, $\Delta\Phi$ the betatron phase difference between two points $\Delta\tau$ difference away from each other in the RF bucket in time.

### *Single Kick Based Method*

The approach was first worked out at the SPS by R. Jones [1] with theoretical analysis by Fartoukh [2]. A single kicked method was used with the sampling occurring at 1/2 synchrotron period from the time of the applied kick. This was because phase difference was maximal at this point since the phase difference would oscillate with $(cos(\omega_s t) - 1)$, where $\omega_s$ is the synchrotron frequency.

Although the approach was fist tested in the SPS, it was never used for actual operations. This was due to the fact that the non-linearities of the fields in the SPS caused very rapid decoherence of the kicked oscillations thus making it very difficult to obtain a good signal at 1/2 synchrotron period after the kick (about several hundred turns). Also this approach was destructive to the beam causing emittance blow up and thus only could be possibly used during machine tune up.

Later the approach was also tested at the Tevatron [3]. In this case there was more success due to the fact that the Tevatron at injection had a much longer coherence time. Thus it was actually used for tune up during operations for a while. Then when octupoles were used to help control the head-tail instability, this created decoherence times similar to that in the SPS.

## TESTS AT RHIC

Concurrently with the work at the Tevatron tests were also performed at RHIC, however there is little in the way of published documentation for this work. Later we conducted several tests at RHIC, which we now present here.

During the FY14 APEX studies, we used the Artus kicker to excite the beam and acquired turn-by-turn data in the vertical and horizontal planes. This was done using a Tektronics scope attached to the yellow meter long stripline located at A0 house.

The data acquisition was done in a similar manner as was performed in the Tevatron system. The difference signal was sampled as a poxy for the average relative beam position. The reflection of the signal which creates a doublet signal was separated by splitting, delaying and re-summing. The final signal was digitized by the scope sampling turn-by-turn.

We performed 18 measurements at 100 GeV using the Au beam, while scanning through different chromaticity settings. In Fig. (1, 2) the turn by turn difference signal is shown for the horizontal and vertical planes as well as the FFT for the signal.

When compared to the signals we used to get in the Tevatron (see Fig. 3) it is immediately obvious that the decoherence is much faster and the signal to noise worse. We barely could acquire a signal through one decoherence period (1/2 synchrotron period).

### *Simulation*

One major difference in the RHIC accelerator from the SPS's and Tevatron is the nature of the RF system. RHIC runs with at least two RF harmonics for the longitudinal motion stability at higher intensities. We were concerned that the additional RF component might alter the betatron phase dependence on chromaticity. So to understand this better we simulated this using M. Blaskiewicz RF modeling code (BTFTranf). We compared the case with two versus a single RF component (see Fig. (4,5)) and found that while there was some distortion in the phase oscillations, generally the phase difference scaled with chromaticity and longitudinal $\Delta\tau$ magnitude and it was possible to extract correct chromaticity values despite this.

### *Analysis*

As can be seen in Fig. (1) and (2) by about 6-800 turns when the synchrotron period is at 1/2, the signal was rather

* Work supported by the URA., Inc., under contract DE-AC02-76CH03000 with the U.S. Dept. of Energy.

ISBN 978-3-95450-177-9

# STATUS OF BEAM CURRENT TRANSFORMER DEVELOPMENTS FOR FAIR

M. Schwickert, F. Kurian[1], H. Reeg, T. Sieber, GSI Helmholtzzentrum für Schwerionenforschung, Darmstadt, Germany
[1]also at Helmholtz-Institute Jena, Germany
R. Neubert, P. Seidel, Friedrich-Schiller University Jena, Germany
K. Hofmann, Technical University Darmstadt, Darmstadt, Germany
E. Soliman, German University in Cairo, Cairo, Egypt

*Abstract*

In view of the upcoming FAIR project (Facility for Antiproton and Ion Research) several long-term development projects had been initiated with regard to diagnostic devices for beam current measurement. The main accelerator of FAIR will be the fast ramped superconducting synchrotron SIS100. Design parameters of SIS100 are acceleration of $2\times10^{13}$ protons/cycle to 29 GeV for the production of antiprotons, as well as acceleration and slow extraction of p to U ions at $10^9$ ions/s in the energy range of 0.4-2.7 GeV/u and extraction times of up to 10 s. For high-intensity operation non-intercepting devices are mandatory, thus the developments presented in this contribution focus on purpose-built beam current transformers. First prototype measurements of a dc current transformer based on a Tunnelling Magneto Resistance sensor are presented, as well as recent achievements with a SQUID-based Cryogenic Current Comparator.

## FAIR ACCELERATOR FACILITY

Presently, the technical layout of the FAIR accelerator complex is being finalized and civil construction of the accelerator tunnel will start soon. FAIR consists of the fast-ramped superconducting synchrotron SIS100, the high-energy beam transport system (HEBT) interconnecting the synchrotrons with the pBar-Target for production of anti-protons, the super-fragment separator (SFRS) for the production of rare isotopes, the collector ring (CR) for stochastic pre-cooling of rare isotopes and anti-protons, and the high-energy storage ring (HESR) for internal target experiments [1]. Existing GSI accelerators serve as injectors for the FAIR machines. Primary goal of the novel facility is the production of heavy ion beams with unprecedented intensities close to the space charge limit of the synchrotron. The workhorse of FAIR will be SIS100, designed to produce up to $5\times10^{11}$ $U^{28+}$ ions/s with energies of 400-2700 MeV/u. Particles will be extracted either in single bunches of e.g. 30 ns as required for the production of anti-protons, or as slowly extracted beam with extraction times of several seconds for the radioactive ion beam program of FAIR.

For effective usage of the accelerator chain a multiplexed machine operation is foreseen which will allow to provide beams to up to four different physics experiments inside one machine super-cycle. Especially the planned high-intensity operation calls for a reliable online transmission control system. Beam current transformers will be the main source of intensity signals along the accelerator chain. Each section of the FAIR complex has special requirements and, ideally, beam current transformers are purpose-built instruments for each use case.

## REQUIREMENTS FOR BEAM CURRENT MEASUREMENT

The accelerator control system of FAIR will require the measurement data of beam current transformers for various applications. Besides regular transmission monitoring, operating and archiving systems will monitor the beam currents during injection, accelerating ramp and during fast and slow extraction to calculate extraction efficiencies online. This is done e.g. to prevent recurring beam losses leading to unnecessary activation of machine components. Additionally, the planned machine protection system requests the generation of a ‘beam-presence flag’ and a ‘setup-beam flag’ from the current transformer signals. The setup-beam flag identifies beam settings that are used for preliminary test runs and accelerator commissioning, typically performed at low beam intensities. A signal threshold is monitored for beam current monitors along the related accelerator chain to verify the conditions for the setup-beam flag. The beam-presence flag on the other hand identifies machine settings that have previously been validated for high-current operation of the machine. In this state the online transmission control based on transformer signals is set to very small tolerance bands to protect the accelerator chain from potential beam-induced damages.

Since many years commercial solutions for beam current transformers are available on the market. However, for special use cases, demanding e.g. for very high dynamic range of beam intensities, or the measurement with ultra-high sensitivity in the nanoampere range, purpose-built transformers are required.

## TUNNELING MAGNETO RESISTANCE DC CURRENT TRANSFORMER

The goal of the research project for a novel DC current transformer (DCCT) was to create an instrument that allows for precise online measurement of accelerated and stored beams with a large dynamic range of beam intensi-

ISBN 978-3-95450-177-9

# MICRO PATTERN IONIZATION CHAMBER WITH ADAPTIVE AMPLIFIERS AS DOSE DELIVERY MONITOR FOR THERAPEUTIC PROTON LINAC

E. Cisbani*, A. Carloni, S. Colilli, G. De Angelis, S. Frullani, F. Ghio,
F. Giuliani, M. Gricia, M. Lucentini, C. Notaro, F. Santavenere,
A. Spurio, G. Vacca, Istituto Superiore di Sanità, 00161 Rome, Italy
E. Basile, Azienda Ospedaliera Papardo, 98158 Messina, Italy
A. Ampollini, P. Nenzi†, L. Picardi, C. Ronsivalle,
M. Vadrucci, ENEA C.R. Frascati, 00044 Frascati (Rome), Italy
D. M. Castelluccio, ENEA (FSN-SICNUC-PSSN), 40129 Bologna, Italy
C. Placido, Sapienza University of Rome, 00185 Rome, Italy
[1]also at Istituto Superiore di Sanità, 00161 Rome, Italy

*Abstract*

A dedicated dose delivery monitor is under development for the TOP-IMPLART proton accelerator, the first LINAC for cancer therapy. It is expected to measure the beam intensity profile to precisely monitor the fully active 3+1D (x/y/z and intensity) dose delivery of each short pulse (few µs, 0.1-10 µA pulse current at ~ 100 Hz) of the therapeutic proton beam (up to 230 MeV). The monitor system consists of planar gas chambers operating in ionization regime with cathode plane made of micro pattern pads alternately connected by orthogonal strips. The dedicated readout electronics features trans-impedance amplifier that dynamically adapts its integrating feedback capacitance to the incoming amount of charge, then opportunistically changing its gain. The measured absolute sensitivity is about 100 fC (better than 0.03 relative sensitivity), the dynamic range up to 10000 (2 gain settings) with time response at the level of few ns, and virtually no dead time. Small scale chamber prototype (0.875 mm pitch pads) and readout electronics have been tested and characterized under both electron (5 MeV) and proton (up to 27 MeV) beams.

## INTRODUCTION

According to the World Health Organization, cancers are the leading causes of morbidity and mortality; the annual cases are expected to rise by about 70% in the next 2 decades [1]. The clinical issue is exacerbated by the relevant costs of the cancer care (compare to euro 126 billion/years in European Union in 2009 [2]). Several approaches have been developed for cancer control and cure: surgery, chemotherapy, immunotherapy, radiotherapy, hormonal therapy, ultrasound therapy. Hadrontherapy, which mainly uses accelerated protons or ions, is rapidly expanding in cancers treatment, especially for the control of tumours in the proximity of vital organs or close to radiosensitive healthy organs. In fact hadrontherapy is an intrinsically highly accurate technique, due to the peculiar hadron property to release the largest amount of dose at the end of its path in the tissue while the lateral spread is small and the entrance integral dose is relatively low. Moreover the penetration in the body depends on the initial energy of the hadron. This accuracy results in effective irradiation of the tumour, thereby reducing the dose to the surrounding healthy tissues and thus leading to lower morbidity. However hadrontherapy construction and operation costs are large compared to the other therapies and this represents a serious drawback for its diffusion.

The innovative TOP-IMPLART project [3] moves in the direction of highest therapeutic impact and at the same time costs reduction by the exploitation, for the first time in cancer therapy, of a dedicated LINAC proton accelerator. Key features offered by the LINAC are the pulse current modulation (fully intensity modulated therapy), high repetition rate (better organ motion compensation), negligible power loss from synchrotron radiation (easier radioprotection), simpler injection and extraction than in circular accelerators, modular construction.

The highest conformation of the dose delivery achievable by the TOP-IMPLART requires an accurate monitoring of the beam parameters on a pulse by pulse basis; the dose delivery shall provide real-time measurements of the beam intensity profile, beam centroid position and its direction in order to guarantee that the prescribed dose is optimally delivered. The peculiar characteristics of the TOP-IMPLART LINAC[1] reflect on the following main requirements for the dose delivery monitor: good spatial resolution ~ 0.1 mm, large input dynamic range $\geq 10^4$, good sensitivity ~ 100 fC, rapid response < 1 ms.

## DOSE DELIVERY DETECTOR AND MULTI GAIN READOUT ELECTRONICS

The dose delivery monitor will be based on a set of 2 independent transmission ionization chambers with segmented readout planes (~ $30 \times 30$ cm$^2$ active transverse area). Design of the chamber cathode exploits recent developments in

* evaristo.cisbani@iss.it, contact person
† paolo.nenzi@enea.it, presenter at the conference

[1] Beam specifications: cross section ~ 1 mm, peak current 0.1–10 µA, average current 10 nA, pulse width 1–5 µs, pulse frequency 1–100 Hz.



ISBN 978-3-95450-177-9

# BUNCH ARRIVAL-TIME MONITORING FOR LASER PARTICLE ACCELERATORS AND THOMSON SCATTERING X-RAY SOURCES

J. Krämer, J.P.Couperus, A. Irman, A. Köhler, M. Kuntzsch, U. Lehnert, P. Michel, U. Schramm, O.Zarini
Helmholtz-Zentrum Dresden-Rossendorf, Dresden, Germany

*Abstract*

The ELBE center of high power radiation sources at Helmholtz-Zentrum Dresden-Rossendorf combines a superconducting CW linear accelerator with Terawatt- and Petawatt- level laser sources. Figure 1 shows a layout of the facility and an overview of the secondary sources. Key experiments rely on precise timing and synchronization between the different radiation pulses. An online single shot monitoring system has been set up in order to measure the timing between the high-power Ti:Sa laser DRACO and electron bunches generated by the conventional SRF accelerator. This turnkey monitoring system is suitable for timing control of Thomson scattering x-ray sources and external injection of electron bunches into a laser wakefield accelerator.

## INTRODUCTION

### *ELBE Accelerator and High-Power Lasers*

The ELBE accelerator produces electron bunches up to an energy of 40 MeV in continuous wave (CW) operation [1]. The nominal repetition rate is 13 MHz while various pulse patterns can be generated by the two injectors. The first injector is a thermionic DC-gun operating at 235 kV followed by two normal conducting buncher cavities. It provides electron pulses with a charge of up to 100 pC. The second injector is a superconducting photo gun (SRF-Gun) that will provide electron bunches with a charge of up to 1 nC [2]. The main accelerator consists of two cryo modules, each equipped with two 9-cell TESLA-type cavities [3].

Adjacent to the conventional accelerator, two high power lasers have been set up, enable new experiments with high electric fields and ultra-fast time scales. The chirped pulse amplification Ti:sapphire system DRACO (Dresden laser acceleration source) produces laser pulses up to 6 J at a repetition rate of 10 Hz or 45 J at 1 Hz [4].

A fully diode-pumped laser system - PEnELOPE (Petawatt, Energy-Efficient Laser for Optical Plasma Experiments) is being constructed in the same area. A five stage amplifier system relying on Yb:CaF2 as gain medium is designed for pulse energies of 150 J and a pulse duration of <150 fs at a repetition rate of 1 Hz [5].

Main fields of research are the development of novel compact and brilliant sources of energetic particle beams and potential applications, e.g., in the field of radiation oncology [6].

### *Thomson X-ray Source*

The combination of high power lasers and the ELBE accelerator offers the opportunity to explore the physics of high-intensity laser-electron interaction. One application is the operation of a picosecond narrow-bandwidth Laser-Thomson-backscattering X-ray source. Here both beams are interacting in a dedicated target chamber. The generated narrowband X-rays are highly collimated and can be reliably adjusted from 12 keV to 20 keV by tuning the electron energy (24–30 MeV) [7].

In order to provide a constant photon flux the spatial as well as the temporal overlap between both pulses have to be ensured. Both beams are transpoerted up to 100 meters so that temperature drifts and mechanical vibrations affect the pointing and arrival-time stability at target position.

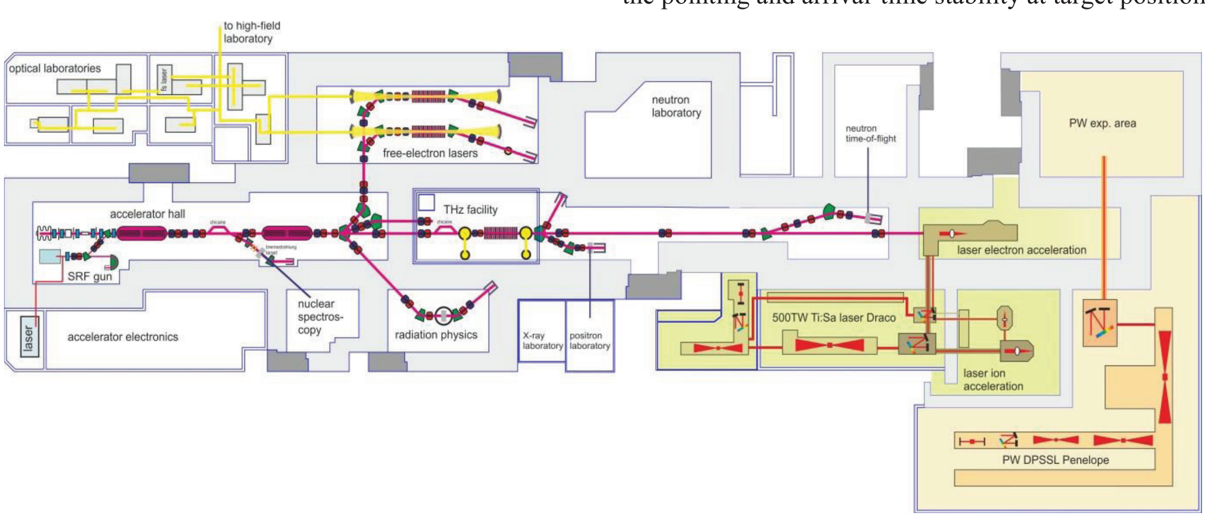


Figure 1: Layout of the ELBE - Center for high power radiation sources.



ISBN 978-3-95450-177-9

# NOVEL APPROACH TO THE ELIMINATION OF BACKGROUND RADIATION IN A SINGLE-SHOT LONGITUDINAL BEAM PROFILE MONITOR

H. Harrison,* G. Doucas, A. J. Lancaster, I. V. Konoplev, H. Zhang,
The John Adams Institute, Department of Physics,
University of Oxford, Oxford OX1 3RH, United Kingdom
A. Aryshev, M. Shevelev, N.Terunuma, J. Urakawa,
KEK: High Energy Accelerator Research Organization, 1-1 Oho, Tsukuba, Ibaraki 305-0801, Japan

*Abstract*

It is proposed to use the polarization of coherent Smith-Purcell radiation (cSPr) to distinguish between the cSPr signal and background radiation in a single-shot longitudinal bunch profile monitor. A preliminary measurement of the polarization has been carried out using a 1 mm periodic metallic grating installed at the 8 MeV electron accelerator LUCX, KEK (Japan). The measured degree of polarization at $\theta = 90°$ (300 GHz) is $72.6 \pm 3.7\%$. To make a thorough test of the theoretical model, measurements of the degree of polarization must be taken at more emission angles - equivalent to more frequencies.

## INTRODUCTION

Developments in particle accelerators place increasing demand on beam diagnostic tools. At facilities operating with sub-ps bunch lengths or experiencing large bunch-to-bunch variation, a non-destructive single-shot longitudinal bunch profile monitor is essential. cSPr has been suggested as a technique for non-destructive longitudinal bunch diagnostics, using spectral analysis of the radiation to determine the bunch profile [1]. This has been successfully demonstrated for a "multi-shot" system [2], now a "single-shot" monitor is being designed. The new monitor will be able to extract all the information needed from each bunch to reconstruct its longitudinal profile. The proof-of-principle "multi-shot" experiments carried out at FACET, SLAC (USA) faced the challenge of extracting the cSPr signal from a high background environment, a problem that needs to be taken into account for any future monitor. It is proposed to use the polarization of cSPr to separate the signal from the background radiation - which is likely to be unpolarized [2] - according to the relation shown in Eq. 1:

$$G_{\parallel} = gG_{\perp} = g\left(\frac{I_{\parallel} - bI_{\perp}}{a - b}\right) \tag{1}$$

where the cSPr signal $G_i$ is expressed in terms of the measured signal $I_i$ and the ratios of the two orientations of radiation $a = \frac{G_{\parallel}}{G_{\perp}}$ and $b = \frac{B_{\parallel}}{B_{\perp}}$.

Previous studies have shown that cSPr is polarized [2–4], however, there has not yet been an extensive study of this property or a conclusive comparison with any theoretical model. Before this idea can be incorporated into the design of the single-shot cSPr monitor it is necessary to perform accurate measurements of the polarization of cSPr and demonstrate that it is possible to predict its degree of polarization via simulation. This paper will demonstrate a good preliminary agreement between the experiment and theory.

* hannah.harrison@physics.ox.ac.uk

## THEORY AND SIMULATION

Smith-Purcell radiation is emitted when a charged particle travels above a periodic grating. The particle induces a surface current on the grating surface which emits radiation at the discontinuities of the grating. The radiation is spatially distributed according to the following dispersion relation:

$$\lambda = \frac{l}{n}\left(\frac{1}{\beta} - \cos\theta\right) \tag{2}$$

where $\lambda$ is the measured wavelength at observation angle $\theta$, $\beta = \frac{v}{c}$ is the normalized electron velocity, $l$ is the grating periodicity and $n$ is the order of emission of radiation.

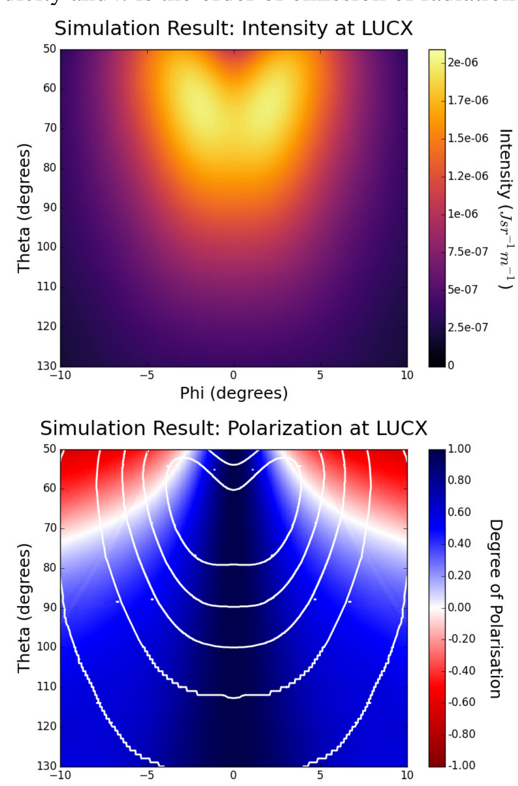


Figure 1: Simulation of intensity (top) and degree of polarization (bottom, contours show intensity), of cSPr generated by the interaction of a 1 mm period grating and an 8 MeV beam. $\theta$ and $\phi$ are the angles along and around the beam.

ISBN 978-3-95450-177-9

# DESIGN OF A TIME-RESOLVED ELECTRON DIAGNOSTICS USING THz FIELDS EXCITED IN A SPLIT RING RESONATOR AT FLUTE

M. Yan*, E. Bründermann, S. Funkner, A.-S. Müller, M. J. Nasse, G. Niehues, R. Ruprecht, M. Schedler, T. Schmelzer, M. Schuh, M. Schwarz, B. Smit, Karlsruhe Institute of Technology, Karlsruhe, Germany
M. Dehler, N. Hiller, R. Ischebeck, V. Schlott, Paul Scherrer Institute, Villigen, Switzerland
T. Feurer, M. Hayati, Universität Bern, Bern, Switzerland

*Abstract*

Time-resolved electron diagnostics with ultra-high temporal resolution is increasingly required by the state-of-the-art accelerators. Strong terahertz (THz) fields, excited in a split ring resonator (SRR), have been recently proposed to streak electron bunches for their temporal characterisation. Thanks to the high amplitude and frequency of the THz field, temporal resolution down to the sub-femtosecond range can be expected. We are planning a proof-of-principle experiment of the SRR time-resolved diagnostics at the accelerator test-facility FLUTE (Ferninfrarot Linac und Test Experiment) at the Karlsruhe Institute of Technology. The design of the experimental chamber has been finished and integrated into the design layout of the FLUTE accelerator. Beam dynamics simulations have been conducted to investigate and optimise the performance of the SRR diagnostics. In this paper, we present the design layout of the experimental setup and discuss the simulation results for the optimised parameters of the accelerator and the SRR structure.

## INTRODUCTION

Temporal characterization of electron bunches is an important diagnostic tool for the control and optimisation of accelerators.The generation of ultra-short electron bunches in the femtosecond regime demands for time-resolved diagnostics with appropriate resolution. RF transverse deflecting structures have been demonstrated to be capable of providing few-femtosecond temporal resolution [1]. Recently, a new time-resolved diagnostics using THz fields excited in a split ring resonator (SRR) has been proposed [2, 3]. Thanks to the short pulse duration, high resonant frequency and high field enhancement of the THz pulses [4], such SRR diagnostics could allow for femtosecond resolution with single shot capability. Moreover, the small size of the SRR structures in the sub-millimeter range makes them more flexible in the integration into the accelerator, and combining several of them provides potentials for even better resolutions.

Analog to systems using RF deflecting structures, the SRR setup maps the temporal coordinate onto a transverse coordinate. As illustrated in Fig. 1, a driving laser system generates intense single cycle THz pulses though optical rectification. The THz pulses are absorbed in the split ring resonator structure and excite electric field enhancement for the resonant frequency inside the gap. The electron bunches, which are generated by the same driving laser system through the photoelectric effects on a cathode, interact with the high amplitude THz field in the gap and are deflected in the transverse direction. The longitudinal density distribution of the electron bunch is translated into a transverse density distribution, which can be measured using a transverse beam imaging screen.

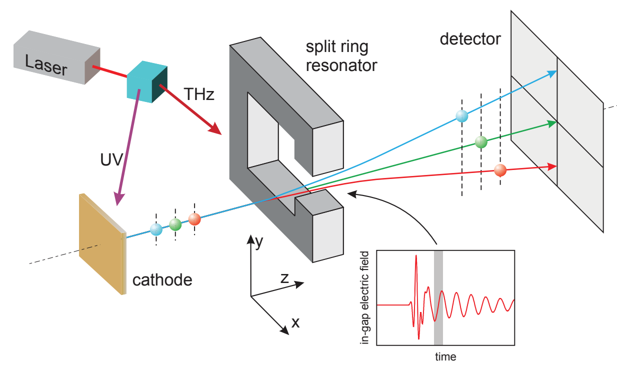


Figure 1: Principle of the SRR diagnostics [2].

In the following, the physical formulation of the streaking effect is shortly introduced for a SRR deflecting in the vertical direction. For an electron at a location $z$ relative to the reference particle, the accumulated transverse momentum obtained from the THz field is

$$p_y = \frac{e}{c} \cdot V_0 \sin(kz + \Psi_0), \tag{1}$$

where $V_0$ is the integrated deflecting field through the gap, $k$ the wavenumber of the THz field, $\Psi_0$ the phase of the THz field. For operation around the zero-crossing phase with $\Psi_0 = 0$, the vertical momentum can be approximated by

$$p_y = \frac{e}{c} \cdot V_0 k z, \tag{2}$$

which is in linear dependence on the longitudinal position $z$ of the electrons inside the bunch. After a beam transport section to a downstream imaging screen, this vertical deflection is further translated into a vertical offset of

$$y = Sz, \quad S = \sqrt{\beta_{y,\mathrm{SRR}}\beta_{y,\mathrm{screen}}} \cdot \sin(\Delta\mu_y)\frac{eV_0 k}{\gamma E_0}, \tag{3}$$

where the streak parameter $S$ describes the strength of the streaking effect, $\beta_{y,\mathrm{SRR}}$ and $\beta_{y,\mathrm{screen}}$ are the beta-functions at the locations of the SRR and the screen, respectively, $\Delta\mu_y$

* minjie.yan@kit.edu

ISBN 978-3-95450-177-9

# 5 MeV BEAM DIAGNOSTICS AT THE MAINZ ENERGY-RECOVERING SUPERCONDUCTING ACCELERATOR MESA

S. Heidrich *, K. Aulenbacher, Institute of Nuclear Physics, Mainz, Germany

*Abstract*

Within the next few years, a new energy-recovering superconducting electron accelerator will be built at the Institute of Nuclear Physics in Mainz. For injection into the main accelerator the beam parameters need to be known. This requires a high resolution longitudinal beam diagnostic system at the 5 MeV-injection arc. The system employs two 90° vertical deflection dipoles, which aims to achieve an energy resolution of 240 eV and a phase resolution of 46 µm.

As a second challenge, the transverse emittance measurements will take place at full beam current. This demands an extremely heat resistant diagnostic system, realised by a method similar to flying wire.

## MAINZ ENERGY-RECOVERING SUPERCONDUCTING ACCELERATOR

The **M**ainz **E**nergy-recovering **S**uperconducting **A**ccelerator **MESA** will run in two different beam modes. The energy recovering mode allows beam currents up to 1 mA at a maximum beam energy of 105 MeV, while the external beam mode achieves an energy of 155 MeV but limits the maximum current to 150 µA. The part of the beam diagnostics discussed in this article will be installed downstream of the normal-conducting pre-accelerator at 5 MeV. Here, the beam will have a normalized transverse emittance of about 1 µm, an energy spread in the order of 2 keV and a bunch length of about 240 µm. For the second stage of MESA, 10 mA beam current is envisaged. The preinjector **MAMBO** (**Mi**lliampere **Bo**oster) is already designed for this average current. [1]

## LONGITUDINAL BEAM DIAGNOSTICS

The design of the longitudinal beam diagnostic combines a magnetic energy spectrometer with a dipole cavity for bunch length measurements. A set-up sketch of the system is displayed in Figure 1. First, the beam is guided through a 90° deflection dipole which causes a transverse spread depending on the energy distribution of the beam. By then collimating the dispersed beam through a 100 µm-gap, an energy window of ±240 eV is cut out. As displayed in Figure 2, the beam shows a large phase dispersion caused by the $R_{51}$ element of the dipole transformation matrix at this point. This phase smearing compromises the subsequent bunch length measurement and needs to be compensated with an additional quadrupole directly behind the collimator and a second 90° dipole. By that, the energy measurement system becomes achromatic and the phase smearing vanishes.

Then, the energy collimated beam is guided to the phase measurement system which consists of a focusing quadrupole, a 500 W 1.3 GHz dipole cavity, a defocusing quadrupole and a tungsten wire which cuts out a 60 µm long part of the bunch. The radiation caused by the interaction between the beam and the wire is proportional to the integrated current of the selected phase space and is measured with a scintillation detector. To scan the whole longitudinal phase space, the phase of the dipole cavity is shifted and the beam is steered over the energy collimator. To compensate the influence of the steerer on the $R_{51}$ matrix element, a second steerer has to be employed downstream of the energy collimator.

The measured phase space can be displayed in real time with a repetition rate of 10 Hz.

Contrary to the transverse diagnostics it is not possible to operate at full beam current. Instead, a pulsed or single bunch mode needs to be implemented.

It has to be mentioned that the energy spectrometer deflects the beam vertically while the injection arc has a horizontal set up. However, it may be assumed that the longitudinal phase space does not depend on the observation direction.

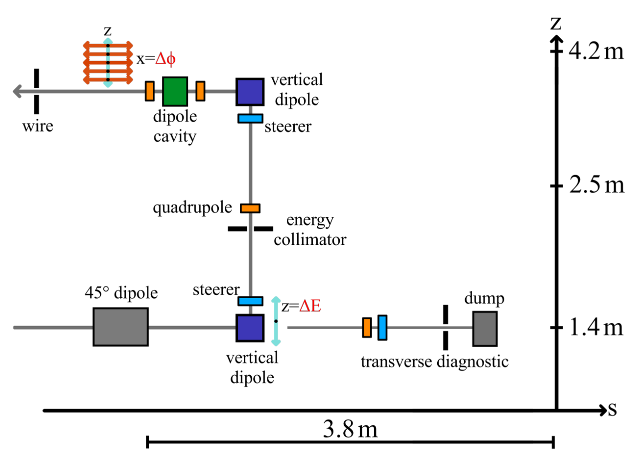


Figure 1: The longitudinal beam diagnostic consists of a vertically deflecting 90° energy spectrometer with subsequent chromatic correction and a dipole cavity which is used to measure the extension of the beamlets.

---
* s.heidrich@uni-mainz.de



ISBN 978-3-95450-177-9

# MEASUREMENT OF FEMTOSECOND ELECTRON BEAM BASED ON FREQUENCY AND TIME DOMAIN SCHEMES

K. Kan[#1], M. Gohdo, T. Kondoh, I. Nozawa, J. Yang , Y. Yoshida[#2]
The Institute of Scientific and Industrial Research (ISIR), Osaka University, Osaka 567-0047, Japan

*Abstract*

Ultrashort electron beams are essential for light sources and time-resolved measurements. Electron beams can emit terahertz (THz) pulses using coherent transition radiation (CTR). Michelson interferometer is one of candidates for analyzing the pulse width of an electron beam based on frequency-domain analysis. Recently, electron beam measurement using a photoconductive antenna (PCA) based on time-domain analysis has been investigated. The PCA with enhanced radial polarization characteristics enabled time-domain analysis for electron beam because of radially polarized THz pulse of CTR. In this presentation, measurement of femtosecond electron beam with 35 MeV energy and < 1 nC from a photocathode based linac will be reported. Frequency- and time- domain analysis of THz pulse of CTR by combining the interferometer and PCA will be carried out.

## INTRODUCTION

Short electron bunches with durations of picoseconds to femtoseconds are useful for generation of light in terahertz (THz) range [1]. Such electron beams are used in time-resolved studies of ultrafast phenomena and reactions, including ultrafast electron diffraction (UED) [2] and pulse radiolysis [3-5]. Electro-optic sampling [6], which is one of detection techniques of THz light pulse, is used in diagnostics of electron bunches. In EO samplings for electron bunch length measurement, the birefringence of EO crystals is induced by the beam electric field, and laser polarization corresponding to the longitudinal electron beam profile is detected [7,8]. EO monitors based on the temporal decoding have revealed the Coulomb field of a root mean square (rms) width of 60 fs from femtosecond electron bunches [8]. Interferometers [9] have been also used for the detection of single mode or multimode THz pulses generated by electron bunches and slow-wave structures [10,11]. Smith-Purcell radiation, which uses metallic gratings, has also been analyzed by interferometers [12,13]. Coherent transition radiation (CTR), which is generated by electron bunches crossing a boundary between different media, has been measured by interferometers and grating-type spectrometers [14-16]. Photoconductive antennas (PCAs), which are composed of semi-insulating semiconductor with electrodes, are widely used for both generation and detection of THz pulses in THz time-domain spectroscopy [17-20]. PCAs could be good candidates for analyzing temporal electric field profiles of electron bunches due to the correlation between electric-field-induced current output and THz electric field strength [20]. THz pulses of CTR are radially polarized [21] due to the diverging electric fields from the beam center. Therefore, a PCA with radial polarization characteristics is considered to be useful for the measurement of THz pulse from an electron bunch. Recently, Winnerl *et al.* reported fabrication of a large-aperture PCA, and the radially polarized field pattern of focused THz pulses was measured [22]. Generation of high-power THz pulses from a PCA using a high-voltage source has been studied for acceleration of electron beam [23]. Polarization components of radially polarized THz pulses from a PCA with interdigitated electrodes were also investigated using a wire grid polarizer [24]. Time-domain measurement of CTR using the PCA as a detector has been also conducted. The scheme is based on measurement of radially polarized THz pulses of CTR with a large-aperture PCA [24], which has radial polarization components. The combination of an interferometer and PCA will enable frequency and time-domain analysis of THz pulse of CTR.

In this paper, measurement of CTR from a femtosecond electron beam was conducted based on frequency and time-domain schemes. The energy and charge of the electron beam were 35 MeV and <1 nC at a repetition rate of 10 Hz, respectively. Frequency spectra of CTR were measured by a Michelson interferometer. On the other hand, time profiles of CTR were measured by a PCA driven by a femtosecond laser.

## EXPERIMENTAL ARRANGEMENT

Femtosecond electron bunches were generated by a photocathode-based linac, which consists of a 1.6-cell S-band radio frequency (RF) gun with a copper cathode, a 2-m-long traveling-wave linac, and an arc-type magnetic bunch compressor. The photocathode of RF gun was excited by UV pulses (262 nm) of a picosecond laser with an energy of <180 μJ/pulse and a pulse width of 5 ps FWHM at 10 Hz. The electron bunches generated in the gun were accelerated in the linac using a 35-MW klystron at a repetition rate of 10 Hz. In the linac, the electron bunches were accelerated to 35 MeV at a linac phase of 100° which is suitable for the bunch compression [16]. The accelerated electron bunches were compressed to femtosecond by the magnetic bunch compressor, which was composed of bending magnets, quadrupole magnets, and sextupole magnets. THz pulses of CTR were generated by the compressed electron bunches and measured.

Schematic diagram and picture of measurement system for CTR using the interferometer and PCA [24] were shown in Fig. 1. CTR was generated on the interface of a mirror (M1) as shown in Fig. 1 (a). The beam energy and bunch charge were 35 MeV and 740 pC/pulse, respectively. Collimated THz pulses of CTR were separated by a beam

#1: koichi81@sanken.osaka-u.ac.jp
#2: yoshida@sanken.osaka-u.ac.jp

ISBN 978-3-95450-177-9

# BUNCH EXTENSION MONITOR FOR LINAC OF SPIRAL2 PROJECT

R. Revenko†, J.-L. Vignet,
GANIL, Caen, France

*Abstract*

A semi-interceptive monitor for bunch shape measurement has been developed for the LINAC of SPIRAL2. A Bunch Extension Monitor (BEM) is based on the registration of X-rays emitted by the interaction of the beam ions with a thin tungsten wire. The time difference between detected X-rays and accelerating RF gives information about distribution of beam particles along the time axis. These monitors will be installed inside diagnostic boxes on the first five warm sections of the LINAC. The monitor consists of two parts: X-ray detector and mechanical system for positioning the tungsten wire into the beam. Emitted X-rays are registered by microchannel plates with fast readout. Signal processing is performed with constant fraction discriminators and TAC coupled with MCA. Results of bunch shape measurements obtained during commissioning of RFQ for SPIRAL2 are presented.

## INTRODUCTION

Semi-interceptive beam diagnostics for measurements of longitudinal bunch profile have been designed for LINAC of SPIRAL2 [1, 2]. It will be used for measurement and control of bunch extension during LINAC tuning and optimization of beam parameters. The operation principle of BEM is based on the registration of X-rays emitted by interaction of ions of the accelerator beam with a thin tungsten wire. The monitor performs precise measurements for X-rays arrival time that gives information about average distribution of ions along the time axis. The LINAC of SPIRAL2 is operated at 88 MHz that corresponds to period 11.36 ns between bunches and its extension of phase typically $\sigma_\varphi$ rms = 7°–8° (or $\sigma_t$ rms = 220–260 ps). Main beam parameters for LINAC specified in Table 1. Five BEMs will be installed at the beginning of the LINAC inside the first five warm sections.

Table 1: Parameters of LINAC Beam

| Parameter | Value |
|---|---|
| Frequency | 88.0525 MHz |
| Period | 11.36 ns |
| Energy at LINAC entrance | 0.75 MeV/A |
| Maximum intensity (deuterons) | 5 mA |
| Maximum power (deuterons) | 7,5 kW |
| Minimum $\sigma_\varphi$ rms | 7° |
| Minimum $\sigma_t$ rms | 220 ps |

The BEM will operate with high-intensity beams up to 5 mA and must provide reliable measurements with temporal resolution not worse than 1° of phase at 88 MHz of accelerated frequency. Some restrictions are imposed to the BEM design. A lack of space inside of the diagnostic box imposes to have a compact system. Also materials used for the BEM should not contaminate the superconducting cavities of cryomodule. These requirements were taken into account during the BEM design.

Different working principles of longitudinal bunch measurements were compared. Registration of SEs emitted from the wire would have required an accelerating potential of few kV. That leads to steering effect for the beam ions and requires an additional electrostatic compensation system. Using of backscattered ions does not provide required temporal resolution due to energy spread and a considerable difference of ions drift times depending on the point of interaction on the wire. Registration of X-rays is more suitable to avoid the use of accelerating potential and to minimize time spread for different drift paths. A disadvantage of this method is a longer time of acquisition related to low efficiency for X-rays registration. In our case it varies between 0.5 and 3 minutes.

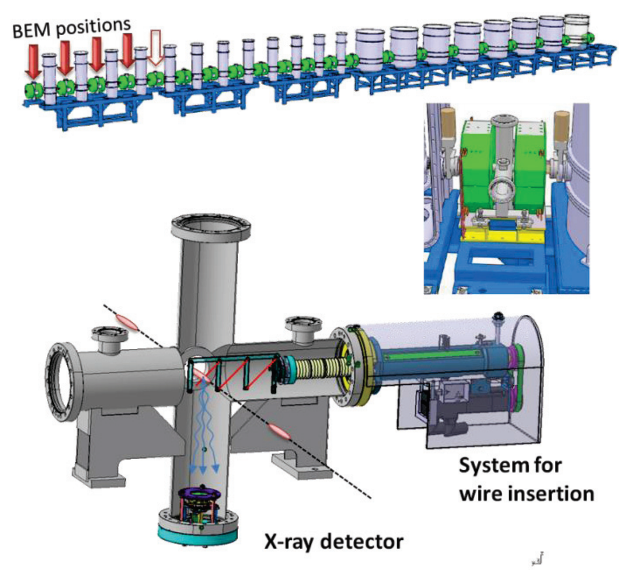


Figure 1: BEM installed at diagnostic box and its positions on LINAC warm sections.

## HARDWARE

The BEM is mounted inside of warm section and occupies two flanges of diagnostic box (Fig. 1). It consists of an X-ray detector and a mechanical system for positioning the wire inside the beam.

The mechanical system of wire insertion is able to perform positioning of the wires with accuracy better than few tens of microns. A wire holder has three identical positions with wires and allows replacing one wire with another in case of damage (Fig. 2, right). Integrity of the wire can be verified using measurements of collected beam current. The wire holder is electrically isolated from the other mechanical parts of actuator and connected to I/V converter



ISBN 978-3-95450-177-9

# STABLE TRANSMISSION OF RF SIGNALS AND TIMING EVENTS WITH ACCURACY AT FEMTOSECONDS

M. Liu*, X. L. Dai, C. X. Yin, SINAP, Shanghai, China

*Abstract*

We present a new design of femtosecond timing system. In the system, the RF signal and timing events are transmitted synchronously in one single optic-fibre with very high accuracy. Based on the theory of Michelson interferometer, the phase drift is detected with accuracy at femtoseconds. And phase compensation is accomplished at the transmitter with two approaches afterwards. Moreover, the traditional event timing system is integrated into the new system to further reduce the jitter of timing triggers. The system could be applied in synchrotron light sources, free electron lasers and colliders, where distribution of highly stable timing information is required. The physics design and the preliminary results are demonstrated in the paper.

## INTRODUCTION

Timing information with high precision is required to synchronize devices and equipments in large accelerator facilities. The SINAP timing system, as one of the traditional event timing systems, distributes triggers and clocks with jitter at picoseconds. [1] The delay and width step of the timing signals is in different levels from picoseconds to nanoseconds. [2] The SINAP timing system is successfully applied in Pohang Light Source II [3][4], Shanghai Synchrotron Radiation Facility, Beijing Electron-Positron Collider II, SuperKEKB [5], Chinese Spallation Neutron Source, Brazil Sirius Light Source, Shanghai Advanced Proton Therapy Facility [6] and so on.

However, the traditional event timing system can't meet the requirement of new experiment methodology like pump-probe technology in the third generation light sources. Moreover, the synchronization of electron gun, lasers and experiment equipment in the fourth generation light sources, free electron lasers, demands higher accuracy. A level of 10-100 femtoseconds should be achieved for the accuracy of the triggers and clocks.

Laser modules but not electronic ones are mainly utilized to form the new highly stable timing system. One technical route makes use of mode locked laser as the reference base, and detects the variation of the transmission delay by the technique of balanced cross-correlation, and compensates the delay with optical feedback methods. [7] The other technical route makes use of continuous wave laser as the reference base, and detects the variation of the transmission delay by the theory of Michelson interference, and compensates the delay with electronic feedback method. [8]

We designed the system, which is based on the theory of the Michelson interference. The RF signal is modulated in continuous wave laser carrier. The phase drift of laser carrier is detected by sensing the phase of the beat frequency signal, which increases the measuring precision remarkably. The phase drift is compensated by optical approaches. The system aims to stabilize the phase of transmitted RF signal to 0.01°. The traditional event timing system is integrated to transmit event stream in the same fibre, from which the timing triggers benefit to decrease the original jitter.

## SYSTEM DESIGN

The detection and compensation of the phase drift is accomplished at the transmitter side. Therefore, the transmitter is much more complex than the receiver. Such design improves the scalability and reduces the cost for large systems.

The transmitter of the system is divided into the optical part and the electronic part. A collection of available commercial modules is utilized to form the optical part, which is primarily the Michelson interferometer. The core modules are the continuous wave laser, the analog modulator, the acousto-optic frequency shifter and the optical delay modules. The RF signal is modulated in continuous wave laser carrier. The photodiode receives the beat frequency signal by heterodyne interference. An optical delay line and a fibre stretcher compensate the drift along the fibre.

The phase drift caused by ambient temperature change is sensed in the electronic part, and then the optical path variation is calculated and is used to control optical delay modules. A wavelength division multiplexer multiplexes the event stream and modulated RF signal onto one single fibre.

The receiver of the system is less complex. It reflects the optical wave as one arm of the Michelson interferometer, recovers the RF signal and event codes.

The structure of the system is illustrated in Fig. 1.

*liuming@sinap.ac.cn

ISBN 978-3-95450-177-9

# X-RAY SMITH-PURCELL RADIATION FOR NON-INVASIVE SUBMICRON DIAGNOSTICS OF ELECTRON BEAMS HAVING TeV ENERGY*

A.A. Tishchenko†, D.Yu. Sergeeva, National Research Nuclear University MEPhI, Moscow, Russia

*Abstract*

We present the general theory of X-ray Smith-Purcell radiation from ultrarelativistic beams proceeding from our earlier results. The theory covers also the case of oblique incidence of the beam to the target, which leads to the conical effect in spatial distribution of Smith-Purcell radiation and allows one to count the divergence of the beam; also, the analytical description of the incoherent form-factor of the beam is given.

## INTRODUCTION

Non-invasive diagnostics is one of the topical problems for the facilities like DESY, SLAC and the future ones like CLIC, ILC, etc. All modern diagnostics schemes are based on optical radiation which restricts limitation on the beam length and diagnostic resolution due to the diffraction (Rayleigh) limit. We suggest X-ray Smith-Purcell radiation as an instrument operating with smaller wavelengths and hence much more suiting for non-invasive submicron beam diagnostics.

Diffraction radiation (DR) arises when a charged particle moves near a target. The Coulomb field of the particle polarized the target material and the polarization currents arise, which leads to the radiation generation. Smith-Purcell radiation (SPR) is a special case of DR occurring when the target is a periodic structure.

Both these types of radiation are usually called the polarization radiation because the source of the radiation in these schemes is the target material rather than the charged particles itself [1].

As it follows from the definitions given above, when both DR and SPR are generated, there is no direct interaction between the particle and the target. It means that DR and SPR can be a base for noninvasive diagnostics. And, generally speaking, the information obtained can be both about the beam and about the target [2, 3].

We construct the theory of Smith-Purcell radiation at frequencies

$$\omega >> \omega_p, \qquad (1)$$

where $\omega_p$ is the plasma frequency, which usually has values about $20-30\,eV$. In this frequency region the response of dielectric or metal to the external field is similar, because behavior of the conductivity electrons and electrons bounded in atoms coincides in the electromagnetic field acting at frequencies higher than the atomic ones. Consequently, the properties of target material are defined by the function $\varepsilon(\omega)$, which has the form:

$$\varepsilon(\omega) = 1-\omega_p^2/\omega^2 . \qquad (2)$$

DR in the high-frequency limit $\omega >> \omega_p$, was investigated in the papers [4] for non-relativistic particles, and in [5] for gratings, i.e. X-ray SPR. Non-relativistic particles, however, emits DR only for impact-parameters of the order of the wavelength, which is not the case for X-ray domain. The analytics in the paper of M.J. Moran [5], on the other hand, was based on the theoretical description given in [6] by M.L. Ter-Mikhaelyan, who developed the theory an infinitely thin perfectly conducting target. This makes these results inapplicable for frequencies larger than optical ones. After that, the basis of the X-ray DR theory was given in [7] and for X-ray SPR in [8] for single-particle radiation.

## PROPERTIES OF RADIATION

Let us consider the generation of SPR from the beam consisting of $N_e$ electrons. The target is a grating of $N$ elements (slabs, strips, grooves, etc) with the period $d$. The slab sizes in $x$, $y$, $z$ directions are $a$, infinite, half-infinite, correspondingly, see Fig. 1. The beam is supposed to move at a constant distance $h$ from the target surface. The particle velocity is $\mathbf{v} = v(\cos\alpha, \sin\alpha, 0)$.

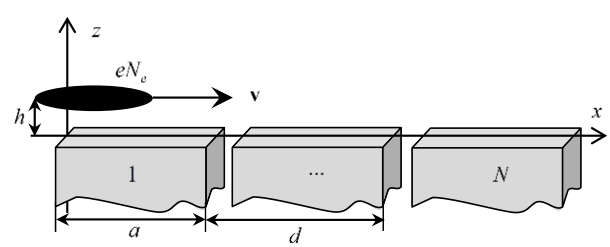


Figure 1: Generation of the Smith-Purcell radiation from a beam of electrons.

The main characteristic of the radiation we will operate with is the spectral-angular distribution of the radiation, which can be written in form

*This work was supported by the Leverhulme Trust International Network, grant IN-2015-012, grant RSF 16-12-10277 and by the Competitiveness Programme of National Research Nuclear University “MEPhI”.
†Tishchenko@mephi.ru



ISBN 978-3-95450-177-9

# BUNCH LENGTH MEASUREMENT BASED ON INTERFEROMETRIC TECHNIQUE BY OBSERVING COHERENT TRANSITION RADIATION

I. Nozawa†, M. Gohdo, K. Kan, T. Kondoh, J. Yang, Y. Yoshida
The Institute of Scientific and Industrial Research, Osaka University, Osaka, Japan

*Abstract*

Generation and diagnosis of ultra-short electron bunches are one of the main topics of accelerator physics and applications in related scientific fields. In this study, ultra-short electron bunches with bunch lengths of femtoseconds and bunch charges of picocoulombs were generated from a laser photocathode RF gun linac and an achromatic arc-type bunch compressor. Observing coherent transition radiation (CTR) emitted from the electron bunches using a Michelson interferometer, the interferograms of CTR were measured experimentally. The bunch lengths were diagnosed by performing a model-based analysis of the interferograms of CTR.

## INTRODUCTION

Generation of ultra-short electron bunches with femtosecond bunch lengths has been progressed with the development of accelerator technologies such as photocathode RF (Radio Frequency) guns, bunch compression techniques and plasma acceleration techniques. The femtosecond electron bunches are essential for physical application in accelerator science such as free-electron lasers[1], laser-Compton scattering x-ray sources[2] and terahertz-light sources based on coherent radiation[3]. In addition to the application mentioned above, it takes an important role in time-resolved measurement like pulse radiolysis in radiation chemistry. The pulse radiolysis is one of the most powerful tools in radiation chemistry to investigate ionizing radiation-induced phenomena. As for this measurement, the ultra-short electron bunch is used as a pump source to ionize the chemical sample, and the kinetics of the radiation-induced phenomena is measured as transient absorption using an ultra-short laser pulse stroboscopically, so the time resolution of the system is mainly determined by the electron bunch lengths. So far, much effort has been paid to improve the time resolution, and the best time resolution of 240 fs was attained using 100-fs electron bunches generated from a laser photocathode RF gun linac and a magnetic bunch compressor at Osaka University in 2011[4].

On the other hand, longitudinal diagnosis of the ultra-short electron bunches is also one of the key topics in accelerator physics and its related fields. The main reason to activate this study is that there is no established bunch length measurement technique for <100-fs electron bunches. Hitherto, many bunch length measurement techniques have been proposed and experimentally demonstrated to diagnose the <100-fs electron bunches. For example, bunch length measurements using coherent radiation (CR)[5,6], electro-optic (EO) crystals[7] and deflecting cavities have been proceeded to diagnose the temporal bunch length of femtosecond electron bunches.

In this study, bunch length measurement based on interferometric technique was demonstrated by monitoring coherent transition radiation (CTR). Details will be described below, but the bunch lengths were estimated by analyzing an autocorrelation of CTR measured using a Michelson interferometer.

## EXPERIMENTAL SETUP

### Photocathode RF Gun Linac

Figure 1 shows the schematic of the linac system at Osaka University. The linac system has three beam lines, and achromatic-arc beam line was used to generate the ultra-short electron bunches. The linac system is mainly composed of three sections: a photocathode RF gun with a copper cathode, an S-band acceleration cavity and an achromatic arc-type magnetic bunch compressor. The photocathode is driven by a 266-nm femtosecond UV pulse of the third harmonic of a Ti:sapphire femtosecond laser with a regenerative amplifier (Tsunami with Spitfire, Spectra Physics). The electron bunch is accelerated at 4 MeV at the exit of the gun and the solenoid mounted at the exit of the gun is used for emittance compensation. The electron bunch is accelerated by the RF electric field inside the 2-m long S-band traveling wave cavity. The beam energy of the electron bunch at the exit of the linac is 35 MeV, and the electron bunch is energy-correlated inside the cavity for bunch compression using the achromatic arc-type magnetic bunch compressor. The bunch compressor is composed of two bending magnets, four quadrupole magnets and two sextupole magnets. The sextupole magnets in the compressor served to compensate for the second-order effect due to the fringing fields of the magnets, which will cause bunch length growth because of the nonlinear transformation of the energy-phase correlation.

### Bunch Length Measurement System

Figure 2 shows the schematic diagram of the bunch length measurement system based on a Michelson interferometer. In this scheme, the CTR was emitted from the electron bunches at a boundary between a vacuum and an aluminium mirror (M1). The mirror (M1), scintillators (ZnS) and an infrared light source (IRS, IRS-001C, IR System) for calibration of the measurement system were mounted on the rotational stage, so the transverse beam shape could be checked during the measurement. The CTR was collimated to parallel light by an off-axis parabolic mirror (OAP1) since it could be considered to be a point source of electromagnetic (EM) waves in infrared region. After that,

†nozawa81@sanken.osaka-u.ac.jp



ISBN 978-3-95450-177-9

# OTR MEASUREMENTS WITH SUB-MeV ELECTRONS*

V. A.Verzilov†, P. E. Dirksen, TRIUMF, Vancouver, Canada

*Abstract*

It is a quite common belief that beam imaging using Optical Transition Radiation (OTR), produced by sub-MeV electron beams, is impossible or at least requires special highly sensitive instrumentations. The TRIUMF electron linac, presently undergoing a commissioning stage, is capable of delivering up to 10 mA of CW electron beams. Simulations showed that such a powerful beam generates substantial amount of OTR light even at electron energies available at the output of the thermionic electron source. The experiment was then setup to test the prediction. This paper reports OTR measurements for the range of electron energies 100 - 300 keV performed with an ordinary CCD camera.

## INTRODUCTION

In spite of the fact that Optical Transition Radiation has become a standard diagnostics tool in beam imaging techniques, grey areas still exist where its application requires additional studies. In particular, OTR imaging of sub-MeV electron beams is often considered impossible or at least unpractical due to low light intensity that quickly goes down with the beam energy. However, OTR techniques still remain attractive even at low energies; since they do not suffer from saturation effects inherent to scintillating materials, OTR targets do not charge up and can typically sustain much higher beam powers. Several studies were dedicated to the subject over the last few decades. Successful observation of beam images from 1 MeV electron beam with a CCD camera was reported in Ref. [1]. A decade later OTR imaging was applied to an 80keV electron beam [2]. This time a weak light dictated the use of an intensified camera. With the help of an intensifier, OTR images were obtained even for 10 keV electrons [3].

Higher beam intensities available with long pulse or CW superconducting accelerators make low energy OTR imaging nearly as routine as at multi-MeV beam energies. At the TRIUMF electron accelerator, an ordinary CCD camera was adequate to observe beams with the energy of 100 - 300 keV ($\beta$ in the range of 0.2 - 0.6).

## GEOMETRY OPTIMIZATION

Planning of low energy OTR measurements requires careful optimization of the experimental geometry in order to maximize the light intensity. It is very well known that for highly relativistic ($\gamma \gg 1$) particles, OTR light from a metallic mirror is highly collimated around a direction which makes an angle with the normal to the mirror surface that is equal and opposite to an angle of the particle incidence, measured with respect to the same normal. When $\gamma \sim 1$ the properties are quite different: the radiation is emitted in a broad range of angles. For the case of an ideally conducting perfect mirror, the OTR energy emitted in the backward direction per unit solid angle and unit frequency interval in the plane formed by the particle momentum and normal to the surface can be found to have a simple form (see Ref. [4] and references therein):

$$W_\omega = \frac{e^2}{\pi^2 c}\beta^2\cos^2\psi\left(\frac{\sin\theta-\beta\ \sin\psi}{(1-\beta\cos(\theta+\psi))(1+\beta\cos(\theta-\psi))}\right)^2 \quad (1)$$

In this equation $\psi$ is the angle between the beam and the surface normal and $\theta$ is angle between the normal and radiation direction. If, as it is typically the case, radiation is observed at right angle to the beam, then $\theta = \pi/2 - \psi$ and Eq. (1) is reduced to

$$W_\omega{}^{90^\circ}(\psi) = \frac{e^2}{4\pi^2 c}\beta^2\left(1+\frac{\cos 2\psi}{1-\beta\sin 2\psi}\right)^2 \quad (2)$$

In Figure 1 the quantity $W_\omega{}^{90}$ is plotted as function of the angle $\psi$ for two beam energies of 100 keV and 300 keV.

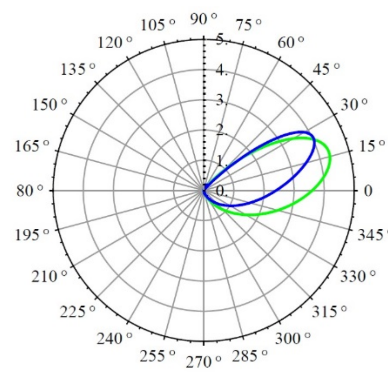


Figure 1: OTR intensity emitted at 90° to the beam direction as function of the angle $\psi$ for beam energies 100 keV (green) and 300 keV (blue). Data plotted by the green line were multiplied by a factor of 3.

From Eq. (2) one can find that the radiation intensity reaches its maximum value

$$W_\omega{}^{90^\circ}(\psi_{max}) = \frac{e^2}{4\pi^2 c}\beta^2(1+\gamma)^2 \quad (3)$$

for an angle $\psi_{max}$ entirely determined by the velocity of beam particles:

$$\psi_{max} = \frac{1}{2}\arcsin\beta \quad (4)$$

From Eq. (4) it follows that $\psi_{max} \to \pi/4$ when $\beta \to 1$ as one would naturally expect for a highly relativistic beam. However, for the energies of interest the intensity is rather low for $\psi = \pi/4$. Instead, Eq. (4) tells us that, optimally,

*Finding is received from National Research Council of Canada
†verzilov@triumf.ca

ISBN 978-3-95450-177-9

# HIGH-ENERGY X-RAY PINHOLE CAMERA FOR HIGH-RESOLUTION ELECTRON BEAM SIZE MEASUREMENTS*

B. Yang, S.H. Lee, J. Morgan and H. Shang,
Advanced Photon Source, Argonne National Laboratory, Argonne, IL 60439 USA

*Abstract*

The Advanced Photon Source (APS) is developing a multi-bend achromat (MBA) lattice based storage ring as the next major upgrade, featuring a 50 – 80-fold reduction in emittance. Combining the reduction of beta functions, the electron beam sizes at bend magnet sources may be reduced to reach 5 – 10 µm for 10% vertical coupling. The x-ray pinhole camera currently used for beam size monitoring will not be adequate for the new task. By increasing the operating photon energy to 120 – 200 keV, the pinhole camera's resolution is expected to reach below 4 µm. The peak height of the pinhole image will be used to monitor relative changes of the beam sizes and enable the feedback control of the emittance. We present the simulation and the design of a beam size monitor for the APS storage ring.

## INTRODUCTION

A new generation of storage-ring based synchrotron radiation sources using multi-bend achromat (MBA) lattices are being planned, designed, constructed, and commissioned worldwide [1,2]. These rings are expected to operate with total emittance two-orders of magnitude lower than many of the third-generation synchrotron radiation sources. Table 1 lists the expected beam sizes at the bend magnet sources after the APS Upgrade (APS-U) at 66 pm total emittance. Due to small beta functions inherent to the MBA lattices, the electron beam sizes in these rings are in the micrometre range, with the potential of reaching sub-micrometre level for vertical couplings under 1%. Robust and accurate diagnostics for these minute beam sizes are important for the operations of these new sources.

In this work, we will discuss the plans and design of the beam size monitor (BSM) for the APS-U MBA storage ring. We will cover the simulated performance of the high-energy x-ray pinhole camera, conceptual design, and alternative techniques to be implemented in parallel.

Table 1: Expected e-beam Sizes for APS-U Storage Ring

| Plane | Horizontal | | Vertical | |
|---|---|---|---|---|
| Beta function | 1.8 m | | 3.9 m | |
| Vertical coupling | Full | 10% | Full | 10% |
| Beam size (µm) | 7.8 | 10.4 | 11.3 | 5.0 |

## COMPUTER SIMULATION

Pinhole images can be modelled using the well-known Fresnel diffraction algorithm. At wavelength $\lambda$, the photon intensity at the image plane can be expressed as, $I_0(x') = |A(x')|^2$ where the photon wave amplitude is

$$A(x') = \frac{A_0'}{1+i}\left\{F\left[\sqrt{\frac{2}{\lambda f}}\left(f\varphi + \frac{d}{2}\right)\right] - F\left[\sqrt{\frac{2}{\lambda f}}\left(f\varphi - \frac{d}{2}\right)\right]\right\}. \quad (1)$$

The length parameter $f$ is given by $1/f = 1/S + 1/S'$, where $S$ is the distance from the source to the pinhole, $S'$ is the distance from the pinhole to the image plane. Furthermore, $\varphi = x'/S'$, $d$ is the total width of the pinhole slit, $A_0'$ is an amplitude constant, and the complex Fresnel integral is defined as

$$F(x) = C(x) + iS(x) = \int_0^x e^{i\pi t^2/2} dt \cdot \quad (2)$$

If we map the image coordinates $x'$ back to the source plane coordinates $x$ using the optical magnification of the beamline, $x = x'/M = x'S/S'$, the intensity at the mapped source can be obtained simply by using $\varphi = x/S$ and a different amplitude constant in Eq. (1). Finally, for finite source sizes, the calculated intensity distribution needs to be convolved with the source distribution. The program *sddsfresnel* implements these algorithms and can be used to calculate the one-dimensional Fresnel profile for a given geometry and a source profile.

For the planned APS bend magnet beamline with $S$ = 8.5 m, $S'$ = 11.5 m, numerical calculation shows that the resolution of the pinhole camera is near optimal for slits width of 10 µm for photon energy of 120 keV. Figure 1 shows the normalized diffraction profiles from such a pinhole with source sizes ranging from 0 to 20 µm. We can see that the profiles can be clearly resolved down to 5 µm, but not below 3 µm. Since photons with energy of 100 – 500 keV are often referred to as soft gamma rays, this work is really about soft gamma ray pinhole camera techniques.

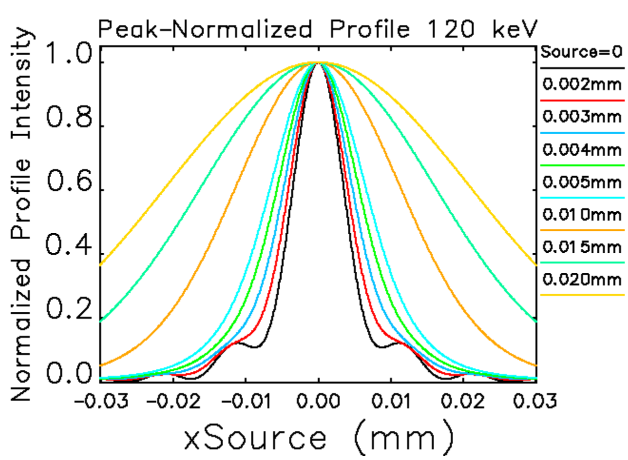


Figure 1: Fresnel diffraction profile using monochromatic 120 keV photons for zero source size; and convolution with Gaussian source with rms width of 2 – 20 µm. All profiles are normalized at the peak for easy comparison.

* Work supported by U.S. Department of Energy, Office of Science, under Contract No. DE-AC02-06CH11357.



ISBN 978-3-95450-177-9

# RECENT RESULTS FROM NEW STATION FOR OPTICAL OBSERVATION OF ELECTRON BEAM PARAMETERS AT KCSR STORAGE RING

O. Meshkov[†,1], V. Borin, V. Dorokhov, A. Khilchenko, A. Kotelnikov, A. Kvashnin, L. Schegolev, A. N. Zhuravlev, E. I. Zinin, P. V. Zubarev, BINP SB RAS, Novosibirsk, 630090, Russia
V. Korchuganov, G. Kovachev, D. G. Odintsov, A. Stirin, Yu. Tarasov, A. Valentinov, A. Zabelin, NRC Kurchatov Institute, Moscow, 123182, Russia
[1]also at NSU, Novosibirsk, 630090, Russia

*Abstract*

The new station for optical observation of electron beam parameters at electron storage ring SIBERIA-2 is dedicated for measurement of transverse and longitudinal sizes of electron bunches with the use of synchrotron radiation (SR) visible spectrum in one-bunch and multi-bunch modes and for the study of individual electron bunches behavior in time in the conditions of changing accelerator parameters. The paper briefly describes the main components of the diagnostics and experimental results obtained with them.

## OPTICAL OBSERVATION STATION

### *SR Beam Line*

Fig. 1 represents the model of SR beam line and optical table. The beam line has two collimators forming round shape of a SR beam and supressing a stray light.

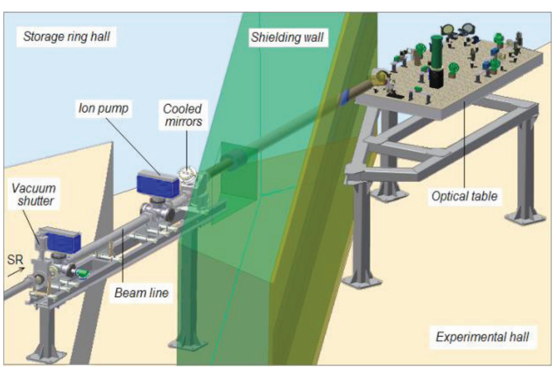


Figure 1: Model of SR beam line with the diagnostics devices placed on the optical table.

First collimator (cooled) is installed at SR beam line entrance. The second collimator (non-cooled) is installed after the quartz vacuum window. The inlet part of vacuum SR beam line (is not shown in Fig. 1) comprises SR absorber and ion pump. The optical part of SR spectrum is separated from the SR fan with two mirrors. The first optically polished cooled copper mirror is installed inside the vacuum unit at the distance about 6 m from source point. The mirror is coated with gold. The second Al – coated mirror reflecting the optical radiation is manufactured from the glass.

[†]O.I.Meshkov@inp.nsk.su

Both mirrors can be mechanically adjusted for precise alignment of the light beam. Lead beam stopper is installed inside the part of beam line passing through the shielding wall for to absorb scattered X-rays. The complete length of the beam line from source point to the main lens of diagnostics placed at the optical table is about 10 m. The computed values of synchrotron radiation from bending magnet at $\lambda$ = 500 nm are presented in Table 1.

Table 1: Computed Parameters of Synchrotron Radiation from Bending Magnet at $\lambda$ = 500 nm

| | |
|---|---|
| Divergence, $\sigma_{SR} = (3\lambda/4\pi R)^{1/}$ | $1.8\cdot10^{-3}$ rad |
| Diffraction limit, $\sigma_D \approx (\lambda^2 R/12\pi^2)^{1/3}$ | ≈0.011 мм |
| Minimal radial size, $\sigma_R \approx R(\sigma_{SR})^2/2$ | ≈0.03 мм |

### *Layout of the Optical Diagnostics*

The measurement part of the optical diagnostics [1] consists of six independent devices with different functions located on the optical table outside the storage ring shielding wall. We use the STANDA optical table.

**Transverse beam sizes precise measurement system** is based on the double-slit interferometer serves to measure bunch vertical size with a resolution about several µm.

**Bunch longitudinal sizes measurement system** is based on the optical dissector tube with electrical focusing and deflection is also used for the diagnostics of longitudinal multi-bunch instability caused by electron bunches interaction with high modes of cavity electromagnetic field. The marker is used for determining and controlling the temporal scale of the dissector. Dissector tube temporal resolution is 40 ps FWHM [2]. The light reflects to dissector from the Edmund Optics 6’’ pellicle beamsplitter

**TV camera** is used for observation of the electron beam cross-section image on the video monitor in main control room.

**The CCD camera** is based on high resolution Allied Vision Technology 1280×960 pixels EG1290 CCD camera with a 100 Mbit Ethernet interface. The result of computer processing of signal from CCD-matrix is a visual two-dimension image of electron beam cross-section, x - and y - curves of electron density distribution within beam, FWHM of Gaussian curve on both coordinates and position of center of electron beam [4].



ISBN 978-3-95450-177-9

# STUDY OF THE RADIATION DAMAGE ON A SCINTILLATING FIBERS BASED BEAM PROFILE MONITOR

E. Rojatti*, G. Calvi, L. Lanzavecchia, A. Parravicini, C. Viviani, CNAO, Pavia, Italy

*Abstract*

The Scintillating Fibers Harp (SFH) monitors are the beam profile detectors used in the High Energy Beam Transfer (HEBT) lines of the CNAO (Centro Nazionale Adroterapia Oncologica, Italy) machine. The use of scintillating fibers coupled with a high-resolution CCD camera makes the detector of simple architecture and with high performances; on the other hand, fibers radiation damage shall be faced after some years of operation. The damage appears in multiple ways, as efficiency loss in light production, delayed light emission, attenuation length reduction. The work presents measurements and analysis performed to understand the phenomenon, in such a way to deal with it as best as possible. The connection between dose rate, integral dose and damage level is investigated as well as the possible recovery after a period of no irradiation. The influence of the damage effects on profiles reconstruction and beam parameters calculation is studied. Data elaboration is modified in such a way to compensate radiation damage effects and protract the SFH lifetime, before the major intervention of fibers replacement. Methods and results are discussed.

## THE SCINTILLATING FIBERS HARP MONITORS

The Scintillating Fibers Harp (SFH) monitors [1] are beam profile detectors installed along the High Energy Beam Transfer (HEBT) lines of the CNAO (Centro Nazionale di Adroterapia Oncologica) accelerator. Their active area is made up of two orthogonal harps of scintillating fibers (for the horizontal and the vertical beam profiles reconstruction) which are guided up to the chip of a CCD camera and mapped for the signal read out. The CCD output signal per fiber (12 bits digital signal) is proportional to the number of particles crossing the fiber, to their energy and depends on the camera configuration parameters. A different correction factor (called "calibration factor") is applied to each fiber at profiles reconstruction in order to equalize the different fibers response, which can vary due to fibers geometry, composition and coupling with camera chip.
The CNAO beam extraction takes 1 to 10 seconds, and thus several beam profile acquisitions, with a good compromise between acquisition rate[1] and integration time, are needed to monitor the beam longitudinal profile during the extraction time and to correctly measure beam parameters (barycenter and width). Fig.1 shows the 3D reconstruction, on the horizontal plane, of one extracted spill.

* elisa.rojatti@cnao.it

[1] The maximum camera acquisition rate is 50 Hz.

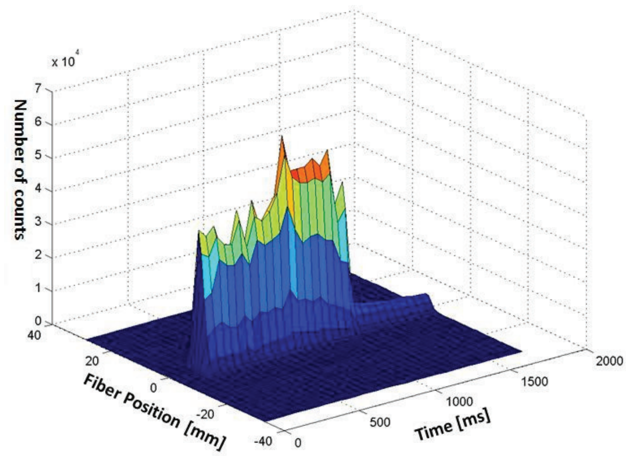


Figure 1: Example of one extracted spill longitudinal profile, reconstructed on the horizontal plane from one SFH measurement.

## RADIATION DAMAGE ON SCINTILLATING FIBERS

Several studies concerning the radiation damage on scintillating fibers have been published [2]. The topic is very complex and far from being fully understood. In case of the SFH detectors, the radiation damage appears both as reduction of light production and as reduction of fibers transparency, mainly involving the central region of the SFH sensitive area which is mostly hit by the beam. The first effect emerges clearly taking one image of the beam profile after having enlarged the beam on purpose (Fig.2): the enlarged-beam profile shows a depression indicating a reduced light production efficiency for the most irradiated fibers.

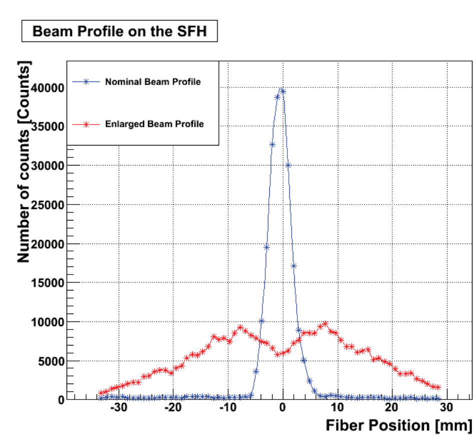


Figure 2: Nominal (blue line) and enlarged (red line) beam profiles on one SFH.



ISBN 978-3-95450-177-9

# TEST OF THE IMAGING PROPERTIES OF INORGANIC SCINTILLATION SCREENS USING FAST AND SLOW EXTRACTED ION BEAMS*

A. Lieberwirth[1,2,3], W. Ensinger[2], P. Forck[1,3,#], O. Kester [1,3], S. Lederer[1,2], T. Sieber[1], B. Walasek-Höhne[1], GSI Helmholtz-Zentrum für Schwerionenforschung, Darmstadt, Germany
also at [2] Technical University Darmstadt, Institute for Material Science, Germany
also at [3] University Frankfurt, Institute of Applied Physics, Germany

*Abstract*

Inorganic scintillation screens (phosphor P43 and P46, single crystal YAG:Ce, ceramic Alumina and Chromium-doped Alumina), as used for transverse profile determination, were investigated concerning light output, profile reproduction and spectral emission. The screens were irradiated with ion pulses extracted from the synchrotron SIS18 at 300 MeV/u and intensities from about $10^6$ to $10^{10}$ particles per pulse using either 1 µs fast extraction or ≈ 300 ms slow extraction. The light output coincides for both extraction modes. For all materials the optical emission spectrum is independent on the ion species and beam intensities. Radiation hardness tests were performed with up to $10^{12}$ accumulated Nickel: The phosphor P46 and single crystal YAG:Ce show no significant decrease of light output, while for P43 and Chromox a decrease by 5 to 15 % was measured.

## OVERVIEW OF INVESTIGATIONS

Intersecting scintillation screens determine two dimensional beam images and are frequently used for transverse profile measurements in beam transfer lines [1]. The following properties have been investigated:

- emission characteristics for different ion species (p, N, Ni, Xe, U) with a kinetic energy of 300 MeV/u
- dynamic range and linearity between the incident particle intensities and the light output within a range of $10^6$ to $10^{10}$ particles per pulse (ppp)
- spectral emission for various ions and intensities
- radiation hardness i.e. possible variation of the emission characteristics as a function of fluence.

As scintillators we investigated phosphor screens P43 and P46 consisting of crystalline powder with a typical gain size of 10 µm, two different single crystal YAG:Ce and ceramics disks made of pure Alumina A999 (99.99 % purity) and Chromium-doped Alumina (Cr with 0.04 % weight), the properties are compiled in Table 1. All screens were irradiated in air.

The ion beams were extracted from the synchrotron SIS18 at GSI with intensities varying from $6{\cdot}10^6$ ppp up to $2{\cdot}10^{10}$ ppp. The pulse duration was 300–400 ms for slow and 1 µs for fast, single turn extraction at a general requested kinetic energy of 300 MeV/u. One standard deviation of the beam profile was typically σ ≈ 3 mm.

A resonant transformer was used to measure the current of the fast extracted beam with an accuracy of 15% [2]. For intensity measurements in slow extraction mode a detector was used, that consists of an Ionization Chamber (6.5 mm 80 % Ar +20 % $CO_2$ gas mixture, separated by two 100 µm stainless steel walls from the vacuum, measurement accuracy: 15%) and a SEM (three 100 µm Al plates, measurement accuracy: 15%) [3]. Additionally, the beam passed a 50 µm thick stainless steel foil to air 72 cm before the target ladder. Thus the beam was stripped and the kinetic energies at the target surface were calculated numerically by the code LISE [4] as summarized in Table 2.

Table 1: Investigated Scintillation Screens, ∅ 5 to 8 cm

| Name | Material | Thick. | Supplier |
|---|---|---|---|
| #1 P43 | $Gd_2O_2S$:Tb | 50 µm | ProxiVision |
| #2 P46 | $Y_3Al_5O_{12}$:Ce | 50 µm | ProxiVision |
| #3 P46 | $Y_3Al_5O_{12}$:Ce | 20 µm | Crytur |
| #4 YAG:Ce | $Y_3Al_5O_{12}$:Ce | 250 µm | Crytur |
| #5 YAG:Ce | $Y_3Al_5O_{12}$:Ce | 1 mm | SaintGobian |
| #6 Alumina | $Al_2O_3$ | 800 µm | BCE |
| #7 Chromox | $Al_2O_3$:Cr | 800 µm | BCE |

Table 2: The Beam Kinetic Energy $E$ in Front of the Target

| Projectile | Slow extr. $E$ [MeV/u] | Fast extr. $E$ [MeV/u] |
|---|---|---|
| Proton $^{1}_{1}H$ | 299.2 | 299.8 |
| Nitrogen $^{14}_{7}N$ | 297 | 299 |
| Nickel $^{58}_{28}Ni$ | 298 | 297 |
| Xenon $^{124}_{54}Xe$ | 281 | 295 |
| Uranium $^{238}_{92}U$ | 272 | 292 |

## OPTICAL SETUP AND ANALYSIS

The scintillation screens on the target ladder were mounted with 45° orientation with respect to the beam plane with an optical setup mounted perpendicular to the target surface as shown in Fig. 1. It consists of two types of cameras (blue in Fig. 1):

Camera #1: AVT Marlin or Stingray, 1/2" CCD chip, 8 bit resolution, monochrome, mounted with a distance of 50 cm with respect to the targets slightly below the optic axis and recorded the two dimensional response of the scintillation screen. The camera was equipped with a Pentax C1614ER lens of 16 mm focal length and remote-

* Funded by German Ministry of Science BMBF under contract number 05P12RDRBJ and Frankfurt Institute of Advanced Science FIAS
# corresponding author: p.forck@gsi.de



ISBN 978-3-95450-177-9

# IONIZATION PROFILE MONITOR SIMULATIONS - STATUS AND FUTURE PLANS

M. Sapinski*, P. Forck, T. Giacomini, R. Singh, S. Udrea, D. M. Vilsmeier, GSI, Darmstadt, Germany
B. Dehning, J. Storey, CERN, Geneva, Switzerland
F. Belloni, J. Marroncle, CEA/IRFU, Gif-sur-Yvette, France
C. Thomas, ESS, Lund, Sweden
R. M. Thurman-Keup, FNAL, Illinois, U.S.A.
K. Satou, J-PARC, Tokai, Japan
C. C. Wilcox, R. E. Williamson, STFC/RAL/ISIS, Oxford, United Kingdom

*Abstract*

Nonuniformities of the extraction fields, the velocity distribution of electrons from ionization processes and strong bunch fields are just a few of the effects affecting Ionization Profile Monitor measurements and operation. Careful analysis of these phenomena require specialized simulation programs. A handful of such codes have been written independently by various researchers over the recent years, showing an important demand for this type of study. In this paper we describe the available codes and discuss various approaches to Ionization Profile Monitor simulations. We propose benchmark conditions to compare these codes among each other and we collect data from various devices to benchmark codes against the measurements. Finally we present a community effort with a goal to discuss the codes, exchange simulation results and to develop and maintain a new, common codebase.

## INTRODUCTION

The Ionization Profile Monitors were first buildt in the 1960s as simple devices to measure transverse profiles of particle beams without affecting them. The basic idea of the device is that the distribution of electrons or ions from the rest gas ionization mirrors the original beam distribution, however the effects of guiding field nonuniformities, beam space charge or initial velocities due to the ionization process can affect the measurement. A number of numerical simulations have been written dealing with those aspects. Because of their specificity - for instance tracking of low energy electrons or ions, beam charge distributions - the established codes, like Geant4 [1] or CST Studio [2], are usually not applicable to IPM simulations.

In this paper first we present the most important stages of an IPM simulation. These logical stages can be used to modularize the simulation code. In the second part we present simulation codes known to us. These codes were discussed during the Ionization Profile Monitor simulation kickoff workshop [3]. They show a variety of approaches to IPM simulations. Finally we discuss the collaborative tools prepared in order to compare various codes, benchmark them against measurements and share the results. More information can be found on the collaboration's TWiki pages [4].

It should be stressed that other beam devices, for instance Beam Fluorescence Monitors or even electron lenses, can be simulated using similar techniques.

## SIMULATION COMPONENTS

The simulation can be divided into the following stages, which cover various physics phenomena and can be used to modularize the simulation code:

- **Ionization** - The purpose of this component is to generate the initial momenta of the particles to be tracked. The most promising approach is to use - if available - a realistic double differential cross section (DDCS) for obtaining the energies and scattering angles of ionization products. The ionization process depends on the beam particle type, beam energy and the residual gas species, therefore an appropriate cross section model for each beam configuration can be chosen.

- **Guiding fields** - The purpose of this component is to provide the externally applied electric and magnetic fields in the volume where the particles must be tracked. Usually either uniform fields are used or a field map is imported from an EM-solver. In most applications the field nonuniformities are just sources of errors, but in some cases fields are deeply nonuniform and their precise knowledge is fundamental in order to reconstruct the real beam profile.

- **Beam fields** - This module provides the electromagnetic fields generated by the beam. For highly relativistic beams the electric field is mainly transverse to the beam and its longitudinal component can be neglected. In such case a '2D' approach in which the longitudinal shape of the beam is modelled by a simple shifting of the bunch charge distribution with time is often used. Other approaches include solving Poisson's equation analytically or using EM solvers. This allows for the creation of a three-dimensional field map. The magnetic field of the beam is usually neglected because its impact on slowly-moving ionization products is much smaller than the electric field.

* m.sapinski@gsi.de

# CALIBRATION OF X-RAY MONITOR DURING THE PHASE I OF SuperKEKB COMMISSIONING

Emy Mulyani*, SOKENDAI, 1-1 Oho Tsukuba Ibaraki 305-0801, Japan
J.W Flanagan[1], KEK, 1-1 Oho Tsukuba Ibaraki 305-0801, Japan
[1] also at SOKENDAI, 1-1 Oho Tsukuba Ibaraki 305-0801, Japan

*Abstract*

X-ray monitors (XRM) have been installed in each SuperKEKB ring, the Low Energy Ring (LER) and High Energy Ring (HER), primarily for vertical beam size measurement. Both rings have been commissioned in Phase I of SuperKEKB operation (February-June 2016), and several XRM calibration studies have been carried out. The geometrical scale factors seems to be well understood for both LER and HER. The emittance knob ratio method yielded results consistent with expectations based on the machine model optics (vertical emittance $\epsilon_y$ is ≈8 pm) for the LER. For the HER, the vertical emittance $\epsilon_y$ is ≈41 pm, which is 4× greater than the optics model expectation. Analysis of beam size and lifetime measurements suggests unexpectedly large point response functions, particularly in the HER.

## INTRODUCTION

The SuperKEKB accelerator is designed to collide $e^-e^+$ at a design luminosity of $8 \times 10^{35}$ cm$^{-2}$ s$^{-1}$(40× larger than that of KEKB)[1]. Measuring and controlling parameters of the accelerator beams is essential to achieve maximum performance from the accelerator; e.g., it is necessary to keep the single-beam vertical size small in order to obtain high luminosity. The XRMs have been installed in both SuperKEKB rings for vertical beam size measurement. Several XRM calibration studies have been carried out during the Phase I of SuperKEKB commissioning.

## XRM APPARATUS

Two XRMs have been installed at SuperKEKB: one for electrons (HER) and one for positrons (LER). Each apparatus consists of three primary components: beamline, optical elements and detection system.

### Beamline

Table 1: Beamline Parameters

| Parameter | LER | HER | Unit |
|---|---|---|---|
| Energy | 4 | 7 | GeV |
| Source to optics (L) | 9.259 | 10.261 | m |
| Optics to detector (L′) | 31.789 | 32.689 | m |
| Air gap (f) | 10 | 10 | cm |
| Thickness of Be filter (T) | 0.5 | 16 | mm |
| Thickness of Be window (T′) | 0.2 | 0.2 | mm |

Each of the SuperKEKB rings has four straight sections and four arc-bends. The X-ray sources are the last arc-bends located immediately upstream of the straight sections in Fuji (LER) and Oho (HER). The beamlines are about 40 m long from the source points to the detectors. A list of the parameters for the beamlines are shown in Table 1. The optical elements (pinhole and coded apertures) are located in optics boxes ≈9–10 m from the source points, for geometrical magnification factors of ≈3× for both lines. Beryllium filters are placed between source points and optic boxes to reduce the incident power levels for both lines. A 0.2 mm thick Be window is also placed at the end of each beamline to separate vacuum (beamline) and air (detector box).

### Optical Elements

Three optical elements have been designed and installed in each ring: a single slit, a multi-slit coded aperture (17 slits) and a Uniformly Redundant Array (URA) coded aperture (12 slits) as shown in Fig. 1 [2]. These optical elements consist of 18–20 μm thick gold masking material on 600 μm thick diamond substrates.

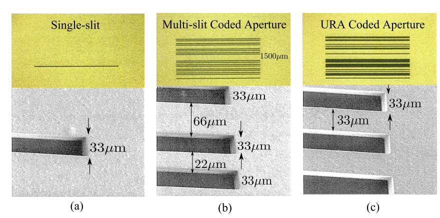


Figure 1: Three types of optical elements at 70× magnification and 1000× Scanning Electron Microscope (SEM): (a)Single-slit, (b) Multi-slit coded aperture and (c) URA coded aperture.

### Detection System

For phase I of SuperKEKB commissioning, a cerium-doped yttrium-aluminum-garnet (YAG:Ce) scintillator is combined with a CCD camera for the x-ray imaging system as shown in Fig. 2. The resolution of this optical systems will be discussed in systematic resolution section.

## GEOMETRICAL SCALE FACTORS

The geometrical scale factors based on beam-based measurement (see Fig. 3) are measured by moving either the beam or optical elements (single slit and coded apertures), observing how the peak features move, then calculating the ratio of geometric magnification $M$ and scintillator camera

* mulyani@post.kek.jp



ISBN 978-3-95450-177-9

# PREPARATORY WORK FOR A FLUORESCENCE BASED PROFILE MONITOR FOR AN ELECTRON LENS

S. Udrea†, P. Forck, GSI Helmholtzzentrum für Schwerionenforschung, Darmstadt, Germany
E. Barrios Diaz, O. R. Jones, P. Magagnin, G. Schneider, R. Veness, CERN, Geneva, Switzerland
V. Tzoganis, C. Welsch, H. Zhang, Cockcroft Institute, Warrington, United Kingdom

*Abstract*

A hollow electron lens system is presently under development as part of the collimation upgrade for the high luminosity upgrade of LHC. Moreover, at GSI an electron lens system also is proposed for space charge compensation in the SIS-18 synchrotron to decrease the tune spread and allow for the high intensities at the future FAIR facility. For effective operation, a very precise alignment is necessary between the ion beam and the low energy electron beam. For the e-lens at CERN a beam diagnostics setup based on an intersecting gas sheet and the observation of beam induced fluorescence (BIF) is under development within a collaboration between CERN, Cockcroft Institute and GSI. In this paper we give an account of recent preparatory work with the aim to find the optimum way of distinguishing between the signals due to the low energy electron beam and the relativistic proton beam.

## BIF SETUP FOR TRANSVERSE DIAGNOSTICS

Electron lenses (e-lens) [1] have been proposed and used to mitigate several issues related to beam dynamics in high current synchrotrons. The e-lens system at CERN will be comparable to those used at FNAL and BNL. The main difference will be the use of a hollow electron beam.

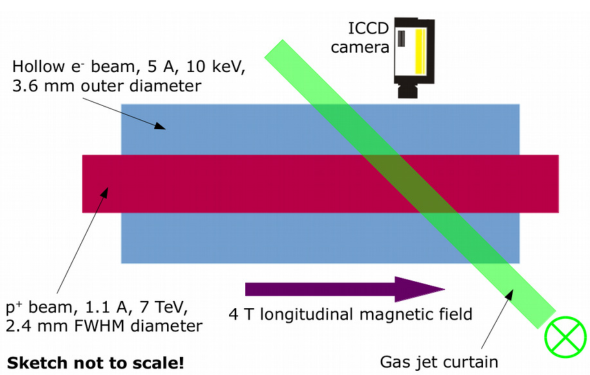


Figure 1: A schematic of the e-lens system planned at CERN for the collimation of the HL-LHC proton beam and the associated transverse beam diagnostics.

The parameters of the CERN e-lens are summarized in Fig. 1: the up to 1.1 A, 7 TeV, 2.4 mm FWHM diameter proton beam of the HL-LHC will be embedded in an up to 5 A, 10 keV hollow electron beam with an outer diameter of about 3.6 mm and an inner one of 2.4 mm. The interaction between the two beams takes place within an approximately 4 T longitudinal magnetic field, which stabilizes the electron beam. The proposed beam induced fluorescence (BIF) setup is composed of a perpendicular supersonic gas jet curtain [2] inclined such as to allow for the observation of the fluorescence radiation resulting from the interaction of the electron and proton beams with the gas molecules. To obtain an image of the transverse profiles of the beams a camera system with suitable optics is intended, which consists of an image intensifier made of micro channel plates (MCP) in chevron configuration and a CCD camera with appropriate optics.

## RELEVANT FLUORESCENCE PROCESSES

From detection perspective the most appropriate gas to be employed in the supersonic gas jet curtain is nitrogen [3]. The main reasons are its high fluorescence efficiency and, based on present knowledge, it may allow distinguishing between the electron and the proton beam.

At wavelengths in the range 300–700 nm most of the fluorescence of $N_2$ molecules and $N_2^+$ molecular ions excited and ionized by protons or electrons results from two processes:

$$N_2 + p/e^- \rightarrow (N_2^+)^* + e^- + p/e^- \rightarrow N_2^+ + \gamma + e^- + p/e^- \quad (1)$$

$$N_2 + e^- \rightarrow (N_2)^* + e^- \rightarrow N_2 + \gamma + e^- \quad (2)$$

The first one is based on the electronic transition $B^2\Sigma_u^+ \rightarrow X^2\Sigma_g^+$ of the molecular ion with wavelengths around 391 nm (depending upon involved vibrational and rotational states) while the second process drives the electronic transition $C^3\Pi_u \rightarrow B^3\Pi_g$ of the neutral molecule with wavelengths around 337 nm. Moreover, the second process cannot be initiated directly by protons because it implies a spin flip mechanism. Thus one expects different photon intensities in the two spectral regions within the areas excited by the proton and ion beams, respectively.

## CROSS–SECTIONS AND INTEGRATION TIMES

### *Proton Excitation*

Data for fluorescence from $N_2$ at relativistic proton energies is provided in [4]. There it is shown that the change of the emission cross-sections with energy closely follows the proton's energy loss as described by a Bethe-Bloch-like expression. From this data one can extrapolate the cross-section at 7 TeV proton energy by the following expression:

$$\sigma_p = A_1 \cdot [(1+e^{-x}) \cdot (x + B_1) - 1] \quad (3)$$

with $A_1 = 1.789 \cdot 10^{-21}$ cm², $B_1 = 10.3$, $x = 2 \cdot \ln(p \cdot c/E_0)$, $E_0 = 0.938$ GeV – rest energy of the proton – and p·c the proton's momentum. At LHC maximum energy $p \cdot c \approx 7$ TeV resulting in $\sigma_p \approx 3.4 \cdot 10^{-20}$ cm², with a 70 % correction made for the main transition of the $N_2$ ion.

† email address s.udrea@gsi.de

ISBN 978-3-95450-177-9

# SPOT SIZE MEASUREMENTS IN THE ELI-NP COMPTON GAMMA SOURCE

F. Cioeta†, E. Chiadroni, A. Cianchi, G. Di Pirro, G. Franzini, L.Palumbo, V.Shpakov, A. Stella, A.Variola, LNF-INFN, Frascati, Italy,
M. Marongiu, A. Mostacci, Sapienza University, Rome, Italy

*Abstract*

A high brightness electron Linac is being built in the Compton Gamma Source at the ELI Nuclear Physics facility in Romania. To achieve the design luminosity, a train of 32 bunches with a nominal charge of 250 pC and 16 ns spacing , will collide with the laser beam in the interaction point. Electron beam spot size is measured with an OTR (optical transition radiation) profile monitors. In order to measure the beam properties, the optical radiation detecting system must have the necessary accuracy and resolution. This paper deals with the studies of different optic configurations to achieve the magnification, resolution and accuracy desired considering design and technological constraints; we will compare several configurations of the optical detection line to justify the one chosen for the implementation in the Linac.

## INTRODUCTION

The goal of this paper is the characterization of different lenses in terms of resolution and magnification for the optical diagnostics for the ELI-NP-GBS LINAC.

The optical diagnostics systems in ELI-NP-GBS will provide an interceptive method to measure beam spot size and beam position in different positions along the LINAC. In a typical monitor setup, the beam is imaged via OTR using standard lens optics, and the recorded intensity profile is a measure of the particle beam spot [1]. In conjunction with other accelerator components, it will also possible to perform various measurements on the beam, namely: its energy and energy spread (with a dipole or corrector magnet), bunch length (with a RF deflector) and the Twiss parameters (with quadrupoles).

The expected beam rms size along the Linac, provided by preliminary beam dynamics simulation, will vary in the 30µm - 1000µm range (as reported in Fig.1).

An evaluation has been done in order to find the best lenses setups and to find a compromise between resolution, magnification and costs for each position.

The optical acquisition system is constituted by a camera Basler scout A640-70 gm with a macro lens (see Fig.2). It has been seen, during the experimental tests, the macro lens is most suitable in order to obtain the requirements of high resolution and magnification. A movable slide is used to move the system between 60 cm and 130 cm of distance from target. These values represent the maximum and minimum distance between the camera sensor and the OTR.

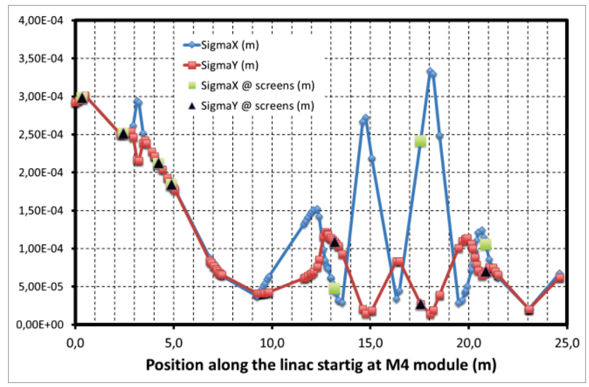


Figure 1: Spot size of the beam in the low energy line after S-band photoinjector.

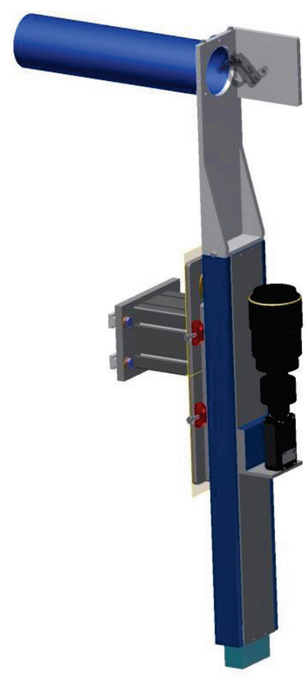

Figure 2: The ELI-GBS optic setup with a camera “Basler Scout A640 70 gm” and a macro lens mounted in a movable slide.

## OPTICS CONFIGURATION

For each ELI-GBS diagnostics station the camera system can be regulated at a distance between 60 and 130 cm from the OTR. The reasons of these values are linked at mechanical and geometric constraints because the beam line is placed at 1.5 meters from the floor (see Fig.3).

† fara.cioeta@lnf.infn.it



ISBN 978-3-95450-177-9

# THERMAL SIMULATIONS FOR OPTICAL TRANSITION RADIATION SCREEN FOR ELI-NP COMPTON GAMMA SOURCE

F. Cioeta†, D. Alesini, A. Falone, V. Lollo, L. Pellegrino, A.Variola
LNF-INFN, Frascati, Italy,
M. Ciambrella, M. Marongiu, A. Mostacci, L. Palumbo, Sapienza University, Rome, Italy
V. Pettinacci, INFN-Roma, Rome, Italy

*Abstract*

The ELI-NP GBS (Extreme Light Infrastructure-Nuclear Physics Gamma Beam Source) is a high brightness electron LINAC that is being built in Romania. The goal for this facility is to provide high luminosity gamma beam through Compton Backscattering. A train of 32 bunches at 100Hz with a nominal charge of 250pC is accelerated up to 740 MeV. Two interaction points with an IR Laser beam produces the gamma beam at different energies. In order to measure the electron beam spot size and the beam properties along the train, the OTR screens must sustain the thermal and mechanical stress due to the energy deposited by the bunches. This paper is an ANSYS study of the issues due to the high quantity of energy transferred to the OTR screen. They will be shown different analysis, steady-state and thermal transient analysis, where the input loads will be the internal heat generation equivalent to the average power, deposited by the ELI-GBS beam in 512 ns, that is the train duration. Each analyses will be followed by the structural analysis to investigate the performance of the OTR material.

## INTRODUCTION

The essential part of the Linac in the ELI-GBS is the beam diagnostics and instrumentation because allows to measure and to observe the spot size of the beam along the machine. In order to measure the beam profile the Aluminum or Silicon Optical Transition Radiation screen are used. The radiation is emitted when a charged particle beam crosses the boundary condition between two media with different optical properties and different dielectric constant. This radiation hits the screen for several cycles during the experiments; thus we want to study, with the finite element analysis (Ansys Code), the OTR material behaviour under thermal stress for 512 ns, train duration. After the thermal analysis the scope is to study the performance of the material through structural analysis in order to investigate the deformation and the equivalent stress for each pulse (of 32 bunches).

It will be demonstrate that the analysis is in agreement with the theoretical study where was evaluated the conduction cooling after the heating of a ELI-GBS beam train. In fact the screen cannot completely cool down in the time between two subsequent pulses; therefore, for each bunch there is an increase of temperature of 0.3° C for Al and 0.4° C for Si. As shown in Fig. 1, it can be seen that after 10 ms from the first pulse, the temperature is 295. 3K for the aluminum and 295. 4K for the silicon. However after few cycles, an equilibrium is reached and the cumulative temperature effect is negligible.[1]

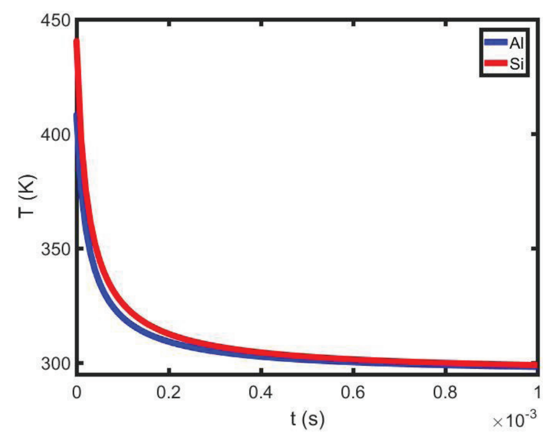


Figure 1: Temporal evolution of the conduction cooling after the heating of a ELI-GBS bunch train ($\sigma x$ =47.5 μm, $\sigma y$ =109 μm). The values refer to the center of the impact area of the beam to the target ($x$ = 0, $y$ = 0).

## ANSYS ANALYSIS

The first step in creating geometry is to build a 3D solid model of the item we are analysing and define the material properties. The target has been modelled with 20x20x1 mm Aluminum plate and the worst case of the dimensions of the area hit by the beam are listed in Tab.1.

Table 1: Instantaneous Temperature Increase for an Impulse Train of 32 Bunches with a Charge of 250 pC Each. It Has Also Been Emphasized the Worst Case Scenario for the ELI-GBS

| $\sigma_x$ ($\sigma_y$)[μm] | $\Delta T^+$ Al [K] | $\Delta T^+$ Si [K] |
|---|---|---|
| 298(298) | 6 | 8 |
| 251(252) | 9 | 12 |
| 211(213) | 12 | 16 |
| 184(184) | 17 | 21 |
| **47.5(109)** | **109** | **141** |
| 241(27.4) | 85 | 110 |
| 106(70) | 76 | 99 |

After the 3D model generation, the OTR has been meshed using hexagonal elements, with size decreasing from the border to the centre. This mapping is crucial to finely impose the energy releasing, concentrating elements only in the target volume that the beam hits. This model is suitable to carry out both steady-state and transient thermal analyses. The cooling mechanism considered is the only

† fara.cioeta@lnf.infn.it

ISBN 978-3-95450-177-9

# PERFORMANCE STUDIES OF INDUSTRIAL CCD CAMERAS BASED ON SIGNAL–TO–NOISE AND PHOTON TRANSFER MEASUREMENTS

G. Kube, DESY, Hamburg, Germany

*Abstract*

Area scan sensors are widely used for beam profile measurements in particle beam diagnostics. They provide the full two–dimensional information about the beam distribution, allowing in principle to investigate shot–to–shot profile fluctuations at moderate repetition rates. In order to study the performance and to characterize these cameras, photon transfer is a widely applied popular and valuable testing methodology. In this report, studies based on signal–to–noise and photon transfer measurements are presented for CCD cameras which are in use for beam profile diagnostics at different DESY accelerators.

## INTRODUCTION

Area scan CCD or CMOS sensors are widely used in beam diagnostics because they provide the full two–dimensional information about the transverse particle beam distribution. For this purpose the information about the particle beam charge distribution is converted in an optical intensity distribution which is recorded by the area scan detector. This light distribution can either be generated in an interaction of the particle beam with material, resulting in atomic excitations which are followed by radiative relaxations (e.g. in scintillating screen or beam induced fluorescence monitors [1, 2]). Alternatively, light extracted from the electromagnetic fields accompanying an ultra–relativistic particle beam can be utilized as it is the case e.g. for synchrotron, transition or diffraction radiation based monitors [3].

For high resolution beam profile measurements, care has to be taken that any resolution broadening introduced by the basic underlying physical process and/or the optical system has to be small. In addition, the conversion process from the charged particle distribution in digital numbers in the data acquisition system has to be linear to avoid any misinterpretation of measured beam sizes and shapes. The linearity may be distorted either by the generation of the photon intensity distribution (e.g. by saturation effects in scintillators or microbunching instabilities in high–brightness electron beams [4]), or in the conversion from a photon distribution into a set of digital numbers in the camera.

The objective of the present study is to focus on the last aspect and to characterize the quality of area scan cameras which are in use for beam profile diagnostics. While there is no principal difference in the characterization between CCD and CMOS sensors, in the following only industrial CCD cameras are considered which are in use at different DESY accelerators. The sensor characterization is based on the Photon Transfer (PT) method which is a valuable methodology employed for solid state imager and camera system investigations. In the next section the PT basic principle is introduced and it is demonstrated how sensor parameters can be derived from Signal-to-Noise Ratio (SNR) measurements. Afterwards, the laboratory setup together with CCD performance measurements is presented.

## PRINCIPLE OF CHARACTERIZATION

PT is widely used for image sensor testing because it is a straightforward method to determine numerous sensor parameters by analyzing only two measured quantities, average signal and rms noise. Detailed information about PT can be found in textbooks (e.g. Ref. [5]), and the European Machine Vision Association even derived the EMVA Standard 1288 according to this method [6]. Following this standard a brief introduction in the underlying mathematical model is given in this section. According to Ref. [6] this model is valid if (i) the amount of photons collected by a pixel depends on the radiative energy density, (ii) noise sources are stationary and white, (iii) only the total quantum efficiency is wavelength dependent, (iv) only the dark current depends on temperature, and (v) the sensor is linear, i.e. the digital signal $y$ increases linear with the number of photons received. It is interesting to point out that the latter condition imposes a lower limit on the applicable wavelength region because the quantum yield in silicon is larger than one for photon wavelengths smaller than 400 nm [7].

As illustrated in Fig.1(a), the digital image sensor converts photons impinging on the pixel area in a series of steps into a

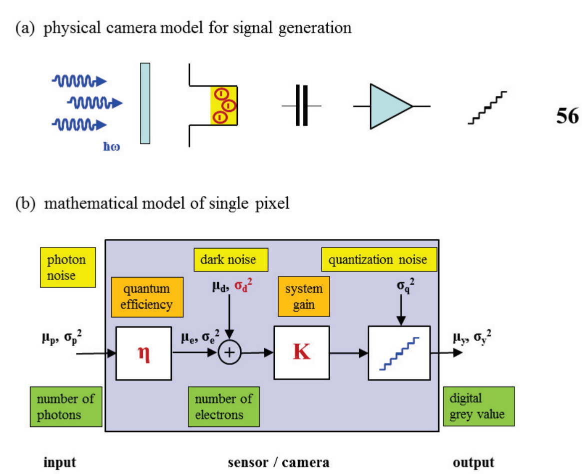


Figure 1: (a) Physical camera model: a number of photons hitting a sensor pixel creates a number of electrons via the photoelectric effect. The resulting charge is converted by a capacitor to a voltage, then amplified and digitized. As result a digital grey value is generated. (b) Mathematical model of a single pixel.



ISBN 978-3-95450-177-9

# EXPERIMENTAL RESULTS OF A COMPACT LASERWIRE SYSTEM FOR NON-INVASIVE H$^-$ BEAM PROFILE MEASUREMENTS AT CERN'S LINAC4

S. M. Gibson*, G. E. Boorman, A. Bosco, Royal Holloway, University of London, UK
T. Hofmann[1], U. Raich, F. Roncarolo, CERN, Geneva, Switzerland
[1] also at Royal Holloway, University of London, UK

*Abstract*

A non-invasive laserwire system is being developed for quasi-continuous monitoring of the transverse profile and emittance of the final 160 MeV beam at CERN's LINAC4. As part of these developments, a compact laser-based profile monitor was recently tested during LINAC4 commissioning at beam energies of 50 MeV, 80 MeV and 107 MeV. A laser with a tunable pulse width (1-300 ns) and ~200 W peak power in a surface hutch delivers light via a 75 m LMA transport fibre to the accelerator. Automated scanning optics deliver a free space < 150 micron width laserwire to the interaction chamber, where a transverse slice of the hydrogen ion beam is neutralised via photo-detachment. The liberated electrons are deflected by a low field dipole and captured by a sCVD diamond detector, that can be scanned in synchronisation with the laserwire position. The laserwire profile of the LINAC4 beam has been measured at all commissioning energies and is found in very good agreement with interpolated profiles from conventional SEM-grid and wire scanner measurements, positioned up and downstream of the laserwire setup. Improvements based on these prototype tests for the design of the final system are presented.

## MOTIVATION

### *Non-invasive Beam Diagnostics at LINAC4*

Conventional beam diagnostics such as SEM-grids and wire scanners inherently obstruct a significant fraction of the particle beam during measurements. To enable quasi-continuous monitoring of CERN's new LINAC4 160 MeV H$^-$ accelerator, a laserwire system is being developed that probes the particle beam properties via photo-detachment interactions as the H$^-$ ions traverse a narrow beam of light. As only $10^8$ of the $10^{14}$ H$^-$ ions in each LINAC4 pulse are typically neutralised by this laserwire, the technique is essentially non-invasive.

The ultimate aim of these developments is to install a permanent dual-laserwire system for use at LINAC4 top energy of 160 MeV, to measure the transverse emittance and beam profile. In our previous studies, a prototype laserwire emittance scanner was successfully demonstrated at the 3 MeV and 12 MeV commissioning phases of LINAC4 [1–3]. By scanning the vertical position of the laserwire with respect to the beam, the transverse emittance was reconstructed from the spatial distribution of neutralised H$^0$ atoms recorded by a downstream segmented diamond detector. The main H$^-$ beam was deflected by a dipole magnet, which for those measurements formed part of the diagnostics test bench at LINAC4.

The main dipole was not present for LINAC4 commissioning at 50 MeV through to 107 MeV beam energies, instead, the opportunity was taken to develop a new setup to measure the transverse beam profile, based on the electrons liberated by the photo-detachment process.

### *Beam Profile Monitor Design*

The design of the beam profile monitor was presented previously [4] and is shown here for completeness in Figure 1. The laser beam delivery optics from the prototype were adapted and reused to direct light into a new, compact interaction chamber, in which the laserwire is orthogonal to the incoming H$^-$ beam. A transverse slice of the H$^-$ beam is neutralised as the H$^-$ beam passes through the laserwire focus, liberating low energy (27 keV for 50 MeV H$^-$) electrons that are readily deflected through 90° by a 0.9 mTm integrated field of a weak dipole magnet. The main H$^-$ beam remains almost undeflected by the weak dipole. The electrons are collected by a fast 4 mm × 4 mm, sCVD diamond detector, that can be moved vertically in synchronisation with the laserwire position, allowing the beam profile to be reconstructed.

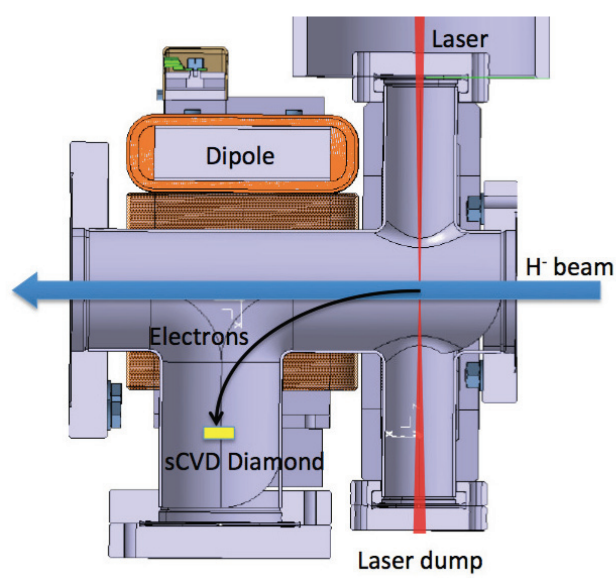


Figure 1: Conceptual design of the H$^-$ beam profile monitor [4].

* stephen.gibson@rhul.ac.uk



ISBN 978-3-95450-177-9

# LANSCE ISOTOPE PRODUCTION FACILITY EMITTANCE MEASUREMENT SYSTEM*

J. Sedillo, D. Baros, J. O'Hara, L. Rybarcyk, R. Valicenti, H. Watkins,
LANL, Los Alamos, NM 87545, USA

*Abstract*

A new beam diagnostic system for emittance measurement is under development for the Isotope Production Facility (IPF) beamline located at the Los Alamos Neutron Science Center (LANSCE). This system consists of two axes; each composed of a harp and slit actuation system for measuring the emittance of 41, 72, and 100-MeV proton beam energies. System design details and project status will be discussed with installation and commissioning of this system scheduled to conclude by February 2017.

## INTRODUCTION

In July 2015, research and development efforts were authorized for the creation of additional beam diagnostic systems at LANSCE's Isotope Production Facility. Among these systems was the inclusion of a new beam emittance and transverse profile monitoring diagnostic located in the IPF beamline. Design efforts have culminated in a dual-axis system comprised of four NI compactRIO embedded controllers capable of driving four actuators (2 orthogonal slits and two orthogonal harps) while simultaneously acquiring beam waveform data from 154 harp wires. After deployment in February of 2017, the system will measure the emittance and transverse profiles of proton beams with nominal energies of 41, 72, and 100 MeV [1].

## SYSTEM LOCATION AND OVERVIEW

The IPF beamline diverges from the LANSCE main beamline at the transition region after the 100 MeV drift tube linac (DTL) acceleration stage. From there, the IPF proton beam passes through a drift space before impinging on the IPF target. Beam properties at the emittance device are: nominal energy of either 41, 72, or 100 MeV; 4Hz macropulse repetition rate; 150µsec pulse width; and 0.1 to 21mA peak beam current.

Figure 1 shows the IPF beamline where the emittance actuators will be located. Two orthogonally mounted slit actuators will reside 7.5 meters upstream of the two orthogonal harp actuators. The IPF target is located approximately 2.7 meters downstream of the harps.

This emittance diagnostic is one of several systems under development for enhancing the beam measurement capabilities of the IPF from which improvements in isotope production reliability, diversity, and yield are expected [1].

*Work supported under the auspices of the United States Department of Energy, Office of Science.

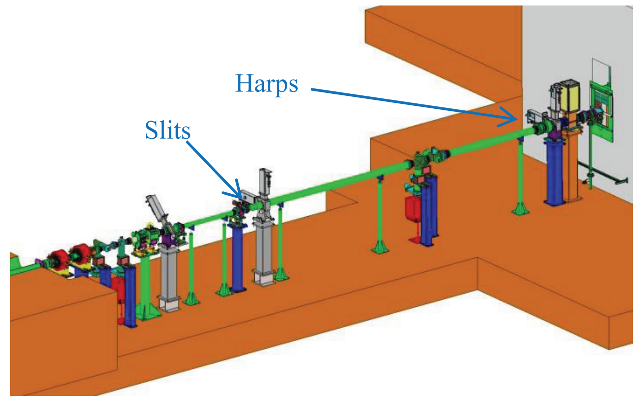


Figure 1: IPF beamline model. Beam direction is left to right.

## SLIT DESIGN

Beam emittance measurement begins with the slit. The IPF slits have been designed with a 0.508-mm slit aperture size and a 14-mm slit thickness. The slit size allows for a relatively higher resolution emittance scan relative to the beam spot size of 48-mm (2-RMS) while minimizing slit-induced scattering. The slit thickness of 14-mm (copper substrate) was specified to fully absorb the intercepted beam. An additional provision for slit biasing has been included via an SHV connection. A computer rendering of the slit design is shown below in Fig. 2.

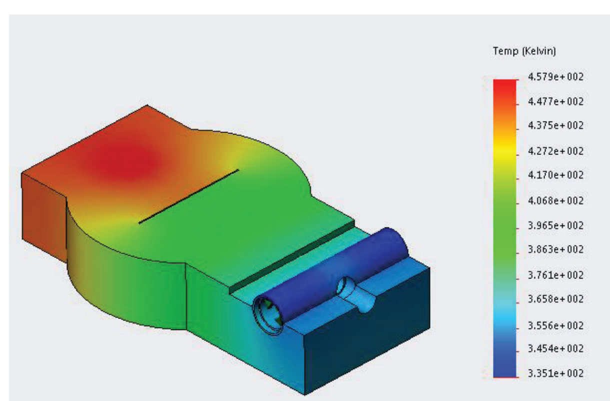


Figure 2: IPF slit model with thermal analysis.

## HARP SENSOR DESIGN

The beam characteristics of interest are sensed by the harps. The IPF harps have been designed with 77-lines of transverse beam resolution spanning a 77-mm plane with 1-mm spacing. This configuration places approximately 49 wires within the beam's spot-size envelope of 48-mm. Sensors are composed of 0.079-mm-thick Silicon-carbide



ISBN 978-3-95450-177-9

# DESIGN AND IMPLEMENTATION OF NON-INVASIVE PROFILE MONITORS FOR THE ESS LEBT

C.A. Thomas*, T. Gahl, T. Grandsaert, H. Kocevar,
H. Lee, A. Serrano, T. Shea, European Spallation Source ERIC, Lund, Sweden

*Abstract*

We present in this paper the design and implementation of the Non-invasive Profile Monitors for the ESS LEBT. Non-invasive Profile Monitors at ESS measure the transverse profile of the high power proton beam. As such the NPM for the LEBT is not different from NPM designed for other sections of the ESS linac, however, it received the requirement to measure the position of the beam accurately with respect to the centre of the vacuum chamber, representing the reference orbit. This particular requirement led to implement a specific design to provide absolute position measurement to the system. In the following we will first describe the design and the associated functionalities, and then we will present the performance measurements of this built system, fully integrated into the control system. Finally we will discuss the performance in comparison to the initial requirements.

## INTRODUCTION

For the commissioning and operation of the ESS source and LEBT, beam transverse profile and r.m.s size are required for the characterisation of the beam lattice along the LEBT and at the entrance of the RFQ. In addition beam position and angle at the entrance of the RFQ is also required. For the measurement of the beam transverse profile and size, Non-invasive Profile Monitors (NPM) have been designed. An NPM for ESS consists of two 1D profile measurements, based on the interaction's by-product of the vacuum chamber residual gas with the accelerated protons. For the LEBT NPM, the beam profile is measured by means of two imaging systems, using the induced gas fluorescence to perform an image of the beam [1]. In the LEBT, no conventional beam position monitor (BPM) is installed, i.e. based on the RF technology. However, the information on the position can be provided by the measurement of the centroid on the beam distribution profile. But to provide this measurement in the ESS general coordinate system, additional knowledge to the usual NPM imaging system has to be provided. In the following, we will present the design and the performance of the NPM for the LEBT, matching the requirement of the beam size and beam position. The requirements for the profile, the beam size and the beam position are summarized in the table 1

## NPM DESIGN FOR THE LEBT

The NPM for the LEBT is based on imaging the proton induced fluorescence. It is composed of an optical system and a camera. The design of the system has been optimised to

Table 1: Requirements for the Beam Profile, Size and Position

| **Profile Error** (%) | **r.m.s Size** (%) | **Beam Error** | **Position Error** (mm) |
|---|---|---|---|
| 1 | 10 | | 0.1 |

satisfy several criteria, based on point spread function, depth of field, capture efficiency, and field of view, sensitivity and signal to noise ratio across the range of current from 1 mA to 70 mA. All these performance criteria together with the geometry of the vacuum chamber define the optical system the sensitivity and the size of the camera sensor. To start with, the viewport size is defined as a requirement to be large enough so that it offers a minimum numerical aperture of NA = 0.22. This condition is matched by design with a viewport on a CF DN-100 flange, with 105 mm aperture, and with the distance to the centre of the vacuum chamber, 230 mm. The main objective for the requirement on the numerical aperture of the viewport of the NPM is to provide a potential capture of 1% of the total solid angle of the emitted photons, $4\pi$. In the design of the optical system, the object numerical aperture may match the one offered by the viewport. However, this might not always be possible to achieve due to additional constraint.

In the following we will expose how the optical system has been selected to match as close as possible the expected performance.

In addition to the optical performance for imaging, the system is expected to deliver information on the centre of the beam with respect to the centre of the vacuum chamber, i.e. in the ESS general coordinate system. This can be achieve on the condition that the position of the sensor with respect to the focal plan image is known with the required accuracy. We will present how this can be achieve with the required precision.

### *System Optimisation for the Imaging Performance*

The system schematic is show in the Fig. 1. The source is composed of point sources distributed with the proton beam transverse distribution and linearly along the beam path, and which are emitting uniformly over $4\pi$ solid angle. The photon flux emitted by the source per unit length of interaction along the beam path, the gas fluorescence excited by the protons, can be estimated by:

$$N_{ph} = \sigma_f \frac{P_g}{\bar{R}T} N_a \quad (1)$$

* cyrille.thomas@esss.se

ISBN 978-3-95450-177-9

# SPACE CHARGE STUDIES FOR THE IONISATION PROFILE MONITORS FOR THE ESS COLD LINAC

C.A. Thomas*, European Spallation Source ERIC, Lund, Sweden
F. Belloni, J. Marroncle, CEA, Saclay, France

*Abstract*

In this paper, we present the results from a numerical code developed to study the effect of space charge on the performance of Ionisation Profile Monitors. The code has been developed from the analytical expression of the electromagnetic field generated by a 3D bunch of charged particles moving along one axis. This transient field is evaluated to calculate the momentum gained by a test moving particle, but not necessary co-moving with the bunch, and included in a non-linear ordinary differential equation solver (Runge-Kutta) to track the 3D motion of the test particle. The model of the IPM is complete when an additional constant electric field is included to project the test particle onto a screen. The results from this code, modelling the IPM to be developed for the ESS Cold Linac, are presented here, and the impact of the space charge on the measurement of the beam profile is discussed.

## INTRODUCTION

One of the challenges brought by high power beam such as provided by the ESS linac is that they can damage or simply destroy any material they interact with. For the measurement of transverse beam profile in two orthogonal axis, established method such as Wire-Scanners can not be applied as the wire breaks under a too long interaction with the beam. At ESS to palliate this, Non-invasive Profile Monitors (NPMs) will be in use for all beam with a pulse longer than 50µs and with a 62.5 mA peak current. NPM as called for ESS are based on the interaction between the residual gas chamber and the proton beam, which gives rise to ionisation and to fluorescence of the gas particles. In the superconducting cavities section of the Linac, NPMs use the ionisation byproduct of the interaction. An NPM at ESS is then composed of two orthogonal instruments called Ionisation Profile Monitors, IPM. This instrument is composed of a High-Voltage cage, which project on choice the ions or electrons produced by the proton beam, onto a screen where the beam profile is detected and read-out. One of the issues with this instrument is that its performance depends on the linearity of the projection. The projectiles being charged particles, they will be also interacting with the electromagnetic field generated by the proton bunches. Therefore, high charged bunches are likely to give an addition transverse to the projectiles, giving an error to the read position of the projected projectile. In this paper, we present a numerical code based on a model of the IPM. With this code we investigate the effect of the space charge on the profiles, showing the range of application of the IPM to the ESS beam.

* cyrille.thomas@esss.se

## MODEL OF THE IPM AND NUMERICAL MATLAB IMPLEMENTATION

The simple numerical model to investigate the influence of the bunched proton beam of ESS on the IPM performance is described by Eq. 1

$$m\frac{d}{dt}\vec{v} = \vec{F} \tag{1}$$

and with $m$ the mass of the particle, $\vec{v}$ its speed in 3D, and $\vec{F}$ the 3D force felt by the particle.

In the case of the force to be generated by a bunch of charged particles moving at the relative speed in one direction that we choose to be given by the unit vector $\mathbf{z}$, one can write the force $\vec{F}$ as:

$$\vec{F} = q\left(\vec{E} + \vec{v}\times\vec{B}\right) = q\begin{cases}\left(1-\beta_b\frac{v_z}{c}\right)E_x\\ \left(1-\beta_b\frac{v_z}{c}\right)E_y\\ E_z+\beta_b\left(E_x\frac{v_x}{c}+E_y\frac{v_y}{c}\right)\end{cases} \tag{2}$$

where $q$ is the charge of the particle, and $\vec{v} = v_x\hat{\mathbf{x}} + v_y\hat{\mathbf{y}} + v_z\hat{\mathbf{z}}$, the speed of the particle in 3D; $\beta_b = v_b/c$ the relativistic speed of the bunch, and $c$ the speed of light; $\hat{\mathbf{i}}$ represents the unit vector in the lab frame.

The field generated by the relativistic bunch moving along $z$ axis is given by [1]:

$$\vec{E} = \begin{pmatrix}E_x\\E_y\\E_z\end{pmatrix} = \begin{pmatrix}\gamma_b\bar{E}_x\\ \gamma_b\bar{E}_y\\ \bar{E}_z\end{pmatrix} \tag{3}$$

with $\gamma_b = \frac{1}{\sqrt{1-\beta_b^2}}$ the Lorentz factor related to the bunch relativistic speed. $\vec{\bar{E}} = \bar{E}_x\mathbf{x}+\bar{E}_y\mathbf{y}+\bar{E}_z\mathbf{z}$ is the field generated by the bunch in the rest frame coordinate of the bunch, with its origin in the center of the bunch and with unit vectors $\mathbf{i}$ colinear to $\hat{\mathbf{i}}$ , and in which the coordinates transform as:

$$\bar{x} = x \quad \bar{y} = y \quad \bar{z} = \gamma_b(z-\beta_b ct) \tag{4}$$

and the dimensions of the 3D Gaussian bunch we consider here is:

$$\bar{\sigma}_x = \sigma_x \quad \bar{\sigma}_y = \sigma_y \quad \bar{\sigma}_z = \gamma_b\sigma_z \tag{5}$$

The expression of the 3D field generated by the 3D Gaussian bunch is given by:

ISBN 978-3-95450-177-9

# PRELIMINARY MEASUREMENT ON POTENTIAL LUMINESCENT COATING MATERIAL FOR THE ESS TARGET IMAGING SYSTEMS

C.A. Thomas*, M. Hartl, Y. Lee, T. Shea, European Spallation Source ERIC, Lund, Sweden
E. Adli, H. Gjersdal, M.R. Jaekel, O. Rohne, University of Oslo, Olso, Norway
S. Joshi, University West, Trollhättan, Sweden

*Abstract*

We present in this paper the preliminary measurements performed on luminescent materials to be investigated and eventually coated on the ESS target wheel, the Proton Beam Window separating the end of the ESS Linac and the entrance of the ESS target area, and the ESS Dump. Among all the properties of the luminescent material required for the target imaging systems, luminescence yield and luminescent lifetime are essential for two reasons. The first one is trivial, since this material is the source for the imaging system and sets its potential performance. The lifetime is not generally of importance, unless the object is moving, or time dependence measurements are to be done. In our case, the target wheel is moving, and measurement of the beam density current may have to be performed at the 10µs scale. Thus luminescence lifetime of the coating material should be known and measured. In this paper, we present the luminescence measurements of the photo-luminescent lifetime of several materials currently under studies to be used eventually for the first beam on target.

## INTRODUCTION

One of the challenges presented by high power proton beams for neutron spallation is the level of control required to prevent any damage on material of the target that must not be illuminated by the beam, or on the target itself not to be damaged. This level of control can be partly achieved by means of imaging the beam power density distribution deposited on the surface of the target. For such a system to be deployed at ESS, a luminescent material has to be identified and qualified. The qualification of such a material goes through reviews and tests of the candidate material properties, such as its luminescence yield, decay time, temperature sensitiveness, but also the thermo-mechanical resistance of the coated material to the beam impact and to high radiation dose, and to its luminescence properties under extremely high fluence, and finally, the qualified control of the industrial coated process. In this paper we address one of these aspect which is the measurement of the luminescence decay time. There are several ways to measure this decay time. Two possible ways are the time domain response, provided by a direct measurement of the luminescent pulse excited by a short proton bunch, and frequency domain response, from the measurement of the amplitude and phase luminescence excited by a frequency modulated source. The first method uses short bunches, and for instance short proton bunches delivered by facility like HiRadMat can be used for such a measurement. The second method is developed on a test bench for luminescent materials which can be photo-excited. The main objective of this test bench is to get time decay without the need of an accelerator of short bunched proton beams, and without time access restrictions. The method developed by Lakowicz *et al.* [1], consists in measuring the amplitude and phase response of the luminescent material under intensity modulated source and as function of the modulation frequency. The method is complementary to the time-domain lifetime measurement. It can provide a fine measurement of multi-exponential intensity decays but also non-exponential decays resulting from resonance energy transfer, time-dependent relaxation or collisional quenching. In the following, we firstly describe the experimental setup for the test bench for the frequency-domain luminescent lifetime measurement. Then we will present results from frequency-domain lifetime measurements on the chromium alumina coated for the SNS target imaging system. We will then discuss the method and the results obtained with it and within the perspective of using a similar luminescent coating material for the ESS target imaging system. Finally, we conclude on the performance and usage of the frequency-domain lifetime bench towards the selection process of the luminescent coated material for the ESS target imaging system.

## EXPERIMENTAL SETUP

### *Frequency-Domain Lifetime Bench Setup*

Our frequency domain lifetime measurement setup is shown in the Fig. 1. It consists of a modulated UV source (Thorlabs UV source DC3100-365), and two optical path, one towards the reference detector (Thorlabs PDA10), and the other towards the photo-luminescent sample. The luminescent light from the sample is detected by means of another fibre coupling assembly, which incorporates a filter for the source wavelength, and a second detector ((Thorlabs PDA10 or PDA36, depending on the bandwidth and sensitivity required). The signals from the two detectors together with the source modulation reference signal are sent to an oscilloscope, where the data is acquired. A detail description of the setup, the method and the analysis is explain in [1] and in [2].

### *Model for the Frequency-Domain Lifetime Measurement*

As described in [2], the lifetime decay can be measured by fitting the amplitude and phase response of the lumines-

* cyrille.thomas@esss.se

ISBN 978-3-95450-177-9

# LONGITUDINAL DIAGNOSTICS METHODS AND LIMITS FOR HADRON LINACS

A. Shishlo†, A. Aleksandrov, ORNL, Oak Ridge, TN 37831, USA

*Abstract*

A summary of the longitudinal diagnostics for linacs is presented based on the Spallation Neutron Source (SNS) linac example. It includes acceptance phase scans, Bunch Shape Monitors (BSM), and a method based on the analysis of the stripline Beam Position Monitors' (BPM) signals. The last method can deliver the longitudinal Twiss parameters of the beam. The accuracy, applicability, and limitations of this method are presented and discussed.

## INTRODUCTION

The SNS linac accelerates $H^-$ ions up to 1 GeV. It has two parts: a normal temperature linac and a SCL which is the world's first of the kind high power hadron superconducting linac. The SCL accelerates negative hydrogen ions from 186 MeV to 1 GeV with 81 six-cell niobium elliptical superconducting RF cavities [1]. The SNS power ramp up started in 2006, and in 2009 SNS reached 1 MW level. During this time, an unexpected beam loss in an SCL was encountered. This beam loss was reduced to the acceptable level by empirically lowering the field gradients of the SCL quadrupoles without understanding the loss mechanism. That led to efforts by the accelerator physics group to understand and to control the beam sizes in all three dimensions in the SNS superconducting linac. Later the mechanism of the unexpected beam loss was identified as the Intra Beam Stripping (IBSt) process [2,3]. This explained our success in the loss reduction, but future improvements depend on our ability to measure and control the linac bunch sizes along the SCL including the bunch length. To measure this parameter the new method of non-invasive longitudinal diagnostics was developed [4].

In the present paper we are going to describe the new approach, its accuracy, conditions of applicability in hadron linacs, and its limitations. In the beginning, we will give the overview of traditional longitudinal diagnostics in the SNS linac. Then we will discuss the possibility and conditions of using the Beam Position Monitor's (BPMs') signal for the bunch length measurements. After that, we will describe the scheme of the new method where we combine a short RF cavity, a drift space, and the BPM to measure the longitudinal Twiss. We are going to present formulas for estimating parameters of the cavity and a drift length necessary for successful application of the method. At the end we will discuss the results of application of this method to the SNS linac.

## SNS BUNCH LENGTH DIAGNOSTICS

At SNS the direct measurements of the bunch length in the linac and transport lines are performed by the Bunch Shape Monitors (BSM) [5]. The SNS linac has 4 BSMs in the warm section right before the SCL part. These BSMs were used to check the bunch shape at the entrance of SCL. The measurements showed that we have a longitudinally unmatched beam in this section, and the longitudinal emittance at the SCL entrance is substantially higher than the design value. The last BSM was also used to benchmark a new BPM-based method [4]. Unfortunately, the BSMs as beam intercepting devices are not used in the superconducting linac because of a possibility of a cavities' surface contamination.

Another method for the bunch length measurement is the widely used acceptance phase scan. This method was used at SNS for the Drift Tube Linac cavities in the warm linac and for SCL [6]. The classical variant of the acceptance scan uses a Faraday cup with energy degrader to measure the transmission of the beam through a long accelerator cavity as a function of the cavity phase. In the case of the SNS superconducting linac the combination of the beam current monitors and beam loss monitors was used [6]. For the SCL this method is very time consuming, creates a lot of beam loss in the SCL during the scan, and it has errors that cannot be evaluated.

The new suggested method uses the BPMs to measure the longitudinal bunch length. The next section will discuss the conditions for reliable measurements of this parameter.

## BUNCH LENGTH AND BPM SIGNALS

The analysis of the spectral density of the sum signal of all four BPM's quadrants was performed a long time ago [7]. The Fourier amplitude of the surface charge density on a beam pipe is defined by geometry, relativistic parameters of the beam, and a Fourier amplitude of the longitudinal density of the bunch [7]

$$u_\omega \propto \frac{A_\omega}{I_0\left(\dfrac{R\cdot\omega}{\gamma\cdot\beta\cdot c}\right)} \tag{1}$$

where $\omega$ is BPM's frequency, $R$ is the beam pipe radius, $c$ is the velocity of light, $A_\omega$ is the Fourier amplitude of the longitudinal density of the bunch, $I_0$ is the modified Bessel function, and $\gamma$, $\beta$ are relativistic parameters.

The modified Bessel function in the formula (1) describes the attenuation of the signal for higher frequencies because of the pure geometry. We can get the detailed longitudinal shape of the bunch only in the ultra-relativistic case, when $\gamma \to \infty$, and the useful frequencies will be limited only by the external circuit. In the

† shishlo@ornl.gov



ISBN 978-3-95450-177-9

# THE WALL CURRENT TRANSFORMER – A NEW SENSOR FOR PRECISE BUNCH-BY-BUNCH INTENSITY MEASUREMENTS IN THE LHC

M. Krupa*,[1], M. Gasior
CERN, Geneva, Switzerland
[1] also at Lodz University of Technology, Lodz, Poland

*Abstract*

The Wall Current Transformer (WCT) is a new bunch-by-bunch intensity monitor developed by the CERN Beam Instrumentation Group to overcome the performance issues of commercial Fast Beam Current Transformers (FBCT) observed during Run 1 of the LHC. In the WCT the large magnetic cores commonly used in FBCTs are replaced with small RF transformers distributed around the beam pipe. Rather than directly measuring the beam current, the WCT measures the image current induced by the beam on the walls of the vacuum chamber. The image current is forced to flow through a number of screws which form the single-turn primary windings of the RF transformers. The signals of the secondary windings are combined and the resulting pulse is filtered, amplified and sent to the acquisition system. This paper presents the principle of operation of the WCT and its performance based on laboratory and beam measurements.

## INTRODUCTION

During the LHC Run 1 (2008-2013) two commercial Fast Beam Current Transformers (FBCT) were installed on each LHC Ring: one used operationally and one spare used mostly for development. The bunch-by-bunch intensity measurements obtained with the FBCTs were observed to be sensitive to both the beam position at the transformer location and the bunch length [1]. This undesirable sensitivity was proven to be linked to the FBCT itself and significantly perturbed the bunch-by-bunch intensity measurements.

As an attempt to improve the situation, two new sensors were designed during the LHC Long Shutdown 1 (2013-2014) and subsequently installed for Run 2 (2015 onwards). The Integrating Current Transformer (ICT) [2], developed in collaboration with Bergoz Instrumentation, was installed on LHC Ring 1 while a Wall Current Transformer (WCT), developed by the CERN Beam Instrumentation Group, was installed on LHC Ring 2. In 2015 the two new monitors replaced the development FBCTs while the two operational FBCTs, upon which multiple intensity data users relied, were left in place to compare the three different technologies. This comparison showed that the best results were obtained with the WCT, leading to the operational systems being replaced with WCTs for the 2016 run.

The WCT design is derived from the Inductive Pick-Up (IPU) developed in 2003 at CERN for the CTF3 Drive Beam Linac [3]. Instruments applying similar ideas had also been developed in the past [4, 5]. Whilst the IPU was designed for beam position measurements, the WCT was carefully optimised for precise LHC bunch current measurements.

## PRINCIPLE OF OPERATION

A simplified cross section of the WCT is shown in Fig. 1. The WCT uses small RF transformers instead of the large magnetic cores typically found in FBCTs. The transformers are mounted on internal Printed Circuit Boards (PCB) and uniformly surround the vacuum chamber. The image current is forced to flow through conducting screws connecting both sides of a dielectric insert brazed to the vacuum chamber. The screws go through the centre of each transformer to form single-turn primary windings. The secondary windings of the transformers are soldered to the PCBs and loaded with resistors of a few ohms, converting the secondary current into voltage. The signals of all RF transformers are passively combined into a single WCT output providing a signal proportional to the instantaneous beam current.

In parallel to the screws, both sides of the dielectric insert are connected by an RF bypass to provide a well-controlled image current path at frequencies above a few GHz, beyond the useful WCT bandwidth. The bypass consists of resistors and capacitors soldered to a flexible PCB that is mounted directly on the vacuum chamber.

The WCT is enclosed in a metal housing. The space between the housing and the conductive screws is filled with ferrite cores which increase the inductance of the housing as seen by the image current. This forces the low-frequency

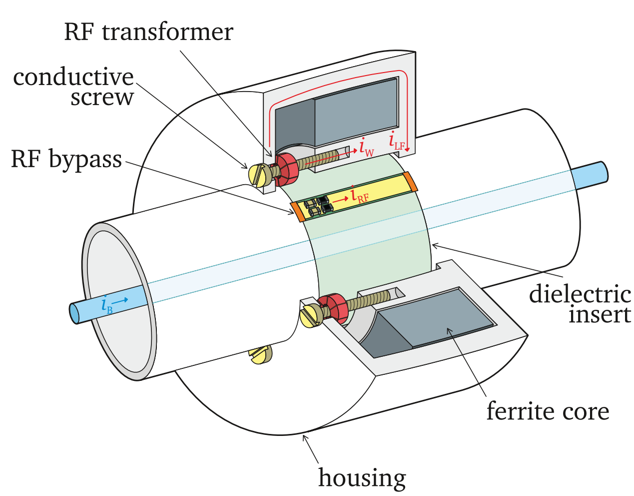


Figure 1: Cross section of the WCT.

---
* michal.krupa@cern.ch

# DIAGNOSTIC DATA ACQUISITION STRATEGIES AT FRIB *

S. Cogan†, S. Lidia, R. C. Webber, Facility for Rare Isotope Beams, East Lansing, MI, USA


## *Abstract*

Strategies for data acquisition and processing will be discussed in the context of the Facility for Rare Isotope Beams (FRIB). Design decisions include selecting and designing electronics hardware, data acquisition cards, firmware design, and how to integrate with EPICS control system. With over 300 diagnostic devices and 16 unique types of devices, timing for synchronous data acquisition is important. Strategies to accelerate development as well as reduce maintenance requirements will be discussed, including using common hardware and firmware whenever possible, and defining a common data reporting structure for use by most devices. MicroTCA.4 platform is used to integrate data acquisition cards, distribute timing information, and machine protection signals.


## FRIB MACHINE REQUIREMENTS

The Facility for Rare Isotope Beams (FRIB) is a new scientific user facility for low energy nuclear science. Under construction on campus and operated by Michigan State University, FRIB will provide intense beams of rare isotopes [1].

FRIB will deliver the highest intensity beams of rare isotopes available anywhere. The superconducting linear accelerator (linac) will accelerate ion species from $^{18}$Ar up to $^{238}$U with energies of no less than 200 MeV/u and provide beam power up to 400 kW. Although designed to support full-scale CW operation, low current and pulsed modes will also be utilized, so diagnostics must support a large dynamic range, from 1 nA to 1 mA of beam current. Figure 1 shows a schematic overview of the accelerator.

### *Machine Protection and Availability*

In order to achieve high reliability and high availability, permanent accelerator component damage should be prevented, beam loss and residual activations should be minimized, and beam downtime minimized. This leads to an array of diagnostic devices which monitor a variety of beam loss mechanisms. A machine protection system (MPS) has been designed to detect and respond quickly (< 35 µsec) to beam loss events and terminate the beam [3]. This is achieved by monitoring not-OK (NOK) signals from a multitude of MPS nodes which digitize diagnostic data and make local NOK decision in less than 15 µsec. The remaining 20 µsec of the time budget is used to communicate the NOK signal to the MPS Master and to terminate beam production and transport. Table 1 is simplified picture of the acute (fast) and chronic (slow) losses which we must detect. Table 2 shows an overview of diagnostic devices utilized not only for machine protection (MPS), but also for tuning, commissioning, and general diagnostic information [2]. *Italicized devices* * will provide input to MPS.

Table 1: Acute and Chronic Beam Loss Detection

| Beam Loss | Diagnostic Response Time |
|---|---|
| 100% (2 J) | 15 usec |
| 10% (0.2 J) | 150 usec |
| Slow (0.1 W/m) | seconds |

Table 2: FRIB Diagnostic Devices

| Device | Total # |
|---|---|
| *Beam Position Monitor* * | 149 |
| *Beam Current Monitor (ACCT)* * | 12 |
| *BLM - Halo Monitor Ring* * | 66 |
| *BLM - Ion Chamber* * | 47 |
| *BLM - Neutron Detector* * | 24 |
| *BLM – Fast Thermometry System* * | 240 |
| Profile Monitor (Lg., Sm. Flapper) | 41 |
| Bunch Shape Monitor | 1 |
| Allison Emittance Scanner (2 axis) | 2 |
| Pepper pot emittance meter | 1 |
| Wire Slit Emittance Scanner (2 axis) | 1 |
| Faraday Cup | 7 |
| Fast Faraday Cup | 2 |
| Viewer Plate | 5 |
| Selecting Slits System - 300 W | 5 |
| Collimating Apertures - 100 W | 2 |
| Intensity Reducing Screen System | 2 |

### *Implications for Data Acquisition*

To achieve MPS requirements (not all of which are discussed here, see [3]), diagnostic devices should have a response time of 5 µsec (analog bandwidth DC to 35 kHz), digitized sample rates of at least 1 MS/sec and support a large dynamic range, from < 1 nA to 1mA, depending on the device. To respond to beam loss events in less than 15 µsec, MPS decisions are made in real-time locally by the data acquisition electronics. Field programmable gate arrays (FPGAs) are utilized to provide real-time signal processing and MPS decision, with close integration to digitizing hardware, often combined in a single electronics board. Additionally, FPGAs allow custom firmware to incorporate accurate timestamp from a global timing system (GTS) and provide ability for improved signal processing, including digital filters, background noise subtraction, advanced threshold triggering, etc.

* This material is based upon work supported by the U.S. Department of Energy Office of Science under Cooperative Agreement DE-SC0000661, the State of Michigan and Michigan State University.
† cogan@frib.msu.edu

ISBN 978-3-95450-177-9

# BEAM DIAGNOSTICS CHALLENGES FOR BEAM DYNAMICS STUDIES

O. R. Jones, CERN, Geneva, Switzerland

*Abstract*

This seminar reviews the performance and limitations of present beam instrumentation systems in relation to beam dynamics studies, and gives an overview of the main requirements from the accelerator physics community for new or improved measurements that need an R&D effort on beam diagnostics.

## INTRODUCTION

Beam dynamics studies are an essential element in the smooth running of all accelerators. Such efforts are important for the commissioning of a machine, modifying initial design parameters to increase performance, and to understand the issues and challenges that arise during accelerator exploitation [1].

Routine measurements during standard operation, such as adjustment of the orbit and optimisation of the tune, coupling and chromaticity are not addressed in this seminar, although some of the diagnostic devices used for such measurements will be covered. The emphasis is instead on specific measurements during machine set-up, such as the measurement and correction of the machine optics in both synchrotrons and linacs or transport lines. Also discussed are more advanced measurements for the understanding of impedance and space charge effects, detecting instabilities, and the identification of sources driving the diffusion of particles to high oscillation amplitudes.

## MEASURING THE MACHINE OPTICS FUNCTIONS IN SYNCHROTRONS

The measurement and correction of optics parameters has been an area of intensive study since the advent of strong focusing synchrotron accelerators, where perturbations from field imperfections and misalignments became a concern. Traditionally, colliders have led the development of methods for optics control based on turn-by-turn centroid position data, while lepton storage rings have focused on closed-orbit-response techniques [2]. Both of these methods rely heavily on the use of the beam position system of the accelerator, and are now often driving its requirements.

### *Turn-by-turn Techniques*

In 1983 a major achievement took place in the CERN-ISR, where the Beam Position Monitors (BPMs) were used successively around the collider to measure the relative amplitude and phase advance of the β-function by observing the amplitude and phase of induced betatron oscillations [3]. This was the first time that machine optics had successfully been reconstructed from individual BPM data, at that time using a BPM system that was entirely based on analogue technology.

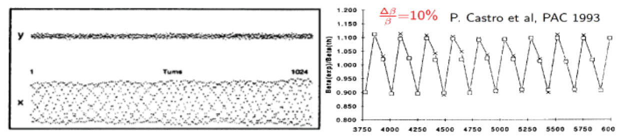


Figure 1: LEP β-beating example. Left: turn-by-turn BPM data. Right: Δβ/β for a section of the machine.

The first optics measurements using digital, turn-by-turn BPM data were performed at CERN-LEP (Fig. 1) [4]. The β-function at each BPM location was extracted from the phase advance between 3 BPMs, assuming a good knowledge of the focusing elements in between (Eq. 1).

$$\beta^{BPM1}_{measured} = \beta^{BPM1}_{model}\left(\frac{\{cot\varphi_{12} - cot\varphi_{13}\}_{measured}}{\{cot\varphi_{12} - cot\varphi_{13}\}_{model}}\right) \quad (1)$$

This method, known as "β from phase", was also used in CESR (Cornell, USA) in 2000 to minimize the β-beating, the difference between the measured β and the design β (Δβ/β), with an rms of only 2% [5]. This is still one of the best optics correction achieved in a lepton collider.

One of the limitation of this method is its reliance on good quality BPM data. Identifying BPMs giving poor readings or BPMs with excessive noise was therefore very important. A major step forward in achieving a more robust analysis was taken at SLAC in 1999, where singular value decomposition (SVD) techniques were used to isolate faulty BPMs and identify noise components affecting the oscillation data [6].

The 3 BPM method developed at LEP has recently been extended for the LHC to take into account any number of BPMs [7], resulting in a much better overall resolution in the measurement of the β-functions.

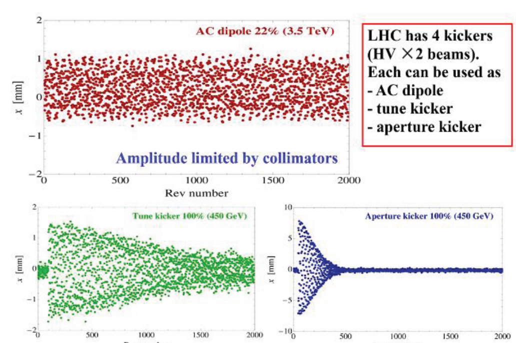


Figure 2: Examples of excitation for optics measurements in the LHC. Top: AC-dipole excitation. Bottom: Examples of single kicks at injection energy.

In order to initiate a sufficient large centroid motion to be visible on a turn-by-turn basis with the BPM system, the beams typically need to be kicked to relatively high

ISBN 978-3-95450-177-9

# BEAM SIZE MEASUREMENTS USING INTERFEROMETRY AT LHC

G. Trad*, E. Bravin, A. Goldblatt, S. Mazzoni, F. Roncarolo, CERN, Geneva, Switzerland
T. Mitsuhashi, KEK, Ibaraki, Japan

*Abstract*

During the long LHC shutdown 2013-2014, both the LHC and its injector chain underwent significant upgrades. The most important changes concerned increasing the maximum LHC beam energy from 4 TeV to 6.5 TeV and reducing the transverse emittance of the beam from the LHC injectors. These upgrades pose challenges to the measurement of the transverse beam size via Synchrotron Radiation (SR) imaging, as the radiation parameters approach the diffraction limit. Optical SR interferometry, widely used in synchrotron light facilities, was considered as an alternative method to measure the 150 µm rms beam size at top energy as it allows measurements below the diffraction limit. A system based on this technique was therefore implemented in the LHC, for the first time on a proton machine. This paper describes the design of the LHC interferometer and its two SR sources (a superconducting undulator at low energy and a bending dipole at high energy), along with the expected performance in terms of beam size measurement as compared to the imaging system. The world's first proton beam interferograms measured at the LHC will be shown and plans to make this an operational monitor will be presented.

## INTRODUCTION

Measuring the transverse emittance of the beam is fundamental in every accelerator. This is particularly true for colliders, since the precise determination of the beam emittance is essential to maximize and control the luminosity. In the LHC, where it is not a directly accessible quantity, the emittance is inferred from the measurement of the transverse beam sizes and the knowledge of the accelerator optics. The LHC Beam Synchrotron Radiation Telescope (BSRT) is the only instrument offering non-invasive, continuous beam size monitoring via direct imaging of the emitted visible Synchrotron Radiation (SR). After the CERN long shutdown in 2013-2014, the maximum LHC beam energy was increased from 4 TeV to 6.5 TeV and the transverse emittance of the injected beam was reduced following upgrades in the injector chain upgrades. This makes the measurement of the transverse beam size via SR imaging a real challenge, as the radiation parameters approach the diffraction limit. Since the optical SR interferometer, widely used in synchrotron light facilities, allows beam size measurements below the diffraction limit, a system based on this technique was therefore implemented in the LHC, for the first time in a proton machine. In this paper, the design of the LHC interferometer is presented and its final version, installed in June 2016, is described. The characterization of its components and the commissioning process with beam will also be discussed. Additionally the LHC beam size measurement via the world's first measured proton beam interferograms will be shown and plans to make the interferometer an operational monitor will be presented.

* georges.trad@cern.ch

## LHC SR SOURCE

The LHC is equipped with two SR monitors (one per beam) used to characterise the transverse and longitudinal beam distributions. The SR source is a combination of a dedicated undulator and a beam separation dipole (D3). The visible SR emission point shifts gradually with the energy ramp from the undulator (at injection energy, 450 GeV) to the D3 which dominates from 1.2 TeV onwards [1]. The D3 is a 9.45 m long superconducting dipole and at 7 TeV, its maximum field is 3.9T giving a bending angle of 1.58 mrad and a radius of curvature of ~6 Km. The undulator was designed to enhance the visible SR component from injection energy up to ~1.2 TeV, until the contribution of visible SR from D3 becomes detectable. The undulator is installed 937 mm upstream of D3 and shares the same cryostat. It is made of two 28 cm periods with a peak field of 5 T, thus resulting in the undulator parameter "K" 0.0712.
The emitted SR is intercepted by an extraction mirror installed in the beam vacuum and sent through a vacuum window to the BSRT. Figure 1 shows the SR intensity distribution on the extraction mirror, as simulated for injection and top energy.

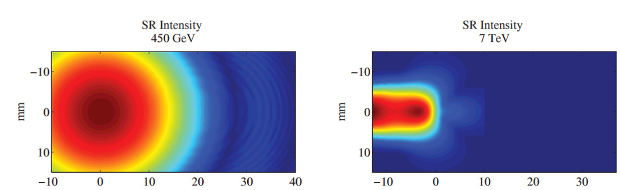


Figure 1: Simulated SR Intensity on the extraction mirror of the LHC at injection (left) and Flat Top (right).

## SR IMAGING LIMITATION

The visible SR imaging system is based on two focusing stages, offering the possibility of switching between two different sets of lenses. One optimized for 400-600 nm operation at injection and the other for Near Ultra-Violet (NUV, 250 nm) imaging at high energy [2]. It is worth mentioning that the NUV operation was found beneficial in terms of resolution at high energy where the beam size is as small as 170 µm. In fact in LHC Run II, the BSRT resulted reliably operational for bunch-by-bunch measurements and crucial

ISBN 978-3-95450-177-9

# BEAM SHAPE RECONSTRUCTION USING SYNCHROTRON RADIATION INTERFEROMETRY

L. Torino, U. Iriso, ALBA-CELLS, Cerdanyola del Vallès, Spain

*Abstract*

Synchrotron Radiation Interferometry (SRI) through a double-aperture system is a well known technique to measure the transverse beam size using visible light. In many machines the beam is tilted in the transverse plane, but the SRI technique only allows to directly measure the size of the projection of the beam shape along the axis connecting the two apertures. A method to fully reconstruct the beam in the transverse plane using SRI has been developed and successfully tested at the ALBA synchrotron light source. This report shows the full beam reconstruction technique and presents the results at different couplings. We also discuss how this technique could improve the measurement of very small beam sizes, improving the resolution of standard SRI.

## INTRODUCTION

Transverse beam size measurements are used to monitor the beam quality in accelerators. In synchrotron light sources, a direct image of the beam transverse plane can be provided by x-ray pinholes [1], while direct imaging using the visible part of the synchrotron radiation cannot be performed due to diffraction limitations.

Another widely used method to measure the transverse beam size is the Synchrotron Radiation Interferometry (SRI), which is based on the analysis of the spatial coherence of the synchrotron light and has been used in accelerators since the late 90s [2].

As opposed to the imaging techniques like the x-ray pinhole camera, the standard SRI technique using a double-aperture system only provides the projected beam size (in the aperture axis direction), and therefore information about possible beam tilt is lost.

A method to reconstruct the full transverse beam profile using a rotating double-aperture system, which allows to properly measure the beam size and relative beam tilt angle has been developed. The technique can also be used to perform ultra-low vertical beam size measurements, crucial for the newest machines.

## SYNCHROTRON RADIATION INTERFEROMETRY AT ALBA

The SRI setup is located in the ALBA diagnostic beamline Xanadu [3]. The radiation is produced by a bending magnet, the visible part is extracted and imaged by a Young-like interferometry.

The interferometry system is composed by two pinholes, a lens to focus the interference fringes, a telescopic ocular to magnify the interferogram, a narrow band color filter and a polarizer to select the wavelength and polarization of the light. The final results are captured by a CCD. A sketch of the measurement setup is presented in Fig. 1.

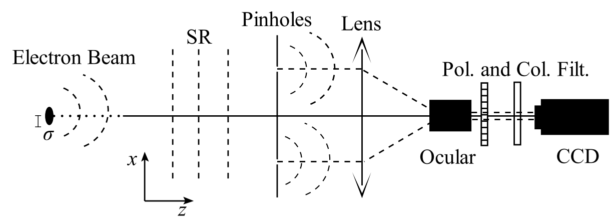


Figure 1: Sketch of the SRI experimental setup: The synchrotron radiation (SR) produced by the beam passes through the double-pinhole system and is imaged through a lens and an objective ocular to the CCD. The radiation polarization and the wavelength are selected through a polarizer (Pol.) and a color filter (Col. Filt.).

The formula describing the interferogram intensity along the direction parallel to the axis passing through the pinholes ($x$) is:

$$I(x) = I_0 \left\{ \frac{\mathrm{J}_1\left(\frac{2\pi a x}{\lambda f}\right)}{\left(\frac{2\pi a x}{\lambda f}\right)} \right\}^2 \times \left\{ 1 + V \cos\left(\frac{2\pi D x}{\lambda f}\right) \right\}, \quad (1)$$

where $I_0$ is the light intensity, $a$ is the pinholes radius, $\lambda$ is the radiation wavelength, $f$ is the focal length of the imaging system, $D$ is the distance between the pinholes and $V$ is the visibility. The visibility is the contrast of the interferogram fringes: $V = \frac{I_{Max}-I_{Min}}{I_{Max}+I_{Min}}$, where $I_{Max}$ and $I_{Min}$ are respectively the maximum and the minimum of the interferogram fringe at the center.

Equation 1 is used to fit a slice of the measured interferogram, letting the visibility as free parameter. Assuming that the beam has a Gaussian distribution along the direction of the pinholes axis, the beam size is obtained as:

$$\sigma = \frac{\lambda L}{\pi D} \sqrt{\frac{1}{2} \log\left(\frac{1}{V}\right)}, \quad (2)$$

where $L$ is the distance between the source point and the pinholes. The larger is the visibility the smaller is the beam size. Examples of interferograms used to measure the beam size projections are presented in Fig. 2.

## FULL BEAM RECONSTRUCTION

Since the SRI only measures the projection of the beam on the double aperture axis, we proceed to measure the projection along different axis by rotating the pinholes system. Figure 2 presents interferograms obtained for pinholes rotated at 0°, 45°, 90° and 135°, and the corresponding fit.

ISBN 978-3-95450-177-9

# THE NEW OPTICAL DEVICE FOR TURN TO TURN BEAM PROFILE MEASUREMENT

V. Dorokhov*, A. Khilchenko, A. Kotelnikov, A. Kvashnin, O. Meshkov[1], P. Zubarev
BINP SB RAS, Novosibirsk, 630090, Russia
also at [1]NSU, Novosibirsk, 630090, Russia
V. Korchuganov, A. Stirin, A. Valentinov, NRC Kurchatov Institute, Moscow, 123182, Russia

*Abstract*

The electron beam quality determines the main synchrotron radiation characteristics therefore beam diagnostics is of great importance for synchrotron radiation source performance. The real-time processing of the electron beam parameters is a necessary procedure to optimize the key characteristics of the source using feedback loops.

The frequency of electron beam cycling in the synchrotron storage ring is about 1 MHz. In multi-bunch mode electrons are grouped into a series of bunches. The bunch repetition frequency depends on the total number of bunches and usually reaches hundreds of MHz. The actual problem is to study the separate bunch dimensions' behavior under multi-bunch beam instabilities.

To solve this problem a turn-to-turn electron beam profile monitor is developed for siberia-2 synchrotron light source. The linear avalanche photodiodes array is applied to imaging. The apparatus is able to record a transversal profile of selected bunches and analyze the dynamics of beam during 106 turns. The recent experimental results obtained with the diagnostics are described.

## INTRODUCTION

We have developed the same device several years ago and successfully used it at VEPP-4M electron-positron collider [1-4]. The Fast Profile Meter (FPM) based on the Multi-Anode Photomultiplier Tube is a part of the VEPP-4M optical diagnostic system. We have successfully applied the FPM for determination of synchro-betatron resonances, phase oscillation monitoring, measurement of the beam spread and study of collective effects.

The device includes a MAPMT, a 12-byte ADC, a controller module, an internal memory of 4Mb and 100 Mb ethernet interface. It can record $2^{17}$ profiles of a beam at 16 points. Discontinuity of the records can vary within $1 \div 2^8$ turns of a beam. Revolution time of a beam in the VEPP-4M is 1220 ns and the recording time can last between 0.16 s to 20 s. As a result, the device can analyze the frequency oscillation of a beam in the range of 10 Hz — 1MHz. Fig. 1 represents a single beam profile fitted with Gaussian function.

*dorohov_vl@mail.ru

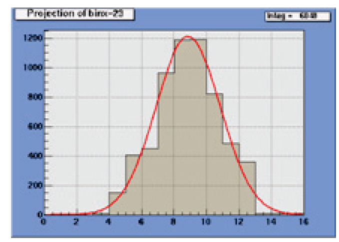

Figure 1: Example of the single beam profile fitted by the Gauss function.

The optical arrangement (Fig. 2) allows us to change the beam image magnification on the cathode of MAPMT from 6× to 20×, which is determined by the experimental demands. The set of remote controlled grey filters, included into optical diagnostics, allows selecting a suitable level of the light intensity with the dynamic range about $10^3$.

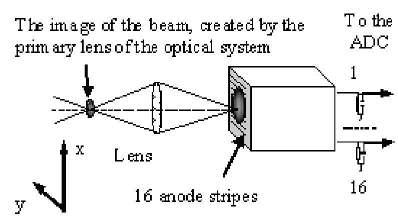


Figure 2: Optical layout of the diagnostics. The lens sets up a beam image on the photocathode of the MAPMT. The radial profile measurement is shown.

Fig. 3 presents the beam size and position behavior in the case of beam-beam instability, restored from FPM data.

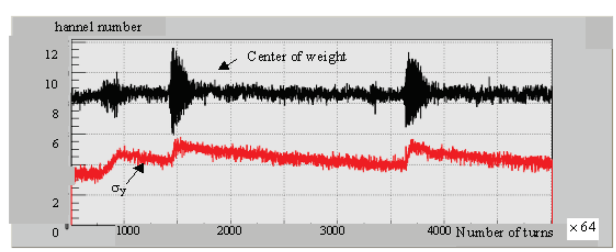


Figure 3: Beam dipole oscillations (black plot) and $\sigma_y$ behavior (red plot) during the beams convergence at the interaction point. Duration of the single turn is 1220 ns. The channel constant is 0.12 mm.

The currents of the electron and positron beams were restricted by beam-beam effects (Ie = 3 mA, Ip = 3.4 mA), and the positron beam was the "strong" one. Both the di-

ISBN 978-3-95450-177-9

# LONGITUDINAL PHASE SPACE DIAGNOSTICS FOR ULTRASHORT BUNCHES WITH A PLASMA DEFLECTOR

I. Dornmair* [2], K. Floettmann [3], A. R. Maier [3], B. Marchetti [1], C. B. Schroeder [1]
[1]Center for Free-Electron Laser Science & Department of Physics, University of Hamburg, Germany
also at [2]Lawrence Berkeley National Laboratory, Berkeley, California, USA
also at [3]DESY, Hamburg, Germany

*Abstract*

The plasma-based deflector is a new method to diagnose the longitudinal phase space of ultrashort electron bunches. It harnesses the strong transverse fields of laser-driven plasma wakefields to streak an electron bunch that is injected off-axis with respect to the driver laser. Owed to the short plasma wavelength and the high field amplitude present in a plasma wakefield, a temporal resolution around or below one femtosecond can be achieved with a plasma length of a few millimeters. Limitations arise from beam loading, synchronization and higher order correlations of the transverse fields. Amongst the possible applications are experiments aiming at external injection into laser-driven wakefields, or the diagnostics of laser-plasma accelerated beams.

## INTRODUCTION

Laser Plasma Accelerators (LPA) can provide high accelerating gradients in the order of 10 to 100 GV/m, and the acceleration of electron bunches to several GeV has been shown over few centimeter distances [1, 2]. The technology is therefore a promising candidate especially for drivers of next generation light sources. However, the beam quality is still a major challenge for the field, especially in terms of energy spread, emittance and divergence after the plasma.

In a laser plasma accelerator, a high power laser pulse is focused into a plasma target. Typical laser parameters here are a few Joules pulse energy, several tens of femtoseconds pulse length and a focal spot size around 15 $\mu$m. In the plasma, the laser pulse trails a wakefield. The ponderomotive force of the laser pulse causes a charge separation leading to large electric fields both in the longitudinal and in the transverse directions. The characteristic length scale is the plasma period with around 10 to 100 $\mu$m length for typical parameter ranges. Short electron bunches can be injected into the wakefield internally, i.e. from the plasma background, or externally from a conventional accelerator [3, 4], which has not been demonstrated so far. The usually large energy spread of plasma accelerated beams can be connected to the finite electron bunch length in combination with the short plasma period. For both injection strategies it is therefore vital to gain access to the longitudinal phase space of the injected bunch, in order to optimize the beam quality.

The bunch length of LPA beams has been measured to around 1.4 to 1.8 fs rms with coherent transition radiation [5] or to 2.5 fs rms employing Faraday rotation of a probe laser [6]. The resolution of a longitudinal phase space diagnostic consequently needs to be around or below one femtosecond, a feat that so far has only been achieved with X-band TDS cavities [7]. The use of those cavities in LPA is extremely challenging, not only due to their large size and cost, but also due to the lack of synchronization of the RF to the LPA driver laser. We therefore proposed [8] to employ the strong fields and short periods in plasma wakefields to streak the electron bunch.

## PLASMA BASED DEFLECTOR

In the linear regime, i.e. for a normalized peak vector potential of the driver laser $a_0^2 = (eA/m_e c^2)^2 \ll 1$, the electric fields in the wake exhibit a longitudinally sinusoidal structure [9]. The transverse shape of the longitudinal field follows the laser intensity profile, while the shape of the transverse fields follows the derivative of the laser intensity profile in the respective transverse coordinate. An electron bunch that is injected at a transverse offset with respect to the driver laser and at a phase where the transverse fields have a zero-crossing will then experience streaking fields. For a Gaussian driver laser, the optimum transverse offset is one standard deviation of the laser intensity profile, since there the transverse fields are maximal. An illustration of the setup can be seen in figure 1.

The temporal resolution of the setup can be calculated in a similar manner as for conventional TDS cavities, and is given by

$$\Delta\xi/c \geq \frac{\epsilon_{ny} m_e c}{\sigma_y e k_p V}. \tag{1}$$

Here, $\xi$ is the internal bunch coordinate, $\epsilon_{ny}$ is the normalized transverse emittance, $\sigma_y$ is the rms electron beam size inside the plasma, $k_p = (ne^2/m_e\epsilon_0 c^2)^{1/2}$ is the plasma wavenumber at a density $n$, and $V$ the effective voltage given by the integral of the peak transverse fields over the plasma length.

The resolution of a plasma-based deflector profits from the short plasma period and consequently large wavenumber, as well as from the strong fields present in the wakefield. Also, a low emittance of LPA beams has been measured with 0.1 - 0.2 mm mrad [10, 11]. On the other hand, a resolution reduction can be expected from the electron beam size $\sigma_y$, as it needs to be significantly smaller than the laser spot size, and will consequently be around 10 $\mu$m even for large laser spot sizes.

* irene.dornmair@desy.de

ISBN 978-3-95450-177-9

# ACCURATE MEASUREMENT OF THE MLS ELECTRON STORAGE RING PARAMETERS

R. Klein, G. Brandt, T. Reichel, R. Thornagel,
Physikalisch-Technische Bundesanstalt (PTB), Berlin, Germany
J. Feikes, M. Ries, I. Seiler,
Helmholtz-Zentrum Berlin für Materialien und Energie (HZB), Berlin, Germany

*Abstract*

The Physikalisch-Technische Bundesanstalt (PTB, the German national metrology institute) uses the Metrology Light Source (MLS) as a primary radiation source standard. This requires the accurate measurement of all storage ring parameters needed for the calculation of the spectral radiant intensity of the synchrotron radiation. Therefore, instrumentation has been installed in the MLS for the measurement of, e.g., the electron beam energy, the electron beam current or the electron beam size that outperforms that usually installed in electron storage rings used as a common synchrotron radiation source.

## INTRODUCTION

The PTB, the German metrology institute, utilizes the electron storage ring Metrology Light Source (MLS) [1] in Berlin - Adlershof for the realization of the radiometric units in the near infrared, visible, ultraviolet and vacuum ultraviolet spectral range. For this purpose the MLS can be operated as a primary source standard, i.e. the spectral radiant intensity of the synchrotron radiation (SR) is calculated by means of the Schwinger equation [2]. The primary source can then be used for the calibration of other radiation sources or of wavelength- or energy dispersive instruments [3]. The input parameters for the calculation of the spectral radiant intensity are the electron beam energy, electron beam current, the effective vertical size of the electron beam and the magnetic induction at the source point of the SR. For calibration applications, e.g. the spectral radiant power transmitted through a flux-defining aperture also is of interest. For this, also the geometrical parameters of the experiment have to be measured which are the distance to the source point and the vertical observation angle with respect to the orbital plane. These parameters have to be measured accurately since there measurement uncertainty determines the uncertainty of the calculated spectral radiant intensity. PTB operates equipment for the measurement of the storage ring parameters over a wide range. Especially the electron beam energy and electron beam current can be varied over a wide range (see below) to create tailor-made conditions for various calibration tasks. Table 1 summarizes typical storage ring parameters and the related uncertainties in their determination. The influence of the uncertainty of the measured parameter in the calculation of the spectral power depends on the wavelength. For the uncertainties listed in Table 1 the spectral radiant power can be calculated with a relative uncertainty well below 0.1 % for wavelength longer than 10 nm. In this spectral range the MLS is used for UV and VUV radiometry. The relative uncertainty gradually rises to almost 1 % for a wavelength of 1 nm as can be seen in Fig. 1. In this shorter wavelength range it might sometimes be better to use the neighboring BESSY II electron storage ring, that is operated by PTB in special user shifts as a primary source standard, mainly for the X-ray spectral range [4].

Table 1: Typical Operation Parameters of the MLS as a Primary Source Standard and Related Uncertainty in the Measurement of these Parameters.

| **Parameter** | **Typical value** | **Typical (rel.) uncertainty** |
|---|---|---|
| electron energy $W$ | 628.5 MeV | $2 \cdot 10^{-4}$ |
| magnetic induction $B$ | 1.38 T | $1 \cdot 10^{-4}$ |
| electron beam current $I$ (example) | 20 mA | $2 \cdot 10^{-4}$ |
| eff. vert. source size $\Sigma_y$ | 1.5 mm | 10 % |
| vert. observation angle $\psi$ | 0 µrad | 5 µrad |
| distance $d$ | 20 m | 5 mm |

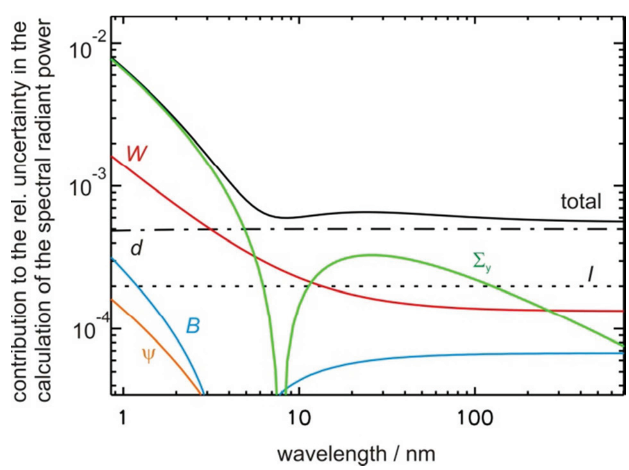


Figure 1: Contribution of the parameters' uncertainties to the calculation of the spectral power. The symbols marking the various lines are explained in Tab. 1, first column; the uncertainty in the parameters is listed in the third column of this table.



ISBN 978-3-95450-177-9

# MEASUREMENT OF THE BEAM RESPONSE TO QUADRUPOLE KICK BY USING STRIPLINE PICKUP MONITOR AT J-PARC MAIN RING

Y. Nakanishi, A. Ichikawa, A. Minamino, K. G. Nakamura, T. Nakaya, Kyoto University, Japan
T. Koseki, H. Kuboki, M. Okada, T.Toyama, KEK, Japan

*Abstract*

In high intensity proton synchrotrons, linear and nonlinear betatron resonances cause beam loss. When the betatron tune spreads over a resonance line, the betatron oscillation amplitude will get larger, causing large beam loss. Our study aims for a direct measurement of the betatron tune spread by using a quadrupole kicker and a four-electrode monitor. The monochromatic RF signal is transfered to the kicker and we induce an oscillation by kicking the beam. The amplitude of the quadrupole oscillation will depend on the number of particles having a certain tune. In the beam test at J-PARC MR, the dipole kicker was used as a quadrupole kicker by exciting the two facing electrodes in-phase. We measured the response to the kick at several frequencies. We observed that the amplitude of the quadrpole oscillation depends on the kicker frequency and the number of particles per bunch. This demonstrates that the quadrupole oscillation can be induced by a kicker and the possibility of measuring the number of particular tune particles from the response. We will present the result of the beam test and our prospect and the comparison between the experimental result and a numerical calculation.

## INTRODUCTION

J-PARC, Japan Proton Accelerator Research Complex, has a high intensity accelerator. J-PARC accelerator consists of three parts, LINAC (Linear accelerator), RCS (3 GeV Synchrotron) and Main Ring (30 GeV Synchrotron).

It is important to consider the beam loss upon increasing the beam power [1,2]. The beam loss is caused by the coherent motion and the incoherent motion of the beam. The incoherent motion is mainly induced by space charge, and this effect make the incoherent tune spread. In J-PARC, tune spread has estimated by not a direct measurement but a simulation. If tune spread can be measured, we can know a betatron bare tune which makes tune spread smaller than under current operation.

We aim for measuring tune spread caused by the space charge effect in this measurement. The response by a normal quadrupole kicker was measured in J-PARC MR.

When the beam run under an unideal operation, for instance the injection mismatch and the error field effect, the beam circulates involving the small quadrupole oscillation. After the injection, the beam width gradually increases until it becomes stable. Kickers, which use monochromatic RF signal and make the normal quadrupole force, kick the beam and induce the quadrupole oscillation.

## THE METHOD OF MEASUREMENT

This measurement was carried out on J-PARC MR. Table 1 shows the parameter of the used beam.

Table 1: Beam Parameter

| | |
|---|---|
| Horizontal tune | 22.40 |
| Vertical tune | 20.75 |
| Revolution frequency | 185743.5Hz |

Table 2: Kicker Setting Parameter

| | |
|---|---|
| Maximum power | 3kW×2 |
| RF frequency | 222854 Hz, 215854 Hz, 208854 Hz, 201854 Hz, 194854 Hz, 247615 Hz |
| Kicker angle | 102μrad / m / turn |

Table 3: Beam Intensity

| | The number of protons per bunch |
|---|---|
| (I) | $0.99(\pm0.01)\times10^{13}$ |
| (II) | $1.28(\pm0.01)\times10^{13}$ |
| (III) | $1.39\ (\pm0.02)\times10^{13}$ |

Two power amplifier are connected to kickers. The maximum power is 3 kW for each amplifier. Three kickers are arranged in series. The kicker consists of two electrodes in the vacuum pipe. We use it as a dipole kicker in the usual operation, but in this measurement, as a quadrupole kicker by exciting the two facing electrodes in-phase [3]. The beam passes through the kicker, particles having a certain tune oscillate larger. The relationship between a resonance tune of particles and the kicker RF frequency is given by Eq. (1), (2). [4]

$$2\nu_x = n_x \pm f_{RF}/f_{rev} \tag{1}$$

$$2\nu_y = n_y \pm f_{RF}/f_{rev} \tag{2}$$

$\nu_{x,y}$ is betatron tune in x and y direction, $n_{x,y}$ is an integer, $f_{RF}$ is the kicker RF frequency, and $f_{rev}$ is revolution frequency in MR.

The response is measured by four-electrode monitor [5]. Table 2 shows the parameters of kicker operation. Maximum power is sum of three kicker power. Two means the number of electrodes in each kicker. The angle gradient per turn is 102 μrad/m in this quadrupole kicker. The beam was kicked after 1s from the beam injection. This is because the beam is affected by the injection mismatch and the beam largely oscillates just after the injection. Figure 1 shows the



ISBN 978-3-95450-177-9

# NUMERICAL COMPARATIVE STUDY OF BPM DESIGNS FOR THE HESR AT FAIR

A. J. Halama, C. Böhme, V. Kamerdzhiev, F. Klehr, S. Srinivasan
Forschungszentrum Jülich, Germany

*Abstract*

The Institute of Nuclear Physics 4(IKP-4) of the Research Center Jülich (FZJ) is in charge of building and commissioning the High Energy Storage Ring (HESR) within the international Facility for Antiproton and Ion Research (FAIR) at Darmstadt. Simulations and numerical calculations were performed to characterize the beam position pickup design that is currently envisaged for the HESR, i.e. a diagonally cut cylindrical pickup. The behavior of the electrical equivalent circuit has been investigated with emphasis on capacitive cross coupling. Based on our findings, performance increasing changes to the design were introduced. A prototype of the BPM pickup was constructed and tested on a dedicated test bench. Preliminary results are presented. Another proposed design was characterized and put into comparison, as higher signal levels and higher position sensitivity are expected. That is a symmetrical straight four-strip geometry. Additionally an extensive study was conducted to quantify the effect of manufacturing tolerances. Driven by curiosity an eight-strip pickup design was considered, which would allow for beam size measurements, utilizing the non-linearity.

## CAPACITIVE PICKUPS

Capacitive pickups are widely used in particle accelerators as intensity and position monitors. Being non-destructive devices these pickups are of great interest especially in ring accelerators and those where beam may not be lost. Capacitive pickups such as the cylindrical diagonally cut electrodes facilitate the image current, which is influenced by the beam with close resemblance to a perfect current source, as it is mostly modelled in the equivalent circuit. Its pulse shape is given by the time derivative of the longitudinal beam recorded at the pickup location. As a design choice for the HESR the voltage of an electrode shall reflect the longitudinal time structure proportionally. For this case the main frequency contribution of the signal must lie above the cut-off frequency of the RC couple. This is achieved by the high input impedance of the attached preamplifier. The voltage of a centered beam is [1]:

$$U_{img}(t) = \frac{1}{\beta c C_{el}} \frac{A}{2\pi b} I_{beam}(t) \tag{1}$$

With $\beta$:=normalized velocity, c:= speed of light, A:= electrode inner surface area and b:= BPM radius. If at least two opposing electrodes are used, a linear response of the voltage versus the beam position can be seen in the centre region of nonlinear BPM such as strip types or buttons. Whereas the cylindrical diagonally cut BPM offers a linear response in the entire region. The linear response can be generalized as the normalized difference signal. Thus the difference over sum ratio is used to describe the linear behaviour [1][2]. For x and similarly y, with S being the sensitivity:

$$x = \frac{1}{S_x}\frac{U_r - U_l}{U_r + U_l} - x_{off} = \frac{1}{S_x}\frac{\Delta_x}{\Sigma_x} - x_{off} \tag{2}$$

To account also for higher order behaviour, ether a lookup table or use a two-dimensional polynomial can be used. For x and similarly y:

$$x = \sum_{i=1}^{N}\sum_{j=1}^{N} K_{x,ij}\left(\frac{\Delta_x}{\Sigma_x}\right)^i\left(\frac{\Delta_y}{\Sigma_y}\right)^j \tag{3}$$

### *Simulation Boundary Conditions and Formalism*

An equivalent circuit has been used to model the voltage response driven by a current source. The circuit evaluation for these studies was carried out using LTspice IV.

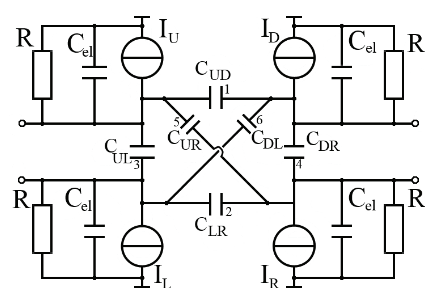


Figure 1: Equivalent circuit of a capacitive four electrode pickup.

For the case of 4 electrodes there are 10 capacitances, i.e. four capacitances against ground, which correspond to $C_{el}$ in Eq. (1). The remaining ones are interconnecting all electrodes, all as illustrated in Fig. 1. The capacitances for the presented results have been determined using COMSOL Multiphysics 5.0 AC/DC analysis, as it allows for static electric field simulations with fixed and floating potentials. The dependence on the beam position is introduced as a geometrical scaling factor, $\Gamma$, which would be $\Delta\phi/2\pi$, for a centred beam. It increases for a beam that approaches the electrode. $\Delta\phi$ is the average angular coverage. The scaling factor can be determined for any geometry.

$$\Gamma(\phi_1, \phi_2, r, \theta) = \frac{\int_{\phi_1}^{\phi_2} \frac{l_{BPM}(\phi)}{(\vec{r}_{BPM}(\phi)-\vec{r}_{Beam}(\theta))^2}\,\mathrm{d}\phi}{\int_{0}^{2\pi} \frac{l_{BPM}(\phi)}{(\vec{r}_{BPM}(\phi)-\vec{r}_{Beam}(\theta))^2}\,\mathrm{d}\phi} \tag{4}$$

With $\theta$ and $\vec{r}_{Beam}$ pointing at the beam. Eq. (4) has been derived empirically with the intention to reflect the position dependent influence, driven by the electrical field of the



ISBN 978-3-95450-177-9

# COMMISSIONING OF THE BUNCH-BY-BUNCH TRANSVERSE FEEDBACK SYSTEM FOR THE TPS STORAGE RING

Y. S. Cheng†, K. H. Hu, K. T. Hsu, C. H. Huang, C. Y. Liao
NSRRC, Hsinchu 30076, Taiwan

*Abstract*

Taiwan Photon Source (TPS) finished its Phase II commissioning in December of 2015 after installation of two superconducting RF cavities and ten sets of insertion devices in mid-2015. The storage ring achieved to store beam current up to 520 mA. Intensive insertion devices commissioning were performed in the second quarter of 2016 and delivered beam for beam-line commissioning and performed pilot experiments. One horizontal stripline kicker and two vertical stripline kickers were installed in May 2015. Bunch-by-bunch feedback system were commissioning in the last quarter of 2015 and the second quarter of 2016. Commercial available feedback processors and power amplifiers were selected for the feedback system integration. Beam property and performance of the feedback system were measured. Problems and follow-up measures are also addressed. Results will be summarized in this report.

## INTRODUCTION

The TPS is a 3 GeV synchrotron light source which was performed Phase I commissioning without insertion devices (ID) and with two 5-cell Petra cavities in the last quarter of 2004 and the first quarter of 2015 up to 100 mA stored beam [1]. Phase–II commissioning was done in the last quarter of 2015 with 10 sets of IDs and two KEKB-type superconducting RF modules and reached 520 mA stored beam maximum. Transverse coupled-bunch instability, caused by the resistive wall impedance and fast ion will deteriorate beam quality. Bunch-by-bunch feedback will suppress various transverse instabilities to ensure TPS achieve its design goals. Vertical bunch by bunch feedback loop was commissioning [2] in the first quarter of 2015 with prototype vertical kicker to test functionality includes feedback, bunch cleaning, single bunch transfer function, tune measurement. Power amplifier from AR and R&K were tested. One horizontal kicker and two vertical kickers were installed in the shutdown period of the second and the third quarter of 2015. Commissioning of both planes with insertion devices operation was started in the last quarter of 2015 and the second quarter of 2016.

Threshold current for the longitudinal instability appeared at ~80 mA when using with two 5-cell Petra cavities without insertion devices. Longitudinal instability disappeared up to 500 mA stored beam current during phase-II commissioning equip with two KEK-B type superconducting cavities with 10 sets of insertion devices in the last quarter of 2015. Transverse instabilities are dominated by wall resistivity and ion in TPS storage ring.

† cheng.ys@nsrrc.org.tw

## STATUS OF THE FEEDBACK SYSTEM

Two vertical kickers and one horizontal kicker were installed during mid-2015 shutdown. Concept of these kickers is derives from the design of PSI/SLS [3] and adapt to fit vacuum duct of TPS at ID straight. Length of the electrode is 300 mm. Shunt impedance at low frequency is about 40 kΩ and 25 kΩ for vertical and horizontal kicker respectively, Perspective drawing and installation at the storage ring are shown in Fig. 1. To save space to accommodate more insertion devices, all kickers install at upstream of in-vacuum undulator (IU22) at three 7 m long straight. Three kickers are distributed at three short straight. This prevents the option to install all feedback electronics at the same site. Three in-vacuum insertion devices were install at these kickers respectively.

The horizontal kicker was installed at upstream of SR03 (upstream straight of lattice cell #3), and two vertical kickers were installed at upstream cell SR11 and SR12. Feedback electronics for horizontal and vertical planes where installed at different areas in which shared RF front-end is impossible. The kicker electrodes are not well match to 50 Ohm. Measured impedance is around 75~95 Ohm between the feedthrough structure and electrode respect to the vacuum chamber. This leads to large broadband beam power picked up which prevent power amplifier work properly, high power low pass filter with cut off frequency 350 MHz were installed at each power amplifier output to block high frequency beam power to enter power amplifier output.

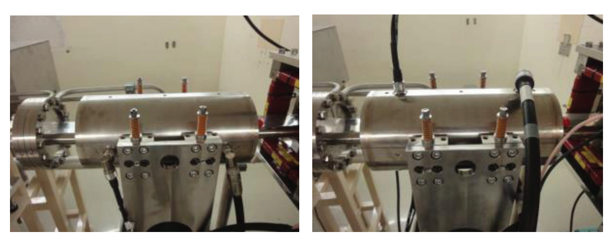

Horizontal kicker x 1 set  Vertical kicker x 2 sets

Figure 1: Transverse kickers install at upstream of three 7 m short straight which in-vacuum undulators located.

Feedback electronics of bunch-by-bunch equip feedback functionality, such as housing keep, filter design, timing adjustment, etc. It supports bunch oscillation data capture for analysis to deduce rich beam information, tune measurement, bunch clearing, beam excitation, etc. Features of the planned system include the latest high dynamic range ADC/DAC (12 bits), high performance FPGA, flexible signal processing chains, flexible filter design, bunch feedback, tune measurement, bunch



ISBN 978-3-95450-177-9

# HOM CHARACTERIZATION FOR BEAM DIAGNOSTICS AT THE EUROPEAN XFEL INJECTOR*

N. Baboi#, T. Hellert[1], L. Shi[2], T. Wamsat,
DESY, Hamburg, Germany
[1]also at The University of Hamburg, Hamburg, Germany
R.M. Jones[2], N. Joshi[2]
Cockcroft Institute, Daresbury, UK
[2]also at The University of Manchester, Manchester, UK

*Abstract*

Higher Order Modes (HOM) excited by bunched electron beams in accelerating cavities carry information about the beam position and phase. This principle is used at the FLASH facility, at DESY, for beam position monitoring in 1.3 and 3.9 GHz cavities. Dipole modes, which depend on the beam offset, are used. Similar monitors are now under design for the European XFEL. In addition to beam position, the beam phase with respect to the accelerating RF will be monitored using monopole modes from the first higher order monopole band. The HOM signals are available from two couplers installed on each cavity. Their monitoring will allow the on-line tracking of the phase stability over time, and we anticipate that it will improve the stability of the facility. As part of the monitor designing, the HOM spectra in the cavities of the 1.3 and 3.9 GHz cryo-modules installed in the European XFEL injector have been measured. This paper will present their dependence on the beam position. The variation in the modal distribution from cavity to cavity will be discussed. Based on the results, initial phase measurements based on a fast oscilloscope have been made.

## INTRODUCTION

Higher Order Modes (HOM) [1] are excited by electron bunches passing the superconducting accelerating cavities of the European X-ray Free Electron Laser (E-XFEL) in the north of Germany [2]. While HOMs can harm the beam, they can also be used for beam monitoring, since their properties depend on the beam properties, such as offset, charge and arrival time.

It is planned to build specialised monitors for the E-XFEL, on one hand for beam alignment and transverse position monitoring [3], and, on the other, for direct, on-line tracking of the beam phase with respect to the accelerating RF [3,4]. These monitors are currently under design [5,6], based on the experience at the Free Electron Laser in Hamburg (FLASH) [7]. There, monitors are installed at so-called TESLA accelerating cavities [3], as well as at 3rd harmonic cavities [8,9], working at 1.3 and respectively 3.9 GHz. The advantages of such monitoring are information on the beam at locations where there is no standard diagnostics, the relatively low cost, the possibility to align the beam in the cavities and reduce harmful HOMs. Also one can obtain information on the cavity alignment inside the cryo-module. The phase measurement will be the first direct, on-line measurement in superconducting cavities.

In the *European XFEL*, energetic electron pulses will produce extremely intense X-ray flashes in the undulator sections. The electrons are accelerated by ca. 100 superconducting cryo-modules, each containing eight cavities. Some of the main parameters of the electron beam are shown in Table 1.

Table 1: Main Parameters of the E-XFEL Electron Beam

| Electron beam parameter | |
|---|---|
| Max. energy [GeV] | 17.5 |
| Bunch charge [nC] | 0.02 - 1 |
| Max. bunch frequency [MHz] | 4.5 |
| Max. bunch number / pulse | 2700 |
| Pulse repetition frequency [Hz] | 10 |
| Max. pulse length [μm] | 600 |

While the commissioning of the complete accelerator is planned to start by the end of 2016, the first E-XFEL injector started operation in December 2015 [10]. This contains a 1.3 GHz and a 3.9 GHz cryo-module [11]. The latter shapes the bunch energy profile in order to increase the peak current.

A picture of a *TESLA and* a *3rd harmonic cavity* is shown in Fig. 1. The 1.3 GHz TESLA Nb cavity has 9 cells and is ca. 1 m long. RF power is input through the power coupler, while the HOM power generated by the beam is extracted through 2 special couplers mounted in the beam pipes at either end. The 3.9 GHz cavity is basically scaled down by a factor 3 from the TESLA cavity, except mainly the beam pipes which are larger. These enable the propagation of the HOMs through the entire eight-cavity module so that the HOM power is extracted more efficiently. Eight cavities are mounted in either type of module with the power coupler downstream. In this paper we name the cavities by their position within the module, e.g. C4 is the 4th cavity. H1 will denote the HOM coupler close to the input coupler (downstream for 1.3 GHz modules), and H2 at the other cavity end.

The *HOM-based beam position monitoring* idea relies on the fact that the dipole mode strength depends linearly on the beam position and charge. In the TESLA cavities, a dipole mode at ca. 1.7 GHz, with a high R/Q, giving the

* The work is part of EuCARD-2, partly funded by the European Commission, GA 312453
# nicoleta.baboi@desy.de

# DESIGN OF STRIPLINE BEAM POSITION MONITORS FOR THE ESS MEBT

S. Varnasseri, I. Bustinduy, A. Ortega, I. Rueda, A. Zugazaga, ESS Bilbao, Bilbao, Spain
R.A. Baron, H. Hassanzadegan, A. Jansson, T. Shea, ESS- ERIC, Lund, Sweden

*Abstract*

There will be overall 8 Beam Position Monitors (BPM) installed in the ESS MEBT. Seven of them will be used for the measurement of beam position, phase and intensity. One BPM will be used for the fast timing characterization of the chopped beam. The design is based on shortened stripline to accommodate the signal level for low velocity proton beam within MEBT. Due to mechanical space limits, all the BPMs are embedded inside quadrupoles; which requires special care on the magnetic properties of the materials within BPM sets and in particular the feedthroughs. The prototype electromagnetic and mechanical design is finished and its manufacturing is underway. This paper gives an overview of the electromagnetic and mechanical design and related analysis including position signal sensitivity of the BPMs.

## INTRODUCTION

ESS MEBT (Medium Energy Beam Transport) with energy of 3.62 MeV is part of the European Espallation Source (ESS) to be operational at Lund, Sweden early 2020 [1]. It requires various beam diagnostics instruments including the position, phase and intensity measurement devices. As part of the beam diagnostics instruments necessary for future commissioning and normal operation of accelerator, we have designed and manufactured a prototype of stripline beam position monitor (BPM). The proton beam has a repetition frequency of 14 Hz of pulses of 2.8 ms and nominal amplitude of 62.5 mA. The BPM pick ups are of stripline type which are housed inside quadrupole magnets (Figure 1). The main reason is due to lack of longitudinal mechanical space within compact MEBT to install all the BPMs. The BPM sensitivity to displacement, voltage signal level, frequency response and mechanical restrictions are the main factors in the design of stripline. Table 1 shows the main beam parameter related to BPM design analysis.

Table 1: BPM Related Beam Parameters

| Parameter | Value | Unit |
|---|---|---|
| Beam energy | 3.62 | MeV |
| Beam current (avg.) | 62.5 | mA |
| Particles/bunch | 1.1e9 | |
| Readout frequency | 704 | MHz |
| RF frequency | 352 | MHz |
| Bunch length | 60-180 | ps |
| Pulse length (max.) | 2.8 | ms |

In principle the second RF harmonic of 704.42 MHz of the electrode signal is used for BPM signal processing readout system. The BPM sensitivity with the nominal MEBT beam requires to be larger than 0.8 dB/mm and the voltage amplitude reaching to electronics has to be compatible with margin to input level of electronics. The design of stripline monitors is based on transmission line with 50 Ω characteristics impedance. Furthermore the bunch length is not fixed during the passage within MEBT, so the voltage amplitude on electrodes slightly varies depending on the physical location of BPMs. In the following sections, the electromagnetic design, characteristics and mechanical realization of the first prototype is described.

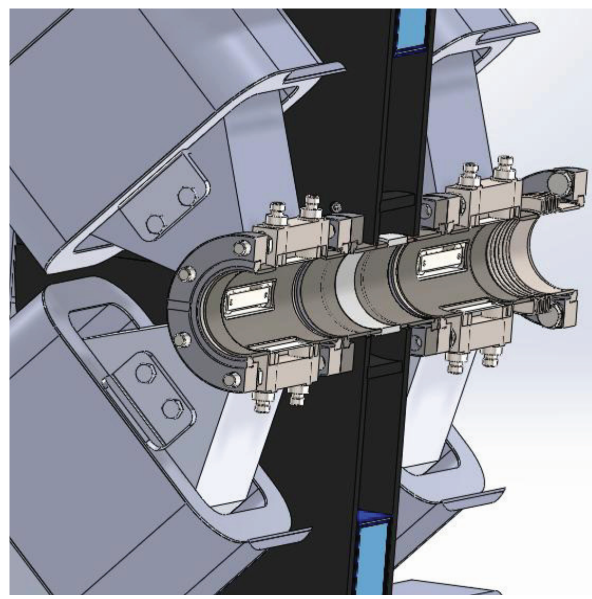

Figure 1: A CAD image of two BPM blocks embedded within two adjacent quadrupole magnets.

The overall BPM accuracy shall be smaller than +/-200 μm. This includes electronics errors, BPM sensor tolerances, errors of BPM welding on the beam pipe and alignment errors. Furthermore the BPM stripline shall be fabricated so that error contribution due to mechanical tolerances and electrodes imperfections does not exceed +/- 100 μm of the overall BPM accuracy. These values implied by other elements and overall tolerances within MEBT section.

## ELECTROMAGNETIC ANALYSIS

The bunches passing through the BPMs distributed within MEBT section vary in length at different locations. This will change the bunch charge frequency spectrum and therefore the BPMs will generate slightly different signal amplitudes at different physical locations. This is true also for the signal timing shape which goes out of the BPM striplines due to different frequency components.



ISBN 978-3-95450-177-9

# ORBIT FEEDFORWARD AND FEEDBACK APPLICATIONS IN THE TAIWAN LIGHT SOURCE

C.H. Kuo, P.C. Chiu, K.T. Hsu, K. H. Hu
NSRRC, Hsinchu 30076, Taiwan

*Abstract*

Taiwan Light Source (TLS) is a 1.5 GeV third-generation light source with circumference 120 meters. TLS is operated at 360 mA top-up injection mode. The storage ring is 6-fold symmetry with 6-meter straight sections for injection, RF cavity, and insertion devices. There are three undulators were installed in three straight sections to delivery VUV and soft X-ray for users. Beside there undulators, a conventional wiggler (W200 installed at straight sections to provide hard X-ray to serve user. Working parameters of hard X-ray sources are fixed without cause problem on operation. However, undulators should be changing its working parameters during user experiments performed. These undulators during its gap/phase changing will create orbit perturbation due to its field errors. Orbit feedback is main tool to keep orbit without change. However, some correctors setting of the orbit feedback system are easy to saturation due to large perturbation come from U90. To keep functionality of the orbit feedback system working in good condition, combines with orbit feedback and feed-forward is proposed and reported in this conference.

## INTRODUCTION

The current orbit feedback system was deployed in ten years ago. There are various correctors are installed in the storage of TLS. The corrector open loop gain is from 30 Hz to 100 Hz with vacuum chamber. Therefore, the orbit feedback system cannot be operated at full bandwidth. These correctors are shared with same power-supply for close orbit correction and feedback. The main setting range of corrector is for close orbit request. There is one fifth setting range of full scale for orbit feedback. That is easy to saturate for corrector. The main orbit perturbation source is from insertion device by the operation experience during the past twenty years. To accommodate fast operation of various insertion devices and provide better orbit stability, the BPM electronics and corrector power supplies are replaced step by step. Figure 1 shows the beam position reading during the phase change of EPU5.6 undulator with and without orbit feedback response at the R1BPM0 and R1BPM8 which are equipped with Libera Brillance [1,2]. Orbit perturbation due to EPU5.6 is suppressed by feedback system while high speed operation of the insertion devices is still restrained by low closed loop bandwidth of the orbit feedback system. The feed-forward orbit control for insertion is also applied with orbit feedback system to reduce corrector strength of orbit feedback and keep from saturation.

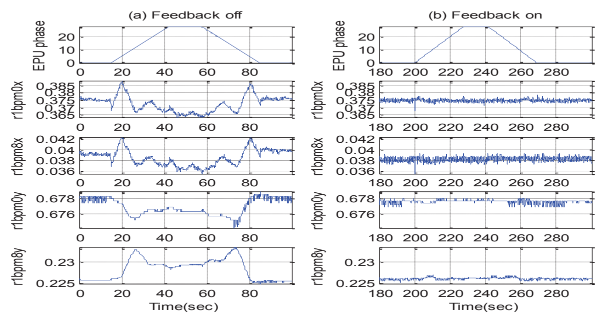


Figure 1: Effectiveness of the orbit feedback loop versus phase change of the EPU5.6 undulator. (a) without feedback; (b) with feedback.

To satisfy stringent orbit stability requirement of the TLS, low noise corrector power supply, and reliable orbit feedback system for long-term operation are necessary.

## FEEDBACK SYSTEM

### *BPM Electronics*

Libera Brilliance's integration had risen from 2007. The migration is gradually deployed not to interfere with the routine operation. To reduce GbE jitter and achieve better performance, numbers of Libera Brilliances are grouped together to produce a packed GbE UDP packet to reduce the number of IP packets. All Libera Brilliance will be grouped together [3].

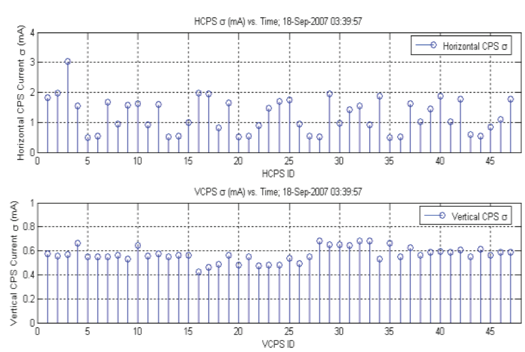


Figure 2: Power supply performance of the old power supply and the MCOR 30 power supply.

The corrector power supply is already replaced by MCOR 30. Standard deviation of the vertical power supplies (vertical corrector) and horizontal power supplies (horizontal corrector) in 100 sec readings are shown in Fig. 2. The power supply current readings of the vertical corrector power supply have the around 0.5 mA standard deviation since it is limited by the 16 bit ADC module.



ISBN 978-3-95450-177-9

# A HETEROGENEOUS FPGA/GPU ARCHITECTURE FOR REAL-TIME DATA ANALYSIS AND FAST FEEDBACK SYSTEMS

M. Vogelgesang*, L.E. Ardila Perez, M. Caselle, S. Chilingaryan, A. Kopmann, L. Rota, M. Weber
Karlsruhe Institute of Technology, Karlsruhe, Germany

*Abstract*

We propose a versatile and modular approach for a real-time data acquisition and evaluation system for monitoring and feedback control in beam diagnostic and photon science experiments. Our hybrid architecture is based on an FPGA readout card and GPUs for data processing. To increase throughput, lower latencies and reduce overall system strain, the FPGA is able to write data directly into the GPU's memory. After real-time data analysis the GPU writes back results back to the FPGA for feedback systems or to the CPU host system for subsequent processing. The communication and scheduling processing units are handled transparently by our processing framework which users can customize and extend. Although the system is designed for real-time capability purposes, the modular approach also allows standalone usage for high-speed off-line analysis. We evaluated the performance of our solution measuring both processing times of data analysis algorithms used with beam instrumentation detectors as well as transfer times between FPGA and GPU. The latter suggests system throughputs of up to 6 GB/s with latencies down to the microsecond range, thus making it suitable for fast feedback systems.

## INTRODUCTION

The repetition rates of modern linear accelerators such as European XFEL and TELBE [1, 2] cause increasing challenges for the development of detectors and beam diagnostics tools. With the recent developments of fast analog to digital readout systems, beam diagnostics has therefore become a big data problem. Although FPGAs emerged as ideal devices to perform on-line data analysis on large amounts of data, the implementation of particular data analysis algorithms still requires specific in-depth knowledge of the hardware and is, compared to software solutions, associated with significantly higher development costs despite efforts of FPGA vendors. At the same time, the data transmission link between the detector and the computational units or external storage is typically the bottleneck that limits the amount of data that can be processed in a given time frame.

Processing the acquired data off-line is a potential solution for most applications, however as soon as on-line monitoring or a feedback control loop is an essential part of the application, stable *real-time* data analysis with guaranteed low latencies is required. In case of on-line monitoring, data must be transferred to the processing machine as fast as possible with low variance in time. Conventional systems either based on a local temporary storage or network interconnects are not suitable due to insufficient transfer times.

* matthias.vogelgesang@kit.edu

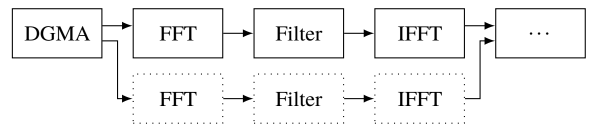


Figure 1: Overview of multi-GPU data stream processing: after inserting the data into a buffer within the DGMA filter, the data processing steps consisting of filtering in the frequency domain can be executed on separate GPUs for higher throughput.

In this paper, we will present a hardware/software architecture that bridges fast data acquisition using FPGAs and fast data processing with GPUs. Using direct memory accesses, we can decrease latency as well as increase throughput by utilizing the entire connection bandwidth. This data acquisition infrastructure is accessible from within our data processing framework which – in this particular use case – is used to analyse digitized spectrometer data in a heterogeneous compute environment. It automatically distributes data among multi-core CPUs and GPUs and uses multi-level parallelism to achieve a higher processing throughput than conventional single-threaded computing. The processing pipeline is flexible and can be re-arranged as well as extended by the user to accommodate for different applications. By adopting the proposed solution, the development time of a particular experimental setup can be reduced significantly.

## ARCHITECTURE

### *FPGA-based Data Acquisition Platform*

Our core data acquisition platform is based on our custom "Hi-Flex" FPGA board, that uses a Xilinx Virtex 7 device and is connected to the host computer through a PCI-Express (PCIe) 3.0 8-lane connection. The board has integrated DDR3 memory of 4 GB and an internal maximum throughput of 120 Gbit $s^{-1}$. Two industry standard FMC connectors (fully populated) are used to interface different mezzanine boards, which host the frontend electronics of different application-specific detectors such as 2D pixel detectors [3] or 1D linear array detectors [4]. The FPGA has an in-house developed Direct Memory Access (DMA) engine for PCIe 2.0 / 3.0 compatible with Xilinx FPGA families 6 and 7 supporting DMA data transfers between main system memory and GPU memory. The DMA engine is described in more detail in [5].

### *Data Processing Framework*

The basis for processing the input data in real-time is our heterogeneous data processing framework, initially devel-



ISBN 978-3-95450-177-9

# FAST ORBIT FEEDBACK WITH LINUX PREEMPT_RT

Yaw-Ren Eugene Tan, Australian Synchrotron, Clayton, Australia
Daniel de Oliveira Tavares, LNLS, Campinas, Brazil
David J. Peake, The University of Melbourne, Melbourne, Australia

*Abstract*

The fast orbit feedback (FOFB) system in development at the Australian Synchrotron (AS) [1] aims to improve the stability of the electron beam by reducing the impact of insertion devices and targeting orbit perturbations at the line frequency (50 Hz, 100 Hz and 300 Hz). The system is designed to have a unity gain at a frequency greater than 300 Hz with a simple PI controller with harmonic suppressors in parallel (as was done at Elettra). With most of the system in place (position aggregation, power supplies and corrector coils) we decided to implement a PC based feedback system to test what has been installed as well as the effectiveness of the proposed control algorithms while the firmware for the FPGA based feedback processor is being developed. This paper will report on effectiveness of a feedback system built with CentOS and the PREEMPT patch running on an Intel CPU.

## INTRODUCTION

The ultimate goal of the feedback system is to ensure that the transverse RMS beam motion up to 100 Hz is kept to less than 9.0 µm horizontally and 1.6 µm vertically.

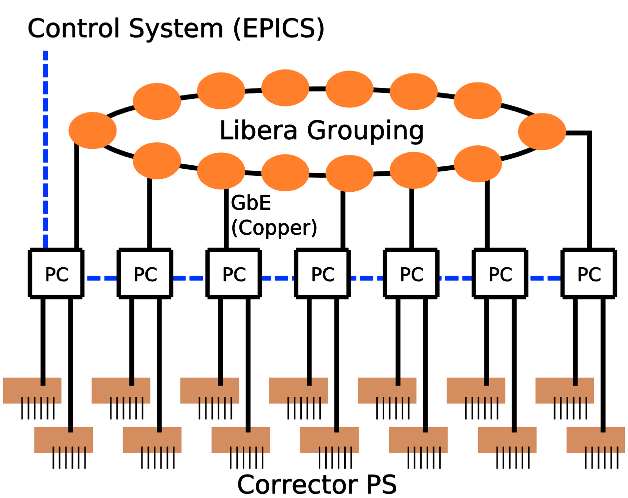


Figure 1: Distributed PCs processing the Fast Acquisition Data from the EBPMs and calculating the correction for the power supplies. No direct synchronisation between PCs. Control of the feedback system is through EPICS process variables running on a virtual server.

Figure 1 shows the distributed configuration of the seven PCs used to control the 14 power supplies around the storage ring. Each of the seven PCs receive real-time Fast Acquisition (FA) position data from the Libera Electron beam position processors (EBPMs), calculate and transmit the correction to the magnet power supplies through a 10 MBaud serial link. The synchronisation of the corrections between the PCs depends on the ability of the application to process the data in a repeatable time period and the synchronicity of the FA data transmitted by the EBPMs.

## LINUX PREEMPT_RT PATCH

To achieve a repeatable processing period, with a tolerance of 10s of µs, a "realtime" operating system is required. There are many potential candidates, such as RTEMS and VxWorks, however in the interest of minimising the development time, a decision was made to attempt it with our nominal production operating system at the AS (CentOS) with a PREEMPT_RT patched kernel.

The PCs use a PCI-x serial card by Axxon to communicate with the power supplies (the Linux serial driver had to be patched to get the card to operate at the maximum rate). The test the "realtime" nature of the operating system and applications, a test program was written to transmit data packets at a rate of 5 kHz (using *clock_nanosleep* to set the period) and the period of the transmitted serial data measured on an oscilloscope. The program was tested with CentOS 5 (kernel 2.6.29.6-rt24; Intel Core2 Q8400 2.66 GHz) and CentOS 7 (kernel 3.10.75-rt80; Intel Celeron G1840 2.80 GHz).

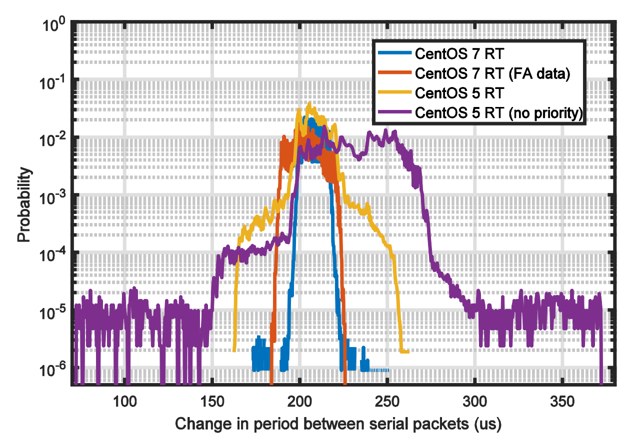


Figure 2: The newer kernel performs better and by setting a high scheduling priority the peak to peak jitter can be reduced to <100us. In the best case the peak to peak jitter is < 80 us with greater than 99.995% occurring within a 30 us window. If the serial output is triggered by the incoming FA data the jitter is subsequently worse due to jitter on the processing of the incoming data. (The sample size varies from 350k to 1300k).

The results of the measurements shown in Figure 2 indicate that upgrading from CentOS 5 to CentOS 7 reduces the jitter by almost half. In the best case more than



ISBN 978-3-95450-177-9

# DEVELOPMENT OF A PROTOTYPE ELECTRO-OPTIC BEAM POSITION MONITOR AT THE CERN SPS

A. Arteche*, A. Bosco, S. M. Gibson, Royal Holloway, University of London, Egham, UK
N. Chritin, D. Draskovic, T. Lefèvre, T. Levens, CERN, Geneva, Switzerland

*Abstract*

A novel electro-optic beam position monitor capable of rapidly (< 50 ps) monitoring transverse intra-bunch perturbations is under development for the HL-LHC project. The EO-BPM relies on the fast optical response of two pairs of electro-optic crystals, whose birefringence is modified by the passing electric field of a 1 ns proton bunch. Analytic models of the electric field are compared with electromagnetic simulations. A preliminary opto-mechanical design of the EO-BPM was manufactured and installed at the CERN SPS in 2016. The prototype is equipped with two pairs of 5 mm cubic $LiNbO_3$ crystals, mounted in the horizontal and vertical planes. A polarized CW 780 nm laser in the counting room transmits light via 160 m of PM fibre to the SPS, where delivery optics directs light through a pair of crystals in the accelerator vacuum. The input polarization state to the crystal can be remotely controlled. The modulated light after the crystal is analyzed, fibre-coupled and recorded by a fast photodetector in the counting room. Following the recent installation, we present the detailed setup and report the latest status on commissioning the device in-situ at the CERN SPS.

## MOTIVATION AND CONCEPT

An electro-optic beam position monitor (EO-BPM) is being developed for high frequency, intra-bunch measurements at the High-Luminosity Large Hadron Collider [1]. The main aim of the new instrument is to determine the mean transverse displacement along each $4\sigma = 1$ ns proton bunch, with a time resolution of < 50 ps. Existing head-tail monitors based on stripline BPMs are capable of measuring intra-bunch instabilities, with a bandwidth of 3–4 GHz that is limited by the pick-ups, cables and acquisition system [2]. In contrast, an EO-BPM is essentially a conventional button-BPM in which the pick-ups have been replaced with electro-optic crystals, to target bandwidths of 10–12 GHz or more, due to the fast optical response of the crystal in the transient electric field of the bunch.

The electro-optic response is measured using polarized light from a continuous wave, 780 nm laser source, housed away from the accelerator in the low radiation, accessible environment of a counting room. The light is conveyed in 160 m PM delivery fibre to collimation and polarization optics at each pick-up, and transmitted through the crystal, parallel to the particle beam direction. The light that emerges after the crystal typically has a different polarization state, due to the natural birefringence of the crystal. When the particle bunch passes, the electric field penetrates the crystal and via the Pockels effect, induces a change in the birefringence of the crystal, thus rapidly modifying the polarization state of the emerging light. An analyzer is placed after the crystal and the subsequent intensity of light is coupled into a return SM fibre and recorded by a fast photodetector. By taking the difference signal between pick-ups on the opposite sides of the beam pipe, the transverse displacement along the bunch can be deduced. In an alternative interferometric layout, coherent light is exploited to optically suppress the common mode signal, such that the detector directly measures the difference signal between the two pick-ups [1].

As a proof of these concepts, a prototype EO-BPM has been developed and was recently installed for tests in the CERN SPS. The following sections report on the detailed opto-mechanical design of the electro-optic pick-ups that were installed, including electromagnetic simulations of the geometry to assess the electric field strength penetrating the crystal. The installed layout in the CERN SPS is reviewed, including the fibre coupled, remotely controlled polarization optics. Finally, experimental validation of the sensitivity of the crystal to electric fields equivalent to those expected from the simulation is presented.

## ELECTRO-OPTIC PICK-UP DESIGN AND SIMULATION

### *Prototype Opto-Mechanical Design*

The conceptual design of the EO-BPM has compact, fibre-coupled optics directly mounted to the eo pick-up. For the CERN SPS prototype, however, a more flexible approach was decided, to enable reconfiguration and investigation of the polarization states. Therefore the fibre-coupled collimation and polarization optics were mounted on a small external breadboard adjacent to the pick-up, with light coupled into and out of the pick-up by a free space laser beam. The opto-mechanical design of the pick-up [3] is illustrated in Figure 1, showing the superposed path of the laser beam.

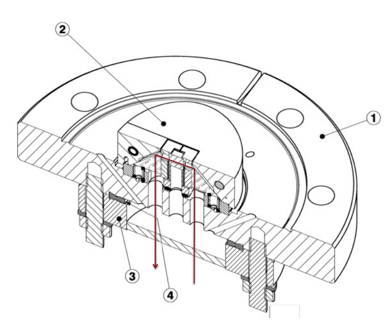


Figure 1: Laser beam trace inside the eo pick-up: 1. Flange. 2. Button. 3. Viewing port. 4. Copper gasket.

* alberto.arteche.2014@live.rhul.ac.uk



ISBN 978-3-95450-177-9

# PHASE AND ENERGY STABILIZATION SYSTEM AT THE S-DALINAC

T. Bahlo*, C. Burandt, L. Jürgensen, T. Kürzeder, N. Pietralla, J. Wissmann
Institut für Kernphysik, TU Darmstadt, Darmstadt, Germany
F. Hug, JGU Mainz, Germany

*Abstract*

The **S**uperconducting **Da**rmstadt **Lin**ear **Ac**celerator S-DALINAC is a recirculating electron accelerator with a design energy of 130 MeV operating in cw. Before entering the 30 MeV main accelerator the low energetic electron beam passes both a normal-conducting injector beamline preparing the beam's 3 GHz time structure as well as a superconducting 10 MeV injector beamline for preacceleration. Since the superconducting injector accelerates on-crest while the main accelerator accelerates off-crest the beam phase is crucial for the efficiency of the acceleration process and the minimization of the energy spread. Due to thermal drifts of the normal- conducting injector cavities this injection phase varies by about 0.2 degree over a timescale of an hour. In order to compensate for these drifts, a high level phase controller has been implemented. Additionally a low energy scraper system has been installed between the injector and main linac in order to lock both the phase and the energy spread at the linac entrance.

## MOTIVATION

The S-DALINAC (see Fig. 1) is a recirculating electron accelerator providing electron beams with energies up to 130 MeV in cw operation. It provides beam currents between several nA and 60 $\mu$A for nuclear structure and astrophysical experiments since 1987 [1]. The electron beam can be produced by two alternatively usable sources. The thermionic electron gun produces an unpolarized beam while the **S**-DALINAC **P**olarized **In**jector [2] creates polarized electron beams by illuminating a GaAs cathode with a laser beam. After beam preparation in the n.c. injector beamline including chopper and prebuncher cavities the electron bunches enter the s.c. 10 MeV injector. There the electrons are preaccelerated on-crest by niobium cavities working at a resonance frequency of 3 GHz. Leaving the s.c. injector the electron beam can either be used for nuclear resonance fluorescence experiments at the **D**armstadt **H**igh **I**ntensity **P**hoton **S**etup DHIPS [3] or it can be guided to the main accelerator by a 180°-arc. The main accelerator can be used up to four times using the three recirculations in order to reach the design energy of 130 MeV. It has been shown that the energy spread can be reduced significally from 120 keV to 30 keV by using a non-isochronous recirculating mode [4]. Theoretically this mode reproduces the same energy spread as before the first injection to the main linac. This depends heavily on the correct injection phase since a mismatch of 2° can increase the relative energy spread from $8 \cdot 10^{-5}$ to $3 \cdot 10^{-4}$. Experience shows that the beam phase behind the s.c. injector drifts and oscillates on a timescale of several hours. An example measurement of these dynamics without compensation can be seen in Fig. 2. The reason for these phase shifts still is not fully understood. One possible explanation are instabilities of the high voltage supply of the source, that already have been observed. Another possibility is a thermal drift of the n.c. beam preparation cavities. To compensate for these drifts a high-level phase controller has been developed. This controller now locks the exit phase of the s.c. injector. To decrease the energy spread even further an additional low energy scraper system has been installed. This system can eliminate the beam halo and it can prevent any energetically mismatched electrons leaving the s.c. injector. Furthermore it can reduce the energy spread of the beam arbitrarily but reduces the intensity simultaneously.

## PHASE CONTROLLER

To adjust the phase behind the s.c. injector it has to be changed before entering it. The following three devices have a significant influence on the exit phase, that has been measured by a rf monitor.

**Chopper** The Chopper forces the continuous electron beam of the electron gun on a cone-shaped trajectory that wanders over an aperture converting the continuous beam into a bunched one. This obviously defines the reference phase for every adjacent rf device.

**Prebuncher** The buncher cavity introduces a velocity gradient within every electron bunch by decelerating the early electrons and accelerating the late ones while leaving the reference particle's velocity unchanged. This focuses the bunch longitudinally after a defined distance. By shifting the buncher's phase an overall acceleration or deceleration can be introduced that changes the travel time to the injector entrance and therefore the entrance phase.

**s.c. 2-cell cavity** The 2-cell cavity is used to preaccelerate the low-energy electrons for the not sufficiently $\beta$-graded cavities of the injector. Although it is operated on-crest, it can be used similary to the buncher to adjust the exit phase using time-of-flight effects.

The results shown in Fig. 3 motivate the use of the buncher for beam phase adjustments since it is the most efficient and linear device that has been tested.

### *Implementation*

**Hardware** The low-level control system of the rf cavities is implemented on an in-house developed board [5]

* tbahlo@ikp.tu-darmstadt.de



ISBN 978-3-95450-177-9

# OPERATION OF THE BEAM POSITION MONITOR FOR THE SPIRAL 2 LINAC ON THE TEST BENCH OF THE RFQ

P. Ausset†, M.B. Abdillah, F. Fournier, IPN, Orsay, France
S.K. Bharade, G. Joshi, P.D. Motiwala, BARC, Mumbai, India
R. Ferdinand, D. Touchard, GANIL, Caen, France

*Abstract*

SPIRAL2 project is based on a multi-beam superconducting LINAC designed to accelerate 5 mA deuteron beams up to 40 MeV, proton beams up to 33 MeV and 1 mA light and heavy ions (Q/A = 1/3) up to 14.5 MeV/A. The accurate tuning of the LINAC is essential for the operation of SPIRAL2 and requires measurement of the beam transverse position, the phase of the beam with respect to the radiofrequency voltage, the ellipticity of the beam and the beam energy with the help of Beam Position Monitor (BPM) system. The commissioning of the RFQ gave us the opportunity to install a BPM sensor, associated with its electronics, mounted on a test bench. The test bench is a D-plate fully equipped with a complete set of beam diagnostic equipment in order to characterize as completely as possible the beam delivered by the RFQ and to gain experience with the behavior of these diagnostics under beam operation. This paper addresses the first measurements carried with the BPM on the D-plate: intensity, phase, transverse position and ellipticity under 750 KeV proton beam operation

## GENERAL DESCRIPTION OF SPIRAL2

SPIRAL2 facility is being installed in Caen, France. It includes a multi-beam driver accelerator (5mA/40Mev deuterons, 5mA/14.5MeV/A heavy ions). The injector is constituted by an ECR ion source (Q/A= 1/3), an ECR deuteron/proton source, a low energy beam transfer line (LEBT) followed by a room temperature RFQ which accelerates beam up to an energy of 0,75MeV/u. A medium energy transfer line (MEBT) transfers the beam to the superconducting Linac.

The Linac is composed of 19 cryomodules: 12 contain one β = 0.07 cavity and 7 contain two β = 0.12 cavities. All cavities in the cryomodules operate at F = 88.0525MHz.

The superconducting Linac is designed to accelerate deuterons, protons, heavy ions Q/A= 1/3 and Q/A = 1/6 for a future injector. (Table 1)

Table 1: SPIRAL 2 Main Beam Parameters

| Particle | Current Max (mA) | Energy (MeV/u) |
|---|---|---|
| Proton | 5 | 2 - 33 |
| Deuteron | 5 | 2 - 20 |
| Q/A = 1/3 | 1 | 2 - 14.5 |
| Q/A= 1/6 | 1 | 2 - 8 |

†ausset@ipno.in2p3.fr

SPIRAL2 nominal mode of operation is planned to be C.W. mode. The considerations on commissioning and tuning periods of the LINAC lead to consider also pulsed mode operation in order to minimize the mean power of the beam. The shortest duration of a macro-pulse will be 100 µs. The repetition rate may be as low as 1Hz and as high as 1 kHz. The intermediate configurations have to be taken in account in order to reach the C.W. operation. The step to increase or decrease either the macro pulse duration or the repetition rate will be 1µs.

## SPIRAL2 BEAM POSITION MONITORS

### General Description

A doublet of magnetic quadrupoles is placed between the cryomodules for the horizontal and vertical transverse focusing of the beam. Beam Position Monitors (BPM), of the electrostatic type, is inserted in the vacuum pipe located inside the quadrupoles of the LINAC.

Each BPM sensor contains four probes on which beam image currents induce bunched-beam electrical signals. The electronics board associated with each BPM sensor processes the electrical signals and enables the measurement of beam transverse position, phase, energy and transverse beam ellipticity$\sigma_x^2 - \sigma_y^2$, where $\sigma_x$ and $\sigma_y$ are the standard deviations of the transverse size of the beam.

### BPM Acquisition Modes

The BPMs data and measures are acquired under CW or pulsed mode operation in three modes: Normal, post mortem and electrode signal reconstruction.

A synchronizing signal “SF” is distributed simultaneously to the SPIRAL2 diagnostics, including the BPM to indicate that the beam is present during its high level.

Normal mode: the electronics module acquires the data on the SF rising edge after a delay and during a given integration time. The integration time must be less than the time where the SF signal is high. Both the delay and the integration times are selected by the operator.

Data: beam centroid transverse position and beam ellipticity, electrode received signal amplitude and vector sum in phase and magnitude of the four electrodes are transferred to the VME local memory on the fall of “SF” signal. EPICS driver reads the data every 200ms from the local VME memory.

### BPM Specifications

The main specifications for the BPM system are summarized in Table 2.



ISBN 978-3-95450-177-9

# A VERSATILE BPM SIGNAL PROCESSING SYSTEM BASED ON THE XILINX ZYNQ SOC*

R. Hulsart†, P. Cerniglia, N.M. Day, R. Michnoff, Z. Sorrell,
Brookhaven National Laboratory, Upton, Long Island, New York, USA

*Abstract*

A new BPM electronics module (V301) has been developed at BNL that uses the latest System on a Chip (SoC) technologies to provide a system with better performance and lower cost per module than before. The future of RHIC ion runs will include new RF conditions as well as a wider dynamic range in intensity. Plans for the use of electron beams, both in ion cooling applications and a future electron-ion collider, have also driven this architecture toward a highly configurable approach [1]. The RF input section has been designed such that jumpers can be changed to allow a single board to provide ion or electron optimized analog filtering. These channels are sampled with four 14-bit 400MSPS A/D converters. The SoC's ARM processor allows a Linux OS to run directly on the module along with a controls system software interface. The FPGA is used to process samples from the ADCs and perform position calculations. A suite of peripherals including dual Ethernet ports, µSD storage, and an interface to the RHIC timing system are also included. A second revision board which includes ultra-low jitter ADC clock synthesis and distribution and improved power supplies is currently being commissioned.

## SYSTEM ARCHITECTURE

A VME form factor was chosen for the initial design of this BPM system (Fig. 1), which leverages off of the existing VME infrastructure found throughout RHIC and its injector facilities. A VME bus interface was not included in the design, only power and serial timing links are distributed on the VME backplane. The V301 name designates it as a third-generation VME design.

## ANALOG INPUT SECTION

### Analog Filters

Much of the versatility available on this BPM platform is due to the options for the RF filtering section (Fig. 2). Three separate signal paths are available on the PCB which can be selected by altering soldered jumpers. For most ion beam measurements (RHIC), the pulse length which is received from the pickup electrodes is sufficient to be oversampled by the 400MSPS A/D converters, and so only a low-pass filter (nominally 39MHz) is used to remove unwanted high-frequency components. Filters with different cut-off frequencies can also be substituted,

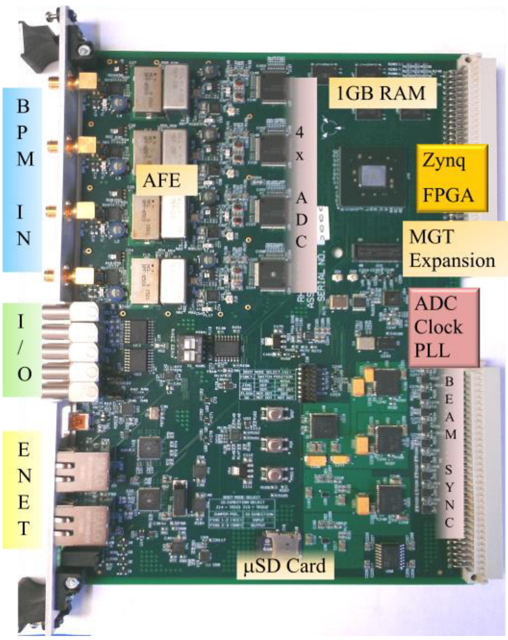


Figure 1: BPM Electronics

such as a 200MHz low pass which has been used for the BLIP raster BPM. The second and third signal paths are used to connect band pass filters of different package styles, used for measuring very narrow electron beam pulses. When used for low-repetition rate or single-bunch e-beam measurements the ringing response of a 503MHz filter is used to extend the sampling period. Narrowband processing at other frequencies is also possible by choosing similar band pass filters in the same package style. A smaller footprint SAW type band pass filter centered at 707MHz is the third option which will find use in the LEReC project which uses a 704MHz bunch frequency.

Low pass filters (nominally 800MHz) are also included at the board input and around each gain stage, to remove any high-frequency noise and/or aliased frequencies.

### Gain and Attenuation

Each RF input channel has a set of two gain stages, nominally +20dB each. An Analog Devices RF amplifier (ADL5536) is used, which has a good response over the frequency range, and only uses a single +5V supply. Before each of the gain stages, a 7-bit programmable digital step attenuator allows adjustments in 1/4dB increments, from 0-31.75dB of attenuation. In addition, each gain stage can be bypassed by moving soldered jumpers. This is important for applications (such as RHIC stripline BPMs) where large input signals are present and high gain is not necessary.

*Work supported by Brookhaven Science Associates, LLC under Contract No. DE-AC02-98CH10886 with the U.S. Department of Energy
† rhulsart@bnl.gov

# A FPGA BASED COMMON PLATFORM FOR LCLS2 BEAM DIAGNOSTICS AND CONTROLS*

J. Frisch, R. Claus, M. D'Ewart, G. Haller, R. Herbst, B. Hong, U. Legat, L. Ma, J. Olsen, B. Reese, L. Ruckman, L. Sapozhnikov, S. Smith, T. Straumann, D. Van Winkle, J. Vasquez, M. Weaver, E. Williams, C. Xu, A. Young.
SLAC National Accelerator Laboratory, Menlo Park CA USA

*Abstract*

The LCLS2 is a CW superconducting linac driven X-ray free electron laser under construction at SLAC. The high beam rate of up to 1MHz, and ability to deliver electrons to multiple undulators and beam dumps, results in a beam diagnostics and control system that requires real time data processing in programmable logic. The Advanced Instrumentation for Research Division in the SLAC Technical Innovation Directorate has developed a common hardware and firmware platform for beam instrumentation based on the ATCA shelf format. The FPGAs are located on ATCA carrier cards, front ends and ADC /DAC are on AMC cards that are connected to the carriers by high speed serial JESD links. External communication is through the ATCA backplane, with interlocks and low frequency components on the ATCA rear transition module (RTM). This platform is used for a variety of high speed diagnostics including stripline and cavity beam positon monitors (BPMs).

## KEY FEATURES

A new instrumentation / control platform has been developed for LCLS2 in order to provide the following features that were not all available with existing platforms:

- Ethernet communication within a c to simplify hot-swapping and control of distributed systems.
- Timing data stream distributed to all application cards to allow beam parameter dependent processing.
- Analog front ends integrated with ADCs / DACs, but separate from digital systems to allow digital and analog engineers to work independently and to provide independent upgrade paths
- Large application card area with vertical space for RF shielding to simplify the design of high performance RF systems
- High system density with efficient use of rack space for analog connections.
- Widely-used telecom hardware.

## HARDWARE OVERVIEW

The "Common Platform" is based on the Advanced Telecommunications Computing Architecture [1] (ATCA) that is widely used in industry. The SLAC common platform is based on the following components (figure 1, 2):

- ATCA Shelf: This is the "crate" that holds the electronics cards, power supplies, etc.
- Backplane: Provides high speed data connections from all cards to slots 1 and 2.
- Management: Provides IPMI for shelf components (commercial)
- Network Switch: This is an ATCA carrier card that is located in slot 1 with access to Ethernet to each carrier card, and which provides a 10Gb, or 40Gb uplink. (typically commercial, custom also available)
- Carrier Card: This card contains a FPGA and has serial connections to the backplane Ethernet, and to the RTM and dual AMC cards. The carrier card also contains DC-DC power supplies from the -48V to a variety of voltages used by the AMC cards.
- AMC card: These contain the analog front ends, ADCs and DACs, and timing chips
- RTM card: These are connected directly to the FPGA on the carrier card and are used for miscellaneous I/O and network connections.

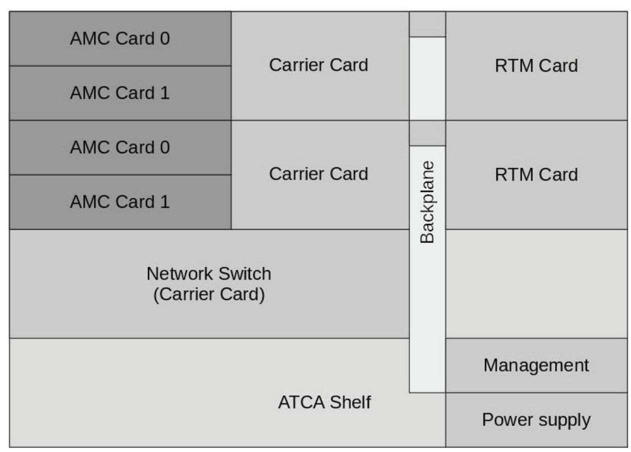


Figure 1: Common platform components.

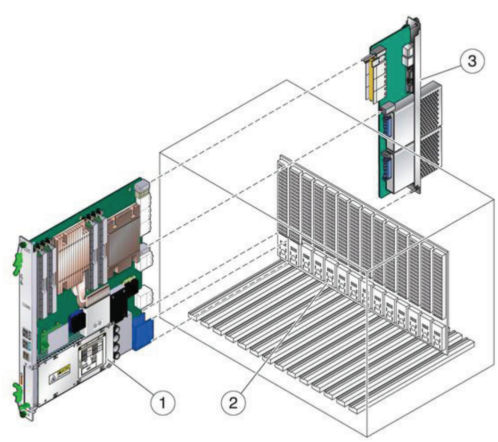


Figure 2: ATCA shelf and cards.

*Work supported by US Department of Energy, Office of Science under contract DE-AC02-76SF00515



ISBN 978-3-95450-177-9

# THE SLAC LINAC LLRF CONTROLS UPGRADE*

D. Van Winkle†, M. D'Ewart, J. Frisch, B Hong, U. Legat, J. Olsen, P. Seward, J. Vasquez, SLAC National Accelerator Laboratory, Menlo Park, USA


*Abstract*

The low level RF control for the SLAC LINAC [1] is being upgraded to provide improved performance and maintainability. RF control is through a high performance FPGA based DDS/DDC system built on the SLAC ATCA common platform. The klystron and modulator interlocks are being upgraded, and the interlocks are being moved into a combination of PLC logic and a fast trip system. A new solid state sub-booster amplifier will eliminate the need for the 1960s vintage high RF phase shifters and attenuators.


## OVERVIEW

The legacy RF system at SLAC has been in operation for over 50 years. Despite working extremely well for many years, many parts of the system are showing signs of wear including effects as esoteric as copper erosion in some water cooled chassis. A rough block diagram of the legacy RF system is shown below in Fig. 1.

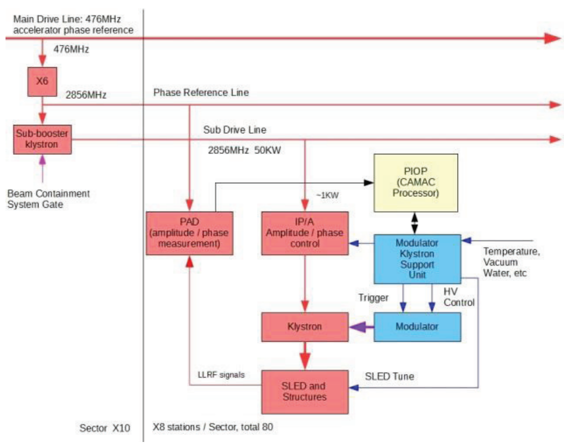


Figure 1: Legacy RF system.

To mitigate these effects and to provide for upgradeability well into the future, the US Department of Energy is investing in upgrading the system using modern FPGA based technology. When upgrading a system such as this, many conflicting requirements must be met at once. During the design process, many platforms were evaluated for applicability and maintainability. We evaluated: VME, PXI, mTCA for physics, ATCA, and conventional chassis. At the same time this evaluation was going on for LLRF upgrades at SLAC, the diagnostics, machine protection and other groups were evaluating their own common platform solution and had decided on ATCA as their platform of choice. Because of that decision and our own evaluations, it was decided that the system will be designed into the ATCA platform. A high level block diagram of the new LLRF system is shown in Fig. 2.

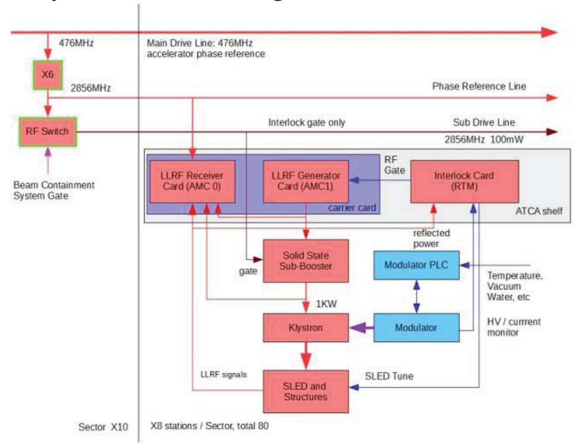


Figure 2: Upgraded RF system.

## DETAILS OF NEW SYSTEM

The system is being designed into a new platform based upon the telecommunications system ATCA [2]. The system incorporates two advanced mezzanine cards (AMC cards) which plug into a carrier card that contains the FPGA for all signal processing functions. The overall common platform system allows for enough flexibility that the design can be used for other diagnostic and machine protection functions simply by designing other AMC cards with the specific functionality required for those systems. Further details of the common platform system are covered at another paper in this conference [3].

### *Specifications and Backwards Compatibility*

The LLRF system has to completely replace the old system which was based upon CAMAC controls and other custom chassis within the larger LINAC system. In addition, the system will not be able to be upgraded as a whole at one time; the design incorporates a method for upgrading as little as one station at a time. To that end, there are several requirements on the new system for it to fit into the existing infrastructure of beam containment (BCS), timing systems and other legacy systems:

- The new system must maintain compatibility with the existing BCS system without compromising the beam containment functions as currently implemented.
- The new system must replace the legacy Modulator Klystron Support Unit (MKSU) that serves to protect the high power pulsed klystrons and modulators.
- The new system must use solid state sub-boosters for each Klystron, rather than the legacy sector (8 klystron) sub-booster klystron.

* Work supported by US Department of Energy, Office of Science under contract DE-AC02-76SF00515
† dandvan@slac.stanford.edu



ISBN 978-3-95450-177-9

# BATCH APPLICATIONS OF DIGITAL BPM PROCESSORS FROM THE SINAP *

L.W. Lai, F.Z. Chen, J. Chen, Z.C. Chen, Y.B. Leng#, Y.B. Yan, W.M. Zhou
SSRF, SINAP, Shanghai, China

*Abstract*

During the past several years a digital BPM (DBPM) processor has been developed at the SINAP. After continuous development and optimization, the processor has been finalized and has come to batch application on the signal processing of cavity BPMs and stripline BPMs at the Dalian Coherent Light Source (DCLS) and the Shanghai Soft X-ray FEL (SXFEL). Tests have been done to evaluate the performances, such as the noise level, the SNR and the cross talk. The system resolution of the cavity and stripline BPMs can achieve 1um and 10um respectively. The test results on the Shanghai Deep-Ultra-Violet (SDUV) and the DCLS will be introduced.

## INTRODUCTION

A prototype of the DBPM has been developed successfully at the SINAP during the past few years [1~5]. Some tests and applications have been carried out at the Shanghai Synchrotron Radiation Facility (SSRF)[6]. Since 2015, two FEL facilities, DCLS and SXFEL, have been under constructions. Dozens of stripline BPMs and cavity BPMs are planted along the LINAC accelerators and the undulators. To handle the BPM data acquisitions and the position calculations, a new in-house BPM processor has been designed.

The main system structure of the previous DBPM has been kept for the new design, and some optimizations and modifications are implemented aiming at the application on FEL. Figure 1 is an overview of the system structure. It consists of 4 input RF signal conditioning blocks, 4 analogue to digital converters (ADC), a digital signal processing module, and a CPU running control system.

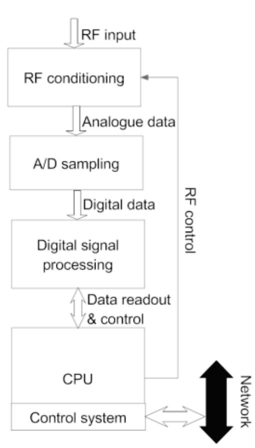


Figure 1: DBPM processor architecture.

*Work supported by National Natural Science Foundation (No. 11305253, 11575282)
#lengyongbin@sinap.ac.cn

## HARDWARE DESIGN

The processor includs four input channels, and it mainly consists of three boards: a carrier board implementing the RF conditioning and digitizer with ADCs, a mother board holds FPGA and other peripheral components and interfaces, and an ARM board conducting system control (as shown in Figure 2).

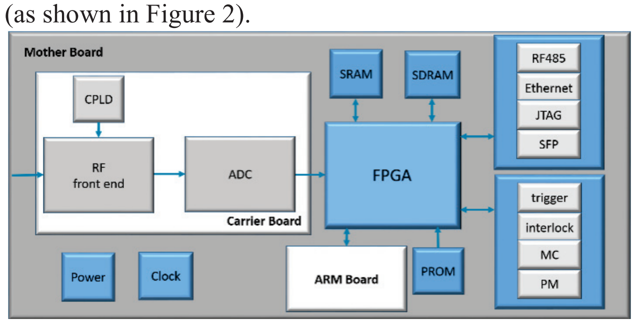


Figure 2: Hardware diagram.

### *RF Carrier Board*

There are four input channels on RF carrier board. Each channel has two functions: the RF conditioning and the ADC digitizer. Figure 3 is the signal conditioning flow of one channel. The brief descriptions are:

- Two surface acoustic wave (SAW, TFS500A) bandpass filters, whose centre frequencies are 500MHz and their 3dB bandwidths are 12MHz.
- Three low pass filters (LFCN-575) located at different processing sections.
- Three fixed amplifiers and one 31dB digital step attenuator with 31dB dynamic range, which is controlled by a CPLD on the board.

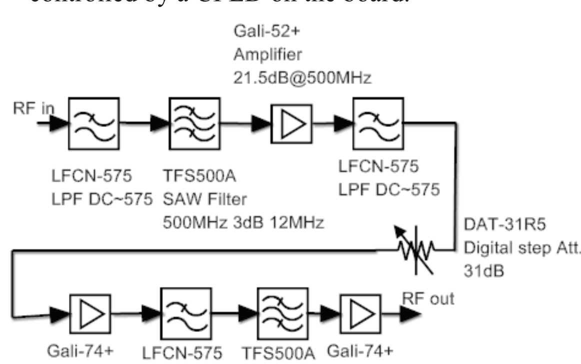


Figure 3: RF conditioning flow.

After conditioning, the RF signal is digitized by a 16bits ADC at the rate is 117.2799MHz. Clock source can be selected to be internal or external.



ISBN 978-3-95450-177-9

# CAVITY BPM SYSTEM FOR DCLS*

Jian Chen, Jie Chen, Longwei Lai, Yongbin Leng†, Yingbin Yan, Luyang Yu, Renxian Yuan,
SSRF, SINAP, Shanghai, China

*Abstract*

Dalian Coherent Light Source (DCLS) is a new FEL facility under construction in China. Cavity beam position monitor (CBPM) is employed to measure the transverse position with a micron level resolution requirement in the undulator section. The design of cavity, RF front end and data acquisition (DAQ) system will be introduced in this paper. The preliminary measurement result with beam at Shanghai Deep ultraviolet (SDUV) FEL facility will be addressed as well.

## INTRODUCTION

In order to meet the growing demands of the biological, chemical and material science research, an increasing number of FEL user facilities have been constructed and being proposed in the world. Dalian Coherent Light Source is a extreme ultraviolet (EUV) coherent light source based on ultra-fast lasers and electron accelerator techniques, it will be the first FEL user facility operating exclusively in the EUV wavelength region based on the principle of high-gain harmonic generation (HGHG) scheme and the aim is to generate the FEL radiation with wavelength range from 50 to 150 nanometer [1].

The DCLS facility is located in the northeast of China and under commission now. The entire facility consists of the following parts:

1. A photo-injector will produce electron pluses of 500 pC with normalized emittance below 1 mm • mrad.
2. The linear accelerator will accelerate the electrons to 300 Mev which consists of 6 S-band accelerator structures and a movable chicane for electron bunch compression.
3. The undulator complex where the seed laser induces an energy modulation for the electron beam in the modulator and then converted into a density modulation in the dispersion chicane, a selected higher harmonic is then amplified in the radiator to generate the FEL radiation with wavelength of 50 ~ 150 nm.
4. The photo beam line and diagnostic line.

For the electron beam in the undulator section, the demanded position resolution is less than 1 um@0.5nC because the electron beam and the generated photo beam must be overlapped in the undulator section for sufficient FEL interaction between them. In SXFEL and DCLS, a C-band cavity BPM worked at 4.70 GHz for both position cavity and reference cavity is employed in order to achieve this requirement. In total, 10 CBPMs were utilized in the undulator sections of the DCLS. The schematic layout is shown in Fig. 1.

*Work supported by National Natural Science Foundation of China (No.11575282 No.11305253)
†lengyongbing@sinap.ac.cn

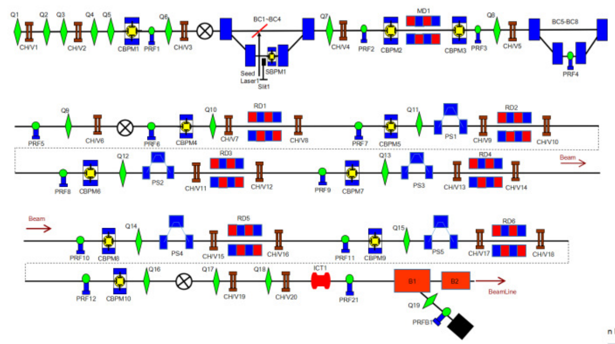

Figure 1: Schematic layout of CBPMs in the undulator section.

The CBPM system of DCLS is comprised of cavity pickup, a dedicated RF front end and DAQ system. Fig. 2 show the diagram of the system. More details and relevant results are described in the following section.

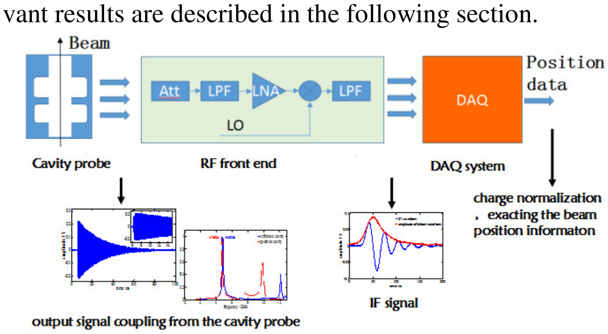


Figure 2: Diagram of the CBPM system.

## DESIGN AND FABRICATE OF THE CAVITY PICKUP

A low Q factor cavity BPM was designed and tested in the last year [2,3], although it has the strengths of high efficient coupling structure and better SNR but the performance was limited by the DAQ system due to the short duration time about 2~5 ns. Considering the single-bunch working mechanism both in SXFEL and DCLS, we redesigned a high Q factor CBPM to matching with the electronics for getting a better performance. Table 1 illustrate the high Q factor CBPM design parameters.

Table 1: Design Parameters of the CBPM

| Parameter | TM110 | TM010 |
|---|---|---|
| Frequency | 4.70 GHz | 4.70 GHz |
| Q | ~ 8000 | ~ 8000 |
| Number of ports | 4(X:2, Y:2) | 2 |

Comparing to the low Q cavity we designed before, the material changes from stainless steel of 304 to oxygen-

ISBN 978-3-95450-177-9

# CONCEPTUAL DESIGN OF LEReC FAST MACHINE PROTECTION SYSTEM*

S. Seletskiy†, Z. Altinbas, M. Costanzo, A. Fedotov, D. M. Gassner, L. Hammons, J. Hock, P. Inacker, J. Jamilkowski, D. Kayran, K. Mernick, T. Miller, M. Minty, M. Paniccia, I. Pinayev, K. Smith, P. Thieberger, J. Tuozzolo, W. Xu, Z. Zhao
BNL, Upton, USA

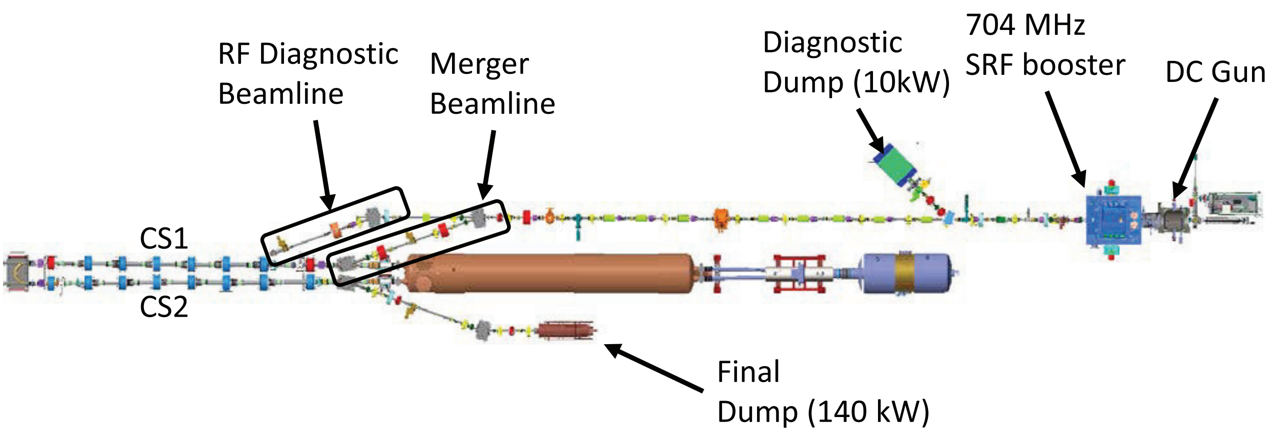


Figure 1: LEReC layout.

*Abstract*

The low energy RHIC Electron Cooling (LEReC) accelerator will be running with electron beams of up to 110 kW power with CW operation at 704 MHz. Although electron energies are relatively low (< 2.6 MeV), at several locations along the LEReC beamline, where the electron beam has small (about 250 um) RMS radius design size, it can potentially hit the vacuum chamber with a large incident angle. The accelerator must be protected against such a catastrophic scenario by a dedicated machine protection system (MPS). Such an MPS shall be capable of interrupting the beam within a few tens of microseconds. In this paper we describe the current conceptual design of the LEReC MPS.

## LEREC LAYOUT AND PARAMETERS

The LEReC accelerator [1] consists of the 400 keV DC photo-gun followed by the 1.6-2.4 MeV SRF Booster, the transport line, the merger that brings the beam to the two cooling sections (CS1 and CS2) and the cooling sections followed by the 140 kW dump. The LEReC also includes two dedicated diagnostic beamlines: the low-power beamline capable of accepting 10 kW beam and the RF diagnostic beamline.

The LEReC layout is schematically shown in Fig. 1.

We are planning to start the gun commissioning in the winter of 2017 with the short beamline that does not include the SRF Booster and ends at 10 kW beam dump.

The LEReC beam train consists of 9 MHz macro-bunches. Each macro-bunch consists of $N_b$=30 bunches repeated with 704 MHz frequency. The length of each bunch at the cathode is 80 ps. The charge per bunch ($Q_b$) can be as high as 200 pC.

We will have the ability to work with macro-bunch trains of various length (Δt), various number of macro-bunches per train ($N_{mb}$), and various time delay (T) between the trains.

Also, as an alternative to our nominal operational mode with continuous train of 9 MHz macro-bunches, we will have the capability to run a continuous wave (CW) of 704 MHz bunches.

Table 1: LEReC Beam Modes

| Beam modes | Goals |
|---|---|
| Low Current Mode (**LCM**) $Q_b$=30-130 pC; $N_b$ = 30; $N_{mb}$ = 1; T = 1 s | Optics commissioning: beam trajectory, beam envelope, rough RF setting, emittance measurement |
| RF Studies Mode (**RFSM**) $Q_b$=130 pC; $N_b$ = 10,15,20,25,30; Δt ≤ 250 us; T = 1 s - 10 s | RF fine-tuning. Study beam longitudinal dynamics. |
| Transitional Mode 1 (**TM1**) $Q_b$=130 pC; $N_b$ = 30; Δt ≤ 1000 ms; T = 1 s | Gradual transition from LCM to HCM with nominal $Q_b$. |
| Transitional Mode 2 (**TM2**) $Q_b$=30 - 130 pC; $N_b$ = 30; | Alternative to TM1 |
| High Current Mode (**HCM**) $Q_b$=130 pC; | Get to the design parameters |
| CW mode (**CWM**) $Q_b$=50 pC; 704 MHz CW | Alternative to HCM |

* Work supported by Brookhaven Science Associates, LLC under Contract No. DE-AC02-98CH10886 with the U.S. Dept. of Energy.
† seletskiy@bnl.gov

# AN OPTICAL FIBRE BLM SYSTEM AT THE AUSTRALIAN SYNCHROTRON LIGHT SOURCE

M. Kastriotou*[1, 2], E.B. Holzer, E. Nebot del Busto [1, 2], CERN, Geneva, Switzerland
[1] also at University of Liverpool, Liverpool, UK
[2] also at Cockcroft Institute, Warrington, UK
C.P. Welsch, Cockcroft Institute, Warrington; University of Liverpool, UK
M. Boland, SLSA, Clayton, Australia; University of Melbourne, Australia

*Abstract*

Increasing demands on high energy accelerators are triggering R&D into improved beam loss monitors with a high sensitivity and dynamic range and the potential to efficiently protect the machine over its entire length. Optical fibre beam loss monitors (OBLMs) are based on the detection of Cherenkov radiation from high energy charged particles. Bearing the advantage of covering more than 100 m of an accelerator with only one detector and being insensitive to X-rays, OBLMs are ideal for electron machines.

The Australian Synchrotron comprises an 100 MeV 15 m long linac, an 130 m circumference booster synchrotron and a 3 GeV, 216 m circumference electron storage ring. The entire facility was successfully covered with four OBLMs. This contribution summarises a variety of measurements performed with OBLMs at the Australian Synchrotron, including beam loss measurements during the full booster and measurements of steady-state losses in the storage ring. Different photosensors, namely Silicon Photo Multipliers (SiPM) and fast Photo Multiplier Tubes (PMTs) have been used and their respective performance limits are discussed.

## INTRODUCTION

Optical fibre beam loss monitors comprise an optical fibre coupled to a photosensor. Their operation principle is the detection by the photosensor, of Cherenkov photons [1], which are generated in the fibre by high energy charged particles produced through a beam loss. With the advantages of covering long distances while being sensitive to electrons and insensitive to X-rays, these monitors can be favorable for the machine protection of light sources.

The position reconstruction of OBLMs for electron storage rings has been discussed in past studies [2]. In the present paper the potential of covering the complete machine and the performance of OBLMS during normal operation of a light source is examined at the Australian Synchrotron Light Source.

## EXPERIMENTAL SETUP

### *The Australian Synchrotron*

In the Australian Synchrotron [3], electrons are generated in a 500 MHz thermionic gun and enter a 15 m linac, which accelerates them to 100 MeV. The electrons are then injected into a 130 m booster ring that further accelerates them up to 3 GeV. During the last few tens of milliseconds of the 600 milliseconds ramping cycle, the closed orbit is altered via a slow bumping technique. This allows the beam to be centered at the extraction point within the field of the fast magnet that kicks the beam into the Beam To Storage ring (BTS) transfer line. At the end of the BTS, another kicker magnet injects the beam into Sector 1 of a 216 m circular storage ring that consists of 14 sectors with a double bend achromat lattice. Sector 11 contains the beam scrapers used to concentrate the beam losses at this location and so protect the multiple insertion devices located elsewhere in the ring.

During standard operation, the storage ring holds a beam current of 200 mA, injected in trains of 75 bunches and a current of approximately 0.5 mA. Nominally, the beam fills 300 out of the 320 available 500 MHz buckets. Beam lifetimes as good as 200 hours can be reached. When operating in single bunch mode, the bunch charge can be varied in the range of $10^{+5} - 10^{+9}$ electrons [4].

### *Installation*

The entire accelerator complex of the Australian Synchrotron Light Source was covered for the observation of beam losses with a set of only four optical fibres. Each fibre consists of a 200 µm pure silica core, 245 µm cladding and a 345 µm acrylate coating. A dark nylon jacket provides protection against ambient light and mechanical breakage.

The schematic of the installed cables and their respective photon sensors is shown in Fig. 1. Two fibres were installed symmetrically on the inner and outer side of the linac, each covering half of the booster ring. One of these also covered a large fraction of the BTS transfer line as well as the booster extraction point. Only one optical end of each of these fibres is extracted to the roof of the facility, at Sector 2. The other two fibres cover half of the storage ring, each with photosensors installed in both ends [2].

### *Photosensors*

Two types of photosensors have been examined in the present study: A Hamamatsu fast photomultiplier tube (H10721-10) and a Silicon Photomultiplier (Multi Pixel Photon Counter S12572-015C) [5]. The latter is coupled to a transimpedance amplifier (comprised of a Texas Instruments THS3061 operational amplifier [6] and a feedback resistor)

* maria.kastriotou@cern.ch

ISBN 978-3-95450-177-9

# RELATION BETWEEN SIGNALS OF THE BEAM LOSS MONITORS AND RESIDUAL RADIATION IN THE J-PARC RCS

M. Yoshimoto#, H. Harada, M. Kinsho, K. Yamamoto
J-PARC, JAEA, Tokai, Ibaraki, 319-1195, Japan

*Abstract*

To achieve routine high power MW-class beam operation requires that the machine activations are within a permissible level. Thus, our focus has been to reduce and manage beam losses. Following the issues with the ring collimator in April 2016, the GM counter now measures the residual dose along the ring. These detailed dose distributions can now provide more details of the beam loss. Here, a new BLM is proposed that detects the spot area beam loss to determine the relation between the residual dose distribution and the beam loss signals. The new BLM will allow for a detailed map of the beam losses.

## INTRODUCTION

The 3-GeV Rapid Cycling Synchrotron (RCS) of the Japan Proton Accelerator Research Complex (J-PARC) accelerates protons from 400 MeV to 3 GeV kinetic energy at 25 Hz repetition rate. The average beam current is 0.333 mA and the design beam power is 1 MW [1]. In addition, the RCS has two functions as a proton driver for neutron/muon production at the Material and Life science experimental Facility (MLF) and as a booster of the Main Ring synchrotron (MR) for the Hadron experimental facility (HD) and Neutrino experimental facility (NU). In order to maintain such routine high power MW-class beam operation, the machine activations must be kept within a permissible level. Therefore, we adopt a ring collimator system to remove the beam halo and localize the beam loss at the collimator area [2]. Fig. 1 shows the schematic view of the RCS ring and the ring collimator system. The RCS ring collimator system consists of a primary collimator, also referred to as "scatter", which scatters the halo particles, and five secondary collimators, so-called "absorbers", which absorb those scattered particles.

During April, 2016, the ring collimator system experienced serious trouble. A collimator control system failure occurred followed by a vacuum leak at the secondary collimator no. 5 (Col-Abs. no. 5). In order to restart the user beam operation, the Col-Abs. no. 5 was replaced with spare ducts, which did not have radiation shielding. In addition, as a precaution, every other collimator from this system must be stopped. As a result, it is difficult to maintain localization of the beam loss in the RCS after the restart of the beam operation. Therefore, a series of particle tracking experiments were carried out to examine how the particles were lost under various collimator arrangements. The change in the beam loss profile and variations in the radiation dose were estimated in advance. After solving the problem with the collimator, we tried tuning the beam to minimize the beam loss without adjusting the collimator. Subsequently, the user beam operations are restarted [3]. In addition, we measured the residual dose along the ring every short maintenance period to investigate the influence of the collimator trouble.

In this paper, we report measurement results of the residual dose distribution along the ring. The relation between the residual dose distribution and the beam loss signals indicates new knowledge of the RCS beam loss sources and mechanism. In addition, we introduce a new beam loss monitor (new BLM), which detects the spot area beam loss to evaluate the residual radiation of the ring.

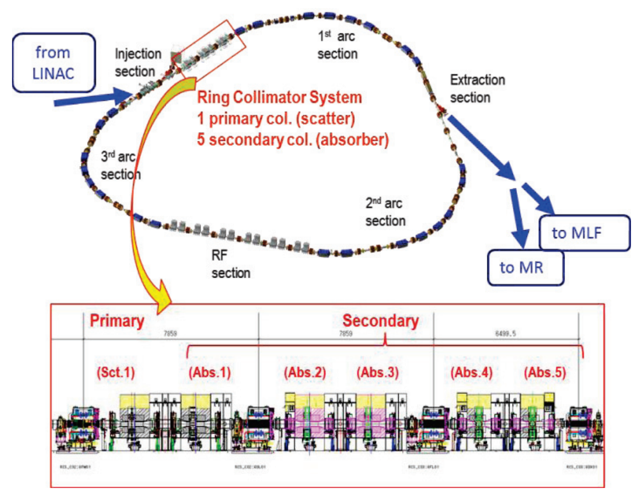


Figure 1: Schematic view of the Japan Proton Accelerator Research Complex (J-PARC) rapid cycling synchrotron (RCS) and the ring collimator system.

## RESIDUAL DOSE MEASUREMENT

The beam loss profiles along the ring were predicted to change drastically due to the replacement of the Col-Abs. no. 5 with the spare ducts. Thus, detailed distributions of the residual dose along the ring were measured using a Geiger–Müller counter and compared with the distribution of the beam loss signals obtained by proportional counter-type beam loss monitors (P-BLMs). Fig. 2 shows the comparison between the beam loss signals and the residual dose distributions on four sides of the duct along the ring. The P-BLMs are installed along the ring and beam lines, and they are mainly used in the interlock system for machine protection [4]. The P-BLM signals are integrated and archived at every beam-shot. The RCS has a threefold symmetric lattice that partitions

# yoshimoto.masahiro@jaea.go.jp

ISBN 978-3-95450-177-9

# EVALUATING BEAM-LOSS DETECTORS FOR LCLS-2*

Alan S. Fisher#, Clive Field, Ludovic Nicolas, SLAC, Menlo Park, California 94025, USA

*Abstract*

The LCLS x-ray FEL occupies the third km of the 3-km SLAC linac, which accelerates electrons in copper cavities pulsed at 120 Hz. For LCLS-2, the first km of linac will be replaced with superconducting cavities driven by continuous RF at 1300 MHz. The normal-conducting photocathode gun will also use continuous RF, at 186 MHz. The laser pulse rate will be variable up to 1 MHz. With a maximum beam power of 250 kW initially, and eventually 1.2 MW, the control of beam loss is critical for machine and personnel safety, especially since losses can continue indefinitely in linacs, and dark current emitted in the gun or cavities can be lost at any time. SLAC protection systems now depend on ionization chambers, both local devices at expected loss sites and long gas-dielectric coaxial cables for distributed coverage. However, their ion collection time is over 1 ms, far slower than the beam repetition rate. We present simulations showing that with persistent losses, the space charge of accumulated ions can null the electric field inside the detector, blinding it to an increase in loss. We also report on tests comparing these detectors to faster alternatives.

## INTRODUCTION

### *LCLS and LCLS-2*

The Linac Coherent Light Source (LCLS) is an x-ray free-electron laser (FEL) that began operation in 2009 [1]. It occupies the third kilometer of SLAC's 3-km copper room-temperature linac. Both the linac and the photo-cathode radio-frequency (RF) gun are pulsed at 120 Hz with 2856 MHz. The first km of the linac was removed in the past year to make way for LCLS-2, which will use continuous 1300-MHz RF in superconducting cavities, with a normal-conducting photocathode RF gun at 186 MHz and a bunch rate of up to 1 MHz. Operation will begin (before upgrades) at an electron energy of 4 GeV and a beam power of 250 kW, increasing to 1.2 MW. Table 1 compares the parameters of both machines.

### *Beam Loss and Safety Systems*

Beam-loss instrumentation follows a tiered structure. During normal operation, diagnostics monitor and locate sources of loss, and aid in tuning. The machine protection system (MPS) blocks the beam or halts it if losses exceed a threshold, or for other causes (insertion of an obstacle such as a valve, an excessive temperature). Beam containment (BCS) stops the accelerator if a loss of beam current or radiation from beam loss would indicate possible harm to people or to devices like protection collimators. Safety-systems detectors are deployed in twos for redundancy.

Table 1: Parameters of the LCLS Normal-Conducting Linac and the LCLS-2 Superconducting Linac

| **Parameter** | **LCLS** | **LCLS-2** |
|---|---|---|
| Electron energy | 15 GeV | 4 (later 8) GeV |
| Bunch charge | 20 to 250 pC | 20 to 250 pC |
| Beam power | 450 W | **0.25 (later 1.2) MW** |
| Gun frequency | 2856 MHz | 185.7 MHz |
| Linac frequency | 2856 MHz | 1300 MHz |
| RF pulse rate | 120 Hz | Continuous |
| $e^-$ bunch rate | 120 Hz | 92.9 (later 929) kHz |
| Photon energy | 0.2 to 5 keV | 1 to 15 (later 25) keV |

The detectors discussed here are evaluated primarily for BCS, but their signals will be split outside the tunnel for independent processing for BCS, MPS, and diagnostics.

The highest level of protection, the personnel protection system (PPS), interlocks access to the machine and shuts it off if radiation is found in occupied areas. PPS instrumentation will not be further considered here.

Unlike LCLS, which has 8 ms (a 120-Hz period) to shut off, LCLS-2 has continuous RF. Losses must be detected in as little as 100 µs, after which the beam must be shut off within 100 µs (see Table 2). Losses can arise from high-power photocurrent, or from dark current due to field emission in the gun or linac modules. Dark current can be emitted at any time and can travel through several cryomodules in either direction depending on the RF phase at emission.

## IONIZATION DETECTORS

BCS at SLAC has long relied on two types of ionization detector. We describe these here and discuss whether ion collection is sufficiently fast for LCLS-2.

### *Protection Ion Chamber (PIC)*

A PIC is a point loss detector, placed within 0.5 m of a site such as a collimator needing protection against damage. Figure 1 shows the design, a stainless-steel cylinder containing a stack of 32 plates biased alternately at ground or (typically) −300 V. At this voltage, collection of electrons takes 2 µs, but ions require 1 ms.

Both the PICS and the LIONs discussed next are generally filled to 125 to 150 kPa with a mixture of 95% Ar and 5% $CO_2$. However, the LCSL-2 model and the experiment (both discussed below) use 100% Ar.

*SLAC is supported by the U.S. Department of Energy, Office of Science, under contract DE-AC02-76SF00515
#afisher@slac.stanford.edu

ISBN 978-3-95450-177-9

# BEAM DIAGNOSTICS FOR CHARGE AND POSITION MEASUREMENTS IN ELI-NP GBS

G. Franzini†, F. Cioeta, O. Coiro, D. Pellegrini, M. Serio,
A. Stella, A. Variola, INFN-LNF, Frascati (Rome), Italy
A.Mostacci, S. Tocci, University of Rome "La Sapienza", Rome, Italy

*Abstract*

The advanced source of Gamma-ray photons to be built in Bucharest (Romania), as part of the ELI-NP European Research Infrastructure, will generate photons by Compton back-scattering in the collision between a multi-bunch electron beam and a high intensity recirculated laser pulse. An S-Band photoinjector and the following C-band Linac at a maximum energy of 720MeV, under construction by an European consortium (EurogammaS) led by INFN, will operate at 100Hz repetition rate with trains of 32 electron bunches, separated by 16ns and a 250pC nominal charge. The different BPMs and current transformers used to measure transverse beam position and charge along the LINAC are described. Design criteria, production status and bench test results of the charge and position pickups are reported in the paper, together with the related data acquisition systems.

## INTRODUCTION

The ELI-NP GBS (Extreme Light Infrastructure-Nuclear Physics Gamma Beam Source) is a high intensity and monochromatic gamma source under construction at IFIN-HH in Magurele (Romania). The photons will be generated by Compton back-scattering at the interaction between a high quality electron beam and a high power recirculated laser. Two interaction regions are foreseen: one with electrons accelerated up to 280 MeV (low Energy LINAC), the other with electrons up to 720 MeV (high Energy LINAC). The LINAC will deliver a high phase space density electron beam, whose main parameters are listed in Table 1 and depicted in Figure 1 [1].

Table 1: Main Characteristics of the GBS Electron Beam

| Parameter | Value |
|---|---|
| Maximum Energy | 720 MeV |
| Macro Pulse rep. rate | 100 Hz |
| Number of bunches per Macro Pulse | up to 32 |
| Bunch Spacing | 16.1 ns |
| Bunch Length ($\sigma_t$) | 0.91 ps |
| Bunch Charge | 25 pC – 250 pC |

Various diagnostics devices have been foreseen to be installed in the LINAC, in order to measure the properties of both the macropulses and the single bunches. Both intercepting and non-intercepting type of measurements will be implemented. The devices used for the intercepting type of measurements are Optical Transition Radiation (OTR) screens. A total of 23 stations will be installed along the LINAC: 12 on the Low Energy LINAC, 11 on the High Energy LINAC. They will be used to measure the Beam Position (Centroid) and the Spot Size of the beam. They will also be used to measure the beam energy and its spread, the bunch length and the Twiss parameters, in conjunction with a dipole, an RF deflector and quadrupoles respectively.

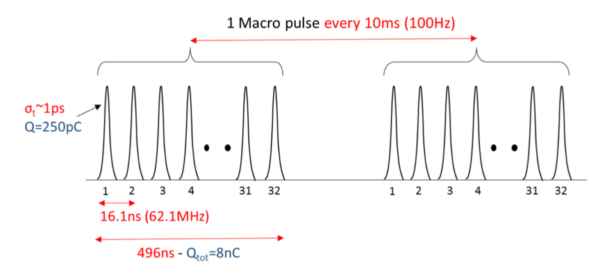


Figure 1: GBS Electron Beam representation.

The devices used for non-intercepting measurements are Beam Charge Monitors (BCM) and Beam Position Monitors (BPM).

The former ones are based on the Integrating Current Transformers (ICT) [2], which will be installed in 4 different positions (3 in the low energy LINAC, 1 in the high Energy LINAC).

Concerning the Beam Position Monitors, two different types will be installed: Stripline Beam Position monitors are the most common. 29 of them will be installed, specifically 13 in the Low Energy LINAC, 16 in the High Energy LINAC. Moreover, near the interaction points (both at low energy and high energy), a total of 4 Cavity Beam Position Monitors will be installed (see Fig.2).

## BEAM CHARGE MONITORS

Beam charge monitors (BCM) will be installed in four positions: the first one will be located right before the first S-band accelerating structure; the second one will be located at the end of all the accelerating structures of the Low Energy LINAC, before the so-called "dogleg"; the third and the fourth will be installed before the low energy and the high energy interaction points. These four locations will allow studying the losses of charge of the beam at the key-points of the LINAC.

BCMs will have the capability to measure the charge of every single bunch, within the macro pulse. The ICT [2] (see Fig.3) could be seen as a band-pass filter and the passage of the beam bunches could be considered as the input signal.

# COMMISSIONING RESULTS OF THE TOP-IMPLART 27 MeV PROTON LINEAR ACCELERATOR*

P. Nenzi†, A. Ampollini, G. Bazzano, L. Picardi, M. Piccinini, C. Ronsivalle, V. Surrenti, E. Trinca, M. Vadrucci, ENEA C.R. Frascati, Frascati, Italy

*Abstract*

The results of a 27MeV proton LINAC commissioning are presented. The LINAC, operating at the ENEA Frascati Research Center, consists of a 425MHz injector followed by a 3GHz booster. The injector is a commercial LINAC, the PL7 model produced by ACCSYS-HITACHI, composed by a duoplasmatron proton source with einzel lens, a 3MeV RFQ (Radio-Frequency Quadrupole) and a 7MeV DTL (Dritf-Tube LINAC). Wide injection current range (0-1.5mA) is obtained varying extraction and lens potentials. The booster LINAC consists of sequence of 3 SCDTL (Side-Coupled DTL) modules whose output energies are 11.6MeV, 18MeV and 27MeV, respectively. Each of the 3 modules requires less than 2MW peak power. All modules are powered by a single 10MW peak-power klystron. The output beam has been characterized at 10Hz PRF (Pulse Repetition Frequency) using fast AC transformers, Faraday cup and ionization chamber for current (and, by integration, charge) monitoring, whereas energy has been measured using a novel detector based on LiF (Lithium-Fluoride) crystals. Systematic measurements have been performed to investigate the sensitivity of output beam to machine operating parameters (SCDTL temperatures, stability of injector and RF power) highlighting the existing correlations. The LINAC is part of a 150MeV protontherapy accelerator under development in the framework of the TOP-IMPLART Project.

## INTRODUCTION

TOP-IMPLART (Terapia Oncologica con Protoni – Intensity Modulated Proton Linear Accelerator for Radio Therapy) is a Regione Lazio (local government) founded project [1] for the development of a compact-size proton LINAC for cancer treatment with the main characteristics shown in table 1.

Table 1: TOP-IMPLART Accelerator Characteristics

| Parameter | Value |
|---|---|
| Depth in tissue (max) | 15 g/cm$^2$ |
| Proton energy (max) | 150 MeV |
| Dynamic energy variability | 90-150 MeV |
| Dose rate | 1-10 Gy/min |

The TOP-IMPLART LINAC, is a 150MeV pulsed accelerator, under development at the ENEA Frascati Research Center, where it is currently under assembling and testing, inside a dedicated 30 meter concrete bunker.

* Work supported by Regione Lazio, agreement TOP-IMPLART Project
† paolo.nenzi@enea.it

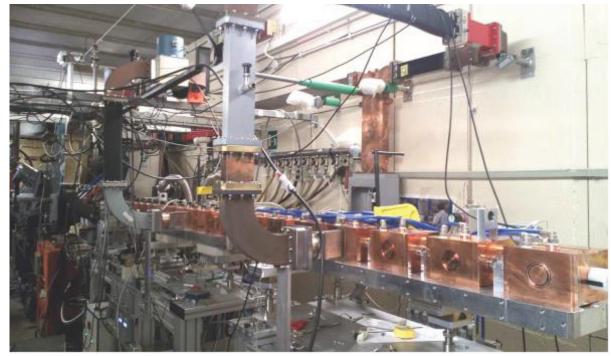

Figure 1: Actual layout of the TOP-IMPLART LINAC.

TOP-IMPLART is composed by two main sections: a commercial 7 MeV injector, produced by AccSys-Hitachi company, operating at 425 MHz, followed by a high-frequency booster operating at 2997.92 MHz designed by ENEA. The two frequencies have no harmonic relation and, thus, no RF synchronization between the sections has been adopted.

The injector is composed by a duoplasmatron ion source followed by an RFQ and a DTL. The booster is composed by SCDTLs [2,3] up to 65 MeV and CCLs up to 150 MeV. Actually only three, of the four SCDTLs (see Fig. 1) in the medium energy section are operational, reaching an output energy of 27MeV, with the fourth SCDTL expected to be installed by the end of the year, to reach 35MeV. The principal design parameters of the medium energy section are summarized in Table 2. The four SCDTLs are powered by a single TH2090 klystron tube (15MW peak-power, 15kW average) installed into a PFN (Pulse Forming Network) modulator developed in around 1990. Klystron and modulator have been adapted to the requirements of the TOP-IMPLART project and integrated into the accelerator.

The pulse length is 15µs-80µs for the injector and, 1µs-4µs for the booster. The PRF can be varied between 1 and 100Hz. In its present layout, closed loop feedback is fully operational in the duoplasmatron source (current control) and in the RFQ (frequency, phase and amplitude feedback), and only partially in the DTL (only frequency and phase feedback). The booster section operates in open-loop.

Table 2: Medium Energy Section Characteristics

| SCDTL # | 1 | 2 | 3 | 4 |
|---|---|---|---|---|
| # tanks | 9 | 7 | 7 | 5 |
| Cells/tanks | 4 | 5 | 6 | 6 |
| Bore Hole diameter (mm) | 4 | 4 | 5 | 5 |
| Total Length (m) | 1.12 | 1.1 | 1.4 | 1.1 |
| Output Energy (MeV) | 11.6 | 18 | 27 | 35 |



ISBN 978-3-95450-177-9

# UPGRADES TO THE LANSCE ISOTOPE PRODUCTION FACILITIES BEAM DIAGNOSTICS *

H. Watkins, D. Baros, D. Martinez, L. Rybarcyk, J. Sedillo, R. Valicenti,
Los Alamos National Laboratory, 87545, USA

*Abstract*

The Los Alamos Neutron Science Center (LANSCE) is currently upgrading the beam diagnostics capability for the Isotope Production Facility (IPF) as part of an Accelerator Improvement Project (AIP). Improvements to measurements of: beam profile, beam energy, beam current and collimator charge are under development. Upgrades include high density harps, emittance slits, wire-scanners, multi-segment adjustable collimator, data acquisition electronics and motion control electronics. These devices will be installed and commissioned for the 2017 run cycle. Details of the hardware design and system development are presented.

## INTRODUCTION

### *IPF Purpose*

The purpose of the Isotope Production Facility (IPF) is to produce isotopes, not commercially available, for research, development and treatment in the United States. They currently produce Strontium-82 isotopes for cardiac imaging as well as a variety of other isotopes used for medical treatment and study. The isotopes produced at IPF impact approximately 30,000 patients per month [1]. The facility uses beams at 41, 72 and 100MeV for isotope production.

### *IPF Upgrades*

The IPF facility is planning an upgrade as part of its scheduled beam window replacement in 2017. This upgrade is focused on increasing yield of the facility, reducing programmatic risk and improving beam diagnostics. The improved diagnostics capability will ensure that the beam profile, intensity and incident energy are well understood in an effort to improve target survival at increased beam currents [2].

## PROFILE MEASUREMENTS

Three upgrades to beam profile measurements will be completed as part of the IPF upgrade. The existing harp will be replaced with a higher resolution device. An emittance measurement and wire scanner measurement will be added upstream of the harp. These measurements will be placed at three separate locations along the IPF drift length to characterize the beam. The harp will serve a dual purpose as both a profile measurement and a collector for emittance.

*Work supported by the U.S. Department of Energy, Contract No. DE-AC52-06NA25396 LA-UR-16-26712

### *Actuators*

The IPF beam line transitions from a 4” diameter beam pipe to a 6” diameter beam pipe after the raster magnets and prior to the target. The challenge for actuators in these locations is the large stroke length required to scan wires and harps. This sets a requirement for actuators to achieve a 20 cm stroke and 1 mm scan resolution. Figure 1 shows three new designs created to meet the profile measurement requirements that all used a common off the shelf (COTS) slide table and actuation stage.

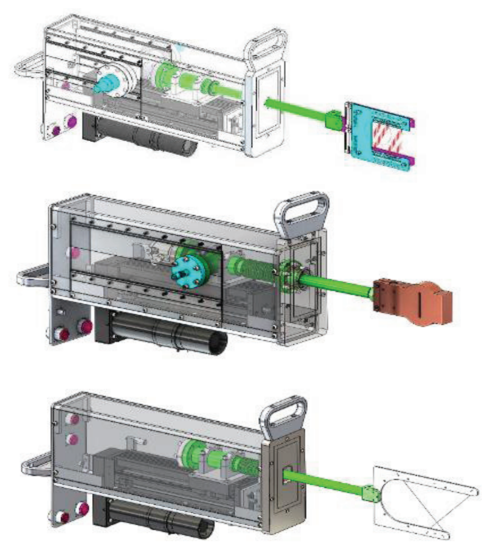

Figure 1: Three Types of Actuators

### *High Density Harp*

Another challenge of the IPF upgrade was the high density harp. The requirements were to design a device with a 7.6cm profile width and 1mm wire resolution. The harp head assembly needs 77 wires in both the horizontal and vertical planes.

The harp head design achieved this high density requirement by using a dual sided printed circuit board (PCB) that spaced wires 2 mm apart on each side. Figure 2 shows how the hook and spring were used to tension a silicon carbide (SiC) wire across the PCB.



ISBN 978-3-95450-177-9

# FIRST HEATING WITH THE EUROPEAN XFEL LASER HEATER*

M. Hamberg†, Uppsala University, Uppsala, Sweden,
F. Brinker, M.Scholz, DESY, Hamburg, Germany

*Abstract*

The EU-XFEL laser heater is installed and commissioning phase is ongoing. In this paper I discuss the steps undertaken and report the first heating of electron beams observed in the injector section.

## INTRODUCTION

The European XFEL is a 3.4 km long free-electron laser (FEL) which will deliver radiation in the wavelength regime of 0.05 to 4.7 nm. To avoid problems with longitudinal micro bunching instabilities a laser heater is implemented. The interaction region is located in a chicane and consists of a 0.7 m permanent magnet undulator in which IR-laser pulses are overlapping electron bunches during the passage and induces a phase space modulation. When the electron bunches leave the chicane section via two bending magnets the modulation is smeared out and leave a net "heating effect". This in turn increases the overall stability and therefore the overall brightness level of the FEL. The principle has previously been proven [1-2].

The EU-XFEL Laser Heater is a Swedish in kind contribution and has earlier been described in detail [3-5]. In this paper I report the commissioning steps undertaken and the first recorded heating outputs observed in the injector section and finish with a conclusion and outlook.

## USER INTERFACE

Most of the Laser Heater features are controlled through the DESY Distributed Object Oriented Control System (DOOCS) control system via the JAVA DOOCS DATA DISPLAY (JDDD) interface [6-7]. The interface displays the laser heater in a schematic way. Each optical station such as the laser laboratory on level 5 in the injector building, optical stations 0 and 1 (OS0 & OS1 close before and after the interaction region on level 7 respectively) can easily be operated separately.

## PRECONDITIONING

Given the default electron energy of 130 MeV, a laser wavelength ($\lambda_L$) of 1030 nm and the wiggler period ($\lambda_w$) of 7.4 cm the undulator gap had to be 42.43 mm to fulfill the known resonance condition :

$$B_w = \frac{2\pi \cdot m_e \cdot c}{q_e \cdot \lambda_w} \cdot \sqrt{2\left(\frac{\lambda_L}{\lambda_w} \cdot 2 \cdot \gamma^2 - 1\right)}$$

The laser pulse was set to 22 ps flattop FWHM for IR (which corresponds to 22 ps for the UV cathode laser as well), laser pulse energy was limited to ~4μJ per pulse at interaction region since the foreseen heater amplifier was not yet installed. Due to preliminary conditions waiting for the amplifier the laser spot size in the interaction region was tuned to σ≈0.6 mm as opposed to the e-beam σ≈0.3 mm.

## TRANSVERSE OVERLAP & SETTING THE STAGE

To accomplish heating of the electron bunches overlap of the laser beam has to be assured. The transverse overlap is obtained by reading out the positions on Cromox screens directly before and after the interaction region of the undulator where both, the electron and the laser beams can be observed. The laser beam position is adjusted with the two orthogonal linear stages making up the periscope on OS0. Due to the design the overlap can be adjusted in the X- and Y-direction independently by one translation stage each. An example of illustrated laser spot and, electron beam and laser simultaneously can be seen in Fig. 1.

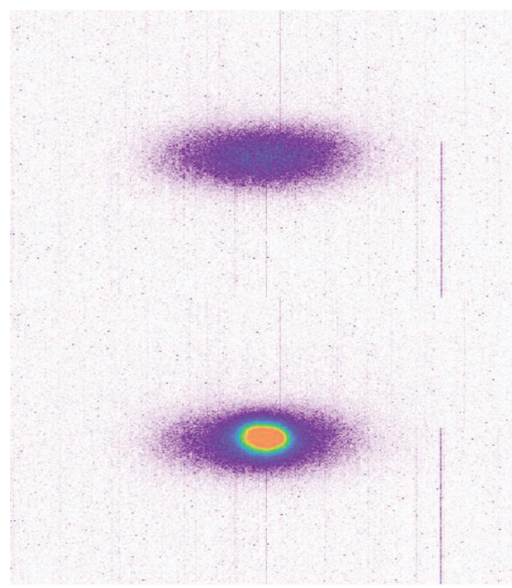

Figure 1: Cromox screen directly before undulator with top only laser, bottom, e-beam and laser illustrating transverse overlap.

## TEMPORAL OVERLAP & HEATING

The temporal overlap was first controlled via a rough delay line adjusted by hand and adjusted after read out from a photo diode at the inlet of OS1 after the undulator. A 4 GHz oscilloscope was used to display the signal from the laser and undulator synchrotron light respectively.

Once the course overlap was found a fine delay line based on a retroreflector mounted on a 210 mm motorized linear stage with ~μm resolution was ready for use. Due

* Work supported by Swedish Research council, Sweden, and DESY, Hamburg, Germany
† mathias.hamberg@physics.uu.se



ISBN 978-3-95450-177-9

# THE MEASUREMENT AND CONTROLLING SYSTEM OF BEAM CURRENT FOR WEAK CURRENT ACCELERATOR

Junhui Yue, Lingda Yu, Yuguang Xie, Yulan Li, Zhongjian Ma, IHEP, CAS, Institute of High Energy Physics, Chinese Academy of Sciences, Beijing 100049, China

*Abstract*

For some detectors' calibration, a very weak electron current provided by accelerator is necessary. In order to control the beam current to the detector, 8 movable slits in which the position resolution of the stoppers is better than 5μm are installed along the accelerator. For the weak current measurement, 9 movable current monitors based on scintillator are installed along the beam line. These monitors can measure the very weak current, even to several electrons. The monitors can be pulled away the beam axis when the electron beam goes to the downstream.

## INTRODUCTION

In order to calibration some detectors, a small linac is designed and installed in the campus of IHEP. This accelerator consists of a weak current electron gun, a RF chopper, a 1.0m-long accelerator tube and a 3.0m-long accelerator tune, 8 movable slits, 9 current monitors, and other systems. It can provide 0.1~5MeV beam and 5~50MeV beam. These two kinds of beams are sent to the same target chamber by the bending magnets. The schematic diagram of weak current is shown in Fig. 1.

For the charge of pulse is above 1nC, ordinary monitor is enough. In pC region, a charge sensitive and low noise detector has been development. In fC region, thermo luminescence dosimeters (TLD) and two dimensional radiation dosimeters would be candidates [1]. For aC region, that means there are only several electrons in the pulse, plastic scintillator is used to detector the electron, the detailed description is in this paper.

## THE SELECT OF MATERIAL AND THICKNESS OF STOPPER

In order to step by step decrease the beam intensity, 8 movable slits are installed along the accelerator. Slit 1 is horizontal and Slit 2 is vertical, they can decrease the beam intensity to 1/20 with the help of solenoid because of the space change. Slit 3 and Slit 4 have the same effect. Slit 5 also decrease the beam intensity with the RF chopper because of time change. Other horizontal slits cooperate with the bending magnet to decrease the beam intensity. In order to effectively block the electrons, the material of stopper is carefully selected and the thickness is needed to calculate. Lead target, aluminium target and tungsten target are calculated by FLUKA program. Tungsten target is effect to block the electron and avoiding other effects. The result is showed in Fig. 2. For the 50MeV electrons, 90 percent energy are deposited in tungsten target, the thickness is not more than 2.25cm, so all the stoppers, 2.25cm thickness tungsten is used. Other target needs thicker material, it is not easy to design and manufacture.

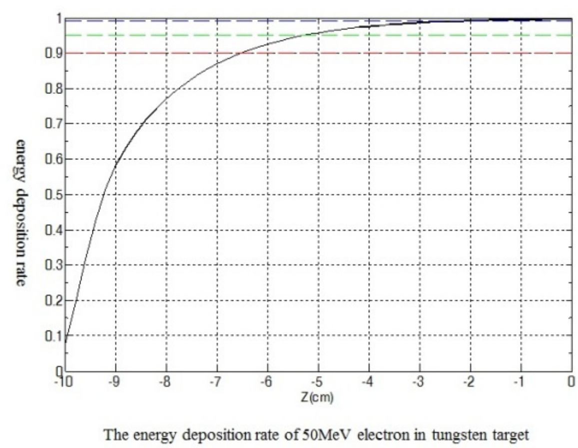


Figure 2: The energy deposition of 50MeV electron in tungsten target.

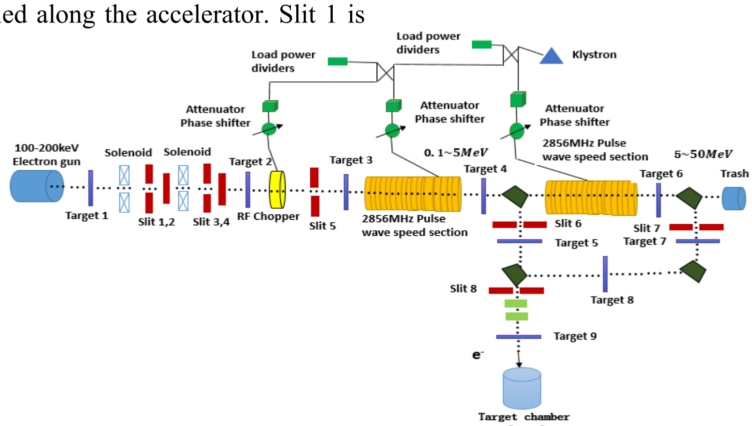


Figure 1: The Schematic diagram of weak current accelerator.

ISBN 978-3-95450-177-9

# HEAVY ION BEAM FLUX AND IN-SITU ENERGY MEASUREMENTS AT HIGH LET*

S. Mitrofanov†, I.Kalagin,V. Skuratov, Y. Teterev
FLNR JINR, Dubna, Moscow Region, Russia
V. Anashin, United Rocket and Space Corporation, Moscow, Russia

*Abstract*

The Russian Space Agency with the TL ISDE involvement has been utilizing ion beams from oxygen up to bismuth delivered from cyclotrons of the FLNR JINR accelerator complex for the SEE testing during last seven years. The detailed overview of the diagnostic set-up features used for low intensity ion beam parameters evaluation and control during the corresponding experiments is presented. Special attention is paid to measurements of ion flux and energy at high LET levels and evaluation of ion beam uniformity over large (200x200 mm) irradiating areas. The online non-invasive (in-situ) time of flight technique designed for low intensity ion beam energy measurements based on scintillation detectors is considered in details. The system has been successfully commissioned and is used routinely in the SEE testing experiments.

## INTRODUCTION

Onboard equipment of spacecraft is exposed to ionizing radiation from the Earth's natural radiation field, as well as galactic and solar cosmic rays during its operation. There are two types of effects in microelectronic circuits caused by radiation: 1—those related to accumulated dose; and 2—those caused by a singular hit of a swift heavy ion (single event effect, SEE). Despite its relatively minor contribution (~1%) of the total amount of charged particles, it is heavy ions that cause the most damage to microelectronics hard ware components due to the high level of specific ionization loss. Hence, to reproduce the effects of the heavy ion component of cosmic radiation for the prediction of electronic device radiation hardness usage of low intensity (up $10^6$ ions $cm^{-2}$ $s^{-1}$) heavy ion beams with linear energy transfer (LET—the measure of energy losses per path length in the material) levels in silicon, specific for the ion energy range of 50–200MeV/nucleon, is supposed. Taking into account that actual integrated circuits in metal and plastic packages, as well as ready to use electronic boards need to be tested, ion beams with energies in the range of 3–50 MeV/nucleon are used in model experiments. This entire means that the accepted method of SEE testing requires measurements of ion flux in the range from 1 to $10^5$ ions ($cm^{-2}*s^{-1}$), ion fluence up to $10^7$ ions/$cm^2$, beam uniformity at the device under test (DUT) and energy of ions. The SEE testing facility is established [1] at the U400M and U400 cyclotrons at the accelerator complex of the Flerov Laboratory of Nuclear Reactions (FLNR) of the Joint Institute for Nuclear Research (JINR) [2]. Ion beam parameters used for SEE testing, like ion type and energy, the LET and ion flux range, are listed in Table 1.

*This work was sponsored by the Russian Federal Space Agency by special agreement between Institute of Space Device Engineering and Joint Institute for Nuclear Research.
†mitrofanov@nrmail.jinr.ru

Table 1: Ion Beam Parameters Used for the Low Energy SEE Testing

| Accelerated ion | Extracted ion | Energy, MeV | LET, MeV/(mg/cm$^2$) | Ion flux, $cm^{-2}s^{-1}$ |
|---|---|---|---|---|
| $^{16}O^{2+}$ | $^{16}O^{8+}$ | 56±3 | 4.5 | 1 ÷ $10^5$ |
| $^{22}Ne^{3+}$ | $^{22}Ne^{10+}$ | 65±3 | 7 | 1 ÷ $10^5$ |
| $^{40}Ar^{5+}$ | $^{40}Ar^{16+}$ | 122±7 | 16 | 1 ÷ $10^5$ |
| $^{56}Fe^{7+}$ | $^{56}Fe^{23+}$ | 213±3 | 28 | 1 ÷ $10^5$ |
| $^{84}Kr^{12+}$ | $^{84}Kr^{32+}$ | 240±10 | 41 | 1 ÷ $10^5$ |
| $^{136}Xe^{18+}$ | $^{136}Xe^{46+}$ | 305±12 | 67 | 1 ÷ $10^5$ |
| $^{209}Bi^{22+}$ | $^{209}Bi^{58+}$ | 490±10 (820±20) | 95 (100) | 1 ÷ $10^5$ |

Since becoming operational in 2010, the low energy beam (3÷6 MeV/nucleon) facility has been available to users. The facility for the SEE testing at high energy (15÷64 MeV/nucleon) was successfully commissioned in January'14. The third line is based on U400 (commissioned in December'14) and after modernization of this cyclotron in 2018 there will be the possibility to make the SEE testing with the fluent energy variation for every ion.

## BEAM FLUX CONTROL

The wide range of beam control systems are used during irradiation. To catch the beam movable probes inside the U400M are used. Diagnostic elements such as the luminophor and the Faraday cup are used during rough beam adjusting at high intensity. For the fine beam tuning and beam profile control, double side Si strip detector (Fig.1) and arrays of scintillators detectors are installed.

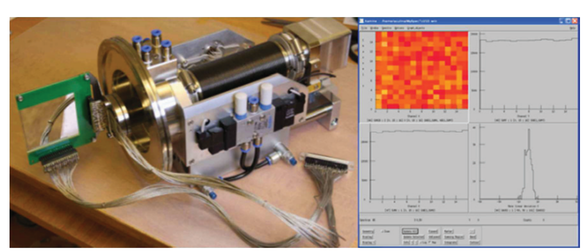

Figure 1: Double-side Si strip detector. Dual axes (X-Y) orthogonal beam detection Kr beam profile as example.



ISBN 978-3-95450-177-9

# DESIGN OF AN ELECTRON CLOUD DETECTOR IN A QUADRUPOLE MAGNET AT CesrTA*

J. P. Sikora†, S.T. Barrett, M. G. Billing, J. A. Crittenden, K. A. Jones, Y. Li, T. O'Connell
CLASSE, Cornell University, Ithaca, NY 14853, USA

*Abstract*

We have designed a detector that measures the electron cloud density in a quadrupole magnet using two independent techniques. Stripline electrodes collect electrons which pass through holes in the beam-pipe wall. The array of small holes shields the striplines from the beam-induced electromagnetic pulse. Three striplines cover a roughly 0.45 radian azimuth near one of the pole tips. The beam-pipe chamber has also been designed so that microwave measurements of the electron cloud density can be performed. Beam-position-monitor-style buttons have been included for excitation and reception of microwaves and the chamber has been designed so that the resonant microwaves are confined to be within the 56 cm length of the quadrupole. This paper provides some details of the design including CST Microwave Studio® time domain simulation of the stripline detectors and eigenmode simulation of the $TE_{11}$ modes in the resonant chamber. The detector is installed in the Cornell Electron Storage Ring and is part of the test accelerator program for the study of electron cloud build-up using electron and positron beams from 2 to 5 GeV.

## INTRODUCTION

At the Cornell Electron Storage Ring (CESR) we have been comparing electron cloud (EC) measurements with the results of simulations both with and without external magnetic fields for several years as part of the test accelerator (CESRTA) program [1, 2]. One measurement technique uses an electrode to sample the electron current that impacts the beam-pipe wall [3]. The simulation of EC buildup in a quadrupole shows that for a 20-bunch train of 5.3 GeV positrons, there is a non-linear increase in EC density with bunch populations greater than $1.0\times10^{11}$ [4]. At low bunch populations, the impact of the electrons on the beam-pipe wall is centered on the poles of the quadrupole since the low energy cloud electrons generally follow the magnetic field lines. At bunch populations above $1.0\times10^{11}$, there is a splitting of the area of electron impact about the pole face. This splitting is large enough that our previous detector, centered on the pole face and 6 mm wide, was not wide enough to include the peak electron currents [4]. As a result, while the data shows a non-linear increase in electron current, it is not as large as predicted by the simulation.

In order to confirm the simulation results we designed and constructed a new detector (Fig. 1) with three 6-mm-wide segments, so that it would cover a wider azimuth about the pole face. Since a new vacuum chamber was to be constructed for the detector, the chamber was also designed to support measurements of EC density made using resonant microwaves [5], an independent measurement technique.

The detector is positioned inside a new quadrupole magnet (Fig. 2) that is placed near an existing quadrupole of the same polarity. Since they are powered independently, the field of the detector quadrupole can varied from zero to about 3.6 T/m with beam in the storage ring by applying a compensating reduction in the strength of the nearby quadrupole. The new quadrupole has an aperture of 150 mm dia., leaving a radial space of about 25 mm for the new detector, between the outer diameter of the beam-pipe and the pole face.

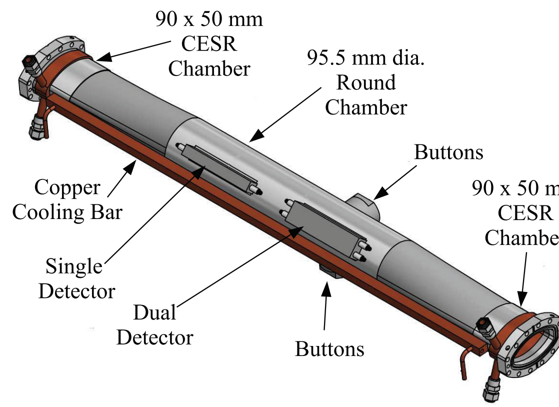


Figure 1: The detector chamber with electron detectors and the button electrodes used for microwave measurements.

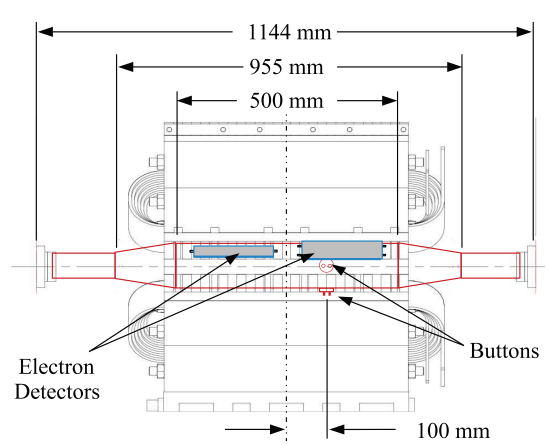


Figure 2: Detector chamber within the quadrupole magnet.

* This work is supported by the US National Science Foundation PHY-0734867, PHY-1002467 and the US Department of Energy DE-FC02-08ER41538, DE-SC0006505.
† jps13@cornell.edu

# NONDESTRUCTIVE HIGH-ACCURACY CHARGE MEASUREMENT OF THE PULSES OF A 27 MeV ELECTRON BEAM FROM A LINEAR ACCELERATOR

A. Schüller*, J. Illemann, R.-P. Kapsch, C. Makowski, F. Renner
Physikalisch-Technische Bundesanstalt (PTB), Braunschweig, Germany


*Abstract*

This work presents instruments and measurement procedures which enable the non-intercepting absolute measurement of the charge of single beam pulses (macro-pulses) from a 0.5 to 50 MeV electron linear accelerator (LINAC) with high accuracy, i.e. with a measurement uncertainty < 0.1 %.[1] We demonstrate the readout and calibration of a Bergoz integrating current transformer (ICT) for a 27 MeV beam. The signal from the ICT is calibrated against a custom-made Faraday cup (FC) with a high degree of collection efficiency (> 99 %) for electron beams in the energy range of 6 to 50 MeV.


## INTRODUCTION

The National Metrology Institute of Germany, the Physikalisch-Technische Bundesanstalt (PTB), operates a custom-designed electron LINAC for fundamental research in dosimetry for radiation therapy (see Fig. 1). The LINAC works on the same principle as medical LINACs applied for cancer treatment. A pulsed electron beam is shot at a metal target for the generation of bremsstrahlung with therapeutically relevant dose rates. In contrast to medical LINACs, all beam parameters can be continuously adjusted and measured with a high degree of accuracy. In this way, it is possible to study radiation effects as a function of their fundamental physical quantities. One crucial quantity is the charge per beam pulse which is directly proportional to the dose of the generated photon radiation. Due to the discontinuous operating principle of a LINAC the charge of the pulses fluctuates somewhat (typical for PTB's research LINAC: 3 %). For the non-intercepting absolute measurement of the charge of the beam pulses, a beam intensity monitoring system based on an ICT, commercially available from Bergoz Instrumentation [1], is used. The signal from this monitoring system is calibrated against the charge measurement by means of a temporarily installed FC in combination with an electrometer, calibrated traceably to PTB's primary standards. The collection efficiency of the FC is determined by a cancellation measurement.

## SETUP

The ICT (transformer winding: 50:1) is mounted directly as a vacuum component in the beamline ("G" in Fig. 1). A bare wire called a "Q-loop" is mounted within the ICT aperture by means of two additional flanges with an electrical feedthrough on both sides of the ICT as shown in Fig. 2. Via the Q-loop, the FC current can be conducted through the ICT for the determination of the collection efficiency of the FC.

The FC is temporarily installed behind the ICT (at "H" in Fig. 1). It shares the same vacuum as the beam. A photo of the FC glued into a vacuum adapter is shown in Fig. 3. The design of the FC is optimized with regard to high collection efficiency for electron beams with energies of 6 to 50 MeV. Its structure is shown in Fig. 4. The FC is composed of a sequence of 1.5 cm C, 2 cm Al, 2 cm Cu, and 4.2 cm WCu-alloy (80 % W).

The measurement of the charge collected by the FC is carried out by a precise electrometer (Keithley 616). In order to avoid saturation effects during a pulse, a 33 nF capacitor is installed at its input. The electrometer is thus suitable for pulse resolved charge measurements.

The ICT output voltage is recorded by means of a waveform digitizer (WD) also referred to as a transient recorder (Spectrum M3i.4142). Due to the high radiation exposure in the vicinity of the beamline, the WD is placed outside the radiation protection bunker. In order to improve the signal-to-noise ratio at the end of the required 40 m coaxial cable, a voltage amplifier (FEMTO HVA-200M-40-B) is used as a preamplifier at the output of the ICT. The preamplifier is enclosed by a pile of lead bricks. The wiring of the setup is shown in the block diagram in Fig. 5.

## SIGNAL ACQUISITION

### *Faraday Cup*

Every charge pulse from the FC fed into the electrometer input causes a voltage step at its analog output. The output voltage $U_{\mathrm{out}}$ is measured by a high-accuracy digital multimeter (Agilent 3458A). It is controlled by a LabVIEW program (see Fig. 5). At every LINAC trigger event, the device records 200 data points with an interval of 200 $\mu$s (6 ms pre-trigger, 34 ms post-trigger). The voltage difference $\Delta U_{\mathrm{out}}$ between before and after the charge pulse is determined. If $U_{\mathrm{out}}$ exceeds $-100$ V, then the electrometer is discharged by closing the remote "zero" contact. The electrometer is calibrated by a reference charge $Q_{\mathrm{ref}}$ generated by means of custom-made air capacitors with traceably calibrated capacitance $C_{\mathrm{air}}$ and a reference voltage $U_{\mathrm{ref}}$. The charge $Q_{\mathrm{ref}}$ collected by the electrometer at a change in the reference voltage by $\Delta U_{\mathrm{ref}}$ amounts to

* andreas.schueller@ptb.de

[1] All uncertainties quoted in this article are expanded uncertainties based on a coverage factor $k = 2$ (two standard deviations), providing a coverage probability of about 95 %.

ISBN 978-3-95450-177-9

# MEASUREMENT UNCERTAINTY ASSESSMENTS OF THE SPIRAL2 ACCT/DCCT

S. Leloir#, T. André, C. Jamet, G. Ledu, S. Loret, C. Potier de Courcy,
GANIL, Caen, France

*Abstract*

Four instrumentation chains with AC and DC Current Transformers (ACCT-DCCT) will equip the lines of SPIRAL2 facility to measure the beam intensity and line transmissions. These measures are essential to tune and supervise the beam, to assure the thermal protection of the accelerator and to control that the intensities and transmissions are below the authorized limits. As such, the uncertainties of measurement chains must be taken into account in the threshold values.

The electronic has been designed with high requirements of quality and dependability by following different steps; from prototyping, the qualification through an Analysis of Failure Modes and Effects Analysis (FMEA) [1] until final fabrication.

This paper presents the measurement uncertainty assessments of the ACCT/DCCT chains.

## INTRODUCTION

The SPIRAL2 facility at GANIL in France is planned to accelerate deuteron, proton and heavy-ion beams with a RFQ and a superconducting linear accelerator. Table 1 recalls the main beam characteristics.

Table 1: Beam Specifications

| Beam | P | D+ | Ions (1/3) |
|---|---|---|---|
| Max. Intensity | 5 mA | 5mA | 1 mA |
| Max. Energy | 33 MeV | 20 MeV/A | 14.5 MeV/A |
| Max. Power | 165 kW | 200 kW | 43.5 kW |

A DCCT bloc is set up at the entrance of the Radio Frequency Quadrupole (RFQ) and three ACCT/DCCT blocs (Fig. 1) will be installed at the Linac entrance, the Linac exit and the Beam Dump entrance (Fig. 2). [2]

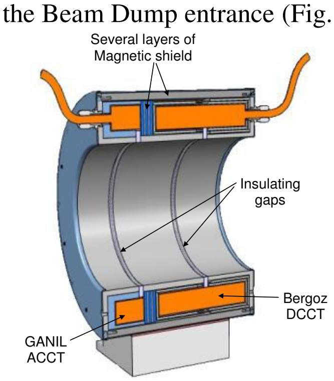


Figure 1: ACCT-DCCT bloc section.

# sebastien.leloir@ganil.fr

These non-destructive beam intensity diagnostics are required to:

- ✓ Control and monitor the beam intensity
- ✓ Control and monitor the transmissions (intensity differences between two blocs),
- ✓ Control the intensity quantity sent to the Beam Dump Linac over 24 hours.

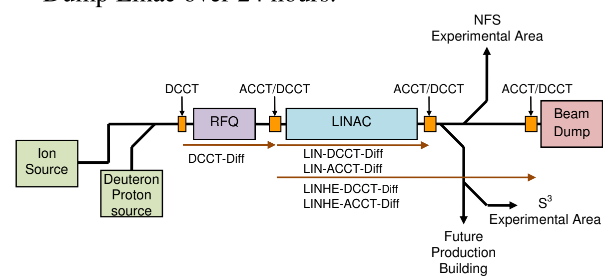


Figure 2: Beam Intensities and transmissions.

## MEASURING CHAIN DESCRIPTION

### *DCCT Measuring Chain*

The figure 3 shows a schematic overview of the DCCT chain. The transformer and the first electronic are commercial devices (Bergoz ref: NPCT-175-C030-HR).

In order to decrease the offset fluctuation, the DCCT is maintained at a temperature of 40°C±1°C.

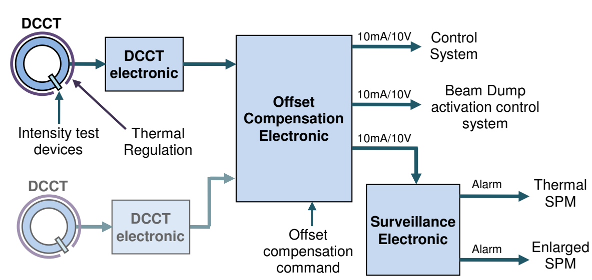


Figure 3: DCCT chain.

The electronic card "offset compensation":

- ✓ sets the zero point, with a manual command before each start of new beam tuning
- ✓ generates the transmission signal (difference of two intensity signals)
- ✓ distributes the intensity and transmission signals at different systems

The surveillance cards carry out moving averages of their input signal. These averages are compared to thresholds and the cards generates alarms in case of overtake. The alarms (a cut-off request) are sending to the Machine Protection Systems (Thermal and Enlarged MPS) [3].



ISBN 978-3-95450-177-9

# OPTIMIZATION STUDIES FOR AN ADVANCED CRYOGENIC CURRENT COMPARATOR (CCC) SYSTEM FOR FAIR*

T. Sieber[1†], J. Golm[2,3], P. Kowina[1], F. Kurian[2,3], R. Neubert[4], M. Schwickert[1], T. Stöhlker[1, 2, 3], V. Tympel[4]

[1]GSI Helmholtz Center for Heavy Ion Research, Darmstadt, Germany
[2]Institute for Optics and Quantum Electronics, Friedrich-Schiller-University Jena, Germany
[3]Helmholtz-Institute Jena, Germany
[4]Institute for Solid State Physics, Friedrich-Schiller-University Jena, Germany

*Abstract*

After successful tests with the GSI-CCC prototype, measuring beam intensities down to 2 nA at a bandwidth of 2 kHz, a new advanced Cryogenic Current Comparator system with extended geometry (CCC-XD) is under development. This system will be installed in the upcoming Cryring facility for further optimization, beam diagnostics and as an additional instrument for physics experiments. After the test phase in Cryring it is foreseen to build four additional CCC units for FAIR, where they will be installed in the HEBT lines and in the Collector Ring (CR). A universal cryostat has been designed to cope with the various boundary conditions at FAIR and at the same time to allow for uncomplicated access to the inner components. To realize this compact cryostat, the size of the superconducting magnetic shielding has to be minimized as well, without affecting its field attenuation properties. Hence detailed FEM simulations were performed to optimize the attenuation factor by variation of geometrical parameters of the shield. The beam tests results with the GSI-CCC prototype, and the developments for FAIR, as well as the results of simulation for magnetic shield optimization are presented.

## INTRODUCTION

For the FAIR [1] project at GSI various new developments in the field of beam diagnostics are necessary to cover the enhanced spectrum of beam parameters. The slow extracted beams from the SIS100 synchrotron can – due to the long extraction times – have intensities which are far below the sensitivity range of regular beam transformers. For that reason it is planned to install ultrasensitive Cryogenic Current Comparators (CCC), based on superconducting SQUID technology at five locations at FAIR. With this device current measurements in the nA range have been achieved with high bandwidth (10 kHz) at GSI [2].

The CCC consists basically of a superconducting niobium torus, which represents shielding and pick-up at the same time, and a SQUID system with related electronics. The geometry and attenuation properties of the Nb torus were optimized by extensive simulation calculations. In parallel a new cryostat, enclosing the pickup and sensor unit has been developed, which fulfils the requirements at FAIR.

In addition, the analysis of spills from the FAIR synchrotrons requires a high bandwidth in combination with an excellent long term stability of the system. Since a temperature dependent baseline drift was observed during the measurements with the GSI prototype [3, 4] (as well as with the CERN/AD CCC [5]), the temperature dependence of offset and bandwidth are currently investigated in detail. Figure 1 shows the planned distribution of CCCs at FAIR.

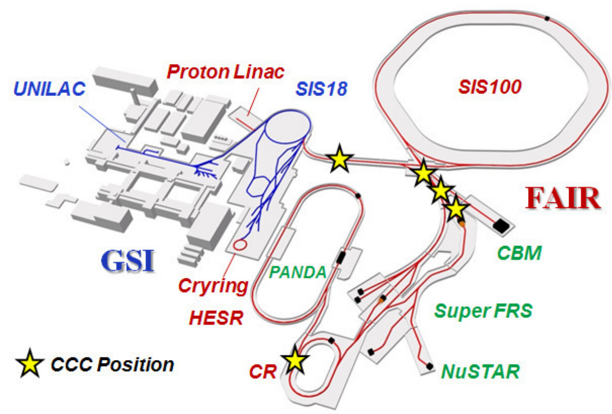


Figure 1: CCC locations at FAIR.

## INTENSITY MEASUREMENTS WITH THE GSI PROTOTYPE CCC

The CCC measures the absolute beam current by detecting the beam magnetic field with a SQUID sensor, which is shielded from external fields by a pickup/shielding combination [6]. In practice the CCC voltage output is calibrated to a known current, applied through a current loop. The calibration loop is wound around the magnetic shield producing an azimuthal magnetic field which is detected by the SQUID analogue to the beam current measurement. Following that scheme, the prototype CCC measured a test current down to 4 nA with a signal to noise ratio of 6dB. The noise limited current sensitivity of the CCC installed in the beam line was calculated to 0.2 nA/√(Hz) at 1 Hz and to 2 pA/√(Hz) at 100 Hz.

* work supported by the BMBF under contract No. 05P15SJRBA
† T.Sieber@gsi.de

ISBN 978-3-95450-177-9

# MEASUREMENT OF COUPLING IMPEDANCES USING A GOUBAU LINE

F. Stulle*, J. Bergoz, Bergoz Instrumentation, Saint-Genis-Pouilly, France
H. W. Glock, Helmholtz-Zentrum für Materialien und Energie GmbH, Berlin, Germany

*Abstract*

Longitudinal coupling impedances can be deduced from S-Parameter measurements performed on a Goubau Line. The Goubau Line, also known as single wire line, is a variant of the coaxial wire method. Both setups use a wire for mimicking the particle beam. Coaxial tapers at the wire ends adapt the wave impedance to the 50 Ω impedance of coaxial cables, sources and receivers. But for guiding the electromagnetic wave, the Goubau Line relies on the realistic boundary conditions imposed by an insulated wire instead of using a coaxial shield. Equations for the deduction of longitudinal coupling impedances are reviewed and applied to Goubau Line measurements. Goubau Line measurements and CST Studio simulations are compared, showing good agreement.

## INTRODUCTION

The coaxial wire method is a well-established technique for the deduction of coupling impedances [1-3]. The wire is mimicking the particle beam. A coaxial shield is used to guide the electromagnetic fields. Coaxial tapers on both ends adapt the wave impedance to the 50 Ω impedance of coaxial cables, sources and receivers. Using a vector network analyzer, S-parameters of the setup with and without device under test (DUT) are obtained. These measurements are sufficient to mathematically deduce coupling impedances of the DUT with high accuracy.

The Goubau Line [4] is a variant of the coaxial wire method. The important difference is that for guiding the electromagnetic wave it relies on the realistic boundary conditions of an insulated wire, instead of using a coaxial shield. That a single wire in open space can act as a waveguide had already been shown in the early days of electrodynamics [5-7].

Such a setup allows for more flexibility because it does not need to be adapted to the DUT geometry. Additionally, the DUT can be easily placed off-axis. On the other hand, it cannot be considered lossless, which is a usual assumption when analyzing S-parameters obtained by the coaxial wire method. Consequently, the standard equations, which are used to analyze data taken with the coaxial wire method, should be carefully examined before applying them to Goubau Line measurements.

We review the calculation of the longitudinal coupling impedance from S-parameter measurements. Assumptions and simplifications are discussed in view of their applicability to Goubau Line measurements. Afterwards, longitudinal coupling impedances are compared which were obtained from Goubau Line measurements and by CST Studio wakefield simulations [8].

*stulle@bergoz.com

The DUT was a pair of vacuum flanges intended to house a current transformer (Fig. 1). However, no current transformer was installed inside.

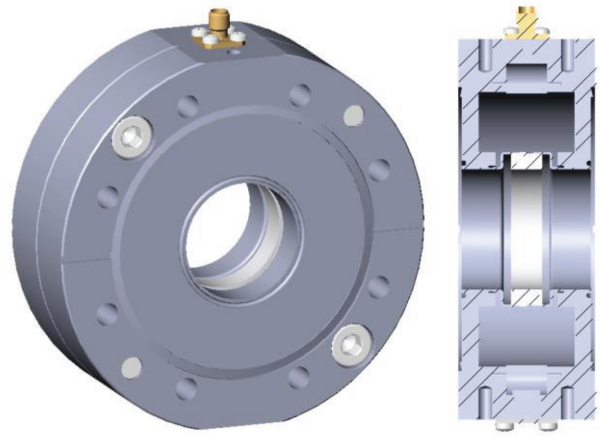

Figure 1: Drawing of the tested vacuum flanges.

Of interest is the coupling impedance induced by the ceramic gap and the surrounding cavity, which can be considered a single lumped impedance. For the particle beam, the metal parts left and right of the gap are like pieces of the vacuum chamber.

Note that such a DUT was chosen to demonstrate Goubau Line measurements and to facilitate simulations. The results are not representative for the real beam instrumentation installed in an accelerator.

## CALCULATION OF LONGITUDINAL COUPLING IMPEDANCES

Coupling impedances are the frequency-domain equivalent to the time-domain wake potentials. One can be obtained from the other by (inverse) Fourier transform.

The impact of these coupling impedances on a highly relativistic particle beam is like that of a complex impedance on a current flowing in an electronic circuit. Consequently, they can be analyzed by using scattering parameters (S-parameters) (Fig. 2).

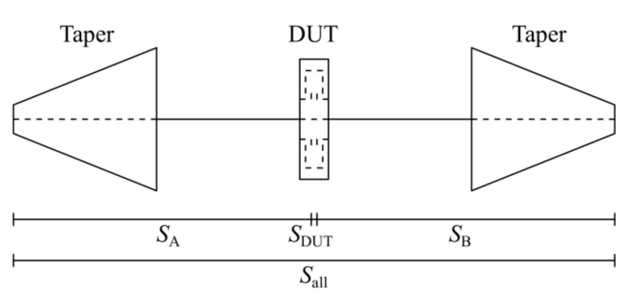


Figure 2: Definition of scattering matrices. The setup is in general asymmetric, i.e. $S_A$ and $S_B$ differ.

ISBN 978-3-95450-177-9

# ENERGY AND LONGITUDINAL BUNCH MEASUREMENTS AT THE SPIRAL2 RFQ EXIT

C. Jamet #, W. Le Coz, G. Ledu, S. Loret, C. Potier de Courcy
GANIL, Caen, France

*Abstract*

A new step of the SPIRAL2 commissioning started in December 2015 with the acceleration of a first proton beam at the RFQ exit. A test bench, with all the different diagnostics which will be used on the SPIRAL2 accelerator, was installed directly after the first rebuncher of the MEBT line in order to qualify beams but also to test and make reliable the diagnostic monitors.

In 2016, different ion beams are qualified by the diagnostic test bench. This paper describes the results of the energy measurements done by a Time of Flight monitor and the longitudinal measurements using a fast faraday cup.

## INTRODUCTION

The SPIRAL2 driver is designed to accelerate and deliver proton beams, deuteron and ion beams with q/A=1/3 to NFS (Neutron for Science) and S3 (Super Separator Spectrometer) experimental rooms. Table 1 shows the main beam characteristics.

Table 1: Beam Specifications

| Beam | P | D+ | Ions (1/3) |
|---|---|---|---|
| Max. Intensity | 5 mA | 5mA | 1 mA |
| Max. Energy | 33 MeV | 20 MeV/A | 14.5 MeV/A |
| Max. Power | 165 kW | 200 kW | 43.5 kW |

Currently, an Intermediate Test Bench is installed in the MEBT line. The commissioning is in progress in the accelerator part composed by 2 sources (a proton/deuteron source and an ion source with a q/A=1/3), the LEBT lines, a chopper, a RFQ, a rebuncher as shown in the figure 1.

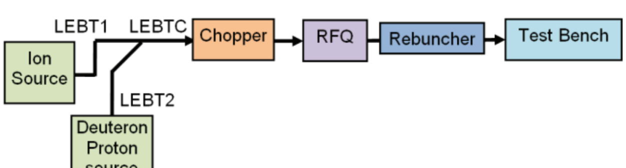


Figure 1: Injector diagram.

A first proton beam was accelerated through the RFQ in December 2015. In the first semester of 2016, the commissioning was done with proton and helium beams in pulse and CW mode, up to the nominal beam intensities. In parallel, the installation of the accelerator process continues.

## INTERMEDIATE TEST BENCH

The "Intermediate Test Bench" or "Diagnostic Plate" was built to test all the different diagnostics which will be used on the SPIRAL2 Accelerator.

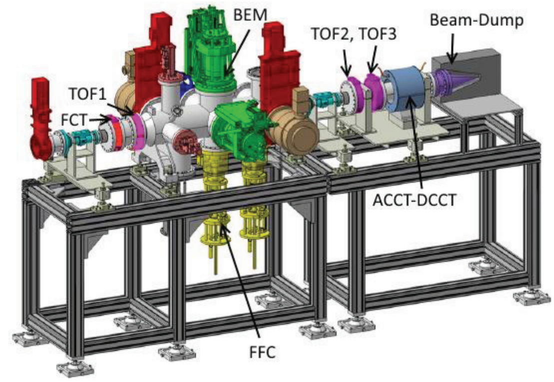


Figure 2: View of the intermediate test bench.

The Test Bench is installed after 3 quadrupoles and the first-rebuncher of the MEBT in order to validate the RFQ, the diagnostics by measuring the following beam characteristics (Figure 2):

- Intensity with ACCT, DCCT transformers and Faraday Cup (FC)
- Transverse Profiles with Multiwires beam profile monitors (SEM) and Ionization Gas monitor
- Transverse emittance with an Allison Scanner Emittancemeter (H an V)
- Phases and Energy with the Time of Flight (TOF) monitor
- Longitudinal profile with a Fast Faraday Cup (FFC) and a Beam Extension Monitor (BEM)
- Beam Position, Phase and Ellipticity with 2 Beam Position Monitors (BPM)

## BEAM ENERGY PRINCIPLE

The beam energy is measured by using 3 electrodes pick-up (TOF1, TOF2 and TOF3). The energy is calculated, with a Time of flight method [1].

A dedicated electronic measures, using an I/Q demodulation method, the In-phase component I(t) and the Quadrature component Q(t) of the first harmonic [2]. An EPICS Interface, connected to the TOF electronic device by a Modbus-TCP communication, calculates the phases and the amplitudes from these components [3]. From the difference phases, the energy is determined.

## BEAM ENERGY MEASUREMENTS

### *Beam and TOF Features*

The beam features were the following (table 2):

- Proton Intensity: from few 10µA to 5mA
- Helium $^{4}He^{2+}$ Intensity: few 10 µA to 1 mA
- Slow Chopper duty cycle: From 1/10000 to 1/1
- Chopper Frequency: 1Hz to 5 Hz

ISBN 978-3-95450-177-9

# A PROCEDURE FOR THE CHARACTERIZATION OF CORRECTOR MAGNETS

S. Gayadeen *, M. Furseman, G. Rehm, Diamond Light Source, Chilton, U.K.

*Abstract*

At Diamond Light source, the main assumption for the Fast Orbit Feedback (FOFB) controller design is that the corrector magnets all have the same dynamic response. In this paper, a procedure to measure the frequency responses of the corrector magnets on the Diamond Storage Ring is presented and the magnet responses are measured and compared in order to assess whether this assumption is valid. The measurements are made by exciting a single corrector magnet with a sinusoidal input and measuring the resulting sinusoidal movement on the electron beam using electron Beam Position Monitors (eBPMs). The input excitation is varied from 10 Hz to 5 kHz using a 10 mA sine wave. The amplitude ratio and the phase difference between the input excitation and the beam position excitation are determined for each input frequency and the procedure is repeated for several magnets. Variations in both gain and phase across magnets are discussed in this paper and the effect of such variations on the performance of the FOFB controller performance is determined.

## INTRODUCTION

The Fast Orbit Feedback (FOFB) Controller at Diamond performs global orbit correction to 172 horizontal and vertical correctors respectively using the position from 171 horizontal and 171 vertical electron Beam Position Monitors (eBPMs). The main assumption of the FOFB design is that all corrector magnets in the Storage Ring have the same dynamic effect on beam position. This assumption allows the FOFB controller to be decoupled into a static part (implemented as the inverse of the Response Matrix) and a dynamic part (implemented as IIR filters on the outputs of the inverse Response Matrix). If the dynamics of the corrector magnets are dissimilar, then the decoupled control approach may no longer be valid and significant differences in dynamics may limit the ability of the FOFB controller to attenuate disturbances.

Two straights in the Diamond Storage Ring (I13 and I09) were modified with vertical mini-beta and horizontally focusing optics [1], resulting in the need for two extra correctors in each modified straight in both planes. The additional correctors are different in design to the standard correctors used around the rest of the Storage Ring. Moreover the mini-beta correctors are fitted around a different vacuum chamber cross section. A method to measure the dynamic response of the Storage Ring correctors was developed so that the dynamics of the mini-beta correctors can be compared to the standard corrector magnets and the impact on the FOFB performance can be determined. The procedure to obtain the required measurements for such characterisation and the analysis of the measurements are presented in this paper.

* sandira.gayadeen@diamond.ac.uk

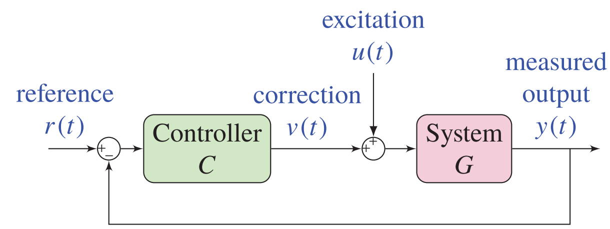


Figure 1: System representation.

## FREQUENCY RESPONSE OF A SYSTEM

A general representation of the system to be characterised is shown in Fig. 1 where the system to be characterised is represented by $G$ (referred to as the open loop system) which includes dynamics contributed by the magnet power supplies, the magnet itself and the vacuum vessel. Also included in $G$ are external disturbances acting on the electron beam. The FOFB controller is represented by $C$, which takes the difference of the beam position at all eBPMs, $y(t)$ and the golden orbit, $r(t)$ as an input. An external excitation, $u(t)$ can be added to the calculated output $v(t)$, which then becomes the correction applied to the corrector magnets.

A common way of modelling the system $G$, is to find the frequency response, or response to a sinusoid. An input signal $u(t)$ that is a harmonic signal with angular frequency $\omega$, can be expressed as

$$u(t) = u_0 \sin(\omega t) \quad (1)$$

If the system is properly damped, then after some time the transient behaviour of the system will damp and the output $y(t)$ is also harmonic with the same frequency and its amplitude and phase with respect $u(t)$ are determined by the complex value of $G(j\omega)$ i.e. the complex number that is obtained when $s = j\omega$ is substituted in the expression of the transfer function $G(s)$ [2]. Specifically, the gain $|G(j\omega)|$ equals the ratio of the amplitudes of the output and input signals and the phase angle $\angle G(j\omega)$ is equal to the phase shift. The gain and phase shift are shown as functions of the angular frequency in a Bode plot. The information in such a plot is used as a model of the linear, time-invariant system $G(s)$ and can be used to compute the output of the system for a given input.

To measure the frequency response, the system is excited at a user defined set of $M$ excitation frequencies $\{\omega_i\}_{i=1,\ldots,M}$ and associated amplitudes $\{u_{0_i}\}_{i=1,\ldots,M}$. When the system is excited, information is only obtained at the chosen excitation frequencies, so that the frequency grid should normally



ISBN 978-3-95450-177-9

# LONGITUDINAL PHASE SPACE MEASUREMENT AT THE ELI-NP COMPTON GAMMA SOURCE

L. Sabato[1]*, University of Sannio, Dept. of Engineering, Corso G. Garibaldi, 107, Benevento, Italy
P. Arpaia, A. Liccardo, Federico II University of Naples,
Dept. of Electrical Engineering and Information Technology, Via Claudio 21, Naples, Italy
D. Alesini, G. Franzini, C. Vaccarezza, A. Variola, Istituto Nazionale di Fisica Nucleare -
Laboratori Nazionali di Frascati (INFN-LNF), via Enrico Fermi, 40, Frascati, Italy
A. Giribono, A. Mostacci, L. Palumbo, Sapienza University of Rome,
Dept. Scienze di Base e Applicate per l'Ingegneria (SBAI), Via Antonio Scarpa, 14, Rome, Italy
[1]also at Istituto Nazionale di Fisica Nucleare (INFN) Naples, via Cintia, Naples, Italy

*Abstract*

Virtual bunch length measurement can be carried out by means of ELEGANT code for tracking the bunch particles from RF deflector to the screen. The technique relies on the correlation between the bunch longitudinal coordinate and transverse coordinates induced through a RF deflector. Therefore, the bunch length measurement can be carried out measuring the vertical spot size at the screen, placed after the RF deflector. The deflecting voltage amplitude affects the resolution. Adding a dispersive element, e.g. a magnetic dipole between RF deflector and the screen, the full longitudinal phase space can be measured. In this paper, we discuss some issues relevant for the electron linac of the Compton source at the Extreme Light Infrastructure - Nuclear Physics (ELI-NP).

## INTRODUCTION

The Gamma Beam Source (GBS) at ELI-NP is going to be an advanced Source of up to 20 MeV Gamma Rays based on Compton back-scattering, i.e. collision of an intense high power laser beam and a high brightness electron beam with maximum kinetic energy of about 720 MeV. This infrastructure is going to be built in Magurele, near Bucharest (Romania) [1, 2]. The GBS electron linac can run at maximum repetition rate of 100 Hz. Therefore, at room temperature the specifications on the requested spectral density can be reached only by multiple bunch collisions. The final optimization foresees trains of 32 electron bunches separated by 16 ns, time needed to recirculate the laser pulse in order to allow the same laser pulse to collide with all the electron bunches in the RF pulse, distributed along a 0.5 $\mu$s RF pulse [1].

The properties of the single bunch and the whole train of bunches have to be measured in order to achieve high brightness in high repetition rate machine [3, 4]. In particular, bunch length measurement can be done using a Radio Frequency Deflector (RFD) and a screen in an electron linac. This disruptive measurement technique is well-known and widespread used in high brightness Linacs around the world, e.g. at the SLAC free electron laser [5, 6] or at SPARC-LAB linac [7].

* luca.sabato@unisannio.it

In this paper, the effect of a non-negligible energy chirp on bunch length virtual measurements is treated. Moreover, the energy chirp affects energy spread measurements. The simulations are carried by means of ELEctron Generation ANd Tracking (ELEGANT) code [8]. In section **MEASUREMENT TECHNIQUE**, the basic idea, the working principle and the procedure of the bunch length measurement technique using a RFD are explained. In section **SIMULATION RESULTS**, the RFD and bunch parameters of GBS linac case are reported and the bunch length virtual measurements are discussed.

## MEASUREMENT TECHNIQUE

### *Basic Idea*

Different types of measurements can be done with a RFD. Bunch length measurements can be done using only a RFD and a screen. Adding a dispersive element, e.g. a magnetic dipole between RF deflector and the screen, the full longitudinal phase space can be measured. The basic idea of these measurements is based on the property of the RFD transverse voltage to introduce a correlation between the longitudinal and vertical coordinates of the bunch at the screen position. Therefore, the bunch length measurement can be carried out measuring the vertical spot size at the screen, placed after the RF deflector [7, 9].

### *Working Principle*

When the particles pass through the RFD, they feel a deflecting voltage when they pass through the RFD. The effect on every particle is a change in vertical divergence [10]. Considering the bunch length much smaller than RF wavelength (i.e. $kz_0 \ll 1$), we can assume the RFD voltage is [6, 11]:

$$V(z_0) \approx V_t\left[kz_0 cos(\varphi) + sin(\varphi)\right]. \tag{1}$$

where $z_0$ is the position of the particles along the beam axis with the origin in the RFD, $k = 2\pi/\lambda_{RF}$, $\lambda_{RF}$, $V_t$, and $\varphi$ are the deflecting voltage wavelength, amplitude, and phase, respectively.

Therefore, RFD gives a vertical divergence change [6]:

$$\Delta y_0'(z_0) = C_{rfd}\left[kz_0 cos(\varphi) + sin(\varphi)\right], \tag{2}$$



ISBN 978-3-95450-177-9

# PRESENT STATUS OF THE LASER CHARGE EXCHANGE TEST USING THE 3-MeV LINAC IN J-PARC

H. Takei†, E. Chishiro, K. Hirano, Y. Kondo, S.I. Meigo, A. Miura, T. Morishita, H. Oguri, K. Tsutsumi, J-PARC Center, Japan Atomic Energy Agency, Tokai, Ibaraki, JAPAN

*Abstract*

The Accelerator-driven System (ADS) is one of the candidates for transmuting long-lived nuclides, such as minor actinide (MA), produced by nuclear reactors. For efficient transmutation of the MA, a precise prediction of neutronics of ADS is required. In order to obtain the neutronics data for the ADS, the Japan Proton Accelerator Research Complex (J-PARC) has a plan to build the Transmutation Physics Experimental Facility (TEF-P), in which a 400-MeV negative proton ($H^-$) beam will be delivered from the J-PARC linac. Since the TEF-P requires a stable proton beam with a power of less than 10 W, a stable and meticulous beam extraction method is required to extract a small amount of the proton beam from the high power beam using 250 kW. To fulfil this requirement, the Laser Charge Exchange (LCE) method has been developed. The LCE strips the electron of the $H^-$ beam and neutral protons will separate at the bending magnet in the proton beam transport. To demonstrate the charge exchange of the $H^-$, a preliminary LCE experiment was conducted using a linac with energy of 3 MeV in J-PARC. As a result of the experiment, a charge-exchanged $H^+$ beam with a power of about 5 W equivalent was obtained under the J-PARC linac beam condition, and this value almost satisfied the power requirement of the proton beam for the TEF-P.

## INTRODUCTION

The Accelerator-driven System (ADS) is one of candidates for transmuting long-lived nuclides such as minor actinide (MA) produced by nuclear reactors [1]. For the efficient transmutation of MA, precise prediction of the neutronic performance of ADS is required. In order to obtain the neutronics data for the ADS, the Japan Proton Accelerator Research Complex (J-PARC) has a plan to build the Transmutation Physics Experimental Facility (TEF-P) [2]. The critical assembly installed in the TEF-P, which is a small and low power reactor, operates below 500 W to prevent excessive radio-activation. To perform the experiments at the TEF-P with such reactor power, with an effective neutron multiplication factor ($k_{eff}$) of around 0.97, the incident proton beam power must be less than 10 W. Because the J-PARC accelerators focus on much higher beam power, a low power proton beam extraction device of high reliability is indispensable.

The development of a laser charge exchange (LCE) technique for extraction of the low power proton beam from the high power proton beam is now underway. The LCE technique was originally developed to measure the proton beam profile [3]. To apply the LCE technique to the beam separation device for the TEF-P, it is important to evaluate the efficiency of conversion to the low power proton beam and the long-term power stability of the low power proton beam in order to keep the thermal power of the assembly constant. Thus, a preliminary LCE experiment to measure the power of the low power proton beam was conducted using a linac with energy of 3 MeV in J-PARC. In this paper, the preliminary results of the LCE experiment are presented.

## LASER CHARGE EXCHANGE

Figure 1 illustrates the concept of the LCE device for the TEF-P [4]. When a laser beam is injected into a negative proton ($H^-$) beam with energy of 400 MeV from the J-PARC linac, the charge of the $H^-$ beam crossed with the laser beam becomes neutral ($H^0$). Since the outer electron of the $H^-$ is very weakly bound to the atom, it can easily be stripped by a laser light in the wavelength range of 800~1100 nm as shown in Fig.2 [5]. These $H^0$ protons do not sense the magnetic field of a bending magnet, and are completely separated from the remaining $H^-$ beam at the exit of the bending magnet. However, it is well-known that pre-neutralized $H^0$ particles are produced by collision with the remaining gas in accelerator tubes and are transported with the main proton beam. When we apply the LCE technique to the $H^-$ beam with the pre-neutralized protons, it becomes impossible to predict the total power of the extracted beam.

To eliminate the pre-neutralized protons, we were trying to perform laser injection and beam bending simultaneously in one magnet. When the laser is injected in the magnetic field of the bending magnet, the pre-neutralized proton goes straight along the beam inlet direction and can be separated from the clean low power proton beam at the exit of the bending magnet. The charge-exchanged $H^0$ beam reaches the stripping foil. After passing the stripping foil, the $H^0$ beam is converted to a positive proton ($H^+$) beam and then delivered to the TEF-P target. A material with a low melting temperature will be used as the stripping foil to avoid high power beam injection to the TEF-P target. Hereafter, the low power $H^+$ beam extracted from the high power $H^-$ beam by using this LCE strategy is referred to as "the stripped $H^+$ beam."

Figure 2 shows the photoneutralization cross-section of $H^-$ ions as a function of photon wavelength in the centre-of-mass frame. We chose a fundamental wavelength of 1064 nm from the commercial Nd:YAG laser because this wavelength is near the peak of the photoneutralization cross-section of $H^-$ ions. Even taking the Lorentz contraction effect into consideration, the photoneutralization cross-section for the $H^-$ beam with energy of 400 MeV using the fundamental wavelength of Nd:YAG laser is

† takei.hayanori@jaea.go.jp

ISBN 978-3-95450-177-9

# KALYPSO: A Mfps LINEAR ARRAY DETECTOR FOR VISIBLE TO NIR RADIATION

L. Rota*, M. Balzer, M. Caselle, M. Weber, IPE-KIT, Karlsruhe, Germany
G. Niehues, P. Schönfeldt, M. J. Nasse, A.S. Mueller, LAS-KIT, Karlsruhe, Germany
N. Hiller, A. Mozzanica, PSI, Villigen, Switzerland
C. Gerth, B. Steffen, DESY, Hamburg, Germany
D. R. Makowski, A. Mielczarek, TUL-DMCS, Lodz, Poland

*Abstract*

The acquisition rate of commercially available line array detectors is a bottleneck for beam diagnostics at high-repetition rate machines like synchrotron lightsources or FELs with a quasi-continuous or macro-pulse operation. In order to remove this bottleneck we have developed KALYPSO, an ultra-fast linear array detector operating at a frame-rate of up to 2.7 Mfps. The KALYPSO detector mounts InGaAs or Si linear array sensors to measure radiation in the near-infrared or visible spectrum. The FPGA-based read-out card can be connected to an external data acquisition system through a high-performance PCI-Express 3.0 data-link, allowing continuous data taking and real-time data analysis. The detector is fully synchronized with the timing system of the accelerator and other diagnostic instruments. The detector is currently installed at several accelerators: ANKA, the European XFEL and TELBE. We present the detector and the results obtained with Electro-Optical Spectral Decoding (EOSD) setups.

## INTRODUCTION

Electro-Optical Spectral Decoding (EOSD) is a well-established technique to measure the longitudinal bunch profile in a non-destructive way [1, 2] and with sub-picosecond spatial resolution [3]. A detailed description of EOSD can be found in [4]. In a typical EOSD setup, a chirped laser pulse is modulated inside an Electro-Optical crystal by the Coulomb field of the electron bunch. In this way the information on the temporal profile of the bunch is contained in the spectrum of the laser pulse. A spectrometer with a linear array detector is commonly used to measure the spectrum and reconstruct the bunch profile. While, in principle, this diagnostic technique allows single-shot measurements over many bunches, the bottleneck of current experimental setups lies in the linear array detector used in the spectrometer.

In particular, the acquisition rate of the detector has to match the bunch repetition rate of the accelerator machine (*e.g.:* 4.5 MHz at the European XFEL, 2.7 MHz during single-bunch operation at ANKA) to obtain single-shot resolution on a turn-by-turn basis. Moreover, the data acquisition system (DAQ) must be able to sustain high data-rates to allow the analysis of the beam dynamics over long time scales (*i.e.:*, a large number of samples). To the best of our knowledge, the line rates of commercial linear detectors reach only a few hundreds of kHz [5, 6].

An alternative approach, based on the method of photonic time-stretch, has been recently implemented by Roussel *et al.* [7] to lift the aforementioned limitation on the acquisition rate. This method enables an unprecedented acquisition rate in EOSD experiments (up to 62.5 MHz, an order of magnitude higher than what can be currently accomplished with linear array detectors) by using an oscilloscope to sample the signal of a fast photodiode. However, because of the finite memory depth of oscilloscopes, only a limited amount of samples can be acquired in a given time frame. This method is therefore not suitable for long observation times or experiments where real-time data analysis and fast-feedback are required.

In order to overcome such limitations, we have developed KALYPSO (KArlsruhe Linear arraY detector for MHz-rePetition rate SpectrOscopy ), a novel linear array detector operating at line-rate of up to $2.7 \cdot 10^6$ fps (frames per second). In this contribution, we describe the architecture of the system and its application as beam diagnostic tool in the near-field EOSD setup of ANKA.

## DETECTOR ARCHITECTURE

KALYPSO consists of a detector board and an FPGA-based readout card. The detector board mounts the sensor, the front-end amplifier and the Analog-to-Digital Converter (ADC). The sensor is a Si or an InGaAs linear array, with

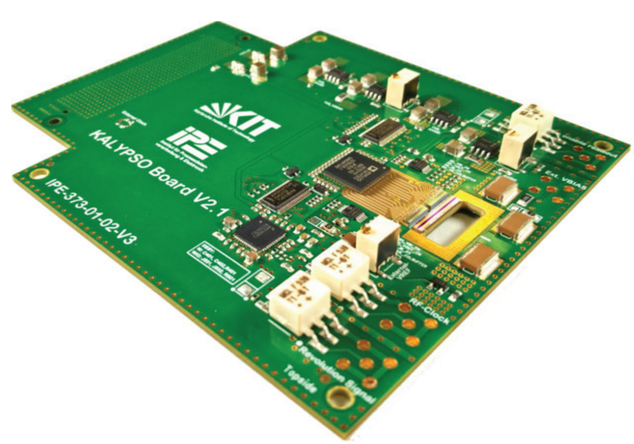


Figure 1: Picture of the KALYPSO detector board with InGaAs sensor.

* Author's contact: lorenzo.rota@kit.edu



ISBN 978-3-95450-177-9

# PROGRESS ON THE PITZ TDS

H. Huck*, P. Boonpornprasert, L. Jachmann, W. Koehler, M. Krasilnikov, A. Oppelt, F. Stephan, DESY, Zeuthen, Germany
L. Kravchuk, V. Paramonov, A. Zavadtsev, INR of the RAS, Moscow, Russia
C. Saisa-ard, Chiang Mai University, Chiang Mai, Thailand

*Abstract*

A transverse deflecting system (TDS) is under commissioning at the Photo Injector Test Facility at DESY, Zeuthen site (PITZ). The structure was designed and manufactured by the Institute for Nuclear Research (INR RAS, Moscow, Russia) as prototype for the TDS in the injector part of the European XFEL. Last year the deflection voltage was limited for safety reasons, but after thorough investigations of the waveguide system we are now able to operate the cavity close to design specifications. The PITZ TDS streaks the electron beam vertically, allowing measurements of the longitudinal bunch profile, and, in combination with a subsequent horizontal bending magnet, also of the longitudinal phase space and slice energy spread. Furthermore, several quadrupole magnets and screen stations can be employed for horizontal slice emittance measurements using the TDS. This paper describes the progress in commissioning of the hardware, measurement techniques and simulations, and outlines the prospects of reliable slice emittance measurements at 20 MeV/c, where space charge forces complicate the determination of transfer matrices.

## INTRODUCTION

X-ray Free Electron Lasers (XFELs) pose stringent requirements on the quality of their driving electron beams, especially in terms of peak current and emittance. Higher peak currents and lower emittances yield higher radiation power and reduce the total undulator length necessary to reach FEL saturation. In particular, the small normalized transverse core slice emittance (i.e. the emittance or "focusability" of the central, high-current parts of the electron bunches), is a major figure of merit. Measurements of the longitudinal charge profile to determine the peak current as well as slice emittance measurements can be performed using a transverse deflecting RF cavity or multi-cell structure (TDS).

Transverse fields inside the structure deflect electrons depending on their arrival time with respect to the RF phase. Near the zero-crossing phase the beam is sheared, linearly mapping the longitudinal charge profile to a transverse, e.g. vertical axis on an observation screen downstream. The horizontal axis can then be utilized for other longitudinally resolved measurements: In combination with a horizontally dispersive bending magnet, live images of the full longitudinal phase space can be observed on the screen, while the quadrupole-scan emittance measurement technique allows for slice emittance measurements [1, 2].

In the simple case of a pure drift space (length $L$) between TDS and screen, a longitudinal slice of the bunch (relative position $z$) hits the screen at vertical position [3]

$$y = S \cdot z = \frac{eV_0k}{pc} \cdot L \cdot z, \tag{1}$$

where $p$ denotes the electron momentum, $c$ the speed of light, and the shear parameter $S$ depends on the deflecting voltage $V_0$ and wave number $k$. In the general case, the longitudinal resolution can be expressed as [3, 4]

$$\sigma_z \gtrsim \frac{2}{eV_0k} \frac{m_0c^2}{\sin(\Delta\psi)} \sqrt{\frac{\gamma\epsilon_n}{\beta_{\mathrm{TDS}}}} \tag{2}$$

with the beta function $\beta_{\mathrm{TDS}}$ in the TDS, normalized emittance $\epsilon_n$, relativistic factor $\gamma$ and betatron phase advance $\Delta\psi$ between TDS and screen.

## PITZ LAYOUT

At the Photo Injector Test Facility at DESY, Zeuthen site (PITZ), electron guns for the European XFEL and the Free-electron laser FLASH are being tested and optimized. Projected emittance requirements for the nominal European XFEL run parameters have been met [5], recently for the start-up phase as well [6]. In order to measure and optimize also the slice emittance (and other parameters), a TDS is installed in the high energy section of the PITZ beamline, between the first emittance measurement station and the phase space tomography module (Fig. 1). The TDS, designed [7] and manufactured by the Institute for Nuclear Research of the Russian Academy of Sciences as a prototype of the TDS in the injector section of the European XFEL [8, 9], is under commissioning since 2015 [10]. The cell dimensions were selected to have the same cells for all three structures in the European XFEL TDS and are realized in its prototype for PITZ [11]. Table 1 summarizes the most important parameters of the cavity.

Table 1: Design Parameters of the PITZ TDS

| | |
|---|---|
| Deflecting voltage | 1.7 MV |
| Input power | 2.11 MW |
| RF Frequency | 2997.2 MHz |
| Pulse length | 3 µs |
| Structure Length | 0.533 m |
| Number of cells | 14+2 |
| Phase advance per cell | $2\pi/3$ |
| Quality factor at 20 °C | 11780 |

* holger.huck@desy.de



ISBN 978-3-95450-177-9

# A THz DRIVEN TRANSVERSE DEFLECTOR FOR FEMTOSECOND LONGITUDINAL PROFILE DIAGNOSTICS

S.P. Jamison†, E.W. Snedden, D.A. Walsh
Accelerator Science and Technology Centre,
STFC Daresbury Laboratory, Warrington WA4 4AD, United Kingdom
M.J. Cliffe, D.M. Graham, D.S. Lake
School of Physics and Astronomy & Photon Science Institute
The University of Manchester, Manchester M13 9PL, United Kingdom

*Abstract*

Progress towards a THz-driven transverse deflecting longitudinal profile diagnostic is presented. The deflector is driven with sub-picosecond quasi-single cycle THz fields generated by non-linear optical rectification. To utilize the large deflection field strength of the source for longitudinal diagnostics it is necessary to maintain the single-cycle field profile of the THz pulse throughout the interaction with the relativistic beam. Our scheme allows for the octave spanning bandwidth of the single-cycle pulses to propagate without dispersion at subluminal velocities matched to co-propagating relativistic electrons, by passing the pulse distortion and group-carrier walk-off limitations of dielectric loaded waveguide structure. The phase velocity is readily tuneable, both above and below the speed of light in a vacuum, and single-cycle propagation of deflecting fields at velocities down to 0.77c have been demonstrated.

## INTRODUCTION

Measurement of coherent diffraction or transition radiation (CDR and CTR), together with methods of phase retrieval promise the ability to characterise bunch longitudinal charge density profile at the few-femtosecond level, although issues of ambiguity in phase retrieval remain. A range of electro-optic techniques have been demonstrated that provide unambiguous temporal profile, but they have yet to achieve capability in the few femtosecond regime. Transverse defecting structures are currently the only diagnostic devices that are capable of unambiguous femtosecond resolution longitudinal profile, and in addition they are capable of characterising electron-bunch 'slice' parameters which are inaccessible to the CDR/CTR and electro-optic techniques. Transverse deflecting structures however come with significant demands on location and space within an electron transport system, along with large RF infrastructure costs. Here we describe progress towards developing a THz driven transverse deflection diagnostic that offers significantly smaller footprint and flexibility in location, reduced infrastructure costs, and potential for sub-femtosecond temporal resolution.

In a transverse deflecting structure the measurement of temporal properties is driven by a time varying transverse kick and drift space and electron beam optics converting the temporally dependant kick into a transverse displacement. The achievable time resolution of the transverse streak is underpinned by the longitudinal gradient of the deflection force, $\frac{\partial F_\perp}{\partial z} \sim \omega \int dz\, E_\perp^{peak}\,(z - tc\beta_s)$ , where $c\beta_s$is the phase velocity of the deflection field and the synchronised particle beam, and $\omega$ the frequency of the deflection field. For deflection fields at THz frequencies, with a 2-orders of magnitude increase in the longitudinal gradient compared to an RF driven structure with the same peak deflection fields, high time-resolution can be obtained with either significantly reduced peak field strengths, or reduction in physical interaction space (or a combination of both). Laser generated single-cycle sources are well established within the ultrafast laser and THz spectroscopy communities, and sources with 10-100MV/m field strengths in single-cycle sub-picosecond pulses have been widely demonstrated in conventional THz non-linear materials [1,2], while sources of GV/m field strengths have been demonstrated in more exotic organic materials [3]. While much of the historic development of THz sources has been driven by demand in materials science, within the accelerator community there has been significant interest in generating high-field sources for atto-second photon diagnostics. For such an application the electric field of a THz pulse provides a time dependent acceleration of soft-xray liberated photoelectrons, and from analysis of the photo-electron energy spectra the arrival time and temporal duration of the xray pulse can be inferred.

The application of THz pulses for particle acceleration has been previously proposed by several groups [4,5,6], and more recently acceleration of low energy electron beams has been demonstrated [7,8]. Deflection of relativistic beams with THz pulses has been considered recently by Fabianiska et al. [9], where it was proposed to use split ring resonators to enhance the field strength and provide a significant deflection force within the gap of the resonator. To further enhance the time resolution or provide deflection on higher energy beams it is natural to consider an extended interaction length, which introduces the necessity to match the THz carrier-wave velocity with the electron bunch velocity. Waveguide or resonant structures offer a route to slow the phase velocity to less than the velocity of light in vacuum for a 'phase-matched' interaction, but such an approach inherently comes with unavoidable dispersion and distortion of the single-cycle pulse. The dispersion gives rise to a decaying field

† email address: steven.jamison@stfc.ac.uk



ISBN 978-3-95450-177-9

# A HIGH RESOLUTION SINGLE-SHOT LONGITUDINAL PROFILE DIAGNOSTIC USING ELECTRO-OPTIC TRANSPOSITION*

D.A. Walsh†, S.P. Jamison[1], E.W. Snedden, ASTeC, STFC Daresbury Lab, Daresbury, UK
[1]also at The Photon Science Institute, University of Manchester, Manchester, UK
T. Lefevre, CERN, Geneva, Switzerland

*Abstract*

Electro-Optic Transposition (EOT) is the basis for an improved longitudinal bunch profile diagnostic we are developing in ASTeC as part of the CLIC UK research program. The scheme consists of transposing the Coulomb field profile of an electron bunch into the intensity envelope of an optical pulse via the mixing processes that occur between a CW laser probe and Coulomb field in an electro-optic material. This transposed optical pulse can then be amplified and characterised using robust laser techniques – in this case chirped pulse optical parametric amplification and frequency resolved optical gating, allowing the Coulomb field to be recovered. EOT is an improvement over existing techniques in terms of the achievable resolution which is limited by the EO material response itself, reduced complexity of the laser system required since nanosecond rather than femtosecond lasers are used, and insensitivity of the system to bunch-laser arrival time jitter due to using a nanosecond long probe. We present results showing the retrieval of a THz pulse (Coulomb field stand-in) which confirms the principle behind the EOT system.

## INTRODUCTION

The use of electro-optic (EO) techniques for the measurement of longitudinal bunch profiles has for many years held the potential to provide high temporal resolution, non-destructive measurements, and single shot aquisition. The core principle behind all EO techniques is that for suitably relativistic energies the Coulomb field of each electron flattens out, becoming more disc like, resulting in the overall Coulomb field of the bunch becoming an accurate representation of the charge distribution. When this Coulomb field propagates through an EO material the most common, but not always appropriate, approximation is that the refractive index is then modulated through the Pockels effect. A laser pulse is then used to probe this E-field induced change using techniques borrowed or developed from the fields of generation and detection of ultrashort THz pulses, which have very similar properties.

A number of schemes have been developed but there are often trade-offs in system performance or practicality. Spectral decoding [1] whilst simple to implement has a practically limited resolution of a few hundred fs, has a limited (few ps) sampling window, and requires a potentially complex ultrashort pulse laser. However, demonstrations using fibre lasers have been made alleviating this last drawback. Spatial encoding [2] and temporal encoding [3, 4] have higher temporal resolutions, but also have finite sampling windows, and due to the necessary cascaded nonlinear processes require high pulse energy regeneratively amplified laser systems which are very complex and sensitive. There are also methods that improve upon the resolution of Spectral Decoding via the implementation of standard optical pulse diagnostics such as Temporal E-field Cross-correlation (TEX) [5]. This is based on Spectral Interferometry and inherits both the associated resolution enhancement (tens of fs is possible), but also the significant alignment sensitivity associated with interferometric measurements. It has also been suggested that FROG methods could be used to analyse the spectral decoding signals for enhanced resolution (PG-FROG, BMX-FROG [6, 7]), but again this has a limited sampling window along with the requirement of high energy ultrashort pulse lasers to drive the required cascaded nonlinear optical processes.

EOT [8-10] is significantly different to the previously mentioned techniques in that the probe laser field is not necessarily derived from an ultrashort laser pulse. Instead of a compressed or chirped femtosecond pulse, the Coulomb field is probed with a single frequency laser. By applying a more fundamental description of the EO effect as one of nonlinear frequency mixing it can readily be shown, and has been demonstrated [11], that this maps the spectrum of the Coulomb field onto optical sidebands of the probe laser. As nonlinear optical mixing preserves the relative phase information of the spectral components of the Coulomb field this process also transfers information of its temporal profile into the electric field of the new optical waves, as

$$E^{out}(t) \propto \left(\frac{d}{dt}E^{in}(t)\right) \cdot E_{eff}^{bunch}(t), \tag{1}$$

where $E^{out}(t)$ is the newly generated EOT pulse, $E^{in}(t)$ is the input probe, and $E_{eff}^{bunch}(t)$ is the Coulomb field temporal profile accounting for spectral variations in the material response. What this indicates is that the amplitude of the Coulomb field is now mapped into the *envelope* of the new optical wave, with sign changes effectively becoming π phase jumps in the optical carrier wave.

This process now allows the use of Frequency Resolved Optical Gating (FROG) [12] – a standard and robust optical pulse diagnostic – to recover the Coulomb field profile from this new wave. Traditional FROG methods cannot be applied directly to the THz frequency range to recover the field directly as this would necessarily require recov-

* Funded by CERN contract KE1866/DG/CLIC and carried out at STFC Daresbury Laboratory
† david.walsh@stfc.ac.uk



ISBN 978-3-95450-177-9

# NON-INVASIVE BUNCH LENGTH DIAGNOSTICS OF SUB-PICOSECOND BEAMS*

S.V. Kuzikov†,1,2, A.A Vikharev, Institute of Applied Physics, Russian Academy of Sciences, Nizhny Novgorod, Russia
S. Antipov, Euclid Techlabs LLC, Bolingbrook, IL, USA
also at [1]Euclid Techlabs LLC, Bolingbrook, IL, USA
also at [2]Lobachevsky University of Nizhny Novgorod, Nizhny Novgorod, Russia

*Abstract*

We propose a non-invasive bunch length measurement system based on RF pickup interferometry. A device performs interferometry between two broadband wake signals generated by a single short particle bunch. The mentioned wakes are excited by two sequent small gaps in beam channel. A field pattern formed by interference of the mentioned two coherent wake signals is registered by means of detecror's arrays placed at outer side of beam channel. The detectors are assumed to be low cost integrating detectors (pyro-detectors or bolometers) so that integration time is assumed to be much bigger than bunch length. Because rf signals come from gaps to any detector with different time delays which depends on particular detector coordinate, the array allows to substitute measurements in time by measurements in space. Simulations with a 1 ps beam and a set of two 200 micron wide vacuum breaks separated by 0.5 mm were done using CST Particle Studio. These simulations show good accuracy. One can recover the detailed temporal structure of the measured pulse using a new developed synthesis procedure.

## RF PICK-UP INTERFEROMETRY FOR BUNCH LENGTH MEASUREMENTS

We propose to design a device that will effectively perform interferometry between two broadband wake signals generated by the beam. At high repetition rates, interferometer scans at accelerators can be performed quickly. In a matter of seconds, the data can be averaged to improve the signal to noise ratio and allow the use of inexpensive pyro-detectors as opposed to bolometers. As a result one get spatial autocorrelation function for single shot measurement.

### *Measurements of ~10 ps Bunch Length*

In the case of relatively long beams (10 ps) we propose to utilize power diodes with coaxial RF pickups arranged in pairs. A beam pickup intercepts a small fraction of the image current flowing along the beam pipe (Fig. 1). Two signals are combined with a time delay in a coaxial combiner.

*This work was supported by the Russian Scientific Foundation (project #16-19-10448).
†email address: sergeykuzikov@gmail.com

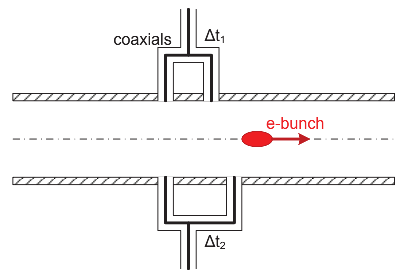


Figure 1: 10 ps resolution non-invasive bunch length measurement setup based on coaxial pairs placed along the z-direction.

Depending on the time delay between the RF pickups, the combined power varies as a function of time.The figure 2 shows the results of a simulation that involves a 10 ps beam passing by two RF pickup probes combined with variable delays. By using several pairs with different delays an autocorrelation function can be produced (Fig. 3).

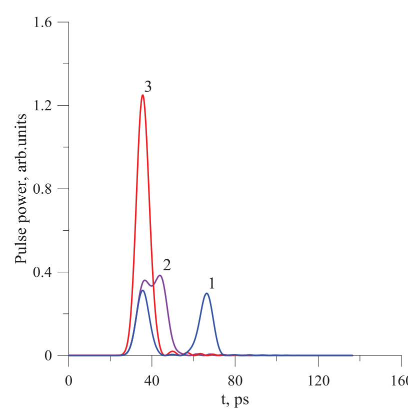


Figure 2: Power time dependence for various time delays.

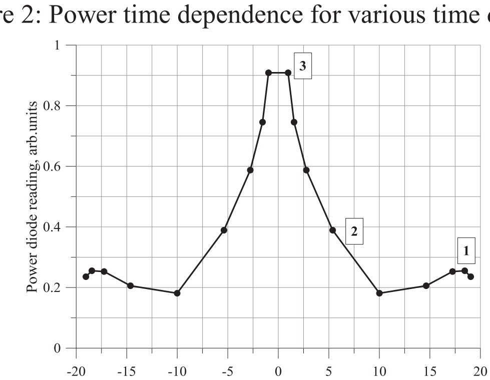


Figure 3: Pyro-detector's output for various time delay pairs.



ISBN 978-3-95450-177-9

# A TRANSVERSE DEFLECTING STRUCTURE FOR THE PLASMA WAKEFIELD ACCELERATOR EXPERIMENT, FLASHForward

R. D'Arcy*, V. Libov, J. Osterhoff
DESY, Hamburg, Germany

*Abstract*

The FLASHForward project at DESY is an innovative plasma-wakefield acceleration experiment, aiming to accelerate electron beams to GeV energies over a few centimetres of ionised gas. These accelerated beams must be of sufficient quality to demonstrate free-electron laser gain; achievable only through rigorous analysis of both the drive- and accelerated-beam's longitudinal phase space. The pulse duration of these accelerated beams is typically in the few femtosecond range, and thus difficult to resolve with traditional diagnostic methods. In order to longitudinally resolve these very short bunch-lengths, it is necessary to utilise the properties of a transverse RF deflector, which maps longitudinal onto transverse co-ordinates. It is proposed that this type of device – commonly known as a Transverse Deflecting Structure (TDS) due to its 'streaking' in the transverse plane – will be introduced to the FLASHForward beam line in order to perform these single-shot longitudinal phase space measurements. The initial investigations into the realisation of this diagnostic tool are outlined.

## INTRODUCTION

The FLASHForward facility [1] at DESY aims to accelerate electron beams to GeV energies over a few centimetres of ionised gas through the principle of Plasma Wakefield Acceleration (PWFA). The FLASHForward beam line utilises sections of the FLASH Linac [2] to extract compressed electron bunches for injection into plasma. Longitudinal diagnosis of both the drive beam entering – as well as the witness beam exiting – the plasma are necessary to the understanding of PWFA physics processes. The resulting accelerated witness bunches, with bunch lengths limited by the plasma wavelength, exit the plasma with a priori unknown bunch parameters. Expected bunch parameter ranges for both driver and witness bunches on FLASHForward can be seen in Table 1, demonstrating the diverse nature of these beams. It is therefore essential to diagnose these beams in full 6D phase space.

The longitudinal and transverse diagnostics provided by a Transverse Deflecting Structure (TDS) system would reveal key information about these drive beams, allowing for the maximising of energy gain in the plasma through bunch shaping. The capability to diagnose witness beams would also yield invaluable insight into the results of acceleration, providing a tool to differentiate between the nuances of distinct injection schemes (thus confirming the validity of particle-in-cell codes), as well as an additional resource in optimising the system for FEL gain. No prior PWFA facility has benefitted from the functionality of an X-band TDS to diagnose both drive and witness bunches. This paper will concern itself with the design, implementation, and simulations of such a system.

* richard.darcy@desy.de

## PROPOSED TDS SYSTEM

Due to the proximity of the FLASHForward and FLASH2 beam lines, it is proposed that an X-band RF system is shared in order to mitigate costs. The proposed experimental plan can be seen in Fig. 1. In this setup, a low-level RF source would supply power to a klystron and modulator unit. These components would sit outside the experimental hall in the adjacent corridor. A high-power acceptance mechanical X-band RF switch would then direct 100% of the RF power to either the FLASHForward or FLASH2 waveguides and X-band TCAV sections. Once this system has been commissioned, a pulse compression unit will be installed to increase the peak power supplied to the cavities.

The voltage kick experienced by a beam travelling through a deflecting cavity is defined by

$$V[MV] = R[MV/m\sqrt{MW}]\, l[m]\, \sqrt{P[MW]} \quad , \qquad (1)$$

where $R$ and $l$ are the shunt impedance and length of the cavity, respectively, and $P$ is the power supplied to the cavity. Although designs for the cavity and RF source have yet to be finalised, initial figures of $R \sim 6\ MV/m\sqrt{MW}$, $l \sim 1.0\ m$, and $P \sim 25\ MW$ are expected. For this reason, a voltage kick of 30 MV will be assumed in all further calculations unless otherwise stated.

## BEAMLINE DESIGN

It is common practice to employ a TDS system for both longitudinal phase space and transverse slice emittance measurements. In order to successfully measure these param-

Table 1: Driver and Witness Bunch Parameters Expected at FLASHForward

| Parameter | Driver | Witness |
|---|---|---|
| $E$ [GeV] | 0.5–1.2 | 1.2–2.5 |
| $\Delta E/E$ (uncorrellated) [%] | <0.1 | 1 |
| $\varepsilon_{n,(x,y)}$ [$\mu$m] | 2–5 | 0.1–1 |
| $\beta_{x,y}$ (in plasma) [mm] | 20 | 1 |
| $\sigma_t$ [fs] | 50–500 | 1–100 |
| $Q$ [pC] | 20–1000 | 1–500 |

ISBN 978-3-95450-177-9

# LASER ARRIVAL TIME MEASUREMENT AND CORRECTION FOR THE SwissFEL LASERS

M. Csatari Divall[†], C. P. Hauri, S. Hunziker, A. Romann, A. Trisorio, Paul Scherrer Institut, 5232 Villigen PSI, Switzerland

*Abstract*

SwissFEL will ultimately produce sub-fs X-ray pulses. Both the photo-injector laser and the pump lasers used for the experimental end stations therefore have tight requirements for relative arrival time to the machine and the X-rays. The gun laser oscillator delivers excellent absolute (including reference jitter) jitter performance at ~25 fs integrated from 10 Hz-10MHz. The Yb:$CaF_2$ regenerative amplifier, with an over 1 km total propagation path, calls for active control of the laser arrival time. This is achieved by balanced cross-correlation against the oscillator pulses and a translation stage before amplification. The experimental laser, based on Ti:sapphire laser technology will use a spectrally resolved cross-correlator to determine relative jitter between the optical reference and the laser, with fs resolution. To be able to perform fs resolution pump-probe measurements the laser has to be timed with the X-rays with <10 fs accuracy. These systems will be integrated into the machine timing and complemented by electron bunch and X-ray timing tools. Here we present the overall concept and the first results obtained on the existing laser systems.

## INTRODUCTION

Excellent timing jitter can be achieved in modern mode-locked solid state lasers [1]. They are standardly used as master oscillator to act as the heart of large accelerator complexes, as timing signals can be distributed in stabilized fiber links over many km's [2]. However to reach required energy to drive photo-injectors, as well as for experiments in FEL's, further amplification is needed. To reach mJ levels of energy in each pulse at up to kHz repetition rates, regenerative and multi-pass amplifiers are used. These include many roundtrips and propagation both in material as well as in air and make the output pulse arrival dependent on environmental factors, such as temperature, humidity, pressure, vibrations and air-flow [3]. To reach required specification, active stabilization of the laser arrival time is necessary. In the following section we describe the laser systems to be used at SwissFEL as well as the required timing stability and present a general concept for laser timing stabilization.

### *Laser Systems at SwissFEL*

Table 1 summarizes the laser parameters and timing requirements for both laser systems. The experimental laser system [4] is based on chirped-pulse amplification in Ti:Sa from Coherent. The system is seeded by Vitara Oscillator and pulses are amplified in Legend Elite Duo HE+ amplifier, with a custom made post amplifier stage and Revolution pump lasers. With this layout it provides a compressed output energy > 20 mJ, centred at 800 nm and at 100 Hz repetition rate.

Table 1: Laser Specifications and Timing Requirements

| Parameter | Experiment Laser | Gun Laser | Units |
|---|---|---|---|
| Wavelength | 800 | 260 | nm |
| Meas. resolution | 10 (1) | 25 | Fs |
| Overall rms jitter | 150 | 40 | Fs |
| Pulse length | 0.03 | 4-10 | ps |
| Rise and falltime | 10 | 700 | fs |
| Pulse Energy | 10 | 2 | mJ |
| Reference wavelength | 1560 | | nm |
| Pulse length | 180 | | fs |
| Pulse energy | 0.2 | | nJ |

The gun laser is a hybrid fiber front-end Yb:$CaF_2$ CPA system, operating at 1041 nm [5]. The oscillator from OneFive[1] at 71.4 MHz delivers broadband pulses and seeds the regenerative amplifier (Amplitude Systeme[2]), which is operating at up to 100 Hz repetition rate. The pulses reach 2.5mJ energy before compression. The system has a UV output, a short probe diagnostic output and an IR beam for the laser heater, all with their individual compressors.

The reference laser is also delivered by OneFive, operating at 1560 nm, delivering 180 fs pulses in stabilized and dispersion compensated fiber links, with 0.2 nJ energy in each pulse. The repetition rate of the master oscillator is at 142.8 MHz, which is twice of the seed oscillators, used for the laser systems. It is expected that the added timing jitter of the links is below 10 fs rms, with a drift of less than 10 fs peak to peak over 24h [6].

### *Timing Overview*

Figure 1 shows the general concept for obtaining timing overlap between the laser output and the master reference link. In both cases the pulse train from the link is compared on a fast ADC with the output pulses from the laser and coarse overlap is obtained via free-space delay stages.

† marta.divall@psi.ch

[1] http://www.onefive.com/

[2] http://www.amplitude-systemes.com/amplifiers-s-pulse.html

ISBN 978-3-95450-177-9

# UNAMBIGUOUS ELECTROMAGNETIC PULSE RETRIEVAL THROUGH FREQUENCY MIXING INTERFERENCE IN FREQUENCY RESOLVED OPTICAL GATING

E.W. Snedden*, D.A. Walsh and S.P. Jamison[1],
Accelerator Science and Technology Centre, STFC Daresbury National Laboratory,
Warrington, WA4 4AD, United Kingdom
[1]also at Photon Science Institute, The University of Manchester,
Manchester, M13 9PL, United Kingdom

*Abstract*

We demonstrate a method for full and unambiguous temporal characterization of few-cycle electromagnetic pulses, including retrieval of the carrier envelope phase (CEP), in which the interference between non-linear frequency mixing components is spectrally resolved using Frequency Resolved Optical Gating (FROG). We term this process Real-Domain FROG (ReD-FROG) and demonstrate its capabilities through the complete measurement of the temporal profile of a single-cycle THz pulse. When applied at THz frequencies ReD-FROG overcomes the bandwidth limitations relating probe and test pulses in Electro-Optic (EO) sampling. The approach can however be extended generally to any frequency range and we provide a conceptual demonstration of the CEP retrieval of few-cycle optical field.

## INTRODUCTION

Few-cycle electromagnetic pulses offer a means to both control and probe physical processes active on femtosecond timescales. State-of-the-art accelerator facilities incorporate or produce such pulses at multiple levels of operation, including: the output of 4$^{\text{th}}$ generation light sources, such as the CLARA free electron laser test facility [1]; the production of coherent transition radiation from a relativistic electron bunch [2]; and the intrinsic coulomb field of a relativistic electron bunch. In the latter two examples the radiation is directly related to the longitudinal properties of the bunch and thus can be utilized for diagnostic purposes [3] . The characterization of such ultrashort radiation is therefore often a crucial element of accelerator operation [4].

All information relating to the temporal properties of an ultrashort field can be derived from knowledge of the pulse spectrum and spectral phase: $\tilde{E}(\omega) = \tilde{A}(\omega)e^{i\tilde{\phi}}(\omega)$. The spectral phase can be mathematically described by the series expansion:

$$\tilde{\phi}(\omega) = \phi^{CE} + \tilde{\phi}^{(1)}(\omega) + \frac{1}{2}\tilde{\phi}^{(2)}(\omega) + \ldots \tag{1}$$

The zero-order term of Eq. (1) ($\phi^{CE}$) is referred to as the carrier envelope phase (CEP). For pulses in which the electric field envelope consists of many cycles this term can be identified as a time-shift of the carrier within the envelope. In few or single-cycle pulses however the distinction between the carrier and envelope components is no longer appropriate and the CEP plays a fundamental role in determining the temporal profile.

While many methods are available to measure relative changes in CEP (for example, f-2f interferometery [5]), schemes to measure the absolute value of CEP are more specific, being limited by constraints in frequency and often involve complex experimental arrangements [6]. Obtaining the full temporal field profile typically requires a separate system dedicated to the measurement of the pulse envelope and higher-order spectral phase components. Towards this latter case Frequency Resolved Optical Gating (FROG) has found common application due to its robustness and ease of experimental implementation [7]. In all forms FROG incorporates the measurement of an intensity spectrogram which is derived from a non-linear interaction between multiple pulses. As a measurement of intensity however it has been widely held that FROG techniques are incapable of determining the CEP.

In beam diagnostic applications, Electro-Optic (EO) sampling has found extensive use as a means of characterizing the complete temporal profile – including the CEP – of few and single-cycle THz pulses produced by relativistic electron sources [3]. EO sampling requires that the THz field is interrogated by a $\delta$-like optical probe field and thus is subject to bandwidth limitations relating the probe and test fields. EO sampling has been utilized in recent work [8,9] to characterize the CEP of far-infrared pulses; as $\phi^{CE}$ presents as a spectral invariant, knowledge of the CEP at THz frequencies within the pulse (as can be obtained through EO sampling) is sufficient for reconstruction of the complete temporal profile following a separate FROG measurement.

In this work we demonstrate that unambiguous retrieval of an ultrashort pulse including the CEP can proceed directly from a single FROG measurement in which the interference between harmonic components is resolved. We develop a theoretical framework for this method termed Real-Domain FROG (ReD-FROG) [10], describing how it conceptually relates to EO sampling. A proof-of-principle experiment is presented in which the CEP of a single-cycle THz pulse is accurately retrieved. We finally demonstrate the conceptual application of self-referenced ReD-FROG to the recovery of an octave-spanning optical field.

* edward.snedden@stfc.ac.uk

ISBN 978-3-95450-177-9

# BUNCH SHAPE MEASUREMENTS AT THE NATIONAL SUPERCONDUCTING CYCLOTRON LABORATORY ReAccelerator (ReA3)*

R. Shane†, S. M. Lidia, Z. Liu, S. Nash, A. C. C. Villari, O. Yair
Facility for Rare Isotope Beams, East Lansing, USA

*Abstract*

The longitudinal bunch shape of a reaccelerated heavy-ion beam at the National Superconducting Cyclotron Laboratory's (NSCL) ReA3 beamline was measured using an Ostrumov-type bunch-shape monitor. The phase of the last accelerating cavity was varied to change the bunch length, while the energy was kept constant by adjusting the amplitude of the voltage on the cavity. Two peaks were observed in the longitudinal projection of the bunch shape distribution. The widths of the two peaks did not vary much when the cavity phase was changed, while the peak separation decreased to the point that the two peaks became unresolvable as the bunching was increased. The relative amplitudes of the two peaks was very sensitive to tuning parameters. This, coupled with a lack of information about the transverse profile of the bunch, complicated the analysis and made a simple width assignment difficult. Measurements were also made with an MCP timing grid for comparison. The general shape and trend of the two data sets were similar; however, the widths measured by the timing grid were about 30-50% smaller.

## INTRODUCTION

We have utilized a borrowed bunch shape monitor (BSM) [1] to perform measurements at the ReAccelerator (ReA3) facility at the National Superconducting Cyclotron Laboratory (NSCL) [2,3]. For this measurement, a beam of $^{42}$Ar was stopped in a gas stopper and subsequently reaccelerated by ReA3. The beam had a pulse structure at 5 Hz with a duty factor of 20%, and an average current of about 6-30 epA.

The ReA3 accelerator uses prototypes of the RF cavities for the Facility for Rare Isotope Beams (FRIB). Bunch-shape measurement is required at the charge-stripping area of the FRIB accelerator. The experience and understanding gained in this set of measurements will help to reduce future development cost of the bunch-shape monitoring system for FRIB.

A schematic showing the principle of operation for the BSM is shown in Fig. 1. Secondary electrons are emitted when beam ions strike a tungsten wire. The wire is held at a large negative potential (up to -10 kV), which causes the electrons to accelerate away. A collimating slit selects a narrow beamlet of electrons. These collimated electrons pass between RF deflection plates which provide transverse modulation of the electrons. The deflector is synced to the accelerator frequency ($\omega$ = 80.5 MHz).

* This material is based upon work supported by the U.S. Department of Energy Office of Science under Cooperative Agreement DE-SC0000661, the State of Michigan and Michigan State University.
† email address: shane@frib.msu.edu

The electrons, now spread transversely, impinge on an MCP, and a camera is used to view the electron distribution on the phosphor screen. Varying the phase offset ($\varphi_0$) between the deflector and accelerator shifts the spatial distribution on screen.

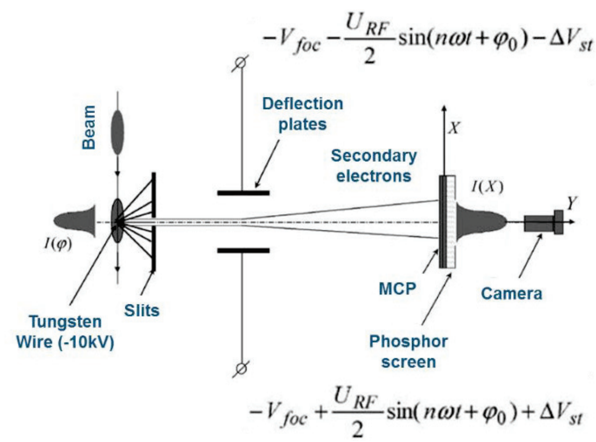


Figure 1: Schematic of bunch-shape measurement technique, adapted from Ref. [1].

## DATA

The raw greyscale images from the camera are averaged over 127 captures, and then a threshold is applied on the intensity to produce black and white images as shown in Fig. 2 (top). These are projected onto the horizontal axis to produce a one-dimensional waveform of the longitudinal bunch shape, as shown in Fig. 2 (bottom). Three waveforms were recorded at each RF deflection phase, with a variance of about 10% of the peak intensity. A running average reduces this to about 3%.

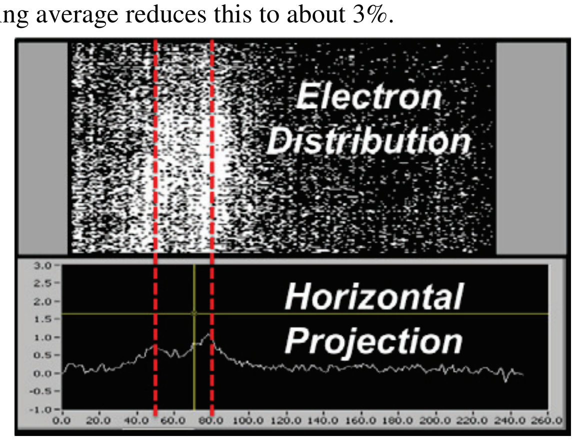


Figure 2: (top) Raw camera image showing the electron distribution intensity. (bottom) Projection of the distribution onto the horizontal axis.

ISBN 978-3-95450-177-9

# SYNCHRONIZATION OF ps ELECTRON BUNCHES AND fs LASER PULSES USING A PLASMONICS-ENHANCED LARGE-AREA PHOTOCONDUCTIVE DETECTOR

E. J. Curry*, M. Jarrahi, P. Musumeci, N. T. Yardimci†, UCLA, Los Angeles, CA 90095, USA
B. T. Jacobson, RadiaBeam Technologies, Santa Monica, CA 90405, USA

*Abstract*

Temporal synchronization between short relativistic electron bunches and laser pulses at the ps and sub-ps level is required for accelerator applications like inverse Compton scattering based light sources. Photoconductive antennas with THz and sub-THz bandwidth which are gated by fs lasers provide this level of timing resolution. This paper describes the operating principals of the diagnostic along with bench-top experimental results with recently developed plasmonics-enhanced large-area devices. A vacuum chamber with robust electronic noise reduction has been designed for upcoming beam-based experiments.

## INTRODUCTION

Modern high-brightness photo-injectors have evolved to produce bunched beams of relativistic electrons with ps and sub-ps duration, while commercial laser technology has reduced pulse lengths of high-power IR sources to 100 fs and below. These two advances have led to a merging of these disciplines into a new scientific field where each core technology must operate at peak performance and be synchronized in time with a resolution better than the pulse lengths involved, such as in inverse Compton scattering, where the electron bunch and laser pulse must arrive simultaneously and collide at the interaction point.

## SYNCHRONIZATION MEASUREMENT METHODS

A traditional way for synchronizing electron beam and laser pulses is by using signals from button or stripline beam position monitor for electrons timing [1] while monitoring laser pulses with a biased photodiode. To acquire sub-ps resolution, optical and cable delays must be characterized and the analog signals must be sampled by a high-bandwidth oscilloscope.

Instead of directly measuring beam or laser signal, several techniques have been developed for bunch length measurements and synchronization known as electro-optic sampling (EOS) methods, where the bunch profile is encoded in a signal [2]. Each scheme exploits the changes in optical properties, e.g. birefringence, of some material due to the presence of the passing electric field of the beam. Our EOS setup uses a Wollaston prism configured for doubly-balanced diode detection.

Another method for beam and laser synchronization uses a photoconductive antenna (PCA) which behaves like an optically gated THz sensor. The gate is provided by a fs laser pulse which allows charge flow in a photoconductive substrate for the duration of the illuminating pulse. THz fields generated by the ps or sub-ps electron bunches can be extracted via a transition radiation foil, or measured directly by placing the PCA detector in close proximity to the electron beam. Bunch length measurements have been made [3] using transition radiation and specially designed radially polarized PCA detectors [4]. However, we pursue directly measuring the Coulomb field of the electron bunches by placing the detector inside of the beam vacuum chamber [5].

## EXPERIENCE WITH COMMERCIALLY AVAILABLE PCA SENSORS

Last year we made attempts to adapt a commercially available PCA sensor for beam measurements at the UCLA Pegasus beamline [6]. The sensor had a 5 µm gap in the dipole antenna structure. A large laser spot illuminating a movable pin-hole was used to limit the probe beam size and position the spot in the dipole gap. Bench test of the device mounted in this manner [5] showed this detector should be sensitive to the peak THz field amplitudes excited in close proximity to the Pegasus beam.

However, these beam measurements were unsuccessful. Three issues have been identified that contributed to the failed measurement attempt: maintaining laser alignment one the pinhole assembly was pumped down, the presence of large electronic noise backgrounds, and the overall device sensitivity to THz fields. Over the past year, we have addressed each of these issues, as described in the remainder of this contribution.

## DESCRIPTION OF PLASMONICS-ENHACED LARGE-AREA PHOTOCONDUCTIVE DETECTORS

Incorporation of plasmonic contact electrodes into PCAs has been proven to be an efficient concept to increase the sensitivity and responsivity of the conventional photoconductive detectors [7]. In this project, a novel large-area plasmonic photoconductive device based on a 2-D plasmonic nano-antenna array is used. By using a large-area design, the optical beam doesn't have to be focused tightly anymore. Therefore, the device can accommodate higher optical pump power levels without any thermal breakdown and offers much easier optical alignment. Moreover, the nano-antennas are designed to have low RC parasitic loading; hence, the detector offers a

*ejcurry99@gmail.com
†yardimci@ucla.edu (photoconductive detector design)



ISBN 978-3-95450-177-9

# SINGLE-SHOT THz SPECTROSCOPY FOR THE CHARACTERIZATION OF SINGLE-BUNCH BURSTING CSR

J. Raasch†, M. Arndt, K. Ilin, A. Kuzmin, A. Schmid, M. Siegel, S. Wuensch, Institute of Micro- and Nanoelectronic Systems, Karlsruhe Institute of Technology (KIT), Karlsruhe, Germany
A.-S. Mueller, J. L. Steinmann,
Laboratory for Applications of Synchrotron Radiation, KIT, Karlsruhe, Germany
G. Cinque, M. D. Frogley, Diamond Light Source, Didcot, United Kingdom
J. Hänisch, B. Holzapfel, Institute for Technical Physics, KIT, Karlsruhe, Germany

*Abstract*

An integrated array of narrow-band high-$T_c$ $YBa_2Cu_3O_{7-x}$ (YBCO) detectors embedded in broad-band readout was developed for the future use at synchrotron light sources as a single-shot terahertz (THz) spectrometer. The detection system consists of up to four thin-film YBCO nanobridges fed by planar double-slit antennas covering the frequency range from 140 GHz up to 1 THz. We present first results obtained at the ANKA storage ring and at Diamond Light Source during operation of two and four frequency-selective YBCO detectors, respectively.

## INTRODUCTION

Brilliant Coherent Synchrotron Radiation (CSR) from short, relativistic electron bunches opens a broad range of applications, amongst them terahertz (THz) imaging and spectroscopy. One prominent way to generate CSR is the use of dedicated low-alpha optics in an electron storage ring [1]. Herein, the bunch length is reduced to sub-mm dimensions leading to the coherent emission at wavelengths longer than the overall bunch length, thus in the THz frequency range. The low-alpha mode, however, entails electron beam instabilities, the so-called micro-bunching, once the beam current exceeds a certain threshold [2]. This leads to a variation in the temporal and spectral shape of the emitted THz radiation pulses. The micro-bunching is characterized by the occurrence of bursts of THz radiation at wavelengths shorter than the overall bunch length. These instabilities restrain the possible range of usage of CSR. Moreover, the micro-bunching instabilities limit the possible bunch compression and thus the level of emitted THz radiation power. Optimization of the emitted CSR requires a deeper understanding of the micro-bunching mechanisms. To this end, single-shot and turn-by-turn resolution of the THz signal is needed.

The short pulse lengths during low-alpha operation (ps/sub-ps) combined with high revolution frequencies (above 100 kHz) prevents the use of most room-temperature and liquid helium cooled semiconductor THz detectors. Response times of commercial pyroelectric sensors and semiconducting bolometers are limited at around tens of milliseconds and several hundred nanoseconds, respectively [3]. As compared to that, the characteristic times during the measurements at ANKA are 15 – 20 ps full width at half maximum (FWHM) for the pulse lengths and 2 ns between two consecutive pulses, corresponding to 500 MHz repetition rate [4]. At Diamond Light Source the characteristic pulse length was about 8 ps FWHM, the repetition frequency is the same as at ANKA [5]. Superconducting detectors offer both a high sensitivity and fast response times. First bunch-by-bunch resolution of CSR pulses was demonstrated by the use of superconducting NbN hot-electron bolometers with response times of 165 ps FWHM by Semenov et al. [6]. However, the resolution of the single pulse's temporal shape is not viable with those detectors.

Highest temporal resolution in direct detection is offered by detectors based on the high-$T_c$ material $YBa_2Cu_3O_{7-x}$ (YBCO). Response times as fast as 16 ps FWHM have been demonstrated [7]. Here the limiting factor was identified to be the readout electronics rather than intrinsic response times of YBCO that lie in the range of 1 – 2 ps only [8]. Moreover YBCO THz detectors offer zero bias detection combined with the unique feature of electrical field sensitivity, both of them being based on the intrinsic detection mechanism for direct THz irradiation [9, 10].

At ANKA the overall bunch length of individual CSR pulses could be observed using the YBCO detection system [7]. The substructure on the bunch that arises during bursting can however not be resolved with state-of-the-art electronics. Therefore single-shot THz spectroscopy is a promising new candidate to gain further insight into the bunch profile. For that, single-shot spectral resolution needs to be combined with the ability to resolve individual bunches in a multi-bunch environment. By transforming the information from the single-shot spectra to the time domain, even shorter bunch lengths and substructures can be observed.

Due to its fast intrinsic relaxation processes YBCO was selected as detector material and embedded into narrow-band antennas combined with broad-band readout, as described in the next section. The second part of this report focuses on first tests of planar double-slot antennas under pulsed irradiation that have been conducted at the ANKA storage ring. The narrow-band operation of an array consisting of four detectors has been demonstrated

This work was supported by the German Federal Ministry of Education and Research (Grant 05K13VK4), by the Helmholtz International Research School for Teratronics and the Karlsruhe School of Elementary Particle and Astroparticle Physics: Science and Technology.
† juliane.raasch@kit.edu



ISBN 978-3-95450-177-9

# SINGLE-SHOT THz SPECTROMETER FOR BUNCH LENGTH MEASUREMENTS*

S.V. Kutsaev, A. Murokh, M. Ruelas, H. To
RadiaBeam Systems, LLC, Santa Monica, CA, 90403, USA
V. Goncharik
Logicware Inc, New York, NY, 11235, USA

*Abstract*

We present a new diagnostic instrument designed to measure bunch length in RF particle accelerators. Typically, scanning-type Michelson or Martin-Puplett interferometers are used to measure the coherent radiation from a short bunch to deduce the bunch length. However, this requires averaging over several shots, revealing only the average bunch length. We propose to measure the emitted coherent spectrum of a short bunch emission that contains the same spectral information as the bunch shape using single-shot spectrometry. In this paper, we present design considerations and first experimental results obtained at FACET for this instrument that allows shot-to-shot measurement of the spectrum emitted by a short electron bunch.

## INTRODUCTION

Electron bunch length monitors are an important diagnostic tool for current and upcoming accelerators. The short bunch lengths of single-pass linacs have traditionally made use of RF transverse deflecting cavities [1,2,3] or interferometric methods [4,5]. RF deflecting cavities streak the electron bunch onto a screen and is a destructive measurement limited by available RF power. Interferometric methods exploit the fact that the emitted coherent spectrum of a bunch contains the spatial information of the bunch structure. This technique is attractive in that it is potentially non-destructive when paired with coherent synchrotron radiation or diffraction radiation. However, scanning-type Michelson or Martin-Puplett interferometers are incapable of shot-to-shot measurements.

A single-shot, non-destructive, high-repetition-rate bunch length monitor is a greatly desired diagnostic. A cascaded multi-stage grating spectrometer has the potential to fill this gap in diagnostic techniques [6].

## SINGLE-SHOT SPECTROMETER

Since a single-shot spectrometer allows for reliable detection and measurement of RF pulse shortening, it can be used for identification of occurrences of RF breakdown (RFBD). The first prototype of our THz spectrometer was designed for RFBD detection in 120 GHz high-gradient accelerating sections developed at the SLAC National Accelerator Laboratory [7]. Operations with short pulses required narrow bandwidth (2GHz) and high frequency resolution (100 MHz).

This version of the spectrometer was designed, prototyped and built by RadiaBeam Systems, LLC [8]. It was tested at SLAC and the proof-of-principle operation was demonstrated. It was revealed that the alignment and optics systems must be enhanced, as well as more robust electronics added.

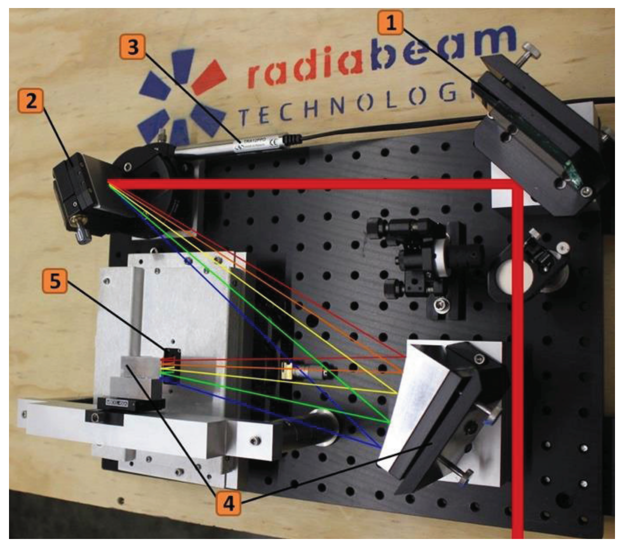


Figure 1: Physical layout of final spectrometer design, shown with dimensions and optical path

The design of the THz single-shot spectrometer is an adaptation of the DESY broadband multi-channel spectrometer [9], and consists of several core elements shown in Figure 1:

1) Reflecting mirror to deflect the signal to the grating,
2) Diffraction grating to spatially separate the signal by frequencies,
3) Motorized mounting to rotate the grating,
4) Aluminum 2D parabolic mirrors to focus the signal on the linear detector array,
5) Electronic board with pyroelectric detector to acquire the THz radiation signal

## DESIGN UPGRADE

Unlike the spectrometer for RFBD detection, for which a narrow-band, high-resolution spectroscopy is required, the bandwidth of the spectrometer for bunch length measurements must be much larger than the RFBD design. This upgrade can be accomplished with two simultaneous techniques: adding additional stages with

* This work was supported by the U.S. Department of Energy, Office of High Energy Physics, under contract DE-SC0013684



ISBN 978-3-95450-177-9

# THERMAL SIMULATIONS OF WIRE PROFILE MONITORS IN ISIS EXTRACTED PROTON BEAMLINE 1

D. W. Posthuma de Boer*, A. Pertica, ISIS, STFC, Rutherford Appleton Laboratory, Oxfordshire, OX11 0QX, UK

*Abstract*

Wire scanners and secondary emission (SEM) grids are used for measurements of transverse beam profile at the ISIS neutron and muon source. Silicon carbide-coated carbon fibre wires are used in profile monitors throughout the ISIS accelerator. One such SEM grid is currently installed close to the target in Extracted Proton Beamline 2 (EPB2) and is intercepted by the 800 MeV proton beam at a repetition rate of 10 Hz. Future profile measurements will require another of these monitors to be installed close to the target in EPB1; intercepted with a repetition rate of 40 Hz.

Wires intercepting the ion beam are heated due to the deposition of beam-energy. Thermal simulations for the higher repetition rate were performed using ANSYS and a numerical code. The numerical code was then expanded to include various beam, wire and material properties. Assumptions for temperature dependent material emissivities and heat capacities were included in the simulation. Estimated temperatures due to the energy deposited by protons, and approximate values of deposited energy from the expected neutron flux are presented. The effects on wire-temperature of various beam and wire parameters are also discussed.

## INTRODUCTION

Intercepting wires are used at accelerator facilities around the world to measure transverse and longitudinal beam properties. Beam particles either knock electrons from the wire or deposit some charge, inducing a current which is proportional to the flux of the beam. By measuring the relative current at multiple transverse positions, a beam profile can be obtained [1].

The ISIS facility at the Rutherford Appleton Laboratory is a spallation neutron and muon source delivering an average of 0.2 MW of proton beam power to two target stations (TS1 & TS2). During acceleration and extraction wire-based monitors are used to measure the transverse beam profile. At ISIS the intercepting wires are silicon-carbide (SiC) coated carbon fibres with a diameter of 142 µm.

A wire grid is currently installed in EPB2 close to the TS2 target, with the wires intercepting the beam at a rate of 10 Hz. Future profile measurements will require a second grid to be installed in EPB1 close to the TS1 target. These wires will intercept the 800 MeV proton pulses at a repetition rate of 40 Hz. Thermal simulations are required to verify that wires in EPB1 will be able to withstand temperatures resulting from this higher repetition rate.

* david.posthuma-de-boer@stfc.ac.uk

## THEORY

### *Charged Particles in Matter*

Energetic charged particles passing through a medium interact electromagnetically with atomic electrons, depositing energy by ionising constituent atoms. For a singly charged particle with a velocity $v = \beta c$, energy $E$ and relativistic factor $\gamma$, passing through a material with atomic number $Z$ and number density $n$, the energy deposited into the material per unit particle path length $x$; the stopping power $S(E)$, follows the Bethe-Bloch equation

$$S(E) = -\frac{\mathrm{d}E}{\mathrm{d}x} \approx \frac{4\pi\hbar^2\alpha^2 nZ}{m_e\beta^2}\left[\ln\left(\frac{2v^2\gamma^2 m_e}{I_e}\right) - \beta^2\right], \quad (1)$$

where $\alpha$ is the fine structure constant, $I_e$ is the effective ionisation potential, $m_e$ is the electron mass, $c$ is the speed of light and $\hbar$ is the Dirac constant [2]. An example of this for 800 MeV protons travelling in a tungsten medium is shown in Fig. 1. As the protons travel through the medium they lose kinetic energy to atomic electrons, increasing the value of $S(E)$ [2]. A sharp increase in the stopping power; known as the Bragg peak, is seen towards the end of the range.

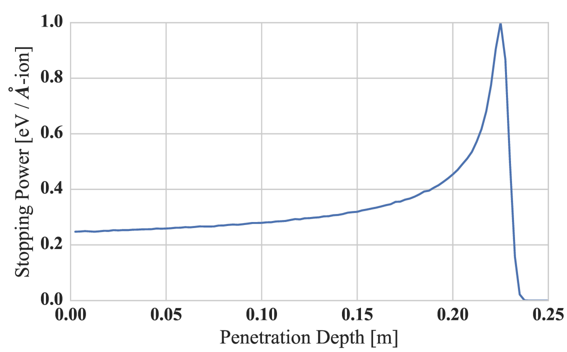


Figure 1: Results of a SRIM simulation showing the stopping power for 800 MeV protons in tungsten [3].

### *Thermal Effects*

From the definition of the constant-volume heat capacity it can be found that the change in temperature, $\Delta T$, of an object is given by:

$$\Delta T = \int \frac{1}{Mc_v}\,\mathrm{d}U, \quad (2)$$

where $U$ is the internal energy of an object, $M$ is the energy-absorbing-mass and $c_v$ is the constant-volume specific heat capacity of the material. Equation (2) shows that when energy is deposited into an object there is an associated increase in temperature [4].

ISBN 978-3-95450-177-9

# THEORY OF X-RAY TRANSITION RADIATION FROM GRAPHENE FOR TRANSITION RADIATION DETECTORS*

A.A. Tishchenko†, A.S. Romaniouk, D.Yu. Sergeeva, M.N. Strikhanov, National Research Nuclear University MEPhI, Moscow, Russia

*Abstract*

We present the theory of transition radiation for monolayers in X-ray domain from the first principles and consider the pros and cons of using graphene-monolayer in transition radiation detectors.

## INTRODUCTION

Transition Radiation Detectors (TRD) are used in many modern experiments like ATLAS and ALICE in CERN, FENIX in BNL, AMS-02 experiment in space, etc. Usually they are used to separate particles with gamma factor less than 500 and more than 1500. However, to increase separation threshold TRD technique requires significant improvement.

Cut-off frequency of the transition radiation (TR) spectrum is proportional to the Lorenz-factor $\gamma$, which extends the spectrum to the X-ray domain, see Fig. 1. The cut-off frequency is defined as:

$$\omega_c = \gamma\omega_p. \tag{1}$$

This frequency is proportional to the plasma frequency $\omega_p$ of the material which depends on the electron density and the effective mass of electron $m_e$:

$$\omega_p^2 = 4\pi NZe^2/m_e, \tag{2}$$

with $e$ being the electron charge, $NZ$ being the number of electrons in the unit volume of the target.

In paper [1] it was suggested to use TR radiators based on graphene-monolayer. The idea is based on the fact that some fraction of conductivity electrons in graphene has zero (or very little) mass and, hence, as plasma frequency is inversely proportional to the mass of electron it could shift the TR spectrum to the region of higher frequencies with respect to the ordinary materials. Indeed, it is seen from Eq. (2) that if the effective electron mass goes to zero, then both the plasma frequency and the cut-off frequency from Eq. (1) go to infinity:

$$m_e \to 0, \quad \Rightarrow \quad \gamma\omega_p \to \infty. \tag{3}$$

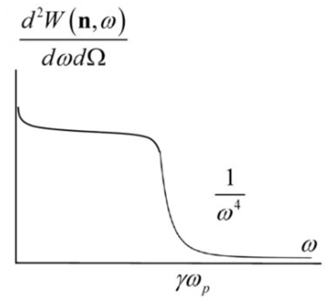


Figure 1: Cut-off of the transition radiation spectrum at high frequencies.

Calculation of the characteristics of the radiation from any monolayer can not be a limiting case of zero-thickness film from the theory for the film of arbitrary thikness, because the latter uses normally boundary conditions, which is not the case for monolayer.

Below we present the theory of transition radiation for monolayers in X-ray domain from the first principles [2, 3] and consider the pros and cons of using graphene-monolayer in TRDs.

## MICROSCOPIC THEORY OF RADIATION FROM A MONOLAYER

Let us consider the generation of TR by a single charged particle, for example, by an electron. The target is a monolayer consisting of $N$ atoms or molecules or any small particles with the size less than the wavelength.

Microscopic Maxwell's equations for such a system have the form:

$$\begin{cases} rot\mathbf{H}^{mic}(\mathbf{r},\omega) = \frac{4\pi}{c}\mathbf{j}'(\mathbf{r},\omega) - \frac{i\omega}{c}\mathbf{E}^{mic}(\mathbf{r},\omega), \\ rot\mathbf{E}^{mic}(\mathbf{r},\omega) = \frac{i\omega}{c}\mathbf{H}^{mic}(\mathbf{r},\omega), \\ div\mathbf{H}^{mic}(\mathbf{r},\omega) = 0, \\ div\mathbf{E}^{mic}(\mathbf{r},\omega) = 4\pi\left(\rho^0(\mathbf{r},\omega) + \rho^{mic}(\mathbf{r},\omega)\right), \end{cases} \tag{4}$$

where

$$\mathbf{j}'(\mathbf{r},\omega) = \mathbf{j}^0(\mathbf{r},\omega) + \mathbf{j}^{mic}(\mathbf{r},\omega). \tag{5}$$

The exact solution of the system Eq. (4) is :

*This work was supported by the grant RFBR 14-22-03053 (ofi-m) and, partially, by the Competitiveness Program of National Research Nuclear University MEPhI.

†tishchenko@mephi.ru



ISBN 978-3-95450-177-9

# INCOHERENT AND COHERENT POLARIZATION RADIATION AS INSTRUMENT OF THE TRANSVERSAL BEAM SIZE DIAGNOSTICS*

D.Yu. Sergeeva†, M.N. Strikhanov, A.A. Tishchenko, National Research Nuclear University MEPhI, Moscow, Russia

*Abstract*

Polarization radiation, which includes diffraction radiation (DR), transition radiation (TR), Smith-Purcell radiation, and others, can be a good instrument for beam diagnostics. All information about the beam size is contained in the so-called form-factor of the beam. The form-factor represents the sum of two parts corresponding to the coherent and incoherent radiation. Contrary to the general opinion the incoherent part does not always equal unity. In this report we give theoretical description of the incoherent and coherent parts of the form-factor both for Gaussian and uniform distribution of the ultrarelativistic particles in the bunch. The theory constructed describes also the case of beam skimming the target, which leads to mixing of DR and TR. We show that the incoherent part depends on the transversal size of the beam, and dependence differs for different distributions. The role of the incoherent part of the form-factor of the bunch for different parameters is discussed.

## INTRODUCTION

Diffraction radiation (DR), Smith-Purcell radiation (SPR), transition radiation (TR) have the similar nature: they arise due to the dynamic polarization of the target material by the Coulomb field of a charged particle. So, they can be called polarization radiation. The theory of polarization radiation from a single particle are well developed, except for X-ray polarization radiation.[1]

X-ray radiation makes the sub-micron beam diagnostics possible, because for such short waves the Rayleigh limitation is not a problem.

The spectral-angular distribution of the energy of radiation from a beam can be obtained as the distribution of energy for radiation from a single particle $d^2W_1/d\omega d\Omega$ multiplied by form-factor $F$ [2]:

$$\frac{d^2W(\mathbf{n},\omega)}{d\Omega d\omega}=\frac{d^2W_1(\mathbf{n},\omega)}{d\Omega d\omega}F. \quad (1)$$

The form-factor has two terms, corresponding to the coherent and incoherent radiation:[2-6]

$$F=NF_{inc}+N(N-1)F_{coh}, \quad (2)$$

with $N$ being the number of the particles in the bunch.

Usually the incoherent form-factor is supposed to be equal to unity, like it occurs for synchrotron radiation or transition radiation from an infinite media of an infinite slab. For polarization radiation from the target edge (DR, SPR, TR from a finite slab) the incoherent form-factor does not equal unity:

$$F_{inc}\neq 1. \quad (3)$$

This fact was explained in detail in the paper [2].

One of the main features of the spectral-angular distribution of the polarization radiation is its dependence on the impact-parameter, i.e. the shortest distance between the moving charge and the target surface; see the parameter $h$ in Fig. 1. This dependence is:

$$\frac{d^2W_1(\mathbf{n},\omega)}{d\Omega d\omega}\propto\exp(-2\rho h), \quad (4)$$

where $\rho$ is some function which will be defined below. From Eq. (4) it is clear that the far the particle from the target surface is, the less intensive the radiation is:

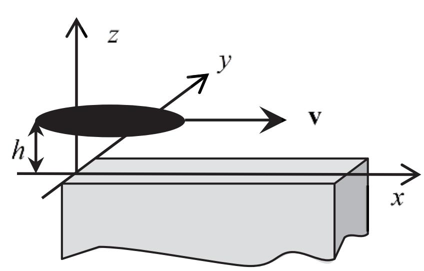


Figure 1: Generation of the radiation by moving the bunch near the target.

## FORM-FACTOR

The way to obtain the formula for the coherent and incoherent form-factor was described in [7] for the Diffraction radiation and Smith-Purcell radiation:

$$\begin{aligned}F_{inc}&=\int_V d^3r\left|e^{-i\mathbf{rq}}\right|^2 f(\mathbf{r}),\\ F_{coh}&=\left|\int_V d^3re^{-i\mathbf{rq}}f(\mathbf{r})\right|^2,\end{aligned} \quad (5)$$

where the integral is over the bunch volume $V$, $f(\mathbf{r})$ is the function of distribution of the particles in the bunch written in the system where the bunch is at rest.

*This work was supported by the Leverhulme Trust International Network, grant IN-2015-012, and by the Competitiveness Program of National Research Nuclear University "MEPhI".
†DYSergeyeva@mephi.ru



ISBN 978-3-95450-177-9

# PERFORMANCE EVALUATION OF MOLYBDENUM BLADES IN AN X-RAY PINHOLE CAMERA

L.M. Bobb, A.F.D. Morgan, G. Rehm, Diamond Light Source, Oxfordshire, U.K.

*Abstract*

At Diamond Light Source transverse profile measurements of the 3 GeV electron beam are provided by x-ray pinhole cameras. From these beam size measurements and given knowledge of the lattice parameters the emittance, coupling and energy spread are calculated. Traditionally, tungsten blades are used to form the pinhole aperture due to the opacity of tungsten to x-rays in the keV spectral range. The physical properties of tungsten also make it difficult to work. To achieve the 25 $\mu$m $\times$ 25 $\mu$m aperture size required for high resolution measurements it is necessary to mount these tungsten blades in an assembly whereby the pinhole aperture size is defined by precisely machined shims. Here we propose to replace the tungsten blade and shim arrangement with machined molybdenum blades and evaluate the performance of the resulting imaging system.

## INTRODUCTION

In order to provide high brilliance x-rays for user experiments, third generation synchrotron radiation facilities must operate with low vertical emittance beams. The emittance of the electron beam is derived from measurements of the transverse beam profile [1, 2] and may be controlled via a feedback system [3]. This necessitates the need for high resolution, robust and online beam size monitoring.

There are various non-invasive techniques to measure the transverse beam profile using synchrotron radiation in the visible to x-ray spectral range [4–7]. In this paper we focus on the use of x-ray pinhole cameras.

Currently there are two pinhole cameras in the vertical emittance feedback system which are referred to as “pinhole 1” and “2” respectively. The layout of these pinhole cameras is shown in Fig. 1. Two different bending magnet locations provide synchrotron radiation to each of the pinhole cameras. The synchrotron radiation is passed from the storage ring vacuum to air through a 1 mm thick aluminium window. Due to the spectral transmission of aluminium the transmitted beam is filtered. The beam is filtered further by its transmission through air from the window to the pinhole and from the pinhole to the PreLude 420 scintillator screen. The source has a spectrum from approximately 15 keV to above 60 keV [1]. To prevent oxide growth the pinhole assemblies are kept under nitrogen.

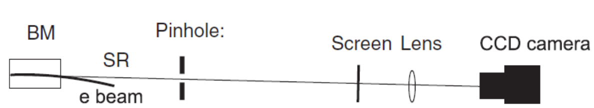


Figure 1: Schematic of the pinhole camera system [1].

The pinhole assembly arrangement of pinhole systems 1 and 2 are identical. The pinhole apertures are formed by stacking two orthogonal sets of (25 mm(h) $\times$ 1 mm(v) $\times$ 5 mm(d)) tungsten blades separated by precisely machined shims. The thickness of the shims between the tungsten blades sets the aperture size e.g. to form a 25 $\mu$m aperture a pair of 25 $\mu$m thick shims are positioned between the ends of a pair of tungsten blades.

The spatial resolution of an imaging system may be described by the point spread function (PSF). The PSF is assumed to be constant on relatively long timescales for a given imaging system and is approximated by a Gaussian distribution of standard deviation $\sigma_{PSF}$. For a pinhole camera imaging system the overall PSF may be represented as

$$\sigma^2_{PSF} = \sigma^2_{pinhole} + \sigma^2_{camera} \tag{1}$$

with

$$\sigma^2_{pinhole} = \sigma^2_{diffraction} + \sigma^2_{aperture} \tag{2}$$

and

$$\sigma^2_{camera} = \sigma^2_{screen} + \sigma^2_{lens} + \sigma^2_{CCD} \tag{3}$$

where the subscripts denote the sources of the PSF contributions. The PSF contribution associated with imaging the scintillator screen denoted $\sigma_{camera}$ may be measured using a knife-edge. The PSF contribution from the pinhole denoted $\sigma_{pinhole}$ may be calculated given the aperture size is known [1].

Due to the tungsten and shim arrangement, although the thickness of the shim is known, the absolute effective aperture size available to pass beam is not well defined. The

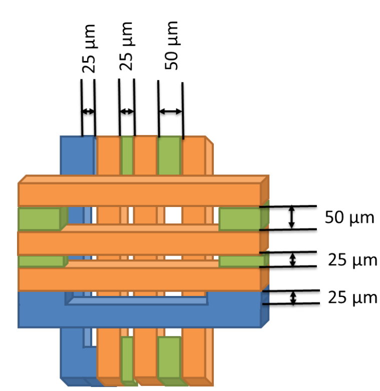


Figure 2: A schematic of the downstream view of the pinhole 3 assembly showing the arrangement of the machined molybdenum blades (blue), tungsten blades (orange) and shims (green).



ISBN 978-3-95450-177-9

# BEAM INDUCED FLUORESCENCE MONITOR R&D FOR THE J-PARC NEUTRINO BEAMLINE

M. Friend*, High Energy Accelerator Research Organization (KEK), Tsukuba, Japan
C. Bronner, M. Hartz, Kavli IPMU (WPI), University of Tokyo, Tokyo, Japan

*Abstract*

Proton beam monitoring is essential for the J-PARC neutrino beamline, where neutrinos are produced by the collision of 30 GeV protons with a long carbon target. Along with continued upgrades to the J-PARC beam power, from the current 420 kW to 1.3+ MW, there is also a requirement for monitor upgrades. A Beam Induced Fluorescence monitor is under development, which would continuously and non-destructively measure the proton beam profile spill-by-spill by measuring fluorescence light from proton interactions with gas injected into the beamline. Monitor design is constrained by the J-PARC neutrino beamline configuration, where a major challenge will be getting sufficient signal to precisely reconstruct the proton beam profile. R&D for a pulsed gas injection system is under way, where injected gas uniformity and vacuum pump lifetime are main concerns. Design of a light detection system is also under way, where light transport away from the high radiation environment near the proton beamline, as well as fast detection down to very low light levels, are essential.

## J-PARC PROTON BEAM OVERVIEW

The J-PARC proton beam is accelerated to 30 GeV by a 400 MeV Linac, a 3 GeV Rapid Cycling Synchrotron, and a 30 GeV Main Ring (MR) synchrotron. Protons are then extracted using a fast-extraction scheme into the neutrino beamline, which consists of a series of normal- and super-conducting magnets used to bend the proton beam towards the neutrino production target for generation of a neutrino beam pointing towards the Super-Kamiokande detector for the T2K Long-Baseline Neutrino Oscillation Experiment [1]. Beam monitoring is essential for both protecting beamline equipment from possible mis-steered beam, as part of a machine interlock system, and as input into the T2K analysis.

Table 1: J-PARC Proton Beam Specifications

| | Protons/Bunch | Spill Rate |
|---|---|---|
| Current (2016) | $2.75 \times 10^{13}$ | 2.48 s |
| Upgraded (2018~) | $2.75 \rightarrow 4.00 \times 10^{13}$ | 1.30→1.16 s |

The J-PARC 30 GeV proton beam has an 8-bunch beam structure with 80 ns ($3\sigma$) bunch width and 581 ns bucket length. J-PARC currently runs at 420 kW with the plan to upgrade to 750+ kW by 2018 and 1.3+ MW by 2026. This will be achieved by increasing the beam spill repetition rate from the current 1 spill per 2.48 s, to 1.3 s and finally 1.16 s, along with increasing the number of protons per bunch from $2.75 \times 10^{13}$ to $4 \times 10^{13}$ as shown in Table 1. With this increased beam power comes increased necessity for minimally destructive beam monitoring, as each of the currently-in-use beam profile monitors cause 0.005% beam loss (where all but the most down-stream beam profile monitor is remotely inserted into the beam orbit only during beam tuning).

* mfriend@post.kek.jp

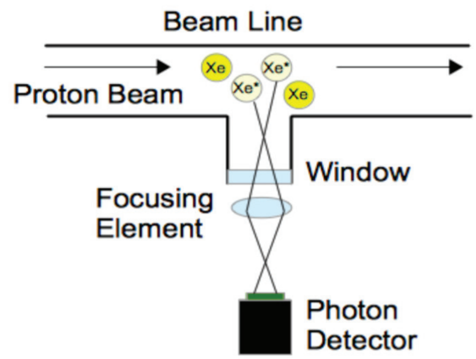


Figure 1: Schematic diagram of BIF monitor.

The proton beam spot size varies along the neutrino line from ~2–8 mm ($1\sigma$) and is ~4.2 mm at the neutrino production target. Current non-destructive beam position monitors continuously measure the beam position with a precision of 450 $\mu$m, while destructive monitors measure the beam width with a precision of 200 $\mu$m during beam orbit tuning. Any new monitoring system should exceed this beam position precision and match this beam width precision if possible.

Development of a new non-destructive Beam Induced Fluorescence (BIF) monitor [2] for the J-PARC neutrino beamline is underway. In a BIF monitor, the beam profile is measured when the passing beam ionizes some of the gas particles in the beamline. The particles then fluoresce when returning to the ground state, and the transverse profile of this fluorescence light will match the transverse profile of the proton beam. A simple BIF monitor schematic is shown in Fig. 1.

## NON-DESTRUCTIVE MONITOR REQUIREMENTS

The BIF monitor must be designed taking into account the specific requirements of the J-PARC neutrino beamline as given below.

ISBN 978-3-95450-177-9

# NON-INVASIVE BEAM PROFILE MEASUREMENT FOR HIGH INTENSITY ELECTRON BEAMS

T. Weilbach, M. Bruker, Helmholtz-Institut Mainz, Germany,
K. Aulenbacher, KPH Mainz, Helmholtz-Institut Mainz, Germany

*Abstract*

Beam profile measurements of high intensity electron beams below 10 MeV, e.g. in energy recovery linacs or magnetized high energy electron coolers, have to fulfill special demands. Commonly used diagnostic tools like synchrotron radiation and scintillation screens are ineffective or not able to withstand the beam power without being damaged. Non-invasive methods with comparable resolution are needed.

Hence, a beam profile measurement system based on beam-induced fluorescence (**BIF**) was built. This quite simple system images the light generated by the interaction of the beam with the residual gas onto a PMT. A more elaborated system, the Thomson Laser Scanner (**TLS**) — the non-relativistic version of the Laser Wire Scanner — is proposed as a method for non-invasive measurement of all phase space components, especially in the injector and merger parts of an ERL. Since this measurement suffers from low count rates, special attention has to be given to the background.

Beam profile measurements with the BIF system will be presented as well as a comparison with YAG screen measurements. The recent status of the TLS system will be presented.

## INTRODUCTION

High-intensity electron beams are getting more and more popular. Because of their high beam power, the use of conventional destructive diagnostic tools is limited. Energy recovery linacs (ERL) can make use of the emitted synchrotron radiation for profile measurements, but this is only possible after the main linac. In the injector and merger section, they need non-intercepting beam diagnostic devices which can withstand the beam power of several 100 kW. The planned electron cooling devices easily reach several MW of beam power. Because of energy recuperation in the collector, they allow only a very small beam loss, which is not compatible with normal destructive diagnostics.

There are already several non-destructive beam diagnostic methods established, which are used in different accelerators, such as a scintillation profile monitor [1] at COSY or the laser wire scanner at the synchrotron source PETRA III [2]. These methods can be adapted for the profile measurement of high-intensity electron beams with energies in the MeV range.

## EXPERIMENTAL SETUP

All measurements are done at the polarized test source (PKAT) [3] shown in Fig. 1 at the Mainzer Mikrotron (MAMI). In this source, a NEA-GaAs [4] photo cathode is used to generate an electron beam with an energy of 100 keV.

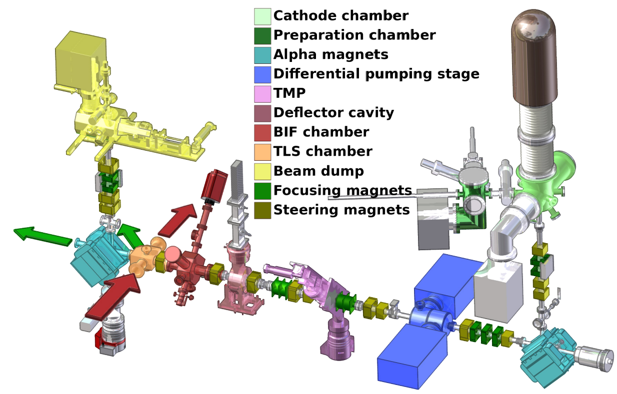


Figure 1: The polarized test source PKAT. The first differential pumping stage (blue) separates the source vacuum (green) from the beam line vacuum. A second differential pumping stage (purple) separates the BIF (red) and the TLS chamber (orange) from the rest of the beam line. The Faraday cup (yellow) monitors the beam current throughout the measurements.

The NEA-GaAs cathode requires a pressure much lower than $10^{-10}$ mmbar for stable operation. Therefore, a first differential pumping stage separates the source vacuum from the beam line vacuum (blue). A second differential pumping stage, consisting of two turbo molecular pumps (purple), surrounds the BIF and TLS chambers. This allows local pressure bumps of up to $10^{-5}$ mbar while maintaining the UHV condition at the cathode.

The beam transport system consists of dipole (alpha and steering magnets) and quadrupole magnets as well as two solenoid doublets. Several conventional (luminescent and scintillating) screens and the Faraday cup at the end of the beam line allow for a setup of the electron beam and also for comparison measurements with the new non-invasive diagnostic methods.

The PKAT can operate in several modes which differ in the time structure of the electron beam. For the BIF measurements, we use the dc mode, in which a blue laser diode generates either a dc beam or a pulsed beam with a repetition rate of several Hz with a length of a few 100 µs. In that mode, the source is limited to 500 µA.

For the TLS measurements, a larger current is needed. Since the power supply can only provide 3 mA of dc current, a pulsed system with a pulse length of about 20 ns and a rep. rate of 150 kHz was built. Thus the PKAT can create an electron beam with a peak current of 30 mA while the average current is approximately 90 µA. The red arrows in Fig. 1 show the incident laser while the green arrows show

ISBN 978-3-95450-177-9

# AN INVESTIGATION INTO THE BEHAVIOUR OF RESIDUAL GAS IONISATION PROFILE MONITORS IN THE ISIS EXTRACTED BEAMLINE

C. C. Wilcox†, B. Jones, A. Pertica, R. E. Williamson, STFC, Rutherford Appleton Laboratory, UK

*Abstract*

Non-destructive beam profile measurements at the ISIS neutron source are performed using Multi-Channel Profile Monitors (MCPMs). These use residual gas ionisation within the beam pipe, with the ions being guided to an array of 40 Channeltron electron multipliers by a high voltage drift field.

Non-uniform transverse electric fields within these monitors are caused by the drift field and the beam's space charge. Longitudinally, a saddle point located between the drift field plate and the opposing compensating field plate introduces extra complexity into the ion motion. To allow for detailed studies of this behaviour, an MCPM has been placed in Extracted Proton Beamline 1 (EPB1) where the beam is well defined. Simulations of the profiles obtained by this monitor are performed using machine measurements, CST EM Studio and a simple C++ particle tracking code.

This paper describes the process used to simulate MCPM profiles along with a comparison of simulated and measured results. Trajectories of detected ions from their creation to the Channeltrons are discussed, together with a study of Channeltron detection characteristics carried out in the ISIS diagnostics laboratory vacuum tank.

## INTRODUCTION

ISIS is a spallation neutron and muon source based at the Rutherford Appleton Laboratory in the UK. The facility consists of a 70 MeV $H^-$ linear accelerator, an 800 MeV proton synchrotron and two EPBs, which transport the accelerated protons to two target stations (TS1 & TS2). The synchrotron operates at a repetition rate of 50 Hz, with four out of every five proton pulses being delivered to TS1 at a rate of 40 Hz and the remaining pulses being delivered to TS2 at a rate of 10 Hz.

Non-destructive profile measurements at ISIS are performed with residual gas ionisation monitors. These utilise the interaction between the proton beam and molecules of the residual gas within the monitor's volume, which creates electron-ion pairs. A drift field, typically of 15 kV, is applied across the monitor to guide the created ions towards an array of detectors. As the level of ionisation at any point within the monitor is directly proportional to the beam intensity at that location [1], a 1D beam profile can be constructed by comparing the quantities of ions arriving at each detector in the array.

Over the past decade, the ISIS design of ionisation profile monitor has undergone multiple stages of evolution to improve both the acquisition speed and accuracy of the measured profiles [2]. The monitors consist of two high voltage electrodes, placed on opposing sides of the monitor to ensure there is no overall influence on the beam trajectory, as shown in Fig. 1. The primary electrode applies a drift field which drives residual gas ions towards a 240 mm wide array of 40 Channeltron electron multipliers. This part of the monitor is referred to as the MCPM, and uses the 4800 series Channeltrons manufactured by Photonis [3], arranged with a regular spacing of 6 mm between each Channeltron centre. The compensating electrode drives ions towards a single, larger 4700 series Channeltron which is connected to a linear motor. This single channel monitor (SCPM) is scanned across the beam aperture and used to calibrate the gains of each of the MCPM Channeltrons, as described in [2].

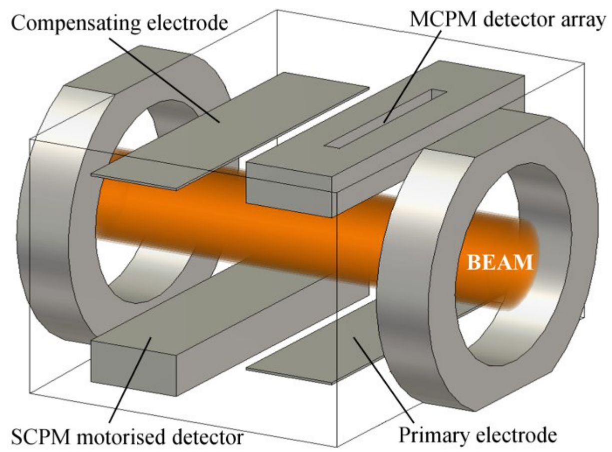


Figure 1: The layout of an ISIS profile monitor.

## MEASUREMENT ERRORS

In order to understand high intensity loss mechanisms in the synchrotron and to establish good beam models, it is essential that accurate profile measurements can be taken both quickly and non-destructively.

Accurate measurements depend on the created residual gas ions travelling directly towards the detectors without undergoing any additional transverse motion. For example, in a horizontal profile monitor the ideal ion trajectory is a direct vertical path between the creation and detection points, resulting in an accurate horizontal measurement. However, both the shape of the drift field generated by the electrodes and the effect of the beam's space charge field cause additional transverse ion motion, introducing a broadening effect into the profile measurement (Fig. 2). Furthermore, a saddle point in the electric field exists in the centre of the monitor, created by the interaction between the primary and compensating electrodes.

A profile correction scheme has been developed from previous studies [4] to account for the effects of the drift field and space charge on measurements. Previous investigations have yielded good results when this correction is applied to the monitors located in the synchrotron [5, 6].

† christopher.wilcox@stfc.ac.uk



ISBN 978-3-95450-177-9

# PROFILE MEASUREMENT BY THE IONIZATION PROFILE MONITOR WITH 0.2T MAGNET SYSTEM IN J-PARC MR

Kenichirou Satou†, Hironori Kuboki, Takeshi Toyama, J-PARC/KEK, Tokai, Japan

*Abstract*

A non-destructive Ionization Profile Monitor (IPM) is widely used to measure transverse profile. At J-PARC Main Ring (MR), three IPM systems have been used not only to measure emittances but also to correct injection miss matchings. To measure beam profiles at the injection energy of 3GeV, the high external E field of +50kV/130mm at the maximum is used to guide ionized positive ions to a position sensitive detector; transverse kick force originating from space charge E field of circulating beam is a main error source which deteriorates profile.

The strong B field is also used to compensate the kick force. To measure bunched beam at the flat top energy of 30GeV in the fast extraction mode in good resolution, the strong B field of about 0.2T is needed. One set of magnet system, which consists of a C-type and two H-type magnets, were developed and installed in one IPM system. The IPM chamber was inserted between the 2 poles of the C-type magnet. To make the line integral of B field along the beam axis zero, the H-type magnets have the opposite field polarity to that of the C-type magnet and were installed on both sides of the C-type magnet. Details of the magnet system and its first trials will be presented.

## INTRODUCTION

The residual-gas ionization profile monitor (IPM) is one of the most ideal diagnostic tools to measure a transverse profile non-destructively. The most promising way to obtain a clear profile is to measure positive ions using a strong dipole E field (Eext), because this system does not being affected with electron contaminations from electron clouds, a discharge problem on HV feeder. The Eext should be much larger than the strong beam space charge E field (Esc). However, due to the technical limitation of HV being able to apply to an insulator between electrodes, profile distortion will be set in case of high density beams of J-PARC, SNS, LHC, and so on. To reconstruct the original profile from an obtained profile, the numerical calculation methods were developed [1-3], however, before calculation, original profile shape should be assumed.

Another method is to use a uniform magnetic guiding field (Bg), which is parallel to Eext, to collect detached electrons. The Bg converts Esc kick force to gyro-motion along Bg and so called E×B drift along beam axis, where the initial momentum of a detached electron and also a velocity gain from Esc determines radius of the gyro-motion. And this radius determines profile measurement accuracy. However the electron contamination problems are left to be settled. Due to this contamination issue, it is hard to measure the beam tail profile.

Our choice is to use the both methods [4, 5]. We have developed a magnet system for one IPM system (Horizontal type IPM) out of three, and started operation from this June. The Fig. 1 shows photo of horizontal IPM system with new developed magnet system. After describing the details of the magnet, the first measurement results are reported.

Figure 1: Photo of horizontal IPM system installed at address 76 of J-PARC MR.

## MAGNET REQUIREMENTS AND PERFORMANCES

The magnet system consists of one C-type main magnet and two H-type correction magnets. The correction magnets are used to cancel the B field integral along the beam axis (BL product) so as not to kick the beam; magnet polarity is opposite

To check the Bg intensity required to measure profiles within 1% accuracy, the profile simulation code IPMsim3D [6, 7] was used. The profile distortions for different Bg settings were checked for a designed maximum beam pulse at the flat top energy of 30GeV. In these calculations, the Gaussian shape was assumed for initial transverse and longitudinal profiles. The expected beam parameters are listed as follows, where 1σ beam emittance for x, and y were set as, 4.4πmm·mrad, and 7.0πmm·mrad, respectively.

- Beam energy:30GeV
- Beam intensity: 4E13 particles per bunch (ppb)
- Transverse beam size: $\sigma_x$=2.7mm, $\sigma_y$=4.4mm
- Longitudinal beam size: $\sigma_t$=10ns

At the IPM centre, the beta function for x and y is β_x=13.1m, β_y=21.6m, respectively, and dispersion function is 0. The initial momentum of an electron was calculated based on the double differential ionization cross section of ref [8]. And Eext was set as -

† kenichirou.satou@j-parc.jp



ISBN 978-3-95450-177-9

# 3D DENSITY SCANS OF A SUPERSONIC GAS JET FOR BEAM PROFILE MONITOR

H. Zhang#, V. Tzoganis, K. Widmann, C. Welsch
Cockcroft Institute and The University of Liverpool, Warrington, WA44AD, UK

*Abstract*

Recently, we have developed a novel beam profile monitor based on a supersonic gas jet. It can be applied to some extreme situation while other methods are not applicable such as for the high intensity and energy beams with destructive power and for the short life beam which requires minimum interference. The resolution of this monitor depends on the jet thickness and homogeneity, and thus we developed a movable gauge to investigate the gas jet distribution in a 3D manner. In this paper, we will present the measurement of the distribution of the gas jet and discuss the future improvement for the jet design.

## INTRODUCTION

Beam profile monitors are essential diagnostics for particle accelerators. With undergoing constructions of proposed high intensity and high power machine like ESS or HL-LHC, the conventional invasive diagnostics are not well suited because of the destructive beam power. Previously, IPM and BIF were used in similar situations based on the ionization or excitation of residual gas by the projectile beams [1]. The usage of the residual gas makes the diagnostic non-invasive but the signal level is low requiring long integration. Recently, a supersonic gas jet based monitor [2-4] was developed at the Cockcroft Institute .Using the gas jet with a high directional speed and high density, the probability of ionization or excitation of the gas molecules will increase dramatically. Therefore, the integration time will be much reduced, even to a level where shot to shot measurement will be possible.

Previously, we reported the results of such monitor to measure a two-dimensional profile of a 5 keV, 7uA electron beam. [4]. Preliminary results have shown that the jet properties could affect the monitor performance. However, the jet homogeneity and density distribution is still unknown.

In this paper, we will present a subsystem dedicated to measure the gas jet profile in 3D and results about the jet density and homogeneity will be discussed in details.

## GAS JET SETUP AND MEASUREMENT

The details of the setup are shown in figure 1 and were described previously [4-6]. The supersonics gas jet is generated by injecting high pressure gas (1-10 bar) from gas tank pass through a small nozzle with diameter 30 $\mu$m into a low pressure region ($10^{-4}$ mbar). With further collimations, the gas jet can travel mono-directionally and be shaped into a screen-like curtain for diagnostic purpose. The differential pumping sections were designed to remove collimated gas molecular and maintain an ultra-high vacuum environment in the interaction chamber. Dumping sections are used for dumping the jet.

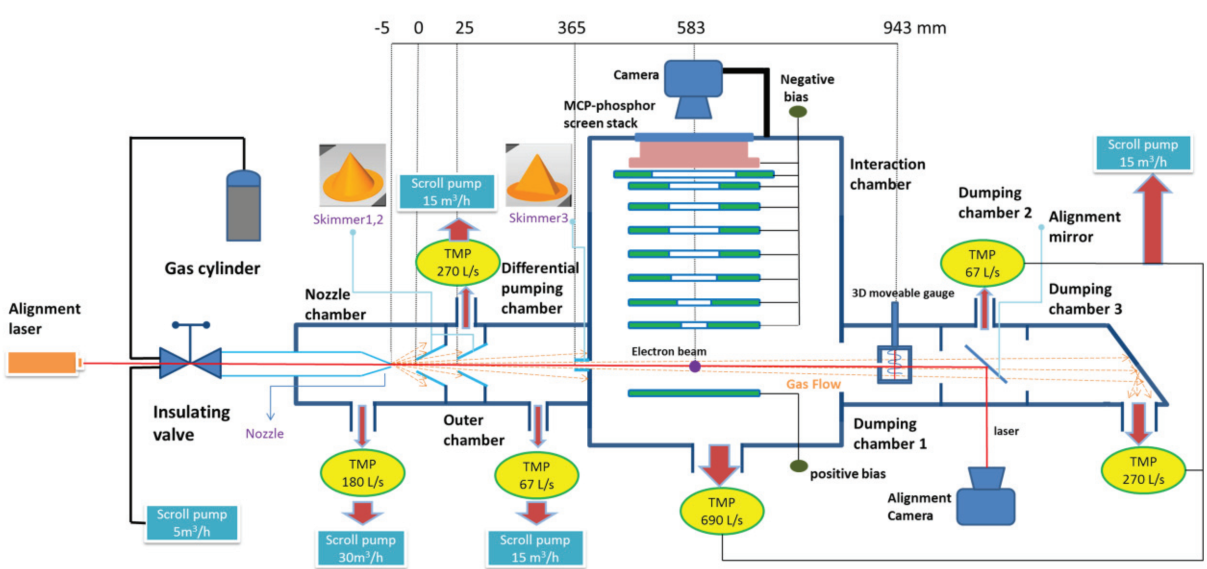


Figure 1: Schematic drawing of the complete setup.

#hao.zhang@cockcroft.ac.uk

ISBN 978-3-95450-177-9

# A HARDWARE AND SOFTWARE OVERVIEW ON THE NEW BTF TRANSVERSE PROFILE MONITOR

B.Buonomo, C. Di Giulio, L.G. Foggetta†, INFN – Laboratori Nazionali di Frascati, Frascati, Italy
P.Valente, INFN – Sezione di Roma, Rome, Italy

*Abstract*

In the last 11 years, the Beam-Test Facility (BTF) of the DAFNE accelerator complex, in the Frascati laboratory, has gained an important role in the EU infrastructures devoted to the development of particle detectors. The facility can provide electrons and positrons, tuning at runtime different beam parameters: energy (from about 50 MeV up to 750 MeV for e- and 540 MeV for e+), intensity (from single particle up to 1010/bunch) and pulse length (in the range 1.5–40 ns). The bunch delivery rate is up to 49 Hz (depending on the operations of the DAFNE collider) and the beam spot and divergence can be adjusted, down to sub-mm sizes and 2 mrad (downstream of the vacuum beam-pipe exit window), matching the user needs. In this paper we describe the new implementation of the secondary BTF beam transverse monitor systems based on ADVACAM FitPIX® Kit detectors, operating in bus synchronization mode externally timed to the BTF beam. Our software layout includes a data producer, a live-data display consumer, and a MEMCACHED caching server. This configuration offers to BTF users a fast and easy approach to the transverse diagnostics data using TCP/IP calls to MEMCACHED, with a user-friendly software integration of virtually any DAQ system. The possibility of sharing mixed data structures (user-generated and BTF diagnostics) allows to completely avoid the complexity of hardware synchronization of different DAQ systems.

## THE DAΦNE BEAM TEST FACILITY (BTF)

The BTF (Beam Test Facility) is part of the DAΦNE accelerator complex: it is composed of a transfer line driven by a pulsed magnet allowing the diversion of electrons or positrons, usually injected into to the DAΦNE damping ring, from the high intensity LINAC towards a fully equipped experimental hall. The facility can provide runtime tuneable electrons and positrons beams in a defined range of different parameters. The beam energy can be selected from about 50 MeV up to 750 MeV, for electrons, and 540 MeV for positrons. In dedicated mode (DAΦNE off), the beam pulse length can also be adjusted in 0.5 steps from 1.5 to 40 ns. The delivery rate is depending on the DAΦNE injection frequency (25 or 50 Hz) with a duty cycle also changing according to the DAΦNE injection status, up to 49 bunches/s. Two major modes of operations are possible, depending on the user needs: high and low intensity. In the high intensity mode the LINAC beam is directly steered in the BTF hall with a fixed energy (i.e. the LINAC one, fixed to 510 MeV during the collider operations) and with reduced capability in multiplicity selection (typically from 1010 down to 104 particles/bunch). In the low intensity mode a step Copper target, allowing the selection of three different radiation lengths (1.7, 2 or 2.3 X0), is inserted in the first portion of the BTF line for intercepting the beam: this produces a secondary beam with a continuous full-span energy (from LINAC energy down to 50 MeV) and multiplicity (down to single particle/bunch), according to the setting of a 43° selecting dipole and of two sets of horizontal and vertical collimators. The typical momentum band is well below 1% down to 50 MeV. A pulsed dipole magnet at the end of the LINAC allows alternating the beam between the DAΦNE damping ring and the test beam area, thus keeping a pretty high BTF duty cycle, assuring an average of at least 20 bunches/s during the injection in DAΦNE, when BTF operates in the low intensity regime.

## BTF PIXEL DETECTOR LAYOUT

A general overview of the BTF detectors and a description of the related software can be found here [1, 2].

Detector beam-testing generally require a fast transverse beam imaging during runtime, with some pre-analysis capability and, as in the BTF case, with a stable, reproducible and well-known response in the full range of energy, multiplicity and transverse dimensions of the particle beam. In addition, taking into account the BTF heavy work-cycle (beam is generally allocated in one-week slots for a minimum of 25 up to 40 weeks/years, including BTF-dedicated shifts), the equipment has to be reliable, robust, and with an easy maintenance, in order to guarantee full readiness and high-availability for the users purposes. For the same reasons, the related low-level software has to comply with these demanding requirements: not only very high reliability, but also easy and efficient integration in the vast variety of user acquisition software codes. Concerning the high level software, we decided to have the possibility of a fully featured runtime data display using LabVIEW®.

### *ADVACAM Silicon Pixel Detector*

In [1], we described the setup based on a MEDIPIX-like silicon pixel detector with ADVACAM FitPIX® Kit electronics, at first made routinely available to the users via the basic version of the provided software, PIXET®, implemented in the BTF timing and virtual machine sub-systems. This solution well accomplished data acquisition and data-logging tasks (customizable thanks to the possibility of python scripting), but we decided to move to a completely custom low level C-code to better match our facility

†luca.foggetta@lnf.infn.it

ISBN 978-3-95450-177-9

# BRIDGING THE GAP; UPDATING LANSCE DIGITIZERS*

D. Baros, J. Sedillo, H. Watkins, Los Alamos National Laboratory, 87545, USA

*Abstract*

The Los Alamos Neutron Science Center (LANSCE) is currently upgrading equipment that is used to digitize transverse beam profile measurements. Emittance measurements were originally digitized using legacy equipment, known as RICE (Remote Indication and Control Equipment). This required 38 RICE modules distributed along the half-mile long accelerator simultaneously recording 4 channels each to populate the 76 data points needed to create a single emittance profile. The system now uses a National Instruments cRIO controller to digitize the entire profile in a single chassis. Details of the hardware selection and performance of the system for different timing structures are presented.

## INTRODUCTION

LANSCE is a National Research Facility which contains a half-mile-long linear accelerator. (LINAC). The LANSCE LINAC creates proton beams with energies up to 800 million electron volts and is capable of accelerating protons to 84% the speed of light. LANSCE achieved full energy on June 9, 1972 and continues to run to this day with much of its late 1960's – early 1970's technology intact.

An example of this late 1960's technology is the data acquisition and control system for the LANSCE LINAC better known as RICE (Remote Indication and Control Equipment).

## RICE

RICE was custom built as part of the first large-scale effort to use computers to control an accelerator. Designed in the late 1960's, before CAMAC and VME standards, it was created to provide control and data readout (industrial I/O) for most devices in the LANSCE LINAC. Its architecture was designed to directly map onto the architecture of the LINAC and thus is tightly coupled to the LINAC hardware.

An average RICE module contains 30 analog inputs, 50 digital inputs, 8 analog commands and 30 digital command channels. There are 66 RICE modules distributed along the LANSCE LINAC.

The layout of the LANSCE LINAC is illustrated in Figure 1 (individual RICE modules are represented by circled numbers). The 66 RICE Modules are connected to one uVAX computer in a star topology configuration.

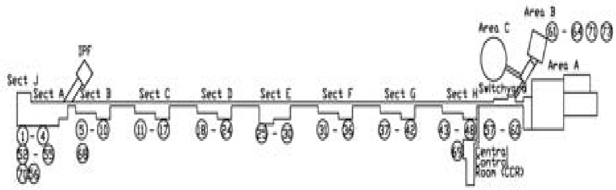

Figure 1: LANCE LINAC.

A RICE module consists of three separate components: the RICE chassis, the RICE Input/Output (I/O) chassis and the Analog Data System (ADS) chassis. The RICE chassis is a serial to parallel and parallel to serial word encoder/decoder. The RICE I/O chassis is used to interface the RICE system with the accelerator inputs/outputs and can address up to 128 binary channels. The ADS chassis is a 128 channel differential A/D converter used for analog readback of accelerator devices [1].

## EMMITTANCE (RICE)

Beam emittance at LANSCE was originally obtained by utilizing 4 analog data point channels on 38 separate RICE modules. These RICE modules simultaneously record the data to produce the 76 data points needed for a single emittance profile. The data points (12-bits) were generated by inserting a 20 mil copper slit and a 76 wire collector with 1 mm pitch into the beam line and simultaneously recording data on each of the wires as it passes through the beam.

The EMRP (EMittance Replay Program) software program plots the emittance data with amplitude as a function of position and collector wire index. The data in the plot is correlated by the same time offset from the beginning of the beam pulse. In order to observe beam behaviour in different points of time along the beam pulse, the hardware triggering offsets need to be changed and scans retaken. This process can take upwards of 8 hours to collect longitudinal measurements across the pulse.

Currently LANSCE utilizes six Emittance systems:

- IBEM – H- Injector
- TAEM – H+ Transport
- TBEM – H- Transport
- TDEM – Low Energy Beam Transport
- TREM – Transition Region Transport
- IDEM – Ion Source Test Stand.

Each system represents a specific beam species in a critical location along the accelerator. These systems are primarily used for beam tuning to detect the position of the beam in the accelerator and to characterize beam quality. An example of a TAEM02 Horizontal emittance scan is shown in Figure 2.

*Work supported by the U.S. Department of Energy, Contract No. DE-AC52-06NA25396 LA UR 16 26713



ISBN 978-3-95450-177-9

# THE BEAM PROFILE MONITORING SYSTEM FOR THE CERN IRRAD PROTON FACILITY*

F. Ravotti†, B. Gkotse[1], M. Glaser, E. Matli, G. Pezzullo, CERN, 1211 Geneva 23, Switzerland
K.K. Gan, H. Kagan, S. Smith, J. D. Warner, Ohio State University, Columbus, OH 43210, USA
[1]also at Université Européenne de Bretagne, Brest, France

*Abstract*

To perform proton irradiation experiments, CERN built during LS1 a new irradiation facility in the East Area at the Proton Synchrotron accelerator. At this facility, named IRRAD, a high-intensity 24 GeV/c proton beam is used. During beam steering and irradiation, the intensity and the transverse profile of the proton beam are monitored online with custom-made Beam Profile Monitor (BPM) devices. In this work, we present the design and the architecture of the IRRAD BPM system, some results on its performance with the proton beam, as well as its planned upgrades.

## INTRODUCTION

In High Energy Physics (HEP) experiments such the one at the CERN Large Hadron Collider (LHC), devices are frequently required to withstand a certain radiation level. As a result, detector materials, equipment and electronic systems must be irradiated to assess their level of radiation tolerance. To perform these irradiations, CERN built a new irradiation facility on the T8 beam-line of the East Area at the Proton Synchrotron (PS) accelerator. At this facility, named IRRAD, a Gaussian 24 GeV/c proton beam of variable size ranging from ~5×5 mm$^2$ to ~20×20 mm$^2$ is used to irradiate experimental devices [1].

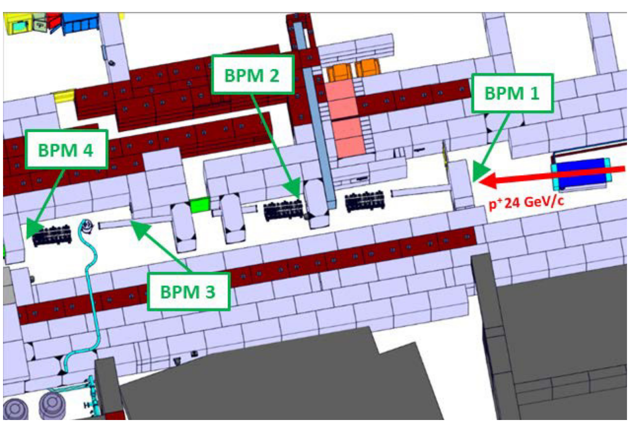


Figure 1: Position of the four BPM devices along the IRRAD facility at CERN.

The proton beam on T8 is delivered in spills with a maximum intensity of 5×10$^{11}$ proton per spill and about 400 ms duration. Several spills per PS accelerator super cycle (CPS) are delivered to IRRAD resulting in a variable beam intensity, depending on the number of users simultaneously served by the whole CERN accelerator complex. As a figure of merit, three spills per CPS of 30 basic periods are delivered to IRRAD, resulting in an average flux >8×10$^{13}$ p/cm$^2$/h over one centimetre squared surface. During irradiations, it is thus necessary to monitor in real-time the intensity and the transverse profile of the proton beam.

The IRRAD BPM uses a 39-channels pixel detector to monitor the beam position. The pixel detector, that must withstand high-cumulated radiation levels, is constructed using thin foil copper pads positioned on a flex circuit. When protons pass through the copper pads, they induce a measurable current. To measure this current and thus determine the proton beam intensity, a new data acquisition system was designed as well as a new database and on-line display system. In its final configuration, the IRRAD facility exploits four BPM detectors located along the path of the irradiation beam as shown in Fig. 1.

The new BPM data acquisition system uses low noise integrators. The voltages from each integrator are scaled and limited before connection to a 16-bit ADC. Furthermore, an Arduino Yún collects the data from the ADC and controls its transmission over the Ethernet port to a server for further processing and storage. Finally, the live beam position and intensity data are available to the IRRAD users, as well as to the operators at the CERN Control Centre (CCC), via a dedicated web-based display.

Two BPM data acquisition systems were assembled in 2014 and were used to read out two BPM detectors during the commissioning of the new facility. Four additional BPM data acquisition systems were later installed at the beginning of the irradiation run 2015 and, since then, are operational.

In this work, we detail the design and the architecture of the IRRAD BPM system, as well as its performance and foreseen upgrades.

## OPERATION PRINCIPLE AND CHOICE OF THE DETECTOR MATERIAL

The need for an on-line method to determine the position and the profile of the high-intensity proton beam of IRRAD motivated the feasibility study of an instrument based on the proton-induced Secondary Electron Emission (SEE) from thin metal foils [2]. Secondary emission of electrons from the surface of a plate occurs when a charged particle beam crosses it. The liberated charge comes mainly from delta rays escaping from the plate, with a small contribution due to the secondaries produced in the interactions of the beam particles with the plate. The total collected charge is proportional to the intensity of the impinging beam. For

* Work supported by the European Union's Horizon 2020 Research and Innovation programme under Grant Agreement no. 654168 as well as from the European Commission project AIDA.
† e-mail address: Federico.Ravotti@cern.ch

ISBN 978-3-95450-177-9

# STATUS OF THE TWO-DIMENSIONAL SYNCHROTRON RADIATION INTERFEROMETER AT PETRA III*

A.I. Novokshonov, A.P. Potylitsyn,Tomsk Polytechnic University (TPU), Tomsk, Russia
G. Kube, M. Pelzer, G. Priebe, Deutsches Elektronen-Synchrotron (DESY), Hamburg, Germany

*Abstract*

Synchrotron radiation based emittance diagnostics at modern $3^{rd}$ generation light sources is mainly based on beam profile imaging in the X-ray region in order to overcome the resolution limit imposed by diffraction. A possibility to circumvent this limitation is to probe the spatial coherence with a double-slit interferometer in the optical spectral region. The light source PETRA III at DESY is using this type of interferometer since several years in order to resolve vertical emittances of about 10 pm.rad. The device is set up behind a 30 m long optical beamline, connecting the accelerator tunnel and the optical hutch. In order to increase the measurement stability, a much shorter optical beamline with reduced number of optical elements was recently commissioned. At the end of the beamline, a two-dimensional interferometer was installed which allows to deduce transverse emittances in both planes simultaneously. This contribution summarizes the status of beamline and interferometer commissioning.

## PRINCIPLE

The principle of the interferometric method is based on the investigation of the spatial coherence of SR. In order to quantify the coherence properties usually the first order degree of mutual spatial coherence $\gamma(D)$ is used (c.f. for example Ref. [1]) with $D$ the distance between two wave-front dividing slits, see Fig. 1. The interferometer itself is a wave-front–division-type two-beam interferometer which uses polarized quasi monochromatic radiation. The intensity of the interference pattern (interferogram) measured in the detector plane directly depends on $\gamma$ [2]:

$$I(y_0) = I_0 \left[\mathrm{sinc}(\frac{2\pi a}{\lambda R} y_0)\right]^2 \left[1 + |\gamma| \cos(\frac{2\pi D}{\lambda_0 R} + \varphi)\right] \quad (1)$$

with $a$ the half of the single slit height and $D$, $R$ as indicated in Fig. 1, $\lambda_0$ the wavelength of observation and $I_0$ the sum of the incoherent intensities from both slits. If the condition of Fraunhofer diffraction (i.e. far–field limit) holds, the van Cittert–Zernicke theorem [3] relates the degree of coherence $\gamma$ with the normalized source distribution $f(y)$:

$$\gamma(\nu) = \int \mathrm{d}y\, f(y) \exp(-i2\pi\nu y)\,, \quad (2)$$

where $\nu = \frac{D}{\lambda_0 R_0}$ denotes the spatial frequency. The beam size information is encoded in the interferogram such that as smaller the beam size, as deeper the modulation depth of

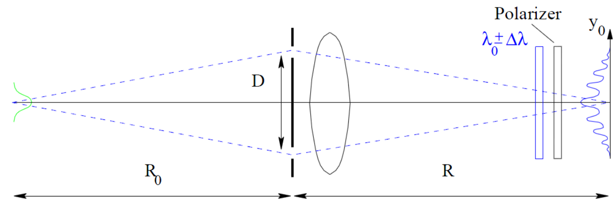


Figure 1: Principle setup for interferometric beam size measurements.

the interference pattern. In the case of an ideal point source, the intensity in the minima of the pattern would amount to $I_{min} = 0$, resulting in a visibility of $V = \frac{I_{max}-I_{min}}{I_{max}+I_{min}} = |\gamma| = 1$. The visibility of an extended source will always have a visibility $V < 1$.

If the beam shape $f(y)$ is known to be normal distributed with width $\sigma_y$, the integral in Eq. (2) can be solved analytically which results in an equation by which the beam size can directly be determined:

$$\sigma_y = \frac{\lambda_0 R_0}{\pi D} \sqrt{\frac{1}{2} \ln \frac{1}{\gamma(D)}}\,, \quad (3)$$

while $\gamma(D)$ has to be fitted from the recorded interferogram. A comprehensive overview and more details about the development of SR interferometers can be found in Ref. [4].

## EXISTING SETUP

Since 2011 an interferometric measurement is in use at the $3^{rd}$ generation light source PETRA III at DESY, Hamburg (Germany) in order to resolve the small vertical emittance of $\varepsilon_y = 10$ pm rad. The setup is installed behind an about 30 m long optical beamline which is described in Ref. [5]. However, this setup suffers from many problems:

(i) Due to the long distance between source point and slits the setup is very sensitive on temperature drifts, a correlation between measured emittance values and ambient temperature is visible. (ii) The beamline is equipped with several optical elements (3 lenses and 6 mirrors), each of them introducing additional uncertainties. (iii) The interferometric setup occupies the place of the streak camera, i.e. simultaneous measurements of vertical and longitudinal beam sizes are not possible. (iv) The present interferometric setup allows to measure only vertical beam sizes, a simultaneous horizontal interferometric measurement would be preferable.

In order to overcome these problems, a new optical beamline with extended interferometric setup was installed in

* This work was partly supported by the Russian Federation Ministry of Science and Education within the program "Nauka" Grant # 3.709.2014/K.

ISBN 978-3-95450-177-9

# SUB-fs RESOLUTION WITH THE ENHANCED OPERATION OF THE X-BAND TRANSVERSE DEFLECTING CAVITY USING AN RF PULSE COMPRESSION SLED CAVITY*

P. Krejcik#, G.B. Bowden, S. Condamoor, Y. Ding, V.A. Dolgashev, J.P. Eichner, M.A. Franzi, A.A. Haase, J.R. Lewandowski, T. Maxwell, S.G. Tantawi, J.W. Wang, L. Xiao, C. Xu, SLAC, Menlo Park, CA 94025, USA

*Abstract*

The successful operation of the x-band transverse deflecting cavity (XTCAV) installed downstream of the LCLS undulator has been further enhanced by the recent addition of an RF pulse compression "SLED" cavity that doubles the temporal resolving power of this powerful diagnostic system for measurement of the longitudinal profile of both the electron bunch and the x-ray FEL pulse. RF pulse compression has allowed us to use the existing SLAC X-band klystron with nominal output power of 50 MW and extend the RF pulse length by a factor 4 to give us 4 times the peak power after compression. A new, innovative SLED cavity was designed and built at SLAC to operate efficiently at X-band. The elegant design uses a small spherical cavity combined with a polarizing mode coupler hybrid. We report on the installation, commissioning and beam measurements demonstrating the sub-femtosecond resolution of the XTCAV system.

## INTRODUCTION

The X-band RF deflecting structure, commonly referred to as the XTCAV, installed at the SLAC National Accelerator Laboratory Linac Coherent Light Source, LCLS, has been in operation for two years now, serving as a diagnostic for both the electron beam and the x-ray photons[1]. The features setting this device apart from other RF deflecting cavities are the x-band operation together with the placement of the device at the end of the FEL undulator in the electron beam dump line. Operation at X-band has resulted in about a factor 8 greater kick strength than the S-band devices installed in the linac. This allows us to measure and resolve the femtosecond long bunches that we are able to produce in the LCLS. By installing the device downstream of the undulator and viewing the streaked beam on a screen in a region with vertical dispersion we are able to both observe the longitudinal phase space of the electron bunches and witness the time-dependant energy loss within the bunch due to the FEL process. The location of the deflecting structure and observation screen relative to the undulator is shown schematically in Fig. 1. Since these components are downstream of the undulator their operation is non-invasive to normal operation for photon users. There is one caveat to this statement which we will mention when the RF jitter performance is discussed.

* This work was supported by Department of Energy Contract No. DE-AC0276SF00515
#pkr@slac.stanford.edu

The XTCAV system has allowed a multitude of diagnostics to be performed that characterize the temporal profile of both the electron and photon beams [2]. The temporal profile of the photon beam is reconstructed from the energy loss temporal profile of the electrons, and is recorded on a shot by shot basis by the photon users to correlate with their experiment data. The XTCAV has also enabled exotic set-ups to be implemented at the LCLS such as twin bunch operation, two-color experiments and slotted spoiler foil operation [3].The XTCAV system is invaluable in this set up since one can observe which slices of the bunch are lasing and at what relative energy.

To make this versatile system even better we have sought to boost the temporal resolution of the measurements by doubling the transverse kick strength of the XTCAV which in turn requires increasing the input RF power by a factor 4.

## SLED PRINCIPLE

SLED is an acronym used at SLAC that originally meant *SLAC Linac Energy Doubler*, where RF pulse compression was used to double the accelerating gradient of the SLAC linac by adding RF storage cavities to the output of the klystron. The S-band output power of the klystron could be compressed a factor 4 with two high-Q cavities connected by a hybrid coupler. SLED has since become a generic name for any RF pulse compression cavity scheme. Although a two cylindrical cavity SLED scheme with hybrid coupler could be designed for X-band operation it was considered too complex and costly to implement at this shorter wavelength.

Instead, a new and elegant SLED cavity design was recently conceived, built and tested at SLAC [4] based on a single, compact spherical cavity with a polarizing, mode converting coupler.

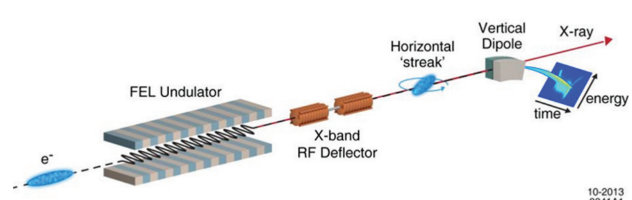


Figure 1: Layout of the X-band RF deflecting structure at the exit of the LCLS undulator where the beam is streaked horizontally and the electrons are bent vertically onto a spectrometer screen.



ISBN 978-3-95450-177-9

# BPM BASED OPTICS CORRECTION OF THE SOLARIS 1.5 GeV STORAGE RING

A. Kisiel*, P. Borowiec, P. P. Goryl, M. Jaglarz, M. Kopeć, A. M. Marendziak, S. Piela, P. Sagało, M. J. Stankiewicz, A. I. Wawrzyniak, Solaris NSRC, Krakow, Poland

*Abstract*

The Solaris is a novel approach for the third generation synchrotron light sources. The machine consists of 600 MeV linear injector and 1.5 GeV storage ring based on 12 compact Double Bend Achromat (DBA) magnets designed in MAX-IV Laboratory in Sweden. After the commissioning phase of the Solaris storage ring the optimization phase has been started along with the commissioning of the first beamline. An essential part of the beam diagnostics and instrumentation system in the storage ring are Beam Position Monitors (BPMs) based on 36 quarter-wave button BPMs spread along the ring. Proper calibration allowed to measure and correct several beam parameters like closed orbit, tune, chromaticity, dispersion and orbit response matrix. The results of the latest machine optimization including the orbit correction, beam-based alignment and BPM phase advance will be presented.

Table 1: Solaris Storage Ring Design Parameters

| Parameter | Value |
|---|---|
| Energy | 1.5 GeV |
| Beam current | 500 mA |
| Circumference | 96 m |
| Number of bending magnets | 12 |
| Main RF frequency | 99.931 MHz |
| Number of bunches | 32 |
| Horizontal emittance (bare lattice) | 6 nm rad |
| Tune $Q_x$, $Q_y$ | 11.22, 3.15 |
| Natural chromaticity $\xi_x$, $\xi_y$ | -22.96, -17.4 |
| Corrected chromaticity $\xi_x$, $\xi_y$ | +1, +1 |
| Beam size (straight section) $\sigma_x$, $\sigma_y$ | 184 µm, 13 µm |
| Beam size (dipole) $\sigma_x$, $\sigma_y$ | 44 µm, 30 µm |
| Total lifetime | 13 h |

## INTRODUCTION

The first polish third generation light source Solaris is based on the linear accelerator and the storage ring connected with dog-leg transfer line. The linac provides the beam with maximum 600 MeV energy which can be injected to the storage ring and ramped up to the nominal energy 1.5 GeV. A storage ring layout consists of 12 novel highly integrated Double Bend Achromat (DBA) magnets designed by MAX-IV Laboratory in Sweden. One year period of the machine assembling has started in May 2014. Then the commissioning phase started and the process of fine-tuning for reaching the designed parameters is still ongoing. Most important parameters of this 1.5 GeV storage ring are presented in Table 1. A detailed description of the machine and the layout can be found in [1–4].

Recent optimization of linear injector and storage ring allowed to reach 600 mA of injected beam at 525 MeV energy stored in the ring and 400 mA beam ramped to the nominal 1.5 GeV energy. Machine optics, which is described in [5, 6], was corrected closely to the designed values. Sufficiently stable beam along with good reproducibility of beam parameters from injection to injection allowed to start the commissioning of the first beamline — UARPES.

## BPM LAYOUT IN SOLARIS

Properly configured Beam Position Monitor (BPM) system is an essential part of the beam diagnostics subsystem for both the linac and the storage ring. The single passing beam in linear structures is monitored in terms of position and stability by 8 stripline BPMs placed along the linac and transfer line. Each quarter-wave directional stripline is 15 cm long and has 50 Ω impedance, what corresponds to the 500 MHz resonant frequency. In order to couple the resonance of the beam with the stripline, mixed-frequency chopper with 500 MHz harmonics will be used.

Storage ring layout includes 36 quarter wave diagonal button BPM sensors distributed evenly along the ring — each DBA is equipped with 3 sensors in two different architectures. The first type of BPM (BPM I) are placed at the ends of each DBA and has button sensors aligned directly along diagonal coordinates, when second type of BPM (BPM II) is placed at the centre of each DBA and has the sensor buttons shifted along the vertical axis on top and bottom of the vessel. BPM made in this architecture is more sensitive to well-centred beam and less sensitive to off-centred beam position, what implies the necessity of separate calibration.

## BUTTON BPM CALIBRATION

An electron beam passing the BPM sensors induces on the sensor heads the voltage pulse which magnitude is proportional to the distance between the beam and the sensor head. Comparing the signals from all four BPM channels the position can be calculated as a relative proportion of inducted signals. All position monitors in Solaris are oriented diagonally and horizontal ($X$) and vertical ($Y$) positions can be calculated with respect to the formulas:

$$X = K_x \frac{(V_A + V_D) - (V_B + V_C)}{V_A + V_B + V_C + V_D} + X_{off}, \qquad (1)$$

$$Y = K_y \frac{(V_A + V_B) - (V_C + V_D)}{V_A + V_B + V_C + V_D} + Y_{off}, \qquad (2)$$

* arkadiusz.kisiel@uj.edu.pl

# TIME-RESOLVED MEASUREMENT OF QUADRUPOLE WAKEFIELDS IN CORRUGATED STRUCTURES*

Chao Lu[†1,2], Feichao Fu[1,2], Shenggunag Liu[1,2], Tao Jiang[1,2], Libing Shi[1,2], Rui Wang[1,2], Dao Xiang[‡1,2], Lingrong Zhao[1,2], Pengfei Zhu[1,2],
[1]Key Laboratory for Laser Plasmas (Ministry of Education), Shanghai Jiao Tong University, Shanghai, China
[2] also at Collaborative Innovation Center of IFSA (CICIFSA), Shanghai Jiao Tong University, Shanghai, China
Zhen Zhang , Department of Engineering Physics, Tsinghua University, Beijing, China

*Abstract*

Corrugated structures have recently been widely used for manipulating electron beam longitudinal phase space and for producing THz radiation. Here we report on time-resolved measurements of the quadrupole wakefields in planar corrugated structures. It is shown that while the time-dependent quadrupole wakefield produced by a planar corrugated structure causes significant growth in beam transverse emittance, it can be effectively canceled with a second corrugated structure with orthogonal orientation. The strengths of the time-dependent quadrupole wakefields for various corrugated structure gaps are also measured and found to be in good agreement with theories. Our work should forward the applications of corrugated structures in many accelerator based scientific facilities.

## INTRODUCTION

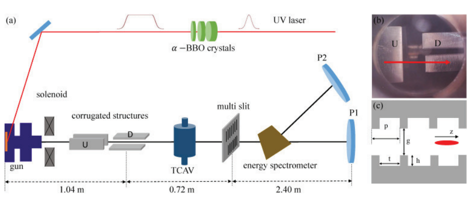


Figure 1: (color online). (a) Schematic layout of the time-resolved measurement of quadrupole wakefields experiment (distances not shown in scale); (b) side view of the CS: upstream CS has a horizontal gap and downstream CS has a vertical gap (the red arrow indicates the beam direction); (c) geometry of the planar CS parameters (the red ellipse represents a beam propagating along the $z$ axis).

When relativistic electron beams pass through metallic pipes or plates with corrugations, electromagnetic waves (wakefields) that propagate with the beams are excited. Such quasi-single frequency radiation on the one hand is a promising candidate for intense THz source (see, for example [1–3]); on the other hand it may be used to manipulate electron beam longitudinal phase space through the interaction between the electron beam and the electromagnetic waves inside the structure (see, for example [4–6]).

* Work supported by the National Natural Science Foundation of China (Grants No. 11327902)
† j.j.lucertainfeel@gmail.com
‡ dxiang@sjtu.edu.cn

## EXPERIMENT METHODS TO QUANTIFY QUADRUPOLE WAKEFIELDS

Recently the corrugated structures (CS) have been used to tailor beam longitudinal phase space in three different ways, namely removing linear chirp (correlation between beam's longitudinal position and beam energy), removing quadratic chirp and imprinting energy modulation. For instance, when the electron bunch length is much shorter than the wavelength of the wakefield, the beam sees a deceleration field that increases approximately linearly in longitudinal direction when it passes through a CS. This longitudinal wakefield can be used to "dechirp" the beam after bunch compression to reduce beam global energy spread [4–11]. Alternatively, when the electron bunch length is comparable to the wavelength of the wakefield, the beam sees a longitudinal wake that approximates a sinusoid. This wakefield can be used to compensate for the beam quadratic chirp [12–14] that otherwise increases free-electron laser (FEL) bandwidth in seeded FELs (see, e.g. [15]) and degrades the MeV ultrafast electron microscope (UEM) performance [16, 17]. Yet another scenario is when electron bunch length is much longer than the wavelength of the wakefield. In this regime the longitudinal wakefield can be used to produce energy modulation in beam longitudinal phase space that may be further converted into density modulation for producing THz radiation [18–20].

In this paper the beam emittance and transverse phase space in presence of CS are measured with multi-slit method. We show that the time-dependent focusing or defocusing introduced by quadrupole wakefields mainly results in mis-

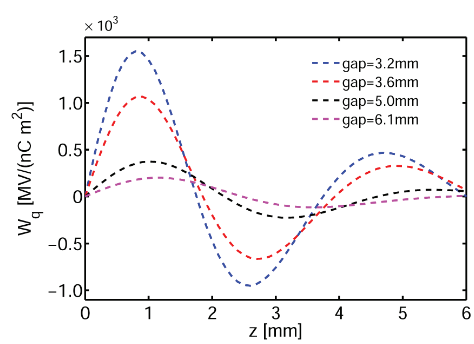


Figure 2: (color online). The point charge quadrupole wake fields at various CS gaps respectively $g = 3.2, 3.6, 5.0, 6.1$ mm.



ISBN 978-3-95450-177-9

# OPTICAL EFFECTS IN HIGH RESOLUTION AND HIGH DYNAMIC RANGE BEAM IMAGING SYSTEMS

J. Wolfenden†, R. Fiorito, C.Welsch, University of Liverpool, Liverpool, UK
P. Karataev, K. Kruchinin, JAI at Royal Holloway University of London, Egham, UK
M. Bergamaschi, R. Kieffer, T. Lefevre, S. Mazzoni, CERN, Geneva, CH

*Abstract*

Optical systems are used to transfer light in beam diagnostics for a variety of imaging applications. The effect of the point spread function (PSF) of these optical systems on the resulting measurements is often approximated or misunderstood. It is imperative that the optical PSF is independently characterised, as this can severely impede the attainable resolution of a diagnostic measurement. A high quality laser and specially chosen optics have been used to generate an intense optical point source in order to accomplish such a characterisation. The point source was used to measure the PSFs of various electron-beam imaging systems. These systems incorporate a digital micro-mirror array, which was used to produce very high (>$10^5$) dynamic range images. The PSF was measured at each intermediary image plane of the optical system; enabling the origin of any perturbations to the PSF to be isolated and potentially mitigated. One of the characterised systems has been used for optical transition radiation (OTR) measurements of an electron beam at KEK-ATF2 (Tsukuba, Japan). This provided an application of this process to actively improve the resolution of the beam imaging system. Presented here are the results of our measurements and complementary simulations carried out using Zemax Optical Studio.

## INTRODUCTION

The impact the PSF of an optical system has on a measurement is often ignored as it is usually not the main limiting factor on resolution. When making high resolution measurements this is not true. Any uncertainty can result in a restriction in the precision of the measurement. The imaging systems in use at recent OTR and ODR studies [1, 2, 3] are an example of such a case. The distribution of PSFs usually takes the form of an Airy disc, with the resolution determined by the width. OTR from a single electron is distinct, in that it contains a zero valued central minimum [4]. The detailed shape of the distribution provides a greater effective resolution than its width [1, 2]. The image of OTR from an electron distribution, with a width comparable to the FWHM of the single electron distribution, displays a central minimum but with a finite non-zero value [1, 2]. This convolution with the transverse profile of an electron beam provides a previously unattainable level of resolution on beam size measurements. In practise however the beam size is not the sole contributor to intensity increase found in the centre of the distribution. There are many other effects, all of which restrict the attainable resolution. A prominent example is the PSF of the optical system used to image the OTR. The diffraction and aberration effects of this PSF will broaden the OTR PSF and degrade the resolution of beam size measurements. If the performance of the optics could be independently assessed, then it would be possible to minimise the impact of the optical PSF on the measured OTR profiles. Another limiting factor is the overall intensity of the OTR. For small beam sizes the sensitivity in the centre can be masked by noise and background [1, 2]. If the intensity of the signal could be increased this central value would be lifted away from the background, the rms noise would become statistically less significant, and smaller beam size measurements could be achieved. This intensity increase would also make future studies into high dynamic range (HDR) OTR imaging possible, as this technique currently relies on high signal levels and masking using a digital micro-mirror array (DMD) [5]. It follows that if the low intensity details of the OTR distribution were measured with HDR, this would further increase the resolution of the beam diagnostic measurements utilising OTR. The effect of the DMD on the optical PSF has been investigated previously [3], but the impact on OTR measurements is still to be assessed.

† joseph.wolfenden@liverpool.ac.uk

## OPTICAL SYSTEM

### PSF Measurements

After an investigation into the PSF of an OTR imaging system currently in use [3], an achromatic imaging system with comparable performance has been designed. Figure 1 shows a schematic of this system. The PSF of a similar system was measured following the technique outlined in [3]. This system differed from system in Fig. 1 in that the focal length of the third lens was changed. This was to change the overall magnification of the system from 25 to 10, as this improved the intensity of the OTR signal measured.

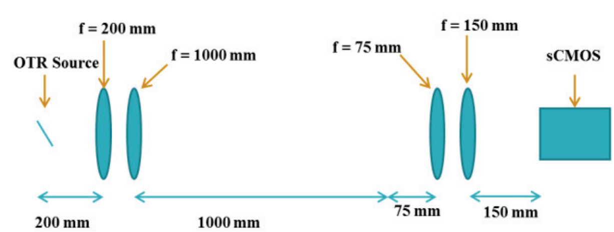


Figure 1: Schematic of OTR imaging system.

As the PSF of an optical system is dominated by the first aperture of the system, the substitution of the third lens for another similar lens would have had a negligible impact on the PSF. The PSF measured is shown in Fig. 2.



ISBN 978-3-95450-177-9

# PALM CONCEPTS AND CONSIDERATIONS

Pavle Juranić, Rafael Abela, Ishkhan Gorgisyan, Rasmus Ischebeck, Balazs Monoszlai,
Luc Patthey, Claude Pradervand, Milan Radović, Volker Schlott, Andrey Stepanov (PSI, Villigen PSI) Rosen Ivanov, Peter Peier (DESY, Hamburg)
Christoph P. Hauri, Leonid Rivkin (EPFL, Lausanne; PSI, Villigen PSI)
Kanade Ogawa, Shigeki Owada, Tadashi Togashi, Makina Yabashi
(RIKEN SPring-8 Center, Sayo-cho, Sayo-gun, Hyogo)
Jia Liu (XFEL.EU, Hamburg)

*Abstract*

The accurate measurement of the arrival time of a hard x-ray free electron laser (FEL) pulse with respect to a laser is of utmost importance for pump-probe experiments proposed or carried out at FEL facilities around the world. This manuscript presents the Photon Arrival and Length Monitor (PALM), the latest device to meet this challenge, a THz streak camera, and discusses the challenges in its design, use, and analysis of results.

## INTRODUCTION

Laser pump, x-ray probe experiments performed at FEL facilities around the world [1, 2, 3, 4, 5] typically want to use short pulse length and intense coherent x-ray radiation to perform experiments with sub-picosecond time resolution. As they go towards improved temporal resolutions, the experiments require accurate measurements of the arrival times of the FEL pulses relative to a laser pump on the sample they are probing. This measurement must also be non-invasive, allowing the experimenters the maximum use of the X-ray beam for their work rather than for diagnostics.

Several methods have been proposed and implemented in the past to meet this diagnostics challenge: transmission/reflectivity spatial and spectral encoding used for soft and hard x-rays at FLASH, SACLA, and LCLS [6, 7, 8, 9], the THz streak camera for soft x-rays at FLASH [10, 11] and other methods [12, 13, 14]. These methods all have their advantages and drawbacks, and the only one that has been attempted for hard x-ray arrival time measurement is the spatial/spectral encoding setup, which has an arrival time accuracy of on the order of 10 fs RMS [6, 9]. The potentially more accurate THz streak camera has not been attempted for use at hard x-ray sources due to the small photoionization cross-section of the gas target and the difficulties in differentiating jitters in the photon energy of the FEL beam from an arrival time signal of the FEL beam by electron spectroscopy. The Photon Arrival and Length Monitor (PALM) prototype chamber [15] developed at the Paul Scherrer Institute (PSI) for the future SwissFEL facility mitigates both of these problems, measuring the pulse length, and the arrival times of hard x-ray FEL pulses relative to a THz pulse and the laser it is generated from.

## CONCEPTS

The concept of the THz streak camera has been explained in the past in literature [16, 17, 18], and has shown itself capable of measuring pulse lengths of high-harmonic-generation (HHG) soft x-rays in table-top laser laboratories. The device can also be used to measure the arrival time of the x-ray relative to the THz pulse.

The THz streak camera uses a gas that is photoionized by the x-ray light as an electron emitter. The electrons are then subject to a time-varying vector potential generated by co-propagating THz radiation, the duration of which is longer than the pulse length of the x-ray pulse. A shift in the arrival time of the x-ray pulse translates to a shift in the kinetic energy gained by the electrons in the vector potential. The final kinetic energy of the photoelectrons $K_f$ streaked by the vector potential $U_p$ is

$$K_f = K_0 + 2U_p sin^2(\varphi_0) \pm \sqrt{8K_0U_p}\sin(\varphi_0) \qquad (1)$$

where $K_0$ is the initial kinetic energy of the electrons at the time of ionization, $\varphi_0$ is the phase of the vector potential at the time of the ionization, and

$$U_p = \frac{e^2E_{THz}^2(t)}{4m_e\omega_{THz}^2} \qquad (2)$$

$E_{THz}(t)$ is the (sinusoidal) THz electric field, $e$ is the electron charge, $m_e$ is the mass of the electron, and $\omega_{THz}$ is the frequency of the THz f in radians/s.

The time delay between the external THz field and the FEL pulse is controlled by a translation stage, and time of flight of the electrons under different time delays ise recorded, forming a two dimensional (2D) streaked spectrogram. As shown in Eq.1, the shape of the spectrogram is determined by the THz frequency, initial electron kinetic energy and the vector potential. The time-to-energy map can be extracted by recording the center of mass (COM) kinetic energy of each time delay and shot-to-shot arrival time of the FEL pulses related to the THz pulse are retrieved by recording the single-shot electron kinetic energy when the stage is set at the middle of the time-to-energy slope.

The pulse lengths are measured by looking at the change in spectral width of the kinetic energy of the electrons. A longer pulse will give a longer width, as described in [10, 11].

Since x-ray photoionization cross sections decrease as the x-ray photon energy increases [19], fewer electrons are thus expected to generate from single-shot ionization of the noble gas atoms for hard x-rays. However, the PALM setup



ISBN 978-3-95450-177-9

# RECENT DEVELOPMENTS FOR INSTABILITY MONITORING AT THE LHC

T.E. Levens*, K. Łasocha, T. Lefevre, CERN, Geneva, Switzerland

*Abstract*

A limiting factor on the maximum beam intensity that can be stored in the Large Hadron Collider (LHC) is the growth of transverse beam instabilities. Understanding and mitigating these effects requires a good knowledge of the beam parameters during the instability in order to identify the cause and provide the necessary corrections. This paper presents the suite of beam diagnostics that have been put into operation to monitor these beam instabilities and the development of a trigger system to allow measurements to be made synchronously with multiple instruments as soon as any instability is detected.

## INTRODUCTION

The first run of the Large Hadron Collider (LHC), from 2009 to 2013, saw transverse beam instabilities at injection and during physics fills while running with 50 ns bunch spacing at an energy of 3.5 TeV [1]. The second physics run, beginning in 2015, has moved to 25 ns bunch spacing, increasing electron cloud and other collective effects [2]. Other changes, such as tighter collimator settings at 40 cm $\beta^*$ [3] and strict limits on beam loss at the increased operating energy of 6.5 TeV [4], mean that the mitigation of beam instabilities has continued to be an important consideration.

The availability of diagnostics to characterise beam instabilities is important, both for qualifying experimentally the LHC impedance model [5] and for making the correct adjustments to the machine settings if instabilities occur during operation.

The recently deployed LHC Instability Trigger Network [6], based on White Rabbit technology [7], enables bi-directional trigger distribution between instruments capable of detecting and observing beam instabilities. The first major use of the network has been to trigger the LHC head-tail monitor [8] with a trigger algorithm running on the base-band tune (BBQ) system [9].

## HEAD-TAIL MONITOR

A workhorse instrument used for characterising beam instabilities is the LHC head-tail monitor. The system, shown in Fig. 1, is based on the high speed acquisition of a long stripline type beam-position monitor (BPM). A commercial wideband 180° hybrid generates the sum and difference of the BPM electrodes and these signals are directly digitised with a 10 GSPS 8 bit digitizer located close to the beam line in a service gallery.

The head-tail monitor was originally installed in the CERN-SPS for chromaticity measurements by the observation of the phase shift between the head and tail of the bunch [8]. Because of the high bandwidth of the BPM and acquisition system, it can also be used for direct time-domain measurements of intra-bunch motion. Although it can provide direct information about the beam stability, the minimum detectable oscillation amplitude is limited by the dynamic range of the acquisition system. A second limitation is the available acquisition memory and data readout speed. The commercial oscilloscopes used in the LHC are limited to 11 turns for all bunches (1 ms of data) and take approximately 10 seconds to read out. These two factors require that the head-tail monitor be precisely triggered once the oscillation amplitude has reached a sufficient level to be visible, but before significant beam loss leads to a beam abort.

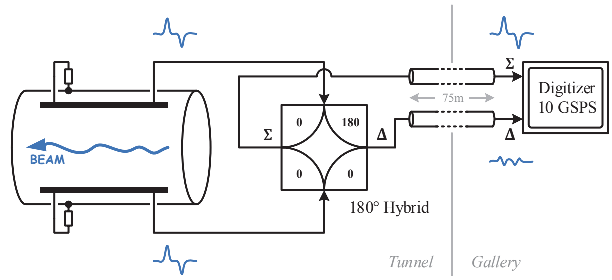


Figure 1: Block diagram of the LHC head-tail monitor.

New digitizers [10] are being tested that feature much larger acquisition memories, capable of storing up to 1.6 s of data. While easing the trigger requirements, the increased data size of up to 64 GB per acquisition poses serious challenges for data storage and processing.

### *Data Processing*

The raw data from the head-tail monitor requires a number of post processing steps in order to obtain useful information about the bunch stability. During the first LHC run, where the head-tail monitor was primarily used for measurements during machine development sessions, the processing was performed manually. In order to understand instabilities that occur during normal operation, the head-tail monitor is now used on a day-to-day basis generating large quantities of data. To help with extracting useful information from these large data sets, an automatic method for determining if an acquisition contains an instability has been developed.

The first step is to determine which, bunch slots are actually filled with beam. For this, a single turn of data from the sum signal of the head-tail pickup is divided into 25 ns intervals. Each of these “bunch slots” is then further sub-divided into five 5 ns segments and the maximum signal amplitude in each of these is calculated. For a slot where no

* tom.levens@cern.ch



ISBN 978-3-95450-177-9

# MULTI-LASER-WIRE DIAGNOSTIC FOR THE BEAM PROFILE MEASUREMENT OF A NEGATIVE HYDROGEN ION BEAM IN THE J-PARC LINAC *

A. Miura#, K. Okabe, M. Yoshimoto
J-PARC Center, Japan Atomic Energy Agency, Tokai, Ibaraki, Japan
I. Yamane
High Energy Accelerator Research Organization, Tsukuba, Ibaraki, Japan

*Abstract*

One of the major missions of Japan Proton Accelerator Research Complex (J-PARC) is the establishment of high-brilliance beam operation. For this purpose, transverse profile monitors play crucial roles in obtaining information concerning beam-mismatching factors and emittance evolution for the linac beam tuning. A wire scanner monitor using metallic wire is currently reliably operated in the J-PARC linac. Because the beam loading on a wire increases under high-current beam operation, we focus on using a laser-wire system as a nondestructive monitor. Additionally, we propose the use of a new multi-laser-wire system. In this study, we propose the multi-laser-wire system and its application. Finally we discuss its advantages over the present profile monitoring system.

## INTRODUCTION

In the J-PARC linac, the negative hydrogen ion beam is accelerated to 400 MeV. The repetition rate is increased to be from 25 to 50 Hz. Half of the 400-MeV beams are injected into the downstream synchrotron (rapid cycling synchrotron (RCS)), whereas the other half are transported to the planned experimental laboratory of the accelerator-driven transmutation facility.

One of the important issues for high-current, high-brilliance accelerators is the understanding of beam dynamics. A wire scanner monitor (WSM) that employs a thin metallic wire is reliably operated in multiple accelerator facilities around the world to suppress excess beam loss and mitigate beam halo evolution. Because the heat loading on a metallic wire is increased under high-current beam tuning, we focus on using a laser-wire system as the nondestructive beam diagnostic device. In addition, we propose a new multi-laser-wire system [1,2] that uses a pair of concave mirrors with different focal lengths to form multiple laser beam paths, and the beam waists of the laser paths are aligned in principle. In this study, we propose the multi-laser-wire system and its application to beam-profile monitoring.

## BEAM SPECIFICATION OF THE J-PARC LINAC

The linac comprises a 50-keV negative hydrogen ion source (IS), a 3-MeV radio frequency quadrupole cavity (RFQ), a 50-MeV drift tube linac (DTL) a 191-MeV separated-type DTL (SDTL), and a 400-MeV annular ring-coupled structure (ACS) [3] as shown in Fig. 1. The ACS-type bunchers are placed between the SDTL and the ACS cavities for longitudinal matching because the operating frequency is 972 MHz for the ACS, which is a threefold frequency jump over that for the SDTL. The ACS downstream is the beam transport line to the RCS.

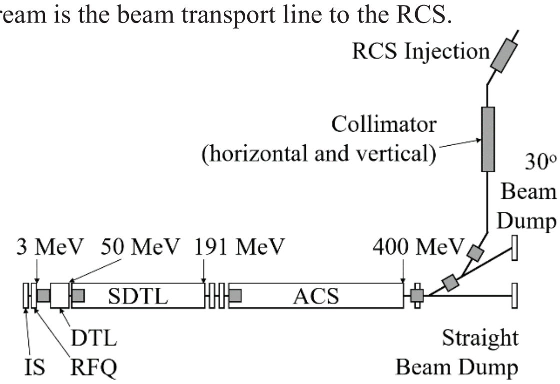


Fig. 1. Beam-line layout of Japan Proton Accelerator Research Complex (J-PARC) linac.

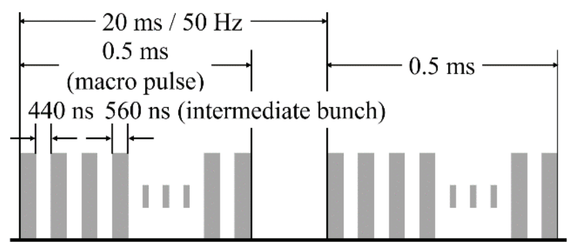


Fig. 2. Time structure of pulsed beam in linac.

The time structure of the pulsed beam in the linac, which is shaped by an RF chopper cavity for RCS injection, is shown in Fig. 2. The beam pulse comprises a 324-MHz micro-bunch, a 560-ns intermediate bunch length, and a 0.5-ms macro-pulse length with 25-Hz repetitions. The shortest pulse duration we can observe occurs during the 3.01-ns micro-pulse.

The metallic wire in a WSM collides with the accelerated beam and destroys a part of it as beam loss. Because it has a high dynamic range in principle [4], we have used it to tune the quadrupole magnets. Tungsten wire has been used due to its high melting point, and its diameter was decided based on the thermal balance and signal gain [4]. However, high beam-current resistance will be required in a device for beam profile measurement. In addition, because the radiation during a high peak current operation should be mitigated, it is important to realize a nondestructive profile monitor based on the laser-wire system.

#akihiko.miura@j-parc.jp



ISBN 978-3-95450-177-9

# SiPMs FOR BEAM INSTRUMENTATION. IDEAS FROM HIGH ENERGY PHYSICS

D. Gascon[†], D. Ciaglia, G. Fernandez, S. Gomez, R. Graciani, J. Mauricio, N. Rakotonavalona, D. Sanchez, A. Sanuy

Dept. de Física Quàntica i Astrofísica, Institut de Ciències del Cosmos (ICCUB), Universitat de Barcelona (IEEC-UB), Martí Franquès 1, E08028 Barcelona, Spain

*Abstract*

Silicon Photomultipliers (SiPM) enable fast low-level ight detection and even photon counting with a semiconductor device. Thanks to a now matured technology, SiPMs can be used in a variety of applications like: Medical imaging, fluorescence detection, range-finding and high-energy physics. We present different possible application of SiPMs for beam instrumentation. First, we discuss timing properties of SiPMs, and how to optimize them for high rate environments enabling photon counting. This requires to understand the dependence of SiPM pulse shape on its configuration (total area, cell size, capacitances, etc.) and analyse dedicated front end electronics techniques. Finally, based on the experience of several projects aiming to develop trackers for high-energy physics, we present some ideas to develop beam monitoring instrumentation based on SiPMs.

## INTRODUCTION

The two main applications of photo-sensors for the detection of elementary particles are the scintillation detectors and the Cherenkov radiation detectors. Scintillators have been extensively used in calorimeters, and recently also in trackers based on scintillating fibres. Time of flight measurement often requires scintillators detectors as well. The most classical example of Cherenkov detector is the Ring Imaging Cherenkov (RICH), used for particle identification.

The photo-sensor requirements are different according to the specific detector. Usually, RICH detectors require blue and Ultra-Violet (UV) sensitivity and single photon detection. On the contrary, scintillator light yield is much higher and the emission is shifted to the blue/green region of the spectrum. However, calorimeters have large dynamic range, up to 100s or 1000s of photons, whereas scintillating fibre trackers are used for Minimum Ionizing Particle (MIP) signals, producing few photons.

For a long time the main photo-detector for such detection systems was the Photomultiplier Tube (PMT), which was created more than 50 years ago [1]. As alternatives to the PMTs, in the last decade, a new type of photo-detector was developed on the basis of the semiconductor technology, the Silicon Photomultiplier (SiPM) [2].

* † dgascon@fqa.ub.edu

## SIPM TECHNOLOGY

The basic element of a SiPM is the Single Photon Avalanche Diode (SPAD) [3], consisting on an Avalanche Photo-Diode (APD) and a quenching element. If the bias voltage of an APD is greater than the junction breakdown voltage (this excess voltage is often called over-voltage), a charge multiplication process occurs and becomes a diverging self-sustaining process (Geiger regime). A quenching resistor, connected in series with the junction, is used to interrupt the avalanche: when the current in the junction is high enough to generate a voltage drop across the resistor close to the applied overvoltage (i.e. the difference between the bias voltage and the breakdown voltage), the current flowing becomes low enough that statistically the avalanche can be quenched and the junction is recharged.

A SiPM ([2], [4], [5], [6]) (also known as Geiger-mode avalanche photodiode, G-APD) is a device obtained by connecting in parallel several miniaturized SPADs (few tens of $\mu m^2$) belonging to the same silicon substrate so that the output signal of the SiPM is the sum of the SPADs outputs. The small SPADs in the SiPM are named microcells.

The gain of a SPAD is expressed as the ratio between the charge produced by the avalanche and the primary charge produced by the interaction of the optical photon within the device. Since the avalanche is interrupted when the voltage at the two sides of the micro-cell goes down to the breakdown voltage, the gain at the two sides of the micro-cell is can be expressed as the product of the SPAD overvoltage and parasitic capacitance.

The output of the SiPM is proportional to the number of cells that fired, provided that the number of incident photons is much smaller than the number of microcells and provided they are uniformly distributed across sensor surface. Since the overvoltage and cell capacitance uniformity can be quite accurate in modern production processes, an excellent separation between peaks in charge spectrum is achieved. This makes possible to count even tens of photons, which is clearly impossible with PMTs.

Photodetection efficiency (PDE) characterizes the probability that a device triggers on an incoming photon [4]. For a SiPM, PDE includes the transmissivity of the coating, the probability to hit the active area versus dead material between microcells (filling factor), and the probabil-



ISBN 978-3-95450-177-9